



HAL
open science

Study of the role of the lateral habenula in fear conditioning and stress response in rat

Laura Durieux

► **To cite this version:**

Laura Durieux. Study of the role of the lateral habenula in fear conditioning and stress response in rat. Agricultural sciences. Université de Strasbourg, 2021. English. NNT : 2021STRAJ023 . tel-03601506

HAL Id: tel-03601506

<https://theses.hal.science/tel-03601506>

Submitted on 8 Mar 2022

HAL is a multi-disciplinary open access archive for the deposit and dissemination of scientific research documents, whether they are published or not. The documents may come from teaching and research institutions in France or abroad, or from public or private research centers.

L'archive ouverte pluridisciplinaire **HAL**, est destinée au dépôt et à la diffusion de documents scientifiques de niveau recherche, publiés ou non, émanant des établissements d'enseignement et de recherche français ou étrangers, des laboratoires publics ou privés.

ÉCOLE DOCTORALE DES SCIENCES DE LA VIE ET DE LA SANTE (ED414)

Laboratoire de Neurosciences Cognitives et Adaptatives (LNCA-UMR 7364)

THÈSE présentée par

Laura DURIEUX

Soutenue le 12 juillet 2021

Pour obtenir le grade de : **Docteur de l'Université de Strasbourg**

Discipline / Spécialité : **Biologie / Neurosciences**

**Étude du rôle de l'habénula latérale dans la peur conditionnée
et la réponse au stress chez le Rat**

**Study of the role of the lateral habenula in fear conditioning
and stress response in Rat**

THÈSE dirigée par :

Mr Lucas LECOURTIER

Chargé de recherche (CNRS), Université de Strasbourg

Mme Monique MAJCHRZAK

Professeur, Université de Strasbourg

RAPPORTEURS :

Mme Nadine RAVEL

Directeur de recherche (CNRS), Université Claude-Bernard, Lyon

Mr Pierre-Hervé LUPPI

Directeur de recherche (CNRS), Faculté de Médecine Laennec, Lyon

EXAMINATEUR INTERNE :

Mme Ipek YALCIN

Directeur de recherche (CNRS), INCI, Strasbourg

AUTRES MEMBRES DU JURY :

Mr Nelson TOTAH

Assistant professor, University of Helsinki, Finland

ACKNOWLEDGEMENTS

First of all, I would like to thank my jury, Nadine RAVEL, Pierre-Hervé LUPPI, Ipek YALCIN, and Nelson TOTAH, for accepting to review and evaluate my thesis work.

Merci à Jean-Christophe CASSEL de m'avoir accueilli depuis mon master et de m'avoir permis d'effectuer ma thèse au sein du LNCA.

Mes remerciements à Chantal MATHIS, responsable d'équipe, pour son accueil.

Un grand Merci à mes directeurs de thèse, Monique MAJCHRZAK pour ta précieuse contribution, pour le travail sans limite que tu as apporté dans les moments clés et pour les discussions qui défiaient mon point de vue et me permettaient d'avoir une meilleure vue d'ensemble ; Lucas LECOURTIER, pour absolument tout. Tu as été pour moi, un des meilleurs "CHEF" que j'aurai pu souhaiter. Je te dois ce que je suis devenue durant ces 4 ans (excepté mon incapacité à écrire correctement. Ça c'est clairement que moi 😊). Tu as été présent et à l'écoute. Tu m'as apporté ton soutien, ton aide quotidienne, et ta confiance même pour des projets aussi fous que de modéliser des réseaux fonctionnels 😊. Et bien sûr, merci à vous deux pour vos corrections, sans faille, de mes documents écrits, quel qu'ils soient. Je ne peux qu'évoquer la patience et l'application que ce travail représente (ainsi que la migraine qui y est très certainement associée). MERCI !

Karine, je ne sais même pas par où commencer... Tu as été, en plus d'une aide précieuse, un soutien moral hors du commun. Tu as été présente pour moi depuis mon master jusqu'à maintenant, des longues heures passées en salle d'immuno, en mois de comptage, (qui n'est quand même pas la plus stimulante des évaluations à faire 😊) en passant par les différents délires qui nous avons pu avoir ainsi que ta joie de vivre continuelle, qui est contagieuse. Je ne sais pas ce que j'aurais fait sans toi <3

Deux autres piliers de mon temps passé au LNCA : un immense merci à Brigitte et à Romain B., qui en plus des temps inoubliables passés avec vous au laboratoire comme à l'extérieur, vous m'avez apporté votre inconditionnelle aide dans vos différents domaines d'expertise. Et oui, cela n'aurait pas été simple de trouver la tVTA sans Romain 😊

Merci à Demian BATTAGLIA et Christopher pour leur aide dans la compréhension du "Graph Theory". En effet, votre aide a été précieuse. I would also like to thank Nelson TOTAH again for his valuable help in setting up the electrophysiologic system, his patience and the time he took to explain to me how LFP analysis works. Comme je suis dans les remerciements liés aux analyses "informatique", je pense directement à Elouan. Merci, de ton aide, ton soutien, des heures passées à m'expliquer comment fonctionne Python et comment fonctionne l'analyse de vidéos. Ta gentillesse naturelle et ta passion sont des inspirations pour moi. Je te remercie aussi pour les heures de jeu vidéo passées ensemble, et certainement pas assez à mon goût, mais cela n'enlève en rien à la qualité de ces moments.

Alexandra, Anne, Katia et Pascal, merci pour votre présence et votre aide à travers cette aventure qu'a été la thèse. Vos apports théoriques ont été très précieux ainsi que nos temps au Milano, ou ailleurs.

Merci à Catherine pour son aide avec "la paperasse" qu'elle seule a le pouvoir de comprendre et de dompter 😊. Merci à Patrick et Sylvie pour leur confiance.

Wilf, Lauren, many thanks for your support and your help in improving my English. Four years ago, I could not speak English at all and now thanks to you, I made a huge progress. Wilf, I cannot find the words to thank you enough, for the beer, the discussions on electrophysiology, the invitation to Germany, and for everything else along the way. Lauren, thank you for being such a force of life, such a good friend and obviously, for the vacation in USA, I could not have enjoyed it as much without you.

Caroline et Elina, vous avez été les plus « supportive » dans cette aventure. I cannot wait to come back to our evenings together, with beer, VR, singing and dancing 😊😄 I also thank you both for making me practice English, and after all drunken English is definitively the best one 😊. More seriously, I really want to thank you for being by my side, no matter what. Je pense que vous avez préservé mon équilibre mental (ou du moins ce qu'il en restait 😊). Είστε οι καλύτεροι φίλοι που θα μπορούσε κανείς να έχει ! São os melhores amigos que alguém poderia ter ! I really hope that means what I intended 😊.

David, Cristiana, Eliabel, Estelle, Gaelle, Isabel, Laura T, Marion, and Rafael, the LNCA and my PhD would not have been the same without you.

Je remercie aussi toutes les personnes que je n'ai pas la place de citer ici mais qui ont participé à ces quatre années que ce soit au sein du LNCA ou à l'extérieur.

Et enfin, un grand merci à ma famille, mes deux frères, Mathis et Olivier, et ma maman, Arlette, pour le soutien inconditionnel que vous m'apportez, pour votre confiance, sans faille, en moi. Vous êtes tous les trois des inspirations pour moi, chacun à votre manière. J'espère vous avoir persuadé, Olivier, Mathis, que le travail, aussi dur soit-il, paye toujours, et que se "donner à fond" est, en finalité, ce qui est le plus important, quel que soit le défi. J'en profite pour faire un dernier petit remerciement pour Pêche et Phantom, bien que je n'aie pas trouvé de traducteur capable de leur faire passer le message 😊😊

Déclaration sur l'honneur *Declaration of Honour*

J'affirme être informé que le plagiat est une faute grave susceptible de mener à des sanctions administratives et disciplinaires pouvant aller jusqu'au renvoi de l'Université de Strasbourg et passible de poursuites devant les tribunaux de la République Française.

Je suis conscient(e) que l'absence de citation claire et transparente d'une source empruntée à un tiers (texte, idée, raisonnement ou autre création) est constitutive de plagiat.

Au vu de ce qui précède, j'atteste sur l'honneur que le travail décrit dans mon manuscrit de thèse est un travail original et que je n'ai pas eu recours au plagiat ou à toute autre forme de fraude.

I affirm that I am aware that plagiarism is a serious misconduct that may lead to administrative and disciplinary sanctions up to dismissal from the University of Strasbourg and liable to prosecution in the courts of the French Republic.

I am aware that the absence of a clear and transparent citation of a source borrowed from a third party (text, idea, reasoning or other creation) is constitutive of plagiarism.

In view of the foregoing, I hereby certify that the work described in my thesis manuscript is original work and that I have not resorted to plagiarism or any other form of fraud.

Nom : DURIEUX Prénom : Laura

Ecole doctorale : ED414

Laboratoire : Laboratoire de Neurosciences Cognitives et Adaptatives

Date : 07/09/2021

Signature

ABBREVIATIONS

#

5-HT: 5-hydroxytryptamine / serotonin

A

AAV: adeno-associated virus

ACC: anterior cingulate cortex

ACM: adaptive calibration model

ACTH: secretion of adrenocorticotrophic hormone

AMG: amygdala

AMPA: α -amino-3-hydroxy-5-methyl-4-isoxazolepropionic acid receptor

AVP: arginine vasopressin hormone

AW: active wake

B

BAC: bed nucleus of the anterior commissure

BG: basal ganglia

BL: basal amygdala

BLA: basolateral amygdala

BNST: bed nucleus of stria terminalis

C

CA1: cornus ammonis 1

CA2: cornus ammonis 2

CA3: cornus ammonis 3

CaMKII: calcium-kinase calmodulin dependent protein II

cAMP: cyclic adenosine monophosphate

CeA: central nucleus of the amygdala

CNO: clozapine-N-oxide

CORT: corticosterone

CRH: corticotropin-releasing hormone

CS: conditioned stimulus

CSD: current source density

CW: quiet (calm) wake

D

DA: dopamine

DAPI: 4',6-diamidino-2-phenylindol

DBB: diagonal band of Broca

DDCS: dorsal diencephalic conduction system

DG: dentate gyrus

dHPC: dorsal hippocampus

DLC: DeepLabCut

dPFC: dorsal prefrontal cortex

DPM: disruption propagation model

DREADD: Designer Receptor Especially Activated by Designer Drug

E

EEG: electroencephalogram

EMG: electromyogram

Ent: entorhinal cortex

EPM: Elevated Plus Maze

EP: entopeduncular nucleus,

exAMG: extended amygdala

F

FA: factorial analysis

FFT: fast Fourier transform

fMRI: function magnetic resonance imaging

FR: *fasciculus retroflexus*

G

GABA: gamma-Aminobutyric acid

GAS: General Adaptation Syndrome

GC: glucocorticoid

GPCR: G-protein coupled receptors

GPI: internal portion of the globus pallidus

GR: glucocorticoid receptor

H

Hb: habenula

hM3Dq: human muscarinic receptor 3 coupled to Gq protein

hM4Di: human muscarinic receptor 4 coupled to Gi protein

HPA: hypothalamic–pituitary–adrenal
HPC: hippocampus
HPLC: high performance liquid chromatography

I

ICM: intercalated cell masses
IEG: immediate-early gene
IL: infralimbic cortex

L

LA: lateral amygdala
LC: locus coeruleus
LDT: laterodorsal tegmental nucleus
LFP: local field potential
LH: lateral hypothalamus
LHb: lateral habenula
LHbL: lateral part of the lateral habenula
LHbM: medial part of the lateral habenula
LO: lateral orbitofrontal cortex
LS: lateral septal nuclei
LTD: long term depression
LTP: long term potentiation

M

MCC: midcingulate cortex
MD: dorso-medial nucleus of the thalamus
MeA: medial amygdala
MHb: medial habenula
MO: medial orbitofrontal cortex
mPFC: medial prefrontal cortex
MR: mineralocorticoid receptor
MS: medial septum

N

NA: noradrenaline
NAc: accumbens nucleus
NMDA: N-methyl-D-aspartate receptor
NREM: non-REM
NTS: nucleus of solitary tract

O

OFC: orbitofrontal cortex

P

PAG: periaqueductal grey
PBS: phosphate buffered saline
PCA: principal component analysis
PFA: paraformaldehyde
PFC: prefrontal cortex
PRh: perirhinal cortex
PRL: prelimbic cortex
PVH: paraventricular nucleus of the hypothalamus

R

RD: dorsal raphe
Re: reuniens nucleus
REM: rapid eye movement
rLHb: rostral part of the lateral habenula
RM: median raphe
RMTg: rostromedial tegmental nucleus

S

SAM: sympathoadrenal medullary
SCN: suprachiasmatic nucleus
SM: *stria medularis*
SNC: substantia nigra pars compacta
SRM: Selected Reaction Monitoring
SUB: subiculum
SuMM: supramammillary nucleus of the hypothalamus
SWR: sharp-wave ripples
SWS: slow wave sleep

T

TS: *triangularis septi*
tVTA: tail of the ventral tegmental area

U

US: unconditioned stimulus

V

vHPC: ventral hippocampus
VO: ventral orbitofrontal cortex
VP: ventral pallidum
vPFC: ventral prefrontal cortex
VTA: ventral tegmental area

TABLE OF CONTENTS

FOREWORD	I
I. RESEARCH OVERVIEW ON MY PHD SUBJECT	I
II. GOALS & STUDY CONDUCT	I
III. THESIS CONTENT.....	III
INTRODUCTION	1
I. BEHAVIORAL ADAPTATION TO STRESSFUL ENVIRONMENT	1
1. STRESS AND RELATED CONCEPTS.....	1
2. THE STRESS RESPONSE	3
a. <i>The behavioral stress response</i>	3
b. <i>The physiological stress response</i>	4
c. <i>Stress and Memory</i>	8
3. NEUROBIOLOGY OF THE STRESS RESPONSE	10
a. <i>Main structures</i>	11
b. <i>Networks</i>	23
II. HABENULA.....	30
1. GENERALITIES	30
2. LATERAL HABENULA.....	32
a. <i>Anatomy and Neurochemistry</i>	32
b. <i>Connectivity and Network</i>	33
c. <i>Functions</i>	37
III. STUDIES PROBLEMATICS	43
IV. GENERAL KNOWLEDGE ON THE TECHNICAL AND CONCEPTUAL APPROACHES USED IN THIS PROJECT	45
1. DREADD (STUDIES 1 & 2).....	45
a. <i>The different types of DREADD receptors developed</i>	46
b. <i>Viral vectors used for DREADD receptors expression</i>	47
c. <i>Strength and weaknesses of DREADD approach</i>	48
2. WIDE SCALE NETWORK ANALYSIS (STUDY 1 AND 2).....	50
a. <i>General goal of Network analysis</i>	52
b. <i>Factorial analysis</i>	52

c.	<i>Introduction to Graph Theory</i>	57
3.	LOCAL FIELD POTENTIAL (STUDY 3)	62
a.	<i>The origin of brain oscillations</i>	62
b.	<i>What can be the role of brain oscillation?</i>	65
4.	DEEP LEARNING TOOL FOR VIDEO TRACKING (STUDY 3)	73
a.	<i>Introduction to Deep Learning</i>	73
b.	<i>Introduction to DLC</i>	73
c.	<i>Summary of DLC operations</i>	74
MATERIALS AND METHODS		76
I. ANIMALS AND HOUSING CONDITIONS		77
II. SURGICAL PROCEDURES		78
1.	GENERAL CONSIDERATIONS	78
2.	ELECTROPHYSIOLOGY EXPERIMENT (STUDY 3)	80
a.	<i>Building of the electrodes</i>	80
b.	<i>Description of the two experiments</i>	81
c.	<i>Surgery</i>	82
III. BEHAVIORAL EVALUATIONS		84
1.	TRACE FEAR CONDITIONING (STUDY 1)	84
2.	ELEVATED PLUS-MAZE (STUDY 1)	86
3.	LOCOMOTOR ACTIVITY (STUDY 1)	88
4.	RESTRAINT PROTOCOL DURING STUDY 2	89
5.	RESTRAINT DURING ELECTROPHYSIOLOGICAL RECORDINGS (STUDY 3)	89
IV. DREADD VALIDATION USING PATCH CLAMP RECORDINGS		92
V. PLASMATIC CORTICOSTERONE		93
1.	BLOOD SAMPLING	93
2.	MASS SPECTROMETRY COUPLED WITH HIGH PERFORMANCE LIQUID CHROMATOGRAPHY	94
VI. HISTOLOGY		97
1.	BRAIN SAMPLING	97
a.	<i>Brain extraction</i>	97
b.	<i>Brain slicing</i>	98
2.	C-FOS IMMUNOHISTOCHEMISTRY	99
VII. IMAGES OBSERVATION AND PROCESSING		100
1.	VERIFICATION OF THE SPREAD OF MCHERRY (STUDY 1 AND 2) AND OF DII (STUDY 3)	100

2.	QUANTIFICATION OF THE EXPRESSION OF THE C-FOS PROTEIN (STUDY 1 AND 2)	100
a.	<i>Production of the pictures</i>	100
b.	<i>Processing of the pictures using a semi-automated method</i>	100
c.	<i>Development of the semi-automated method</i>	102
VIII.	STATISTICAL ANALYSIS	103
1.	GENERAL STATISTICS	103
2.	MULTIVARIATE STATISTIC (STUDY 1 AND STUDY 3)	104
a.	<i>Principal Component Analysis (study 3)</i>	104
b.	<i>Factorial Analysis (study 1)</i>	105
3.	GRAPH THEORY APPLIED TO FUNCTIONAL NETWORKS (STUDY 2)	105
a.	<i>Evaluation of correlations</i>	106
b.	<i>Networks Modeling (Graph Theory Based)</i>	107
c.	<i>Statistical analyses used on the model</i>	110
d.	<i>Alligiance analysis</i>	113
IX.	LOCAL FIELD POTENTIAL RECORDINGS AND PROCESSING (STUDY 3)	117
1.	RECORDING SYSTEM AND DATA PROCESSING	117
a.	<i>Recording system</i>	117
b.	<i>Video recording system</i>	118
c.	<i>Computer hardware for data processing</i>	118
2.	PROCESSING AND ANALYSIS OF THE VIDEO RECORDINGS	119
a.	<i>Preprocessing of the videos</i>	119
b.	<i>Automatic Video Tracking using Deep Learning Approach</i>	119
3.	ELECTROPHYSIOLOGICAL SIGNAL PROCESSING	123
a.	<i>Preprocessing</i>	123
b.	<i>Assessment of Sleep/Wake Stages</i>	125
c.	<i>Removing the artefacts of the signal</i>	128
d.	<i>Frequency and time domain frequency analyses</i>	129
e.	<i>Connectivity analysis</i>	131
	RESULTS	133
I.	STUDY 1: INVOLVEMENT OF THE LATERAL HABENULA IN FEAR MEMORY	134
II.	STUDY 2: FUNCTIONAL BRAIN-WIDE NETWORK MAPPING DURING ACUTE STRESS EXPOSURE IN RATS. IMPACT OF DREADD-INDUCED LATERAL HABENULA INACTIVATION, WITH A NOTE ON CNO	135
III.	STUDY 3: CHANGES IN LATERAL HABENULA OSCILLATORY ACTIVITY UPON REPEATED STRESS EXPOSURE	136

DISCUSSION	137
I. TECHNICAL CONSIDERATIONS	138
II. PRINCIPAL FINDINGS OF THE THREE STUDIES	139
III. HYPOTHESES LINKING THE LHB AND THE STRESS RESPONSE	140
IV. PERSPECTIVES	142
ANNEXES	145
I. GRAPH THEORY ANALYSIS - RANDOM NETWORK MODELING	146
II. SETTING DEEPLABCUT AND CHECKING RESULTS.....	147
<i>f. Pretrained networks and data augmenter evaluation</i>	<i>147</i>
<i>g. Filtering method assessment</i>	<i>148</i>
III. <i>IN SILICO</i> SILENCING OF THE LHB IN THE RESTRAINT STRESS FUNCTIONAL NETWORK	149
REFERENCES	151
RESUME FRANÇAIS.....	182

TABLE OF FIGURES & TABLES

FIGURES

Introduction

FIGURE 1: STRESS SYSTEM MODEL	2
FIGURE 2: ELECTROENCEPHALOGRAM AND HYPNOGRAM OF SLEEP STAGES	5
FIGURE 3: SCHEMATIZATION OF THE HPA AXIS REGULATION AND THE POTENTIAL ROLE OF THE GLUCOCORTICOIDS.	6
FIGURE 4: TIME-COURSE OF MOLECULAR, CELLULAR, AND BEHAVIORAL RESPONSES TO STRESS HORMONES.	7
FIGURE 5: SCHEMATIZATION OF THE FEAR CONDITIONING PARADIGMS.....	9
FIGURE 6: EFFECTS OF STRESS INTENSITY ON GRS OCCUPANCY AND COGNITIVE PERFORMANCES.....	10
FIGURE 7: MAIN STRUCTURES IMPLICATED IN THE STRESS RESPONSE IN THE HUMAN AND RAT BRAIN	11
FIGURE 8: FUNCTIONAL PFC AREAS IN HUMANS AND RODENTS	12
FIGURE 9: COMPARISON OF THE TWO NOMENCLATURES OF THE PFC	13
FIGURE 10: INTRINSIC AND EXTRINSIC CONNECTIONS OF THE AMG.....	19
FIGURE 11: THEORETICAL DIAGRAM OF THE MODULATION OF THE HPA AND SAM AXIS IN RESPONSE TO ACUTE STRESS.	24
FIGURE 12: ORGANIZATION OF THE LIMBIC STRUCTURE MODULATION ON HPA AND SAM AXIS.	25
FIGURE 13: STRUCTURAL CHANGES OCCURRING WITH REPEATED STRESS IN INTERCONNECTED BRAIN REGIONS.....	26
FIGURE 14: THEORETICAL MODEL OF THE NETWORK OF SEROTONIN DRIVEN STRESS.....	27
FIGURE 15: THEORETICAL CIRCUIT OF FEAR EXPRESSION AND FEAR EXTINCTION MEMORY.....	28
FIGURE 16: THEORETICAL MODEL OF PREFRONTAL CORTICAL REGULATION OF FEAR MEMORY FORMATION.	29
FIGURE 17: LOCALIZATION OF THE HB IN DIFFERENT MAMMAL SPECIES.	31
FIGURE 18: SCHEMATIC REPRESENTATION OF LHB SUBNUCLEI IN RATS.	32
FIGURE 19: SCHEMATIC REPRESENTATION OF THE AFFERENCES AND EFFERENCES OF THE LHB	35

FIGURE 20: SCHEMATIC REPRESENTATION OF THE AFFERENCE OF THE LHB IN A “MACROSYSTEM” PERSPECTIVE	37
FIGURE 21 : LHB INACTIVATION INDUCE SPATIAL MEMORY DEFICITS.	40
FIGURE 22: INTRACELLULAR SIGNALING PATHWAYS OF THE G-PROTEIN-COUPLED PROTEINS.	46
FIGURE 23: MAIN TYPE OF DREADD RECEPTORS USED <i>IN VIVO</i>	47
FIGURE 24: GENERAL EXPRESSION OF AVVS IN THE HPC DEPENDING ON THE VIRUS SEROTYPE IN MICE.....	48
FIGURE 25: METABOLIC PATHWAY OF C-FOS TRANSCRIPTION AND ITS ACTION ON LATE RESPONSE GENES	51
FIGURE 26: FICTITIOUS EXAMPLE OF “DIMENSIONAL REDUCTION”	55
FIGURE 27: EXAMPLE OF SCREE PLOT	56
FIGURE 28: MAIN FOUR STEPS TO CONSTRUCT AND ANALYZE A FUNCTIONAL NETWORK USING GRAPH THEORY AS EXEMPLIFIED IN HUMAN STUDIES.....	59
FIGURE 29: CORRELATION OF THE FUNCTIONAL NETWORK NODE DELETION WITH BEHAVIORAL OUTPUT	62
FIGURE 30: EXAMPLE OF SPATIO-TEMPORAL TOPOGRAPHY OF SOURCE AND SINK	64
FIGURE 31: THEORICAL FUNCTIONS OF PHASE SYNCHRONIZATION	66
FIGURE 32: LOGARITHM POWER SPECTRUM OF HIPPOCAMPAL EEG DURING SLEEP AND WAKING STAGES IN MICE.	68
FIGURE 33: EFFECT OF AN ACUTE STRESS ON DHPC IN RATS	70
FIGURE 34: ELECTROPHYSIOLOGICAL INTERACTION OF THE LHB WITH THE DHPC	72
FIGURE 35: WORKFLOW OF DEEPLABCUT	75

Materials & Methods

FIGURE 36: PHOTOGRAPHY OF FLAT EDGE AND BEVELED EDGE ELECTRODES.....	80
FIGURE 37: SCHEMATIC REPRESENTATION OF WIRES IDENTIFICATION.	81
FIGURE 38: SCHEMATIC REPRESENTATION OF THE POSITION OF THE DIFFERENT HOLES DRILLED IN THE SKULL.	83
FIGURE 39: EIB MAP REPRESENTATION FOR BOTH EXPERIMENTS: CSD VALIDATION AND STRESS EXPERIMENT.	83
FIGURE 40: PICTURES OF THE CONDITIONING CONTEXT (LEFT) AND OF THE MODIFIED CONTEXT (RIGHT) USED DURING THE FEAR CONDITIONING PROTOCOL.....	85
FIGURE 41: PICTURE OF THE ELEVATED PLUS MAZE DEVICE	87
FIGURE 42: PICTURE OF THE DEVICE USED TO ASSESS HORIZONTAL LOCOMOTOR ACTIVITY	88
FIGURE 43: PICTURES OF THE TUBE USED FOR THE RESTRAIN STRESS PROTOCOL.....	89

FIGURE 44: PICTURES OF RATS CONNECTED TO THE ELECTROPHYSIOLOGY RECORDING SYSTEM.	90
FIGURE 45: PICTURES (VIDEO CAPTURES) OF THE DIFFERENT BEHAVIORAL TRAITS ANALYZED.	92
FIGURE 46: SCHEMATIC REPRESENTATION (AND PHOTOS) OF THE MASS SPECTROMETRY COUPLED TO HPLC SYSTEM.	95
FIGURE 47: WORKFLOW OF C-FOS SEMI-AUTOMATIC COUNTING	101
FIGURE 48: WORKFLOW OF FUNCTIONAL NETWORK ANALYSIS	106
FIGURE 49: WORKFLOW OF THE GRAPHICAL REPRESENTATION COMPUTING	108
FIGURE 50: WORKFLOW OF THE BOOTSTRAP ANALYSIS	111
FIGURE 51: WORKFLOW OF THE PERMUTATION STATISTICAL TEST	113
FIGURE 52: WORKFLOW OF THE ALLEGIANCE ANALYSIS	115
FIGURE 53: ELECTROPHYSIOLOGY AND VIDEO RECORDING SYSTEMS	118
FIGURE 54: EXAMPLE OF MANUAL LABELLING OF THE RAT BODY PARTS FOR DLC TRAINING.	120
FIGURE 55: EVALUATION OF THE LEARNING PROCESS OF DLC	121
FIGURE 56: EXAMPLE OF DLC LEARNT LABELING.	122
FIGURE 57: PLOT OF THE PREPROCESSING GUI	124
FIGURE 58: SLEEP/WAKE ASSESSMENT GUI	126
FIGURE 59: RESULT OF THE SLEEP/WAKE STAGES ASSESSMENT	127
FIGURE 60: ARTEFACT REMOVAL GUI	128
FIGURE 61: RESULTS OF THE AUTOMATIC ARTEFACT REMOVAL	129
FIGURE 62: EXAMPLE OF FREQUENCY BANDS DETECTION	131

Discussion

FIGURE 63: SCHEMATIZATION OF THE HYPOTHESIS CONCERNING LHB IMPLICATION IN VARIOUS ASPECTS OF THE STRESS RESPONSE.	142
--	-----

Annexes

FIGURE 64: GLOBAL ASSESSMENT OF THE RANDOM NETWORKS	146
FIGURE 65: HISTOGRAM OF THE ACCURACY OF DIFFERENT FILTERS: MEDIAN AND ARIMA	148
FIGURE 66: COMPARISON OF DLC DETECTION MOTIONNESS AND MANUAL BEHAVIORAL CODING MADE WITH AION.	149
FIGURE 67: CORRELATION HEATMAPS OF THE CTL-VEH, THE DPM AND THE HM4-CNO.	150

TABLES

Introduction

TABLE 1: SUMMARY OF THE DIFFERENCES BETWEEN THE MESOLIMBIC AND MESOCORTICAL DOPAMINE PATHWAYS.	22
---	----

Materials & Methods

TABLE 2: STEREOTAXIC COORDINATES USED FOR THE ELECTROPHYSIOLOGY EXPERIMENTS.	82
TABLE 3: ELUTION GRADIENT FOR CORT SAMPLES	96
TABLE 4: MASS SPECTROMETER IONIZATION, SELECTION, FRAGMENTATION, AND IDENTIFICATION PARAMETERS	97
TABLE 5: STEREOTAXIC COORDINATES OF THE CONSIDERED BLOCS IN STUDY 1.....	98
TABLE 6: STEREOTAXIC COORDINATES OF THE CONSIDERED BLOCS IN STUDY 2.....	99

Annexes

TABLE 7: SUMMARY OF THE ERRORS FROM THE DIFFERENT PRETRAINED NETWORK COUPLED TO A DATA AUGMENTER.....	147
---	-----

FOREWORD

FOREWORD

I. Research Overview on my PhD Subject

The physiological mechanisms underlying behavioral adaptation to a stressful situation have been studied from a long time. Since Cannon's work at the beginning of the last century, it has been established that behavioral adaptation to threat depends in particular on the modulating effect of glucocorticoids and adrenaline on brain activity. Different behaviors have been described in stressful situations and a complex brain network has been associated with them. However more than 100 years later, the processes underlying the selection of behaviors adapted to the stressful situation are still not fully understood.

The LHb is a small epithalamic brain structure highly conserved across the evolution. It receives numerous afferences from the limbic system and from the pallidal structures and projects mainly on monoaminergic structures or structures regulating their activity. Given this connectivity, for a long time the LHb was considered as a simple relay of information from the forebrain to the mesencephalic structures.

Recently, research on this structure have highlighted a more important role of the LHb. Thus, the LHb acted more as an integrator of information from the forebrain, modulating the monoaminergic transmission. From there, the number of studies on LHb has increased significantly and has revealed its involvement in many cognitive and emotional processes. In general, the LHb has been shown to be a key structure for adapting the individual's behavior to the environment, and in particular, to a threat. However, how the LHb is integrated into the extensive network supporting the stress response is not yet fully understood.

II. Goals & Study Conduct

The main objective of my PhD was to study the implication of the LHb in the behavioral adaptation to threat. Many previous studies have shown its involvement in the stress response and memory processes associated with a stressful experience. However, the role of the LHb in this adaptive response still needs to be explored.

Our first study aimed to investigate the role of the LHb in fear conditioning, which is a paradigm used to study memory processes associated with stressor exposure. Knowing the interaction, described in the literature, of the LHb with the medial prefrontal cortex (mPFC) and the hippocampus (HPC), we used a type of conditioning engaging these two structures. Knowing the interaction, described in the literature, of the LHb with the median PFC and the HPC, we used a

FOREWORD - Goals & Study Conduct

type of conditioning engaging both structures (*i.e.*, trace conditioning, in which a delay separates the to be associated stimuli, a tone cue and a footshock in our experiments), and studied their functional interaction with the LHb. In a first experiment, we investigated the expression of the c-Fos protein (cellular activity marker) across several regions (*i.e.*, median prefrontal cortex [mPFC], HPC, amygdala [AMG] and LHb), in a trace fear conditioning paradigm. We found that the median part LHb was preferentially displaying c-Fos⁺ cells. Additionally, using a factorial analysis (FA), we have highlighted a functional interaction between the evaluated structures, suggesting that regions of the LHb may be preferentially involved in distinct sub-processes of fear memory formation (*e.g.*, onset of fear response or associative processes). In a second experiment, we inactivated the LHb using a chemogenetic approach (DREADD; Designer Receptor Especially Activated by Designer Drug) during the learning phase of the trace fear conditioning paradigm. Then, we evaluated the fear response of the animal to the cue and to the conditioning context and found that LHb silencing induced a contextual memory deficit and enhanced cued fear. Together, these results demonstrate the involvement of the LHb in fear memory formation and suggests that different parts of the LHb could be involved in distinct processes supporting the formation of memory. associated with an aversive, stressful situation.

Next, we investigated the functional network engaged by an acute stress exposure and particularly the place of the LHb in this network. Following a restrain stress of 10 min, we evaluated c-Fos expression across 56 brain regions including the limbic structures primarily implicated in the stress response (*i.e.*, mPFC, HPC, AMG). The correlation between c-Fos activation in these structures allowed us to model a functional network engaged in the stress response, based on Graph Theory. The functional interactions across the network revealed several modules (communities), suggesting that the architecture of this functional network allows complex processing. Moreover, we found that the highest LHb correlations were with the main structures involved in the stress response (*e.g.*, mPFC, AMG, HPC and several monoaminergic structures). In addition, we studied the modules of the network, resulting in grouping the LHb with several structures necessary for the management of the behavioral stress response. To demonstrate the necessity of LHb to maintain the integrity of this functional network, we inactivated the LHb using DREADD. Surprisingly, the animals only treated with the “specific” ligand of the DREADD receptor, display a completely reshaped functional network during the restrain stress, unfortunately, shading the effect of the inactivation of LHb on the network. These last results did not help us to further understand the role of the LHb in the functional network of interest but provide important insights on the weakness of DREADD approach.

Based on the results of our previous approaches., the interaction of the LHb with the principal limbic structures in the stress response (mPFC, HPC and AMG) suggests its role in the transfer

FOREWORD - Thesis Content

and integration of information from these structures. However, with c-Fos as a marker of the activated structures, we could not investigate the dynamic of these interactions. Therefore, in our third study we decided to investigate the synchronization of these structures on a temporal scale, using local field recordings during and after an immobilization. We added a second immobilization three hours after the first one to evaluate the adaptation of the network at the stressful situation re-exposure. We first evaluated the occurrence of spontaneous behaviors such as stereotypies, which generally appear in rodents upon stress. We focused our analyses on the different sleep-wake stages to address several mechanisms related to the stress response, whether it is the modulation of vigilance or offline processes occurring during sleep. Behaviorally, we observed a lower activation following the second immobilization, in comparison with the first one, suggesting that rats habituated after the first exposure. This was accompanied, after analyses of electrophysiology signals, by a decrease of the time spent in active wake (AW) and an increase of the time spent in slow wave sleep (SWS) and rapid eye movement (REM) sleep. After clustering the rats in two categories based on the intensity of their response to the first immobilization stress, into high responders and low responders, we found that these groups displayed differential Lhb theta synchronization during AW and SWS periods following the second immobilization stress. In addition, a high Lhb-dHPC coherence was found during AW and REM sleep episodes. These preliminary results suggest an implication of Lhb synchronization in coping with stress exposure, as well as a strong collaboration between the Lhb and the dHPC likely during the various processes taking place during the stress response.

III. Thesis Content

This manuscript, based on the format of scientific articles, is organized as followed.

The introduction is divided in four parts. The first part reviews the literature on the stress response, beginning with the first definition of “stress”, passing through behavioral then physiological responses and their impact on memory. Still in this, the neurobiology of the stress response is described, and an overview of its network is proposed. The second part describes the habenula (Hb), its anatomy, anatomic pathways and functional connections; it also includes a review wrote during my PhD (currently unpublished) on Lhb functions and more particularly on its implication in the response to a threatening environment. The third part is a short chapter resuming our working hypotheses. The last part presents the approaches and the advanced analyses that I used during the PhD.

FOREWORD - Thesis Content

Following, the materials and methods of all the experiments performed during the PhD are described in more detail than in the materials and methods of the studies included in the manuscript.

The results are present in published format for study 1, complete draft for study 2. The study 3 is also presented on this format but because the analysis is still ongoing, the draft is not complete.

The discussion and perspective part summarizes and discusses the main results. Furthermore, a global hypothesis based on the obtained results is proposed and some perspectives of future work are developed.

A supplemental information part is added at the end of the manuscript, providing some additional information and very preliminary results. In this part, there is also a section on the validation of the accuracy of the video tracking algorithm used.

INTRODUCTION

INTRODUCTION

I. Behavioral adaptation to stressful environment

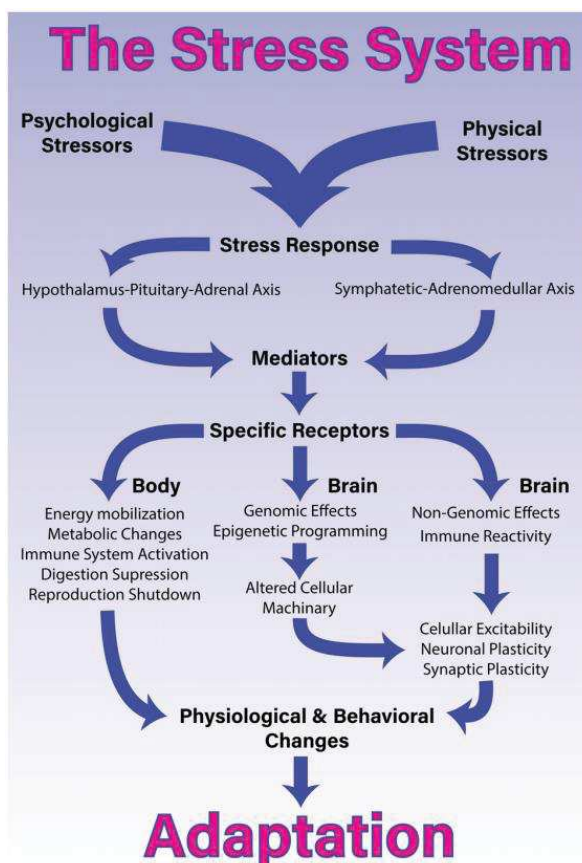
1. Stress and related concepts

In physiology, the concept of stress emerged from the work of Claude Bernard at the end of the 19th century. Then Walter Bradford Cannon, at the beginning of the next century, introduced the notion of **homeostasis**, defined as the ability of living organisms to maintain a stable internal state in a changing environment. This concept was mainly developed, in the middle of the last century, by Hans Selye who defined **stress** as “the nonspecific response of the body to any demand” (Selye, 1976), in the context of the still used today General Adaptation Syndrome (GAS; see Johnson et al., 1992; Godoy et al., 2018 for reviews). This syndrome comprises 3 steps (Selye, 1946, 1950; Johnson et al., 1992; Tonhajzerova and Mestanik, 2017; Godoy et al., 2018): 1) **Alarm reaction**, which is the earliest response to a stressor (“that which produced stress”, Selye, 1976) and defined by a sympathoadrenal medullary (SAM) discharge (*i.e.*, secretion of adrenaline) and the activation of the hypothalamic–pituitary–adrenal (HPA) axis. Its consequences, at the peripheral level, are mainly an increase of muscular tonus, an increase of blood pressure, and tachycardia. At this step of the response, the *fight or flight* response is engaged. 2) **Resistance**, when the body tries to overcome the changes that occurred during the alarm reaction; the body tries to cope with the stressor in order to go back the initial homeostatic state. 3) **Exhaustion**, when the body’s energy resources are so depleted that physical responses are no longer possible. If reached, this last stage may lead to several stress-related pathologies such as anxiety disorders, post-traumatic stress disorder, or depression. The body can also come to a recovery stage instead of exhaustion, *i.e.*, stage 3 is never reached.

Other stress-related concepts have emerged after the GAS model. In 1988, Sterling and Eyer introduced the concept of **allostasis** (Sterling and Eyer, 1988). Allostasis refers to the maintenance of homeostasis through active responses to daily events (*i.e.*, allostasis means: “achieve stability through changes”). Few years later, the concepts of **allostasis load** and **allostasis overload** were introduced (McEwen, 2007). The allostasis load refers to cumulative allostasis process against a stressor, *i.e.*, the cumulated energy spent to reach homeostasis again, whereas its overload refers to the physical or psychological damages resulting from exposure to either acute high intensity, or long duration stressors; it can also result from an ineffective management of allostasis (*i.e.*, prolonged response even if it is not necessary). Allostasis overload results in pathophysiological states (see McEwen, 2007; Tonhajzerova and Mestanik, 2017 for

review). Thus, if stress is essential for survival, it can also precipitate psychiatric disorders such as anxiety-related disorders, depression, and post-traumatic stress disorder (see reviews: Heim et al., 2008; Martin et al., 2009; Walsh, 2011; Saveanu and Nemeroff, 2012; Nemeroff, 2016; Godoy et al., 2018).

Actually, the concept of **stress system** is used to provide an integrated view of all physiological responses to stressors and their interactions to produce a behavioral outcome adapted to the situation (see review, Tonhajzerova and Mestanik, 2017; **Figure 1**); several models have included it in a more complex framework. For example, the model introduced by Del Giudice and colleagues in 2011, the **Adaptive Calibration Model** (ACM; Del Giudice et al., 2011), is based on evolutionary and developmental theories, highlighting individual differences in the functioning of the stress system. The ACM includes the memory of past experiences, the origin and type of stressors, as well as gender, providing an integrated model for future research. According to the authors, the stress response system is central in the adaptation to the context. It takes into account



internal (body) and external (environment) changes and lead to a global response favoring survival through coping with the threats. They further separate this integrated function into three main biological roles: 1) to coordinate the physiological and behavioral responses upon physiological or psychological challenges to restore homeostasis; 2) to filter or amplify the external stimuli (changes in the environment) in order to increase attention and detect predictive cues; 3) to take into account the current psychological state of the individual (*i.e.*, competitive risk taking, attachment, learning, reproductive purpose).

Figure 1: Stress system model
Representation of the stress system defined by Godoy and collaborators (2018).

2. The Stress Response

a. The behavioral stress response

The first description of the behavioral response to environmental stressors (*i.e.*, the exposure to a predator) was the “fight or flight response” by Walter Bradford Cannon ([see Cannon, 1915 for the initial description](#)). Later, other defensive behaviors were described: freeze, a human state of hypervigilance, and fright, also called tonic immobility (*i.e.*, playing dead). The whole sequence of the behavioral response to a threat is often described in the literature as follows: the first response is freezing (being in alert, on guard, with no movement except respiratory ones), a state that can eventually last and become a successful defense mechanism by promoting threat avoidance (for example, freezing can prevent capture by a predator). Freezing, firstly identified as “crouching” ([Blanchard and Blanchard, 1969](#)), is the behavior that rodents engage in when exposed to cues previously associated with aversive stimuli, and is often used as an index of fear. If this behavior does not stop the threat, it can be followed by flight or fight behaviors. Flight, when possible, is the more frequently observed behavior in rats ([Blanchard and Blanchard, 1989](#)). But, if the predator enters in physical contact, the more likely response is “fright” ([see Bracha, 2004](#) for review on the sequence of the stress response). Several other stress responses have been described in the literature. Thus, Taylor and collaborators, suggest that the behavioral stress response depends on the sex of the individual exposed to stress, and is oriented on “tend and befriend” pattern in females: “Tend” indicates the nurturing activities designed to protect the offspring; “Befriend” is the creation and the maintenance of a social network, which could help to get protection ([Taylor et al., 2000](#)).

b. The physiological stress response

The paraventricular nucleus of the hypothalamus (PVH) plays a key role in triggering the physiological response to a stressor by directly activating the SAM and HPA axes (Herman et al., 2003; Ulrich-Lai and Herman, 2009). The limbic structures, such as the PFC, AMG and HPC, are indirectly, through GABAergic (GABA; gamma-Aminobutyric acid) cells groups, connected to the PVH by the bed nucleus of the stria terminalis (BNST) and other subfields of the hypothalamus (Crestani et al., 2013). In addition, the nucleus accumbens (NAc) seems to also participate in the modulation of the HPA axis through the PVH (Noh et al., 2012). In general, activation of the SAM axis is rapid and has short-term effects, whereas activation of the HPA axis is slower and has both short-term and long-term effects. The HPA axis modulates blood levels of glucocorticoids (GCs) that may act in many brain regions during the stress response (de Kloet et al., 2005; de Kloet,

Box 1: Circadian rhythm

Circadian rhythms are periodic variations over approximately 24h in many biological and physiological processes. In mammalian, the suprachiasmatic nucleus (SNC, hypothalamic nucleus) is the principal pacemaker of the circadian rhythm. The rhythmic activity of the clock is endogenous with a period close to 24h and this rhythmic activity is synchronized with the light/dark cycle which has a period of exactly 24h. The internal clock generates a circadian rhythm that synchronizes multiple biological functions in order to anticipate the periodic changes of the external environment. Many physiological functions and parameters have a circadian rhythm, including the sleep/wake cycle and plasma glucocorticoid level. There is a phase relationship between these two rhythms. Glucocorticoid level is highest at the end of the inactivity period (in the morning for diurnal species such as humans, in the evening for nocturnal species such as rats and mice). This increase in glucocorticoid level at this time anticipates the energy needs of the moment of awakening by mobilizing the energy substrates necessary for this period. Glucocorticoid level then decreases progressively throughout the activity phase until it reaches its lowest value during sleep, when the body's energy requirements are lower (see Reppert, 1998; Dunlap, 1999; Gachon et al., 2004; Okamura, 2004; Chung et al., 2011 for more information on the circadian clock).

2013; Joëls, 2018), and may also modulate circadian rhythm (see Box 1) and sleep (see Box 2; Friess et al., 1995; Cleare, 2004; Gamble et al., 2014), or learning and memory (Lupien and Lepage, 2001; Joëls et al., 2006). Adrenaline secreted by the SAM axis is also involved in the modulation of the stress response (Kopin et al., 1988; Musselman et al., 1997) along with others

INTRODUCTION - Behavioral adaptation to stressful environment

monoamines such as noradrenaline (NA), dopamine (DA) and serotonin (5-HT; 5-hydroxytryptamine; [Flügge et al., 2004](#)).

Box 2: Sleep

Sleep can be defined as a periodic and reversible physiological state characterized by a decrease in consciousness and a limitation of perceptual processes. Sleep is divided in two vigilance states: the rapid eye movement (REM) sleep and the non-REM (NREM) sleep. REM sleep is characterized by the presence of rapid eye movement and muscular atonia. During REM, the electroencephalogram (EEG) shows low amplitude and fast activity in the theta range. During non-REM sleep, the EEG is dominated by high amplitude low frequency delta oscillation, and NREM is for this reason also called slow wave sleep (SWS). In humans, non-REM sleep is separated in 4 stages (see [Figure 2](#)) with light (S1 and S2) and deep sleep (S3 and S4), whereas in rats, distinction is only made between REM and non-REM sleep ([Genzel et al., 2014](#)). During the period of sleep, NREM and REM alternate in a cyclic manner (see [Figure 3](#)) with NREM always preceding REM. However, if sleep in humans is monophasic, sleep in rats and mice is polyphasic with very short NREM-REM cycles, which are interspersed with periods of awakening. In both species, sleep functions are numerous and includes brain and body restoration, energy conversion, learning and memory consolidation (see these reviews: [Crick and Mitchison, 1983](#); [Eiser, 2005](#); [Brown et al., 2012](#); [Krueger et al., 2016](#); [Bulkeley, 2017](#), for more information on sleep functions and control of the sleep and wakefulness states).

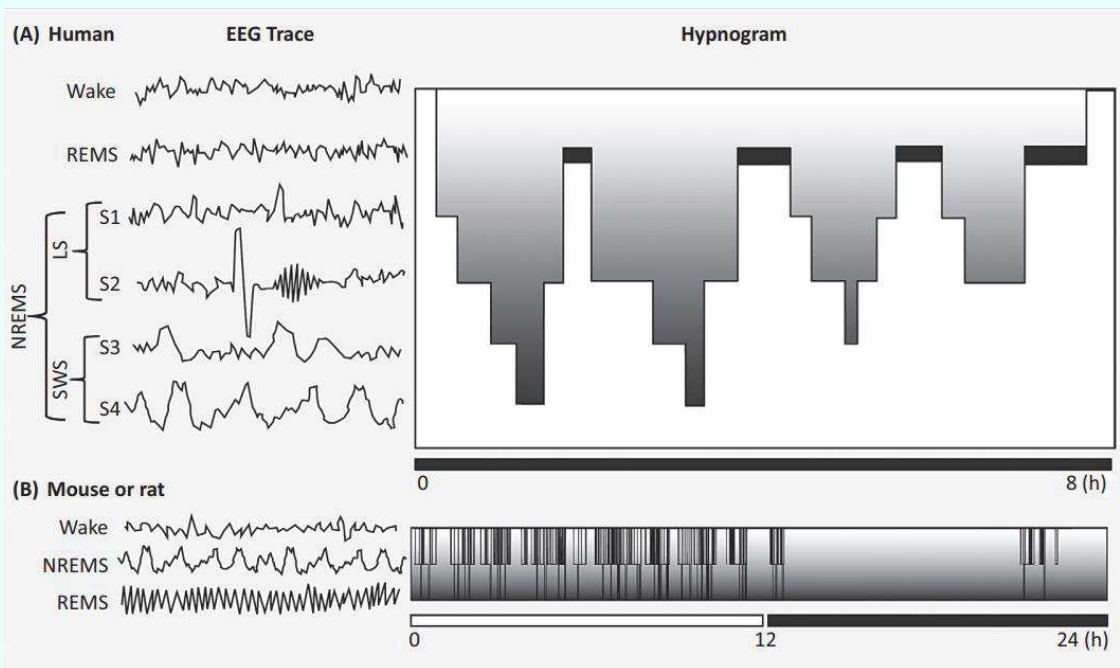


Figure 2: Electroencephalogram and hypnogram of sleep stages
Form [Genzel et al., 2014](#).

Glucocorticoids and the HPA axis

The synthesis of GCs is regulated by the HPA axis activity (see **Box 3**). Two families of receptors are activated by this hormone: the **mineralocorticoid receptors (MRs)** and the **glucocorticoid receptors (GRs)**. The higher density of GRs is found in the PVH (Miklós and Kovács, 2002; Herman et al., 2003). The GRs and MRs are expressed in numerous limbic structures including the HPC (Reul and de Kloet, 1985; Herman et al., 1989; Han et al., 2005), the AMG (Han et al., 2014) and the lateral septal nucleus (LS; Reul and de Kloet, 1985). Note that the distribution of GRs is more widespread than this of MRs (Reul and de Kloet, 1985). The GCs can modulate the HPA axis directly through the PVH and the anterior pituitary, or indirectly through limbic structures (de Kloet et al., 2005; de Kloet, 2013; Godoy et al., 2018).

Box 3: The Hypothalamic–Pituitary–Adrenal axis

The activity of the HPA axis is modulated by the circadian rhythm and stress. The stimulation of the hypothalamus, particularly the PVH (referred to as PVN in figure 3), induces the release of corticotropin-releasing hormone (CRH) and of arginine vasopressin hormone (AVP) which stimulate the secretion of adrenocorticotropic hormone (ACTH) by the anterior pituitary. This hormone stimulates the cortex of the adrenal gland which produces GCs (mainly cortisol in humans, and corticosterone in rodents). The GCs secreted have multiple functions in the body and exert a negative feedback control on the HPA axis (Chung et al., 2011; see **Figure 3**).

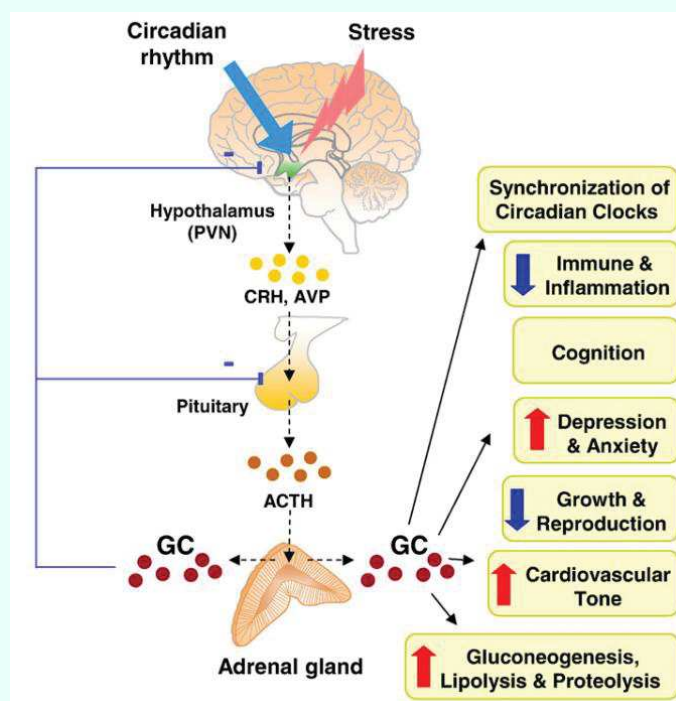


Figure 3: Schematization of the HPA axis regulation and the potential role of the

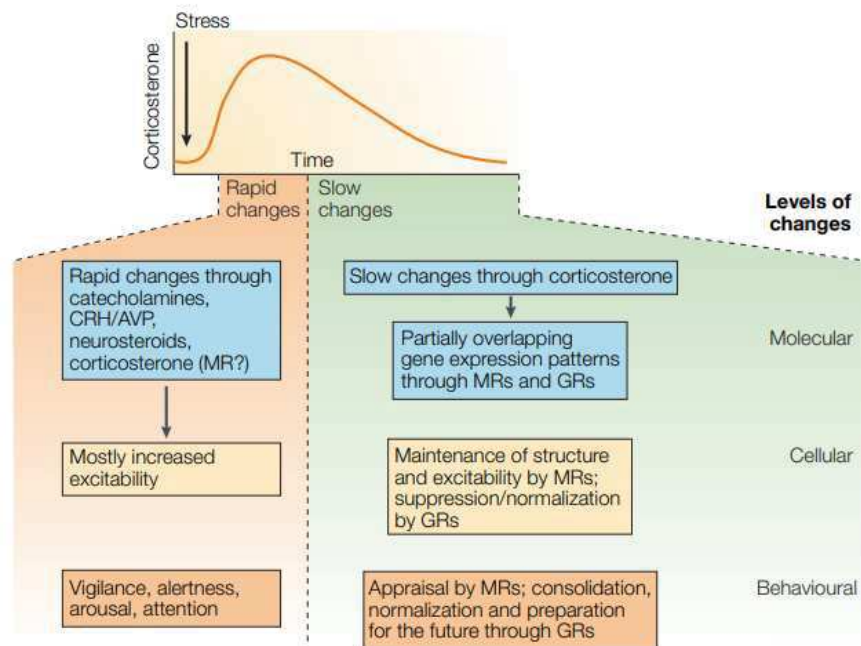
INTRODUCTION - Behavioral adaptation to stressful environment

The GCs also influence memory, and more particularly memory consolidation (McGaugh and Roozendaal, 2002). Small increases of GCs levels are associated, in the HPC, with induction of long term potentiation (LTP; Diamond et al., 1992), whereas high GCs levels have been shown to decrease LTP and increase long term depression (LTD; Pavlides et al., 1996; Xu et al., 1998; Kim and Diamond, 2002). Therefore, whatever the task in rodents, an elevation of corticosterone (CORT) levels seems to be necessary for consolidation processes (Oitzl and de Kloet, 1992; Quirarte et al., 1997; Sandi et al., 1997). In addition, the activation of GRs might promote LTP in the basolateral amygdala (BLA) (Vouimba et al., 2004).

It has been suggested that, under stressful conditions, MR and GR have a complementary role (de Kloet, 2013). Through MRs, CORT has a rapid action that promotes the processing of new information and leads to the selection of the appropriate behavior to cope with the stressor. In contrast, through the GRs, CORT may prevent an “overshooting” of these initial reactions, promoting the formation or consolidation of the memory for its later potential use. In addition,

activation of MRs or GRs appears to play an important role in the time course of CORT effects (see Figure 4), which is essential for an adaptive response to stress (de Kloet et al., 2005).

Figure 4: Time-course of molecular, cellular, and behavioral responses to stress hormones.
From de Kloet et al., 2005.



Adrenaline, Noradrenaline and the SAM axis

The stimulation of the SAM axis leads to the release of adrenaline from the adrenal gland (Cannon, 1915; de Kloet et al., 2005; Joëls and Baram, 2009; Tank and Lee Wong, 2015), and NA from either the sympathetic nerves (Kvetnansky et al., 2009; Tank and Lee Wong, 2015) or the locus coeruleus (LC). The activation of SAM axis affects the autonomic nervous system and modulates vegetative functions (e.g., respiratory, cardiac, metabolic). The LC is involved in numerous circuits including limbic structures implicated in the stress response such as the PFC, the AMG and the

INTRODUCTION - Behavioral adaptation to stressful environment

HPC. The LC, through its NA projections, is involved in the response to an acute stress, acting as an “alarm system” (Myers, 2017). More particularly, these projections are implicated in attention, arousal, and defensive response against a stressor (Cassens et al., 1981; Valentino and Van Bockstaele, 2008). The LC also projects directly onto the PVH (Cunningham and Sawchenko, 1988) to participate to the modulation of the HPA axis (Armario et al., 2012).

One interesting aspect of the stress response is that its actors are engaged in the memorization of stressful events, to favor further coping. For example, in the BLA, the concomitant input of NA and CRH seems crucial for this memory consolidation (Quirarte et al., 1997).

c. Stress and Memory

To be able to adapt ones' response to a threat is crucial for survival. By extend, forging a memory of cues which can be approached and cues which need to be avoided is crucial and relies on associative memory processes underpinned by an evolutionary-conserved neural circuit. Associative memory builds an enduring relationship between two events. To study biological mechanisms supporting associative memory two paradigms are generally used: classical conditioning (or Pavlovian conditioning; defined by Pavlov in 1927), where the two events are external stimuli and which is established independently of the subject's behavior; instrumental conditioning (defined by Thorndike in 1911), in which the subject's behavior is one of two events, the other one being a stimulus (see Wasserman and Miller, 1997; Kandel and Pittenger, 1999; Wang and Cui, 2018 for review). In this manuscript, I have mainly focused on classical conditioning and more particularly on that sustained by a stressor, an aversive stimulus, i.e., **fear (or threat) conditioning**. The main paradigms developed to study memory using such conditioning are presented **Box 4** and the neurobiological substrate involved will be detailed in **Part Neurobiology of the stress response page 10**.

Box 4: Fear conditioning a model to study stress-related memory

Fear conditioning consists of exposing animal to an inescapable stress in a conditioning box (the context) with or without discrete cues predicting the stressor. The contextual fear conditioning occurs when animals are exposed to the context in which an unconditioned stimulus (US; often an electrical shock) is delivered. Animals learn that the context predicts the US. This learning can be tested by replacing the animals in the same context (i.e., conditioning context). If animals have learnt the context-US association, then they will display a freezing behavior. In the cued fear conditioning, either delay or trace, a cue (the conditioned stimulus, CS; often a tone) is also delivered. In the delay paradigm, the US is delivered just after the CS, whereas, in the trace paradigm, the US is delivered several seconds after the CS, creating a gap (i.e., trace) between both stimuli. In cued fear conditioning, animals also associate the conditioning context with the US especially when the cue is not predictive enough of the US delivery. Cued fear memory is assessed by quantifying the freezing behavior induced by re-exposure to the cue, usually in a new context. Context- and cued-conditioned fear can be attenuated/suppressed with an extinction procedure *i.e.*, repeated exposure of the animal to the context and/or sound, without US delivery.

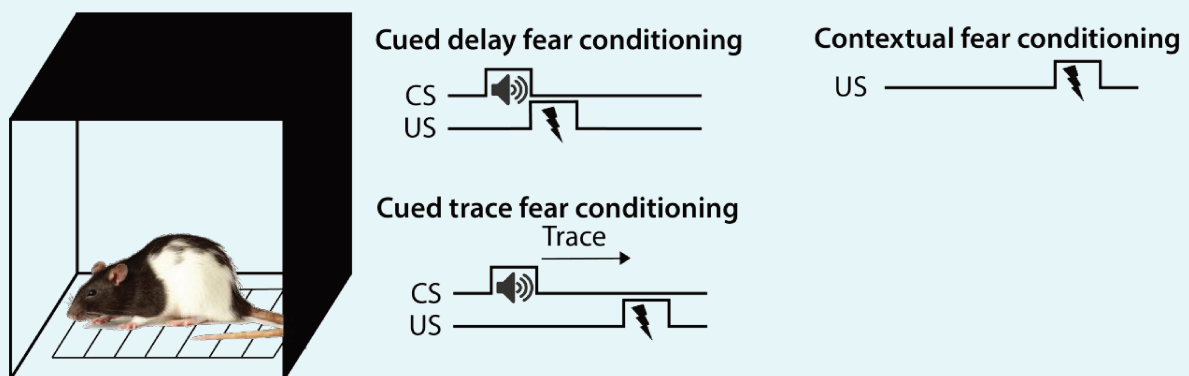


Figure 5: Schematization of the fear conditioning paradigms.
Abbreviation: CS, conditioned stimulus; US, unconditioned stimulus.

In addition to their role in the formation of fear memory, stressors can affect other cognitive processes, with facilitatory or impairing effects depending on the characteristics of the stressors (*i.e.*, intensity, duration, predictability, controllability, and chronicity; see Lupien et al., 2007; Finsterwald and Alberini, 2014; Schwabe, 2016 for review), mainly through their impact on the HPA axis (see part **Glucocorticoids and the HPA axis page 6** for more information). For example, in rats, exposure to an acute strong stressor induced spatial memory impairments (de Quervain et al., 1998; Diamond et al., 1999). Chronic stress, such as chronic restraint, unpredictable randomized stressors or repetitive social stress, led to memory deficits (Luine et al., 1994; Liu et al., 2012; Yuen et al., 2012). The stress intensity determines its beneficial or deleterious impact on memory and cognitive processing according to an inverted U-shaped curve (see **Figure 6**). Stress will enhance cognitive performances until an optimal 'point' is reached. The allostasis load will continue to increase beyond this "optimal point", generating an allostasis

INTRODUCTION - Behavioral adaptation to stressful environment

overload, which may impair memory, and, depending on inter-individual resistance and resilience, may lead to stress-related disorders.

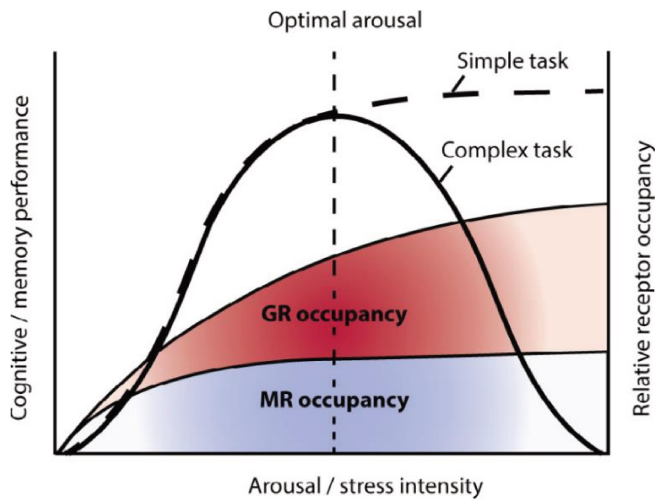


Figure 6: effects of stress intensity on GRs occupancy and cognitive performances

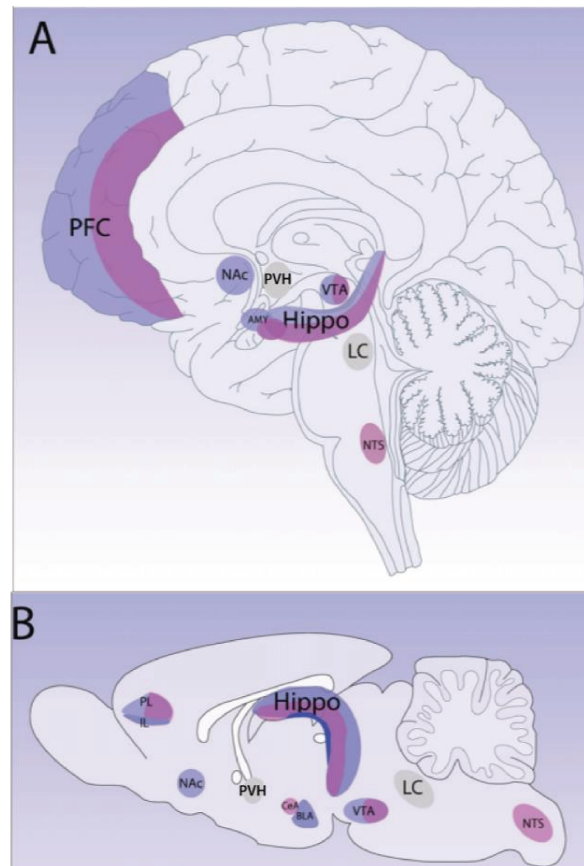
This plot represents the inverted U shape relationship between cognitive performances and stress intensity. Occupancy of GRs and MRs is dependent on the stress intensity. Too high occupancy will decrease memory performances for complex tasks. From Finsterwald and Alberini, 2014.

3. Neurobiology of the stress response

The stress response system recruits a vast network of brain structures, neurotransmitter and hormonal systems, all working in coordination to restore the homeostasis disrupted by physical (e.g., hemorrhage) or psychological (e.g., threat perception or anticipation) stressors. Both kinds of stressors engage two different networks although some structures can be found in both (Figure 7). A growing number of studies focus their research trying to understand networks, in order to take into account interactions between structures. I will first present the main data supporting the involvement of some key structures (because they are particularly relevant to the study of the implication of Hb; see below) in the stress response (restricted to its physiological component) and fear memory, before focusing on studies addressing this response at the network level.

Figure 7: Main structures implicated in the stress response in the Human and Rat brain

Representation of the neuroanatomy of the stress response against a physical stressor (pink) or psychological stressor (blue) in humans (A) and in rodents (B). The neuroanatomical substrate may overlap between both types of stressors (grey). Adapted from Godoy et al., 2018. Abbreviation: AMY, amygdala; BLA, basolateral nucleus of the amygdala; Hippo, hippocampus; LC, locus coeruleus; NAc, accumbens nucleus; NTS, nucleus of the solitary tract; PFC, prefrontal cortex; PVH, paraventricular nucleus of the hypothalamus; VTA, ventral tegmental area.



a. Main structures

The Prefrontal Cortex

Anatomy

The involvement of the PFC in the stress response has been extensively studied; however, due to the lack of homogeneity of PFC subregions across species it remains difficult to obtain a clear view of its exact role (Vogt and Paxinos, 2014; Laubach et al., 2018). The first topological description of the PFC in primates was by Brodmann (Brodmann, 1909). He described a granular layer IV, which is absent (or poorly developed) in non-primate mammals (Carlén, 2017). Currently, another organization is also used in primates, based on the functional implication of its different subregions (see Figure 8A). In rodents, most studies have used a functional nomenclature to describe PFC areas (see Figure 8B). The rodent PFC has been divided in two main subareas: the mPFC and the orbitofrontal cortex (OFC). The mPFC is subdivided as follows: anterior cingulate cortex (ACC), prelimbic cortex (PRL), and infralimbic cortex (IL). The OFC is subdivided in three main parts: medial orbitofrontal cortex (MO), lateral orbitofrontal cortex (LO), and ventral orbitofrontal cortex (VO). However, the names used for primate brain areas do not correspond to

rodent brain areas (Van De Werd and Uylings, 2014), making it difficult to transfer knowledge between species.

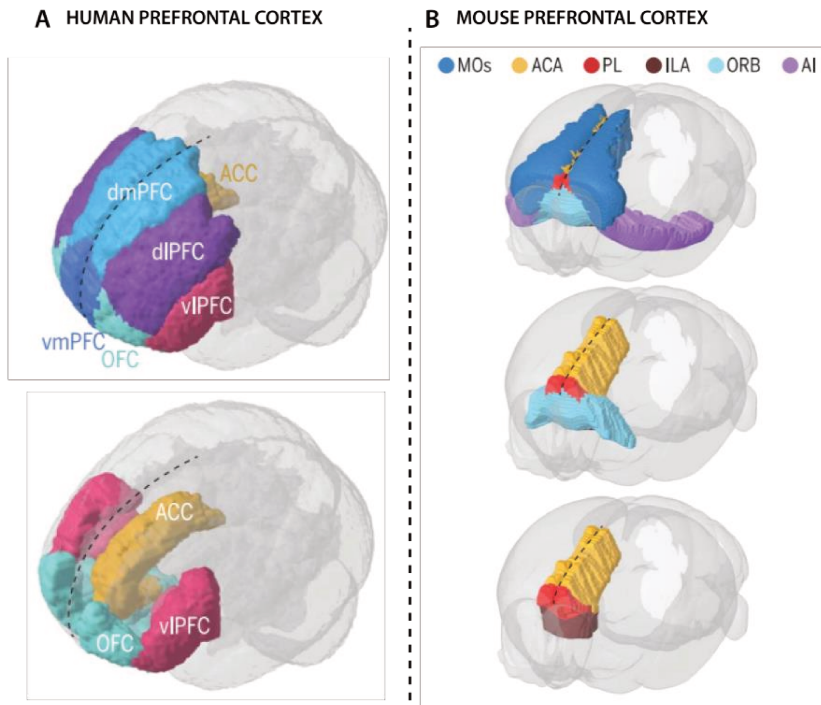


Figure 8: Functional PFC areas in humans and rodents

Representation of the PFC functional divisions in humans (A) and mice (B). Adapted from Carlén, 2017. Abbreviations: ACA, anterior cingulate area; AI, agranular insular area; dIPFC, dorsolateral prefrontal cortex; dmPFC, dorsomedial prefrontal cortex; ILA, infralimbic area; MOs, secondary motor area; OFC, orbital frontal cortex; ORB, orbital area; PL, prelimbic area; vIPFC, ventrolateral prefrontal cortex; vmPFC, ventromedial prefrontal cortex.

Therefore, Vogt and Paxinos proposed a new nomenclature for the rodent mPFC based on cytoarchitectonic analogies with human nomenclature (Vogt and Paxinos, 2014). If some studies begin to use this new nomenclature (Fillinger et al., 2017a, 2017b; Cerpa et al., 2019), most of them, including ours, still refer the previous nomenclature likely because of its extended functional description, still referring to rodent ACC, PRL and IL. However, it is always useful to have an approximate correspondence with the Vogt nomenclature (see Laubach et al., 2018 for comparison of both nomenclatures); the ACC in the Vogt and Paxinos nomenclature refers to the anterior part of the PFC, whereas the posterior part of the PFC is the midcingulate cortex (MCC). In our study, ACC is considered an equivalent of area 32 (dorsal part) and 24b, the PRL is considered an equivalent of area 32 (ventral part) and the 24a, the IL is considered an equivalent of area 25 (except the extreme anterior part represents the MO); however, because their implication in various functions differ we used the MCC such as the Vogt nomenclature has proposed (areas 24b' and 24a') instead of considering the posterior extension of the ACC such as in the previous nomenclature; see Figure 9)

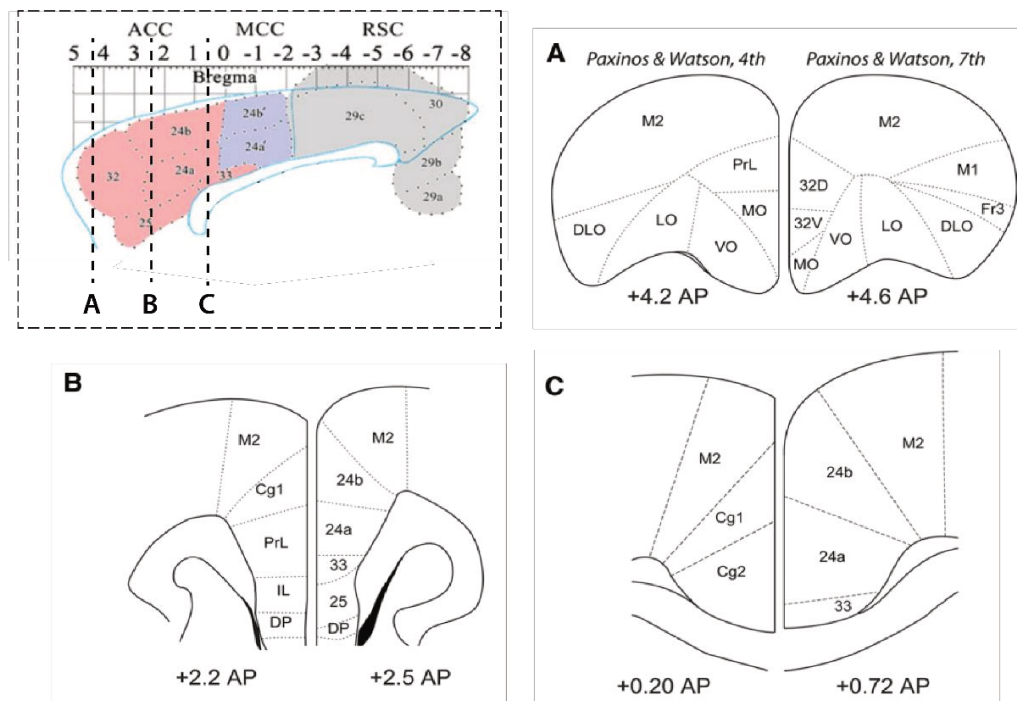


Figure 9: Comparison of the two nomenclatures of the PFC

Abbreviations: ACC, anterior cingulate cortex area; Cg1 & Cg2, anterior cingulate cortex, DLO, dorsolateral orbital cortex; DP, dorsal peduncular cortex; LO, lateral orbital cortex; M1 & M2, motor cortex; MCC, mid cingulate cortex; MO, medial orbital cortex; PrL, prelimbic cortex; RSC, retrosplenial cortex; VO, ventral orbital cortex. Adapted from (A-B-C) Laubach et al., 2018; (top left) Vogt and Paxinos, 2014.

In rats, projections to the mPFC arise in numerous brain regions including several other cortical areas, the basal forebrain, the thalamus, the AMG, the hypothalamus and brainstem structures (see Hoover and Vertes, 2007 for the details). Interestingly, the diversity and density of those projections depend on the subregion targeted (*i.e.*, ACC, PrL or IL), which supports differential roles of those subregions in the stress response. Projections from the mPFC are also numerous (for example, striatum, BLA, lateral hypothalamus [LH], periaqueductal gray [PAG], septum, ventral tegmental area [VTA], dorsal raphe [RD]) and depend on the subregion they arise from (Heidbreder and Groenewegen, 2003; Gabbott et al., 2005).

Role in the stress response

The mPFC is particularly involved in the modulation of the HPA axis (Herman et al., 2003). The mPFC displays a high *c-Fos* response (*c-fos* is an early gene, often used as a marker of activation; see part **Wide Scale Network Analysis (study 1 and 2) page 50** for more information) following exposure to various stressors, including restraint (Cullinan et al., 1995). Interestingly, in rats a lesion of the whole mPFC decreased the plasmatic CORT level before acute restraint (20 min)

INTRODUCTION - Behavioral adaptation to stressful environment

whereas no difference was found after stress (Sullivan and Gratton, 1999). In the same study, the mPFC lesion was also found to decrease circulating CORT level after a chronic restraint (20 min by day for 5 days), when the lesion was bilateral or only on the right hemisphere, but not when only on the left hemisphere; these results suggest a lateralization of mPFC modulation of the HPA axis, which could be explained by a left/right asymmetry of the mesocortical DA system in normal condition and during the stress response (Carlson et al., 1993; Sullivan and Szechtman, 1994; Sullivan and Gratton, 1999). There is also a lateralization of the engagement of the mPFC in rats during chronic social defeat paradigm, as control rats display a higher proliferation of new-born cells in the mPFC in the left hemisphere whereas, in rats exposed to chronic stress, higher levels are found in the right hemisphere (Czéh et al., 2007, 2008).

The implication of the mPFC in the stress response also depends on its subdivisions. For example, bilateral lesion of the PRL, in rats, increases plasmatic CORT concentration and c-Fos expression into the PVH (Diorio et al., 1993; Figueiredo et al., 2003), whereas IL bilateral lesion induces a decrease of plasmatic CORT levels (Sullivan and Gratton, 1999). Also, lesion of the dorsal part of the PFC (dPFC; including the dorsal PRL and the ACC) has anxiogenic effects whereas lesion of the ventral PFC (vPFC; ventral PRL and IL) has anxiolytic effects (Sullivan and Gratton, 2002), suggesting an opposite role of the PRL (at least its dorsal part) and of the IL in the stress response. Anxiogenic effects following dPFC lesion may come from the fact that it indirectly inhibits PVH activity, whereas anxiolytic effects after vPFC lesion might potentially be the consequence of the indirect stimulation of the PVH by the IL (Herman et al., 2003; Radley et al., 2006; Jones et al., 2011). The mPFC innervates several predominantly GABAergic projections onto the PVH including from the BNST, the LH, the dorso-medial nucleus of the thalamus (MD) or the nucleus of the solitary tract (Terreberry and Neafsey, 1987; Hurley et al., 1991; Heidbreder and Groenewegen, 2003). Moreover, the IL and the PRL send projections to the AMG and the raphe nuclei (Hurley et al., 1991; Heidbreder and Groenewegen, 2003; Gabbott et al., 2005) which may in turn participate to the modulation of the HPA axis (see below **page 19 for AMG** and **page 21 for Raphe nuclei**). Finally, the mPFC innervates the paraventricular nucleus of the thalamus (PVT; Hurley et al., 1991; Heidbreder and Groenewegen, 2003) which facilitates HPA activation during the stress response (Bhatnagar and Dallman, 1998).

Unlike the mPFC, the implication of the OFC in the stress response has not been extensively studied. Shiba and collaborators reviewed studies done in animals (rodents and monkeys) concerning the implication of the OFC in fear and anxiety regulation (Shiba et al., 2016). They propose that the OFC contributes to the regulation of emotion through its involvement in outcome prediction.

Role in fear memory

There is a bidirectional modulation of the mPFC on conditioned cued fear expression (Vidal-Gonzalez et al., 2006; Sierra-Mercado et al., 2011). For example, in rodents, in extinction learning (*i.e.*, learning that the CS no longer predicts the US), the vPFC seems necessary for learning the new rule whereas the dPFC seems to promote the expression of the learnt fear (Morgan et al., 1993; Quirk et al., 2006). It can be noticed that studies converge towards the same complementary functional implication of dPFC vs vPFC on the stress response and on the modulation of anxiety. The involvement of mPFC in extinction has been demonstrated in numerous lesion or inactivation studies (Sierra-Mercado et al., 2006; Corcoran and Quirk, 2007; Gilmartin and Helmstetter, 2010), supporting its role in cued-fear extinction learning rather than in cued-fear learning. However, some studies showed that the learning-related associative fear memory is supported by the plasticity of a distributed network (Helmstetter et al., 2008), and Gilmartin and collaborators hypothesized that the PFC may play a role in the plasticity of this network (Gilmartin et al., 2014), although its inactivation or lesion does not impair learning.

In contextual fear learning (see **Box 4**), the mPFC does not seem to participate, at least when the context is the only reliable predictor of the shock (*i.e.*, “foreground” contextual learning; Corcoran and Quirk, 2007; Gilmartin and Helmstetter, 2010). In contrary, when the context is not the only predictor of the shock (*i.e.*, “background” contextual learning), the mPFC is required. Inactivation of the PRL or the ACC prior to cued fear learning impairs the memory of the training context (Zhao et al., 2005; Gilmartin and Helmstetter, 2010) whereas lesion of the vPFC may promote contextual fear memory (Morgan and LeDoux, 1995). The PFC is known to play a role in contextual fear extinction. For example, the PFC is required (in collaboration with the HPC) for the expression of an appropriate fear response in a new context but not in a safe context or in the conditioning context (Orsini et al., 2011).

The PFC seems to be required in learning processes during more demanding variants of fear conditioning. For example, the insertion of a “gap” between the CS and US (*i.e.*, trace fear conditioning; see **Box 4**) makes the learning dependent on the PFC (Gilmartin and Helmstetter, 2010; Guimaraes et al., 2011; Gilmartin et al., 2013, 2013). In this paradigm, the association between CS and US cannot be solely supported by the convergence of information in the AMG as is assumed in delay fear conditioning. Additional brain structures such as the PFC, HPC, entorhinal cortex (Ent), and perirhinal cortex (PRh) are required to appropriately associate the CS and US when several seconds separate them (Gilmartin and Helmstetter, 2010; Guimaraes et al., 2011; Czerniawski et al., 2012; Gilmartin et al., 2012). The PFC would maintain the CS representation, allowing its association with the US. *In vivo* recording of PFC neurons have shown

INTRODUCTION - Behavioral adaptation to stressful environment

that many of them maintain their firing during the trace interval (Baeg et al., 2001; Gilmartin and McEchron, 2005). These particular cells, called “bridging cells”, are observed in the ACC and the PRL but not in the IL (Gilmartin and McEchron, 2005; Takehara-Nishiuchi and McNaughton, 2008). Gilmartin and collaborators also showed that optogenetic silencing of PRL neurons during the trace interval impaired learning of the CS-US association. Interestingly, silencing of these PRL neurons during re-exposure to the CS did not impair cued fear memory expression (Gilmartin et al., 2013). The activity of these ACC and PRL neurons may reflect the local temporary storage of CS information (*i.e.*, short term memory) required for trace conditioning, and/or the maintenance of attentional resources during the trace interval.

The Hippocampus

Anatomy

The HPC consists of the ammonic fields (CA1, CA2 and CA3) and the dentate gyrus (DG). It is subdivided into two main subregions with distinct functional properties, namely the dorsal subregion (dorsal HPC, dHPC) and the ventral subregion (ventral HPC, vHPC). The dHPC is mainly involved in learning and memory processes, while the vHPC is mainly involved in emotional responses and motivation (Fanselow and Dong, 2010).

The HPC is an allocortical structure (4 layers except for CA3 [5 layers]). The intra-HPC circuit is often modelled as a tri-synaptic circuit, each synapse representing a particular type of information transfer: DG granule cells send projections to CA3 pyramidal cells which send projections to CA1 pyramidal cells (Amaral and Witter, 1989; Andersen et al., 2000). A secondary tri-synaptic circuit passing through CA2 has also been described (Kohara et al., 2014). However, the hippocampal circuit is more complex than the tri-synaptic model (see van Strien et al., 2009; Llorens-Martín et al., 2014 for review).

Most of the information reaching the DG arise in the Ent through the perforant path (Witter, 2007). The Ent receives projections from several cortical areas (such as the piriform and insular cortices), from sub-cortical area (including the claustrum, the AMG, several thalamic and hypothalamic areas and from the HPC itself (mainly CA1 and subiculum [SUB]; see Kerr et al., 2007).

The main output regions of HPC is CA1. Its pyramidal neurons send excitatory projections to SUB, mPFC regions such as the PRL and the IL (Herman and Mueller, 2006), hypothalamic nuclei, the PVT, the BNST (Herman and Mueller, 2006), and the BLA, the later sending projection back to the HPC (Herman and Mueller, 2006; Godsil et al., 2013).

INTRODUCTION - Behavioral adaptation to stressful environment

Role in the stress response

The HPC appears essential to respond to stressful situations (McEwen, 1968; Smotherman et al., 1981). Stimulation of the dHPC leads to a phasic increase of CORT levels in rats (Casady and Taylor, 1976). It is hypothesized that the HPC regulates the “ending” of the stress response, as feedback control to bring down GC levels (*i.e.*, when the glucocorticoids return to basal levels). Indeed, in rats, HPC lesion prolongs stress-induced GC release in restraint stress (Sapolsky et al., 1986; Herman et al., 1995). Its role seems to depend on the nature of the stressor, as the prolongation of GCs release is observed following restraint (Sapolsky et al., 1986; Herman et al., 1995), during contextual fear conditioning (Kant et al., 1984), and during open field exposure (Herman et al., 1998), whereas it is not observed in, for instance, hypoxia (Bradbury et al., 1993). Interestingly, HPC outputs are indirectly connected with the PVH and this indirect pathway is inhibitory (Barbas and Blatt, 1995; Herman and Mueller, 2006), suggesting a modulation of the stress response, and more precisely, of the HPA axis using a negative feedback (Jacobson and Sapolsky, 1991; Herman et al., 1996). The inhibition of the HPA axis by the HPC seems to be mediated by the vHPC through its ventral SUB projections; lesion of this area enhances the responsiveness to an open field exposure and restraint (Herman et al., 1995, 1998). The SUB projects onto the BNST, some hypothalamic area (Cullinan et al., 1993), making these regions potential targets to support the negative modulation of the HPC on the PVH. As reviewed by Herman (Herman et al., 2003), the role in negative feedback over the activity of the HPA axis is mediated by GCs acting directly in the HPC which includes a high density of GCs receptors (McEwen et al., 1968; Reul and de Kloet, 1985). Also, direct GC injection into the vHPC flattens the circadian rhythm of glucocorticoid secretion (Slusher, 1966), and that injection of CORT into the dHPC decreases glucocorticoid release in adrenalectomized rats (Sarkar et al., 2002). The response of the HPC to glucocorticoids is very large and support the idea that GRs in the HPC are crucial for the adaptation of the stress response. In CA3, a loss of apical dendrites but an increased basal dendritic tree can be observed after a single stressor exposition (Kole et al., 2004). The GRs have also been shown to be important for the neurogenesis in the DG (Garcia et al., 2004). GCs have been shown to modulate synaptic plasticity phenomenon, *i.e.*, LTP and LTD in the HPC (Diamond et al., 1992; Martin et al., 2000).

Role in fear memory

Overall, the HPC seems to be involved only when contextual representation are required (either temporal or spatial; O'Keefe and Dostrovsky, 1971; Fanselow, 2000; Wiltgen et al., 2006; Maren et al., 2013). In delay conditioning, HPC lesion impairs freezing to the context but not to the CS (Kim and Fanselow, 1992; Fanselow, 2000 but see Quinn et al., 2008). The current hypothesis

regarding the precise involvement of HPC in contextual memory is that it participates to the integration of contextual features and not directly in the association between context and US (Fanselow, 2000; Gilmartin et al., 2014). When animals with HPC lesions receive a shock as soon as they are placed in the conditioning context, so with no time to scan the environment, they present learning deficits (i.e., deficit of context encoding), suggesting less efficient contextual encoding (Wiltgen et al., 2006; Fanselow, 2010).

In trace fear conditioning, the HPC is required to cued conditioning (Knight et al., 2004; Gilmartin and Helmstetter, 2010; Guimaraes et al., 2011), and may participate to bridging of the stimuli (i.e., maintaining the CS representation during the trace interval to allow its possible association with the US) (Wallenstein et al., 1998; Rodriguez and Levy, 2001). However, the firing pattern of CA1 or DG are not consistent with this role (Gilmartin and McEchron, 2005), and the discussion about the exact role of the HPC in trace conditioning is still ongoing.

The extended Amygdala

Anatomy

The extended AMG (exAMG) includes the BNST (separated in subregions; see Dong et al., 2001 for detail on their anatomy), and the AMG itself, which consists of: the Central Nucleus (CeA), the Basal nucleus (BL), the Lateral nucleus (LA), and the Medial nucleus (MeA). However, in the literature, the nomenclature used for AMG nuclei is not always clear. Some authors indicated the Basolateral Amygdala (including BL and LA) by using the abbreviation BLA (this is what we chose to do in our first paper and throughout the manuscript) whereas some other studies use BLA for the BL, which brings confusion into the nomenclature of these subregions.

The intrinsic circuitry of the AMG has been very well described (see **Figure 10A**). The LA projects to the CeA either directly, or indirectly through the BL through glutamatergic projections. The BL send also glutamatergic projection to the CeA. The LA and BL send also indirect projections to the CeA through the intercalated cell masses (ICM) which innervate the CeA with GABAergic projections (Duvarci and Pare, 2014). The AMG receives projections from numerous brain areas (see **Figure 10B**), the LA from sensory cortices, thalamus and PRh, the BL from the hypothalamus, the PFC and the HPC. The LA sends projections to the PFC, such as does the BLA, which also projects to the striatum. The CeA is often considered the output of the AMG (but see Janak and Tye, 2015). It is innervating the BNST, the hypothalamus, the midbrain, the pons, and the brainstem including the PAG (Sah et al., 2003 for an exhaustive review of AMG anatomical connections).

INTRODUCTION - Behavioral adaptation to stressful environment

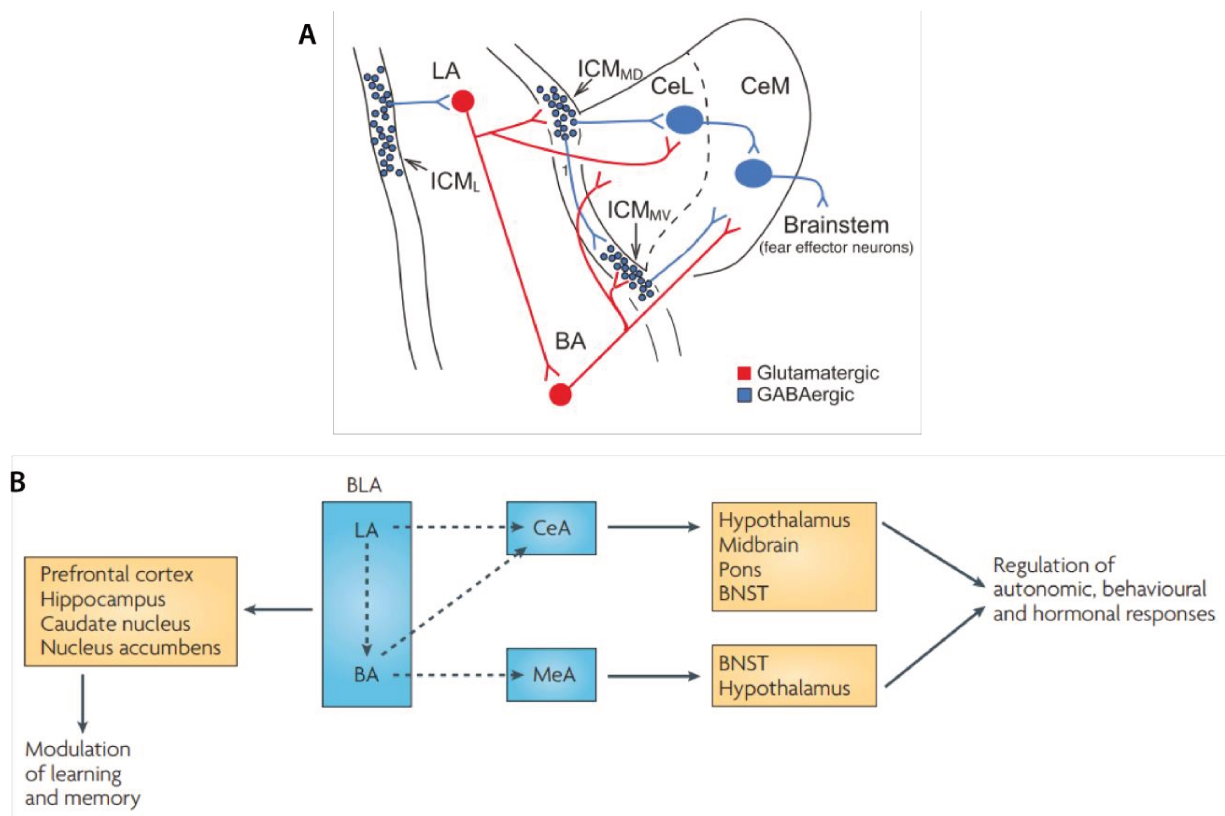


Figure 10: Intrinsic and extrinsic connections of the AMG.

(A) Schematic representation of the intrinsic connections in the amygdala adapted by [Duvarci and Pare, 2014](#). (B) Diagram representing the extrinsic pathways and their functional implications adapted by [Roosendaal et al., 2009](#).

Role in the stress response

The AMG nuclei are involved in different aspects of the stress response ([Roosendaal et al., 2009](#)). The BLA is an essential structure for psychological stressors processing ([Janak and Tye, 2015](#)). It is activated by the anticipation of the stressor ([Cullinan et al., 1995](#)). The BLA has reciprocal connections with the PFC ([Gabbott et al., 2005](#); [McGarry and Carter, 2016](#)), projections which are crucial for aversive learning, fear-related response, anxiety behavior and social interactions ([Felix-Ortiz et al., 2016](#); [Burgos-Robles et al., 2017](#)). The implication of the BLA in stress response is not only restricted to its projections to and from the PFC. Some studies suggest that BLA mediates the stress response also by an indirect pathway to the PVH ([Prewitt and Herman, 1998](#)). However, the lesion of the BLA is ineffective to increase or decrease glucocorticoids levels ([Seggie, 1987](#); [McGregor and Herbert, 1992](#); [Feldman et al., 1994](#)). The BLA would play a more complex role in the regulation of the stress response, for instance by mediating the effect of glucocorticoids on aversive memory ([Roosendaal et al., 2009](#)).

INTRODUCTION - Behavioral adaptation to stressful environment

The AMG participates to the regulation of the HPA axis (Herman et al., 2003) and, contrary to the HPC, its stimulation increases GCs release (Kawakami et al., 1968; Saito et al., 1989), a regulation mediated by the output AMG nuclei, the CeA and MeA, both of them sending projection to the BNST which directly innervates the PVH (Prewitt and Herman, 1998).

Even if the CeA is known to be a central hub in the management of fear response, it is also considered as key structure in the stress response (Ulrich-Lai and Herman, 2009). Lesion of the CeA increase GCs release after restraint or fear conditioning, (Beaulieu et al., 1986; Van de Kar et al., 1991). However, other studies have failed to show an increase of GCs or c-Fos activation in the PVH after restraint (Prewitt and Herman, 1998; Dayas et al., 1999). Herman (2003) evokes the following hypothesis to reconcile the results. He proposes that the CeA is involved in a "reactive" response, depending on the nature of the stress. This proposal could be supported by the c-Fos activation observed in CeA after internal body related-stressors (Sawchenko et al., 1996; Thrivikraman et al., 1997), whereas external stressors lead to a minimal c-Fos response (Cullinan et al., 1995; Emmert and Herman, 1999; Thrivikraman et al., 2000). CeA direct projection to the periaqueductal gray (PAG) are essential to the organization of the response to a threat (LeDoux, 2012).

In contrast to CeA, injury to MeA reduces c-Fos activation in the PVH after restraint in rats (Dayas et al., 1999). Moreover, MeA lesion decreases GCs release after exposure to a stressor (Feldman et al., 1994; Dayas et al., 1999). The MeA appears to be more responsive to external stressors (Cullinan et al., 1995; Emmert and Herman, 1999; Dayas et al., 2001) than to internal stressors (Sawchenko et al., 1996; Thrivikraman et al., 1997; Emmert and Herman, 1999).

As previously mentioned, the BNST plays an important role in the modulation of the HPA axis (Zhu et al., 2001; Choi et al., 2007). It is mostly implicated in the transfer of information from limbic structures (PFC, HPC, AMG) to the PVH.

An interesting fact is that several study in human have shown that the AMG is lateralized over stress effects or emotional processing (Phelps et al., 2001; Baas et al., 2004; Allen et al., 2021). In animal, the lateralization of AMG function is less clear, but has been suggested (see Wilson et al., 2015; Allen et al., 2021 for more details).

Role in Fear Memory

The AMG is known to play a crucial role in formation and expression of CS-US association (Phillips and LeDoux, 1992; LeDoux, 2003).

The BLA is a critical structure for aversive memory consolidation (Roosendaal et al., 2009). Its inactivation impairs aversive memory consolidation (avoidance task in rats; Brioni et al., 1989). It

INTRODUCTION - Behavioral adaptation to stressful environment

is particularly implicated in contextual fear memory (Phillips and LeDoux, 1992) while it was recently shown that its pharmacological inactivation leads to a specific deficit in contextual fear (Calandreau et al., 2005). As mentioned previously, BLA receives a dense input from the HPC. It has been proposed that the BLA relays contextual information to be associated with the US (Phillips and LeDoux, 1992; Maren and Fanselow, 1996). Lesion of the BLA has also been shown to impair conditioned fear extinction (Bouton and Bolles, 1979).

The AMG, especially the LA is a main site of convergence of sensory information allowing the formation of the CS-US association during learning (Romanski et al., 1993; LeDoux, 2000), whereas the CeA, which projects onto the PAG and the hypothalamus, is responsible for the expression of fear behavior. Indeed, its lesion resulted in a generalized deficit in fear expression (Gentile et al., 1986; Hitchcock and Davis, 1986; Campeau and Davis, 1995). However, the CeA may have a more complex role in the CS- and context-US association, as it is also a place of convergence of CS and US information (Turner and Herkenham, 1991; Linke et al., 2000), suggesting its implication in fear learning (Paré et al., 2004; Wilensky et al., 2006).

Brainstem

Dopamine is a key neurotransmitter of the stress response as it is released in many structures upon stress exposure. Main neurons that synthesize DA are located in the substantia nigra (pars compacta [SNc]) and the VTA. For example, stressful experiences, such as restraint or footshocks, increase DA release or DA turn over in the NAc shell (Herman et al., 1982; Abercrombie et al., 1989; Copeland et al., 2005; Ling et al., 2009). The DA system received a particular attention in its potential implication in the stress response, certainly due to its regulation changes in several psychological pathologies. It has been shown that the mesocortical DA system (*i.e.*, liberation of DA in the PFC from the projecting neurons of the VTA) is sensitive to stress (Horger and Roth, 1996). A study showed that a first restraint induced an increased DA release in the PFC whereas a second one, 3 hours later, led to a lower DA levels in the PFC than the first exposition (Jackson and Moghaddam, 2004). These results suggest that the release of DA in the PFC may modulate the stress response and might participate to the “habituation” to stress.

The VTA is a heterogeneous structure, and more precisely, it has been shown that they were different subtypes of the DA neurons, with different efference and afference, distinct anatomical, electrophysiological, and molecular (Margolis et al., 2006, 2008; Ikemoto, 2007; Lammel et al., 2008, 2011). There is a diversity of response of VTA DA neurons to stress so that its implication remains obscure and controversial (Trainor, 2011; Lammel et al., 2014). The mesolimbic pathway (VTA-NAc) is more responding to reward whereas the mesocortical pathway responds to

INTRODUCTION - Behavioral adaptation to stressful environment

punishment/aversive events (see [Table 1](#); [Weele et al., 2019](#)). A study in rats, has shown that, in response to a footshock, neurons from the ventral part of the VTA increased their activity whereas neurons of the dorsal part of the VTA were inhibited ([Brischoux et al., 2009](#)).

	Mesolimbic Dopamine Pathway (VTA-NAc)	Mesocortical Dopamine Pathway (VTA-PFC)
Density of Projection	robust	sparse
Soma Location in VTA	lateral	medial
Ih Current	yes	no
Waveform	conventional	unconventional
Firing Rate	low baseline, low bursting	high baseline, high bursting
Reuptake / Degradation	fast	slow
Presence of Autoreceptors	yes	no
Response to Reward	+++	+ or x
Response to Punishment	+ or -	+++
Major Input(s)	laterodorsal tegmentum	lateral habenula rostromedial tegmentum

Table 1: Summary of the differences between the mesolimbic and mesocortical dopamine pathways.

From Weele et al., 2019.

The Locus Coeruleus (LC) is a brainstem nucleus containing most of the NA-expressing neurons in the brain. The noradrenergic neurons of the LC (LC-NA) are activated by stressors such as restraint, unpredictable shock and social stress ([Wood and Valentino, 2017](#)). The activation of LC-NA occurs in parallel with PVH activation, supporting the cognitive processing needed during the elaboration of the stress response engaging forebrain regions ([Joels and Kloet, 1989](#); [Wood and Valentino, 2017](#)). A study showed that the LC-NA system has a pivotal role in anxiety like behaviors induced by stress by showing that the stimulation of LC activity induce anxiety like behaviors in mice. In addition, its inactivation prevent anxiety like behaviors during stress ([McCall et al., 2015](#)). Interestingly, the LC-NA system is indirectly modulated by CORT ([Valentino and Van Bockstaele, 2008](#)), implicated in the emotional arousal settings state, the facilitating cognition and promoting flexible behavioral responses to stress ([Valentino and Van Bockstaele, 2008](#)).

The raphe nuclei (RD and median raphe [RM] nucleus) are main structures containing neurons expressing 5-HT. The serotonergic system is particularly linked to the stress response. In particular, this system is essential to the selection of the coping strategy. In rat, during a social defeat paradigm, animals who exhibited an active coping style (attack, flight, defensive posture) also had lower 5-HT levels in PFC and AMG ([Diamantopoulou et al., 2012](#)). This is likely to occur

INTRODUCTION - Behavioral adaptation to stressful environment

in coordination with the HPA axis. A study showed that mice using a passive coping strategy facing an acute stress had a hyperactivation of the HPA axis concomitantly to a reduced increase of 5-HT metabolism in the brain in comparison to mice showing an active coping strategy (Veenema et al., 2004). The interaction between 5-HT and CRH may be crucial to switch coping strategy (Puglisi-Allegra and Andolina, 2015). Neurons afferences includes the LC, the hypothalamus, PFC and BNST which play a feedback control over the 5-HT release (Jacobs and Azmitia, 1992; Puglisi-Allegra and Andolina, 2015). In addition, the 5-HT neurons have been implicated in the selection of the coping behavior following an exposition to a stressor (Puglisi-Allegra and Andolina, 2015). The coping behavior can be divided in two main strategies: **active coping** (attempt to act against the stressor) or **passive coping** (no attempt to act against the stressor). The selection of the coping strategy depends on the controllability of the situation and the individual resources. For example, during a controllable situation most of individuals use an active coping to remove the stressor, whereas during an uncontrollable situation, they have the tendency to use passive coping in order to save energy and resources (Vitaliano et al., 1990; Austenfeld and Stanton, 2004).

The PAG is essential to the modulation of the behavioral output upon confrontation to a stressor (LeDoux, 2012). The dorsal part of the PAG is responsive of an unconditioned threat exposition whereas the ventral part is related to conditioned threats. For example, the lesion of the dorsal PAG increase freezing behavior and the lesion of the ventral PAG decrease the freezing response (De Oca et al., 1998; LeDoux, 2012).

b. Networks

In this part of the thesis, I will summarize and assemble the anatomic knowledge we gathered until now, to review the main anatomic networks involve in the stress response and afterwards focus on the fear conditioning networks. We will also discuss about the functional network approach and its contribution to the knowledge of stress response processes and the fear conditioning.

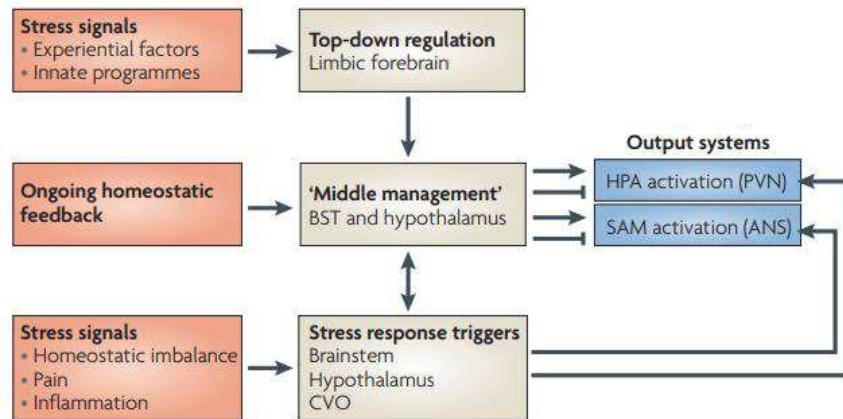
In the stress response

The anatomy of the stress response modulation is very broad. The model proposed by Ulrich-Lai and Herman in 2009, divides the system in three main anatomical “management” (see **Figure 11**): the **top-down regulation system**, including limbic forebrain structures which process the stress signal depending on the individual experience or innate factors; the “**middle management**”, including the BNST and hypothalamus, with modulate the homeostasis and are directly connected to the outputs (*i.e.*, HPA or SAM axis); the **stress response trigger** including the brainstem and

hypothalamus, modulated by stress signals such as homeostasis imbalance, pain or inflammation, and can also activate the outputs systems.

Figure 11: Theoretical diagram of the modulation of the HPA and SAM axis in response to acute stress.

From Ulrich-Lai and Herman, 2009. Abbreviations: ANS, autonomic nervous system; BST, bed nucleus of the stria terminalis; CVO, circumventricular organ; HPA, hypothalamic-pituitary-adrenal; PVN, paraventricular nucleus of the hypothalamus; SAM, sympathoadrenomedullary system.



If we focus on the limbic system (see **Box 5** for limbic system overview) management, we can see that each structure or subregion has a modulatory effect on the stress response by regulating, indirectly, the HPA and SAM axes (see **Figure 12**). The vHPC, more particularly the ventral SUB, has an inhibitory effect on the HPA axis through the hypothalamus, BNST, LS, or mPFC. The AMG has an indirect excitatory effect on HPA and also, for the CeA, on SAM axis. Moreover, the mPFC exercises also a “bimodal” modulatory role. The PRL is implicated in an inhibitory regulation of the HPA et SAM axis whereas the IL stimulates both axes.

Box 5: Limbic system

The concept of the limbic system was introduced in 1952 by MacLean ([Maclean, 1952](#)). It was initially defined in humans by a circuit associating the limbic lobe (defined by Broca as cortical border separating the cortex and the sub-cortical areas; [Pessoa and Hof, 2015](#)) with several sub-cortical areas implicated in emotional and motivational processes (see [Morgane et al., 2005](#); [Roxo et al., 2011](#)). However, today, the limbic system function and neuroanatomy are still controversial, and depend on the authors (see [Kötter and Meyer, 1992](#); [Roxo et al., 2011](#)). In general, this term is associated with the HPC, the cingulate cortex (in humans), the AMG and the NAc. Other brain regions considered as included in the limbic system are the OF, the piriform cortex, the Ent, the fornix, the septal nuclei, the hypothalamus, especially the mammillary nucleus) and the anterior nuclei of the thalamus (see [Kötter and Meyer, 1992](#); [Morgane et al., 2005](#); [Rajmohan and Mohandas, 2007](#); [Roxo et al., 2011](#)). Stressful situations can modulate plasticity mechanisms within the limbic system, which makes this system central in the understanding of the stress response ([Sapolsky, 2003](#)).

INTRODUCTION - Behavioral adaptation to stressful environment

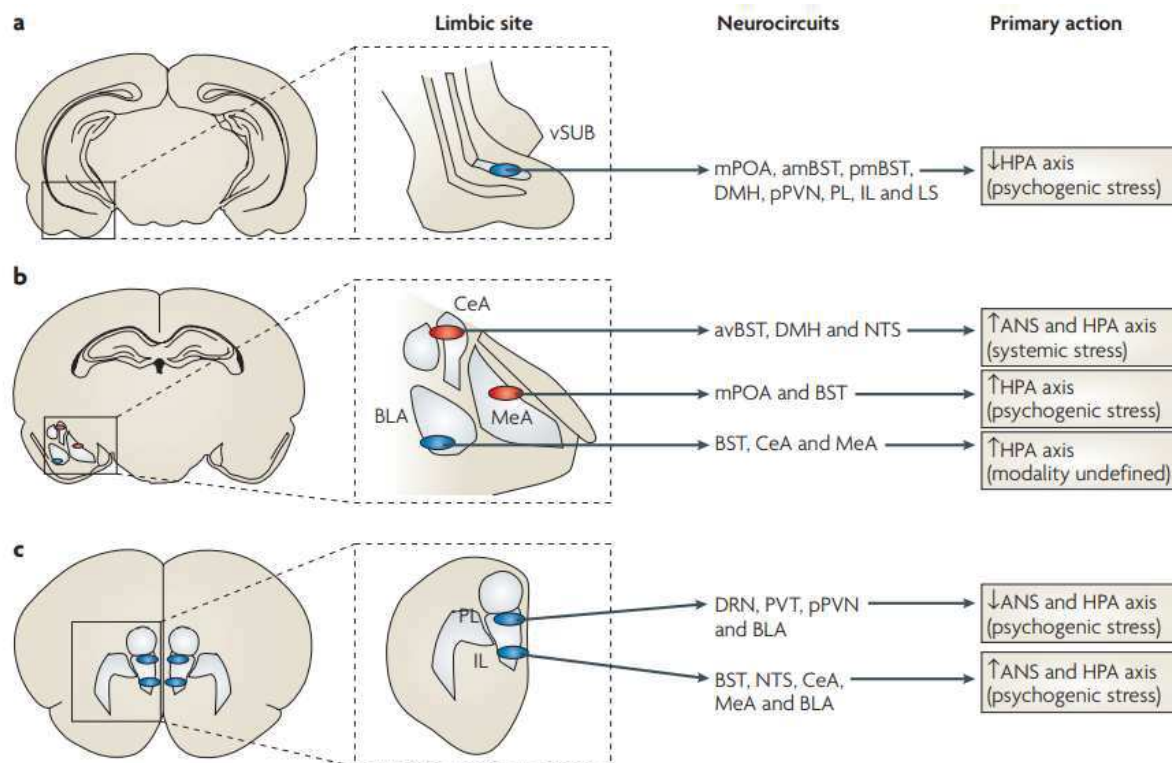


Figure 12: Organization of the limbic structure modulation on HPA and SAM axis.

The blue circles represent excitatory neurons, and the red circles represent inhibitory neurons. From [Ulrich-Lai and Herman, 2009](#). Abbreviation: amBST, anteromedial BST; avBST, anteroventral BST; BLA, basolateral amygdala; BST, bed nucleus of the stria terminalis; CeA, central amygdala; DMH, dorsomedial hypothalamus; DRN, dorsal raphe nucleus; IL, infralimbic cortex; LS, lateral septum; MeA, medial amygdala; mPOA, medial preoptic area; NTS, nucleus of the solitary tract; PL, prelimbic cortex; pmBST, posteromedial BST; pPVN, peri-PVN; PVN, paraventricular nucleus of the hypothalamus; PVT, paraventricular nucleus of the thalamus; vSUB, The ventral subiculum.

The regulation of the stress response is managed by cross-limbic modulations (*i.e.*, communication between limbic structures). As an example, it has been shown that the projections from the HPC to the PFC and the BLA plays a crucial role in memory and in the regulation of the stress response (see [Neurobiology of the stress response page 10](#); [Godsil et al., 2013](#)). The PFC seems to modulate the HPC-BLA system and by extent the stress response, using a top-down control, ([McDonald et al., 1999](#); [Janak and Tye, 2015](#); [Radley et al., 2015](#)). During an intense psychological stress, the connection between the HPC and the mPFC become functionally disrupted ([Zheng and Zhang, 2015](#)). During this type of intense emotional experience, the activity of PFC is suppressed and the HPC-BLA pathway activates synaptic plasticity related to memory consolidation ([Diamond et al., 2007](#)). On top of that, chronic stress induces many structural changes in the limbic system leading to changes in the responsiveness of the structures and affecting the behavioral outputs. However, the effect of chronic stress in the stress network and

INTRODUCTION - Behavioral adaptation to stressful environment

especially in the limbic system depends on the structures considered (see [Figure 13](#); [Roosendaal et al., 2009](#)). The structural change in the AMG leads to a hyperresponsiveness to stressors and is positively correlated to the severity of chronic stress-induced symptoms. In comparison, the structural changes in the HPC and the mPFC are negatively correlated to the severity of these symptoms.

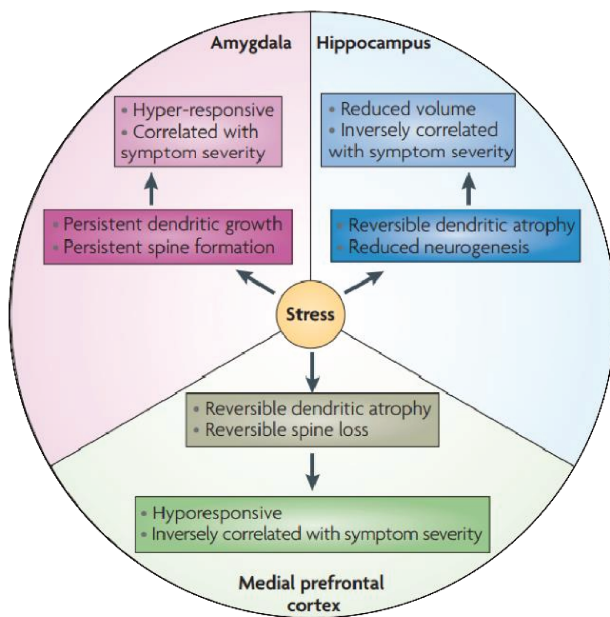


Figure 13: Structural changes occurring with repeated stress in interconnected brain regions

From [Roosendaal et al., 2009](#).

As discussed previously, brainstem structures, more precisely the monoaminergic structures, are implicated in the modulation of the stress response with extraordinarily complex and interactive system. For instance, the stimulation of the RD by GCs leads to the modulation of 5-HT in the mPFC which, by feedback on the RD, regulates 5-HT release in the BLA; this modulation of 5-HT release regulate the effect of DA in the NAc (see [Figure 14](#); [Puglisi-Allegra and Andolina, 2015](#)). All these complex interactions modulate the selection of the coping behavior during stressor exposure.

INTRODUCTION - Behavioral adaptation to stressful environment

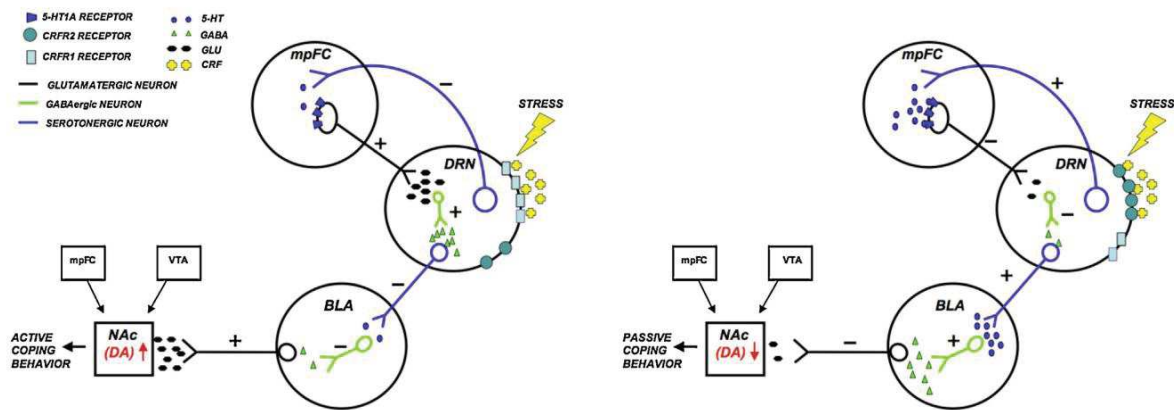


Figure 14: theoretical model of the network of serotonin driven stress.

Model proposed by Puglisi-Allegra and Andolina, 2015. Abbreviation: DRN, dorsal raphe nuclei; CRFR, corticotropin releasing factor receptor; BLA, basolateral amygdala; NAc, nucleus accumbens ; VTA, ventral tegmental area; mpFC, medial prefrontal cortex.

However, the stress response network is more complex than these models. For exploring the stress response at the brain level, researchers have studied functional connectivity through the whole brain in response to acute or chronic exposure to a stressor, trying to better understand how all structures coordinate (Schwabe, 2016; Sousa, 2016). The functional connectivity represents a measure of inter-dependence or synchronization between two brain structures. This interaction is known to represent a support of information processing between these two structures (see part **Wide Scale Network Analysis (study 1 and 2) page 50** for more details on the functional connectivity). This type of study is often conducted with fMRI (function magnetic resonance imaging) or EEG data in humans. However, this approach is currently growing in rodent studies too (Grandjean et al., 2017, 2019).

In humans, a stressful stimulus reproductively activates a set of brain regions (Herman et al., 2003; Dedovic et al., 2009; Ulrich-Lai and Herman, 2009; Sousa, 2016), among which the principal structures of the response such as PFC, HPC, AMG, BNST or PVH (Herman et al., 2003; Dedovic et al., 2009; Ulrich-Lai and Herman, 2009; Sousa, 2016; Godoy et al., 2018). Most of the studies in humans use this approach to find patterns of activation in order to predict pathology development (Franklin et al., 2012; Sousa, 2016). In rodents, few studies used functional connectivity approach to study the stress response and they often focused on chronic stress. In rats, using fMRI, dynamic changes through time following chronic restraint were found. In addition, this study divided the rats in two groups, low responsive and high responsive to chronic stress, to understand the heterogeneity of individual response against a stressor. They found difference in the functional connectome of both group before any restrain stress, providing potentially a

INTRODUCTION - Behavioral adaptation to stressful environment

biomarker to predict individual's resilience or vulnerability to chronic exposition to stressful conditions (Magalhães et al., 2018). In another study, also using fMRI, they showed that the default mode network in rat was affected by chronic restraint and more particularly, that the connectivity strength in the default mode network was increased in the stressed animals compared to control (Henckens et al., 2015). These results indicate an alteration of functional connectivity by a chronic restrain stress.

In fear conditioning

As mentioned before the main actors for the expression of fear and fear extinction are the PFC, the HPC and the AMG (see Figure 15; Sierra-Mercado et al., 2011). For fear expression, the PRL exchanges information directly with the BLA. The vHPC send information to the PRL and the BLA. The BLA processes the inputs and send the information to the CeA which, by its connection to the brainstem, generate fear expression. During extinction, the IL plays the main role in the PFC. IL receives information from the vHPC and the BLA. The IL and the BLA project to the IMC (GABAergic neurons) which projects to the CeA, decreasing the CeA activity and by extend fear expression.

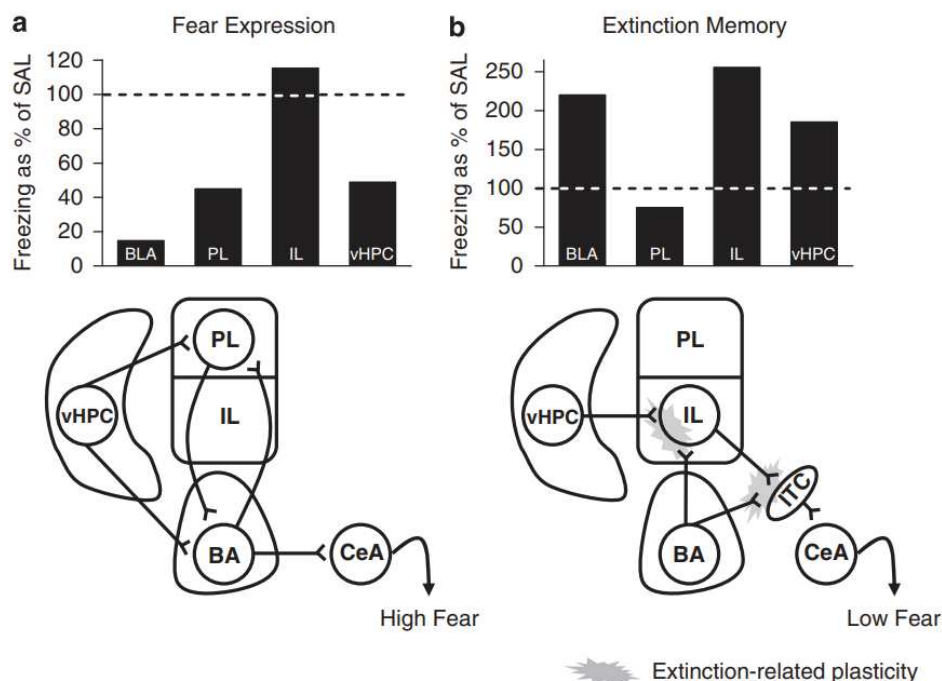


Figure 15: Theoretical circuit of fear expression and fear extinction memory.

From Sierra-Mercado et al., 2011. Abbreviation: BA, basolateral amygdala; CeA, central amygdala; IL, infralimbic cortex; ITC, intercalated cell masses; PL, prelimbic cortex; vHPC, ventral hippocampus.

Gilmartin, in 2014, proposed a model related to the functions of the connections between the main regions involved in trace fear conditioning (Gilmartin et al., 2014). In this model (see Figure 16), the ACC modulates attention and US expectancy processing, and the PRL maintains the CS

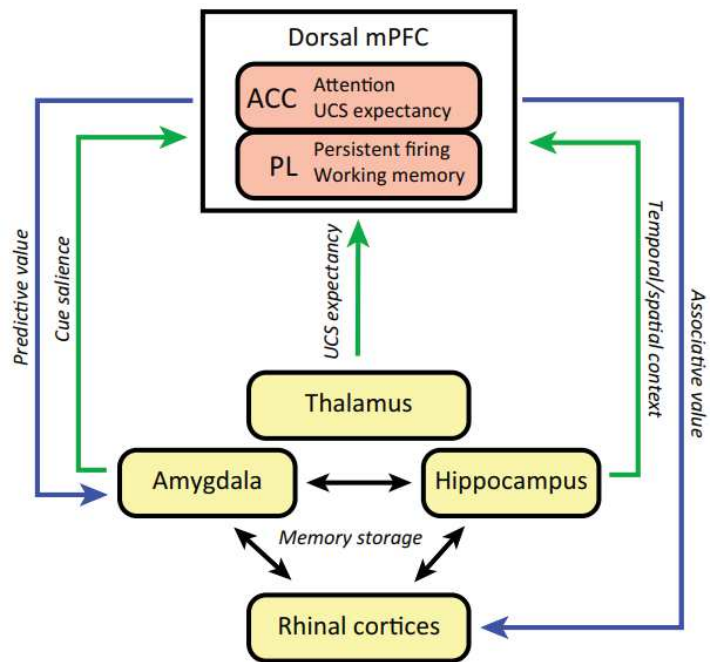
INTRODUCTION - Behavioral adaptation to stressful environment

representation, allowing its association to the US. In this proposed model, the dPFC exchanges information with the AMG and the HPC about cues salience and predictive values (AMG), temporal and spatial context (HPC) and the associative value (rhinal cortices). The thalamus projection to the dPFC is implicated in the USC expectancy information. The connection between AMG, HPC and rhinal cortices is involved in the storage of the memory associated with the experience.

Figure 16: Theoretical model of prefrontal cortical regulation of fear memory formation.

From Gilmartin et al., 2014.

Abbreviations: ACC, anterior cingulate cortex; mPFC, medial prefrontal cortex; PL, prelimbic cortex.



However, one should not forget that fear memory consolidation, or consolidation of fear extinction, are partly done during sleep (Totty et al., 2017; Tempesta et al., 2018), which integrate more potential network interaction to the “basic” model evoked here.

In addition, fear conditioning networks have also been studied with functional connectivity approaches to reach a better understanding of the global network interaction. Studies in rodents are very few but bring interesting insights for future studies. Frankland’s group (Wheeler et al., 2013) did a functional connectome study based on the correlation of c-Fos density through many structures during contextual fear conditioning. They showed that the network supporting fear memory changed with time. The functional network needed to retrieve the memory at 31 days was associated with stronger functional connections over the brain but more particularly between the PFC and the thalamus and between the cortex and the HPC. They also identified several structures (including ACC and PRL) as important key hubs for the long-term fear memory, suggesting a crucial role of these structures in the modulation of the network. Moreover, this analysis provides a global picture of the organization of long-term fear memory in mice. A second

study from the same group (Vetere et al., 2017) validate, on the network they found previously, that the highly connected structures in the functional network influence the behavioral output in fear contextual memory.

II. Habenula

In this part of the introduction, I will focus on the Hb and more particularly the lateral habenula (LHb). I will begin by the generalities on the Hb and its phylogenetic evolution. Then, I will focus on the LHb, addressing its anatomy, its connectivity, and the different functions it is participating to. The part of this introduction will be devoted to a review that we plan to publish, including a general description of its particular involvement in the stress response and fear-related behaviors. I will do my best to avoid overlaps between the introduction on the Hb and the review concerning the LHb and emotional behaviors.

1. Generalities

The Hb is a brain region included in the epithalamus. Its name comes from “*habena*” in Latin meaning “little rein” because of its elongated shape. The Hb is part of the epithalamus, which is located, in mammals, e.g., rodents, cats, monkeys, and humans, along the 3rd ventricle, dorsally to the thalamus (Concha and Wilson, 2001; Díaz et al., 2011; Namboodiri et al., 2016); see **Figure 17**). The Hb receives its input through the *stria medularis* (SM) and projections from the Hb go through the *fasciculus retroflexus* (FR); SM, Hb, and FR form the so-called dorsal diencephalic conduction system (Sutherland, 1982; Roman et al., 2020).

INTRODUCTION - Habenula

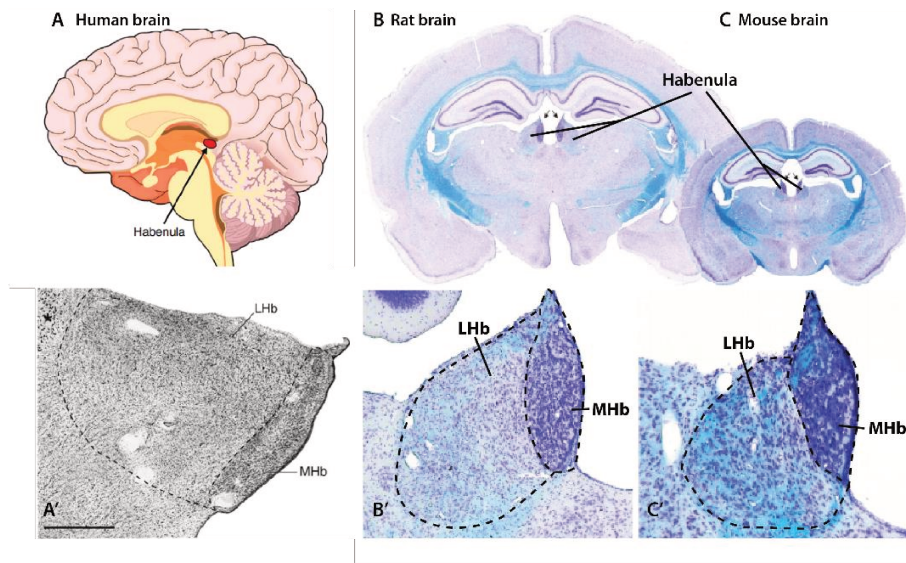


Figure 17: Localization of the Hb in different mammal species.

Localization of the lateral and median habenula in humans (A, A'), in rats (B, B'), and in mouse (C, C'). A', B', and C' are Coronal views zooming on the Hb. Adapted from Diaz et al., 2011, Wagner et al., 2014, Namboodiri et al., 2016.

The medial habenula: a short note

The medial habenula (MHb) is small mostly contains glutamatergic, substance P and cholinergic neurons (Aizawa et al., 2012; Frahm et al., 2015). The MHb receives inputs from the whole septal area [*i.e.*, the *septofimbrialis* and *triangularis septi* (TS) nuclei, the medial septum (MS) and the diagonal band of Broca (DBB)] and from the bed nucleus of the anterior commissure (BAC), ; its principal outputs are the interpeduncular nucleus and the pineal gland (Herkenham and Nauta, 1977, 1979; Qin and Luo, 2009; Viswanath et al., 2014; Namboodiri et al., 2016; Metzger et al. 2019). The MHb is involved in locomotion and anxiety (Otsu et al., 2018), and in the response to various drugs (nicotine: Fowler et al., 2011; Görlich et al., 2013a, 2013b; Zhao-Shea et al., 2013; morphine: Neugebauer et al., 2013; amphetamine: Ellison, 2002; Ciani et al., 2005). It is also involved in fear response. Selective lesion of MHb cholinergic neurons in mice enhance the fear expression to the sound previously associated with an electric shock (Zhang et al., 2016). Conditional deletion of cannabinoid type 1 receptors in MHb neurons lead to a reduced fear-conditioned freezing and abolished conditioned odor aversion (Soria-Gómez et al., 2015). Yamaguchi et al. (2013) found that selective ablation of the TS-MHb pathway was anxiolytic and that selective ablation of the BAC-MHb pathway enhanced the freezing response to electric footshocks (Yamaguchi et al., 2013). Finally, the MHb has been associated to depression, as knocking-down of choline acetyltransferase in the MHb induced anhedonia-like behaviors (Han et al., 2017).

2. Lateral Habenula

The thesis project concerns principally the LHb and its involvement in trace fear conditioning and its implication in the modulation of the stress response. In this part we will introduce the LHb, from anatomical to functional considerations.

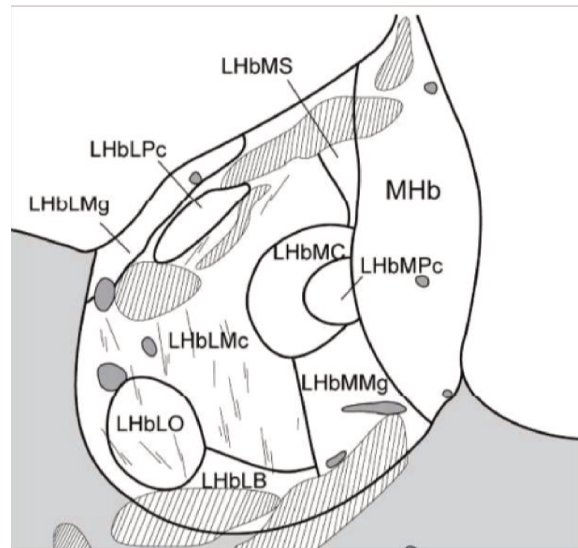
a. Anatomy and Neurochemistry

Anatomical Subfields

In rodents LHb, ten subfields have been described based on tracing experiments, immunological and electrophysiological characterizations (rats: Geisler et al., 2003; Weiss and Veh, 2011, see **Figure 18**; mouse: Wagner et al., 2014, 2016). If this suggests segregated functions across all subnuclei, no study has yet tried to address this question.

Figure 18: schematic representation of LHb subnuclei in rats.

Adapted from Wagner et al., 2014. Abbreviation: LHbLB, basal subnucleus of the LHbL; LHbLMc, magnocellular subnucleus of the LHbL; LHbLMc, magnocellular subnucleus of the LHbL; LHbLMg, marginal subnucleus of the LHbL; LHbLO, oval subnucleus of the LHbL; LHbLPc, parvocellular subnucleus of the LHbL; LHbMC, central subnucleus of the LHbM; LHbMMg, marginal subnucleus of the LHbM; LHbMPc, parvocellular subnucleus of the LHbM; LHbMS, superior subnucleus of the LHbM; MHb, medial habenula.



Receptors present in LHb

Inputs of the LHb (as described after **page 33**) involve several neurotransmission systems (*i.e.*, glutamatergic, GABAergic, monoaminergic, cholinergic, as well as neuropeptidergic). The receptors activated by these various systems can be found across the LHb, supporting the idea of a general role of LHb in the integration of multisystem information. In the following paragraph, we will quickly present the types of receptors present in the LHb. However, the function of each type of receptor is still not correctly defined in the literature.

In rodents, LHb neurons comprise: 1) glutamate receptors: ionotropic, AMPA (α -amino-3-hydroxy-5-methyl-4-isoxazolepropionic acid receptor), and NMDA (N-methyl-D-aspartate receptor) the later in lower proportion (Li et al., 2011; Maroteaux and Mameli, 2012; Meye et al., 2013), and

INTRODUCTION - Habenula

metabotropic: mGluR₁, mGluR₃ and mGluR₅ (Valentinova and Mameli, 2016; Wagner et al., 2016); 2) GABA receptors: GABA_A and GABA_B (Liang et al., 2000; Pirker et al., 2000; Hörtnagl et al., 2013; Meye et al., 2013); DA receptors, *i.e.*, D1, D2, D4 and D5, and 5-HT receptors, 5-HT_{1B}, 5-HT_{2C}, 5-HT_{3A}, 5-HT₄ and 5-HT_{5B} (Bouthenet et al., 1991; Root et al., 2015; Wagner et al., 2016). Interestingly, D4 receptors seem to be activated par NA rather than by DA (Root et al., 2015).

Molecular markers in the LHb

Glutamatergic marker (*e.g.*, vesicular transporter Vglut2) are abundantly found in the LHb, demonstrating that it is almost exclusively glutamatergic in nature (Omelchenko et al., 2009; Brinschwitz et al., 2010; Aizawa et al., 2012; Wagner et al., 2016). To a lesser extent, GABAergic markers are also found, such as the isoform 67 of the glutamate decarboxylase enzyme (Brinschwitz et al., 2010; Wagner et al., 2016; Zhang et al., 2016). As expected according to the presence of monoaminergic receptors, an important expression of tyrosine hydroxylase is found in the LHb (Geisler et al., 2003; Wagner et al., 2016). Even if the cholinergic transmission is prominent in the MHb, some cholinergic markers (*e.g.*, RNA of muscarinic cholinergic receptors type 2) are found in some subfield of the LHb (*e.g.*, central and parvocellular nuclei of LHb; Wagner et al., 2016). Interestingly, peptidergic markers are present, such vasopressin and substance P (Geisler et al., 2003; Wagner et al., 2016). The vasopressin (also called AVP) peptide is part of the HPA axis, regulating the CORT release for circadian rhythm regulation or in response to a stressor (see **The physiological stress response Page 4**). In addition, CRF (corticotropin-releasing factor) has also been shown to modulate LHb neurons excitability (Authement et al., 2018); this modulation of the LHb by CRF, and possibly by AVP, strengthen the view of an existing interaction between the HPA axis and the LHb.

b. Connectivity and Network

An important study designed to map the afferent and efferent pathways of the LHb was done in rats (Herkenham and Nauta, 1977, 1979). Interestingly, they found a quite heterogeneous pattern of inputs between the lateral part of the LHb (LHbL), the medial part of the LHb (LHbM) and the rostral part of the LHb (rLHb), suggesting differential functionality between these three subregions (developed below). We will review the inputs and outputs of the LHb, and their topographical organization, in the following chapter.

Inputs to the LHb

In rodents, one of the principal inputs to the LHb arise in the entopeduncular nucleus (EP; homologous of the internal portion of the globus pallidus (GPi) from humans and non-human primates (Herkenham and Nauta, 1977; Rajakumar et al., 1993). Studies in rats (but also in cats

INTRODUCTION - Habenula

and monkeys), showed that the EP innervates the LHbL (Parent et al., 1981; Rajakumar et al., 1993). The LHb receives other dense projections from the ventral pallidum (VP), the lateral preoptic area, the LH (Herkenham and Nauta, 1977, 1979; Geisler and Trimble, 2008; Hikosaka, 2010; Proulx et al., 2014; Golden et al., 2016).

In addition, LHb present several less dense afferences across the brain. LHb afferences are from the mPFC and more precisely, the IL, PRL and ACC and from the Ins, are mainly glutamatergic and follow an organized topography (Kim and Lee, 2012). The insular projections innervate mostly the center and the ventral part of the LHb. The cingulo-habenular projections seems to innervate mostly the ventro-lateral part of the LHb, whereas the projection from the PRL and IL arrived on the ventral part and the median part of the LHb (Kim and Lee, 2012).

The study of Herkenham and Nauta in 1977 also shown that some LHb afferences come from the AMG but without precising the AMG subfield concerned. Later a tracing study suggests a pathway from the BLA to the LHb, however, there are some doubts still existing concerning this pathway because their example of the LHb marked fibers was not correctly located (Kim and Han, 2016). The existence of this pathway is still to demonstrate. However, a pathway from CeA to LHb has been, recently, demonstrated (Zhou et al., 2019). In addition, Li and collaborators (1993) shown that, in rats, BSNT projects to the LHb (mostly the LHbM). This pathway have been supported by several studies (McLean et al., 1983; Dong and Swanson, 2006; Yetnikoff et al., 2015).

The LHb receives other projections from the NAc, the olfactive bulb, the retina, the suprachiasmatic nucleus (SCN), and the RM (Herkenham and Nauta, 1977, 1979; Greatrex and Phillipson, 1982; Li et al., 1993; Geisler and Trimble, 2008; Hikosaka, 2010; Lammel et al., 2012; Proulx et al., 2014). However, other projections to LHb are described as preferentially projecting to its lateral or median part. The LHbL receives projection from the VTA whereas the LHbM received from the nucleus of the DBB, nucleus triangularis septi (TS). The later also receives very small projection from the lateral septum, the VTA and the PAG (ventral central part; Herkenham and Nauta, 1977). The divers afferences of the LHb are represented in **Figure 19** in the network section.

Outputs from the LHb

The LHb innervates mostly the midbrain monoaminergic centers, including the serotonergic RM and RD (Aghajanian and Wang, 1977; Herkenham and Nauta, 1979), and the dopaminergic SNc and VTA (Herkenham and Nauta, 1979; Bernard and Veh, 2012). Another main projection targets rostromedial tegmental nucleus/tail of the VTA (RMTg/tVTA; Jhou et al., 2009; Kauffling et al.,

INTRODUCTION - Habenula

2009) which is a GABAergic structure known to represent a break for the dopaminergic (Ji and Shepard, 2007) and maybe the serotonergic transmissions. It has been shown that a stimulation of the LHb inhibit the liberation of dopaminergic neurons in the VTA and the SNc (in rats: Christoph et al., 1986; in monkeys: Matsumoto and Hikosaka, 2009; see Lecourtier and Kelly, 2007; Hikosaka et al., 2008 for review). The stimulation of the LHb in rats also leads to an inhibition of the 5-HT neurons in the raphe nuclei (Wang and Aghajanian, 1977; Stern et al., 1979). There is a topographical organization of LHb outputs, the LHbM projecting preferentially onto the RM/RD and VTA/SNc (Bernard and Veh, 2012; Gonçalves et al., 2012), whereas the LHbL projects mainly to the RMTg/tVTA (Gonçalves et al., 2012). A summary of the main outputs and their distribution are represented in Figure 19.

Weaker projections include the supramammillary nucleus of the hypothalamus (SuMM; Kiss et al., 2002), several thalamic nuclei including the DM and the reuniens nucleus (Re), the superior colliculus, the PV, and the laterodorsal tegmental nucleus (LDT; Herkenham and Nauta, 1979; Araki et al., 1984; Semba and Fibiger, 1992).

Network

A summary of the Hb inputs and outputs, forming a complex network, is presented in Figure 19.

Figure 19: Schematic representation of the afferences and efferences of the LHb

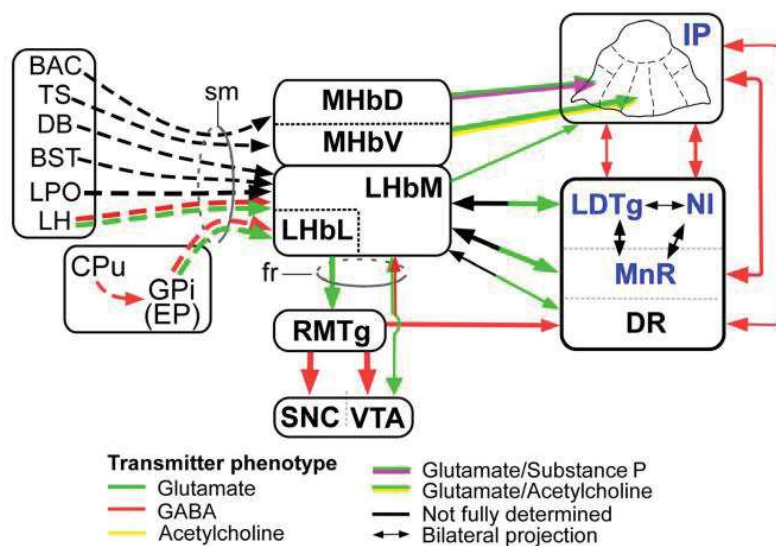


Diagram representing the main inputs and outputs of the habenula. From Metzger et al., 2021. Abbreviation: BAC, bed nucleus of the anterior commissure; BST, bed nuclei of the stria terminalis; CPU, caudate putamen; DB, diagonal band complex; DR, dorsal raphe nucleus; EP, entopeduncular nucleus; fr, fasciculus retroflexus; GPi, globus pallidus, internal part; IP, interpeduncular nucleus; LDTg, laterodorsal tegmental nucleus; LH, lateral hypothalamus; LHbL, lateral habenular nucleus; LHbM, lateral

habenular nucleus; MHbD, medial habenula dorsal part; MHbV, medial habenula ventral part; MnR, median raphe nuclei; NI, nucleus incertus; RMTg, rostromedial tegmental nucleus (same as tVTA); sm, stria medullaris; SNC, substantia nigra, compact part; TS, triangular septal nucleus; VTA, ventral tegmental area.

INTRODUCTION - Habenula

Considering these inputs and outputs, the LHb occupies a particular place in the route of information flow between the forebrain, including key limbic and basal ganglia structures, and the midbrain monoaminergic regions. Through those direct connections the LHb can modulate dopaminergic and serotonergic transmissions towards the PFC, HPC and striatum (see [Lecourtier and Kelly, 2007](#) for review and the review on the LHb and the stress response below).

The LHb is also indirectly connected with the HPC, as two studies in rats have demonstrated a synchronicity of oscillatory activity, at the theta frequency, between the LHb and the dHPC during REM sleep and during exploration of an open field ([Aizawa et al., 2013](#); [Goutagny et al., 2013](#)). In addition, another study in rats shown functional connectivity, based on a mapping of brain activation using cytochrome oxidase, between the LHb and the dHPC during fear conditioning ([González-Pardo et al., 2012](#)). The hypothesis concerning the neuroanatomical support of the interaction between the LHb and the HPC will be discuss further in the chapter [LFP recording in LHb page 71](#).

There is also an indirect influence of the LHb upon the HPA axis as LHb manipulations can modulate CORT release ([Murphy et al., 1996](#); [Jacinto et al., 2017](#); [Mathis et al., 2018](#)). Also, although there are no direct connections between the LHb and the LC, the LHb modulates NA release in PFC, HPC, and striatum ([Kalén et al., 1989](#); [Cenci et al., 1992](#)). Those two features will be discussed later in the review part. Interestingly, some LHb neurons have long dendrites spreading in its entirety, so that there are many contacts between neurons within the structure ([Kim and Chang, 2005](#)). This type of intra-structural network suggests a potential high convergence of the information of different limbic or pallidal structures in the same LHb neurons. With this in mind, along with the diversity of the inputs of the LHb, [Geisler and Trimble, \(2008\)](#) hypothesized that the LHb is integrating information from several so-called macrosystems (*i.e.*, septal hippocampal preoptic, dorsal and ventral striopallidal and amygdalar systems; see [Figure 20](#); [Geisler and Trimble, 2008](#)), to allow the rapid integration of the cortical information by other networks, therefore favorizing behavioral adaptation and flexibility ([Zahm, 2006](#)).

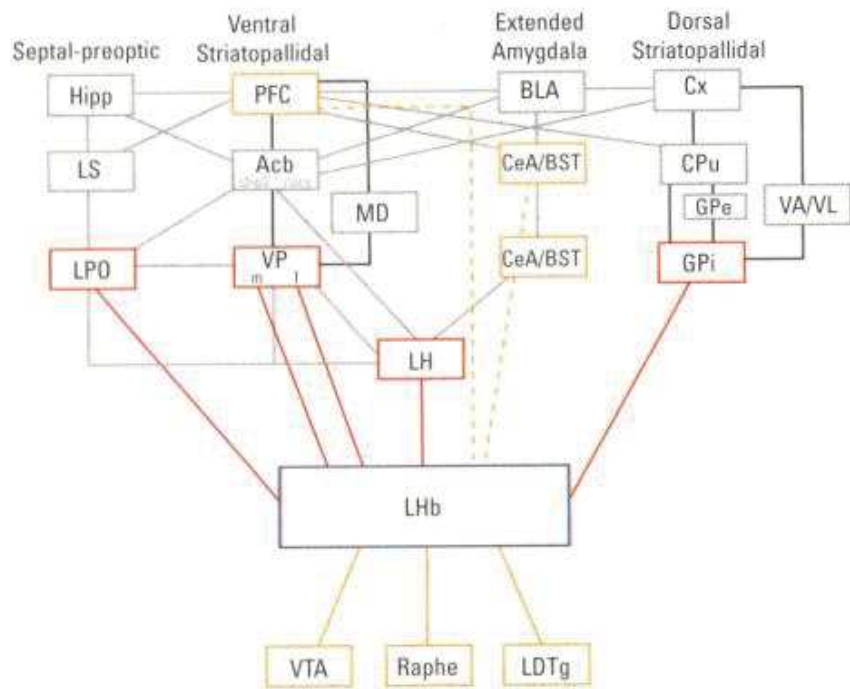
INTRODUCTION - Habenula

Figure 20: Schematic representation of the afference of the LHb in a “macrosystem” perspective

Diagram representing the diverse macrosystem projections on the LHb. The principal inputs are represented by red boxes, while orange boxes represent weaker inputs. The black and grey lines represent the connections between the other structures.

Form Geisler and Trimble, 2008. Abbreviation: LHb, lateral habenula; Hipp, hippocampus; PFC, prefrontal cortex; BLA, basolateral amygdala; Cx, cortex; LS, lateral septum; Acb, accumbens; CeA/BST, central amygdala nucleus/bed nucleus of stria

terminalis; CPu, caudate-putamen; MD, mediodorsal thalamic nucleus; GPe, globus pallidus externus; VA/VL, ventroanterior/ventrolateral thalamic nuclei; LPO, lateral preoptic area; VP, ventral pallidum; m, medial; l, lateral; LH, lateral hypothalamus; GPi, globus pallidus internus; VTA, ventral tegmental area; LDTg, laterodorsal tegmental nucleus.



c. Functions

The LHb is implicated in a variety of functions, from circadian rhythms to cognitive and emotional processes, which I will talk about in the next chapter. Then I decided to integrate a review article, wrote during my PhD, on the role of LHb in the stress response and fear memory, and more particularly its implication as an integrative hub of information participating to the behavioral adaptation in a threatening environment. It will be situated at the end of the section concerning the Hb.

Behaviors related to prediction error and punishment

The most describe and studied role of the LHb, it is implication in the processing of reward-related information; they found a strong activation of LHb neurons upon the presentation of a cue announcing the absence of a reward, or upon the omission of an expected reward, leading the authors to attribute to this structure a role for the signaling of an absence of reward (Matsumoto and Hikosaka, 2007; Bromberg-Martin and Hikosaka, 2011). Further, other experiments were carried out, recording concomitantly midbrain DA neurons as well as neurons of the internal part of the GPi in monkeys; the authors discovered that in fact the LHb was a relay between the basal

INTRODUCTION - Habenula

ganglia (BG) and the DA system in order to cancel a behavioral action, through the inhibition of the activity of DA neurons by the LHb, when it became unnecessary due of the absence of reward (Hikosaka, 2010). Then, it was discovered that the LHb inhibited the activity of DA neurons through the RMTg/tVTA (Hong et al., 2011).

LHb and cognition

Flexibility

In both humans and rats the Hb (or the LHb per se) was shown to play a role in flexibility. Two fMRI studies demonstrated in humans that the Hb (the whole structure takes too few voxels in fMRI images to be able to differentiate the LHb and the MHb) was activated in case a negative feedback was provided following an error (Ullsperger and von Cramon, 2003); later, Shepard et al., (2006) obtained similar results and in addition found that this increased activity of the Hb was concomitant to a decreased activity of midbrain DA area (VTA), here again suggesting that the Hb communicates to the DA system information about negative outcomes, similarly to what was found by Bromberg-Martin and Hikosaka, (2011) in monkeys. These results can suggest that the Hb (and most likely the LHb), participates in the retroactive appreciation of behavioral outputs and probably helps adapting behavior. In rats, Baker and colleagues investigated the involvement of the LHb in behavioral flexibility and found its inactivation (cocktail of GABA agonists, muscimol/baclofen) to impair reversal learning in a T-maze task (Baker et al., 2015), and to impair the use of external cues (tones) in a switching task using a figure 8 maze (Baker et al., 2017). Finally, using a delayed alternation task, they showed that flexibility depended on communication – with at least one relay as there is no direct connection between both structures – between the LHb and dHPC (Baker et al., 2019).

Memory

Very few studies investigated the role of the LHb in memory processes. (Tronel and Sara, 2002) trained rats to retrieve a reward, associated to a specific odor, constantly displaced in an environment; using c-Fos immunostaining, they found that during the retrieval session the LHb, and more particularly its most anterior part, was strongly activated. At the LNCA we have been, in the past few years, investigating the role of the LHb in memory processes in rats, comprising long term-spatial memory and short-term memory. Using the Morris water maze, it was found that LHb inactivation (either with the AMPA/kainate antagonist CNQX or with the GABA-A agonist muscimol), induced encoding, and retrieval - but not consolidation - deficits (Mathis et al., 2015; **Figure 21**) further suggesting the structure is rather involved in online, as opposed to offline, information processing. Earlier, we found LHb inactivation (muscimol) to impair spatial recognition

INTRODUCTION - Habenula

memory, evaluated using an object-based task ([Goutagny et al., 2013a](#)); interestingly, the LHb and the dHPC had synchronized oscillatory activity, at the theta range (6-12Hz depending of the study), including during the exploration of an environment, and this synchrony was positively correlated with behavioral performance, suggesting both structures likely communicate during spatial investigation.

In the meantime, was investigated the role of the LHb in the short-term maintenance of contextual information, a cognitive ability dependent on the mPFC, as the deficits seen in the water maze, at least during encoding, could well have been caused, or worsened, by inactivation-induced short term memory deficits. Using a delayed non-matching to position paradigm in an operant chamber, it was shown that rats with inactivated LHb were not able to maintain an information more than 2 seconds, such as rats with mPFC inactivation ([Mathis et al., 2016](#)); in addition, it was shown that mPFC-LHb disconnection also impaired short-term memory, suggesting the LHb receives top-down cortical information to guide behavior.

As we have seen in the above-cited experiments in rodents, the LHb is likely interacting with the mPFC and HPC during cognitive processes. It is therefore very interesting that, using MRI, [Bocchetta et al., \(2015\)](#) found a significantly reduced Hb volume in patients suffering from behavioral variant frontotemporal dementia, which is, according to the authors, "...a neurodegenerative disorder characterized by atrophy of the frontal and temporal lobes and progressive behavioral and cognitive impairment".

INTRODUCTION - Habenula

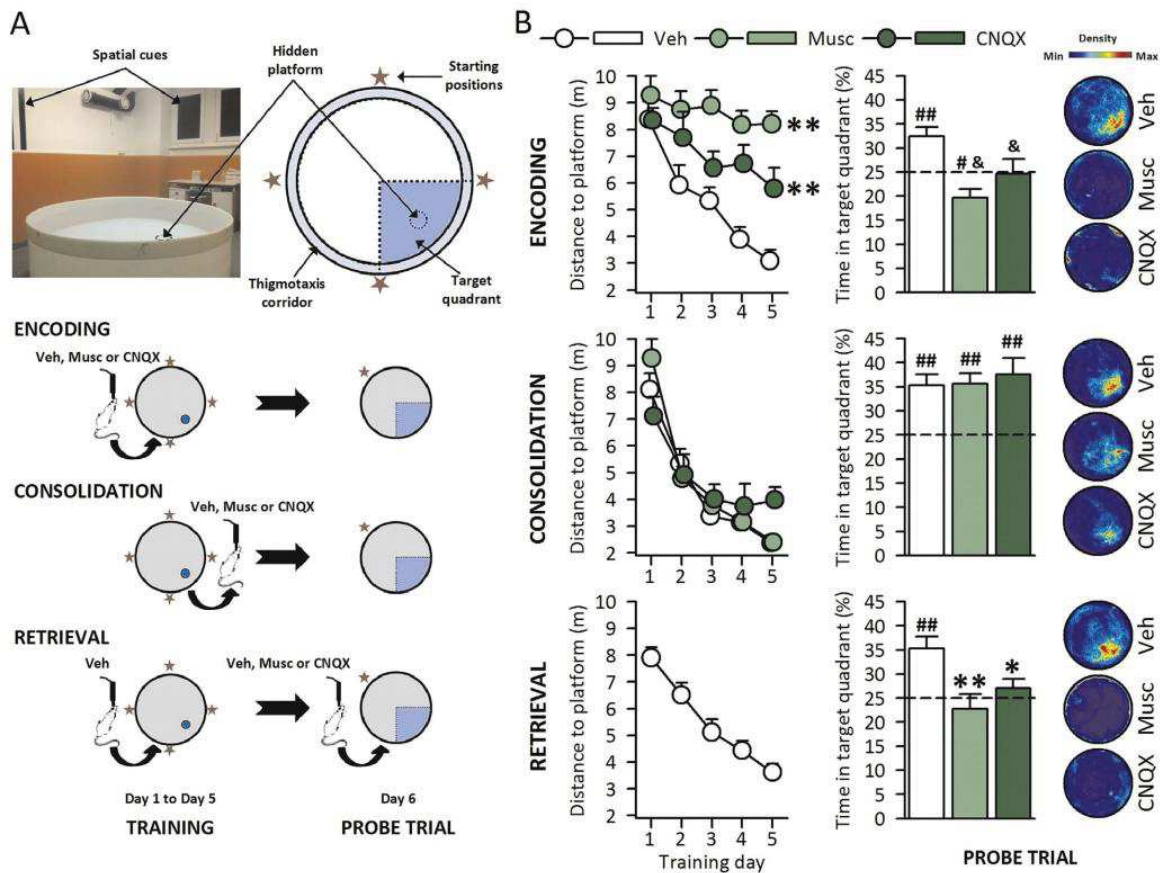


Figure 21 : Lhb inactivation induce spatial memory deficits.

Implication of the Lhb in spatial memory as shown in the Morris water maze. **(A)** The protocol included 5 days of training (4 trials per day) followed by a probe trial on day 6. Lhb inactivation (CNQX or muscimol) was performed either before or following each training session, to impact on encoding or consolidation, respectively, or before a probe trial following normal training, to impact on retrieval. **(B)** Mean distance swum before finding the platform across the 5 days of training (left) and time spent in the target quadrant during the probe trial (right); this shows that Lhb inactivation induces encoding and retrieval – but not consolidation – impairments. Statistics: **p < 0.01, *p < 0.05 Veh, ##p < 0.0, #p < 0.05 vs chance (25%), &p < 0.05 vs the two other groups. Adapted from [Mathis et al. 2015](#) and [Mathis and Lecourtier 2017](#).

Circadian rhythms and sleep/wake cycle

The Lhb receives a direct connection from the retina ([Qu et al., 1996](#); [Hattar et al., 2006](#)). [Zhao and Rusak, \(2005\)](#) showed in rats that Lhb neurons responded, either by an activation or a suppression of activity –but with a larger proportion of activated cells–, to retinal illumination. Noteworthy, a recent fMRI study in humans did not show any reaction of the Hb with increasing illumination; however, they found the Hb to be responsive, by a decreased activity, to changes in the intensity of illumination, irrespective of the direction of the change. This could be a confirmation that the Hb is involved in detecting and processing changes in the environment, to maybe adapt behavior accordingly. The Lhb is also bidirectionally connected with the SCN ([Buijs, 1978](#); [De](#)

INTRODUCTION - Habenula

Vries et al., 1981), suggesting it could be implicated in circadian rhythmicity. Indeed, in rodents the LHb shows circadian rhythmicity (Guilding et al., 2010) and has a higher firing rate at day than at night (Zhao and Rusak, 2005). Interestingly, Chastrette et al., (1991) showed in rats that the increased c-Fos expression that occurs in the LHb following stress exposure was higher when the stress was encountered at nighttime than daytime; as rats are nocturnal animals, this is likely to have preservation purposes as it is more efficient for nocturnal animals to be reactive to stress at nighttime.

The Hb, and the LHb, have been linked to the sleep/wake cycle. Valjakka et al., (1998) found that FR lesion induced a marked reduction of the amount of REM sleep. Aizawa et al., (2013) showed a high coherence (*i.e.*, synchronization; see part **Oscillatory activity in neuronal communication page 65** for details on coherence) of theta activity between the LHb and the dHPC during REM sleep. In addition, they showed, such as Valjakka et al. in 1998, that LHb lesion decreased the number and duration of REM sleep episodes. Interestingly, the synchronized firing was mostly with neurons within the LHbM, which is the LHb region preferentially projecting to the raphe nuclei, so that they postulated that LHb influence over hippocampal theta occurred through the raphe, which they further demonstrated. However, the role of the LHb in modulating HPC theta activity could well occur through the SuMM, to which the LHb projects (Kiss et al., 2002).

Overall, the link between the LHb and brain circadian activity, including sleep, appears very important in an evolutionary point of view, as Mendoza (2017) postulated that it is linked with the regulation of mood and eating, and that disturbances of LHb circadian activity can well participate to the occurrence of depression and eating disorders.

LHb implication in the behavioral adaptation to a threatening environment

The state of the knowledge of the LHb in the behavioral adaptation facing a stressful environment has been summarized in the following review. This review has not yet been published.

REVIEW

THE LATERAL HABENULA AND THE EMOTIONAL BRAIN: FOCUS ON STRESS AND FEAR

The Lateral habenula and the emotional brain: focus on stress and fear

Authors

Laura Durieux^{1,2}, Monique Majchrzak^{1,2}, Lucas Lecourtier^{1,2}

Affiliations

¹Laboratoire de Neurosciences Cognitives et Adaptatives, Université de Strasbourg, Strasbourg, France.

²LNCA, UMR–7364, Centre National de la Recherche Scientifique, Strasbourg, France.

Keywords

Fear Memory; Stress Response; Lateral habenula

Introduction

In higher vertebrate species, the lateral habenula (LHb) is the lateral subdivision [the medial habenula (MHb) representing its medial subdivision] of the habenular complex, or habenula (Hb), an epithalamic structure belonging to the so-called dorsal diencephalic conduction system (**Sutherland 1982; Roman et al. 2020**). Such system, which parallels the more ventrally located medial forebrain bundle, represents a route of information flow between the forebrain and the midbrain. As demonstrated mainly in rodents, the LHb receives projections from structures such as the medial prefrontal cortex (mPFC), the septal area, several hypothalamic and thalamic nuclei, the extended amygdala, the basal ganglia (BG), and midbrain structures such as the raphe (RN) and the ventral tegmental area (VTA); downstream, the LHb projects onto several thalamic and hypothalamic nuclei, and on midbrain monoaminergic structures such as the dopaminergic VTA and substantia nigra pars compacta (SNc), both median (MRN) and dorsal (DRN) raphe, as well as onto the rostromedial tegmental nucleus (RMTg) also called tail of the ventral tegmental area (tVTA), which represents a GABAergic inhibitory break onto the raphe nuclei, the VTA and the SNc (**Zahm and Root 2017; Hu et al. 2020**). **Geisler and Trimble (2008)** have presented such network connections as an indication that the LHb was the processing center of information arising in so-called « macrosystems » and implicated in « mood, cognition and drive »; in addition, the LHb would be viewed as a node through which forebrain structures would regulate their monoaminergic inputs. With such view in mind it is interesting that in humans, the drawing of a map of functional connectivity of the default mode network has shown a strong connectivity between the Hb (comprising both the LHb and MHb) and the prefrontal cortex (PFC), the insular cortex, the auditory and visual primary cortices, the nucleus accumbens (NAc), the dorsal striatum (DS), the pallidum, the thalamus, the VTA, the RN, the periaqueductal gray (PAG), and the cerebellum (**Ely et al. 2019**).

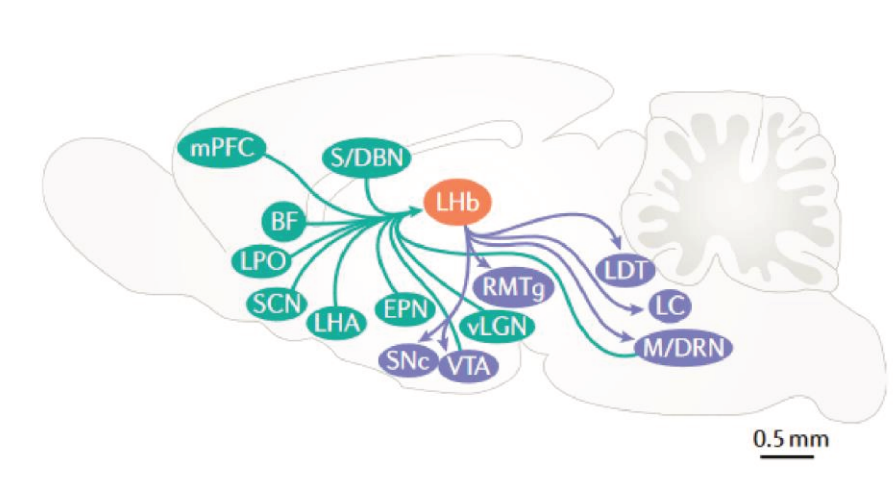


Figure 1: lateral habenula pathways.

From Hu et al., 2020. Abbreviations: BF, basal forebrain; EPN, entopeduncular nucleus; LC, locus coeruleus; LDT, laterodorsal tegmental nucleus; LHA, lateral hypothalamic area; LPO, lateral preoptic area; M/DRN, medial raphe nucleus or dorsal raphe nucleus; mPFC, medial prefrontal cortex; RMTg, rostromedial tegmental nucleus; SCN, suprachiasmatic nucleus; S/DBN, septum and diagonal band nuclei; SNc, substantia nigra pars compacta; vLGN, ventral lateral geniculate nucleus; VTA, ventral tegmental area.

The LHb, since the seminal work of the group of Okihide Hikosaka, is best known as a relay of negative reward information between the basal ganglia (BG) and the dopamine system (**Hikosaka 2010**). In addition, the LHb represents a « center for aversion » as its direct optogenetical stimulation, or the optogenetical stimulation of input to, or output from it, lead to a behavior consisting on the active avoidance of places where such stimulations were performed (e.g., **Shabel et al. 2012; Stamatakis and Stuber 2012; Root et al. 2014**).

The Hb has been present in all vertebrate species through evolution, a medial (medial habenula, MHb) and lateral (LHb) subdivision appearing in mammals whereas they are named dorsal and ventral habenula, respectively, in amphibians and teleosts. This, and the fact that, within the habenula, the volume of the LHb has gained importance in proportion (**Díaz et al. 2011**), suggest the LHb is a structure that serves important « survival » functions, including escape from predators, preservation of the integrity of the body, and reproduction. Indeed, the LHb is involved in defensive behaviors (**Pobbe and Zangrossi 2010; Bowen et al. 2013; Lecca et al. 2020; Velazquez-Hernandez and Sotres-Bayon 2021**), pain processing (**Shelton et al. 2012**), and reproductive and maternal behaviors (**Modianos et al. 1974; Tennent et al. 1982; Corodimas et al. 1993; Pfaus et al. 1993; Matthews-Felton et al. 1995, 1998; de Jong et al. 2010**). It is a fact that the LHb is, in humans, involved in complex cognitive tasks (**Ullsperger and von Cramon 2003**) and associated to pathologies such as depression (**Nuno-Perez et al. 2018; Gold and Kadriu 2019; Hu 2019**), schizophrenia (**Sandyk 1992; Caputo et al. 1998; Zhang et al. 2017; Li et al. 2019**), and drug addiction (**Velasquez et al. 2014**). This suggests the LHb, which has evolved, likely paralleling the evolution of cortical structures and monoaminergic systems, remains an important structure for the integration and processing of cognitive and emotional information, to guide behavioral adaptation and survival. In this review we will first briefly describe the evolution of the Hb, and of the LHb, across vertebrate species; then we will show how the LHb reacts to different emotional situations with a focus on stress and fear; finally, we will try to position the LHb within the broad cerebral network engaged in the response to stressful or threatening situations.

Phylogenetic evolution of the Hb and anatomical considerations in mammals

The Hb is a phylogenetically conserved structure (**Loonen and Ivanova 2016**), found in all vertebrates, including the lamprey (**Grillner et al. 2018**), currently considered as the older vertebrate taxonomic group (**Yañez and Anadon 1994**) as well as in the Teleostei and Sarcopterygii fishes, the frog, the lizard, up to the rodents, monkeys and humans (**Concha and Wilson 2001**). Across the numerous studies that investigated the anatomical evolution of the Hb through taxonomic groups, one of the main finding is that it is displaying left-right structural asymmetry mostly in reptiles, amphibians and fishes (**Bianco and Wilson 2009**), suggesting a differentiation in the neuronal organization and connectivity of right and left Hb in these species. To date no asymmetry or lateralization of function within the Hb or the LHb have been demonstrated in rodents, non-human

primates or humans. Noteworthy, MHb and LHb subdivisions appear in mammals, and are equivalent to zebrafishes dorsal and ventral Hb (dHb; vHb) respectively (e.g., **Amo et al. 2010**). Such an emergence and differentiation of the Hb into MHb and LHb subregions suggests a certain specialization of function, which is demonstrated by the vast body of literature from fishes to rodent studies. Not only both subregions have distinct inputs and outputs, but behaviorally they seem to process different functions; for example, whereas in rodents the LHb is involved in spatial memory (**Mathis et al. 2015**), the MHb is not (**Kobayashi et al. 2013**). In addition, among the multiple drugs of abuse known to disturb emotional processing and affect responses to stress, whereas the LHb processes responses to cocaine (**Maroteaux and Mameli 2012**), the MHb is involved in nicotine reinforcement (**Fowler et al. 2011**). Finally, what is particularly interesting, in terms of evolutionary perspective, is that the proportion taken by the LHb within the Hb is greater in humans than in rats, 91% and 76% respectively (**Díaz et al. 2011**). Although there is no scientific evidence that it is the case, it is tempting to suggest that throughout evolution the importance taken by the LHb has paralleled this of structures like the PFC. Based on this assumption, one can deduce that the engagement of the LHb in processing the external world has become more complex and diverse in humans than it was in lower vertebrates, likely in relation with this of the neocortex. One of its main function could be to preserve the integrity of the individuals by participating to the elaboration of appropriate responses facing the constraints of the environment. This could be why Hb, or LHb, dysfunction in humans participates to the occurrence of psychiatric pathologies such as mood disorders (for reviews: **Proulx et al. 2014; Zhao et al. 2015; Yang et al. 2018; Aizawa and Zhu 2019; Gold and Kadriu 2019; Mendoza and Vanotti 2019; Metzger et al. 2019; Hu et al. 2020; Vitkauskas and Mathuru 2020**; but see **Schafer et al. 2018**) and schizophrenia (**Sandyk 1992; Caputo et al. 1998; Shepard et al. 2006; Stopper and Floresco 2014; Zhang et al. 2017; Hu et al. 2020**; but see **Ranft et al. 2010**).

The LHb under stress and aggression

Across all vertebrates, multiple evidence of a link between the LHb and the physiological and behavioral responses to stressful or threatening situations has been provided.

In zebrafishes **Andalman et al. (2019)** provide interesting insights on the role of the LHb in stress coping, based on the principle that upon repeated, or prolonged, stressful exposure, individuals switch from active to passive coping strategies, in order to spare energy resources; they showed that such switch was mediated by activation of the vHb. In rats LHb activation (electrical or via direct bicuculline administration) induces an autonomic physiological response (cutaneous vasoconstriction and thermogenesis of brown adipose tissue) equivalent to stress-induced hyperthermia response (**Ootsuka and Mohammed 2015**). Maternal separation in rats induce an increased excitability of LHb neurons (**Authement et al. 2018**). According to defensive behaviors, in rats, exposure to cat fur odor induces an important cellular response (c-fos+ cells density) in the LHb (**Bowen et al. 2013**) whereas LHb stimulation increases the latency to escape an aversive

situation in the inhibitory avoidance test (**Pobbe and Zangrossi 2010**). Manipulation of a pathway connecting the basal forebrain and the LHb can modulate the level of aggressivity of mice against an intruder (**Golden et al. 2016**). Whereas LHb inactivation (**Mathis et al. 2015**) or fasciculus retroflexus lesion (**Murphy et al. 1996**) induce anxiety in the elevated plus maze, LHb lesion reverses nicotine-induced anxiety (**Casarrubea et al. 2015**), and reduction in LHb noradrenaline release (through intra-LHb injection of the α_2 adrenergic autoreceptor agonist dexmedetomidine) has anxiolytic effects in the acoustic startle test (**Purvis et al. 2018**). At the structural and cellular levels, several studies have shown the impact of stress exposure on the LHb. **Jacinto et al. (2016)** have shown in rats that exposure to acute stress led to a global bilateral reduction of the LHb volume. In rodents, exposure to stressors strongly enhances LHb activation, as shown by different markers such as c-Fos expression or deoxyglucose staining following a large spectrum of situations, e.g. restraint (**Chastrette et al. 1991; Wirtshafter et al. 1994**), air puff (**Duncan et al. 1996**), foot shocks (**Duncan et al. 1996; Brown and Shepard 2013**), tail shock (**Dolzani et al. 2016**), lithium chloride injection (**Wirtshafter et al. 1994**), exposure to a novel environment (**Wirtshafter et al. 1994**), or peripheral nociceptive stimulation (**Benabid and Jeaugey 1989**). In addition, using calcium imaging in mice, **Wang et al. (2017)** showed a strong LHb activation following different stressors such as quinine oral administration, footshock delivery or following aggression by an intruder. Interestingly, the cellular activation occurs preferentially in the medial portion of the LHb (LHbM; e.g. **Figure 1C-E**), a subregion preferentially connected upstream with mPFC, septal and hypothalamic structures, and downstream with the monoaminergic systems (**Proulx et al. 2014; Aizawa and Zhu 2019; Metzger et al. 2019**). Electrophysiologically, peripheral noxious stimulations in rats induce an increased firing of the majority of the recorded LHb neurons (**Benabid and Jeaugey 1989**), unpredictable chronic stress increases burst firing in the LHb (**Berger et al. 2018**), and exposure to inescapable footshock or restraint facilitates long-term potentiation (LTP) in the LHb (**Park et al. 2017**), linking the LHb to plasticity mechanisms likely at the origin of later consolidation processes. Finally, in monkeys air puff increased the activity of LHb neurons (**Matsumoto and Hikosaka 2009**).

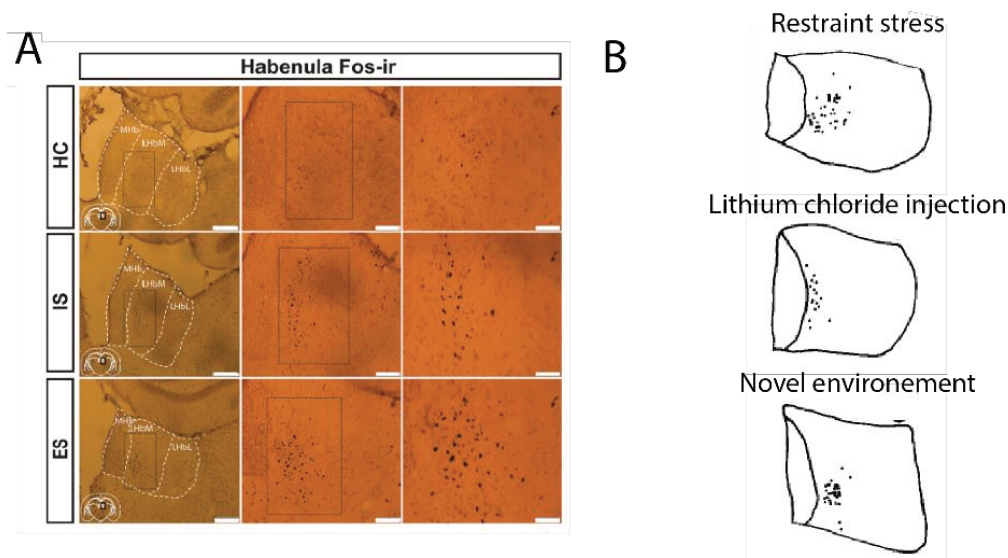


Figure 2: c-Fos+ cells distribution in the LHb.

(A) From Dolzani et al., (2016), c-Fos protein expression by photomicrography in LHb. HC: home cage, IS: inescapable tail shock, ES: escapable tail shock. (B) Drawing of c-Fos+ cells distribution in the LHb (right hemisphere) after a restraint stress, lithium chloride injection or exposition to novel environment, adapted from Wirtshafter and collaborators, 1994.

Noteworthy, several studies, although with some discrepancies, showed that the LHb can influence the release of corticosterone (CORT) by the hypothalamic–pituitary–adrenal (HPA) axis, although there is no direct projection from the LHb to the hypothalamic paraventricular nucleus (PVH). For example, **Murphy et al. (1996)** found that plasma CORT level was chronically increased following lesion of the fasciculus retroflexus (measurements performed several weeks after the lesion procedure). Here (**Mathis et al. 2018**), we have shown that LHb inactivation had different effects on CORT release depending on the situation; whereas LHb inactivation did not affect CORT levels when performed in the home cage or following an elevated plus maze test – although the inactivation induced anxiety, CORT levels were significantly higher following the probe session of the water maze task, concomitantly to memory deficits, suggesting a potential role for the LHb at the interface of emotional and cognitive processing (see below). Finally, it must be noted findings discrepant from ours; **Jacinto et al. (2017)** found that LHb lesions not only suppressed the behavioral response to stress (lack of anxiety in the elevated plus maze), but further blunted the increased CORT release induced by such exposure to a stressful situation; this could be due to the fact that they induced permanent lesions whereas we used acute reversible inactivation.

Besides rodent studies, investigations in humans have also provided evidence of the involvement of the Hb in the processing of aversive situations. Using fMRI, **Hennigan et al. (2015)** have exposed subjects to different types of stimuli, either aversive (electric shock), rewarding (fruit juice), or neutral; they have shown that whereas rewarding stimuli induced a decreased activity of the Hb (such as shown by the group of Okihide Hikosaka in Monkeys in LHb neurons), aversive stimuli induced a strong activation of the Hb.

LHb and aversive memories

Few studies have investigated the role of the Hb, and more particularly the LHb, in the memorization of an aversive experience. An important work linking the LHb and the management of fearful experiences has actually been performed in zebrafishes. **Amo et al. (2014)** demonstrated that the vHb, which is the homologous of the LHb in fishes, is strongly activated during the presentation of cues previously associated to an aversive event (electric shock) and then stimulates the raphe nucleus, delineating here a Hb-serotonergic pathway involved in aversive cues memory. Studies in rodents allowed to make some progress in the understanding of LHb involvement in fear-related processes, even if there are some discrepant findings. **Tomaiuolo et al. (2014)** have studied the role of the LHb on inhibitory avoidance memory: during conditioning rats are placed on a platform and allowed to step down on a grid on which an electric shock was delivered; during memory assessment rats are replaced on the platform and the latency to step down on the grid was recorded and analyzed; the authors showed that muscimol-induced LHb inactivation during conditioning impaired memory retrieval 7 days – but not 24 hours – later. Interestingly, with a weak training (0.4 instead of 0.8 mA shock intensity), whereas for all groups there was no retention at 7 days post-training, LHb inactivation induced an increased step down latency, indicative of more lasting memory; this for the authors suggests that one role of the LHb could be to code the valence of the stimulation, and further that in the case of high intensity stimulation, LHb inactivation had resulted in the processing of the stimulation as « weak » instead of « strong »; finally, the fact that the administration of protein synthesis inhibitors within the LHb had no effect on memory retrieval suggests the LHb is not the place where the memory is actually stored. Using active avoidance paradigms, **Shumake et al. (2010)** demonstrated in gerbils that LHb electric stimulation during active avoidance training impaired acquisition, whereas **Song et al. (2017)** showed that pre-training LHb electric lesion facilitated acquisition, although **Vale-Martínez et al. (1997)** found no effect using similar procedures. Interestingly, **Wilcox et al. (1986)** compared the effects of electric and kainic acid-induced lesions of the LHb on active avoidance, and found that whereas electric lesions markedly impaired learning, kainic acid lesions had no effect; the authors therefore suggested that the effects seen following electric lesions were in fact attributable to damages of septal inputs to the MHb, and not to the LHb per se.

Fear conditioning paradigms, which consist in a trained association between a neutral stimulus (conditioned stimulus, CS; generally, a tone) and an aversive stimulus (unconditioned stimulus, US; generally, a footshock), are widely used in rodents as a way to address the memorization of aversive experiences through the generation of a fear response (freezing) associated with the different elements of the paradigm. There are different ways to perform fear conditioning, either using contiguous CS and US (contextual fear conditioning), or with the insertion of a delay between the end of the CS and the occurrence of the US (trace fear conditioning). The different associations formed are later evaluated by re-exposure to the context (contextual memory) and to the CS in a different environment (CS memory). Depending on the protocol used, the main regions involved are

the extended amygdala, the hippocampus (HPC), the thalamus, the PFC (**Francisco Gonzalez-Lima 1986; Herry et al. 2010; Gilmartin et al. 2013; Herry and Johansen 2014; Connor and Gould 2016**). One issue with the diversity of the protocol used is that the parameters (fear conditioning protocols, inactivation or lesion methods, animal models) are very different from one study to the other, so that results of different experiments are often hard to compare (see **Table 1** for a comparison of studies addressing the role of the Hb). Studies of metabolic activation have suggested that the LHb was actively engaged during fear conditioning. **González-Pardo et al. (2012)**, using cytochrome oxidase in rats, and **Barrett and Gonzalez-Lima (2018)**, using fluorodeoxyglucose in mice, mapped brain activation and both found strong LHb activation during the acquisition phase of classical fear conditioning (CS-US contiguity); however, they both performed functional connectivity analysis, and whereas in the **González-Pardo et al. (2012)** study LHb activity was positively correlated to this of dorsal CA3, in the **Barrett and Gonzalez-Lima (2018)** study LHb activation was positively correlated with this of the ventrolateral PAG. Unfortunately, the more recent paper does not mention nor discuss these discrepancies.

Very few studies investigated the consequences of LHb manipulations on fear conditioning. **Wang et al. (2013)** addressed the consequences of LHb electric lesions on fear memory associated with both the context and the CS using classical fear conditioning and found marked impairments of both associations. According to the authors, who in addition found a marked increase of locomotor activity in lesioned animals, these memory deficits were more the indirect consequence of a locomotor hyperactivation than a decreased fear (and therefore freezing) *per se*; but, if this had been the case the amount of freezing would also have been reduced during conditioning, which was not the case. Considering that the lesions encompassed a great amount of the underlying dorsal thalamic region, which involvement in such fear conditioning paradigm has been demonstrated (**Padilla-Coreano et al. 2012; Do-Monte et al. 2015; Penzo et al. 2015**), the deficits could in fact be partly due to alterations of thalamic function. Part of the study by **Song et al. (2017)**, who demonstrated the beneficial impact of electric LHb lesion on active avoidance acquisition (see above), was to investigate the consequence of the same lesions on fear memory acquisition and extinction; they found that, whereas the lesions impaired neither training nor CS recall, they accelerated extinction; for the authors the same processes can explain both findings (facilitation of active avoidance and extinction in fear conditioning), arguing that LHb lesions improved memory, so that it also improved the new learning during the extinction process.

Table 1 : Characteristics and main results of the different studies that investigated the role of the LHb, or its equivalent, in fear conditioning.

	Targeted Structure	Animal Model	Method	Protocol	CS	US	Context Test	CS Test	Extinction Session
(<i>Amo et al. 2014</i>)	vHb	Zebra Fish	Electrophysiology	Delay	Led 6s	Shock 1s		24h no behavioral data	
(<i>Chan et al. 2017</i>)	LHb	Rat SD	D1 antagonist injection / acquisition	Delay	Tone 19s	Shock 0.7mA 1s (x5)	24h deficit	48h no effect	
			D1/D5 agonist / acquisition				24h deficit	48h deficit	
(<i>Wang et al. 2013</i>)	LHb	Rat LE	Thermo-coagulation lesion (1 min at 60-70°C)	Delay	Tone & light 28s	Shock 2s 0.4mA	24h deficit	24h deficit	
(<i>Wang et al. 2017</i>)	LHb	Mice	Electrophysiology	Trace	Tone 2s	Quinine 0.5s			Tone 24h (x30) no behavioral data
						Shock 0.5s 0.4mA (x30)			
(<i>Song et al. 2017</i>)	LHb	Rat SD	Electrolytic lesion (1mA – 10s)	Delay	Tone 15s	Shock 0.5s 1mA (x5)			Tone 24h (x20) Potentiation

The LHb in a key position in the emotional brain to deal with stress and fear? Anatomical considerations

We have seen above that the LHb can with confidence be linked to the active physiological response to stressful, fearful, or threatening situations, as it is markedly activated by basically all these experiences. What is important now is to try to understand at which place the LHb could be positioned within the brain networks responsible for the response to stress. Which are the brain regions which are the more likely to interact with the LHb, and to which purpose?

We have seen above that the LHb represents a node of reciprocal communication between structures of the forebrain and the midbrain which are important for the management of stressful, aversive, or threatening situations. As seen in **Figure 1**, the LHb shares direct connections with the whole mPFC, the BG via the entopeduncular nucleus/internal globus pallidus, the extended amygdala [bed nucleus of the stria terminalis (BNST), basolateral nucleus (BLA) central nucleus (CeA) of the amygdala], the septal area and the PAG, whereas it likely indirectly communicates with the HPC. In turn, the LHb projects onto the dopaminergic and serotonergic midbrain nuclei and modulate dopamine (DA) and serotonin (5-HT) transmissions, whereas it also modulates noradrenalin (NA) transmission, which are the main neurotransmitter systems implicated in emotional processes. Such modulation includes again key structures processing emotional situations, such as the mPFC and HPC. Finally, we have seen above that the LHb can influence CORT release.

We are now going to see in more details – when they are provided by the literature - how the LHb interacts with these different actors of the stress response and for which purpose.

The HPA axis and CORT release

The engagement of the HPA axis, and the consecutive CORT release, is one of the principal effectors of the physiological response facing a stressful or threatening situation (**de Kloet 1992; de Kloet et al. 1999**). The view is that the peak of CORT occurring upon stress help the individuals to deal with the situation by increasing alertness (**Joëls 2018**). Importantly, CORT levels have been correlated to spatial memory, performances diminishing with increasing levels of CORT (**Luine 1994**). The view that CORT in the HPC can help memory processing has since received physiological support, several studies showing that CORT modulates hippocampal plasticity and trigger LTP at glutamatergic synapses (**Sarabdjitsingh et al. 2014; Sharvit et al. 2015**). A study by **Kaouane et al. (2012)** shed more light on the interactions between CORT and the HPC and the detrimental consequences of excessive stress and altered modulatory processes of the HPA axis; using a fear conditioning procedure, they showed that CORT injection in the HPC following conditioning subsequently biased the animals towards cues with less predictive values, indicative, for the authors, of post-traumatic stress disorder-like memory deficits.

As said above, there are evidence that the LHb interact with the HPA axis, although there are no known direct links between them, as its manipulation can influence blood CORT levels (**Murphy et al. 1996; Jacinto et al. 2017; Mathis et al. 2018**). A recent study by **Berger et al. (2018)** demonstrated that manipulation of the endocannabinoid system within the LHb can affect CORT release. One interesting fact, we have observed that the inactivation of the LHb only altered CORT levels in the water maze by increasing it, an increase concomitant to memory deficits and potentially with signs of excessive stress (increased thigmotaxis; **Mathis et al. 2018**); such an increase was not reproduced when LHb was inactivated in the home cage or during the performance of the elevated plus maze, although it was anxiogenic. Therefore, it seems that the LHb is involve in stress coping, and subsequently interacts with the HPA axis, only in conditions of cognitive demand. A very recent study performed in mice seems to agree with such a view. In fact, **Nuno-Perez et al. (2021)** showed that stress (unpredictable footshocks following training) further biased rats towards non-rewarded choices in a reward-guided task in a T-maze, and that this was correlated to alterations of plasticity mechanisms (reduced AMPA-receptor transmission) in the LHb. Another mechanism through which the LHb participates in stress coping is provided by **Berger et al. (2018)** who demonstrated in rats that the blockade of cannabinoid receptor 1 in the LHb, which increases baseline CORT release, as said earlier, biased coping strategies towards proactivity.

The mPFC

As said elsewhere, the prefrontal cortex is involved in the response to stress mainly in humans (**Uliana et al. 2021**) and sustained stress exposure induces deficits of prefrontal cortex-mediated cognitive function including working memory and cognitive flexibility (**Graybeal et al. 2012; Arnsten**

2015). There is nonetheless multiple evidence of a link between the prefrontal cortex and stress in rodents, whether it is acute or chronic. In rodents it has been shown (c-Fos quantification) that the mPFC is activated by exposure to stressors such as acute restraint (**O'Mahony et al. 2010**), footshock (**Morrow et al. 2000**), or forced swimming (**Cullinan et al. 1995**). In addition, repeated restraint stress in rats induced a marked reduction in apical dendritic spine density in pyramidal neurons of the mPFC (**Radley et al. 2006**) and cognitive deficits similar to what is shown in humans (**Arnsten 2000**). Although it is still not very clear what could be the role of the mPFC in rodent facing stressful situation, it is said to participate to executive functions destined to cope with stress (**Holmes and Wellman 2009**) and, at a more physiological level, in the modulation of the activation of the HPA axis (e.g., anterior cingulate cortex [ACC]; **Diorio et al. 1993**) and the DA system (see below; **Moghaddam 2002**).

There is paucity of investigations on the physiological and behavioral correlates of a potential relation between the mPFC and the LHb. We have seen previously that the LHb receives direct inputs from the mPFC (prelimbic cortex [PRL], infralimbic cortex [IL], ACC; **Kim and Lee 2012**). Interestingly, within the mPFC, the LHb modulates the release of key neurotransmitters involved in the stress response, *i.e.*, DA (**Lisoprawski et al. 1980**; **Lecourtier et al. 2008**) and NA (**Cenci et al. 1992**). It is therefore tempting to postulate that the LHb and the mPFC could communicate during exposure to stressors; the LHb could modulate the release of both DA and NA in the mPFC so that the latter can adequately and timely modulate the HPA axis activity and favor arousal and prepare coping strategies, respectively. Another possible interaction is provided by **Tomaiuolo et al. (2014)**. We have seen earlier that they found LHb inactivation to disrupt long term aversive memory using the inhibitory avoidance task. In addition, they showed that these deficits were reversed when the D1/D5 DA receptor agonist SKF-38393 was injected in the mPFC along with LHb inactivation; this suggests a role for the LHb could be to modulate DA release in the mPFC during training to favor long term aversive memory.

The hippocampus

The HPC is well known for its implication in the stress response, principally as acting as an inhibitor of the activity of the HPA axis providing a negative feedback likely to prevent detrimental consequences of excessive corticosteroid release. On the other hand, stress can alter hippocampal synaptic plasticity (reduction of LTP) and impairs HPC-mediated memory process (**Kim et al. 2007**). The HPC is involved in fear conditioning, mainly by participating to the association between the aversive event and the context (**Rudy et al. 2002**).

There is no known connection between the LHb and HPC, only evidence of indirect links. It is likely that both structures communicate as two studies have shown high coherence of their respective oscillations at the theta frequency (**Aizawa et al. 2013**; **Goutagny et al. 2013**). Past research had already showed such a link. For example, (**Zagami et al. 1995**) showed that LHb stimulation had an overall excitatory effect on HPC neurons, which they postulated occurred through an action on the

RN (see also **Ferraro et al. 1997**). Also, stimulation of the LHb markedly increases acetylcholine (ACh) release in the HPC (**Nilsson et al. 1990**); the authors further postulate that this occurs via the medial septum/diagonal band of Broca, or indirectly via brainstem monoaminergic neurons. Evidence of a link between the LHb and HPC during stressful experience is provided by **Tomaiuolo et al. (2014)** who demonstrated, like for the mPFC (see above) that active avoidance deficits induced by LHb inactivation could be prevented by injecting SKF-38393 in the HPC. Another indirect evidence of a possible communication is provided by **González-Pardo et al. (2012)**; using cytochrome oxidase as a marker of metabolic activation, and subsequently factorial analysis, they found positive correlation between the LHb and dorsal CA3 during acquisition of contextual fear conditioning; they postulated that such communication could be necessary for the establishment of the context-US association. Intriguingly, **Chan et al. (2017)** have shown that intra-LHb administration of both antagonist or agonist of D1 DA receptor not only impaired the acquisition of contextual fear memory, but also reduced LTP in the HPC. Finally, we have seen that the LHb can influence ACh release in the HPC (**Nilsson et al. 1990**); as ACh participates to context encoding during fear conditioning paradigms (**Likhtik and Johansen 2019**), it is tempting to envisage that it is through disturbances of cholinergic HPC inputs that LHb inactivation induced contextual memory deficits in our trace fear conditioning paradigm (**Durieux et al. 2020**).

The extended amygdala

The amygdala is in rodents the main structure involved in emotional processes, including the stress response and fear memory (**Fendt and Fanselow 1999; Balleine and Killcross 2006; Jennings et al. 2013**). An important role is to participate to the memorization of emotional events, especially when associated to a salient stimulus (**Sehlmeyer et al. 2009; Chau et al. 2013; Bergstrom 2016**). In the amygdala, the BLA is particularly implicated in the stress response. Stressors activate the BLA [e.g., restraint (**Park et al. 2017**), footshock and contextual fear conditioning (**Rosen et al. 1998**)] and increase spine density there (**Mitra et al. 2005**). The main role of the BLA remains to participate to the memorization of stressful and aversive events (**Roosendaal et al. 2009**). As discussed by **Belujon and Grace (2015)**, the BLA also serves to « attribute an emotional meaning to environmental stimuli » by serving as an entry point of diverse sensory inputs, which are processed and passed along to the CeA which serves as effector of the behavioral response in relation with the PAG, for example in the genesis of fear responses. The BNST is also of particular interest. It is a site of action of corticotropin-releasing factor (CRF); CRF has been shown in rodents to excite the BNST and modulate anxiety, inhibitory avoidance and conditioned place aversion (**Daniel and Rainnie 2016**). More precisely, in rats **Butler et al. (2016)** showed that CRF+ BNST neurons were activated (c-Fos expression) following stressors such as ferret odor or elevated plus maze exposure. In addition, the BNST has been involved in contextual fear conditioning, but rather under conditions of temporal unpredictability of the occurrence of the US (**Goode et al. 2020**).

There is only little evidence of a connections between the extended amygdala and the LHb. Both the anterior and posterior parts of the BNST project to the LHb (**Dong and Swanson 2004, 2006**). In the amygdala, projections to the LHb from the BLA (**Kim and Han 2016**) and the CeA (**Zhou et al. 2019**) have been shown in rats and mice respectively, although the input from the BLA needs to be confirmed. At the behavioral level, inhibition of the LHb has been shown to blunt the increase 5-HT release within the LHb as a consequence of a stressful social encountering (**Dolzani et al. 2016**). Finally, **Barrett and Gonzalez-Lima (2018)**, using functional connectivity analysis following staining with fluorodeoxyglucose staining, found positive correlation between activity of the LHb and CeA during a contextual fear conditioning protocol.

The periaqueductal gray

The PAG is an important structure involved in the stress response and the expression of aversive emotional behaviors, like fear; it is at the origin of the response of systems such as the sympathetic nervous system, the HPA axis and the motor system (**Lovick 1993**).

Very few papers show connections between the LHb and the PAG. From **Li et al. (1993)**, described in rats, following the injection of a retrograde tracer (WGA-HRP) into the PAG, a direct projection from the LHb to the PAG; the connection is reciprocal as, following injection of the retrograde tracer CTb in the LHb, they show stained neurons in the PAG, a connection confirmed after PHA-L injection in the PAG; interestingly, it is the LHbM, the subdivision preferentially activated by stressors (see above) which is connected to the PAG. In humans, activation the Hb and the PAG have been correlated using fMRI and functional connectivity analyses (**Hétu et al. 2016; Ely et al. 2019**). Therefore, it is harder to speculate for a potential cooperation between both structure during the stress response or fear memory processes. And if the LHb indeed projects onto the PAG, what could be the exact role of such pathway when the network involved in fear-related behaviors, for example, has been well described and link the PAG with structures such as the amygdala, the hypothalamus, or the HPA axis. In fact, the LHb and the PAG could interact indirectly in stressful situations. Indeed, **Pobbe and Zangrossi (2010)** have shown that stimulation of the LHb (60 pmol of kainic acid) improved memory in an inhibitory avoidance paradigm, and that this was blocked by the injection of the 5-HT_{2A/2C} receptor antagonist ketanserin in the PAG; the authors conclude that the expression of fear-related defensive behaviors is mediated by a serotonergic input to the PAG, an input controlled by the LHb.

The monoamine systems: DA, NA and 5-HT

The DA system

Since the seminal work of **Thierry et al. (1976)** it is known that stress exposure induces the stimulation of DA release throughout the brain. **Abercrombie et al. (1989)** later described in rats that the magnitude of the stimulation of DA release was the most important in the PFC, then in the NAc, and then in the striatum. Interestingly, as discussed by **Belujon and Grace (2015)**, the initial

increase in DA excitation produced by exposure to stress is followed by the opposite effect, a dampening of its activity; this chain of events has been theorized under the concept of “opponent process”, postulating that it is useful for homeostasis and to counteracting the detrimental effects of stressors by generating an opposing emotion (relief after fear for example).

We have seen above that in rats the LHb can modulate DA release into the PFC (**Lisoprawski et al. 1980; Lecourtier et al. 2008**). The LHb sends direct projections onto DA neurons of the VTA and SNc. Stimulation of the LHb has been shown to induce a diversity of response of DA neurons; **Christoph et al. (1986)** demonstrated in rats that if 24% of VTA and SNc DA neurons were inhibited following LHb electric stimulation, in 64% of them the initial inhibition was followed by an excitation. **Ji and Shepard (2007)** later demonstrated that the inhibition was mediated by GABA-A receptors. In fact, the LHb projects in rats onto both DA and GABA neurons of the midbrain (**Omelchenko et al. 2009; Balcita-Pedicino et al. 2011**), as well on GABA neurons of the rostromedial tegmental nucleus (RMTg; **Jhou et al. 2009**; also called tail of the VTA by **Kaufling et al. 2009**) which represents an inhibitory break onto DA VTA and SNc neurons. Such a LHb-RMTg-DA neurons circuit has also been demonstrated in monkeys (**Hong et al. 2011**). Therefore, it is not surprising to obtain an inhibition followed by an excitation of DA neurons after LHb stimulation, suggesting complex networks and bidirectional influence of the LHb over the activity of DA neurons.

Although not many, there is some evidence of a link between the LHb and the DA system during emotional processes. **Lammel et al. (2012)** demonstrated that optogenetic stimulation of the LHb-VTA pathway induced conditioned place aversion; interestingly, they also showed that LHb neurons preferentially synapse onto DA neurons projecting to the mPFC, and that the concomitant injection of DA antagonists in the mPFC could reverse the aversion elicited by the LHb-VTA stimulation. As said earlier, the relationship between the LHb and the DA system, comprising the RMTg, is very complex as similar results were obtained in the same behavioral paradigm following optogenetic activation of the LHb-RMTg pathway (**Stamatakis and Stuber 2012**). As we have seen above, DA can also act on the LHb, as **Chan et al. (2017)** demonstrated that intra-LHb injection of DA receptor agonist and antagonist impaired contextual fear conditioning.

It remains difficult to understand what could be the nature and goal of interactions between the LHb and DA system during the processing of emotional experiences. We have seen that the LHb can bidirectionally modulate the activity of DA neurons, and modulate DA release in key regions such as the PFC. One possibility, advocated by several groups (Stuber - Malenka – Jhou) is that the LHb serves to encode aversive experiences, a kind of « anti-reward » structure. We have seen above those aversive experiences can be counterbalanced by opposing emotion in order to preserve the psychological integrity of the individual, and that this is likely to be subserved by opposite changes in DA release. A role for the LHb could be to balance DA transmission towards cortical and subcortical structures in order to control homeostasis and prevent overwhelming effects which could eventually lead to pathological conditions. According to that, **Chaudhury et al. (2013)**, showed that VTA-to-NAc DA neurons were hyperactive in mice susceptible to social defeat stress. Hyperactivity

of the LHb has been shown both in depressive patients and rodent models of depression: therefore, one can postulate that such hyperactivity of DA neurons could be provoked by hyperactivity of LHb neurons.

The NA system

Upon stress, NA is released to participate to the sympathetic reaction to stress. It is also released, as shown in rodents, in various brain structures including the hypothalamus, the amygdala, the thalamus, the HPC, the BG, and the PFC (**Tanaka et al. 1983; Nakane et al. 1994**). It is likely that such response to stress, especially in the PFC, is destined to bring the individual in a level of attention and alertness suited to adequately cope with stress. Also, NA is involved in emotional learning, especially through modulation of the amygdala (**Likhtik and Johansen 2019**).

To our knowledge, despite what can be said in many reviews (e.g., **Lecourtier and Kelly 2007**), a projection from the LHb to the locus coeruleus (LC) does not seem to exist or needs to be confirmed. Nonetheless, it has been shown in rats using microdialysis, that the LHb can modulate NA release; in fact, LHb electric stimulation enhances NA release in the HPC (**Kalén et al. 1989**), and in the mPFC, NAc, and striatum (**Cenci et al. 1992**), a later effect abolished following transection of the *fasciculus retroflexus*, carrying efferent fibers of the LHb. It is still unknown how the LHb can influence NA transmission. In their paper, **Kalén et al. (1989)** discuss their results saying that « *a minor direct projection from the LHb to the LC (Herkenham and Nauta 1979; Araki et al. 1988) [was shown], but these findings have not been confirmed in retrograde tracing studies (Cedarbaum and Aghajanian 1978; Clavier 1979; Aston-Jones et al. 1986)* »; one can add that **Pasquier et al. (1977)** did not report a HbL-LC projection following injection of the retrograde tracer in the LC. Therefore, as said above, it is still to be discovered how exactly the LHb can influence LC activity and NA transmission. Even if indirect, it is still interesting that LHb can influence NA transmission and that such modulation could be important for emotional behaviors. Noteworthy, in humans, **Wills et al. (2020)** found a functional connectivity between the Hb and the LC in anorexia nervosa patients. The LHb could very much modulate NA release in situations of stress. It could explain why LHb inactivation induce anxiety in the elevated plus maze (**Mathis et al. 2015**). The LHb could also modulate NA transmission to the PFC in order to favor alertness and attentional processes; interestingly, Hb lesion was shown to induce attentional deficits in the 5-choice serial reaction time task (**Lecourtier and Kelly 2007**), although these deficits only occurred long time following the lesion. Finally, the LHb could participate to the modulation of NA transmission towards the amygdala and HPC to process CS-US and context-US associations respectively (**Likhtik and Johansen 2019**).

The 5-HT system

Acute stress leads to an increase of the activity of 5-HT neurons in the DRN and an increased 5-HT efflux in the mPFC, amygdala and HPC (**Mahar et al. 2014**). Also, fear conditioning has been shown in rats to induce a rise of 5-HT release in the mPFC (**Hashimoto et al. 1999**) as well as in the

amygdala (**Yokoyama et al. 2005**) likely to encode the aversive aspect of the situation (**Bocchio et al. 2016**).

The LHb is one of the main inputs to the raphe nuclei (**Metzger et al. 2017; Zahm and Root 2017**), and in rats electric stimulation of the LHb has been shown to decrease the firing rate of 5-HT neurons (**Wang and Aghajanian 1977**). Also, **Amat et al. (2001)** showed that electric LHb lesion prevented the stress-induced rise in 5-HT release in the striatum. But the exact influence of the LHb upon the 5-HT system is not that clear. **Soubrié et al. (1981)**, showed in anesthetized cats that LHb stimulation (60 mM KCl administration) induced an increased 5-HT release in both the striatum and the *substantia nigra*. Similarly, **Kalén et al. (1989)**, in anesthetized rats, showed that 5-HT release was enhanced in the striatum following a 15 Hz LHb electrical stimulation. On the contrary, the same group who showed increased 5-HT release in cats following KCl-induced LHb activation showed opposite results, *i.e.*, a decreased 5-HT release in the same structure following 15 Hz electric stimulation (the same paradigm used by **Kalén et al. 1989; Reisine et al. 1982**). **Ferraro et al. (1996)** shed some light on the network linking the LHb and the RN. They identified putative 5-HT and GABAergic neurons and showed that whereas low frequency LHb activation induced an inhibition of both neuronal types, higher frequency stimulation induced a strong activation of GABA neurons and an inhibition of 5-HT neurons, suggesting the complexity of the LHb influence upon the 5-HT system depending on the type of situation and the information exchanged between both structures.

There is no doubt that the LHb and the 5-HT systems are associated during emotional processes. The relationship between the LHb and the serotonergic system and their implication in the stress response has probably been best studied in zebrafishes. **Amo et al. (2014)** have demonstrated that a stimulatory pathway from the vHb, the homologous of the mammals LHb, to the raphe nucleus, was involved in fear learning as its selective ablation induced marked memory impairments, linking the vHb and the 5-HT system to the processing of emotional situations. We have seen earlier that in zebrafishes, under stress the switch from active to passive coping occurred consecutively to a strong activation of the vHb (**Andalman et al. 2019**); in addition, the authors demonstrated that the direct consequence of this activation was to turn down the activity of raphe 5-HT neurons, pointing to a role for a habenulo-raphe pathway in stress coping strategies. Here again must be noted that in zebrafishes, like in rodents, the net impact of vHb or LHb on the activity of 5-HT neurons seems very complex as here also vHb activation induce an excitation of raphe cells in one study and an inhibition in the other. In rats, **Dolzani et al. (2016)** have demonstrated that exposure to an inescapable shock (IS) induced a strong activation of DR 5-HT neurons and a rise of 5-HT release in the amygdala; they further demonstrated that LHb inactivation during IS abolished these responses were abolished, as was the anxiety behavior (assessed by social investigation) normally occurring after IS; this demonstrates that the LHb can modulate the activity of the serotonergic system to control behavior and cope with stress.

Conclusions

The Hb is considered a primitive structure which has constantly evolved and which, early in evolution, has been involved in key behavioral emotional processes ranging from reacting to a stressor to the elaboration of complex coping strategies, such as demonstrated in zebrafishes. The key brain structures involved in emotional processing such as stress response and fear learning, are, besides sensory and association cortices and thalamic relays, the HPA axis, the mPFC, the HPC, the extended amygdala, and the PAG, along with modulatory monoaminergic regions, including the VTA (DA), the RN (5-HT), and the LC (NA). There is not always clear evidence that the LHb interact with these structures regarding emotional processing, as only few investigations have been performed, but there can be reasonable speculations based on the existing literature concerning the LHb (see also review by **Browne et al. 2018**). We have seen that the LHb receives direct inputs from the whole mPFC and bidirectionally interacts with the DA and 5-HT systems. Its link with the extended amygdala, at the exception of the BNST, is less documented and the connection with the PAG needs to be confirmed. Finally, it has no direct connections with the HPC or the paraventricular hypothalamic nucleus and HPA axis, but there is strong evidence to suggest that the LHb and HPC exchange information, and that the LHb is somehow participating to the modulation of the activity of the HPA axis and CORT release. As stated by many groups, the LHb is seen as a relay of descending information from the forebrain to the midbrain; the main pattern one can notice is that there are loops of forebrain-LHb-monoaminergic regions-forebrain connections, so that forebrain structures can modulate their monoaminergic inputs through the HbL. These loops tend to support the hypothesis that the LHb is an integrator of incoming external information and can lead to behavioral adapting according to the “current”/online situation (**Geisler and Trimble 2008; Hikosaka 2010; Lee and Han 2019**). The diversity of external information processed through the LHb include cues associated with aversive events in order to participate in the elaboration of adapted behavioral actions and cope with stress. Further, it can be envisaged that the LHb not only participates to primary reactions upon stress, but also to the building of a memory repertoire so that when encountered again, those situations will allow more efficient reactions and better chances of survival.

III. Studies problematics

The third part of the introduction will address and summarize the different problematics of this project and express the reasons why we performed the different experiments, without referring again to the bibliography which is already cited in the general introduction and in the introduction of each separate study (see **STUDY 1: Involvement of the Lateral Habenula in Fear Memory page 134**, **STUDY 2: Functional brain-wide network mapping during acute stress exposure in rats. Impact of DREADD-induced lateral habenula inactivation, with a note on CNO page 135**, **STUDY 3: Changes in Lateral Habenula Oscillatory Activity Upon Repeated Stress Exposure page 136**).

We have seen that the LHb shows a strong response to barely a large diversity of stressors, as demonstrated using c-Fos immunostaining, cytochrome oxidase, and electrophysiological recordings. At the LNCA it was shown that LHb inactivation induced short-term memory deficits in a delayed non-matching to sample paradigm and spatial reference memory deficits in the water maze, as well as contextual memory deficits in an object-based task; in addition, it was shown, here and elsewhere, that the LHb likely communicates with the HPC. Interestingly, along with spatial memory deficits, induced in the water maze, LHb induced a behavior (thigmotaxis) which could indicate an altered response to the rather stressful experience the test represents. It was further shown that those behavioral alterations (memory deficits and thigmotaxis) were correlated with an excessive CORT release, suggesting that LHb dysfunction somehow disturbed the response of the HPA axis, and that this disturbance might have participated to the behavioral deficits observed. In almost the same line, several teams demonstrated that pathways linking the LHb with the BG, the LH or the VTA and RMTg/tVTA, participate to avoidance behavior. All together these results point to a role for the LHb in the response to stressful and threatening environments, and the elaboration of behavioral outcomes, but without any knowledge of the big picture: within which network of structures is the LHb engaged during exposure to stressful or threatening situations.

According to these considerations, we elaborated our first study in rats (**study 1** below, [Durieux et al., 2020](#)) with two questions in mind: 1) is the LHb engaged in fear memory formation? 2) is the LHb engaged in this process in collaboration with the main regions involved in this type of memory task? We chose to use a trace fear conditioning paradigm, presenting the CS (tone) and US (footshock) with a 30-sec delay apart, so that the context is preferentially associated with the

INTRODUCTION - Studies problematics

US. We made the hypothesis that LHb inactivation in such paradigm will induce deficits of association of the context with the US, regarding the spatial and contextual memory deficits already observed following LHb dysfunction. In addition, we performed in naive rats a conditioning session followed by a c-Fos immunostaining in the LHb, the HPC, the mPFC, and the AMG, in order to try to correlate LHb activation to this of those key structures involved in fear conditioning, and therefore obtain a first idea of the place of the LHb in the network engaged in fear memory processing.

Along with this purely cognitive study, we decided to explore the engagement of the LHb in the response to stress at the network level, but this time considering all the structures engaged in these types of responses. We therefore performed a second study (study 2 below), using a 10-min long acute restraint stress in rats as a behavioral paradigm. Following this, we performed c-Fos immunostaining throughout the whole brain, considering key regions such as, like for the previous study, the mPFC, the HPC, the AMG, and, in addition, other key regions, including cortical regions such as the insular cortex and the parahippocampal cortices, the septum, the BG, thalamic and hypothalamic periventricular nuclei, the monoaminergic structures of the midbrain, the PAG. Then we performed a network analysis based on Graph Theory to model the functional network recruited by the restraint stress, in order to investigate the main information hubs as well as the interaction of the LHb with the other brain structures during restraint stress. In addition, we performed in a group of rats LHb inactivation in order to see if this could somehow disturb/disorganize, the brain network engaged during such experience.

Finally, following these two studies which indicated that during the stress response the LHb was likely communicating with some key regions of the response to stressful and threatening situation, we decided to explore in a finer way how the LHb temporally communicates with these structures (i.e., PRL, ACC, dHPC, BLA), using electrophysiological recordings (local field potential [LFP]). We used restraint stress again, but this time we performed two restraints, 3 hours apart, in order to also investigate behavioral and electrophysiological signs of stress coping upon repeated stress exposure, also addressing sleep/wake stages. To that purpose we not only studied intra-structural modifications (e.g., power analysis) but also inter-structural modifications (e.g., coherence analysis). Moreover, we have also decided to investigate potential inter-individual differences, that could account for a “vulnerability” to restraint stress. This differentiation has already been made in the literature, supporting the idea that the stress response depends on the context but also on the way each individual receives a stressful experience. Our hypothesis was that the LHb could play a role on this susceptibility.

INTRODUCTION - General knowledge on the technical and conceptual approaches used in this project

IV. General knowledge on the technical and conceptual approaches used in this project

As PhD projects often use a wide range of techniques and analyses, I made the choice to devote the last part of the general introduction for introducing those and providing general principles. I will first address the DREADD approach used in **studies 1 and 2**, including pros and cons. Then I will address c-Fos immunostaining and the different network analyses allowed by this type of data, including FA used in **study 1**, and the graph theory approach used in **study 2**. Finally, I will address the electrophysiology technique, the recording of brain oscillations and the type of information they can provide through different analyses (**study 3**). To finish I will introduce the video tracking approach using deep learning algorithm.

1. DREADD (studies 1 & 2)

The DREADD is a pharmacogenetic approach developed by Roth and collaborators and presented for the first time in scientific publication by [Armbruster and collaborators in 2007](#). The DREADD allows to impact on the activity of neuronal populations thanks to genetically engineered G-protein coupled receptors (GPCR; see **Box 6**) which are expressed in brain structures through the injection of viral vectors including their coding sequence. Once expressed at the cell surface, they can be activated by a specific exogenous ligand. There are fundamental principles underlying the DREADD technique: the receptors must be inert (they cannot be activated by endogenous ligands) and the exogenous ligand must only bind to the modified receptors (it cannot activate endogenous receptors).

Box 6: G protein-coupled receptors (GPCR)

The GPCRs are the most important family of membrane receptors. They are composed of seven transmembrane segments and can be activated by diverse types of hormones or neurotransmitters (Rosenbaum et al., 2009). The binding of a ligand on a GPCR leads to the modification of the shape of the receptor, which triggers the interaction of the G proteins with the receptor (Zhu and Roth, 2014). The activation of the G protein is the essential step to trigger the cellular pathway leading to the modification of the cellular activity. The G protein will interact with several molecular effectors (e.g., adenylate cyclase) which will end up by the production (Gs or Gq) or the inhibition (Gi) of cyclic adenosine monophosphate (cAMP) production (see Figure 22), therefore modulating the intracellular concentration of the calcium.

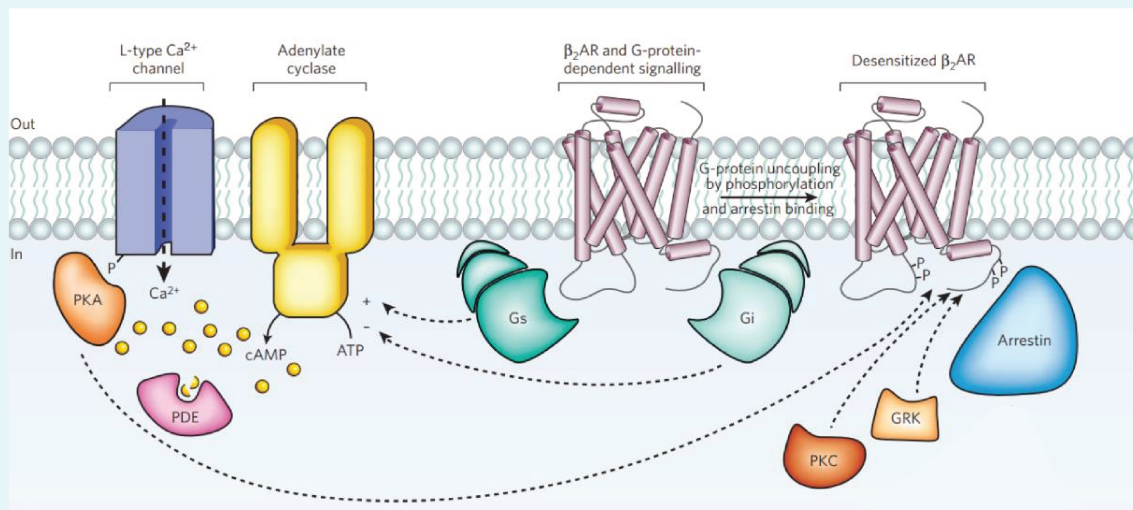


Figure 22: Intracellular signaling pathways of the G-protein-coupled proteins.

Adapted from Rosenbaum et al., 2009. Abbreviations: cAMP, cyclic adenosine monophosphate; Gi, G-protein-coupled-protein, subunit i; GRK, G-protein-coupled receptor kinase; Gs, G-coupled-protein, subunit s; PDE, phosphodiesterase protein; PKA, protein kinase A; PKC, protein kinase C; β_2 AR, type 2 beta adrenergic receptor.

a. The different types of DREADD receptors developed

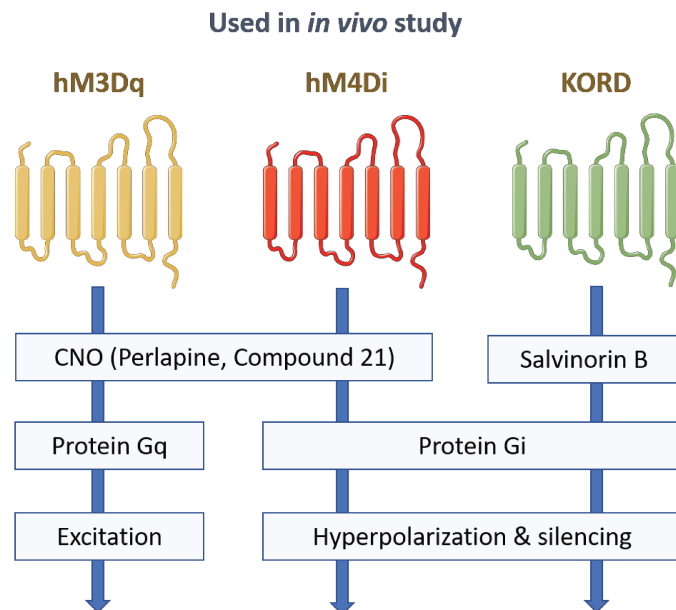
The more widely used DREADD receptors are those resulting from the modification of human muscarinic receptors. They are two types: 1) the hM3Dq is coupled with a Gq protein so that its activation will lead to the stimulation of the cell (i.e., it triggers action potentials); 2) the hM4Di receptor is coupled with a Gi protein so that its activation will lead to an inhibition of the cell (i.e., hyperpolarization of the cell). Finally, another receptor which is more and more used is the KORD which comes from the modification of the kappa-opioid receptor; it is coupled to a Gi protein so that it is also inhibitory, using a different ligand than the muscarinic receptors, i.e., the Salvinorin B (see Figure 23; Urban and Roth, 2015; Roth, 2016).

INTRODUCTION - General knowledge on the technical and conceptual approaches used in this project

Figure 23: Main type of DREADD receptors used *in vivo*.

Representation of the DREADD receptors used *in vivo*: develop from human muscarinic receptor (hM3Dq & hM4Di) or from kappa-opioid receptors (KORD). Their characteristics are indicated: their specific and respective ligands (CNO or Salvinorin B), their G-coupled protein (Gq or Gi), their effect on the cellular activity (excitation or hyperpolarization).

Adapted from [Urban and Roth, 2015](#) & [Roth, 2016](#).



For expressing one of the DREADD receptor, viral vectors are used. These can insert external DNA into the targeted cells and can express, in addition of the modified receptor, a fluorescent molecule. Moreover, we can select the type of neurons/ cells expressing the DREADD receptor by adding a specific promotor to the DNA sequence.

b. Viral vectors used for DREADD receptors expression

There exist many viral vectors that can deliver coding sequences within brain cells. However, their use in Neurosciences is limited by their transfection mechanism and their transport capacity (*i.e.*, how much DNA or RNA they can transport). Their pathogenicity is also a limiting factor. Currently, studies using viral vectors employ retrovirus, lentivirus, Herpes virus, adenovirus and adeno-associated virus (AAV) ([Choudhury et al., 2016](#)). In Neuroscience most of viral vector used are AVV ([Murlidharan et al., 2014](#)) because they have their transport capacity allows the expression of large proteins, because they are do not integrate their DNA to the endogenous ADN of the cell (no risk of random insertion and mutagenesis); the DNA carried will form a episomal concatemers which will be expressed by the host cell and this expression will be stable during several months ([Reimnsider et al., 2007](#); [Choudhury et al., 2016](#)). They have little or no pathogenicity (they trigger a negligieable, if any, immune response; [Tenenbaum et al., 2004](#); [Kotterman and Schaffer, 2014](#)) AAV are small vectors (20 nm). They are linear single-stranded DNA and are able to transport DNA up to 4.8 Kb, encapsulated in a capsid, allowing to include several genes of interest ([Kotterman and Schaffer, 2014](#)). There are different types of AAV (*i.e.*, serotypes; from 1 to 11) classified based on their capsid proteins. As a main consequence, this will induce differential levels

INTRODUCTION - General knowledge on the technical and conceptual approaches used in this project

of expression of the proteins, likely due to the level of interaction between the capsid proteins and the cell membrane, which can vary across the brain structures (e.g., **Figure 24**; the serotypes 1, 2 and 6 will be less effective than serotypes 5, 8 or 9 in the HPC; from [Aschauer et al., 2013](#)). Moreover, the AVV are capable to migrate both anterogradely and retrogradely once captured by neurons ([Tenenbaum et al., 2004](#); [Murlidharan et al., 2014](#)), also likely due to the serotype.

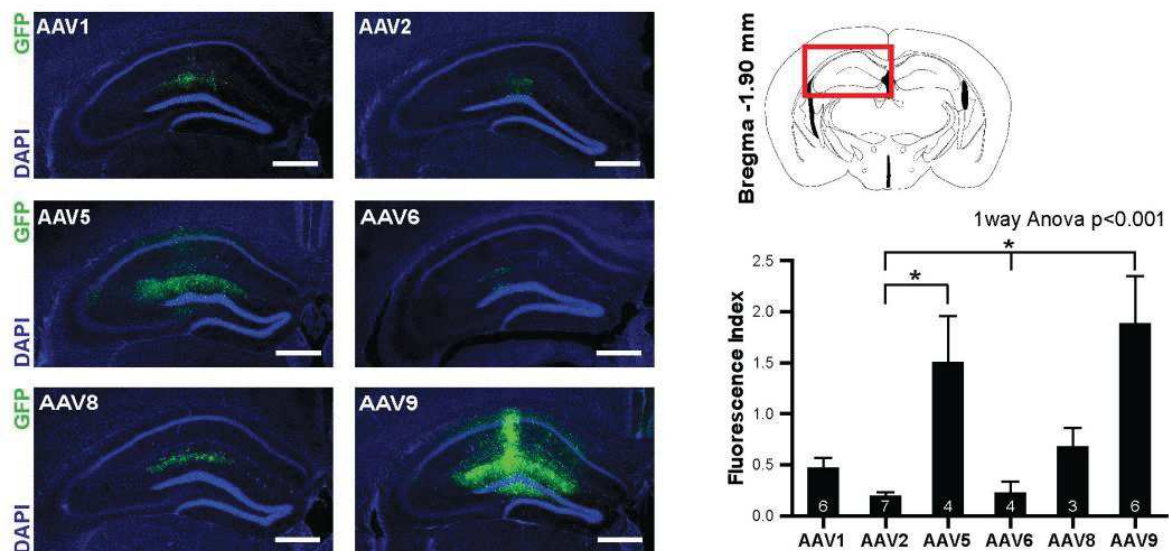


Figure 24: general expression of AAVs in the HPC depending on the virus serotype in mice.
From [Aschauer et al., 2013](#).

For our studies, according to the literature and some preliminary experiments, it was decided that the more efficient serotype for acceptable expression of the DREADD receptor within the LHb would be the 8. The vector selected contained a DNA sequence composed of: CaMKII (calcium-kinase calmodulin dependent protein II) promotor, supposed to allows expression of the protein in excitatory neurons, *i.e.*, glutamatergic, which the LHb is mainly composed of; the coding sequences for the hM4Di receptor and for the fluorochrome molecule, m-Cherry, the latter being used for further histology verification of receptor spreading. The vector is referred to as: AAV8-CaMKII-hM4Di-mCherry.

c. Strength and weaknesses of DREADD approach

The DREADD possess numerous advantages which made it a useful tool to better understand the role of a targeted neuronal population in behavioral processes, through stimulation or inactivation of these neurons. The inactivation or stimulation are reversible, which allow better experimental designs (*i.e.*, causality experiments when one can act at a precise moment of a behavioral

INTRODUCTION - General knowledge on the technical and conceptual approaches used in this project

protocol), in comparison to a permanent lesion of the targeted region; indeed, when the injected ligand has been metabolized and evacuated from the organism, the DREADDed neurons return to their physiological activity). In addition, this technic is not as invasive as the one requiring the local injection of a drug (e.g., muscimol) which requires the chronic implantation of cannulas guide, so that it only requires an intraperitoneal injection to be effective. In comparison to the optogenetic technic, it is also easier to use because it does not require specific equipment and all behavioral paradigms can be tested (including placing rats within a tube) as animals do not have head-caps and optic fibers connected. One more advantage is that DREADD receptors are modified GPCRs so that once activated they trigger physiological molecular pathways to increase or decrease the number of action potential generated by the cell.

Such as every technic used in Neuroscience, the DREADD has its limitations. One of them is that, unlike optogenetics, it does not allow a precise temporal action on the targeted cells; depending of the concentration and the nature of the ligand, the availability of the compound can be extend from 1 to 6 hours post-injection (Whissell et al., 2016), with its pic around 20-30 min post-injection, depending of the study considered. Also, the approach has originally been designed on the principle that the DREADD receptors have no interaction with endogenous molecules and that the ligand will not bind to endogenous receptors. However, several studies have demonstrated that, depending on the ligand considered, is not always true (MacLaren et al., 2016; Manvich et al., 2018). The Clozapine-N-Oxide (CNO) is in fact a metabolite of Clozapine, an atypical antipsychotic, which is known to bind to a large range of receptors, including dopaminergic receptor (D1 and D4), 5-HT (including 5HT1A and 5HT2), noradrenergic (alpha 1 and 2) and histaminergic (H1; Schotte et al., 1993; Ashby and Wang, 1996). In fact, in monkeys and rodents, studies have shown that the CNO is metabolized in clozapine by the P450 enzyme (see Whissell et al., 2016; Raper et al., 2017; Manvich et al., 2018).

Moreover, some studies have shown that CNO can have deleterious behavioral consequences, certainly due to the fact that it is metabolized in clozapine (MacLaren et al., 2016; Manvich et al., 2018). However, these effects seem to occurs only with high CNO doses (Manvich et al., 2018). In addition, clozapine induces interoceptive effects on rats and mice (Manvich et al., 2018). In any case, numerous studies continue to use CNO as a ligand because the other ligands available for hM3Dq and hM4Di have not been as extensively investigated in vivo and the vast majority of studies using CNO do not report any adverse behavioral consequences following CNO administration (e.g., Aponte et al., 2011; Ferguson et al., 2013; Augur et al., 2016; Han et al., 2017).

INTRODUCTION - General knowledge on the technical and conceptual approaches used in this project

2. Wide Scale Network Analysis (study 1 and 2)

During the PhD, we used several types of analyses to extract information about the functional network implicated in the stress response and the trace fear conditioning. In studies 1 and 2, we used the expression of the c-Fos protein as a marker of structural activation (see [Box 7](#); [Wheeler et al., 2013](#); [Ali et al., 2017](#); [Tanimizu et al., 2017](#); [Vetere et al., 2017](#)) to study network functional activity employing two distinct analytical methods: the FA ([study 1](#)) and the Graph Theory analysis ([study 2](#)). Both types of analysis are based on the correlation of c-Fos-positive (c-Fos+) cells densities between structures of interest. Noteworthy, these types of network analysis based on c-Fos expression, are not commonly used in rodents, unlike fMRI studies (*e.g.*, [Zerbi et al., 2019](#)), and they are based on human fMRI or EEG investigations (review: [Bullmore and Sporns, 2009](#); [van den Heuvel and Hulshoff Pol, 2010](#); [Dennis and Thompson, 2014](#)).

INTRODUCTION - General knowledge on the technical and conceptual approaches used in this project

a. General goal of Network analysis

Unlike in the past when it was considered that a function was mainly supported by a single structure, it is now well established that any function is supported by a large network of structures through the coordination of their respective activity (McIntosh, 1999; Sporns, 2012; Park and Friston, 2013). Indeed, it has been shown that the physiological response of cell assemblies to a given stimulus or function supports the emergence of inter-regional synchronicity of oscillatory activity that can represent the substrate of information transfer within specified brain networks subserving specified functions (Singer, 1999; Fries, 2005a). Such networks support information processing and image representation in the brain (Bressler, 1995; Mesulam, 1998; McIntosh, 1999; Friston, 2002). The fact that complex behaviors arise from coordinated activation of brain given regions has led to a growing interest for the types of analytic approach considering broad cerebral activation to understand brain functions. That is why we decided to apply these types of analyses in order to better understand the position of the LHb within the networks engaged in the stress response and trace fear conditioning.

b. Factorial analysis

In this paragraph the basics of the Principal Component Analysis (PCA) will serve to explain the basics of the FA as they both belong to the same family of statistical analyses (*i.e.*, multivariate statistics) and are based on the same main principle (*i.e.*, dimensional reduction). Nonetheless, we need to keep in mind that both analyses have differences and are not used for the same purpose. This particular point will be developed later on. Also, we used the FA to unravel potential functional connectivity and by extend unravel functional networks in **study 1** and, so that our approach of the FA will be explained based on this specific experimental design. In addition, we used the PCA in **study 3**, but the purpose was not to study functional network but to cluster animals according to different behavioral variables (see part **Assessment of Sleep/Wake Stages page 125**). In this part, I will focus on the analysis of functional networks to explain the statistical methods, but the technics principle stays the same whatever the theoretical goal is. As said before, the FA based on the correlation of c-Fos+ cells density in rodents is not that common, but it has already been used in our laboratory (Ali et al., 2017) and elsewhere (Veening et al., 2009). The principle of both technic (PCA and FA) is general knowledge, accordingly, the sources of what is explained in this chapter are books (please see Sá, 2007; Cohen, 2014).

Principles

The goal of the FA was to evidence common factors to all measured variables. According to our immunohistochemistry experiment, the variable considered was the density of c-Fos+ cells within

INTRODUCTION - General knowledge on the technical and conceptual approaches used in this project

regions of interest. The FA allowed to compress a large number of variables, because there was a large number of regions, and therefore a large number of correlations into a smaller number of « factors » (*i.e.*, dimensional reduction; see below *Dimensional reduction*). These factors were generated through the processing of the table of correlation of initial variables, without any *a priori* intervention by the experimenter, and represented groups of variables with high correlation between them. This statistical technique is not based on a *a priori* hypothesis; it is more an exploration of the data. Applied to functional imaging studies, it allows to generate functional networks organized according to those correlations.

General processes

In this part I will first explain the general processes underlying the FA. The first step is called « dimensional reduction » which is quite similar, although simpler, to the PCA. This « dimensional reduction » is followed by the suppression of « weak factors », allowing the generation of a matrix of approximate correlation.

Dimensional reduction

The first step is the reduction of the number of variables. To this purpose the FA acts just like the PCA. The *samples* are the individual values, and the *variables* are what we have actually measured, *i.e.*, c-Fos+ cells density by structure. The samples (our group) should represent, in the better case, the population. The samples of the two first variables are normalized around the 0 value, not changing the distance between them; then the FA seeks for the linear function corresponding best to the data, *i.e.*, the straight-line fitting best with the sample distribution. For this calculation, all distances between the origin (or the 0 value) and each projection of the samples on the straight line (see **Figure 26** for a fictive graphical example) are summed.

$$SS = \sum_{k=1}^n dist_k^2$$

where SS represents the Eigenvalue, *n* is the number of samples, *k* is the index of itemizing of the samples, *dist* is the distance between the origin and the projection of the sample on the linear straight line.

When the sum of the distances is the highest it means that the linear straight-line fits best to our data. This sum is equal to what is called the *Eigenvalue* for the primary extracted component (PC). The straight line allows to calculate the new unit of this system, which will be equal to the *Eigenvector*, as follows:

INTRODUCTION - General knowledge on the technical and conceptual approaches used in this project

$$a = \sqrt{b^2 + c^2}$$

where a is the distance between the origin and the considered dot on the straight line, b is equal to the value of the considered dot on the X axis, c is the value of the considered dot on the Y axis.

Then, all the terms (a , b , and c) are divided by a so that a becomes equal to 1, therefore setting the new unit. The new values of b and c will then represent « from how much of each variable » is the considered component composed; they are called « loading scores ».

Once PC1 is calculated, PC2 is calculated and will be perpendicular to PC1; as such it will be placed to fit best with the rest of the data. Then the cycle starts again until there are no more variables to consider. Such a method explains well how factors can lose « weight » across the different cycles, as there are less and less variance to explain among the remaining variables. Following calculation of all the components, the data are rotated so that PC1 becomes the X axis and PC2 becomes the Y axis. Then the variance explained by each component can be calculated as follows:

$$VarPC_i = \frac{SS_{PC_i}}{n - 1}$$

where $VarPC$ represents the variation of the considered component, SS_{PC} is the Eigenvalue of the considered component, n is the number of samples, i is the index of numbering of the components.

$$totalVar = \sum_{i=1}^p VarPC_i$$

where $totalVar$ represents the overall variance, p is the total number of components.

$$\%VarPC_i = \frac{VarPC_i}{totalVar}$$

where $\%VarFC$ represents the variance explained by the component i .

INTRODUCTION - General knowledge on the technical and conceptual approaches used in this project

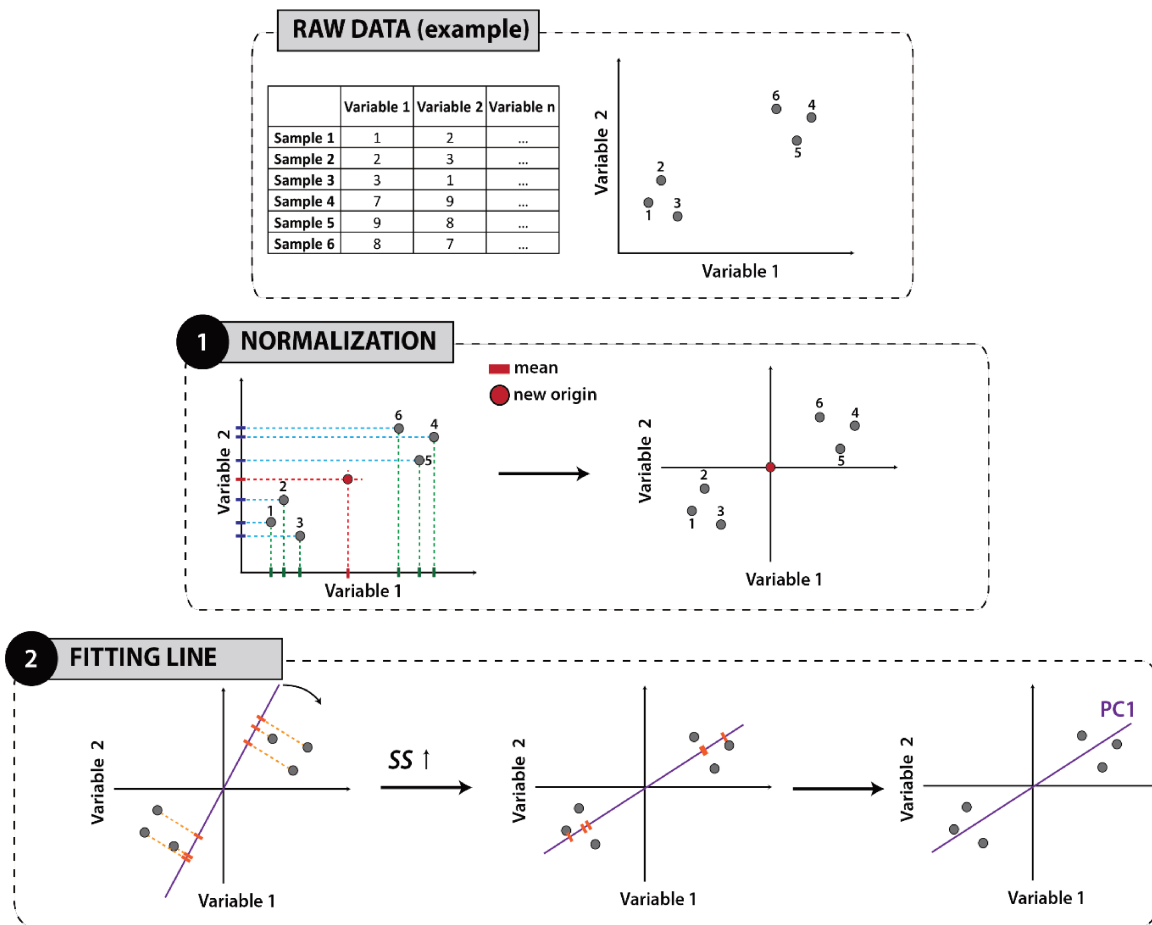


Figure 26: Fictitious example of “dimensional reduction”

Schematic representation of the process engaged to extract the first principal component based on fictitious raw data. The first step is the normalization of the data (1). The normalization is done by calculating the mean of the samples and use this mean as the new origin of the axis. The second step is to find the best fitting line over the samples (2). For this purpose, we calculated the SS (squared sum) of the distance between the projection of the dot on the line and the origin. When the SS is the highest possible then the line is fitting the samples. This line represents the PC1 (principal component). We can extract as many components as allowed by the number of variables.

According to the “dimensional reduction”, one of the differences between the FA and the PCA is that the components are called « factors ». Nonetheless, following this step the two analyses are slightly different, so in the following parts I will only talk about the FA.

The suppression of non-essential factors

Once the Eigenvalues of all factors have been calculated, it is possible to select how many factors (and their corresponding variance) can be kept. For that, several methods exist. The two mostly used in Neuroscience are:

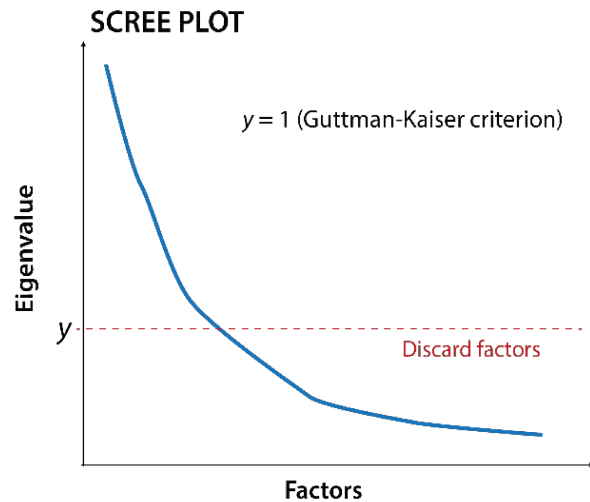
- Selecting the factors that together can explain at least 95% of the variance.

INTRODUCTION - General knowledge on the technical and conceptual approaches used in this project

- Using the Guttman-Kaiser criteria which states that, on normalized data (*i.e.*, correlations), factors with an Eigenvalue below 1 can be eliminated (see Scree plot **Figure 27**), based on the assumption that an Eigenvalue equal to 1 indicates that the factor explains as many variances as one of its variables.

Figure 27: Example of Scree Plot

Scree plot representation allowing to visualize the Eigenvalues of the extracted factors. If the Guttman-Kaiser criterion is selected as the threshold for discarding factors, then y (discard threshold) is equal to one.



The creation of a matrix of approximated correlation

Once the factors with Eigenvalue inferior to 1 eliminated, an approximated table of correlation and a table representing the error (the difference) between the correlation matrix and the original matrix, are generated. To be able to create this new model of correlation, two parameters need to be defined: the *extraction method* and the *rotation*. There exist numerous methods of *extraction* but the most widely used in Neuroscience are:

- The « Principal component method », which considers the whole variance of a sample (unique and shared) to extract the maximum of variance.
- The « Maximum likelihood » which maximize the difference between the factors.
- The « Principal axis factoring » which only considers the shared variance and therefore aims at creating the least number of factors.

There exist two main families of *rotation*: orthogonal and oblique. The oblique rotations are measured seeking a unique relationship between each factor and the variable, so that they are not commonly used in Neurosciences. There exist three main orthogonal rotations:

- Varimax, which reduces as much as possible the number of variables with an extreme loading factor. In other words, limiting the number of loading factors too far from the others loading factors.

INTRODUCTION - General knowledge on the technical and conceptual approaches used in this project

- Quartimax, which reduces as much as possible the number of factors allowing to explain each variable.
- Equimax, which is a combination of the two preceding rotations.

FA outputs

The main result of this technique is the production of factors and « factor loadings » which represent the correlation between the raw variables and the generated variables (or also called estimated variables). Each factor explains a certain percentage of the variation of our samples. These factors represent «clusters » designated as « functional » because the variables included in these factors are highly correlated, and the consecutive hypothesis will be that those highly correlated variables could participate to the same function. Nonetheless, the FA generates other results which are necessary to the validation of the model or to the study of the participation of each sample (value per rat) to each factor. We have then access to the following results:

- « *Communalities* », which represents the variability of the raw variables explained by the factors.
- « *Residues* », which represents the difference between the raw variable and the estimated variable; in other words, it represents the error between the model and the raw data. A negative residue indicates that the model is overestimated, and a positive residue indicates that the model is underestimated for this particular variable. There is always an error between the model and the raw data, it is just that this error should remain reasonable (less than 15 % is often considered reasonable, even if less than 5 % is the perfect condition).
- « *factorial scores* » which represents the normalized value of each animal in each factor.

For a model to be kept as a model adequately representing raw data, it needs to represent at least 50 % of the variability of the samples and the difference between raw and generated data needs to be acceptable (*i.e.*, residues below 15 %). Correlations of factors to variables are considered meaningful when they are superior than + 0.6 or inferior than – 0.6

c. Introduction to Graph Theory

Graph Theory is a mathematic field which purpose is to analyze complex networks (all types of networks, including biological ones). It allows to better perceive the complexity of networks and understand changes that can occur within them, depending on the current situation of the animal. Graph Theory approach on neuronal network is more and more used on human fMRI and EEG data (Bullmore and Sporns, 2009; van den Heuvel and Hulshoff Pol, 2010; Dennis and Thompson,

INTRODUCTION - General knowledge on the technical and conceptual approaches used in this project

2014). However, in rodent, even if analysis methods based on Graph Theory are emerging (see: Wheeler et al., 2013; Tanimizu et al., 2017; Vetere et al., 2017; Brynildsen et al., 2020 for c-Fos based Graph Theory studies), they are still limited and are mostly based on fMRI/EEG data.

As said earlier, analyses based on graph Theory allow to better understand the complexity of brain networks and the associated complex behavioral outputs. Brain complex networks have the characteristic to have a small world architecture (Sporns et al., 2004; Bassett and Bullmore, 2006; Reijneveld et al., 2007; Stam and Reijneveld, 2007). Small world network (originally described in social networks; Bullmore and Sporns, 2009) combine a high number of short connections between structures (connecting almost all the structures of a given network) and a high level of local clustering between structures. In other words, all the structures are connected through relatively few steps. These small world networks have been described in neuronal networks but also in numerous other types of networks (genetical, communication, or computational). The fact that neuronal networks deviate from randomness (*i.e.*, the small world architecture is not random) reflects that their functionality is organized (see review Bullmore and Sporns, 2009, for more details).

Graph generation and evaluation

In this part, I will give the principles governing to the creation of a Graph Theory-based network and the type of analyses that can be conducted on it, as well as their interpretations, with a focus on neuronal networks (a more detailed view will be found in the Materials & Methods section of this manuscript (see **Graph Theory Applied to Functional Networks (study 2) page 105**), as well as in the description of **study 2 (page 135)**).

The type of data used to model a network can vary from histological or imaging data (*e.g.*, fMRI or c-Fos+ cells density) to time series data (*e.g.*, EEG or LFP). The simplest way to modelized a network can be simplified in four steps (see **Figure 28; Bullmore and Sporns, 2009**):

- Define the **node(s)** of the network. In our case the nodes are the brain structures that we evaluated the c-Fos + cell density inside.
- Estimate the measure (continuous) of the association between nodes. In our study we used the c-Fos+ cells density as a representation of structural activation, and we used inter-structural correlations of this density as a representation of their association.
- Calculate the association matrix, also called **adjacency** matrix. This matrix will represent all pairwise associations (in our case, correlations) between the nodes. Most studies at this point use a threshold, keeping only the most significant correlations, producing **binary graphs** (if two nodes are connected, or not), and **edges** (*i.e.*, link) between connected

INTRODUCTION - General knowledge on the technical and conceptual approaches used in this project

nodes. However, another type of Graph can be based on the conservation of all pairwise associations, with the attribution to each the edge of values representing the strength of the connection (called the **weight** of the **edge**); this type of graph is called a **weighted graph**. In addition, if we can have, through the anatomy, a knowledge of the direction of the connection between two structures (for example if we know that a projection goes from structure A projects to structure B and not the other way around), the graph will be **directed**. Finally, a Graph where the edges have no direction (e.g., from c-Fos+ cells density correlations, where there is no way to define which structures influence the others) will be called an **undirected graph**. In our analysis, we used a **weighted and undirected graph** because some studies have shown the limitations of the application of a threshold to a functional network (Langer et al., 2013).

- Calculate the targeted parameters of the graph (e.g., how many structures connect to one particular structure) and compare it to either a **random network** or to another network from another situation, depending on what we are looking for. Many network measures (i.e., parameters) can be evaluated. I will describe the ones we used in our study; however, we can keep in mind that many other exist.

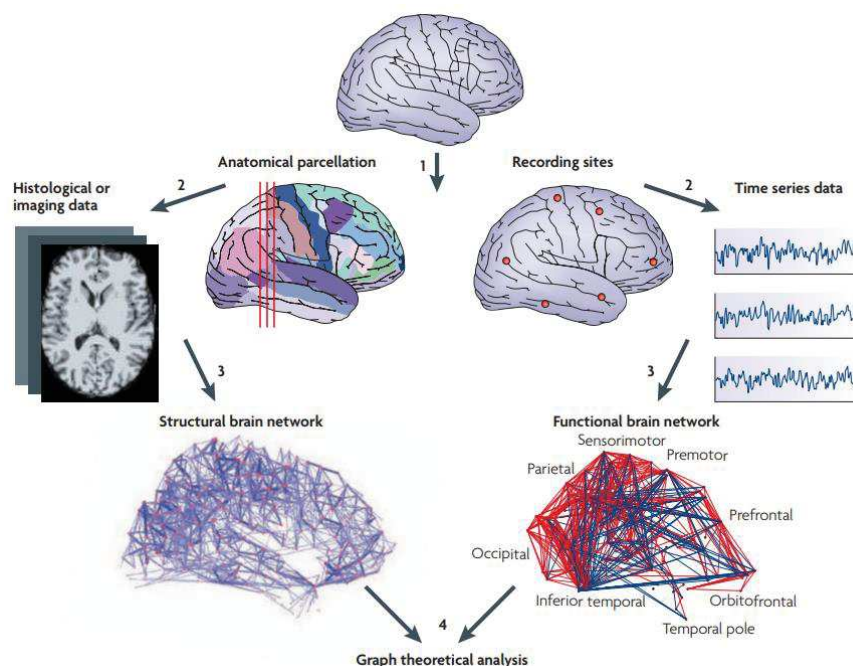


Figure 28: Main four steps to construct and analyze a functional network using Graph Theory as exemplified in human studies.

The numbers (1-4) represent the four main steps to model a functional neuronal network, from Bullmore and Sporns, 2009.

INTRODUCTION - General knowledge on the technical and conceptual approaches used in this project

Main Network Measures and statistical comparisons

For the sake of the following example (quantitative measures on a network), I decided to present them on an undirected binary graph because it is the mostly used in Neuroscience. The measures are quite similar than an undirected weighted network and are extensively explained in the Materials and Methods section ([Graph Theory Applied to Functional Networks \(study 2\) page 105](#)). The goal of this part is not to precisely show how the calculations are done but more to give an overview on what is possible to measure and the meaning of it. However, no consensus has yet been reached whether which measures are more appropriate for neuronal network. Accordingly, I will introduce the most common graph topography measures used in Neuroscience (see [Bullmore and Sporns, 2009](#) for review).

The most common measure to characterize a network is the **node degree** (i.e., the number of nodes connected to one target node). This measure can be evaluated for each node in the network, giving the **degree distribution** of the network ([Amaral et al., 2000](#)). The higher degree a node will have (participating to the flow of information, potentially integrating them), the more important it will be considered for the function of the network, and by extension, for the behavioral process studied. The degree distribution of a complex network (such as a neuronal network) will be non-Gaussian because all nodes do not have the same probability to connect (in comparison to random networks where the probability to have a connection between nodes is equal). The degree distribution is often used as a marker of nonrandom networks (see examples in [Wheeler et al., 2013](#); [Tanimizu et al., 2017](#); [Vetere et al., 2017](#); [Brynildsen et al., 2020](#)).

The **clustering coefficient** is also a measure that is often used. It represents the number of potential clusters into a given network. The cluster is defined by the number of connections between the targeted node and its neighbors, as a proportion of the maximum possible connections. Random networks have low average coefficient clustering whereas complex networks have high average coefficient clustering. A high average coefficient clustering is associated with a high efficiency to transfer information locally, and provide robustness to the network (see [Wheeler et al., 2013](#) for an example).

The **efficiency** of the network is also a very informative measure that can be seen as an image of the speed of information transfer between one node and another, functionally. We can also evaluate the global efficiency of the network (i.e., how much the network is efficient to transfer information across its nodes, see [Wheeler et al., 2013](#); [Vetere et al., 2017](#) for an example).

The last measure often used, which allows to make hypotheses about the sub-network composition (i.e., which structures variate together and, in consequence, may be synchronized to

INTRODUCTION - General knowledge on the technical and conceptual approaches used in this project

support the functionality of the network), is the **modularity**. Many complex networks are composed of different modules. A module is defined by a high connectivity in a group of structure and this group (called module) have a low connectivity with the other structures of the network. The modules or communities represent the structures which are more likely to “work” together upon a same task (see [Tanimizu et al., 2017](#); [Zerbi et al., 2019](#) for an example). Therefore, the modularity estimates whether a given network is actually composed of one, or several, or no modules.

Accuracy of the analytical method considering behavioral processes

The physiological substrate of a functional network is a topic heavily discussed in Neuroscience ([Bullmore and Sporns, 2009](#); [Goni et al., 2014](#); [Vetere et al., 2017](#)). Genetic studies have shown in mice that deletion of a theoretically important gene (coding for a high degree protein in a functional network) was associated with high lethality whereas deleting a gene coding for a low degree protein had no lethal consequences ([Jeong et al., 2001](#); [Babu et al., 2012, 2014](#)). In neuronal networks, studies show that small world organization facilitates the efficient transfer of information and minimize its cost by providing a balance between local integration and global processing ([Sporns, 2013](#)). In addition, psychiatric pathologies such as Alzheimer’s disease or schizophrenia are more likely to impact structures identified as main hubs in human anatomical network ([Crossley et al., 2014](#)). Studies generally support the fact that functional networks represent an image of the brain’s processing, and links with the anatomy can be found (as the previously cited studies show). To the best of my knowledge, only one study, by the group of Paul Frankland, has shown a direct link between a graph theory functional network and a behavioral output. Briefly, the authors performed contextual fear conditioning in mice, followed by c-Fos immunohistochemistry; they process the analyses on the c-Fos data and extracted significant nodes ([Figure 33A](#)); after that they deleted those nodes one after the other to observe the consequences global network efficiency *in silico*. In a second part of the study, they compared the deletion (using DREADD-induced inactivation) of high degree nodes extracted from the *in-silico* model (e.g., Re) with freezing ([Figure 33B](#)). They found that the efficiency of the *in-silico* network was directly correlated with the behavioral output of the behavioral experiment (*i.e.*, freezing; [Figure 29](#)). This study strengthens the idea that the functional networks directly support brain processes and can predicts behavioral outputs.

INTRODUCTION - General knowledge on the technical and conceptual approaches used in this project

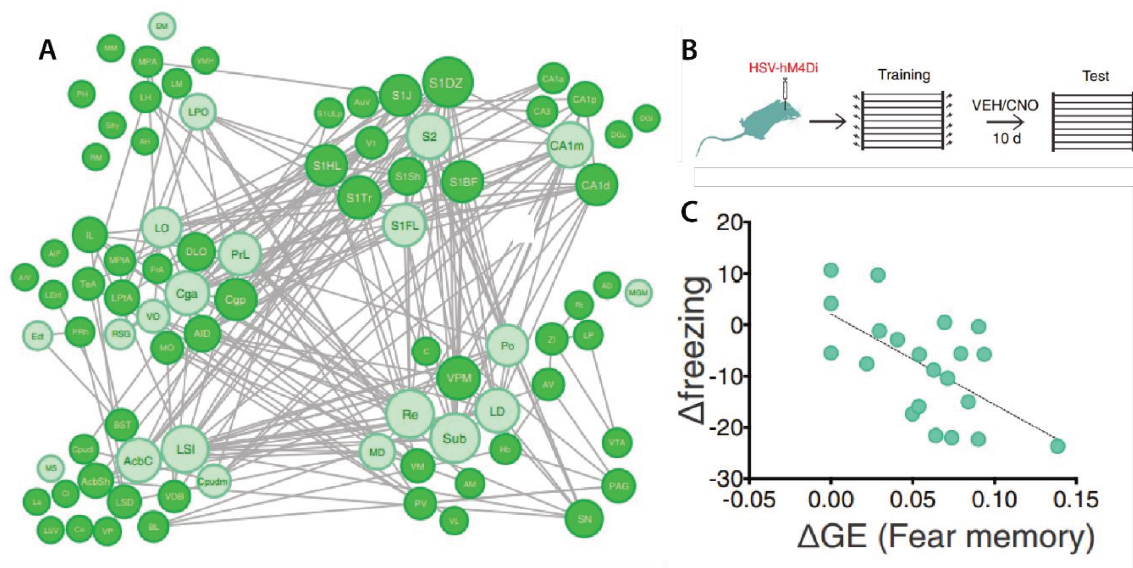


Figure 29: Correlation of the functional network node deletion with behavioral output
(A) represent the modeled network engaged during fear conditioning. The nodes deleted *in-silico* is done in this network (light green: nodes deleted *in silico* and *in vivo*). **(B)** protocol of the structures inactivation in contextual fear conditioning using DREADD. **(C)** Correlation between the alteration of the behavioral output (freezing) during the context test following DREADD-induced inactivation of nodes, and the modification of the global efficiency of the network (inferred from the initial network) following *in silico* nodes deletion.

3. Local Field Potential (study 3)

In this section I will introduce brain oscillations, how they are recorded (*e.g.*, LFPs), their origin, their theoretical functions, with a focus on spatial memory, the stress response and emotional processing. In a last paragraph, I will review what is known about LFPs in the LHb.

a. The origin of brain oscillations

Each electric current generated by each cell of an assembly superpose at a given extracellular medium location (a brain region or a group of brain regions), resulting in a potential (in Volt) based on a reference signal (which is define as the null signal). Such a potential (targeted location signal minus reference signal) can be recorded using various technics: EEG, magnetoencephalogram (MEG), electrocorticogram (ECoG), and LFP. These technics present differences in terms of spatial precision (*e.g.*, the EEG records approximatively 1 cm around the electrodes, whereas the spatial scale of LFP recording is in the mm order).

Brain oscillations are defined by the summation of rhythmic variations of membrane potentials of thousands of cells (Hämäläinen et al., 1993; Buzsáki et al., 2012). In other words, all excitable

INTRODUCTION - General knowledge on the technical and conceptual approaches used in this project

membranes (dendrite, spine, axon or soma) contribute to the extracellular field, ranging from the slowest fluctuation (glia) to the very fast action potentials (Buzsáki et al., 2012). One of the best described contributions to the genesis of LFPs is that of GABAergic interneurons are necessary to the generation of rapid oscillations. For example, a study demonstrated *in vitro* that the exposing CA1 pyramidal neurons to the GABA-A antagonist bicuculline blocked the fast oscillatory waves (Bartos et al., 2007), suggesting that these oscillations are primarily generated by the action of the inhibitory interneurons to the network (the exact role of the interneurons are discussed in Roux and Buzsáki, 2015).

Therefore, many components participate to the generation of LFP signals: synaptic activity; intracellular calcium trafficking (Wong et al., 1979); intrinsic current and resonance, voltage-gated current, modulating the membrane electrical response (but not synaptic currents; e.g., I_h and I_T currents), which also participate to the resonant properties of certain neurons (*i.e.*, their capacity to preferentially response to a particular frequency (Llinas, 1988; Storm, 1988; Silva et al., 1991; Freund and Buzsáki, 1996; Hutcheon and Yarom, 2000); spike hyperpolarization (for example a burst of action potentials is often followed by an hyperpolarization that can impact the LFP signal; (Buzsaki et al., 1988); gap junctions, also called electrical synapses, which participate to the neuronal synchrony (Ylinen et al., 1995; Barth, 2003; Traub et al., 2004); ephaptic effect, which represents, for a neuron, the capacity to have its membrane potential influenced by the surrounding tissues and associated extracellular gradients (Chan and Nicholson, 1986; Anastassiou et al., 2010). Altogether, these existing neuronal properties show that the spatiotemporal fluctuation of the field activity is much more than an epiphenomenon effect, and suggests that LFP have a precise role, for example to synchronize and regulate population neuronal activity (Faber and Korn, 1989).

Nonetheless, the main component of the LFP signal is the synaptic activity, either inhibitory or excitatory currents. The contribution of the synaptic activity to the extracellular current flow is shared by many components and needs to be summed in time to create a measurable signal. This overlap is easier to be achieved through slow events such as synaptic activity (Elul, 1971; Logothetis and Wandell, 2004; Niedermeyer and Lopes da Silva, 2005).

The structure of the dendrites, *i.e.*, its arborization, allows the apex of the neuron to be surrounded by tens of thousands of synapses. The neurotransmitters activating AMPA and NMDA receptors create excitatory currents, involving Ca^{2+} and Na^{+} ions. These ions will flow from the extracellular to the intracellular medium creating a local electrical **sink** (such an entry of cation creates a negatively charged extracellular medium). As many systems in biology, the system tends to reach

INTRODUCTION - General knowledge on the technical and conceptual approaches used in this project

electroneutrality. This implies that an electrical **source** needs to be created to counteract the presence of the sink. This extracellular source is found in an ionic flux, from the intracellular to the extracellular medium, therefore opposite to the one creating the sink. The source and the sink therefore create what is called a **dipole** (see [Figure 30](#) and [Buzsáki et al., 2012](#) for a review).

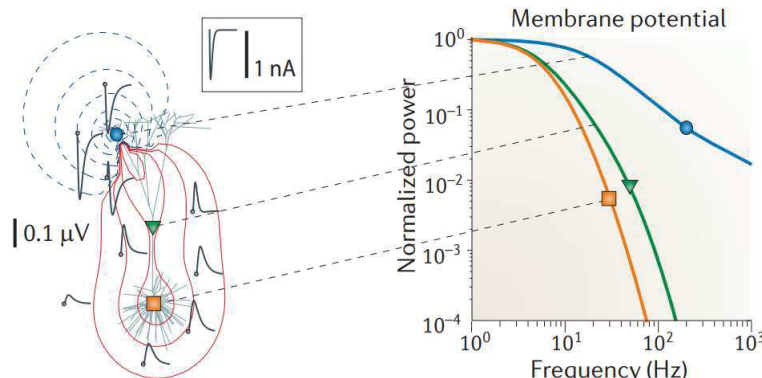


Figure 30: Example of spatio-temporal topography of source and sink

In the left panel, LFP traces are computer-simulated (in grey) responding to an excitatory synaptic current (blue circle, waveform of the current injected is in the box) in the apical dendrite of the pyramidal model neuron, forming the sink. The blue line represents the negative value of the LFP amplitude, and the red line represent the positive value of the LFP amplitude. In the right

panel, the double logarithmic spectra of the membrane potential is represented, following the current injection. Different localization has been measured: near the stimulation site (bleu), mid-apical dendrites (green) and in soma (orange). Remark: the high frequency power (squared amplitude) decreases with the distance from the sink. Adapted from [Buzsáki et al., 2012](#).

The characteristics of the waveform of the LFP, such as the **amplitude**, the **frequency** or the **phase**, depend on the multiple sources contributing to the LFP, as well as the characteristics of the brain tissue where the recording is performed ([Buzsáki et al., 2012](#)). If the recording site is far from the current source, the LFP will be less informative about the changes of the signal occurring at the source location. This is mainly due to the fact that the farthest is the recording site from a source, the more the signal recorded will have intrusions from other sources (e.g., volume conduction). This leads to several issues concerning the recording of sub-cortical LFPs. Indeed, the geometrical organization of neuronal shapes and organization (in layers or not) directly affects the magnitude (amplitude) of the potential recorded (e.g., in higher mammalian cortex, see [Niedermeyer and Lopes da Silva, 2005](#)). In subcortical structures, the localization of the neurons and of their inputs is less organized (neurons are not topologically organized in layers and the projections from other structures have no preferential input localization such as in cortical regions), resulting in lower magnitude of the recorded electrical field. Nevertheless, even with an asymmetric neuronal distribution (non-layered structures), temporally synchronous activity can lead to the generation of source and sink (e.g., in the striatum; [Graybiel, 2008](#)), supporting the fact that subcortical LFP activity can represent the spatially localized field of these subcortical

INTRODUCTION - General knowledge on the technical and conceptual approaches used in this project

structures. However, some precautions should be taken to limit the recording of volume-conducted signal.

The volume conduction represents the propagation through the brain of the electric charge from a distant source (Lindén et al., 2010; Kajikawa and Schroeder, 2011). By definition, a signal that is volume-conducted is not local and often comes from strong dipoles in the brain (e.g., theta oscillation from the HPC). Metaphorically, if a signal source is the point of impact of a drop at the surface of water, the volume-conducted signal is portrayed by the ripples that consecutively form at the surface of the water and propagate centrifugally from this point. In the present study, the volume condition is really an issue in the case of oscillations recorded in the LHb, and more particularly theta oscillations, because the LHb is situated just ventrally to the HPC which is, as said earlier, a powerful source of theta oscillations. Therefore, to minimize, or eliminate, the influence of volume-conducted signal when analyzing LFP signals at a given location, one can use the current source density (CSD) calculation (see **Materials & Methods part Preprocessing page 123**), which allows to identify the source and the sink localization. The CSD formula, gives an approximation of the transmembrane current, which is often considered a more reliable estimation of the local field than the direct recording of the potential (Lindén et al., 2010; Kajikawa and Schroeder, 2011, 2015). Another technic to limit the impact of volume-conducted signal is to perform a local referencing (setting the 0, *i.e.*, the reference, of the potential in the structure where the signal is recorded). This technic is easier to apply but may be less accurate than the CSD (see Goutagny et al., 2013 for an example of study from our laboratory using the local reference).

b. What can be the role of brain oscillation?

Oscillatory activity in neuronal communication

Brain processes trigger interactions of neuronal populations which are supported – or not - by anatomical connections and by the underlying mechanisms which modulate these connections (Womelsdorf and Fries, 2007). Brain oscillations promote the synchronization of neuronal populations and by way of consequence their communication (Fell and Axmacher, 2011; see **Figure 31**). For example, the pic of an oscillation corresponds to a high membrane potential, leading to a higher probability of the emission of action potentials, whereas the cave of the oscillation rather represents a hyperpolarized state which decreases the probability of the emission of action potentials. The oscillatory activity promotes neuronal discharge in a limited time window (just at the time of the hyperpolarization/pic of the wave in our previous example). A synchronized discharge of several neurons making synapse onto the dendrites of a neuron can potentialize the depolarization of the later, increasing the probability to generate an action

INTRODUCTION - General knowledge on the technical and conceptual approaches used in this project

potential. This type of synchronization of neuronal populations has also been hypothesized to potentiate the efficiency of information transfer. In addition, if an action potential, generated in a given structure during the depolarization phase (*i.e.*, the peak of the wave), reach a downstream structure during its own depolarization phase (also during the peak of the wave), will likely trigger the generation of an action potential by this downstream structure. Therefore if the action potential does not arrive at the appropriate phase of the oscillation, the response can be delayed or will not occur (Hutcheon and Yarom, 2000; Fell and Axmacher, 2011).

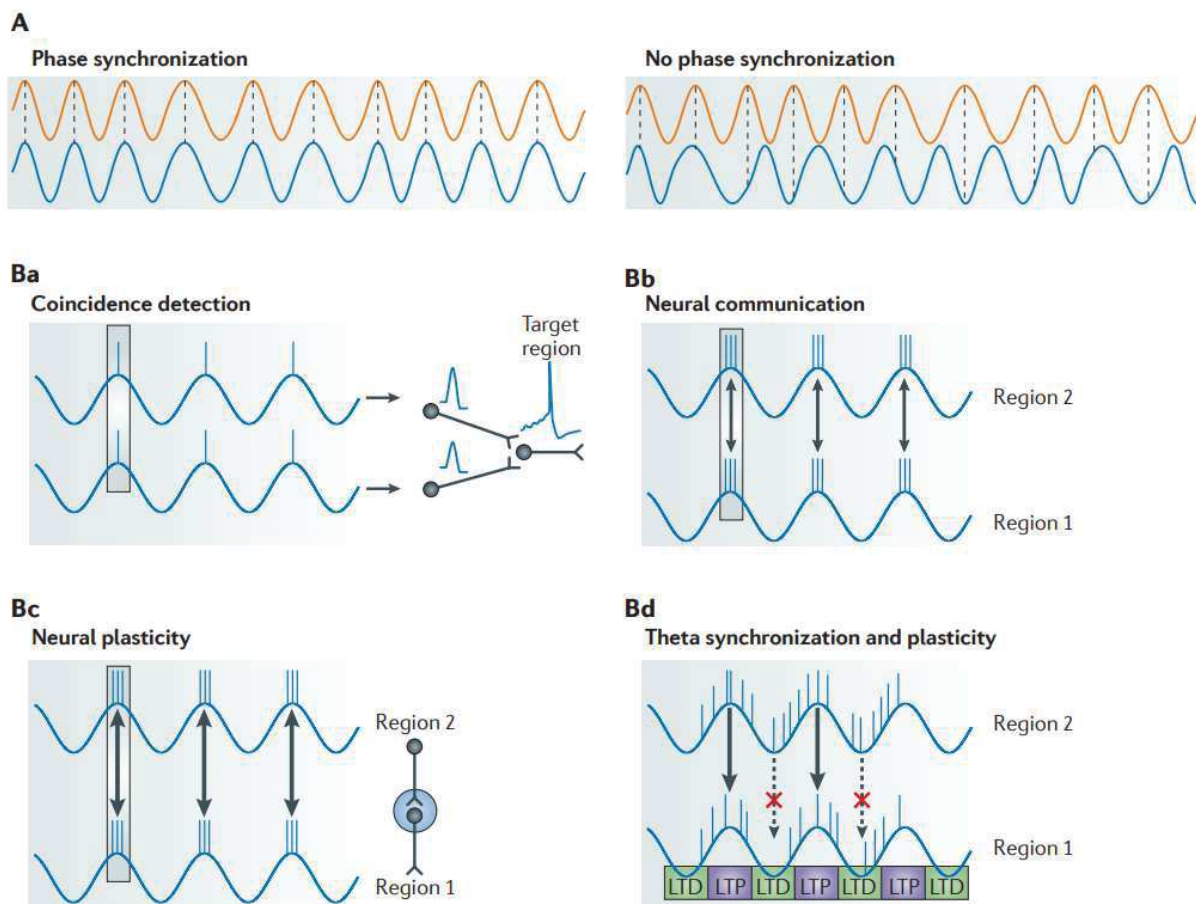


Figure 31: Theoretical functions of phase synchronization

(A) Neuronal oscillation can maintain a stable phase synchronization (left example) or may display no synchronization (right example). (B) Potential role of oscillation synchronization (phase synchronization) in neuronal processing. (Ba) Phase synchronization of neuronal population which coordinate the synaptic input on a common target. (Bb) Phase synchronization which potentialize information transfer (arrow) during excitable windows. (Bc) Precise synchronization of action potential timing promotes synaptic plasticity connection leading to, further, a facilitation of the communication. (Bd) Theoretical influence of the theta phase in the memory related regions (*e.g.*, dHPC). This synchronization in theta range may recruit brain region during the time-windows with a high susceptibility of synaptic plasticity. From Fell and Axmacher, 2011.

INTRODUCTION - General knowledge on the technical and conceptual approaches used in this project

The maintenance of phase relationship between two neuronal populations (called the coherency), is postulated to be the origin of synaptic plasticity mechanisms, promoting the communication between these neuronal populations (Fries, 2005a).

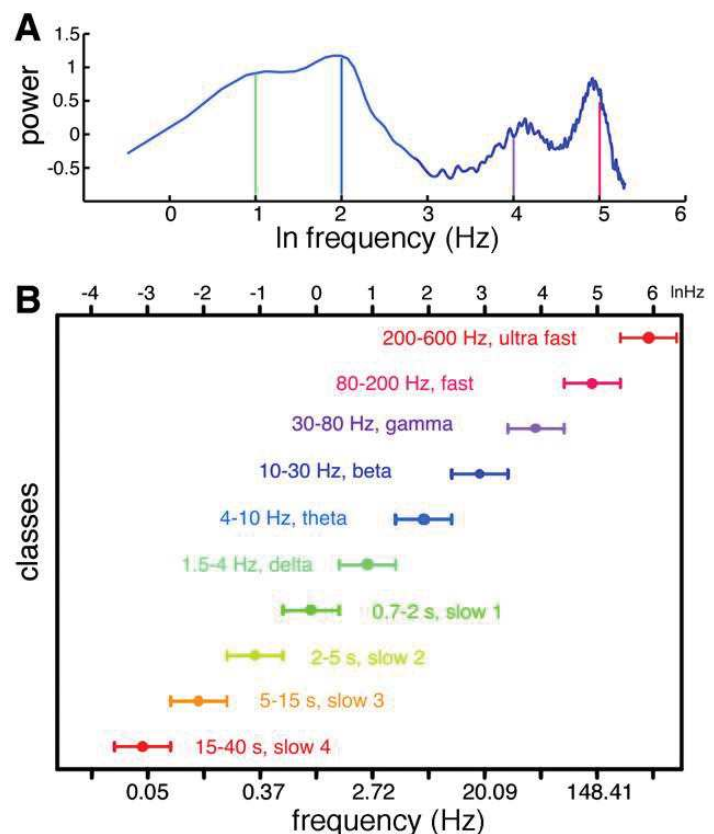
Frequency bands

When a neuronal population is highly synchronized, it induces large deflections in the LFP, leading to an increase in the power (*i.e.*, increase in the amplitude) at a specific frequency band (Pfurtscheller and Aranibar, 1977). The various frequency bands are suggested to play distinct roles in the communication of information across the brain. The low frequency bands are known to promote synchronization of remote neuronal populations because they are more adapted to long conduction delay, whereas high frequency bands are known to promote synchronization of adjacent neuronal population (von Stein and Sarnthein, 2000).

The boundary of a given frequency band can be differentially defined depending on the specie considered and also from one study to another (for example, theta can be from 5Hz to 12Hz or to 6Hz to 10Hz depending on the group). investigated are different depending on the species studied but also from the study (see **Figure 32** for a description of the frequency bands such as defined by Buzsáki's group in mice EEG; Buzsáki and Draguhn, 2004). However, frequency bands are not always defined the same way and can vary around those values across rodent studies. For our study, we attributed ranges to the frequency bands we studied based on the peak observed in the spectrogram (*i.e.*, we took the frequencies before and after the observed peaks and these frequencies were used as the limits of the range considered, see **Materials & Methods part Frequency and time domain frequency analyses page 129**).

INTRODUCTION - General knowledge on the technical and conceptual approaches used in this project

Figure 32: Logarithm power spectrum of hippocampal EEG during sleep and waking stages in mice.
From Buzsáki and Draguhn, 2004.



Implications of the frequency bands

When several brain regions are concomitantly engaged in a given function, the time-dependent synchronization of their oscillations will favor an optimal level of communication between them. For example, in a study cats were trained to engage a given motor action in response to a change in the configuration of visual stimulus, announcing the next trial by an auditory cue led to the synchronization of the

parietal, the visual, the somatosensory and the motor cortical areas in the beta oscillation band (20-25Hz). This synchronization was close to a zero phase lag at the time the visual stimulus appeared (Roelfsema et al., 1996, 1997). Similar task-dependent synchronization has been observed in various executive and cognitive functions requiring a dynamic coordination of distributed brain areas (Buschman and Miller, 2007; Gregoriou et al., 2009; Grothe et al., 2012; Salazar et al., 2012; Dotson et al., 2014).

The most described oscillations in rodent are the one present in the dHPC. In dCA1, theta oscillations are hypothesized to be generated by the input from of the MS and the DBB (Vertes and Kocsis, 1997; Buzsáki, 2002; Colgin and Moser, 2010). Indeed, in rats, lesion or inactivation of the MS/DBB area markedly reduces the amplitude of theta (Mitchell et al., 1982; Bland et al., 1996). Neurons in the MS/DBB present a rhythmic firing at the theta frequency (Petsche and Stumpf, 1962), suggesting that these neurons could act as a peacemaker of theta activity in the dHPC. The generation of the gamma frequency may come from two different oscillators. According to Colgin's theory, slow gamma oscillations (30-60 Hz) are generated in dCA1 by the inputs coming from dCA3, whereas the fast gamma oscillations (60-80 Hz) are generated in dCA1 by the inputs from the Ent (Colgin and Moser, 2010). These theta and gamma oscillations have been particularly implicated in the coding of the spatial information in rodent, by synchronizing the firing

INTRODUCTION - General knowledge on the technical and conceptual approaches used in this project

of the place cells (Jensen and Lisman, 2005; Girardeau and Zugaro, 2011; Hartley et al., 2014). Dorsal hippocampal oscillations have also been shown to be necessary for memory consolidation, including during sleep (see **Box 2: Sleep page 4** for sleep/wake state introduction). For example, the so-called sharp-wave ripples (SWR), which are transient very rapid oscillations (around 200Hz), have been implicated in the “off-line” states (quiet wakefulness and SWS, *i.e.*, when the consolidation of the information may occur) in monkeys (Skaggs et al., 2007) and humans (Bragin et al., 1999; Clemens et al., 2011). In rodent studies, SWR have been implicated in the neuronal replay, described as a mechanism underlying memory consolidation (see Girardeau and Zugaro, 2011 for a review). A particular communication between the dHPC and the mPFC (slow wave synchronization) has also been implicated in memory consolidation processes (Sirota and Buzsáki, 2005), more particularly, when coupled to gamma oscillations (Dalal et al., 2010; Van Someren et al., 2011) and spindles transient oscillations (11-16 Hz; Cox et al., 2012). Finally, the synchronization of slow wave activity with higher-frequency bands has been hypothesized to be a substrate for memory consolidation (Neske, 2015). Hierarchical nesting of frequency band-oscillation, already described in cortical network, may be the marker of high demanding cognitive processes by coordinating cells population activity on different time scales (Buzsáki, 2010; Buzsáki and Watson, 2012). For example, gamma oscillations (40-100Hz) have been found to be couple to theta oscillations (5-10Hz); in the HPC in rats (Bragin et al., 1995), in neocortex in human (Canolty et al., 2006). In rats, the theta-gamma coupling has being found in different tasks. In a T-maze task, Tort et al. (2008), shown a phase-frequency coupling (theta-gamma) in the HPC and in the striatum. They also shown that the coupling present different pattern depending on the action of the rat (*i.e.*, at the beginning of the turn in the T-Maze, the HPC present a high coupling whereas no coupling has been observed in when the rat reaches its goal). These same authors in 2009, also shown that the theta-gamma coupling in the HPC increased through training session in an association item-context. Moreover, they found that this coupling was directly correlated with the increased performance of the animal across the sessions (Tort et al., 2009).

Oscillations during stress response and emotional processing

Not much is known about the dynamics of oscillatory activities in response to a stressor, or in memory processes associated with the stress response. In humans, a psychological stress impairs memory (*i.e.*, in paradigms when subjects need to retrieve a precise memory and suppress other non-relevant memories) and that these deficits were correlated with altered theta oscillation in the parietal cortex (Quaedflieg et al., 2020). In animals, not much is known about the relationship between the stress response and the oscillations in the limbic structures. Electrical stimulation of the CeA mimicking the firing rate induced by an acute stress can induce hormonal and

INTRODUCTION - General knowledge on the technical and conceptual approaches used in this project

electrophysiological acute stress – like responses, (Henke, 1983; Forster et al., 2008). Using the same parameter, Luque-Garcia and collaborators in 2018 studied the interaction of the IL and the CeA in the urethan anesthetized rats. The stimulation of the CeA induced a delayed change in the oscillation frequency of the IL (*i.e.*, increases of theta and gamma oscillation power). They also observed a phase amplitude coupling (mostly slow wave-gamma coupling; as mentioned, implicated in memory consolidation), suggesting that the synchronization of IL neurons may participate to the stress response or to memory consolidation associated to the stress response (Luque-García et al., 2018). A study in rats has shown that exposure to a stressful situation (1 hour on an elevated platform with intense light) enhance the occurrence an oscillatory pattern in the HPC (7-12Hz; called mu in the study; Takillah et al., 2017; see Figure 33 for the spectrogram including the transient mu band). In addition, they show that this stress exposure was correlated with an increased coherence in the mu band between the dHPC and mPFC. Note that they define mu oscillations in the theta band however it is a transient activity and can be see only when the animal does not move. Indeed, theta oscillation can be influence by voluntary movement (Vanderwolf, 1969; Buzsáki, 2002) and lead to cover mu oscillations. Mu oscillation band have been shown to reflect vigilance state (Kramis et al., 1975; Popa et al., 2010) and can be affected by sensory inputs (Fanselow et al., 2001; Fries, 2005b; Tort et al., 2010).

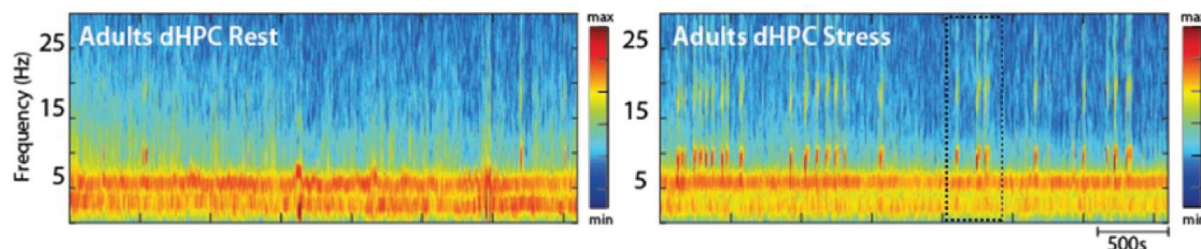


Figure 33: Effect of an acute stress on dHPC in rats

dHPC spectrogram at rest (left) and during the acute stress (elevated platform; right). The emergence of the transient oscillation in the 7-12 Hz under stress is the oscillation identified as mu. Adapted from Takillah et al., 2017.

Some studies aimed at better understanding the communication between limbic structures during emotional processing. For example, (Adhikari et al., 2010) exposed mice to an anxiogenic arena, and observed an increase of the correlation between mPFC and vHPC activities at the theta range. In addition, the increase of theta power in the mPFC was a strong predictor of the behavioral performance (avoiding the aversive part of the arena). These results suggest that the synchronization of theta oscillation between the mPFC and the vHPC plays a role in the modulation of anxiety-like behavior. A study in mice was designed to better understand the brain

INTRODUCTION - General knowledge on the technical and conceptual approaches used in this project

network involved in the capacity of the animals to differentiate between a potentially dangerous (center) and a safe (periphery) environment in an open field (Likhtik et al., 2014). They showed that BLA and mPFC power predicted the center-to-periphery transition of animals displaying an anxiety-like behavior. Moreover, when animals were in the “safe” zone, BLA firing was entrained by of the mPFC theta rhythm. In addition, in a cued fear conditioning paradigm, they showed that animals capable to discriminate the context (*i.e.*, not express fear to another “safe” context), present an increase of theta power in the BLA and the mPFC; they also demonstrated that multi-unit activity in the BLA increase the phase locking on the theta rhythm of the mPFC from before to after the cue. Moreover, they also shown that the probability of the mPFC leads in the BLA-mPFC theta coherency was depending on the freezing percentages that animal presented across trials. These results suggest that the mPFC input to the BLA provide a “safety” signaling, and thereby may modulate amygdalar circuits to diminish fear and anxiety like-behavior.

In rats, theta coherence (4-12Hz) between the AMG, the dHPC and the mPFC has been shown to promote fear memory consolidation during REM sleep. Interestingly, in fear conditioning, the LA and the dHPC present an increase, across learning, of power during the presentation of the cue, which was not seen in the group where the cue was not predicting the shock. This result suggests that the LA and dHPC theta power could improve neuronal communication supporting the association between the cue and the shock. These different studies suggest that theta frequency synchronization within a network composed of the AMG, the HPC and the mPFC is promoting fear conditioning, and more particularly consolidation.

Finally, it can be said that recording and analyzing brain oscillations is not always an easy and sure path. Indeed, whereas Karalis et al., (2016) seemed to have demonstrated that the BLA and the PRL synchronized at 4Hz during freezing behavior in mice, and that the PRL was actually driving the BLA activity during the freezing, two year later a study demonstrated that this 4 Hz oscillation coming from the mPFC and present during freezing was in fact an artefact produced by breathing (Moberly et al., 2018). These results are still controversial.

LFP recording in LHb

Very few studies have performed LFP recordings in the LHb. This can be explained by the technical challenge that represents the safe implantation of electrodes in a very small structure with small nuclear organization (discussed in **study 3 page 136**), and which is located just adjacent to the third ventricle. One of the two seminal studies was conducted in our laboratory (Goutagny et al., 2013). It was first shown in anesthetized rats that the firing of a subset of LHb cells was phase-locked with the dHPC theta oscillation (see **Figure 34 A**); moreover, they

INTRODUCTION - General knowledge on the technical and conceptual approaches used in this project

demonstrated a coherency of theta oscillations between LHb and dHPC was correlated to memory performance in an object-based contextual memory task (**Figure 34 B-C**), suggesting that the LHb participate to spatial information processing in close interaction with the dHPC. Identical findings were provided Aizawa and collaborators ([Aizawa et al., 2013](#)). In addition, they found that the LHb cells which firing was phase-locked with the dHPC theta rhythm of were principally found in the LHbM, which receives projection the DBB. They therefore hypothesized that the DBB may not only pace theta oscillation in the dHPC but also in the LHb.

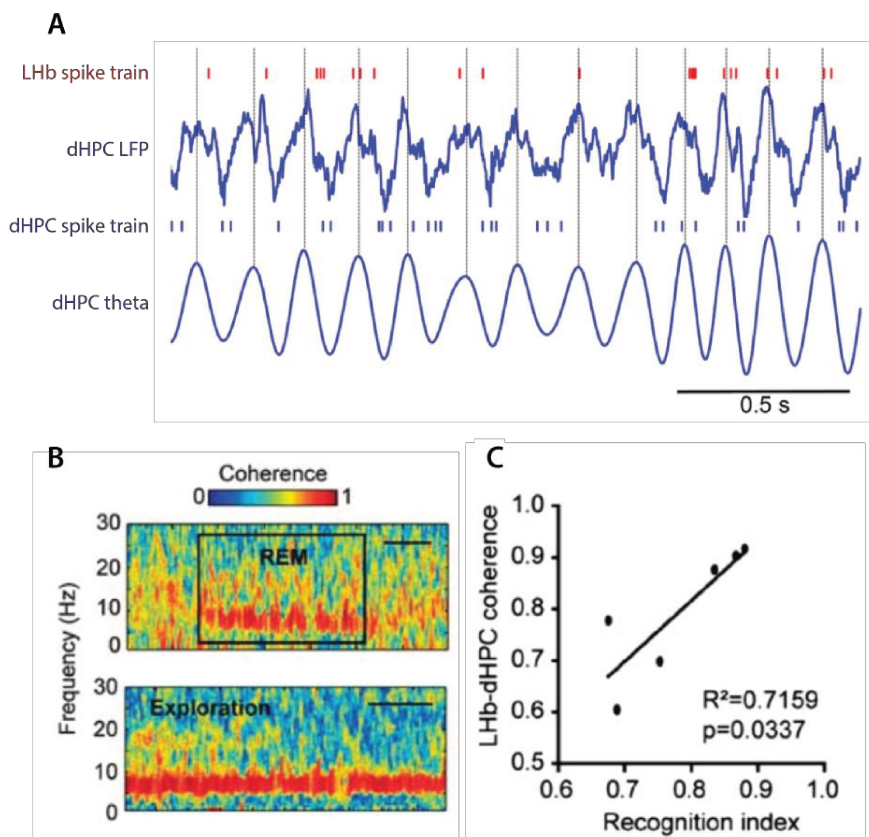


Figure 34:
Electrophysiological interaction of the LHb with the dHPC

(A) red raster represent the spike train of LHb neurons, and the blue raster is the dHPC spike train. The upper blue trace is the raw LFP recording of the dHPC and the lower filtered theta trace from the dHPC during REM sleep, from [Aizawa et al., 2013](#). (B) Coherogram showing the coherence dynamic during REM (upper panel) and exploratory behavior (lower panel) between LHb and dHPC. (C) Correlation between the LHb-dHPC coherence with the memory task performance (i.e., index recognition represents the spatial recognition capability of the animal). (B-C) from [Goutagny et al., 2013](#).

Finally, the third and last study investigating LFP in the LHb demonstrated in rats that the LHb theta power increased when the animal approached the reward area in a maze protocol evaluating behavior flexibility ([Baker et al., 2015](#)).

However, [Bertone-Cueto et al. \(2020\)](#) expressed their concerns of the accuracy to record LFP signal in the LHb. They show that in LHb raw LFP signal that the main recorded signal seems to be volume conducted from the dHPC. However, they did not look at the means to diminish the volume conducted signal from the recording as the CSD or the local referencing.

INTRODUCTION - General knowledge on the technical and conceptual approaches used in this project

A lot remains to be done to better understand how the LHb communicates with other limbic structures, especially during the behavioral adaptation facing a threatening situation.

4. Deep Learning Tool for Video Tracking (study 3)

In this part, we will quickly be explained what the deep learning is, then we will introduce DeepLabCut (DLC) algorithm that we used during the **study 3** and explained the generality of how it works. However, the details of the setting we used will be find the Materials and Methods (see part **Automatic Video Tracking using Deep Learning Approach page 119**) and the validation of the parameters selected will be find in the supplementary data of the manuscript (see part **Setting DeepLabCut and checking results page 147**).

a. Introduction to Deep Learning

Deep Learning is a type of algorithm of machine learning. The principle is based on the artificial neuronal network. This algorithm works based on several layers / level (as neuronal networks) for extracting, progressively, more complex information from raw data. In each layer, the system updates the mathematical model to avoid the mistakes of learning (as during a biological learning when one does a mistake, it learns that its action does not lead to the set goal). For example, the image processing with this type of algorithm will begin by recognize the basic shape base on the first layers (*i.e.*, outlines, colors, orientations). Then, based on the last layers, the algorithm will learn to identify complex images (for example: letters, facial expression, or rats body parts). The creation of this type of algorithm was inspired directly by what we know of the cerebral processing. It is why it is called “artificial neuronal network”. This type of algorithm transforms the research field since several year, offering a powerful tool to further analyze data.

b. Introduction to DLC

DLC was developed by Alexander Mathis and collaborator (Mathis et al., 2018b; Nath et al., 2019). DLC is an open-source Python toolbox for estimating animal poses from video in order to extract different behaviors. The code of DLC is open to everyone on the GitHub platform.

See the following link: <https://github.com/AlexEMG/DeepLabCut/blob/master/README.md> for the source code.

See <https://github.com/DeepLabCut/DeepLabCut/blob/master/docs/functionDetails.md> for more details DLC parameters.

DLC, unlike comparable algorithms, has the advantage of not needing immense amounts of raw data to make an estimate as accurate as the experimenter can do manually, which makes it

INTRODUCTION - General knowledge on the technical and conceptual approaches used in this project

possible to use it on a scientific project scale. DLC offers an efficient and accurate way to analyze videos, where the system relies on the annotation of the animal's body parts (defined by the user) from a few frames of the video to learn, making it adaptable to any situation. In addition, this toolbox solves the issues of background change, light reflection, or motion blur that posed a problem for animal detection with background removal approaches (thresholding or regression). It will detect body parts in a dynamic environment and does not require any particular characteristics regarding the camera used or the quality of the recorded image. The main limitation of using this toolbox is that it is strongly recommended to use a relatively powerful graphics card (GPU) to limit the learning time, even if DLC can adapt to a system without GPU. When DLC is based exclusively on the processor (CPU) the processing time can be slowed down by 10 to 100 times compared to a system with a powerful GPU.

c. Summary of DLC operations

The operation of DLC is organized into several steps (see workflow adapted from [Mathis et al., 2018b](#); [Nath et al., 2019](#)). The first step is to create a project including some videos of the experiment of interest so that a dataset needed to train the network can be created. Then, DLC will extract a user-defined number of frames per video representing the diversity of possible behaviors during the video. Then, the user will be able to annotate the different parts of the animal's body (or objects) of interest on these images. The annotations can be checked and corrected if necessary. Once the images are annotated, the training dataset is created by mixing all the annotated images and then randomly separating them into two groups: training dataset and test dataset. Then, the network is trained from an already pre-trained network (ResNet in our case, but other pretrained networks exist). ResNet will adapt itself to predict the position of the body part requested by the user. The performance of the trained network is evaluated the test dataset. The trained network allows us to extract the postures of the animals on all the videos of the experiment and to create files regrouping all the positions of the body part requested on each video. If the network does not generalize well the position of the points on all the videos, it is possible to filter the images in order to exclude the images where the body part localizations are not placed correctly. Moreover, it is always possible to add new training images and to start the training again with more images.

INTRODUCTION - General knowledge on the technical and conceptual approaches used in this project

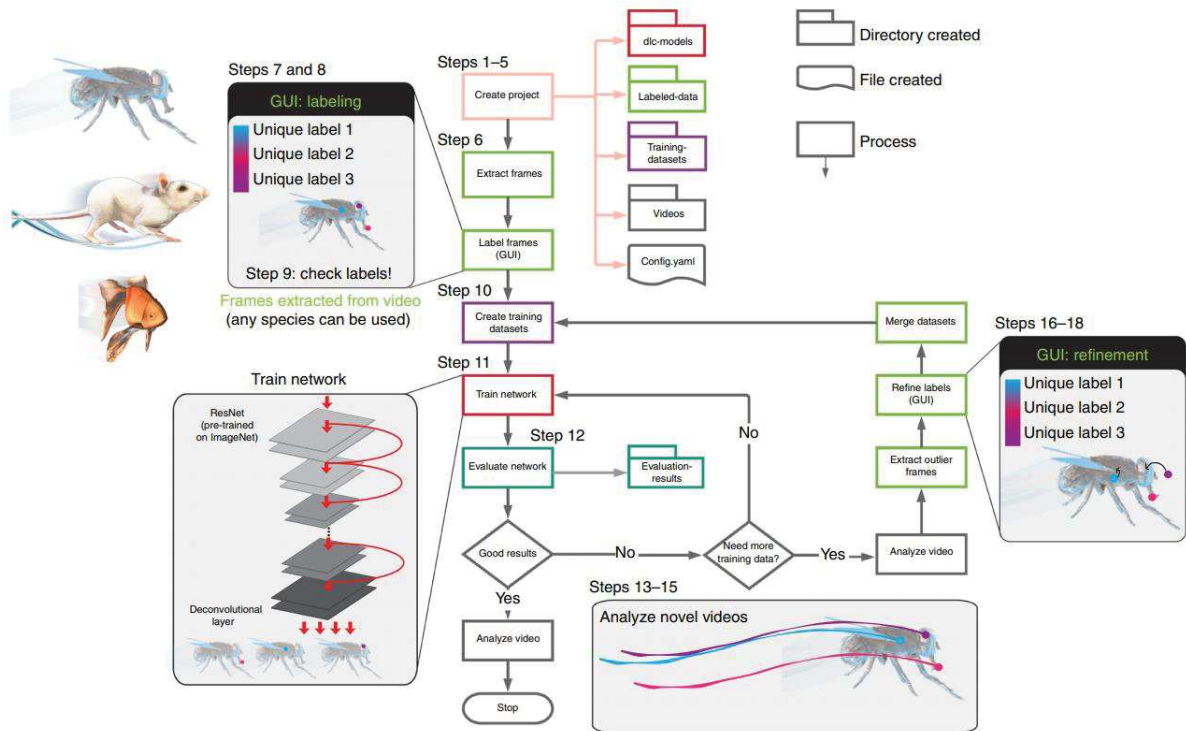


Figure 35: Workflow of DeepLabCut
From Mathis and Nath, 2019.

MATERIALS AND METHODS

MATERIALS AND METHODS - Animals and housing conditions

All experimental procedures have been performed according to national (décret N°2013-118 du 1^{er} février 2013) and European (directive 2010/63/UE du Parlement européen et du Conseil du 22 septembre 2010) guidelines relative to the protection and well-being of laboratory animals. They have been approved by the *Ministère de l'Education Nationale, de l'Enseignement Supérieur et de la Recherche* [APAFIS authorization numbers: 11510 (study 1 and study 2) and 11554 (study 3)].

I. Animals and housing conditions

We used male Long-Evans rats from the breeding center Janvier Labs (Le Genest-St-Isle, France). They arrived in the laboratory at the age of 3 to 4 months. Upon arrival, rats were carefully examined and weighted, and given 7 to 10 days of acclimatization to their new housing conditions without being manipulated. They were housed in pairs in transparent Makrolon cages (40 x 23 x 18 cm) and had constant access to a piece of wood to chew. Cages were stored in rooms with controlled ventilation, temperature ($22 \pm 1^\circ\text{C}$) and humidity ($35 \pm 5\%$) under a cycled light (12 h)/dark (12 h) exposure. They had *ad libitum* access to food and water. Before the start of any experimental procedures, rats were manipulated by the experimenter 1 min/d during at least 3 consecutive days so that they could become used to this type of manipulation. Depending on the type of experiment rats were possibly isolated.

II. Surgical procedures

1. General considerations

Anesthesia was induced through inhalation of isoflurane (Isoflu-Vet[®], Dechra) delivered in O₂ (99.5 % purity; Air liquid, oxygen aviation). Rats were first put in an induction box for 3 min with the percentage of isoflurane set at 4 %; once deeply anesthetized (no reaction to the gentle pinching of the back paw and no palpebral reflex), they were taken out of the box and their skull was quickly shaved with clippers before they were placed in the stereotaxic frame (Stoelting[®]) which ear bars were embedded with a cream comprising lidocaine and prilocaine (Anesderm Gé 5 %[®], Pierre Fabre). Once rats were tightly positioned, with their skull in a flat position, they were wrapped in a survival blanket to keep them warm and their eyes were covered with an ophthalmic gel (Lubrithal[®], Dechra) to prevent drying of the cornea. Then the percentage of isoflurane was set at 1.5% and remained so throughout the whole surgical procedure. The skin was cleaned with an antiseptic solution (Septivon[®] 1.5 %; Omega pharma, France). A local anesthetic (Xylocaïne[®], Xylovet CEVA Santé animal, France, 0.2 mg/ml/100 g) was subcutaneously injected at the incision location and a painkiller (Metacam[®], Boehringer Ingelheim, Germany, Vetmedica, 0.1 mg/ml/100 g) was subcutaneously injected at the level of the neck. The skin was incised, the skull gently cleaned with 0.9 % NaCl, the different locations were identified on the skull and holes were drilled and the dura resected in order to either inject a solution containing the DREADD vector (studies 1 and 2) or implant recording electrodes (study 3). According to studies 1 and 2, once the injections completed, the hole in the skull was filled with bone wax (B/Braun) after what the skin was sutured. According to study 3, once the different electrodes were implanted and secured to skull screws with glue, their tip was uncoated and they were welded to a connector (EIB-16, Neuralynx[®]); then, dental cement was used to mount a head cap. Rats were then placed in cages with clean bedding under a warming lamp until they fully awakened. They were then brought back in the storing room and left quite undisturbed – besides the post-surgery examinations – for 7 to 10 days (or more in the case of the DREADD experiments) to favor a good recovery from the surgical procedure. During this period, they were daily weighted, and their general aspect was checked to potentially detect signs of unease (posture, aspect of the fur, aspect of the eyes and of the ears, presence of vocalization when grabbed). Following recovery, pre-surgery pairs were recomposed (studies 1 and 2) or rats were singly housed, in the case of

MATERIALS AND METHODS - Surgical procedures

the electrophysiology experiments (study 3), to protect their connector from congener chewing. DREADD experiments (studies 1 and 2)

The vector used to inhibit the activity of the LHb was the AAV8-CaMKIIa-hM4D(Gi)-mCherry (7×10^{12} particles/ml), designed and fabricated at UPV (Unitat de Producció de Vectors, Barcelona, Spain – for more information see [\(Piedra et al., 2015\)](#); the plasmid was purchased at Addgene[®] (UK).

Under the surgical procedure describe above, the DREADD solution was bilaterally injected into the LHb by means of a 10- μ l Hamilton[®] syringe placed in a Kopf[®] microinjection unit (Model 5000) mounted on the vertical arm of the stereotaxic frame. In order to favor an optimal expression of the hM4(Gi) receptor within the entire LHb and avoid spreading to surrounding regions, limited amounts of the solution were injected at two different locations in each hemisphere, at the following coordinates and volumes: first injection (0.2 μ L): anteroposterior (AP) = – 3.3 mm from Bregma, mediolateral (ML) = \pm 0.7 mm from the midline of the sagittal sinus, dorsoventral (DV) = – 4.5 mm from dura; second injection (0.15 μ L): AP = – 3.5 mm from Bregma, ML = \pm 0.7 mm from the midline of the sagittal sinus, DV = – 4.4 mm from dura. Two control groups (see below) received equal volumes of phosphate buffered saline (PBS) instead of the DREADD solution. Once the surgery terminated, rats were left undisturbed during 5 weeks to allow a good expression of the hM4(Gi) receptor [\(Reimnsnider et al., 2007\)](#) within the LHb. During the experiments we intraperitoneally injected either Clozapine-N-Oxide (Enzo Life Science, Switzerland; 1 ml/kg), as a ligand for the hM4(Gi) receptor, or vehicle (NaCl 0,9%) in control animals. We chose to inject CNO at a dose of 1 mg/kg which was ineffective behaviorally (e.g., [Campbell and Marchant, 2018](#) for review).

All DREADD experiments included three groups: **group 1** (no-DREADD control group; Sham-Veh) = injection of PBS within the LHb during surgery and injection of vehicle (NaCl 0,9 %) during the experiment; **group 2** (CNO control group; Sham-CNO) = injection of PBS within the LHb during surgery and injection of CNO (1 mg/kg) during the experiment, in order to verify that CNO has no adverse behavioral consequences; **group 3** (mCherry expression control group; hM4-Veh) = injection of AAV8-CaMKIIa-hM4D(Gi)-mCherry within the LHb during surgery and injection of vehicle (NaCl 0,9 %) during the experiment; **group 4** (LHb inhibition; hM4-CNO) = injection of AAV8-CaMKIIa-hM4D(Gi)-mCherry within the LHb during surgery and injection of CNO (1 mg/kg) during the experiment. Control groups, *i.e.*, **group 1** and **group 3**, were *a posteriori* merged (see justification below within the “statistical analyses” section of each experiment).

2. Electrophysiology experiment (study 3)

a. Building of the electrodes

The different electrodes used during our electrophysiology experiments were home-made. To record LFPs we implanted in each region three perfluoroalkoxy-coated tungsten wires (A-M Systems, bare: 50,8 μm , coated: 101,6 μm) twisted together with their tip cut either to form a beveled edge or to form a flat edge (**Figure 36**). Tungsten is commonly used to record LFPs. This metal has peculiar abilities; it has a weak expansion coefficient so that it barely becomes distorted upon changes of temperature or pressure ([Geddes and Roeder, 2003](#)) but remains quite flexible. In addition, tungsten has a good conductance, *i.e.*, $18,94 \times 10^6 \text{ S.m}^{-1}$ ([Sankar et al., 2014](#)). [Hubel \(1957\)](#) have shown that tungsten electrodes had the same recording properties than glass micropipettes.

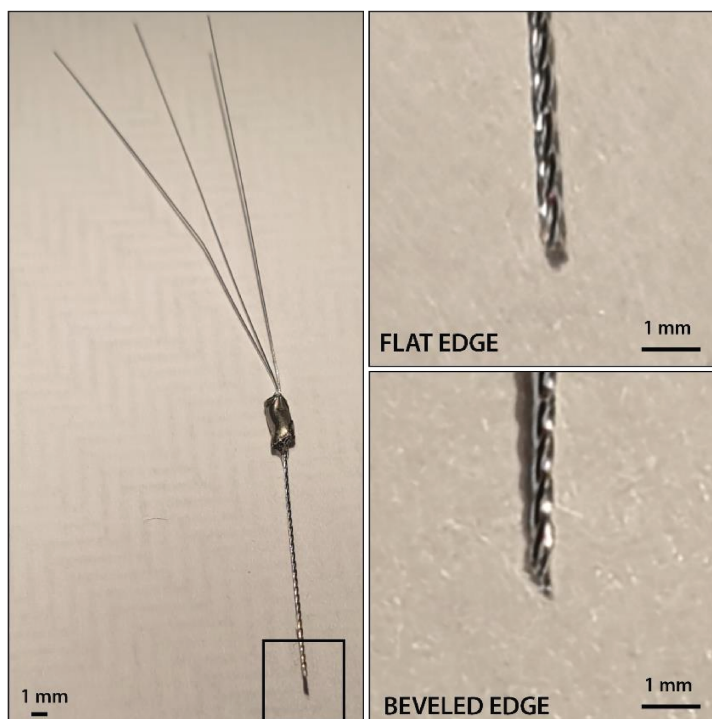


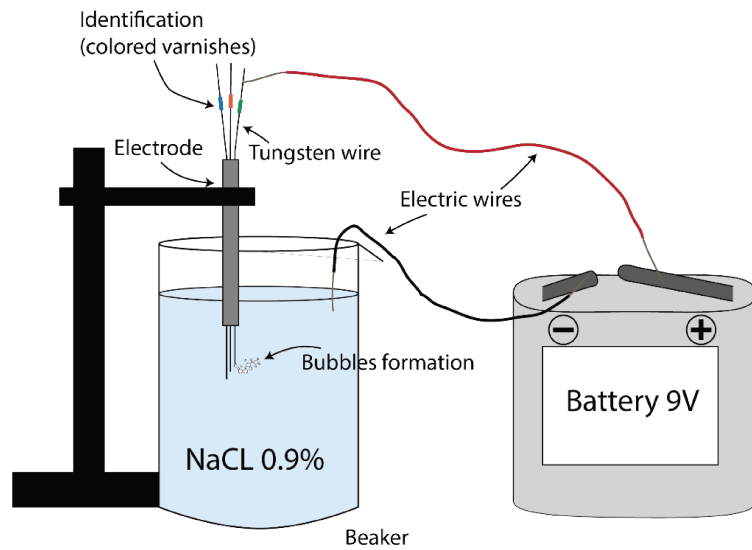
Figure 36: Photography of flat edge and beveled edge electrodes

To build the 3-wire tungsten electrodes we proceeded as follows: the 3 wires of a length of about 2 cm, were passed through a piece of a 18G-needle of a length of approximately 5 mm and glue (Loctite[®] SuperR Glue-3) was applied within the piece of needle so that the wires stuck to it. When the glue was dried, the wires were twisted to make them tighter and more rigid overall. To make the edge beveled - to further apply a

CSD analysis, the electrodes were placed under a binocular and cut at approximately 40° angle. Before that, each of the three wires was identified and labelled (with varnishes of different colors) using a 9-V battery and a beaker filled with 0.9 % NaCl (see **Figure 37**), so that on the day of the surgery, when each electrode was welded on the connector (EIB-16, Neuralynx), we could clearly associate each wire to the correct channel.

Figure 37: Schematic representation of wires identification.

The electrode is maintained so that only the beveled extremity is in the NaCl (0.9%) solution. The outside extremity of the electrode and the NaCl are directly connected to a 9V battery. The current passing through the electrode lead to bubbles formation. With the binocular, we can observe the origin of the bubble and identify the different wires and label them using a color code: green for the shortest, blue for the longest, and orange for the medium. For clarity purpose, the scale of the drawing is not realistic.



To build the electrodes with a flat edge, the 3 tungsten wires were mounted the same way to the piece of needle, then were twisted and the tip cut so that each wire tip was at the same level. These electrodes being not suitable for CSD analysis, the precise identification of each of the three wires was not performed.

Ground and reference electrodes were composed of a screw on which was welded a coated wire of low resistance; the reference electrode was positioned on the Dura whereas the ground electrode was positioned within the skull with no contact with the dura.

b. Description of the two experiments

In the first experiment our goal was to concomitantly record LFPs within the LHb and dCA1 using electrodes including a beveled edge to further perform the CSD analysis and demonstrate that what was recorded within the LHb was not entirely volume-conducted from the dHPC.

In the second experiment we wanted to explore, during our repeated stress paradigm, the communication within the network composed of our regions of interest, *i.e.*, the LHb, the dCA1, the PRL, the ACC, and the BLA ([Table 2](#)).

Table 2: Stereotaxic coordinates used for the electrophysiology experiments.

Structures	Anteroposterior axis (mm from the bregma)	Mediolateral axis (mm for the middle of the superior sagittal sinus)	Dorsoventral axis (mm from the dura)
ACC	+ 0.5	0.7	- 2
PRL	+ 2.6	0.7	- 3
BLA	- 2.5	4.9	- 6.5
LHb	- 3.5	0.8	- 4.2
dCA1	- 3.8	2.7	- 2.1

c. Surgery

Under the procedure described above (see [page 78](#)), holes were drilled in the skull above each region of interest and at the location of the reference (above the most anterior part of the cortex) and ground (approximately above the cerebellum) electrodes (see [Figure 38](#)). Then, the reference and ground electrodes were screwed. Then each 3-wire electrode was gently descended within the targeted structure, one by one, after their tip was covered with a fluorescent dye (DiI, Molecular Probes, Inc.) for further checking of electrode placement; once in place it was glued using UV glue (Metafil Flo[®], Sun Medical CO.LTD), to a nearby screw positioned within the skull, or to the reference electrode in the case of the electrode positioned in the PRL. Once all electrodes in place, they were all glued together and to the skull surface using a thin layer of Superbond glue (C&B[®]). Then the apical tip of each wire was uncoated using the welding device and welded to its respective channel within the EIB-16 (cf. [Figure 39](#)). Finally, the wires and the EIB-16 were covered with dental cement.

MATERIALS AND METHODS - Surgical procedures

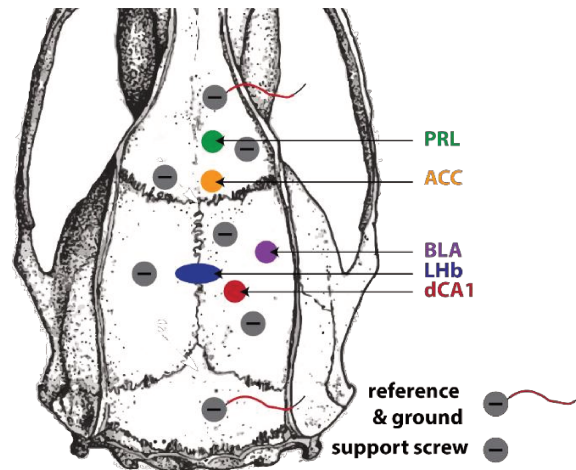


Figure 38: Schematic representation of the position of the different holes drilled in the skull.

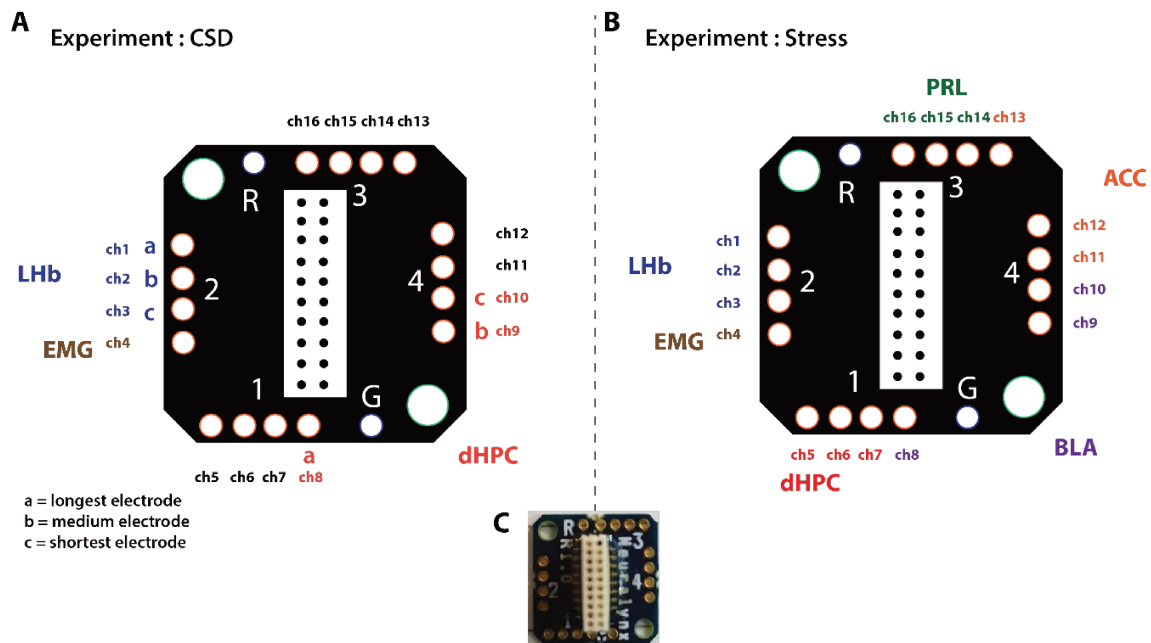


Figure 39: EIB map representation for both experiments: CSD validation and Stress experiment.

(A) The goal of the first experiment was to verify that the signal recorded in the LHb was not entirely volume-conducted from the dHPC. For that we placed 3 wires (ch1-3) in the LHb, three wires into the dHPC (ch8-10) and one wire into the neck muscle (ch4). Each of the three channels had a letter attributed in order to marquer the longest (a), the medium (b) and the shortest (c) electrode. (B) During the stress experiment we recorded the signals within five structures, each implanted with three wires: LHb (ch1-3), dHPC (ch5-7), BLA (ch8-10), ACC (ch11-13), PRL (ch14-16), along with a wire in the neck muscle (ch4). (C) Picture of an EIB.

III. Behavioral evaluations

As described earlier, at least three days before starting a given experiment rats were gently handled 1 min/d. For the experiments involving a DREADD-induced inactivation of the LHb, rats were weighted on the day before the first injection to calculate the exact volume of CNO or NaCl 0.9 % to be administered. In addition, on this same day rats, were given an i.p. injection of NaCl 0.9 % to expose them a first time to this manipulation.

1. Trace fear conditioning (study 1)

Devices

Four conditioning chambers (25 x 27 x 18 cm) were used. Three of the walls and the ceiling were made in transparent Plexiglas, whereas the fourth wall was made of plain metal and comprised a hole including a speaker through which was delivered the CS, *i.e.*, the tone. The grid floor – through which the US, *i.e.*, the electric shock, was delivered – was composed of parallel 0.3 cm diameter stainless-steel bars spaced 0,8 cm apart underneath which a tray containing bedding was placed, to collect feces. Each chamber was positioned within a lit (6 lux) sound–attenuating box (57 cm × 38 cm × 38 cm, Campden Instruments) including a fan displaying background noise (65 – 70 dB). A camera (MCT-210 MS, OptoVision, Toulouse, France; 2.45 mm–wide angle lens) was fixed on the ceiling of each box, above the center of the chamber, and used to record every session. Cameras were connected to a multiplexer (Playback quad, Computar QSMX-II) in the adjacent room so that the image of the 4 boxes could be viewed on the same “video capture” and analyzed together. The video signal was further transmitted to a computer equipped with a video capture software (Scion Corporation, Frederick, Maryland) and to a video recorder so that all session’s videos were stored on tape. Such as described, the chamber constituted the so-called « conditioning context ». During the CS-test a new context, a triangular plexiglass boxes with one gray wall, one black and white striped wall, and a smooth white floor, was inserted in the chamber (see [Figure 40](#)). The speaker and grid floor were connected, through a MED-PC (Med Associates Inc., St Albans, VT, USA) interface, to a computer that controlled the duration and intensity of the sound and of the electric shock.

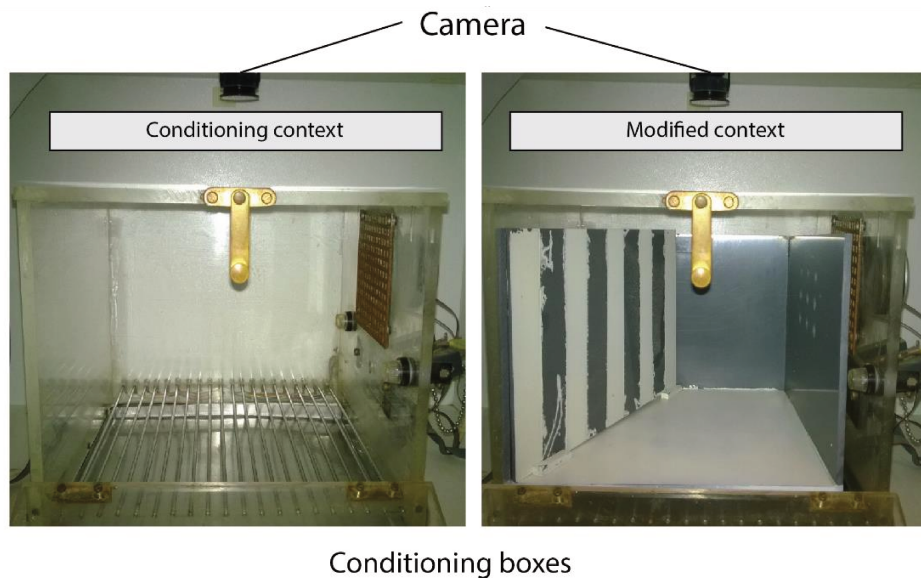


Figure 40: Pictures of the conditioning context (left) and of the modified context (right) used during the fear conditioning protocol.

Protocol

The trace conditioning protocol took place over 4 consecutive days. On day 1 (*conditioning*, 38 min-long session), rats were exposed to 6 CS and US (CS: 15 s tone, 4000 Hz, 10 dB above background; US: 0.5 mA before scrambling, 0.8 s, through the grid floor) with the US delivered 30 s after CS offset (trace interval); the 6 presentations were made with a 4 min 20 ± 26 s intertrial interval. On day 2 (*context test*), rats were replaced in the conditioning chamber for 15 min. On day 3 (*exposure to the CS test context*), rats were placed in the new context for 15 min. On day 4 (*CS test*), rats were placed in the new context, and 2 min later, 5 15 s CS were delivered with a 4min interval. The chamber, as well as the new context, were cleaned with water between each rat. Each session took place between 09:00 and 12:00. Each time rats were brought from the housing room to the experimental room in their home cage, placed on a trolley, each rat being placed in the same chamber throughout the whole experiment. Given the number of animals, rats were divided in three equivalent batches tested 5 days apart from each-other.

In our first study we have performed two distinct experiments (Durieux et al., 2020).

Experiment 1 was designed to assess, on naïve animals, the expression of the c-Fos protein induced by the *conditioning* session of the trace fear conditioning paradigm. For that particular matter we sacrificed our animals 90 min following conditioning (*Fear conditioning* group; n = 4) and compared the levels of c-Fos (see **c-Fos Immunohistochemistry page 99**) in various structures of interest (Hb, HPC, PFC) to those of a group of rats which remained undisturbed in their home cage (*Home cage* group; n = 6), and those of a group of rats which underwent the

same manipulation as our conditioned animals except that they did not received footshocks (*No shock* group; n = 8) (see [Durieux et al., 2020](#), Figure 2 and Table 1 of the publication).

Experiment 2 was designed to address the consequences of DREADD-induced LHb inactivation, during conditioning, on the recall of the conditioning context and of the CS. For that particular matter, CNO (1 mg/kg) vs NaCl 0.9 %, were given in the housing room 30 min prior to the beginning of the conditioning session. Subsequently, NaCl 0.9 % was given to each rat prior the three following sessions so that the routine of the experiment remained stable (see [Durieux, et al., 2020](#), Figure 5 of the publication).

Quantification of freezing behavior

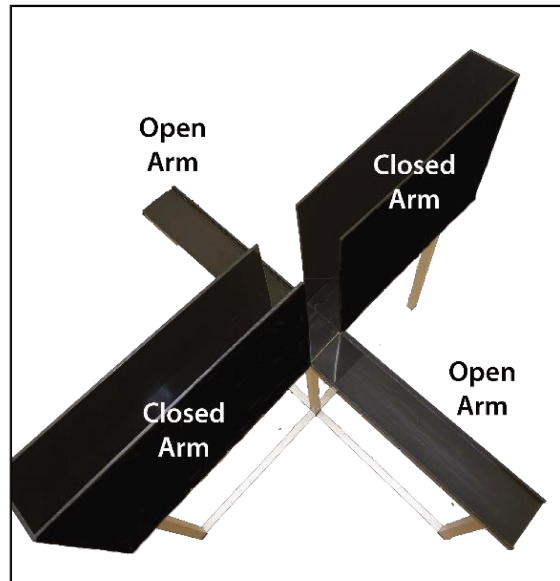
According to a method validated in the laboratory ([Marchand et al., 2003](#)), data acquisition was carried out by with a script written under the video capture software 'Scion Image' (Scion Corporation, Frederick, Maryland). Freezing analysis was conducted with a set of procedures written under Excel (Microsoft®). With this set-up, the 4 conditioning chambers could be monitored at a sampling rate of 1 Hz. After background subtraction, the image corresponding to each chamber was reduced to a single measurement of contrast (standard deviation of pixel values). When the contrast measurement of 3 successive images dropped below as specified threshold, this indicated the absence of movement. Freezing was defined as the absence of movement on 2 successive measures and was expressed as a percentage during predetermined time frames (15 secondes for tone presentation in experiment 1 but also min in experiment 2).

2. Elevated plus-maze (study 1)

Device

The Elevated Plus Maze (EPM) was made of black Plexiglas and positioned 73 cm above the floor of the experimental room. It was composed of 4 arms (see [Figure 41](#); 50 cm long and 10 cm wide) connected by a central squared platform (10 cm for each side). The 2 so-called « open arms », facing each other, had 1.5 cm borders whereas the 2 so-called « closed arms », facing each other, had 40-cm high walls. Light intensity measures at the floor level were 10 lux at the extremity of the open arms, 7 lux in the central platform, and 2.5 lux at the extremity of the closed arms.

Figure 41: Picture of the Elevated Plus Maze device



Protocol

Five min before the beginning of the test rats were placed in an empty transportation cage and placed in the experimental room. Then rats were placed on the central platform facing one of the closed arms. The test lasted 5 min and was video recorded to further assess, if needed, other data than the one collected online by the experimenter. These data collected online comprised the number of entries and the time spent in each arm. An arm entry was validated only when the 4 paws were positioned within the arm. This quantification was performed with the home-made software AION (developed by Elouan Cosquer). Between each rat the EPM was cleaned with water and 70 % ethanol.

Quantification

Besides the number of entries, the percentage of entry and the percentage of time spent in open arms, were calculated as follows:

$$\%OA_{\text{entries}} = \frac{OA_{\text{entries}}}{(OA_{\text{entries}} + CA_{\text{entries}})} \times 100;$$

where $\%OA_{\text{entries}}$ is the percentage of number of open arm entries, OA_{entries} is the total number of entries in open arms, and CA_{entries} is the total number of entries in closed arms.

$$\%OA_{\text{time}} = \frac{OA_{\text{time}}}{(OA_{\text{time}} + CA_{\text{time}})} \times 100;$$

$\%OA_{time}$ being the percentage of time spent in open arms, with OA_{time} being the total time spent in open arms and CA_{time} being the total time spent in closed arms.

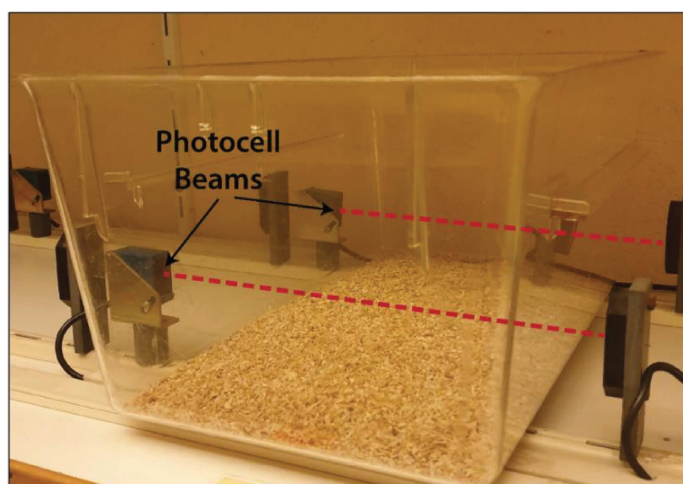
3. Locomotor activity (study 1)

Device

In the dedicated room, rats were put in new cages placed on shelves. Each cage was positioned within the device which comprised 2 photocells positioned 4.5 cm above the cage floor, 28 cm apart, so that each one was positioned 4 cm from one end of the cage (see **Figure 42**). The photocell beams were connected to an interface connected to a computer, so that each time the rat interrupted the photocell beam was counted. Further, the measure of locomotor activity was analyzed in terms of “cage crossings”; a cage crossing was counted when the rat consecutively interrupted the 2 photocells beam.

Figure 42: Picture of the device used to assess horizontal locomotor activity

The picture shows a home cage placed within the device. Photocell beams are represented with red dashed lines.



Protocol

Rats were brought to the experimental room and left on the stabling racks 24 h before the beginning of the test so that they could acclimatize to the room. The experiment started with rats being placed in their respective cage, on the shelves, within the device. They were left undisturbed for 1 h, counted as baseline activity. Then they received their respective treatment, either CNO (1 mg/kg, i.p.) or vehicle (NaCl 0.9 %, i.p.) and replaced in the cage for 2 more hours, counted as post-treatment activity.

Quantification

The number of cage crossing were automatically stored by bins of 15 min.

4. Restraint protocol during study 2

Device

Rats were restrained in an opaque grey PVC tube (length, 80 cm; diameter, 13,5 cm) including several small holes at each extremity so that the rat could breathe (see [Figure 43](#) below).

Figure 43: Pictures of the tube used for the restrain stress protocol.



Protocol

Because in study 2 we also collected blood samples to measure the level of plasmatic CORT before and following restraint stress, this experiment was performed from 9h et 11h in the morning, so quite early within the rat's diurnal phase, when the level of CORT is at its lowest ([Atkinson and Waddell, 1997](#)). Half of the rats first received CNO (1 mg/kg, i.p.) or vehicle (NaCl 0.9 %, i.p.) in the stabling room 30 min prior to being brought in the dedicated room where a first blood sample was taken at the level of the tail (caudal vein; see [Blood sampling page 93](#) for detail on the sampling blood procedure). Then rats were immediately placed within the tube for 10 min. Following restraint, a second blood sample was taken, and rats were brought in another room until they were put to death. The second half of the rats were also administered CNO (1 mg/kg; i.p.) or vehicle (NaCl 0.9 %, i.p.) in the stabling room, then remained undisturbed to serve as non-restrained controls. The same post-treatment delay was applied to them before they were sacrificed to match with the duration of the protocol of the stressed rats (see the timeline [Figure 1 in study 2 page 135](#)).

5. Restraint during electrophysiological recordings (study 3)

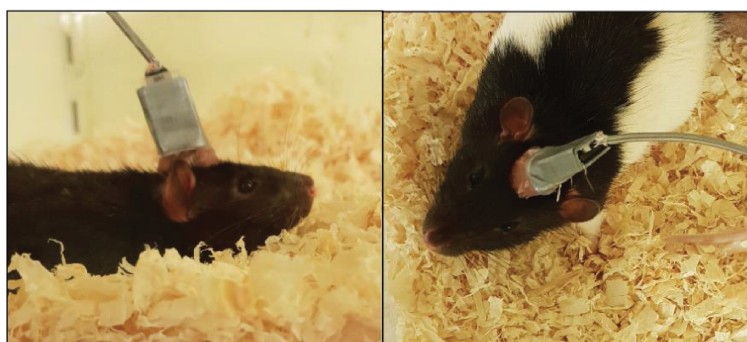
The electrophysiology analyses and the statistics applied are mainly described later in the chapter (see [page 123](#)).

Protocol of the experiment

Ten days following surgery and electrodes implantation, the signals were checked by connecting rats to the recording system. Once it was certain that all electrodes – or most of them – gave correct signals, rats were brought to the surgery room, anesthetized with isoflurane (4 % for induction in the induction box and 1.5 % for maintenance while the rat was placed on the stereotaxic frame) and the preamplifier was secured onto the EIB-16 connector (using two pieces of plastic placed on each side of the preamplifier and glued to it with UV glue, and dental cement to secure the pieces of plastic to the head-cap). Finally, the preamplifier and plastic pieces were wrapped into duct tape. Overall, this procedure, performed early in the morning, lasted 15 min. This way the preamplifier remained connected to the EIB-16 during the entire duration of the experiment (see an example **Figure 44**).

Figure 44: Pictures of rats connected to the electrophysiology recording system.

We can see the preamplifier attached and secured with duct tape.



During each recording session rats were first brought to the recording room from the stabling room and placed in their respective recording cage (the same each time), within the Faraday cage, for 1 h before being connected to the system. During the recording sessions they had only access to water, not food, to avoid frequent contamination of the signals with chewing artifacts if rats would eat. Recordings were performed using an Alpha Omega system (see **page 117** for recording system) while the behavior of the rats was constantly recorded with a webcam placed above the cage and connected to a different computer than the electrophysiology recording system. Video recording was made with OBS Studio (Open Broadcaster Software 25.0.1, free and open source: <https://obsproject.com/fr>). The timeline of the experiment is shown in **Figure 1 in the study 3 page 136**.

During the 3 days following the secured plugging of the preamplifier, rats were brought once a day to the recording room as described above and recordings were performed for 3 h. These 3 sessions were designed to allow habituation to the recording situation (*i.e.*, connection to the cable; overall recording conditions). The following day, the actual immobilization experiment was performed. After the rat was brought to the recording room, it was placed into its recording cage

MATERIALS AND METHODS - Behavioral evaluations

and left undisturbed for one hour. Then, the rat was plugged, and the recording was started. After 1 h, considered as *pre-immobilization baseline*, the first 10-min immobilization was performed. Then the rat was left undisturbed for 3 h (time selected according to (Jackson and Moghaddam, 2004 study), considered as *post-immobilization 1*, after which the second 10-min immobilization was performed. Then rats were left undisturbed for an extra 3 h, considered as *post-immobilization 2*, before the recordings (electrophysiological and video) were stopped. The immobilization lasted 10 min in order to match our previous experiment including c-Fos immunohistochemistry (*cf.* study 2).

Recording and behavioral assessment

In terms of electrophysiological recordings, we were particularly interested in the evolution of the sleep/wake stages throughout the whole experiment, from the baseline to the different post-immobilization periods. Those stages were quantified based on the signals coming from the dCA1, PRL and electromyogram (EMG) electrodes. In addition to this quantification we also evaluated, during the baseline and post-immobilization periods, the different latencies to enter each stage and the duration of the first episode of each stage. In parallel we used the video recordings to check the behavioral status of the rat, *i.e.*, active/moving, or inactive/still; for that particular purpose we used the DLC python toolbox (Mathis et al., 2018; Nath et al., 2019). These data were used for sleep/wake evaluation combine with, or instead of the EMG electrodes. For more details about the quantification of the sleep/wake stages and their analyses please refer to [page 125](#).

We also used the video recordings to manually assess several behaviors amongst those frequently analyzed in studies dealing with stress response and stereotypies (MacLennan and Maier, 1983), before and following the two immobilizations. For that particular purpose we used the home-made AION software (developed by Elouan Cosquer at the LNCA) allowing to code, using different keys of the computer's keyboard, the different behaviors of interest (see [Figure 45](#) for some examples); those included *locomotion* (when rats just moved across the cage ; according to this specific behavior, when rats reached an end of the cage, this was scored as a *cage crossing*), *rearing* (when rats stood on their back paws and sniffed up), *sniffing down* (when rats sniffed compulsively the bedding), *digging* (when rats used their forepaws and nose to dig the bedding and push it to the side), *turning* (when rats, while standing on their four paws, abruptly made a half-turn), *wet-dog shake* (when rats, either on their four paws or on their back paws, shacked their upper body).

MATERIALS AND METHODS - DREADD Validation Using Patch Clamp Recordings

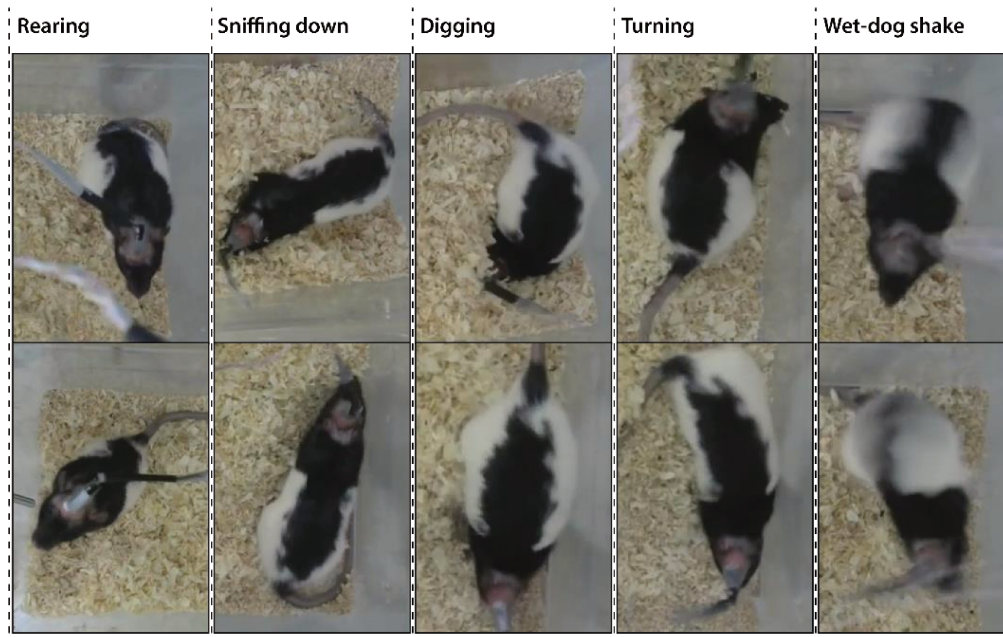


Figure 45: Pictures (video captures) of the different behavioral traits analyzed.

For each of them two examples on the same rat have been selected. For the turning behavior, the upper picture shows the rat before turning and the lower picture show the rat after turning.

IV. DREADD Validation Using Patch Clamp Recordings

Surgery

Rats received a surgical procedure such as described above (see [page 78](#)) and the care, during the recovery period, for the rats used for the behavioral study.

Preparation of the slices

On the day of the experiment rats were brought to the INCI in the laboratory of our collaborator, Dr. Sylvain Hugel, who performed the patch-clamp recordings.

Rats were deeply anesthetized with a mixture of ketamine (82.5 mg/kg, Imalgène 1000, Merial) and xylazine (11 mg/kg, Rompun 2 %, Bayer). They were intracardially perfused with 300 ml of cold (0 - 4°C) sucrose-based artificial cerebrospinal fluid (248 mM sucrose, 11 mM glucose, 26 mM NaHCO₃, 2 mM KCl, 1.25 mM KH₂PO₄, 2 mM CaCl₂, 1.3 mM MgSO₄, and 2.5 mM kynurenic acid; bubbled with 95 % O₂ and 5 % CO₂). Brains were subsequently removed, the hemispheres separated and 300-µm thick sliced were performed with a vibratome (VT1200S; Leica, Nussloch, Germany).

Recordings

Slices were continuously superfused with oxygenated aCSF at 34°C. Lateral habenular neurons were selected based on the presence – or the absence, for control recordings – of mCherry fluorescence and recordings were made in the whole-cell configuration. Patch pipettes were filled with a solution containing 140 mM KCl, 2 mM MgCl₂, 10 mM HEPES, 2 mM MgATP, (pH = 7.3, adjusted with KOH; osmolarity, 310 mOsm, adjusted with sucrose). Recordings were performed under a resting potential at ca. – 60 mV.

In the first experiment we investigated, on LHb neurons including hM4(Gi) receptors (n = 2 rats), the consequences of bath perfusion of CNO (5 μM) on firing frequency in response to intracellular injection of 1 s–lasting current pulses of increasing amplitude (from 0 to 240 pA, increments of 20 pA). Responses were recorded before and following CNO application.

In the second experiment we investigated the consequences of local application of 1 μl CNO (500 μM) on spontaneous firing frequency of LHb neurons, with (n = 1 rat), and without (n = 1 rat) hM4(Gi) receptor expression, by means of puff application through a second pipette positioned just above the recorded neurons.

V. Plasmatic corticosterone

1. Blood sampling

During study 2, blood samples were taken from the caudal vein of the rat's tail, before and following the 10-min restraint procedure. To that purpose, each rat was gently put on a table and covered with a towel, including its head but excluding its tail. Sampling was performed by 2 persons, one, placed in front of the rat, gently restraining it within the towel, with their 2 hands, so it could not move during the sampling, and a second, placed behind the rat, to perform the sampling. In consequence, once a day during the three days preceding the experiment, rats were habituated to being maintained for 1 min within the towel by the same person that later did this particular action during the experiment. The caudal vein was lightly incised with a razor blade and blood, approximately 250 μl each time, was collected by a heparinized capillary tube (Microvette CB 300) while gently stroking the tail from the base of the tip. The pre-stress incision was performed about 3 cm from the tip of the tail, and the post-stress one was performed 2 cm higher. As soon as the blood was collected, the tubes were placed in ice (4°C) before being centrifuged (3000 rpm at 4°C

during 4 min) to collect approximately 150 µl of plasma, which was then stored at -80°C until analyzed.

2. Mass Spectrometry coupled with High Performance Liquid Chromatography

The blood samples were analyzed using the mass spectrometry coupled with HPLC (high performance liquid chromatography) in collaboration with Virginie Chavant and Dr Yannick Goumon (INCI, Strasbourg, France).

Preparation of the blood samples

For each sample, 50 µl of plasma were used and placed in a tube. Samples were kept on ice all along the protocol. First, 10 µl of deuterated CORT (D4-corticosterone 50 pmoles/10 µL [Sigma-Aldrich, St. Quentin Fallavie, France] in H₂O – 0,1 % formic acid – FA) were added; then 1 ml of acetonitril (ACN) 100 % were added. Two centrifugations (20 000 rcf [*i.e.*, Relative Centrifugal Force], 4°C, 20 min) were made, after each of which the supernatant was extracted. The samples were re-suspended in 1 ml of ACN (100%). A second centrifugation was done (20 000 rcf, 4°C, 20 min). The supernatant was collected and dried in vacuum (SeepVacuum, overnight) after what 30 µl of ACN 20 %-0,1 % of formic acid were added, followed by a centrifugation (20 000 RCF, 10 min). Samples were re-suspended in ACN 30% / H₂O 69.9% / formic acid 0.1% solution, then transferred at a volume of 5 µl in the tanks of the HPLC (see [Figure 46](#) for schematization for the system).

MATERIALS AND METHODS - Plasmatic corticosterone

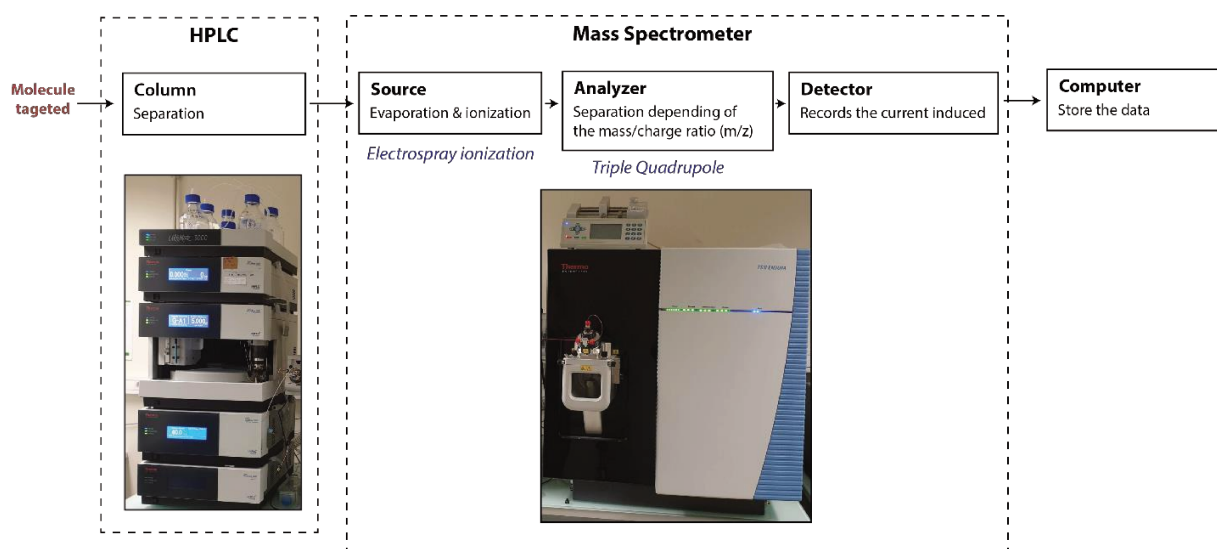


Figure 46: Schematic representation (and photos) of the mass spectrometry coupled to HPLC system.

The sample is injected in the HPLC column where the targeted molecules (CORT) are separated, before being transferred to the mass spectrometer in which the sample pass through three processes: the source, which allows the ionization and the evaporation of the molecules (electrospray ionization in our case), the analyzer, which separates the molecules depending on their mass/charge ratio (m/z), and the detector, which records the current generated by the ion passing through.

Procedure

The analysis is carried out in two steps. First, the different elements were separated by high performance liquid chromatography (HPLC; Dionex Ultimate 3000, Thermo Scientific, San Jose, USA), then injected in the mass spectrometer triple quadrupole (Endura, Thermo Scientific, San Jose, USA) spectrometer to detect the different molecules of interest. The system was controlled by Xcalibur v. 2.0 software (Thermo Electron).

The concentrations of plasmatic CORT were evaluated using the SRM method (Selected Reaction Monitoring). This method is applied when the targeted molecules are known. The principle is that the targeted molecule is fragmented (a predicted fragmentation) and ions will be formed. Only the ionic fragment from the precursor molecule will be analyzed and detected in the mass spectrometer.

HPLC

Samples were loaded on a column (ZORBAX SB-C18, Micro Bore Rapid Resolution 1.0 x 150mm, 3.5 μ m, Agilent). The elution of the HPLC was set with a multi-step gradient between mobile phase A and B. The A phase was composed by 1 % d'ACN – 1% de AF – H₂O and the mobile phase B was composed by 99.9 % d'ACN – 0,1 % d'AF – H₂O (see Table 2 for the elution gradient used).

Table 3: Elution gradient for CORT samples

Retention (min)	Debit (ml/min)	%phase mobile B
0	0,150	0
1	0,150	0
3	0,150	25
10	0,150	30
12	0,150	98
14	0,150	98
15	0,150	0
19	0,150	0

Mass spectrometry

Generally, mass spectrometers are composed by (see **Figure 46**):

- A source: ionize and evaporate the samples. It can work in positive or negative mod.
- An analyzer: separate the molecules depending on their mass-to-charge (m/z) ratio. In the case of this study, the mass analyzer was a triple quadrupole. It is separated in three compartments (Q1, Q2, Q3). Ions enter a state of reasoning passing through the triple quadrupole thanks to the metal rods with opposite polarities they are made of.
- A detector: detect and quantify the targeted ions. In this study, the type of detector was an electron multiplier.

The mass analyzer is composed of three quadrupoles. Q1 sorts the precursor ions (targeted ones) based on their m/z ratio and allows only these ions to pass in the second quadrupole (Q2). This quadrupole is actually a hexapole (even it is called quadrupole) collision cell. This compartment is charged with Argon gas which breaks the precursor passing through Q2 by collision-induced dissociation. The product ions created in Q2 reach Q3 (second mass analyzer). Q3 (as Q1) select the ions based on their m/z ratio. The product ions targeted pass through Q3 and are detected in the detector.

For our experiment, the source was in positive mode. Nitrogen was used as sheath gas (set at 10 Arb) and Aux gas (set 5 Arb). The ion transfer tube temperature was set to 287°C. In the triple

MATERIALS AND METHODS - Histology

quadrupoles, the resolution of Q1 and Q3 were set to 0.7 FWHM (*full width at half maximum* is expressing the amplitude for resolution). The collision gas used was Argon at 2 mTorr. As evoked previously, we used SRM method based on precursor ions (see **Table 4** for RF lens parameter and collision energy depending on the precursor ion).

Table 4: Mass spectrometer ionization, selection, fragmentation, and identification parameters

Compound	Polarity	Precursor (m/z)	Product (m/z)	Collision Energy (V)	RF Lens (V)
Corticosterone	positive	347.11	293.472	17.03	227.49
			311.294	15.91	
			329.169	14.95	
D4-corticosterone	positive	351.179	297.103	17.68	223.55
			315.183	16.88	
			333.24	15.56	

Quantification

The data provided by the spectrometer (*i.e.*, the quantity or intensity [arbitrary unit] by the m/z ratio [representing the mass divided by the charge number – number of electrons removed] were analyzed with the Quan Browser software (Thermo scientific). The concentrations of plasmatic CORT were evaluated as follows: the pic of CORT was located based on the known elution time; the area under the curve (integral) was calculated; this area was compared to the area found for the deuterated molecule (known concentration) allowing to infer the sample concentration. The detection threshold was 3 times the background noise and the quantification threshold was 10 times the background noise.

VI. Histology

1. Brain Sampling

a. Brain extraction

The rats were anesthetized by i.p. injection of a mixture of xylazine (100 mg/kg) and ketamine (10 mg/kg). Once the animal deeply anesthetized (lost corneal reflex and withdrawal reflex from strong pinches of toe and tail), the skin of the abdomen was incised and the rib cage exposed and cut; then the descending aorta was clamped to limit the diffusion of the perfusate in the upper body; the perfusion needle was then inserted in the ascending aorta through the left ventricle and

MATERIALS AND METHODS - Histology

fixed there with a clamp; then the right atrium was incised to allow the fluids to be evacuated from the body. For studies 1 and 2, heparinized phosphate buffered saline (PBS, 1M, heparin 0,1 %; 50 ml) then 4% paraformaldehyde (PFA; 100 ml) were perfused using a peristaltic pump (mini pomp Harvard Apparatus), at a low rate (10 ml/min), to optimizing rinsing then fixing required for immunohistochemistry. For study 3, a syringe was used to only pass 4 % PFA (60 ml) by finger pressure over approximately 2 min, as brain were only collected to check electrode locations. Once the perfusion terminated the brain was extracted, dipped into a small beaker containing 4 % PFA for a 2-h post-fixation duration at 4°C and subsequently dipped for 48 hours into a small beaker containing a 20 % sucrose solution at 4°C for cryoprotection purpose. The brains were then frozen at -40°C in isopentane (ROTH, France) and stored in a freezer at -80°C until they were sliced in a cryostat (Microm HM 560).

b. Brain slicing

In each study, coronal sectioning (40 µm) was done using a cryostat (Microm HM 560). For c-Fos immunohistochemistry (study 1 and 2), slices (up to 6) were placed in 500 µl of cryoprotective solution and stored at -20°C; slices were collected according to predefined blocks, throughout the brain (see [Table 5](#) for study 1 and [Table 6](#) for study 2). For the DREADD experiments (studies 1 and 2) and for the observation of the fluorescence diffused by the presence of Dil (study 3), slices were directly mounted on a slide on which, after the slices had dried, a DAPI medium (4',6-diamidino-2-phenylindol; DAPI Fluoromount®, Clinisciences) was applied before being covered.

Table 5: Stereotaxic coordinates of the considered blocs in study 1

Bloc Name	Bloc Start (AP form bregma)	Bloc End (AP form bregma)
<i>PFC</i>	4.20	2.28
<i>LHb/dHPC</i>	-1.44	-4.44
<i>vHPC</i>	-4.44	-6.60

Table 6: Stereotaxic coordinates of the considered blocs in study 2

Bloc Name	Bloc Start (AP form bregma)	Bloc End (AP form bregma)
<i>PFC</i>	4.68	2.28
<i>Striatum (anterior part)</i>	2.28	-0.36
<i>Striatum (posterior part)</i>	-0.36	-1.44
<i>LHb/dHPC</i>	-1.44	-4.44
<i>vHPC</i>	-4.44	-6.60
<i>Raphe</i>	-6.60	-10.08

2. c-Fos Immunohistochemistry

All rinsing and incubation were made at room temperature under slow agitation (300 rpm). Following 3 10-min rinsing in PBS (1M, pH = 7.4), non-specific sites were blocked with a 1-h incubation into horse serum (0. %). Then slices were incubated with the primary antibody (polyclonal rabbit antibody; SYSY, ref: 226 003, lot: 226003/16, Synaptic System) for 48 h. Following 3 rinsing in PBS (1M, pH 7.4) slices were incubated with the secondary antibody (biotinylated goat anti-rabbit antibody; ref: BA 100, Vector) for 1 h. Then, after 3 rinsing in PBS (1M, pH = 7.4), slices were incubated with the avidin-biotin complex (A et B reagents; Vectastain kit ABC elite standard, PK 6100, Vector Laboratories) for 45 min, allowing the amplification of the signal. Then, after 2 10-min rinsing in PBS (1M, pH = 7.4) followed by 1 10-min rinsing in Tris buffer (0.6 %, pH 7.6), slices were incubated during 13 min in the revelation solution (Kit DAB, SK 4100, Vector Laboratories) including DAB (3,3'-diaminobenzidine) and H₂O₂ (oxygen peroxide). The enzymatical reaction was then stopped by 3 consecutive 10-min rinsing with PBS (1M, pH = 7.4). Finally, slices were placed on a slide and, once they were dry, a mounting medium (Fluoromount®, Clinisciences) was applied and the slices covered.

VII. Images Observation and Processing

1. Verification of the spread of mCherry (study 1 and 2) and of Dil (study 3)

The visualization of the spread of mCherry and Dil was performed using a fluorescence microscope equipped with an apotome module (Apotome.2, Zeiss®) via a camera (Orca Flash 4.0 LT, Hamamatsu) linked to a computer equipped with a picture acquisition and processing software (ZEN 2 Black, Zeiss®). For DAPI (blue – absorption wavelength: 350 nm, emission wavelength: 450-490 nm) slides were exposed to a 365 nm wavelength filtered light; for mCherry (deep red - absorption wavelength: 587 nm, emission wavelength: 610 nm) and Dil (red orange - absorption wavelength: 569 nm, emission wavelength: 551 nm) to a 620 nm wavelength (590 nm to 650 nm; can excite molecule absorbing near this interval without being exactly within it). All pictures of a given slide were acquired with the same zoom parameter (x 2.5) and could subsequently be assembled to reconstruct the whole slide in 2D using the same software (ZEN 2 Black). Images were subsequently superimposed to the images taken in the Paxinos and Watson atlas ([Paxinos et Watson, 2007](#)) in order to determine with precision the different spreads.

2. Quantification of the expression of the c-Fos protein (study 1 and 2)

a. Production of the pictures

Sections were scanned and saved in NDPI format using a NanoZoomer S60 (Hamamatsu) at x 20 thanks to the associated software (NDP.scan, Hamamatsu). All parameters remained unchanged across all experiments.

b. Processing of the pictures using a semi-automated method

The quantification of the c-Fos+ cells has been performed using a home-made method (See workflow of data processing - [Figure 47](#)) developed in Image J (Free License, Wayne Rasband, Research Services Branch, National Institute of Mental Health, Bethesda, Maryland, USA).

The first step was to outline the different regions of interest (see the table of targeted structure in the [supplementary for study n°1 page 134](#), and in the [Supplementary information table S3 for study n°2 page 135](#)) in reference to the Paxinos and Watson atlas ([Paxinos et Watson, 2007](#)). Throughout the different experiments, the outlining of a given region has always been made by the same person.

The second step was fully automated. The counting macro counted the number of dots within the outlined region and results were given by slice, structure, and hemisphere, in a generated excel

file (Microsoft®). Each counting was checked by the experimenter to ensure the validity of the results. To sort the data, given their important amount, we used Matlab (MathWorks®, Natick, Massachusetts, United States).

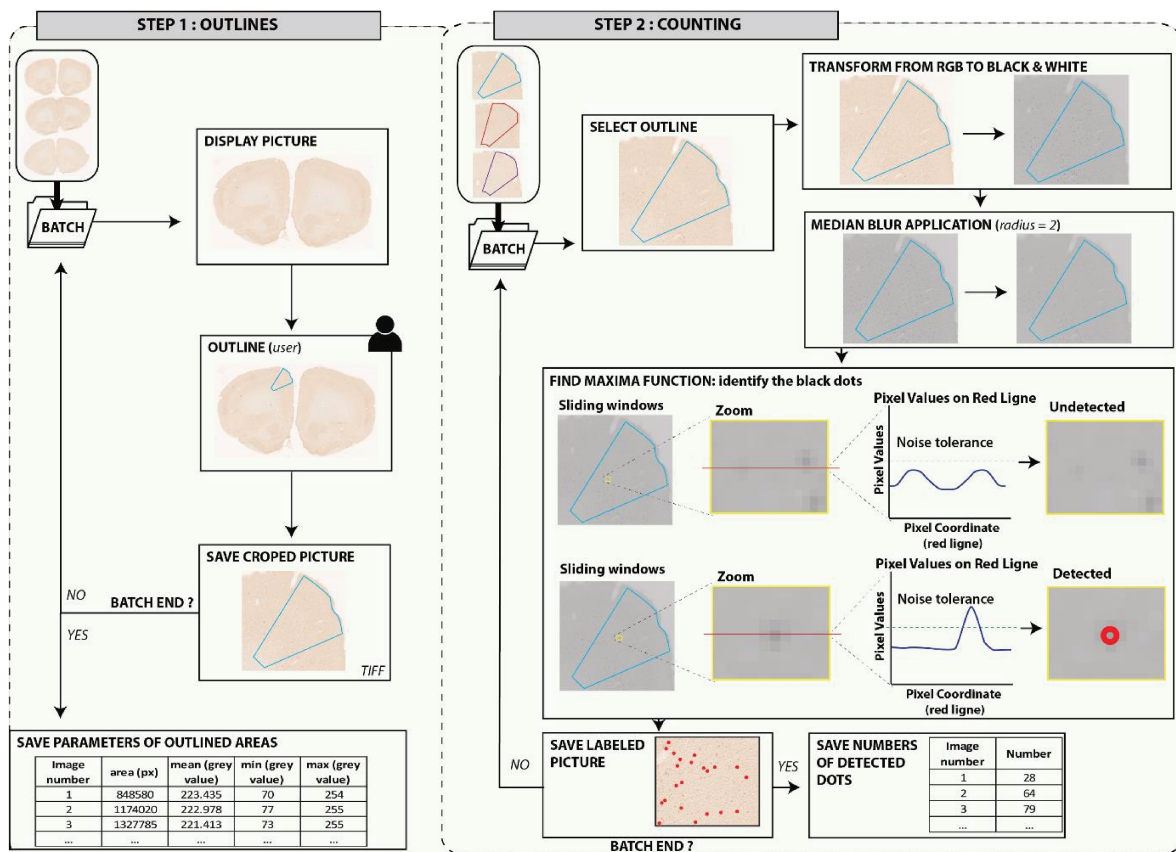


Figure 47: Workflow of c-Fos semi-automatic counting

The home-made semi-automatic counting method is divided into two steps: outlining the regions and counting. The outlines are drawn by the experimenter to surround each region of interest. For faster processing, the script opens the images one by one, crops and saves automatically until the batch of images is completed. Then, the area size, the grey mean, the grey minimum, and the grey maximum are calculated for each batch images and saved in an Excel® file. The counting is totally automatic. The previous pictures, cropped and outlined (forming a new batch), are processed one by one. Image J transforms the RGB images in Black & White, then applies a median blur (radius = 2). The function FindMaxima (from ImageJ) is used on the image for identification of the black dots using a sliding window and a noise tolerance parameter. The window slides through the image and assesses if the pixel values are above the noise tolerance parameter, identifying the black dot. For illustrative purpose, the pixel values distributions are represented on a line (red) however the algorithm is analyzing a square (two dimensions analysis leading to a three dimensions distribution analysis).

c. Development of the semi-automated method

Outlining the regions of interest

The script allowing the outlining of the regions of interest worked as follows. The first step was to select the folder including the pictures of the targeted structure (batch; a batch represented 10 pictures, as processing more than 10 pictures at the time made the script run slower), but several regions of interest could be present on a single picture. The script opened each picture of the batch one by one, and for each picture, the user needed to outline the targeted structure(s) (see **Figure 47** step 1 for an example). Once the outlining was done, the images cropped along the outline were saved in a TIFF format (Tagged Image File). When all regions of interest were outlined, the script saved a general image of the outline locations. Then, another image from the batch opened and this went on until all pictures of the batch had been outlined and saved. Then, the following batch of 10 pictures was processed, and so on until all batches were processed.

Automatic counting of the number of c-Fos+ cells

This macro allowed to count the number of c-Fos+ cells in the outlined areas previously selected (see **Figure 47** step 2 for an overview of the process). The saved pictures were converted from RGB (“red, blue and green”, 32 bit) to BW (“black and white”, 16 bit) to limit the pixel values from 0 (black) to 255 (white). Then, a median blur with a radius of 2 was applied to reduce background noise by replacing each pixel by the median of the adjacent pixels. Following that, the function FindMaxima() from Image J was applied. This function is based on a parameter called « Noise Tolerance » which allows to define a threshold as follows: the « Noise Tolerance » previously defined is subtracted from the maximum value. The area around the maximum value found is analyzed and this processing is applied each time the algorithm finds a local maximum value. In fact, each time the algorithm finds a value which is higher than the local background noise, it is counted as a dot. The advantage of such algorithm is that it acts by a sliding window across the whole picture, so that it allows to adapt to local background noise and therefore override the potential shadows or debris on the picture. The results of this counting are stored in an Excel file (Microsoft®).

Definition of the « Noise Tolerance » threshold within the FindMaxima() function

We have defined the « Noise tolerance » threshold by testing 6 potential thresholds from 50 to 100 (by steps of 10) and selected the appropriate value based on the linear correlation equation obtained by comparing automated to manual counting.

$$Y = (a \times X) + b$$

MATERIALS AND METHODS - Statistical analysis

where Y is equal to the value of the automated counting, a is the slope of the best fitting curve, X is the value of the manual counting, and b is the intersection with the y axis.

Based on this linear equation we were able to find the more relevant « Noise tolerance » value for the FindMaxima() function. To that purpose we needed to have $Y=X$, representing the perfect case where the automated and manual counting methods provide the exact same number of counted dots.

If $a = 1$ and $b = 0$, therefore

$$Y = (1 \times X) + 0$$

$$Y = X$$

The closest parameter found was 78,12 in study 1, represented by the following linear equation:

$$Y = (0.9691 \times X) + 0.09988$$

The correlation with this « Noise tolerance » value was extremely high ($R^2 = 0.95$; $p < 0.0001$), confirming the precision of the semi-automated counting method. For more information, see [Supplementary Figure 7 page 134](#) in [Durieux, et al 2020](#)).

For the second experiment (restraint stress; study 2) we found a parameter equal to 72.84 (see [Supplementary Figure S3 in study 2 page 135](#) for the details), relatively close to study 1. The difference between the two is probably due to differences of background noise, as the immunohistochemistry procedures of the two experiments had not been performed at the same time and different batches of antibodies had been used.

VIII. Statistical analysis

1. General Statistics

The following paragraph describes the general statistical analysis applied on studies 1 and 2. These analyses were performed with the Statistica© (Statsoft, Tulsa, USA) software.

Paired t-test were used to compare the c-Fos⁺ densities from both hemispheres before pooling (Experiment 1 of study 1 and study 2), and to analyze behavioral data obtained in study 3. ANOVAs were used for all the other analysis. The threshold for rejecting the null hypothesis was 0.05 throughout.

MATERIALS AND METHODS - Statistical analysis

For the first experiment of study 1, freezing scores across each 15 s tone presentation were analyzed using one-way ANOVA with Tone as the repeated measure, and c-Fos⁺ cells densities were analyzed using Group (HC, No shock, Fear conditioning) as the between-group factor.

For the experiments using DREADD (experiment 2 of study 1, excepted for the electrophysiological data - see below-, and study 2), after it was checked, using t-tests, that data from the Sham-Veh and hM4-Veh groups did not differ, they were merged into a single control group, called Ctl-Veh ; Group (Ctl-Veh, Sham-CNO and hM4-CNO) was then used as the between-group factor for one- or two-ways ANOVA with post hoc Newman-Keuls multiple range test when appropriate. For study 1, one-way ANOVAs were used for the *Context test* and *New context exposure* sessions of fear conditioning and for plus-maze (percentage of visits, and time spent in open arms; total number of arm visits); two-way ANOVAs were used for the *Conditioning* and *CS test* sessions of fear conditioning and for locomotor activity with CS, baseline vs CS, and 15 min-bins during the 1-h baseline and during the 2 h post-treatment as the repeated factor, respectively.

For study 2, one- and two-ways ANOVAs were used to analyzed c-Fos⁺ cell densities in each brain structure, and plasmatic CORT levels (pre-restraint, vs post-restraint) respectively.

For the electrophysiological experiment of study 1 (experiment 2), data were analyzed with one- and two-way ANOVAs (with Group as the factor and Current pulse amplitude or Time as the repeated measures).

2. Multivariate Statistic (study 1 and study 3)

Multivariate statistics is a family of statistical method that focus on multiple variables, will study the variation that the variables have in common. This family is based on the reduction of the number of variables. These analyses were performed with the Statistica© (Statsoft, Tulsa, USA) software.

a. Principal Component Analysis (study 3)

We used the PCA for separating the rats depending on their post-stress behaviors and clustering them. No particular parameters from the experimenter are need for this analysis. The main principle is to find components explaining the variance between individuals (extensively explained in the Introduction part [Dimensional reduction page 53](#)). Theoretically, the main variance (*i.e.*, PC) of the behaviors output of the animal recorded may represent their vulnerability to stress exposure (*i.e.*, if their behavioral outputs correspond to a post restrain stress situation or not).

b. Factorial Analysis (study 1)

We used the FA for unraveling the structures which the activity (c-Fos activity marker) which covariates between them. This analysis has already used the literature (Veening et al., 2009) and in our laboratory (Ali et al., 2017). Since the technic have been explained in the Introduction (see **Factorial analysis page 52**) and the method is explained in the **study 1** (see **page 134**). For these reasons, we only summarized the method and parameters we used for the FA in the study 1 here.

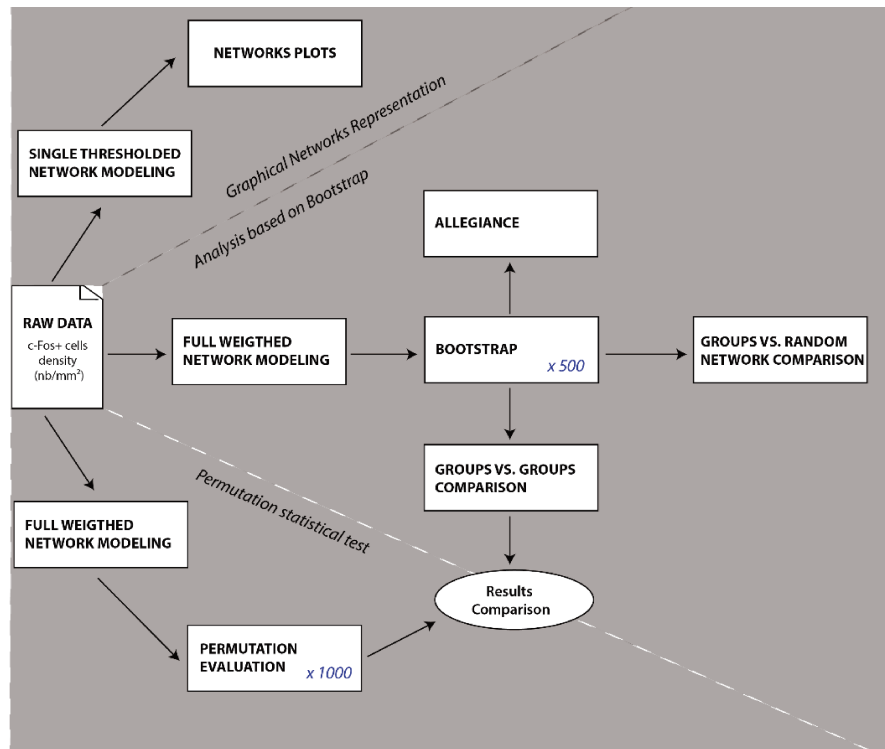
In summary, we have applied the Guttman-Kaiser criteria as a threshold to select the « main » factors. We have used the « Principal component method » to explain most of the variance of our samples, and the « Varimax » rotation to normalize, and therefore minimize the number of extreme data that could be generated. We have made the different verifications, our models always represented more that 50 % of the variation of the totality of our data; also, we have carefully checked that our residues did not exceed 15 % of error between the raw data and data of the model.

3. Graph Theory Applied to Functional Networks (study 2)

We used this analytical method to model functional networks during stress exposure. To better understand LHb implication in the stress response we studied functional networks in naïve animals and following LHb inactivation (using DREADD). Graph theory-based analysis are mostly used on fMRI and EGG data, but, recently, some studies (see Wheeler et al., 2013; Vetere et al., 2017) applied this type of analysis on c-Fos density quantification (see **Introduction page 57** for more details). The workflow of this analysis is schematically represented **Figure 48**.

Figure 48: Workflow of functional network analysis

Based on the raw data (density of c-Fos+, *i.e.*, nb/mm²), we analyzed the data set using three different methods: one for graphical representation (red background), two for statistical comparisons (Bootstrap: blue background & Permutation: green background). Based on the classic bootstrap analysis, we also evaluated the allegiance of the structures of the network.



a. Evaluation of correlations

All data were processed using Python (version 3.7.5, PyCharm edition community – free; <https://www.jetbrains.com/fr-fr/pycharm/>) and several toolboxes. For general coding, we used Pandas (manipulating data as DataFrame and XLSX/CSV export/import; <https://pandas.pydata.org/>), Numpy (managing matrix; <https://numpy.org/>), and Scipy (for general statistic purposes; <https://www.scipy.org/>). The other Python toolboxes eventually used are cited when necessary.

We evaluated inter-structural correlations among 56 structures (see **Quantification of the expression of the c-Fos protein (study 1 and 2) page 100** and **Study 2 page 135**) between the groups exposed to restrain stress: Ctl-Veh, Ctl-CNO, and hM4-CNO. All correlations were calculated using Korr (<https://pypi.org/project/korr/>) according to the Pearson method. The correlation matrix was plotted using Matplotlib (<https://matplotlib.org/>) and Seaborn (<https://seaborn.pydata.org/>). Most of correlation analysis are looking at the covariances between the samples (or individuals) and a time scale. However, in our analysis we correlated the individual values between them at a same time (*i.e.*, value of c-Fos+ cells density of structure 1 vs. structure

2), returning a single correlation matrix. We will see later (see [Statistical analyses used on the model page 110](#)) how do statistic comparison on it.

b. Networks Modeling (Graph Theory Based)

Network modeling was processed using the NetworkX toolbox (<https://networkx.org/>). The networks were modeled based on the R^2 of the correlation (functional connectivity). The principle of modeled network has previously been introduced (see [Introduction page 57](#)). In brief, the nodes of the network represent the brain structures and the edges between two nodes represent the correlation between the activation of 2 two structures. The correlation value can be kept as the weight of the edge. In that case, the network will be called “weighted”. In some other case, the network is based on the significant correlation value (if the correlation is significant then the nodes are connected by an edge, if not, the nodes are not connected to each other) and the values of the significant correlation are kept as weight of the edges. In this shape, the network is called weighted and thresholded. A last case is when, only, the significant correlation associated to edges are kept: the network is called binary. We can define two types of networks: directed and undirected. Directed network indicate the directionality of the information transfer between nodes (for example, the information goes from the LHb to the VTA). The undirected network is when the directionality of the information is not mentioned. Networks based on c-Fos correlations are undirected graph because the directionality of the information between nodes cannot be known with this approach.

For graphical purposes

To display only strong correlations for graphic representation of the network, we decided to create a weighted and thresholded network (*i.e.*, keeping the correlation R^2 as weight of the edge and applying a threshold keeping only the significant correlations). The correlation matrixes were thresholded keeping only the correlations with significance p values lower than 0.05. Each network plot was done using NetworkX, then exported in a JSON format (JavaScript Object Notation) and imported in Cytoscape (open-source software, <https://cytoscape.org/>) for the layout (see [Figure 49](#)).

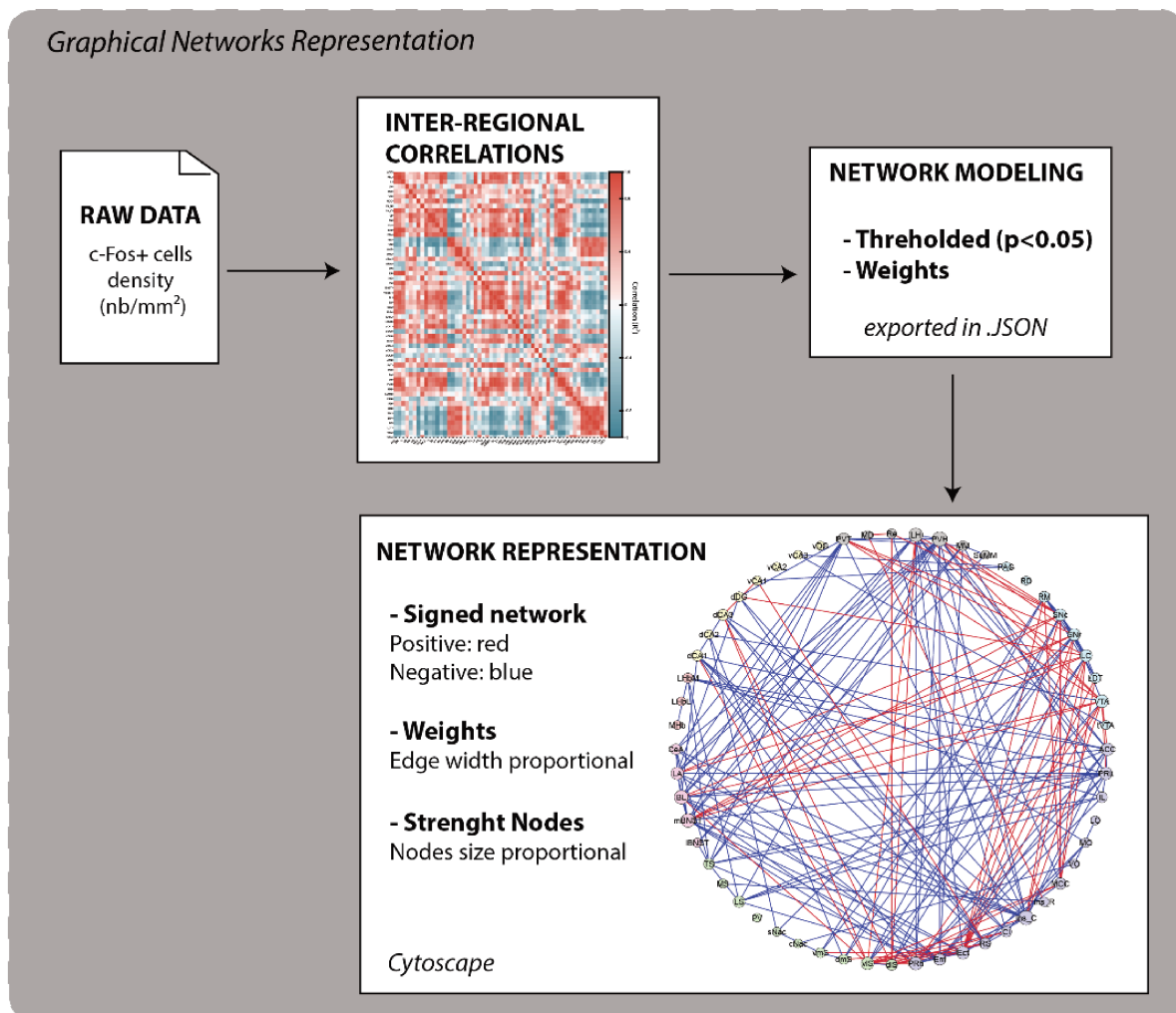


Figure 49: Workflow of the graphical representation computing

For the graphical representation, we kept only the correlations with $p < 0.05$ (Pearson) represented as edges on the network. The positivity and negativity of the correlations were kept (red from positive correlations and blue from negative correlations). The size of each node was proportional to their respective strength. The weight of the edges (*i.e.*, correlations) was represented as proportional to the width of the edges.

For analysis purposes

For the main analysis, we used a full weighted network keeping all the absolute values of the correlations as edges weights connecting the nodes. Graph theoretical analyses were done using NetworkX. We evaluated the **strength** of each node within the network, the **average clustering coefficient**, and the **average of edge weights**.

The strength represents “how much information” the structure receives from the other structures. In other word, a node with a high strength can be considerate as a hub. The strength is calculated as follows:

$$strength_n = \sum e_{n,n_neigh}$$

where n is the targeted node, e is the weight edge between n and n_neigh , n_neigh representing the neighboring nodes. The strength of a given node is the sum of all edge weights connected to this node.

The clustering coefficient is representing the “cumulated strength of a node with its neighbors”. In other words, a node with the strong clustering coefficient means that its neighbors will also have a high coefficient, creating a cluster. For weighted graph, the clustering coefficient can be differentially defined, depending on the method chosen. NetworkX defines the clustering coefficient as the geometric average of the subgraph edge weights as follows:

$$Clustering_n = \frac{1}{deg(n) \times (deg(n) - 1)} \times \sum_{uv} (\widehat{w}_{n,u} \times \widehat{w}_{n,v} \times \widehat{w}_{v,u})$$

where n is the targeted node, $deg(n)$ is a function giving the number of connections of n , u and v represent a pair of nodes connected to n , and $\widehat{w}_{n,u}$ represents the weight of the edge connecting n and u normalized by the maximum weight w in the network, as follows:

$$\widehat{w}_{n,u} = \frac{w_{n,u}}{\max(w)}$$

The average clustering is the average of the clustering coefficient of all nodes.

We also evaluated the modularity of the networks based on the communities. In brief, the modularity is the strength of the fractioning of a network into modules. Modules are also called communities, groups or clusters. Considering a biological network, such network has often high modularity, exhibiting dense connections between nodes in a community/module and less connection in-between modules. Partitions into modules are extracted using iterative optimization procedure (see later). The formula for modularity used by NetworkX is the following:

$$Modularity = \sum_{c=1}^n \left[\frac{L_c}{m} - \left(\frac{k_c}{2m} \right)^2 \right]$$

Where $\sum[x]$ represent the sum of x for all communities (modules) c , L_c is the strength of intra-community connections within the community c , k_c is the sum of node strengths within the community c , and m is the number of edges.

c. Statistical analyses used on the model

This type of analysis gives a single value by variable and by group, which does not allow statistical comparison. To circumvent this issue, we used the **classical bootstrap** approach, which attempts estimating a distribution of values rather than single values by a “resampling” technique. However, due to the low number of samples (animals), this test does not offer a powerful enough statistical comparison. For this reason, we decided to compare the data using another approach, which is to estimate the values which would be obtained under the null hypothesis of no difference between groups and to compare them to the real values obtained. This approach is called the **permutation testing**. We kept only the statistical differences according to the variable (*e.g.*, strength or average clustering) with $p < 0.05$ in both tests (*i.e.*, Bootstrap and Permutation tests, see below), reducing the risk to consider fake positive statistical differences.

Bootstrapping

Bootstrapping is a method using the resampling with replacement, allowing to estimate the distribution of a population based on one value (sample). For example, one can imagine playing with a dice where the number of the dice represent the animals. If $n=6$, then we launch the dice 6 time. From the hazard we can obtain: 1-3-4-4-2-6, 3-3-6-4-2-1, ... These new datasets can be evaluated as the initial data. We can repeat the resampling several times (*e.g.*, 500 times) and obtain 500 different values for the variables targeted as network measurement (*e.g.*, strength or average clustering). These values mathematically estimate the distribution of the population and allow to do statistical comparisons of the distribution (see **Figure 50**).

MATERIALS AND METHODS - Statistical analysis

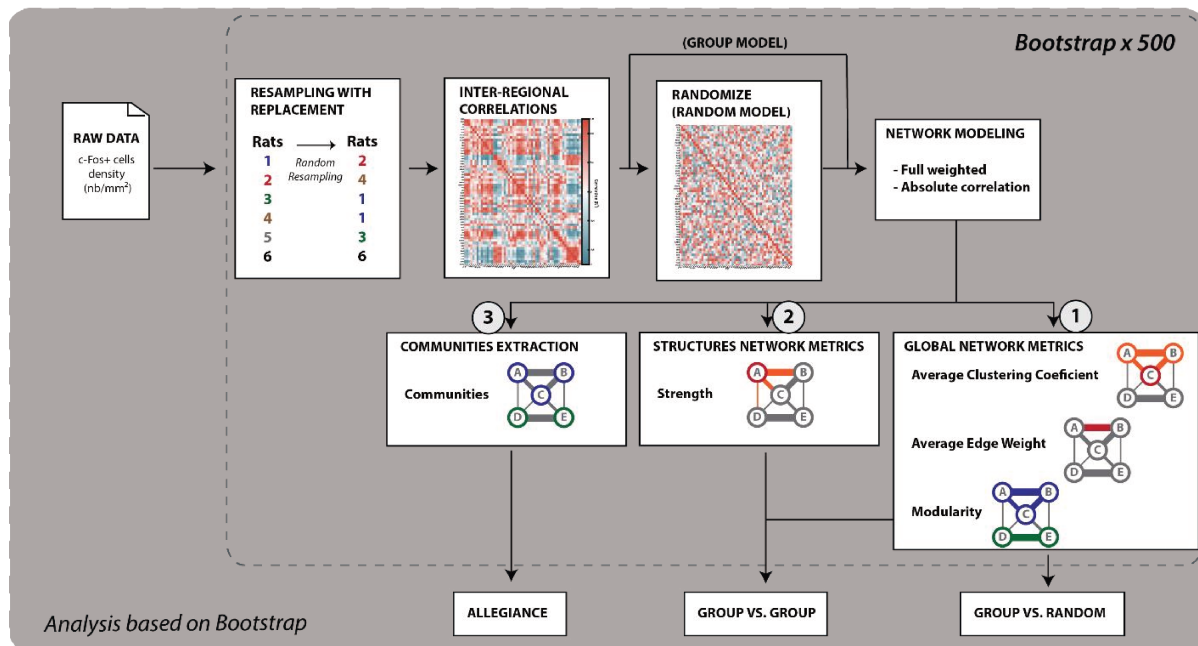


Figure 50: Workflow of the bootstrap analysis

The bootstrap approach is based on the resampling (or replacement) of the animals (or samples), allowing the estimation of the variability of the population. After the resampling, we calculated the correlation map on each new sampling (group model) and, in parallel, we randomized the rows and columns of the correlation matrix (random model). On each model, we analyzed (1) on the global network: the average clustering coefficient, the average edge weight, and the modularity; (2) on the structures of the network: the strength of the nodes; (3) the communities composition. We compare the metrics (1) and (2) between groups and the metrics (1) between the random model and the group associated. The communities extraction (3) was used to calculate the allegiance of the network.

Comparison to random model (H_0)

The modularity based on the processed networks for all groups were relatively low compared to the value we could expect from a binary network (the scale of the modularity in a binary network is from $-1/2$ to 1). Because the graph (network) was weighted, the scale of the modularity was not predictable as it should have been on an unweighted and undirected graph. To make sure that the modularity level obtained was not random we created a random network (hypothesis H_0) and compared the random network of a given group to the network of the same group.

The random network was created by shuffling the rows and columns of the correlation matrix but keeping the main diagonal intact (because structure 1 of a given network is still equal to structure 1 in the network resulting from the random model). We checked several types of random network (see [Annexes part Graph Theory analysis - Random Network Modeling page 146](#)). For each iteration of the bootstrap, a random matrix was created from the correlation matrix, taking into account the population diversity (as well as the initial data). We obtained, for each group (initial data), 500 correlation matrices and 500 random matrices. These iterations allowed us to have a

MATERIALS AND METHODS - Statistical analysis

distribution, for each group, of both the initial and the random networks, making possible their statistical comparison. Note that all links are evaluated simultaneously in a single mathematical step (*i.e.*, the stochastic variable is the matrix itself). Therefore, multiple comparison corrections on the number of pairwise interactions is not needed. Using classic bootstrap comparison (median of the group values compared to the distribution of the random values), we evaluated the significance of the difference between the initial group values and the random values by estimating the p value as follows:

$$p_{value} = 1 - \left(\frac{nb_{obs}}{nb_{iterations}} \right)$$

where nb_{obs} is the number of observations on the distribution of the random network measurement superior or inferior to the median of the group value, and $nb_{iterations}$ is the number of the resampling (bootstrap) done (*i.e.*, $nb_{iterations} = 500$ in our case). We considered a significant difference when $p < 0.05$.

Between-groups comparisons (H1)

To make comparisons between the results obtained for each group (Ctl-Veh, Ctl-CNO, and hM4-CNO) we also estimated the distribution of the population using the bootstrap approach (resampling with replacement – 500 times). We used classic bootstrap approach as explained above (see **Comparison to random model**) and estimated the p value of the comparison the same way.

Permutation test

The permutation test comparison allows to compare groups two by two. It is a statistical test contrasting the actual inter-group differences against chance-level differences expected under the null hypothesis of equivalent groups, based on the calculation of the shuffling of the two groups (creating the null hypothesis), and comparing this distribution of the p value to the real p value of both original group (see **Figure 51**). In other words, the animals of the two groups tested are shuffled randomly (resampling without replacement) creating two new arbitrary groups composed of animals from both initial groups (for example, initial group1 [1,2,3] and initial group 2 [4,5,6]; after resampling shuffled group 1 [5,4,3] and shuffled group 2 [6,1,2]). The network measurements are then calculated (*e.g.*, strength, average clustering coefficient, ...). And between-group differences analyzed. This is repeated 1000 times in our case so that we obtained a distribution of the 1000 calculated differences, therefore representing all the cases when shuffled groups show no difference between each other (because they were mixed). Then, we compared the difference

between the initial groups and the distribution obtained evaluating the p value as previously performed in the bootstrap model (see [Comparison to random model](#)).

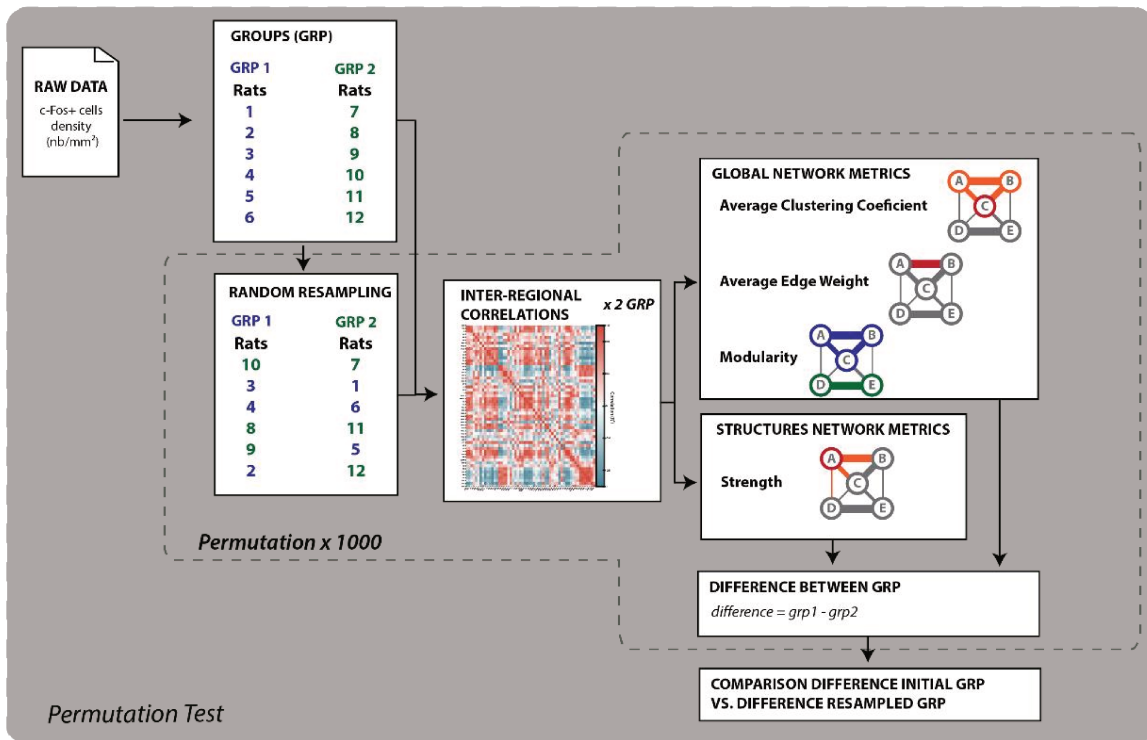


Figure 51: Workflow of the permutation statistical test

The permutation is based on the resampling of the two groups together (mix both groups). Then the correlation matrix is calculated for both resampled groups and the network metrics are computed. We stored the difference between groups for each iteration. At the end of the process (after 1000 iterations), the initial group difference is compared to the distribution of the difference between resampled groups.

d. Allegiance analysis

As explained previously, we can detect the modules (also called communities) of a given network (see [Introduction part Introduction to Graph Theory page 57](#) for details). However, in order to take into account intra-group variability, extracting just one partition into communities based on just the initial correlation matrix is not a powerful approach. To avoid this issue, we decided to calculate the probability of two structures to be in the same community, considering all possible pairs of structures. This probability calculation is called **allegiance analysis**. This analysis exploits both the variance of the samples and the variance of the community extraction algorithm itself, since module extraction include non-deterministic elements (*i.e.*, take into account the variability of the population [resampling with replacement] and the variance of the algorithm used to extract the communities; see below).

Algorithm for the detection of communities

To detect the communities, we used the **Louvain** method, which allows to reveal the potential communities among large networks (Python package <https://pypi.org/project/python-louvain/> called by NetworkX). This algorithm first creates random communities. Then it adapts the composition of each community depending on the modularity obtained, therefore optimizing the theoretical values until the best grouping nodes is found in the network (Blondel et al., 2008). The algorithm can modulate the number of communities extracted using a parameter called **resolution** (in NetworkX). The default value of this parameter is 1. Because the algorithm is based on a random factor (the beginning of the algorithm), the final results can vary. To have the more stable results, we can apprehend the variation of the algorithm by make it run several times. To take into account, the variation of the algorithm, we extracted the communities varying the resolution for 0.88 to 1 over 10 repetitions, so that the number of communities varied from 2 to 5, depending on the group considered (see **Supplemental information S5 from study 2** for an example of the effect of resolution variation on the number of communities).

Allegiance calculation

The **allegiance**, which represents the probability for two structures to be in the same community, was calculated over the bootstraps. For each bootstrap, the correlation matrix was re-calculated, and the communities re-extracted. To extract the community, taking into account the variability of Louvain algorithm in, we calculate the communities 10 times with the resolution interval set between 0.88 and 1 for each bootstrap repetition. We obtained 10 allegiance matrices by bootstrap. To obtain only one matrix by bootstrap we calculate the number of time that two structures were in the same community divided by the number of times the algorithm iterated (*i.e.*, mean of the 10 allegiance matrices). That process gave us a unique probability map for each bootstrap repetition. Over the 500 bootstraps, we calculated the average probability for two structures to be in the same community, across all pair in the network. The final allegiance matrix indicates the probability for each pair of structures to be in the same community (see **Figure 52** for the allegiance workflow).

The allegiance matrix also displays modules, which allows us to extract the communities on this matrix and studying which structures may activate in a functionally coordinated manner. This calculation highlights a high synchronicity, a high functional connection in between the structures of a same community.

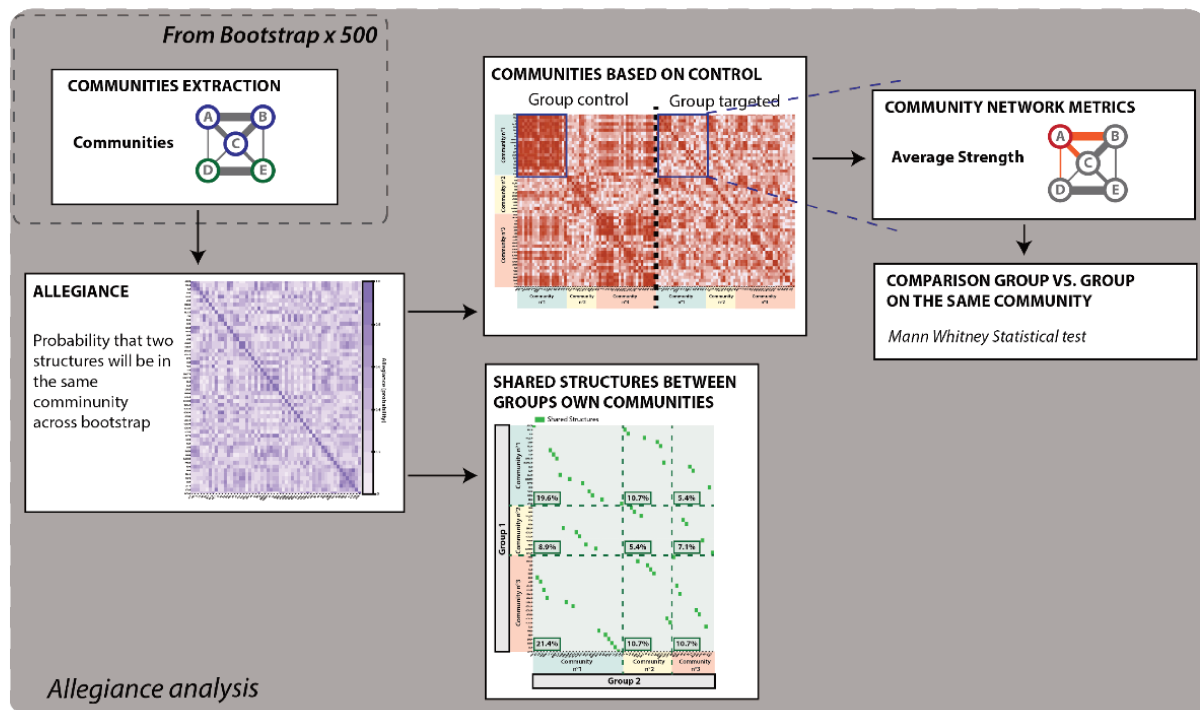


Figure 52: Workflow of the allegiance analysis

For the communities extracted during the bootstrap iterations, we calculated the probability of two structures to be in the same community (allegiance). From the allegiance matrix, we evaluated the communities based on control and the structures of each community, which are shared by the groups.

Group Comparison of Communities Based on the Control group

We were interested in exploring the effect of CNO itself, due to possible side-effects and the consequence of LHb inactivation compared to the naïve network (Ctl-Veh). For this purpose, we extracted the communities of the Ctl-Veh group and calculated the average strength for the structures of each community. We also calculated the average strength in the two other groups (Ctl-CNO and hM4-CNO), still based on communities from the Ctl-Veh group. Given that there are the same structures in the communities of each group, we could compare them using the Wilcoxon-Mann-Whitney non-parametric test. This statistic approach tests the hypothesis that the two medians of each group are close to each other, meaning that there are no differences between the groups. We separately tested the same community for each group. For example, community 1 of the Ctl-Veh group against community 1 of the hM4-CNO group. Cross-community comparisons were not possible because the different communities did not include exactly the same structures. Then, it was relevant to demonstrate the possible differences between the Ctl-CNO and the hM4-CNO in order to figure out if data from the hM4-CNO group were not the sole

MATERIALS AND METHODS - Statistical analysis

consequence of the effect of CNO itself. Therefore, we did the same analysis comparing these two groups based on the Ctl-CNO communities.

Comparison of structures shared between groups

Another way to compare the communities was to identify shared or divergent community memberships of different structures across groups. For this purpose, we created a matrix representing the structures belonging to the between-groups intersection between every possible pair of communities (*contingency matrix*). Noteworthy, communities are numbered in an arbitrary manner by the algorithm for their extraction, so that there is no reason that the k-th community extracted in a group corresponds to the k-th community extracted from the other group (e.g., the community number 1 in group 1 could be equivalent to the community 3 of group 2). Moreover, this type of comparison may give some insight regarding which process or subprocess might be affected by CNO and/or LHb inactivation.

We calculated the Jaccard index gauging the similarity and the diversity between pairs of communities, as follows:

$$J(A, B) = \frac{A \cap B}{A \cup B}$$

where $J(A, B)$ represents the Jaccard index of the set A and the set B (in our case communities A and B), $A \cap B$ is the intersect between A and B (or the number of structures shared between two communities) and $A \cup B$ represent the union of both sets (or the total number of structures in both communities).

IX. Local Field Potential Recordings and Processing (study 3)

1. Recording system and data processing

a. Recording system

All recordings were made within a Faraday cage, directly connected to the ground of the recording system, in order to avoid, or at least minimize, contamination of the signals by 50 Hz oscillations coming from room lights or from other sources, in the room or in adjacent rooms. A preamplifier (16 channels, amplification by a factor 10; AD instruments, UK) is connected to the EIB-16, was fixed to the head-cap with UV glue and dental cement, so that it was not removed for the entire duration of the experiment (see above [Surgery part page 82](#)). The recording system (Alpha Omega GmbH, Ubstadt-Weihe, Germany; see [Figure 53](#)) is composed of a Head Stage (HS), a Signal Integration Unit (SIU) and a Main processing Unit (MPU). The HS (4 x 16 channels) handles the acquisition and digitalization of the signal, the basic hardware filtering (Hardware High Pass Filter: 0.5 Hz; Hardware Low Pass Filter: 8.0 kHz) and has a gain factor of 20. The SIU is mainly responsible for the stimulation waveform generation (which is not use in our study) and offers a two-way digital communication with the MPU. The MPU communicates with the computer through 1Gb Ethernet connection and handles the digital processing (including filtering, segmentation, and down-sampling), the acquisition or emission of the general-purpose digital and analog inputs and outputs, the script processing, and supplies power to all other components of the system. The recorded signal is amplified by a factor 200 in total and is filtered (hardware minimum) from 0.5Hz to 8kHz. The signal is digitalized at a sampling rate of 1375 Hz. Electrode impedance was checked before the start of each recording session; we obtained impedances from ~50k Ω to ~200k Ω at 1kHz.

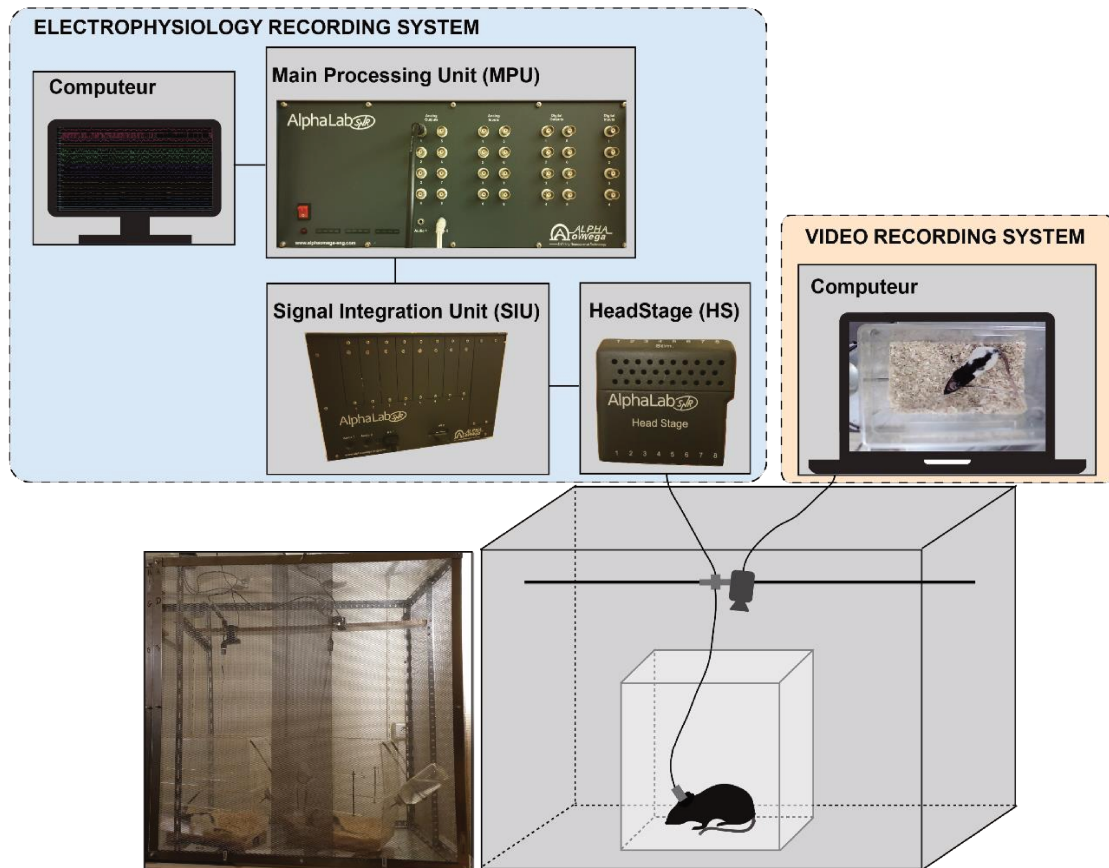


Figure 53: Electrophysiology and video recording systems

Representation of the AlphaLab electrophysiology recording system (with illustrating pictures). The electrophysiological signals pass through the HeadStage, the Signal integration unit and then the Main processing unit, which is connected to a computer. For video recording, the web cam is directly connected to a second computer to record and store the videos.

b. Video recording system

One webcam was placed above the center of each cage. It was connected, by a USB port, to a computer different than the one used to acquire the electrophysiological signals. The video was recorded via a free and open-source software (Open Broadcaster Software 25.0.1; <https://obsproject.com/fr>). Videos were recorded in FLV format (Flash Video format, rendering a high video quality) with the following features: 1280 x 720p, with an image ratio of 16/9 and a frame rate of 30 images by second.

c. Computer hardware for data processing

For video tracking analyses and electrophysiological signal analyses, we used a computer with 2 processors (CPU, Intel® Xeon® Bronze 3106 CPU @ 1.70GHz) allowing a parallel processing of electrophysiological data, 32 Gb of RAM (random access memory) and graphic card (GPU;

NVIDIA® GeForce RTX 2080 Ti), used for a quick learning of the DLC model (Nath et al., 2019) used for video tracking purpose.

2. Processing and analysis of the video recordings

First, we preprocess the videos (*i.e.*, changing the format) then the videos were analyzed either manually (see part **Recording and behavioral assessment page 91** for the details of the behavior analysis) with Aion software or automatically using DLC (algorithm of deep learning; see part **Deep Learning Tool for Video Tracking (study 3) page 73** for the introduction of deep learning algorithm and DLC). This part of the manuscript will quickly explain the preprocessing done on the videos and then details the parameters of DLC used during the study.

a. Preprocessing of the videos

Videos were formatted, using Format Factory software (Freeware, Free Time), in MP4 (MPEG-4 Part 14) which allows a wider compatibility software than the initial format and decreases the size of the files.

b. Automatic Video Tracking using Deep Learning Approach

From the recorded videos, in order to automatically track the animals' position during the different sessions of our protocol, we used a Deep Learning algorithm called DLC (see Introduction **Deep Learning Tool for Video Tracking (study 3) page 73** for more details; version: 2.2) developed by Mathis group (Mathis et al., 2018a; Nath et al., 2019). This approach allowed us to extract the movement of the animals, which was essential to determine, in combination with the electrophysiological data, the different sleep/wake stages. All the DLC parameters were chose to lead to the best accuracy (see **Annexes part Setting DeepLabCut and checking results page 147**).

DeepLabCut algorithm application on our data

We used DLC to assess the presence or absence of movements of the rats throughout the whole protocol, except during the immobilization stress sessions (see **study 3 page 136 Figure 1** for timeline of the experiment). To do so we defined 14 dots of interest on the rat body: nose; head-

MATERIALS AND METHODS - Local Field Potential Recordings and Processing (study 3)

cap + preamplifier; right and left ears; right and left shoulders; upper, middle, and lower back; right and left hips; distal, medium and caudal parts of the tail (see **Figure 54**).

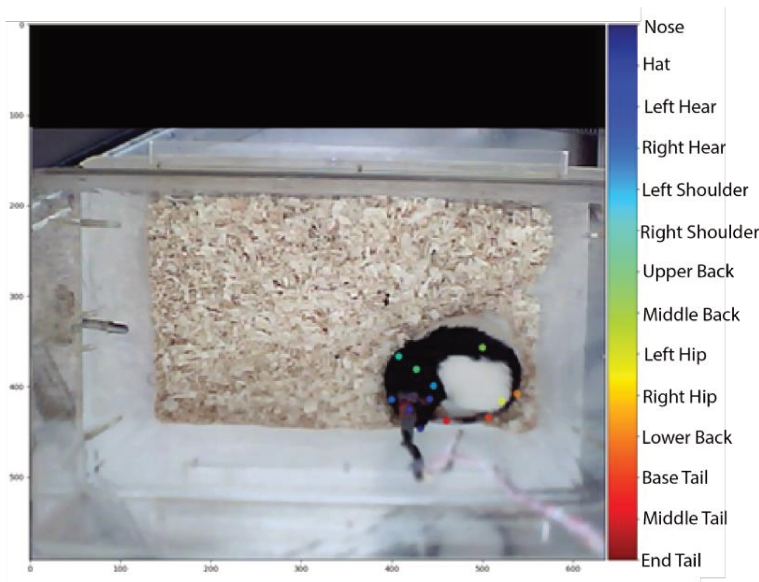


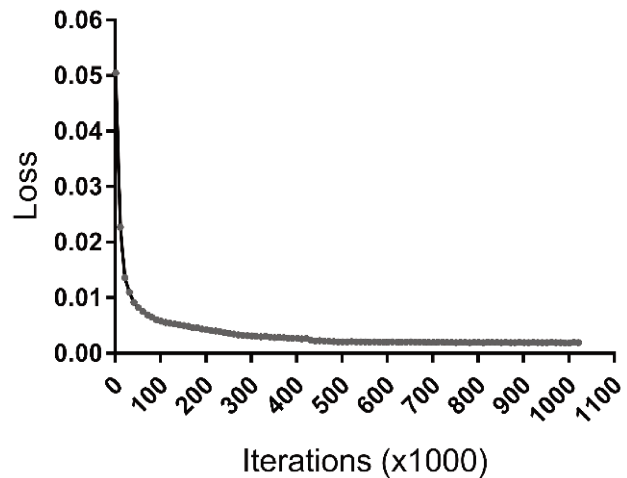
Figure 54: Example of manual labelling of the rat body parts for DLC training.

Each rat's body part is represented by a colored dot and placed manually by the user. 1100 images were labeled as this one, creating the training and testing set of the DLC model.

The training of DLC was performed using 11 videos with 100 images uniformly extracted. For the creation of the training set, we used the pretrained network ResNet152 from ImageNet (<http://www.image-net.org/index> & <https://www.kaggle.com/pytorch/resnet152>). We used `imgaug` (Copyright © 2018 Alexander Jung; <https://github.com/aleju/imgaug-doc>) as image augmenter (recommended by DLC). We used this pre-trained network and this image augmenter based on the comparison we ran on our dataset (see **Annexes part Setting DeepLabCut and checking results page 147**). The training of DLC model ran through 1 030 000 iterations (approximately 24 hours with the computer hardware describe above). This number of iterations potentialized the body part localization after the learning (see **Figure 55**). Potentializing of the learning phase was performed with the loss function, which was used to evaluate and diagnose the model optimization. To train the ResNet pretrained network, it is advised to iterate until the loss is stabilized (loss plateau).

Figure 55: Evaluation of the learning process of DLC

Representative evolution of the loss parameter across the iterations of the learning phase of DLC model. As advised, we obtain the loss plateau suggesting a potential learning phase.



Following the training, the network obtained was evaluated. Basically, the test images and the training images must have a comparable error (mostly due to the human scoring) potentializing the model generation. If the model generation was considered as accurate, then all the videos were analyzed (see [Figure 56](#)). The results extracted by DLC were exported in MultiIndex Pandas Array files (format of data for storing python DataFrame under Pandas library) and in CSV (comma separated values format; readable by Excel©). For each body part to be analyze (dots), DLC gives as result, the x position (on the X-axis), the y position (on the Y-axis) and the probability of the dot to be correctly placed, called likelihood (included between 0 and 1, where 1 means that the dot is correctly placed and 0 means that the dot is not correctly placed). With DLC, we were also able to analyze a predefined skeleton (vector / line connecting the different dots / body parts). The result is the position and the orientation of vector analyzed.



Figure 56: Example of DLC learnt labeling.

The image represents the location of the points labeling each body part placed by DLC algorithm after the training phase. On the image, the five previous locations of each body part are marked inferring the movement of the rat. If the rat moves quickly, for a given body part the different colored dot will be far from each other (Quick Motion), if not, they will be very close (Slow Motion) as this image shows.

Once the analyses of the videos are done, DLC offers the possibility to filter the results. Filtering the results allows to remove the “artifacts” or outliers (*i.e.*, the points which are cannot physically exist). For example, if the nose of the rat is within the left side of the cage in a certain image, and then within the opposite side of the cage in the next image, and then back at the first location in the following image, so that it is very likely that the dot representing the nose in the second image is not where the nose of the rat really was located. The filter will bypass the second image by estimating where the dot should have been (depending on the filter type). There are different types of filters included in DLC. In our study, we filtered the data using the median filter (see [Annexes part Setting DeepLabCut and checking results page 147](#) for the method to choose the type of filter to apply) to remove the outliers.

Movement extraction from DLC coordinates

We estimated the motionness (whether a rat was moving or not) across time. This estimation appeared useful for sleep stages evaluation, and more precisely to distinguish AW and REM sleep phases which both include similar oscillatory patterns in PFC and HPC. To assess the motionness of the rats, we used a Python home-made script. We used only the dots placed on the head of the animal coordinate from DLC because it was more precise for sleep assessment. The first step was to extract the distance between one frame to the next as:

$$dist = \sqrt{(x_b - x_a)^2 + (y_b - y_a)^2}$$

where a is the dot of the current frame, b is the dot of the next frame, x is the X-axis coordinate and y is the Y-axis coordinate.

For each pair of consecutive images, the distance between the dots was stored. Knowing that two images were separated by 1/30 second, we could deduce the motionness. Then a threshold was applied to decide if the rat was moving or not. The threshold was set as 98.5 of the quantiles of the distribution distance. At a given time, if the distance was higher than the threshold, the value was set at 1 (= moving), and if the distance was lower than the threshold, the value was set at 0 (= not moving). To reduce the possibility to make errors in case dot coordinates were not accurate, and to make a final illustration of the dot per second, instead of per 1/30 second, we calculated the mean of the value by second applying the likelihood as coefficient for each value. This allowed to increase the influence of the accurate dots and lower the influence of the non-accurate dots. Following this calculation, if at a particular time the activity of the rat was marked as “1”, it meant that the rat was moving, and if it was marked as “0” meant that the rat was not moving.

3. Electrophysiological signal processing

The analyses of LFP signals were done with MATLAB (MathWorks®, Natick, Massachusetts, United States, R2020b, 9.9.0.1467703). Because it is imposed by the recording system, the data recorded were stored in files containing 10 min of recording (approximately 103280 KB) in the specific format of the Alpha Omega GmbH system (MPX, Alpha Omega proprietary binary format). We used a software developed by the electrophysiology system company Alpha Omega to transform the initial format MPX into MAT (MATLAB data file).

a. Preprocessing

The preprocessing stage was performed using a homemade GUI (graphical user interface) based on MATLAB (see [Figure 57](#)). This interface allows users to check the signal of the three channels of each structure and to select the channels without artifacts in order to do the local referencing (see below).

MATERIALS AND METHODS - Local Field Potential Recordings and Processing (study 3)

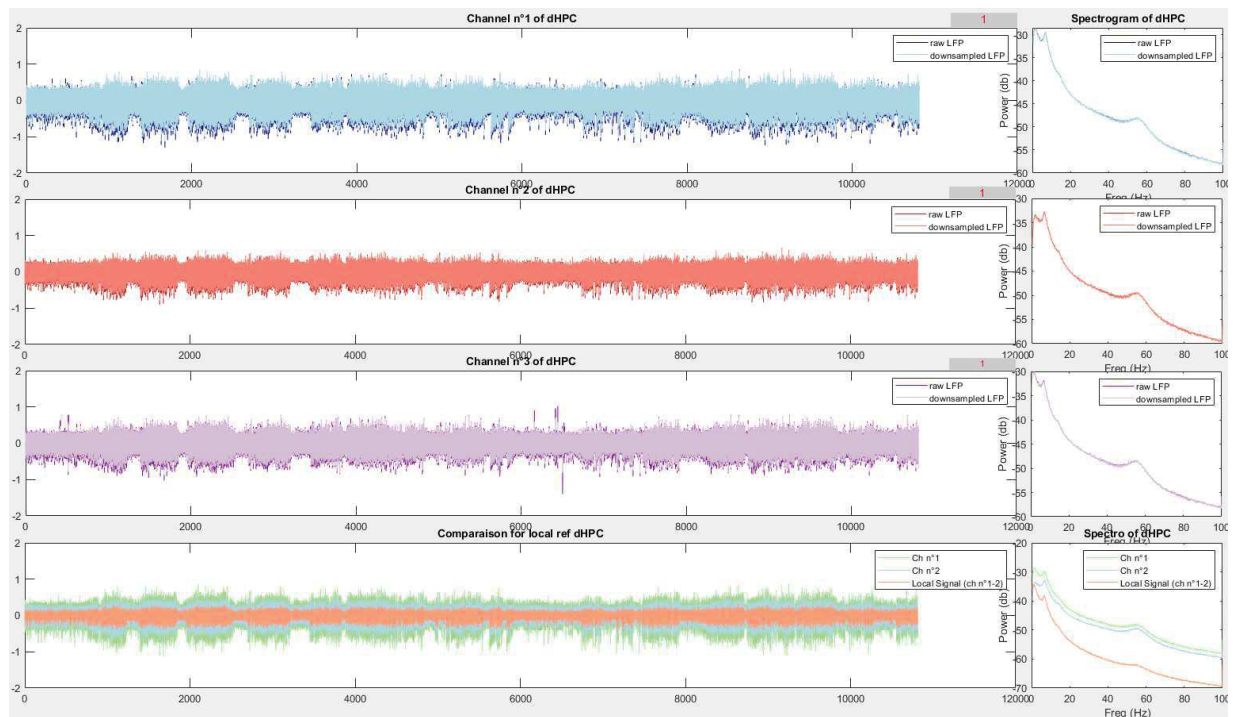


Figure 57: Plot of the preprocessing GUI

This GUI allows to display the three hours of recording for the three channels of the same structure on a single screen (first three plots in the left; represented on mV by second) accompanied with their spectrogram (calculate with Chronux; see below; first three plots on the right; represented in power – dB- by frequency -Hz-). The GUI allows also to select the best quality channel to calculate the local reference (the two last plots at the bottom of the figure).

Whereas stress 1 and stress 2 sessions were 10-min long so that they were included in only one recorded file, for each other session of the protocol (*i.e.*, habituation 1, 2 and 3; baseline prior to stress1; post-stress1; post-stress2), all 10-min files included in the session were concatenated. Then, LFP values (stored in bit) were converted to mV as follows:

$$LFP_{mV} = \frac{LFP_{bit} \times Res_{bit}}{gain} \times \frac{1}{1000}$$

where LFP_{mV} is the potential recorded in mV, LFP_{bit} is the potential recorded in bit, Res_{bit} is the bit resolution (38.1470), $gain$ is the gain of the system (200).

Then, the signals were filtered (MATLAB function `filtfilt()`; zero phase digital filtering; high pass: 0.5 & low pass: 500) and down-sampled (by 5, transforming the sample rate from 1375 Hz to 275 Hz). We planned to analyze the frequencies ranging from 0.5 Hz to 100 Hz. Based on the Nyquist frequency (which states the requirement to have a sampling rate at least two times higher than the maximum of the frequency analyzed), a sampling rate of 275 Hz appeared to be enough to analyze the oscillatory frequencies available in our samples (up to 100 Hz). For the second

experiment, we performed a CSD (limiting the portion of the signal which is volume-conducted from a distant source; [Nicholson and Freeman, 1975](#)) as follows:

$$CSD = -\left(\frac{LFP_{ch3} - 2LFP_{ch2} + LFP_{ch1}}{spacing^2 \times cond}\right)$$

where *CSD* is the current source density in Ampere, *LFP* is the LFP signal, recorded in Volt, from the shortest electrodes (ch1), the medium electrode (ch2) and the longest electrode (ch3), *spacing* is the distance between electrodes in Meters, and *cond* is the conductivity of extracellular medium (0.3 S.m⁻¹).

For the same purpose, during the second experience we performed a local referencing (channel 1 – channel 2). We selected the channels with the best signal based on the display of the signal itself and on a spectrogram representation (done with a MATLAB toolbox Chronux; see later [page 129](#)).

b. Assessment of Sleep/Wake Stages

The sleep/wake stages assessment was also performed using a homemade GUI (see [Figure 58](#)). This interface displays the spectrogram of the signal by hour for the dCA1 and the PRL. It also displays two ratios based on the delta band (0.5 Hz – 3 Hz), the theta band (5 Hz – 12 Hz), and the gamma band (30 Hz – 100 Hz): theta/delta ratio in dCA1 and delta/gamma ratio in the PRL. To distinguish between AW and REM sleep - both including fast activity of low amplitude in PRL and theta in dCA1 - we needed to know if the animal was moving or not. Normally, studies use the EMG (signal to separate AW and REM sleep. However, the signal from our EMG electrodes was not good enough (problem during surgery) for most of the rat. Therefore, we displayed the EMG signal, when possible, along with DLC scoring. Indeed, thanks to DLC the scoring we were able to score and separate AW and REM sleep with a relatively good accuracy (see [Annexes part Setting DeepLabCut and checking results page 147](#)).

MATERIALS AND METHODS - Local Field Potential Recordings and Processing (study 3)

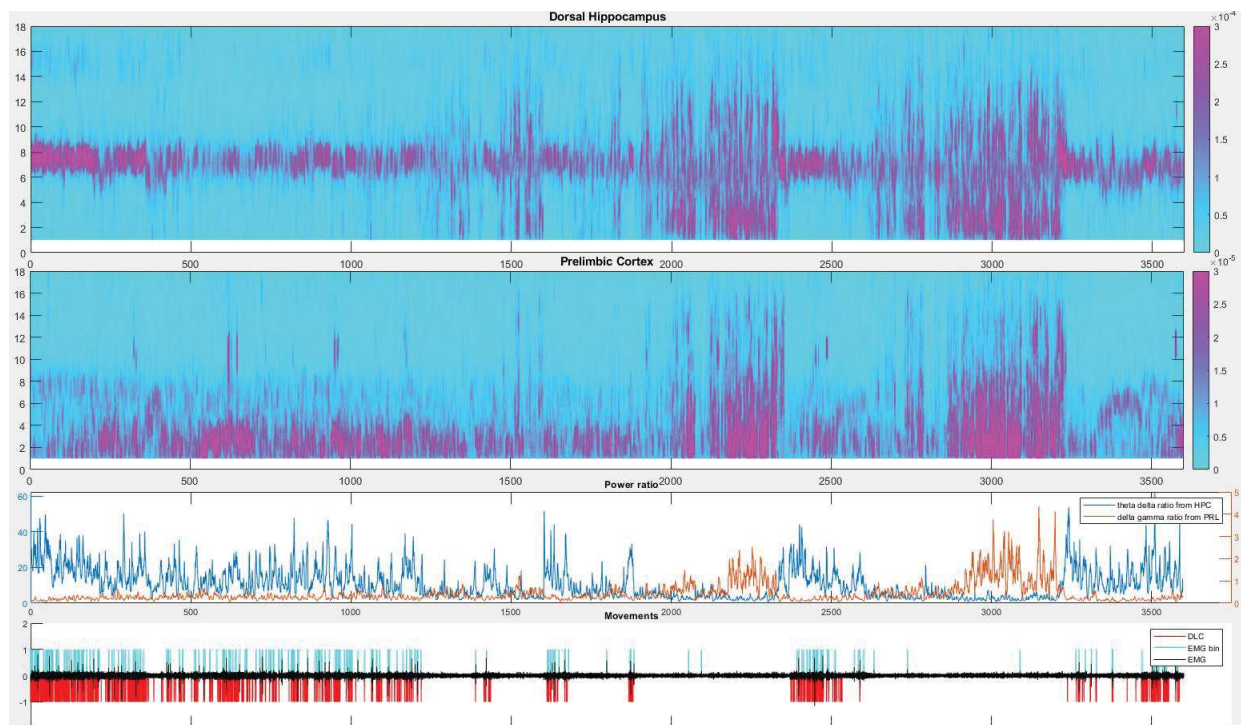


Figure 58: Sleep/wake assessment GUI

The GUI displays the spectrogram of the dHPC (*i.e.*, dCA1) and the PRL by time (1 hour at the time; two upper heatmap); power represented by the colored scale was calculated using Chronux; y axis is the frequency in Hz, and the x axis is the time in s. The third plot represents both ratios: theta-delta frequency band on the dHPC (left y axis) and delta-gamma frequency band on the PRL (right y axis) by time in s. The last plot represents the movement of the animal, either calculated for the EMG (if the quality of the EMG was good enough) or DLC tracking by time in s. In this example, EMG signal was good enough, so we displayed both methods (EMG and DLC).

The scoring was performed manually based on the spectrograms by marking the times when the different stages began and ended, to then create a hypnogram; see [Figure 59](#)). We considered four different stages: **active wake (AW)**, **quiet (calm) wake (CW)**, **slow wave sleep (SWS)**, and **rapid eyes movement sleep (REM sleep)**. AW, as well as REM sleep, are characterized by a high theta power in the dHPC and a high gamma power in the PRL. The presence (AW) or absence (REM sleep) of movements of the animals further separated both stages. SWS is characterized by cortical delta (slow) waves of high power. We defined as CW all other portions of the signal not corresponding to the above-mentioned characteristics. We partitioned the signal so that we could store the different stages separately and saved the results. However, some rats, for a given session, were excluded because the signal was of a bad quality so that we could not assess the sleep/wake stages.

MATERIALS AND METHODS - Local Field Potential Recordings and Processing (study 3)

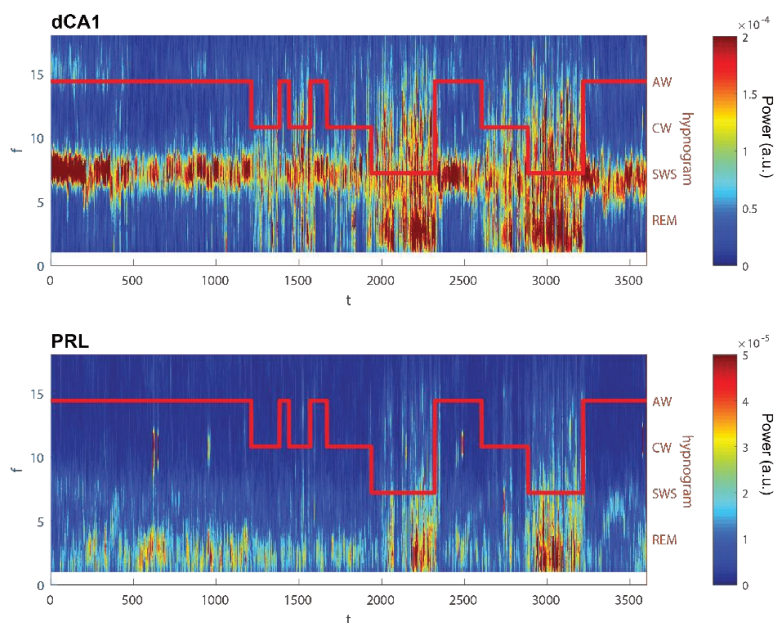


Figure 59: Result of the sleep/wake stages assessment

Spectrograms representing the power [color code on the right, from very low (blue) to very high (red)] of the oscillation frequencies (Y axis, from 0 to 20 Hz) across time (X axis in sec). The two spectrograms (dCA1 at the top, PRL at the bottom) from the previous example (Figure 58) are displayed with the manually evaluated hypnogram (right y axis). The hypnogram shows the different wake (active wake, AW; calm wake, CW) and sleep (slow wave sleep, SWS; rapid eyes movement sleep, REM) stages. In this example, the animal did not do episode of REM sleep during the evaluated hour.

Based on the hypnogram, we also analyzed, for all the different sessions of our protocol, several variables concerning sleep stages: the latency to first enter each stage; the number of occurrences of each stage; the total time spent in each stage; the average episode duration in each state. The results were saved in Excel© files.

Due to a high individual variability, we decided to try to cluster the animals on the basis of the few following selected variables scored during the first hour following immobilization 1: the duration of the first AW episode, the time spent rearing, and the time spent in locomotion. We were interested in figuring out what kind of response could be attributed to the rats by comparing two particular sessions: the 1-h baseline prior to immobilization 1 and the first hour following immobilization 1. To that purpose for each variable, we calculated the difference between both sessions. To evaluate the main variance of these “new” variables, we performed a PCA using Statistica© (Statsoft, Tulsa, USA). The factor 1 resented 88.5% of the total variance (see [study 3 page 136](#)). We further clustered the animals using k-mean algorithm (Matlab function) based on the individual values of the factor 1 of the PCA. It gave back 3 clusters: one including animals considered as showing a high level of activity following immobilization 1 (*high responders*), one including animals considered as showing a low level of activity following immobilization 1 (*low responders*), and one including animals that we considered had a peculiar “opposite” response to what was expected, as they were more active during baseline than following immobilization 1; *opposite responders*).

c. Removing the artefacts of the signal

Following the assessment of the sleep/wake stages we passed the data into another GUI in order, if necessary, to “clean” the signals (*i.e.*, removal of the artefacts, see [Figure 60](#)). This GUI allowed to remove these artefacts either automatically or manually.

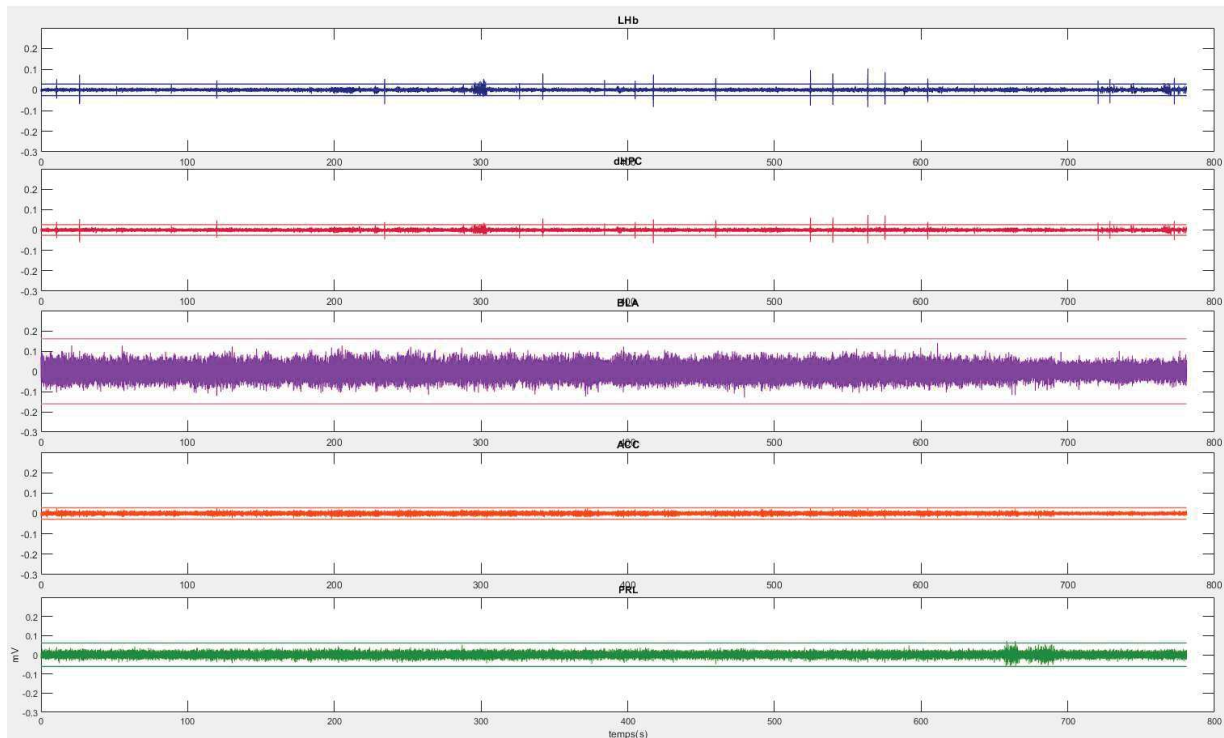


Figure 60: Artefact removal GUI

This GUI plots the signal recorded (in mV by seconds) from each structure (LHb, dCA1, BLA, ACC, PRL). The lines above and below each signal represent the threshold of the automatic signal removal (6 sd).

The automatic method acts as follows: first, a threshold is calculated, 6 times the standard deviation, and, subsequently, each part of the signal with an amplitude higher than the threshold is removed. Noteworthy, if an artefact was only present in one of the 5 structures, the part of the signal was removed from all 5 structures, in order to allow a total time correspondence of the signals across all structures (see [Figure 61](#)).

If the manual method could eventually be used in case the threshold failed to accurately delineate the artefacts, it has not been necessary in the present study so that the automatic method only has been used.

MATERIALS AND METHODS - Local Field Potential Recordings and Processing (study 3)

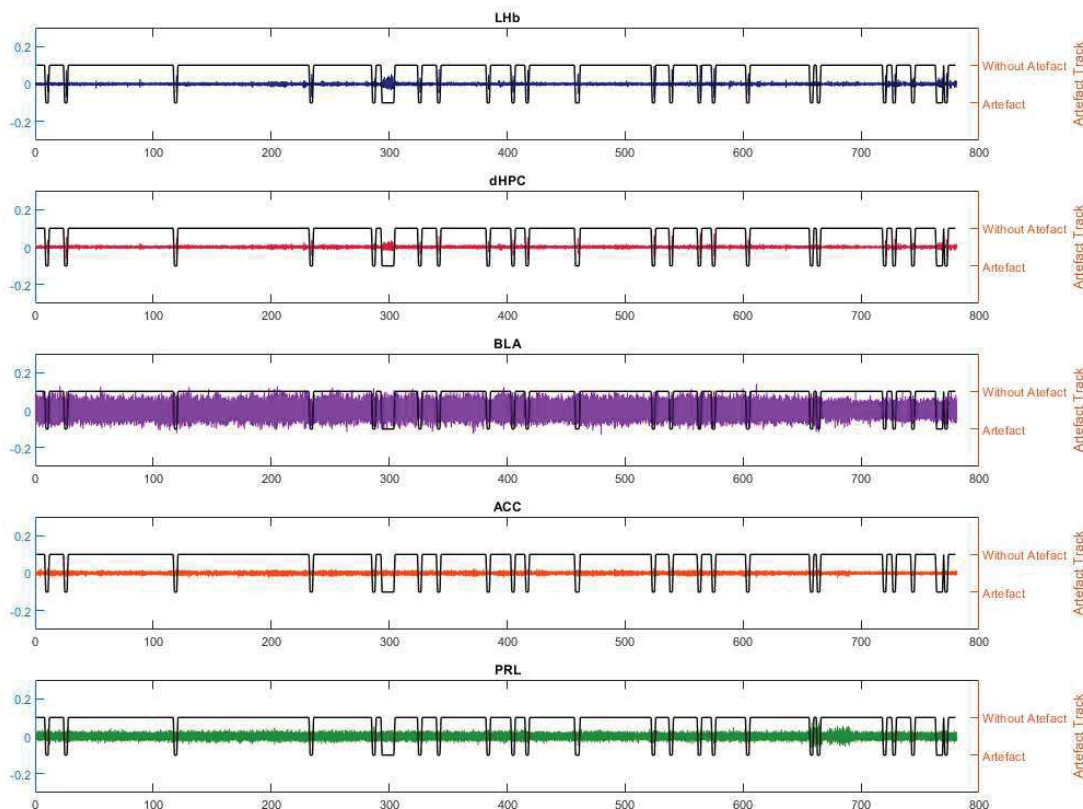


Figure 61: Results of the automatic artefact removal

The signals (in mV by seconds) of the five recorded structures are represented with, superimposed to each of them, what we called the artefact track (right y axis), marking the positions where the signal should be removed (when it is equal to “Artefact”). For each artefact detected, in addition we removed one second before and one second after the point of detections allowing to be sure enough that the entire artefact has been removed.

d. Frequency and time domain frequency analyses

Frequency and time domain frequency analyses were used to evaluate, in each session of our protocol, the different frequencies of the oscillations, as well as their amplitude and phase. For the comparison of the different sessions power, we used the clusters. We also evaluated the frequencies during both immobilization periods. However, the signal could not be separated according to different stages, such as during baseline or post-immobilization periods, as the animals were doing only AW during the 10 min of immobilization. Therefore, because we did not need to separate the sleep/wake stages, the power and the coherency of the oscillations were given directly following the preprocessing.

Chronux FFT

We used the Fast Fourier Transform (FFT) from the Chronux toolbox (<http://chronux.org/>) to check the signal in the preprocessing stage of the analysis and for sleep/wake stages assessment. The

MATERIALS AND METHODS - Local Field Potential Recordings and Processing (study 3)

FFT is pretty quick to run but it needs the assumption that the data are stationary (*i.e.*, mean, variance and frequency composition are not changing over time), which is not really respected in our samples even if we can assume the stationarity on short windows of time. Therefore, we used the Chronux FFT for signal checking in preprocessing stage and for sleep/wake assessment because the algorithm is rapid and the sliding windows and tapers parameters of the Chronux algorithm allow to estimate the stationary status of the signal. We also used the time domain analysis based on FFT, working on a sliding window (5-s windows moving across 0.3 s) and tapers ($k = 9$; $nw = (k+1)/2$; $[nw \ k]$). We analyzed the frequency between 0.5 Hz and 100 Hz in both cases. For the assessment of sleep/wake stages, we also used the Chronux toolbox to calculate the different ratios (*i.e.*, theta-delta ratio in dCA1 and delta-gamma ratio in PRL). These two ratios have been used in the literature to help separating the different sleep/wake stages and, more particularly, to distinguish AW from REM sleep (see [Introduction page 4](#)). For these two ratios, the frequency bands were arbitrary defined as follows: delta: 1 Hz to 3 Hz; theta: 5 Hz to 12 Hz; gamma: 30 Hz to 100 Hz.

Morlet wavelets

Following the global analysis of sleep/wake data, we studied the frequency power (the square of the amplitude) of the different stages (AW, CW, SWS, REM) during each session of the protocol by periods of one hour. We used MATLAB Complex Morlet wavelet definition: $cmor2-Fb-Fc$ where Fb is the bandwidth parameter and Fc is the wavelet center frequency (in our case: $cmor2-0.7958$).

To use the wavelet, transform, we defined a frequency scale (*i.e.*, 277 frequencies from 1 to the Nyquist frequency rate $[275 \text{ Hz}]/2 = 137.5 \text{ Hz}$). Then the wavelet transform is calculated by the Matlab function `cwt(LFP, scales, 'cmor2-0.7958')`, and returns the wavelet transform coefficient (*wt*). The amplitude is the absolute value of *wt* and the power is the squared amplitude. The phase is calculated from `angle(wt)` Matlab function which return the angle (in radian) of every complex number in *wt*. The power was transformed from arbitrary unit (a.u.) in decibel (dB) using the following equation:

$$Power_{dB} = 10 \times \log_{10} (Power_{a.u.})$$

where the *Power* is a vector containing the power values by frequencies.

After evaluating the spectrogram obtained (*i.e.*, the frequency bands present), we considered three bands of frequency: delta, 1 Hz to 3 Hz; theta, 5 Hz to 9 Hz; gamma, 45 Hz to 65 Hz). These frequency bands were defined based on the frequency bands present in the spectrogram (or

MATERIALS AND METHODS - Local Field Potential Recordings and Processing (study 3)

mostly present in the spectrogram, see **Figure 62**) depending on the structures and the sleep/wake stage (e.g., no theta band was observed in dCA1 during SWS). For the results by bands of interest, we normalized the power of a given session by the Baseline session (e.g., PS1[AW] – BL[AW] by structures and by rats) in order to reduce inter-individual variations.

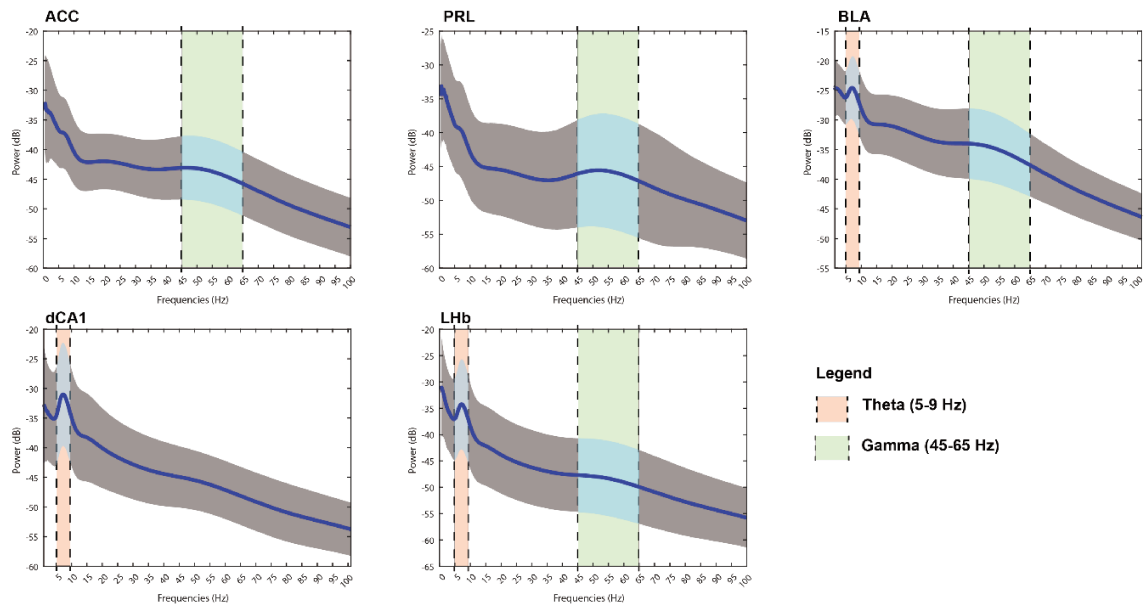


Figure 62: Example of frequency bands detection

Each spectrogram (power in dB by frequency in Hz) of recorded structures is displayed in this figure during AW stage during the habituation 3 session. This example shows when how considered as actual, or not, the presence of a given oscillation band. We considered the frequency band to be present in the structure only when the spectrogram displayed pics or bumps into the defined bands. For instance, we detected the gamma band present in the ACC (bump in between 45Hz and 65Hz), whereas no gamma band was detected in the dCA1 during this session.

e. Connectivity analysis

We wanted to address the question of the potential communication between the different structures we recorded. In electrophysiology, the common way to address that is to perform coherence analysis. If two signals are coherent at the same frequency band, we can analyze their phase locking value, giving clues on the directionality of the communication (*i.e.*, which structure is sending the information to the other). We analyze the coherence between all the structures for each session and each stage. We also analyzed the coherence of the signals during the two immobilization sessions.

Coherence Chronux

Coherence analyses between all recorded structures (PRL, ACC, dCA1, BLA, LHb) led to ten possible comparisons. Coherence was evaluated using the Chronux toolbox, considering all frequency bands from 1 Hz to 80 Hz. Based on the coherogram obtained, we selected, such as we did for power analyses, three frequency bands: delta, 1 Hz to 3 Hz; theta, 5 Hz to 9 Hz; gamma, 45 Hz to 65 Hz. We evaluated the mean of the coherence in these frequency bands for each pair of structures (if the coherence was present in the coherogram). We used the same tapers ($k = 9$; $nw = (k+1)/2$; [nw k]) than for the FFT analysis with Chronux.

Remark: These analyses are still ongoing at the time the manuscript is written, so that the analysis of the coherence across time and other types of analysis we may use (e.g., phase lock value), will not be shown in the manuscript.


RESULTS

RESULTS

I. STUDY 1: Involvement of the Lateral Habenula in Fear Memory



Involvement of the lateral habenula in fear memory

Laura Durieux¹ · Victor Mathis^{1,2} · Karine Herbeaux¹ · Marc–Antoine Muller¹ · Alexandra Barbelivien¹ · Chantal Mathis¹ · Rémy Schlichter³ · Sylvain Hugel³ · Monique Majchrzak¹ · Lucas Lecourtier¹ 

Received: 24 December 2019 / Accepted: 16 June 2020
© Springer-Verlag GmbH Germany, part of Springer Nature 2020

Abstract

Increasing evidence points to the engagement of the lateral habenula (LHb) in the selection of appropriate behavioral responses in aversive situations. However, very few data have been gathered with respect to its role in fear memory formation, especially in learning paradigms in which brain areas involved in cognitive processes like the hippocampus (HPC) and the medial prefrontal cortex (mPFC) are required. A paradigm of this sort is trace fear conditioning, in which an aversive event is preceded by a discrete stimulus, generally a tone, but without the close temporal contiguity allowing for their association based on amygdala-dependent information processing. In a first experiment, we analyzed cellular activations (c-Fos expression) induced by trace fear conditioning in subregions of the habenular complex, HPC, mPFC and amygdala using a factorial analysis to unravel functional networks through correlational analysis of data. This analysis suggested that distinct LHb subregions engaged in different aspects of conditioning, e.g. associative processes and onset of fear responses. In a second experiment, we performed chemogenetic LHb inactivation during the conditioning phase of the trace fear conditioning paradigm and subsequently assessed contextual and tone fear memories. Whereas LHb inactivation did not modify rat's behavior during conditioning, it induced contextual memory deficits and enhanced fear to the tone. These results demonstrate the involvement of the LHb in fear memory. They further suggest that the LHb is engaged in learning about threatening environments through the selection of relevant information predictive of a danger.

Keywords Amygdala · Hippocampus · Prefrontal cortex · c-fos · Chemogenetic · Context

Laura Durieux, Victor Mathis, Sylvain Hugel, Monique Majchrzak and Lucas Lecourtier equally contributed to this study.

Electronic supplementary material The online version of this article (<https://doi.org/10.1007/s00429-020-02107-5>) contains supplementary material, which is available to authorized users.

✉ Monique Majchrzak
majchrzak@unistra.fr

✉ Lucas Lecourtier
l.lecourtier@unistra.fr

- ¹ Université de Strasbourg, Centre National de La Recherche Scientifique, Laboratoire de Neurosciences Cognitives Et Adaptatives (LNCA), UMR 7364, 12 rue Goethe, 67000 Strasbourg, France
- ² Present Address: Department of Neuroscience, Icahn School of Medicine at Mount Sinai, NY 10029–6574, USA
- ³ Institut des Neurosciences Cellulaires et Intégratives (INCI), UPR 3212, CNRS, 8 Allée du Général Rouvillois, 67000 Strasbourg, France

Introduction

The lateral habenula (LHb) plays a key role in the integration of basal ganglia and forebrain limbic information. It is implicated in functions such as reward prediction error, coding of negative motivational value, spatial memory, and subjective decision biases (Matsumoto and Hikosaka 2009; Stamatakis and Stuber 2012; Stopper and Floresco 2014; Mathis et al. 2015, 2018; Baker and Mizumori 2017). One of the main roles of the LHb is to process stressful situations (Stamatakis and Stuber 2012; Amo et al. 2014; Hennigan et al. 2015; Chou et al. 2016). LHb activation has been reported following stressful experiences such as electrical footshocks, immobilization, and tail pinch (Chastrette et al. 1991; Wirtshafter et al. 1994; Cullinan et al. 1995). Moreover, the LHb is a main afferent of the rostromedial tegmental nucleus (RMTg), a modulator of the activity of dopamine (DA) neurons, a structure also activated following repeated foot-shock delivery (Sanchez-Catalan et al. 2017; Li et al. 2019a, b). In addition, activation of afferent pathways to the LHb, from

the globus pallidus, the ventral tegmental area (VTA) or the lateral hypothalamus (LH), promote avoidance behaviors (Lammel et al. 2012; Root et al. 2014; Lecca et al. 2017), whereas silencing of the LH–LHb pathway impairs escape behavior (Lecca et al. 2017). Altogether, these data indicate that the LHb plays a prominent role in the behavioral adaptation to aversive situations. LHb neurons were also reported to progressively increase their activity during the presentation of a conditioned stimulus (CS) that precedes footshock delivery (unconditioned stimulus, US) during avoidance learning (Trusel et al. 2019) and Pavlovian fear conditioning (Wang et al. 2017), while maintaining US responding, suggesting it is involved in the encoding of the predictive relationship between the CS and the US. However, only few studies (Wang et al. 2013; Song et al. 2017; Barrett and Gonzalez-Lima 2018) shed light on its contribution to Pavlovian fear memory. Such a contribution can also be expected given that in rodents the LHb is directly or indirectly connected with the main structures involved in fear conditioning, i.e., the medial prefrontal cortex (mPFC), the amygdala, and the hippocampus (HPC). If contextual fear learning is sensitive to hippocampal manipulation, fear learning to a discrete CS only requires the HPC during trace fear conditioning paradigms, when the CS and the US are separated by an empty temporal interval named the trace interval (Misane et al. 2005; Chowdhury et al. 2005; Esclassan et al. 2009). Importantly, the mPFC is also required for trace conditioning (Gilmartin and Helmstetter 2010; Guimaraes et al. 2011; Gilmartin et al. 2013) as well as for contextual fear learning (Gilmartin and Helmstetter 2010). Anatomically, the LHb receives direct projections from several subregions of the mPFC (Kim and Lee 2012); recently, a connection with the amygdala has been described in mice (Kim and Han 2016; Zhou et al. 2019), although other anatomical investigations fail to report it (e.g. Zahm and Root 2017), so this needs to be confirmed in the Rat. Although the LHb and dorsal HPC (dHPC) are not directly connected, electrophysiological recordings in the head-restrained as well as in behaving rats, demonstrated coherent activity between these two structures (Aizawa et al. 2012; Goutagny et al. 2013), strongly suggesting they exchange information. These findings, along with the known role of the LHb in HPC-dependent spatial memory (Goutagny et al. 2013; Mathis et al. 2015, 2018) and in mPFC-dependent working memory (Mathis et al. 2016), suggest that the LHb could contribute to both CS trace and contextual fear learning. To test this hypothesis, we used a trace conditioning protocol with a trace interval (30 s) long enough to allow fear conditioning to both the context and the tone (Detert et al. 2008). In a first experiment, we questioned whether the LHb was part of the network sustaining trace fear conditioning acquisition by quantifying the expression of the c-Fos protein in the habenular complex, the HPC, the mPFC, and the amygdala; we analyzed the presence of

co-activation among these structures using a factorial analysis design. In a second experiment we used a chemogenetic approach, with a modified muscarinic hM4(Gi) receptor, to perform LHb inhibition during conditioning and assessed its effects on fear elicited by re-exposure to the context and to the CS. In addition, we studied in the same rats the effects of LHb chemogenetic inactivation on plus-maze behaviors and home cage locomotor activity, both previously shown to be sensitive to LHb inactivation (Mathis et al. 2015).

Materials and methods

Animals

This study, authorized by the French authorities (APAFIS#7114), required 66 male Long–Evans rats (250–350 g; Janvier Labs, France). They were housed in pairs on a 12 h light/dark cycle (lights on at 7:00 A.M.) with ad libitum access to food and water, controlled temperature (~23 °C), and a hygrometry of about 55%. Animals were distributed as follows: experiment 1: c-Fos study ($n = 18$); experiment 2: electrophysiological validation of the DRE-ADD technique ($n = 4$) and behavioral study ($n = 44$). Testing took place between 9:30 am. and 2 pm.

Fear conditioning

Four conditioning chambers (25 cm x 27 cm x 18 cm) located in a lit- (6 lx) and sound-attenuating box (57 cm x 38 cm x 38 cm, Campden Instruments) were used. Chambers were made of transparent plastic with a loud-speaker fitted on one of the sidewalls, a transparent ceiling, and a grid floor (parallel 0.3 cm diameter stainless-steel bars spaced 0.8 cm apart) above a sawdust tray. A camera (MCT-210 MS, OptoVision, Toulouse, France) was fitted inside each box, above the center of the chamber, and monitored the entire chamber from the top through a 2.45 mm-wide angle lens. These chambers were used as conditioning context whereas triangular plexiglass boxes with one gray wall, one black and white striped wall, and a smooth white floor could be placed within the chambers and served as a new context. Chambers were cleaned with water between successive rats. Tones and electric shocks were delivered through a computerized interface (Med Associates Inc., St Albans, VT, USA). Fear conditioning (38 min-long session) was conducted as follows: rats were placed in the conditioning chamber and, after a 3 min baseline with no event, received six CS and US presentations (CS: 15 s tone, 4000 Hz, 10 dB above background; US: 0.5 mA before scrambling, 0.8 s, through the grid floor) with the US delivered 30 s after CS offset; the 6 presentations were made with a 4 min 20 ± 26 s intertrial interval. The automatic measurements of freezing

behavior, defined as the suppression of all visible movements except those needed for breathing –and used as a measure of fear–, were performed as previously described (Marchand et al. 2003). A set of procedures written under Excel® Visual Basic®, allowed the computation of the percentage of time spent freezing over blocks of selected duration.

Experiment 1. C-Fos expression related to fear conditioning

A schematic representation of the experimental procedure is given in Fig. 1a.

Tissue preparation and section processing

Rats were conditioned as described above (Fear conditioning, FC, condition), or remained in their home cage (HC) to assess baseline c-Fos expression. An additional group of rats was exposed to the conditioning chambers with tones delivered exactly as during conditioning but without applying electric shocks (No shock, NS). Ninety minutes after the beginning of the session, rats were deeply anesthetized with pentobarbital overdose (120 mg/kg, i.p). Following intracardiac perfusion of phosphate-buffered saline (PBS,

0.1 M) and then 4% paraformaldehyde (PFA)-PBS solution (pH 7.4; 4 °C), brains were removed, post-fixed in 4% PFA-PBS (4 °C, 48 h), transferred into a 0.1 M PBS–20% sucrose solution (4° C, 48 h) and subsequently frozen (isopentane, – 40 °C, 1 min). Serial 40 µm-thick free-floating sections were cut in the coronal plane at – 20 °C and collected then stored in cryoprotectant at – 20 °C.

Immunohistochemistry

Sections were first rinsed three times during 10 min in PBS before being soaked for 1 h in 5% normal horse serum in PBS/0.5% Triton X–100. They were subsequently transferred into the primary anti-Fos rabbit polyclonal antibody (1:750, polyclonal rabbit antibodies; SYSY; ref: 226 003, Synaptic System) solution for 20 h at room temperature, and then in a buffer solution containing biotinylated goat anti-rabbit secondary antibody for 1 h (1:500, Biotin-SP-conjugated affiniPure Goat anti-rabbit IgG, ref: BA1000, Vector). Staining was revealed with the avidin–biotin peroxidase method (Vectastain ABC kit, PK 6100; Vector Laboratories, Burlingame, CA, USA). After two PBS and one Tris (0,6%, pH 7,6) 10 min washes, sections were exposed for 8 min to a revelation solution (Kit DAB, SK 4100, Vector Laboratories) containing DAB (3,3'-diaminobenzidine) and H₂O₂

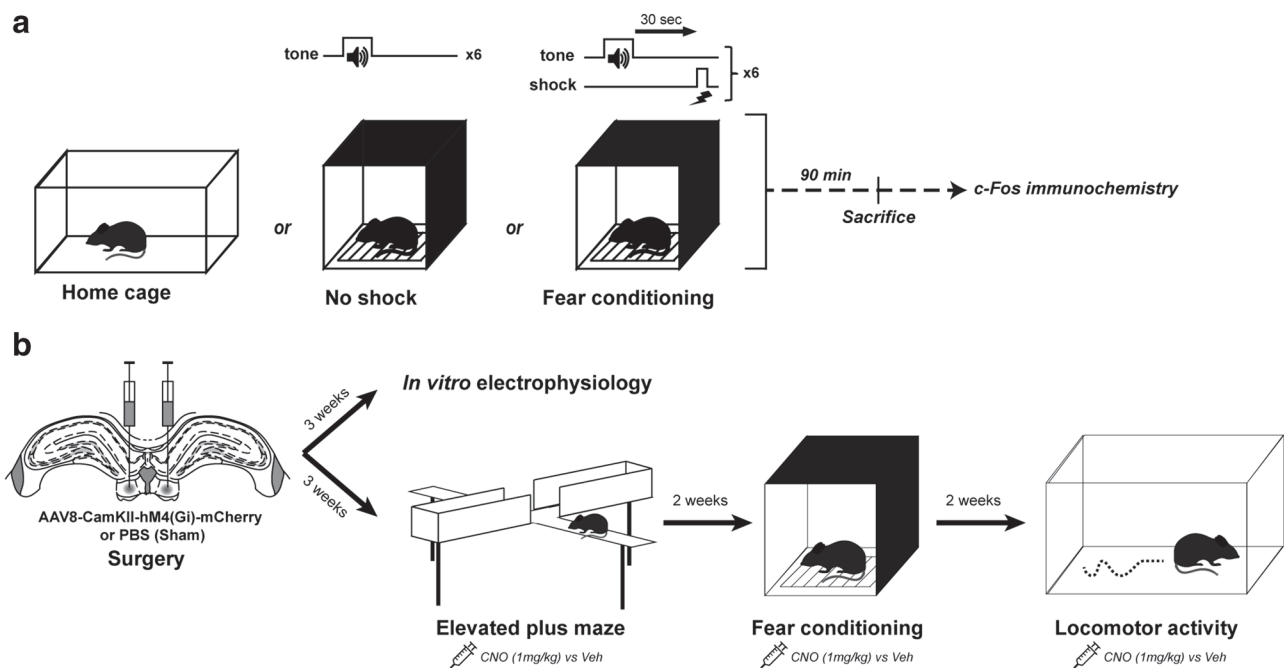


Fig. 1 Schematic representation of the experimental procedure of Experiment 1 (**a**) and Experiment 2 (**b**). **a** Rats exposed to the conditioning session of the trace fear conditioning paradigm (protocol described in Fig. 4a), or to the same procedure without footshocks, were sacrificed 90 min after the start of the session to evaluate c-Fos expression. Home cages rats were used to assess baseline c-Fos

expression. **b** Rats were bilaterally microinjected, within the LHb, with either the viral vector, AAV₈-CamKII-hM4(Gi)-mCherry or PBS as a sham operation. Three weeks later, rats were either used for in vitro electrophysiology experiments or tested first in the elevated plus-maze, then in the fear conditioning paradigm (protocol described in Fig. 4a), before measurement of home cage locomotor activity

(hydrogen peroxide). Sections were then dropped on gelatinated slides, dried for 24 h, dehydrated by incrementally concentrated alcohol baths (70%, 90%, 95%, 100%, 100%), covered with Clearify (Americain MasterTech Scientific), fixed on microscopic slides with Diamount (Diapath S.P.A), and dried for 48 h, protected from light.

Quantification

Quantification of c-Fos+ cells were performed (see Supplementary information and Supplementary Figs 1–6) bilaterally in mPFC [prelimbic (PRL), infralimbic (IL), and anterior cingulate (ACC)], basolateral (BL) and lateral (LA) nuclei of the basolateral complex and central nucleus (CeA) of the amygdala, habenular complex, dorsal and ventral HPC (dHPC and vHPC respectively). The habenular complex was divided into a medial (MHb) subregion, and a lateral (LHb) subregion, the latter being further divided into a lateral (LHbL) and a medial (LHbM) part; in addition, we considered separately the LHb subregion in its most rostral part (rLHb) where LHbL and LHbM do not appear yet according to Paxinos and Watson (Paxinos and Watson 2007). Both the dHPC and vHPC were divided into ammonic fields 1 (CA1) and 3 (CA3), and dentate gyrus (DG). Countings were performed using a semi-automated method with ImageJ (Free License, Wayne Rasband, Research Services Branch, National Institute of Mental Health, Bethesda, Maryland, USA; for more details see Supplementary information and Supplementary Fig. 7) and expressed as mean number of c-Fos positive (c-Fos+) cells by mm². The values of both hemispheres did not differ so that they were pooled (Supplementary Fig. 8).

Factorial analysis

Factorial analysis was conducted using the Statistica software. It was performed to unravel homogeneous functional networks, i.e. regional activities that are consistently correlated in FC and NS groups. The aim of this kind of analyses is to compress a large number of correlations into fewer factors. These factors are created through the computation of the correlation matrix of initial variables, without any prior (hypothesis-driven) input from the experimenter and represent ad hoc variables that show strong correlations with specific clusters of heavily intercorrelated observed variables. In addition to this ability to summarize an overwhelming number of covariations into fewer factors, this analysis is considered a way to unfold the underlying structure organizing these correlations. Applied to functional imaging studies, factorial analysis helps to unravel homogeneous functional networks (i.e. regional activities that are consistently correlated), as previously shown (Veening et al. 2009; Ali et al. 2017). Although this analysis initially extracts a high

number of factors, only a set amount is classically described, as factors show diminishing relevance: they are determined in a series, each new one trying to bind residual correlations that had not yet been explained by preceding factors. The number of factors retained is determined by the observation of each factor's eigenvalue, describing the proportion of total variance that is explained by the adjunction of a supplementary factor relative to initial variables. For instance, an eigenvalue equal to 1 indicates that the corresponding factor explains exactly as much dispersion as one of these variables. To this aim, one of the most widely used criteria is the Guttman–Kaiser's: only factors with eigenvalues superior to 1 are conserved, to keep modeling of raw data from redundancy. When described, factors are associated with factor loadings of each observed variables, which correspond to correlations of the latter with the former, allowing for the description of the computed cluster, these correlations being considered strong above 0.6 or under -0.6 . Computation of factorial analysis was conducted using varimax rotation, which increases discrepancies between these factor loadings on a given factor, thus clarifying the variables critically contributing to this factor's extraction.

Experiment 2. Effects of chemogenetic LHb inactivation on fear memory, anxiety, and locomotor activity

A schematic representation of the experimental procedure is given in Fig. 1b.

Surgery

Rats underwent surgery under isoflurane anesthesia [4% for induction in an induction box (3 min), 1.5% throughout surgery] delivered in O₂. Prior to surgery, they received a painkiller (meloxicam, 1 mg/kg, s.c.). After their head was shaved, rats were secured into a stereotactic apparatus, covered with an aluminum blanket to prevent hypothermia, and lidocaine (0.02 mg in 0.1 ml, s.c.) was injected at the incision location. Following incision, burr holes were drilled above the LHb. AAV8–CamKII–hM4(Gi)–mCherry [Viral Production Unit, Universitat Autònoma de Barcelona (VPU); (Piedra et al. 2015)] or phosphate-buffered saline (PBS) as a Sham operation was bilaterally injected into the LHb, by means of a 33-gauge Hamilton syringe, at the two following locations and volumes: (1) anteroposterior (AP) = -3.3 mm from Bregma, mediolateral (ML) = ± 0.7 mm from the midline of the sagittal sinus, dorsoventral (DV) = -4.5 mm from dura (0.2 μ L); (2) AP = -3.5 mm from Bregma, ML = ± 0.7 mm from the midline of the sagittal sinus, DV = -4.4 mm from dura (0.15 μ L). Among the 44 rats of the behavioral study, 22 were injected with the viral vector

and 22 with PBS. Once the injections terminated the syringe was left in place for 7 min and then slowly removed from the brain, before the skin was stitched. Animals were then placed in cages under a heating lamp until complete awakening. Rats received a second injection of painkiller (meloxicam, 1 mg/kg, s.c.) the following day. After a one week recovery period in individual cages, the same pre-surgery pairs of rats were housed together again. Experiments started three weeks after surgery (Fig. 1b).

In vitro electrophysiological recordings

The efficacy of the chemogenetic strategy was first tested using patch-clamp recordings. Three rats underwent the surgical procedure described above, to express hM4(Gi) receptors within the Lhb, and one rat was used to assess the consequences of Clozapine N-Oxide (CNO) administration on the excitability of Lhb neurons not expressing the hM4(Gi) receptor.

Acute slice preparation

Rats were deeply anesthetized with an i.p. injection of a mixture of ketamine (82.5 mg/kg, Imalgène 1000, Merial) and xylazine (11 mg/kg, Rompun 2%, Bayer). Intracardiac perfusion was performed with 300 ml of cold (0–4 °C) sucrose-based artificial cerebrospinal fluid containing: 248 mM sucrose, 11 mM glucose, 26 mM NaHCO₃, 2 mM KCl, 1.25 mM KH₂PO₄, 2 mM CaCl₂, 1.3 mM MgSO₄, and 2.5 mM kynurenic acid (bubbled with 95% O₂ and 5% CO₂). After 15 min, rats were decapitated, their brain removed and placed in a matrix allowing to split it in two at the level of the longitudinal sulcus and to remove the posterior part using a razor blade. Each brain half was mounted on the vibratome stage (VT1200S; Leica, Nussloch, Germany) by gluing the posterior end, the median plan facing the blade. This allowed us to perform transverse slices (thickness: 300 µm) and to start slicing from the midplane of each brain half. Slices were stored at room temperature in a chamber filled with artificial cerebrospinal fluid (aCSF) containing: 126 mM NaCl, 26 mM NaHCO₃, 2.5 mM KCl, 1.25 mM NaH₂PO₄, 2 mM CaCl₂, 2 mM MgCl₂, and 10 mM glucose (bubbled with 95% O₂ and 5% CO₂; pH=7.3; 310 mOsm measured).

Patch-clamp recordings

Slices were transferred to a recording chamber and continuously superfused with oxygenated aCSF at 34 °C. Lhb neurons, selected based on the presence of mCherry fluorescence (hM4 neurons) or on its absence (no hM4

neurons), were recorded in the whole-cell configuration of the patch-clamp technique. Patch pipettes were pulled from borosilicate glass capillaries (Harvard Apparatus, Edenbridge, UK) with a P-1000 puller (Sutter Instruments, Novato, CA, USA). They were filled with a solution containing 140 mM KCl, 2 mM MgCl₂, 10 mM HEPES, 2 mM MgATP, (pH=7.3, adjusted with KOH; osmolarity, 310 mOsm, adjusted with sucrose) and had final tip resistances of 3.5–4.5 MΩ. Current-clamp experiments were performed with a Multiclamp 700 A amplifier (Molecular Devices, Union City, CA, USA) and recorded with WinWCP or WinEDR softwares (John Dempster, University of Strathclyde). Recordings were performed at a holding current allowing to maintain the resting potential at ca. –60 mV. In the first set of experiments we investigated, on Lhb neurons including hM4(Gi) receptors (*n*=2 rats), the consequences of bath perfusion of CNO (5 µM) on firing frequency in response to intracellular injection of 1 s-lasting current pulses of increasing amplitude (from 0 to 240 pA, increments of 20 pA). Responses were recorded twice, once before and once following CNO bath application. In the second set of experiments, we investigated the consequences of local application of 1 µl CNO (500 µM) on spontaneous firing frequency of Lhb neurons, with (*n*=1 rat), and without (*n*=1 rat) hM4(Gi) receptor expression, by means of puff application through a second pipette positioned just above the recorded Lhb neurons. Spike frequency was analyzed with Clampfit 10.2 (Molecular Devices, Union City, CA, USA). This was done to be more precise and selective of the recorded neurons and to increase the chance to observe a recovery of neuronal firing to baseline levels, through the local administration of a very small amount of CNO solution.

Behavioral study

Drug treatments

CNO (1 mg/kg; freshly prepared before each experiment and dissolved in 0.9% NaCl–0.5% DMSO), or vehicle (Veh, 0.9% NaCl–0.5% DMSO) were administered intraperitoneally. Sixteen hM4 animals and 16 Sham animals were administered CNO (hM4–CNO group and Sham–CNO respectively). Six rats of each surgery condition (hM4–Veh group and Sham–Veh group) were administered vehicle, hM4–Veh animals serving to control for possible adverse effects of the administration of the viral construct and subsequent inclusion of hM4 receptors at the cellular membrane. The Sham–CNO group was used to control for potential adverse effects of CNO (Ilg et al. 2018; Manvich et al. 2018; Campbell and Marchant 2018) in our conditions.

Fear conditioning

The protocol took place over four consecutive days. Rats were subjected to each session in the same chamber. On day 1 (*Conditioning*), rats were conditioned as described above. On day 2 (*Context test; 15 min–long*), they were placed in the conditioning chamber to assess contextual fear. On day 3 (*New context exposure; 15 min–long*), rats were placed in the new context, the CS test context, to reduce baseline fear before CS fear assessment (Jacobs et al. 2010). On day 4 (*CS test; 26 min–long*), after a 2 min baseline in this context with no event, five CS were delivered with a 4 min interval. Rats received CNO or Veh on day 1, 30 min before the start of conditioning, and were administered Veh on each subsequent testing day, 30 min before the start of the session. Freezing scores were averaged on periods of interest on day 1 (the 3 min before the first tone presentation serving to assess baseline freezing), day 2 and day 3 (the 5 first min to capture the primary reaction to the conditioning context, and to the new context, respectively), and day 4 (the 15 s preceding the first tone being used to assess baseline, and the five 15 s tone presentations being used to assess fear conditioned to the CS).

Elevated plus–maze

It was made of black Plexiglas, elevated 73 cm above the floor, and consisted of four arms (50 cm × 10 cm), two comprising 40 cm–high walls (closed arms) and two comprising 1.5 cm–high borders (open arms). Light intensity was 10 lx in open arms, 7 lx at the center of the maze, and 2.5 lx in closed arms. The maze was cleaned with water and 70% ethanol between each rat. Thirty min after CNO or vehicle injections, rat were put in the maze for 5 min. The data analyzed were the total number of visits in the four arms, the number of visits in the open arms (in the percentage of the total number of visits), and the time spent in the open arms (in the percentage of the total time spent in the four arms).

Locomotor activity

Locomotor activity was assessed in the home cage (HC) by means of two infrared light–beams perpendicular to the width of the cage, placed 4.5 cm above floor level and 28 cm apart along the length of the cage. The consecutive interruptions of both light beams were counted as longitudinal crossings, whose numbers were monitored and saved in 15 min bins. Following a 1 h baseline, rats were administered CNO or Veh, and activity was recorded for an additional 2 h.

Histology

Tissue preparation and section processing were conducted as described in experiment 1, and sections were mounted on gelatin-coated slides with a DAPI–fluoromount medium. Observation of the spread of hM4(Gi) receptor expression (visualization of mCherry fluorescence) was performed with a Zeiss Apotome microscope (Zeiss, Muenchen, Germany).

Statistical analyses

For Experiment 1, freezing scores during each 15 s tone presentation and c–Fos + cells densities in the habenular complex were analyzed using one-way ANOVAs with repeated factor (Trial and Subregion, respectively). For the analyses of electrophysiological data from Experiment 2, one– and two–way ANOVAs (with Group as the factor and Current pulse amplitude or Time as the repeated measures) was used. For the analyses of all behavioral data from experiment 2, Group was used as the factor. For fear conditioning, freezing scores during baseline (day 1), reexposure to the conditioning context (day 2), and exposure to the new context (day 3) were analyzed using one–way ANOVAs. Two-way ANOVAs were used to compare groups through conditioning (factor Trial, freezing scores during each 15 s tone presentation, day 1) and during the test of conditioned fear to the CS (factor Tone, 15 s before the first CS presentation vs during CS, day 4). Data collected in the plus–maze and in the home cage were analyzed using one– and two–ways ANOVAs (with Time as the repeated measure), respectively. Post hoc tests used the Newman Keuls multiple range test (except when specified) when appropriate. Values of $p < 0.05$ were considered significant.

Results

Experiment 1

The increase in freezing scores to the tone during the session (Trial, $F_{5,15} = 18.85$, $p < 0.0001$, first tone vs second tone, $p < 0.05$, second tone vs third tone, $p < 0.01$, and asymptotic score— $90\% \pm 6.3$ —thereafter) indicated that FC rats were successfully conditioned. Although a significant Trial effect was found in NS condition ($F_{7,35} = 4.09$, $p < 0.01$), the increase in behaviors coded as freezing by our automated system only reached its low ($26 \pm 9.4\%$) asymptotic level during the fifth tone presentation ($p < 0.05$ vs the previous ones), very unlikely to be indicative of the onset of unconditioned fear responses to this stimulus. As compared to the home cage, NS and FC conditions both induced low to marked c–Fos expression in all the investigated structures (Supplemental Table 1). In

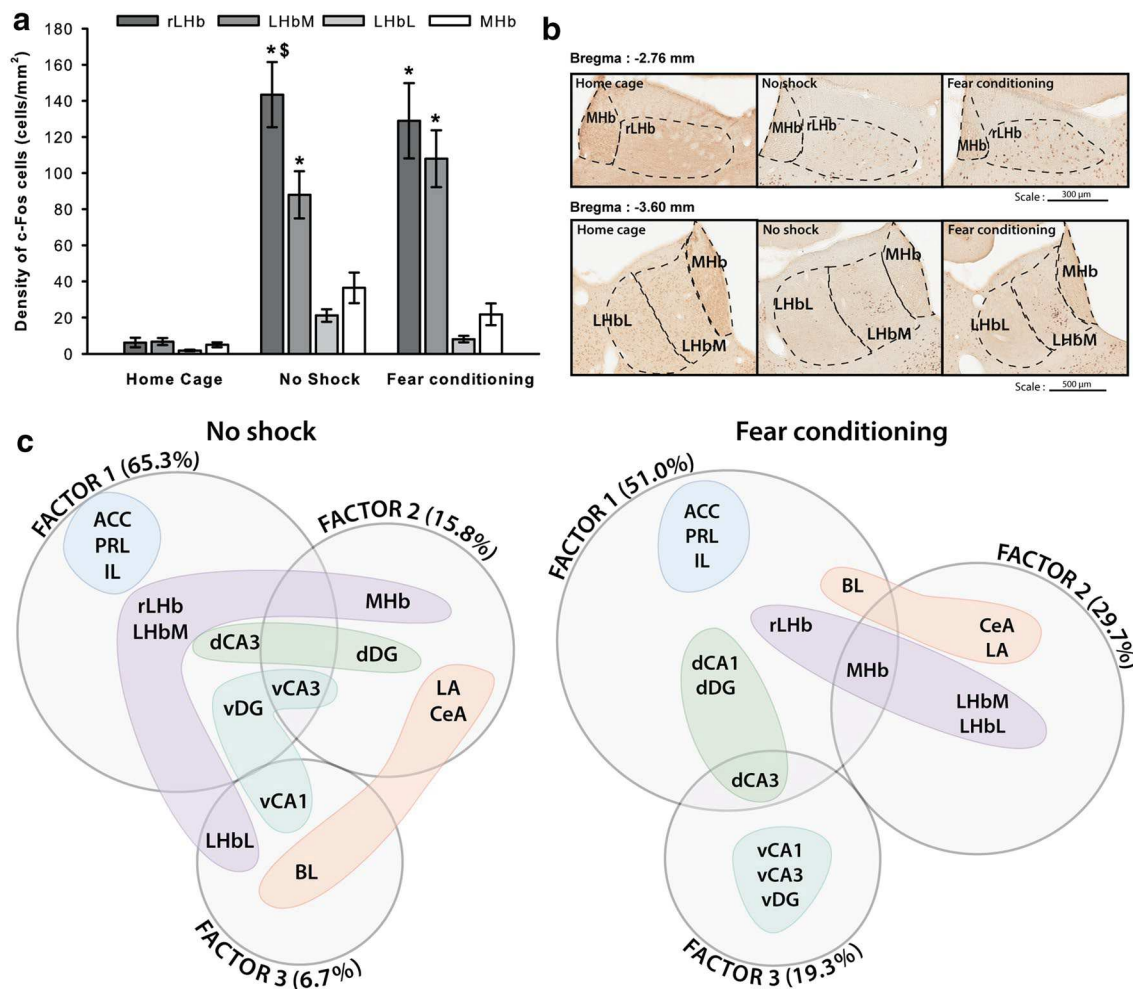


Fig. 2 C–Fos expression in the habenular complex. **a** Density of c–Fos+ cells (mean \pm SEM) in habenular complex subregions of Home Cage (HC), No Shock (NS), and Fear Conditioning (FC) conditions. rLHb and LHbM were highly activated in both NS and FC conditions but differed only in the former one (*, different from LHbL and MHb in the same condition; \$, different from LHbM in the same condition, $p < 0.01$ at least). **b** Photomicrographs showing an example of c–Fos expression in a rat of HC (left), NS (middle), and FC (right) conditions, in a slice including the LHb in its most rostral part (rLHb; top), and in its most caudal part including medial (LHbM) and lateral (LHbL) subdivisions (bottom), according to the atlas of Paxinos and Watson (Paxinos and Watson 2007). Notice the strong c–Fos expression in the rLHb and LHbM of rats of the NS and FC conditions. **c** Diagram depicting networks revealed by the factorial analysis of c–

Fos expression density induced by the NS (left) and FC (right) conditions. Subregions belonging to the same anatomical entity have been gathered following color code: light blue (medial prefrontal cortex), purple (habenular complex), orange (amygdala), green (dorsal hippocampus), light green (ventral hippocampus). Abbreviations: ACC, anterior cingulate cortex; PRL, prelimbic cortex; IL, infralimbic cortex; BLA, basolateral amygdaloid nucleus; LA, lateral amygdaloid nucleus; CeA, central amygdaloid nucleus; d/vCA1, ammonic field 1 of the dorsal/ventral hippocampus; d/vCA3, ammonic field 3 of the dorsal/ventral hippocampus; d/vDG dorsal/ventral dentate gyrus; LHb, lateral habenula; LHbL, the lateral subdivision of the LHb in its most caudal part; LHbM, the medial subdivision of the LHb in its most caudal part; rLHb, rostral part of the LHb

the habenular complex (Fig. 2 a, b), c–Fos+ cells densities differed according to the subregion of both NS and FC rats (HC, $F_{3,15} = 1.56$, $p > 0.2$; NS, $F_{3,21} = 31.17$, $p < 0.0001$; FC, $F_{3,9} = 17.38$, $p < 0.001$). Post hoc comparisons indicated that the density of c–Fos+ cells were higher in rLHb and LHbM than in LHbL and MHb in NS ($p < 0.01$ at least), and FC ($p < 0.01$ at least) conditions, and higher in the rLHb than in LHbM only in NS condition ($p < 0.01$).

Factorial analyses of c–Fos data are shown in Table 1. In the NS condition, analysis of eigenvalues led to the conservation of a 3 factor–model accounting for 87.85% of the total variance observed. *Factor 1* explained 65.34% of this variance and included positive loadings of the whole mPFC, the rLHb and LHbM, the whole CA3 region (ventral and dorsal), and the vDG. *Factor 2* explained 15.8% of the total variance and included positive loadings

Table 1 Networks revealed by the factorial analysis of c-Fos expression density

		No shock			Fear conditioning		
		Loadings (Varimax normalized)			Loadings (Varimax normalized)		
		Factor 1	Factor 2	Factor 3	Factor 1	Factor 2	Factor 3
Medial prefrontal cortex	ACC	0.91	0.09	0.20	0.99	0.01	0.01
	PRL	0.96	0.05	0.23	0.94	-0.20	-0.26
	IL	0.94	0.13	0.22	0.99	-0.05	0.01
Amygdala	CeA	0.00	0.97	0.17	0.21	0.79	0.57
	BL	0.04	0.56	0.75	-0.79	0.40	0.46
	LA	0.48	0.68	0.37	-0.08	0.96	0.28
Habenular complex	rLHb	0.75	0.48	0.04	-0.88	0.26	0.40
	LHbM	0.95	0.12	0.08	0.17	-0.98	-0.14
	LHbL	0.17	0.11	0.83	-0.07	0.94	-0.35
	MHb	0.07	0.88	0.26	0.68	-0.70	0.22
Dorsal hippocampus	dCA1	0.53	0.37	0.54	0.99	0.06	0.12
	dCA3	0.72	0.41	0.44	0.68	0.18	0.71
	dDG	0.45	0.80	0.18	0.91	-0.13	0.40
Ventral hippocampus	vCA1	0.57	0.40	0.68	0.47	0.36	-0.81
	vCA3	0.63	0.64	0.38	0.18	0.10	0.98
	vDG	0.63	0.46	0.55	0.43	-0.50	-0.75
Eigenvalue		10.45	2.53	1.08	8.16	4.75	3.09
Total variance explained (%)		65.34	15.80	6.73	51.00	29.66	19.34

The table indicates, for the NS (left) and FC (right) conditions, the correlation values between the initial variable (i.e. c-Fos+cells density in each subregion) with the common factor extracted. Bolded values correspond to correlations higher than 0.6 or less than -0.6, therefore considered significantly powerful. The percentage of the total variance explained by each factor is shown at the bottom. In the No Shock condition, analysis of eigenvalues led to the conservation of a 3 factor-model accounting for 88% of the total variance observed. In the Fear Conditioning condition, analysis of eigenvalues led to the conservation of a 3 factor-model accounting for 100% of the variance observed

ACC anterior cingulate cortex, PRL prelimbic cortex, IL infralimbic cortex, BL basolateral amygdaloid nucleus, LA lateral amygdaloid nucleus, CeA central amygdaloid nucleus, d/vCA1 ammonic field 1 of the dorsal/ventral hippocampus, d/vCA3 ammonic field 3 of the dorsal/ventral hippocampus, d/vDG dorsal/ventral dentate gyrus, LHb lateral habenula, LHbL lateral subdivision of the LHb in its most posterior part, LHbM medial subdivision of the LHb in its most posterior part, rLHb rostral part of the LHb

of the CeA and LA, MHb, dDG, and vCA3. *Factor 3* explained 6.73% of the total variance and included positive loadings of BL, LHbL, and vCA1. In the FC condition, analysis of eigenvalues led to the conservation of a 3 factor-model accounting for nearly 100% of the variance observed. *Factor 1* explained 51% of the total variance and included positive loadings of the entire mPFC, the MHb, and the entire dHPC, and negative loadings of the BL and rLHb. *Factor 2* explained 29.66% of the total variance and included positive loadings of CeA, LA, and LHbL, and negative loadings of LHbM and MHb. *Factor 3* explained 19.34% of the total variance and included positive loadings of dCA3 and vCA3, and negative loadings of vCA1 and vDG. As illustrated in Fig. 2c, NS, and FC seem to engage the structures of interest but within distinct networks.

Experiment 2

CNO reduced the excitability of hM4(Gi)-containing LHb neurons

CNO reduced action potentials (AP) firing in response to pulses up to 100 pA ($F_{12,48}=4.25$, $p<0.001$; Fig. 3a). For example, the AP frequency in response to 100 pA current pulses in the presence of CNO represented $46 \pm 14\%$ of the frequency recorded in the control condition. Note that under strong current pulses injection (> 100 pA) the inhibitory effect of CNO was overcome (see traces with 240 pA injection in Fig. 3b). To control for possible nonspecific effects of CNO, we examined the consequences of local puff applications of high CNO concentration (500 μM) on the spontaneous firing of LHb neurons with (hM4; $n=1$ rat;

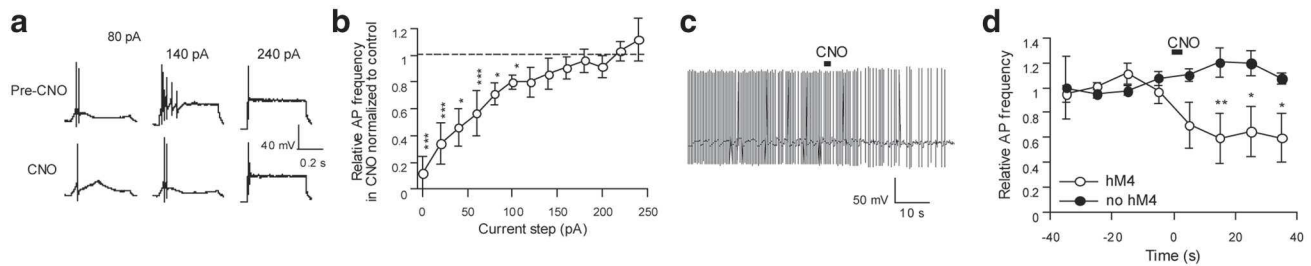


Fig. 3 Electrophysiological validation of the chemogenetic strategy used to reduce the excitability of LHB neurons. **a** Example of patch-clamp recording in current-clamp mode of a hM4(Gi)-containing LHB neuron. Firing in response to intracellular injection of 1 s-lasting 80, 140 and 240 pA current pulses, before (Pre-CNO; top), and during (CNO; bottom) bath perfusion of CNO (5 μ M). **b** Frequency of action potentials in response to intracellular injections of 1 s-lasting current pulses of increasing amplitudes during bath perfusion of CNO (5 μ M) normalized to their frequency before perfusion of CNO. CNO reduced AP firing in response to pulses up to 100 pA (** $p < 0.0001$, * $p < 0.05$ vs normalized control, i.e. dashed line;

Dunnett post-hoc test). **c** Example of spontaneous firing of a LHB neuron expressing hM4(Gi) receptors in response to CNO (500 μ M); one can see the reduction of the frequency of AP following its administration. **d** Global effect of local puff applications of high CNO concentration (500 μ M) on the spontaneous firing of LHB neurons expressing (hM4) or not (no hM4) the DREADD inhibitory receptors. The frequency of AP was normalized with the average frequency during control (time - 30 s to 0 s). CNO was puffed near the recorded neurons at $t = 0$ s. CNO reduced AP firing frequency in hM4 neurons (* $p < 0.05$, ** $p < 0.01$ vs no hM4)

$n = 4$ neurons) and without (no hM4; $n = 1$ rat; $n = 5$ neurons) hM4(Gi) receptors. Whereas CNO significantly reduced the firing frequency of hM4 neurons, it had no effects on the firing of no hM4 neurons (Time X Group, $F_{7,49} = 3.83$, $p < 0.01$; $p < 0.05$ at least, vs no hM4, Duncan post-hoc test; Fig. 3 c, d). Altogether, these results indicate that the effect of CNO was specific to neurons expressing hM4Gi receptors and strongly suggest that such an effect accounts for the behavioral alterations observed in hM4-CNO animals.

Histology and groups size for the behavioral study

Only rats in which mCherry expression was bilaterally mainly present in the LHB were kept. In these rats, hM4(Gi) receptors were expressed within the LHB in its entire rostrocaudal extent in both its lateral and medial parts (Fig. 4). In few of those rats, the expression of hM4 receptors also slightly impinges on the underlying paraventricular thalamic nucleus (PVT), particularly in its posterior part. Five hM4 rats were discarded because hM4(Gi) receptor expression spread to other surrounding structures. In addition, the two groups of rats which were administered Veh (hM4-Veh and Sham-Veh) were pooled into a single Ctl-Veh group after verification that their performances did not differ (Supplementary Information). Therefore, groups were composed as follows: hM4-CNO ($n = 11$), Sham-CNO ($n = 16$), Ctl-Veh ($n = 12$) and indicated as such in the figures.

LHB inactivation altered conditioned fear memory

Conditioning. All groups showed freezing scores close to 0% during baseline ($F_{2,36} = 0.90$, $p > 0.4$), and a similar increase of freezing to the tone during the session (Fig. 5a).

Indeed, the analysis indicated no significant effect of Group ($F_{2,36} = 1.44$, $p > 0.2$), a significant effect of Trial ($F_{5,180} = 20.32$, $p < 0.0001$), and no significant Group x Trial interaction ($F_{10,180} = 1.32$, $p > 0.2$). This suggests that LHB inactivation did not affect the rate of fear learning. **Context test** (Fig. 5b). Reexposure to the training context-induced freezing behavior, but hM4-CNO group showed lower freezing score than the two other groups, the latter displaying similar freezing scores (Group, $F_{2,36} = 3.86$, $p < 0.05$; hM4-CNO vs Ctl-Veh and Sham-CNO, $p < 0.05$ for each comparison). This suggests that LHB inactivation during conditioning impaired conditioned fear of the training context. **New context exposure** (Fig. 5c). Freezing scores were low in all groups and of a similar level (Group, $F_{2,36} = 0.65$, $p > 0.5$), suggesting that exposure to this new context did not induce generalized contextual fear, whatever the group. **CS test** (Fig. 5d). All groups showed similarly low freezing scores during baseline and enhanced freezing during CS presentation (Tone, $F_{1,36} = 54.64$, $p < 0.0001$), especially in the hM4-CNO group (Group, $F_{2,36} = 5.88$, $p < 0.01$; Tone x Group, $F_{2,36} = 5.18$, $p < 0.05$). Post hoc comparisons indicated that hM4-CNO rats showed significantly more freezing than the two control groups only during CS presentation ($p < 0.05$). This suggests that, if all groups displayed fear to the CS, LHB inactivation during conditioning enhanced such fear response.

LHB inactivation induced mild anxiety and increased locomotor activity

In the elevated plus-maze, LHB inactivation did not affect the total number of arm visits (Group, $F_{2,36} = 1.29$, $p > 0.2$; Fig. 6a), nor did it impact the percent time spent in the open

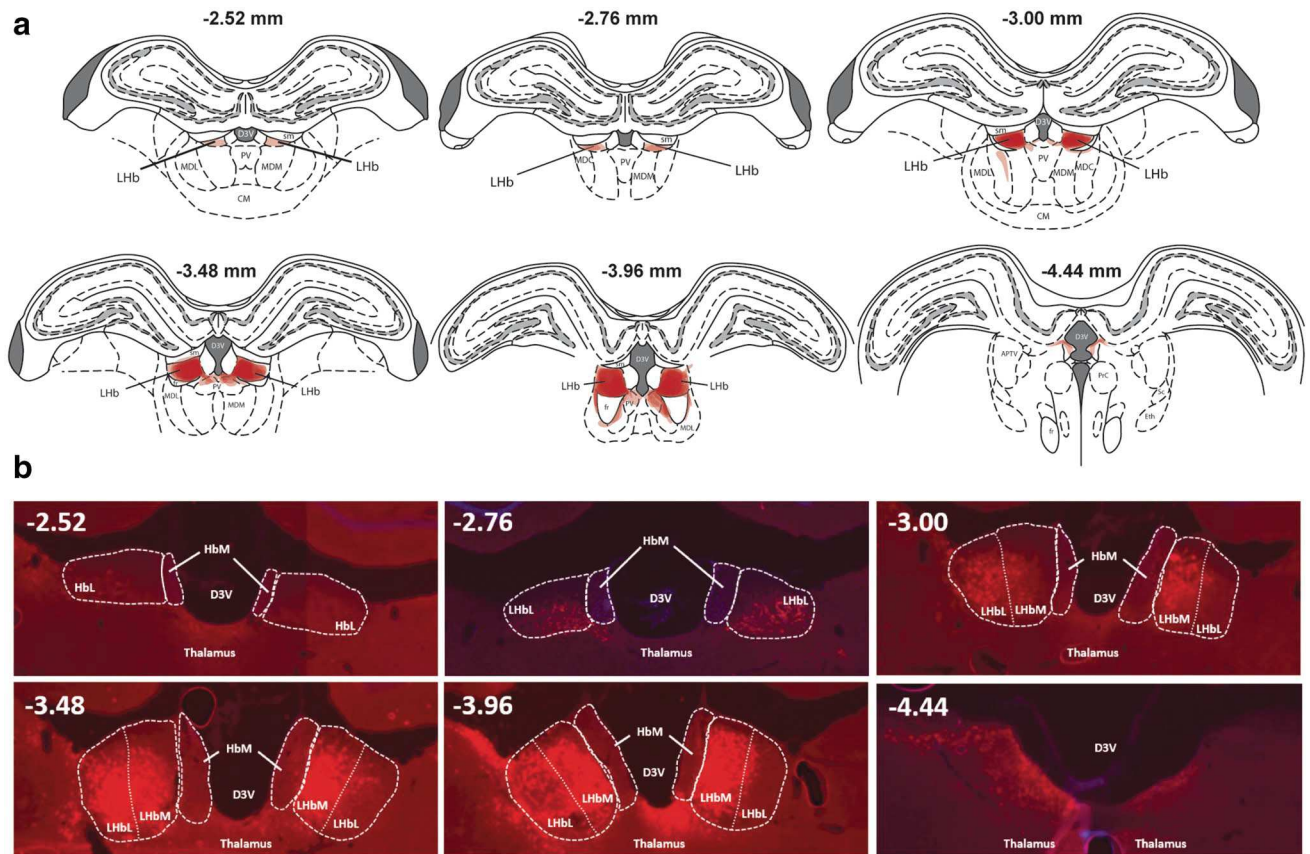


Fig. 4 **a** Schematic representation of the presence of hM4(Gi) receptors in the animals kept following histological verification. For each rat, on each slide used, the area including the expression of the hM4(Gi) receptors was delineated using a pale red color (opacity 20%). Then, for each stereotaxic coordinate [numbers above the slides correspond to AP coordinates from Bregma (mm) (Paxinos and Watson 2007)], the slides of all the animals were piled, creating a color scale from pale red to dark red. Therefore, the darker is the area, the greater is the number of animals presenting an expression of the hM4(Gi) receptors within this area. One can see that hM4(Gi)

receptors were expressed within the LHB in its entire rostrocaudal extent. **b** Typical example of hM4(Gi) expression within the LHB. One can particularly notice the presence of mCherry in both the LHbL and LHbM, as well in the rostral LHB, whereas it was absent in the MHb. White numbers in the top left corner of each photograph are AP coordinates from Bregma (mm). Abbreviations: D3V, third ventricle; LHb, lateral habenula; LHbL, lateral part of the lateral habenula; LHbM, the medial part of the lateral habenula; MHb, medial habenula

arms, despite a tendency (Group, $F_{2,36} = 2.13$, $p = 0.13$; Fig. 6b right). However, the percent of open arms entries were lower in the LHB inactivated group than in the two other groups (Group, $F_{2,36} = 4.21$, $p < 0.05$ for each comparison; Fig. 6b left). With regard to home cage locomotor activity, there was no difference during baseline (Group, $F_{2,36} = 0.89$, $p > 0.4$; Time, $F_{3,108} = 12.09$, $p < 0.0001$; Group x Time interaction, $F_{6,108} = 0.22$, $p > 0.9$; Fig. 6c). LHB inactivation induced marked hyperactivity (bins 5–12; Group: $F_{2,36} = 38.70$, $p < 0.0001$; Time: $F_{7,252} = 16.28$, $p < 0.0001$; Group x Time interaction: $F_{14,252} = 11.36$, $p < 0.0001$). Noteworthy, this hyperactivity peaked 30 min following CNO administration, further validating our strategy to perform behavioral testing 30 min following CNO administration, and lasted approximately 75 min (Fig. 6c). Together, these results indicate that chemogenetic LHB inactivation induced

only mild anxiety and a marked behavioral activation in a familiar (i.e. home cage), but not an unfamiliar –and anxiogenic– (i.e. the elevated plus maze) environment. These behavioral alterations have already been reported following LHB inactivation (Mathis et al. 2015).

Discussion

This study aimed to assess whether the LHB contributes to fear memory formation using a long trace fear conditioning procedure. Our results indicate that it participates to both contextual and CS memories formation. Notably, whereas LHB inactivation did not affect fear expression during learning, demonstrating that it did not impair the ability of the rats to perceive the footshocks, it resulted in poor freezing levels

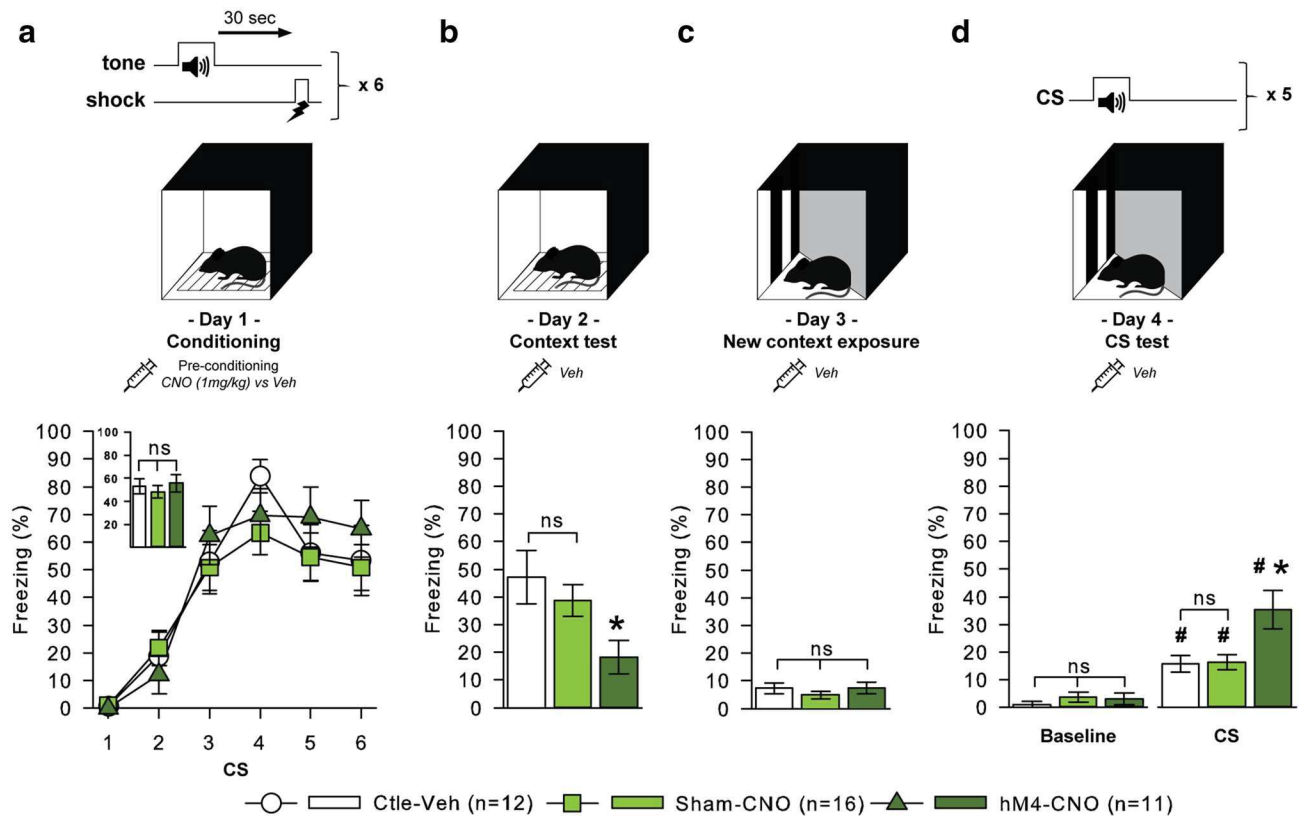


Fig. 5 Lhb inactivation impaired emotional memory. Schematic representation of the protocol used; notice that while rats received an intraperitoneal injection of either CNO (1 mg/kg), or vehicle (Veh), during the conditioning phase, in the subsequent testing days, to maintain rats in the same pre-test routine, including the same amount of manipulations, rats received an intraperitoneal injection of Veh. Values represent the percent time spent freezing (\pm SEM) as an index of fear. **a** During conditioning there was no between-group difference across the six 15 s CS presentations (inset shows the mean freezing over the six CS). **b** During the context test, hM4-CNO rats showed

less freezing ($*p < 0.05$ vs the two other groups). **c** During exposure to the new context, all groups displayed similarly low freezing. **d** During the CS test, whereas there was no between-group difference during baseline (last 15 s; left), during CS presentations all groups showed more freezing ($^{\#}p < 0.05$ vs baseline for the same group), but freezing was higher in hM4-CNO rats ($*p < 0.05$ vs the two other groups during CS presentation). Abbreviations: CNO, clozapine-N-oxide; CS, conditional stimulus (tone); ns, not statistically different; US, unconditional stimulus (electric footshock); Veh, vehicle

upon re-exposure to the context, consistent with contextual memory deficit, whereas it exacerbated fear response to the CS, which is evocative of CS memory enhancement. It is unlikely that those effects resulted from partial inactivation of the adjoining paraventricular thalamic nucleus (PVT); in rats, PVT inactivation before conditioning did not impact fear retention (Padilla-Coreano et al. 2012); also, PVT inactivation during a conditioning phase similar to ours induced in mice a decreased freezing during the CS retention test (Penzo et al. 2015), whereas here hM4-CNO rats showed increased freezing during the CS test.

The contextual memory deficits induced by Lhb chemogenetic inhibition can be discussed according to the two main processes leading to contextual fear conditioning: context encoding per se, and the association between the context and the aversive event. Context encoding rapidly takes place during conditioning through the elaboration of

a conjunctive representation of the various cues of the conditioning chamber, a process mainly dependent on the dHPC (Rudy et al. 2002). An interaction between the Lhb and dHPC might be critical to the proper encoding of contextual information. Such a view is strengthened by the presence of highly correlated metabolic activations in these structures during contextual fear conditioning (González-Pardo et al. 2012), as well as the depiction of electrophysiological communication between them (Goutagny et al. 2013; Aizawa et al. 2013), including in a task involving spatial information processing (Goutagny et al. 2013). Strikingly, in parallel with contextual memory deficits, hM4-CNO rats were able to perform and memorize the CS-US association. Lhb neurons were recently shown to increase CS activity while continuing to be activated by the US during aversive classical conditioning (Wang et al. 2017) and avoidance learning (Trusel et al. 2019) suggesting that the Lhb may be involved

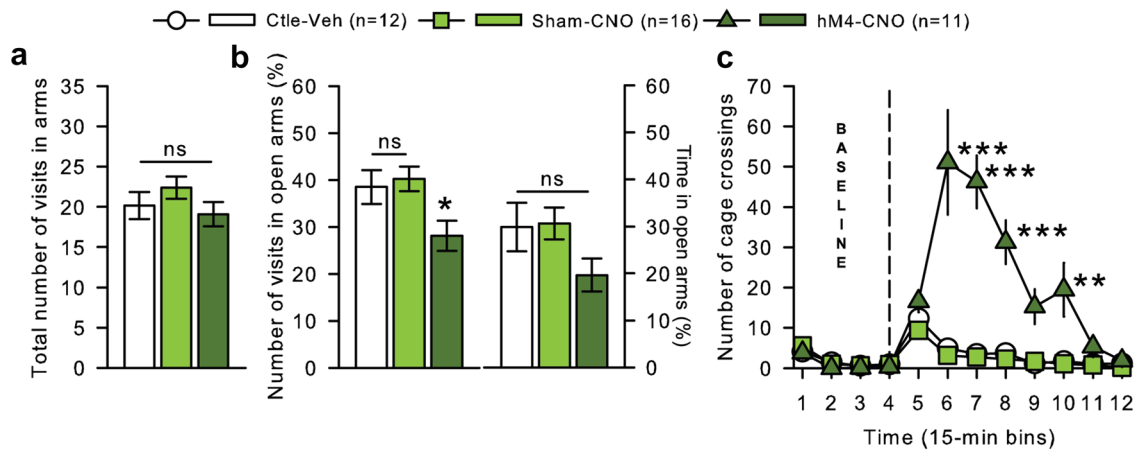


Fig. 6 Lhb inactivation induced mild anxiety in the elevated plus-maze and locomotor hyperactivity in the home cage. Values are presented as mean \pm SEM. **a–b** Lhb inactivation did not alter the total number of arm visits (**a**). Whereas Lhb inactivation decreased the percent of open arms entries (**b, left**; * $p < 0.05$ vs the two other

groups), it did not affect the percent time spent in the open arms (**b, right**). **c** HC locomotor activity. Lhb inactivation markedly increased locomotor activity; such hyperactivity peaked 30 min (bin 6) following CNO administration and lasted approximately 75 min (bins 6–10; *** $p < 0.0001$, ** $p < 0.001$ vs the two other groups)

in the formation of CS-US association supporting predictive learning, at least when the CS is a perfect predictor of the US according to both its temporal and contingent relation with the US. In those conditions and based on this assumption, an alteration of Lhb function may be expected to alter learning about the predictive value of the CS. However, Lhb lesions were shown to facilitate avoidance learning (Song et al. 2017) and contrasting effects of its lesion were reported on CS fear memory (unaffected, Heldt and Ressler 2006; Song et al. 2017; altered fear memory to both the CS and the context, Wang et al. 2013). The recent demonstration of coexistence of two distinct populations of Lhb neurons displaying opposite responses to footshocks indicates that Lhb encoding of aversive cues involves a complex excitation/inhibition process (Congiu et al. 2019), and our current results showing enhanced fear conditioned to a trace CS in hM4-CNO rats suggest a more complex role of the Lhb in predictive learning. Conditioning protocols where the Pavlovian law of temporal contiguity is manipulated—from the introduction of a long time interval to a complete lack of contingency between the CS and the US—typically lead to an increased fear to the context at the expense of the CS. This phenomenon indicates the onset of overshadowing of the CS by the context, a process commonly thought to rely on competition between potential predictors at the time of conditioning (Rescorla 1968; Rescorla and Wagner 1972). The fact that control animals (Ctl-Veh and Sham-CNO) displayed higher levels of freezing to the context than to the CS confirms the overshadowing effect in our long trace protocol. It is likely that an impaired ability to encode the context has led to a lack of competition with the CS, resulting in the ability of the latter to elicit increased fear responses in

hM4-CNO rats. The Rescorla–Wagner model (Rescorla and Wagner 1972) posits that differences in the emotional value acquired by the different cues is based on differences in the perceived salience of the US and of those cues. The lack of alteration of the rate of fear learning in hM4-CNO rats suggests unaltered stimuli salience processing; therefore, the role of the Lhb may be to compute the relative pertinence of potential predictors (to shed light on the strongest one) and favor—or inhibit—their association with the aversive event. The reduced contextual- and enhanced CS-conditioned fear observed in hM4-CNO rats might thus be the consequence of an alteration of this computation. Interestingly, opposite changes in the acquired emotional value of contextual and CS cues were previously reported by Calandrea and collaborators (2005). Indeed, those authors have shown that LA inactivation during conditioning using a delay procedure (*i.e.* no trace interval between the CS and the US, leading to a strong overshadowing of contextual cues by the CS), reduced fear to the more predictive CS and enhanced fear to the less predictive context. Our results suggest that the Lhb might modulate, along with the LA, fear learning according to the predictive value of competing cues.

The c-Fos experiment results, rather than opposing two potential roles of the Lhb in context encoding *vs.* association between stimuli, seem to be congruent with both, although with some anatomical peculiarities. First, the factorial analysis conducted in the NS and FC conditions led to different distributions of the investigated structure among factors. This indicates that even though neuronal activations were observed in the same structures in both conditions, as expected by the fact that all rats were exposed to novelty (see Milanovic et al. 1998; Radulovic et al. 1998; Cho

et al. 2017), the onset of functional associations in these networks can be unraveled through correlational analysis of data. Specifically, the analysis of the FC group led to the extraction of 3 factors gathering neuronal ensembles classically described as sustaining different facets of information processing during fear conditioning. The first factor encompassed the whole dHPC and mPFC subregions, as well as the BL; it may represent the network implicated in contextual information processing (see for review Maren et al. 2013). However, the BL shows a negative loading on this factor, even though it has been repeatedly reported to be the main locus of association between the context representation and the US in contextual fear conditioning (see for review Duvarci and Pare 2014). Thus, this factor likely underlines cognitive facets of information processing in contrast with associative and/or emotional ones. Such an interpretation is congruent with the involvement of both the mPFC and the dorsal HPC in broad cognitive functions (see for review Fanselow and Dong 2010; Connor and Gould 2016). The second factor, characterized by heavy loadings of the LA and the CeA, may sustain the associative process as well as the onset of fear responses (see for review Duvarci and Pare 2014). Indeed, if CS–US association mainly takes place in the LA, the latter also supports context–US association (Calandreau et al. 2005). The mild positive loading of the BL on this factor might reflect associations between the US and its predictors. The third factor, characterized by heavy loadings on the whole ventral HPC, likely reflects emotional processes (Fanselow and Dong 2010). However, this factor puts forward CA3 activations in both dorsal and ventral portions of the HPC, in opposition to ventral DG and CA1 activations. This subfield of the HPC has historically been proposed as a relevant substratum to the encoding of polymodal representations such as a context (Marr 1971). Thus, this factor might also underline the processing of contextual information. The fact that the BL (along with the CeA) also displays a mild positive loading on this factor suggests that it might represent contextual computations relevant to fear conditioning, in contrast with factor 1.

Of utmost interest is the presence of habenular subregions within these ensembles. The association of the MHb with factors 1 and 2 suggests it contributes to both cognitive facets of information processing, *i.e.* associative learning and the onset of fear responses. The implication of the MHb in trace fear conditioning has not yet been investigated. This region in rodents (Yamaguchi et al. 2013; Zhang et al. 2016; Geng et al. 2019), or its equivalent in zebrafish (the dorsal habenula; Agetsuma et al. 2010), modulate fear responses, although Hsu et al. (2016) found no contextual fear conditioning deficits following its lesion. The LHb is also included in these two factors, but with regional specificity. If the inclusion of its rostral part in factor 1 suggests its contribution to the cognitive aspects of fear conditioning,

the inclusion in factor 2 of the LHbM and the LHbL, along with the LA and CeA, suggests they contribute to the associative process and/or to the onset of fear responses. The memory deficits observed following LHb inactivation appear in accordance with the position of the different LHb subdivisions within the clusters of structures revealed by the factorial analysis. Contextual memory deficits are in accordance with rLHb inactivation and the consecutive disturbance of the network including the dHPC (factor 1), whereas inappropriate CS-US association is in accordance with LHbM/LHbL inactivation and the consecutive disturbance of the network encompassing the CeA and the LA (factor 2).

The c-Fos pattern in the LHb is also interesting regarding its potential role as a modulator of DA transmission during fear conditioning. Indeed, the part of the LHb that we defined as “rostral” includes the LHbMA subdivision described by Andres et al. (1999) which neurons send excitatory projection to VTA DA neurons (Metzger et al. 2019). In addition, neurons situated in the more caudal-lateral region of the LHb send excitatory projection on GABA neurons of the RMTg (Petzel et al. 2017) which in turn inhibit VTA DA neurons activity (Brown et al. 2017). The strong activation of these LHb subregions, where hM4(Gi) receptors were abundantly expressed, suggests that the observed deficits could be the consequence of the disturbance of the fine-tuning of DA transmission exert by the LHb during conditioning. Interestingly, infusion of D1-like receptor antagonist during training was shown to reduce trace CS fear memory when infused in the prelimbic region of the mPFC (Runyan and Dash, 2004), and to increase contextual fear when infused in the shell part of the nucleus accumbens (Albrechet-Souza et al., 2013). One can, therefore, postulate that the enhanced CS- and reduced contextual memory seen in hM4-CNO rats is consecutive to an increased DA flow within these two brain regions, due to the disinhibition of DA transmission by LHb inactivation, as suggested by previous work (Lecourtier et al. 2008). However, the fact that D1-like antagonist infusion during conditioning in other VTA DA targets, *i.e.* the dorsomedial PFC (Stubben-dorff et al. 2019), dHPC and BL (Heath et al. 2015) reduces contextual fear rather than increasing it, renders difficult to explain our results just by global disinhibition of the DA transmission. Moreover, D1-like antagonism and agonism were both shown to decrease contextual fear when infused in the LHb during conditioning (Chan et al. 2017). Thus, if numerous evidence pointed to the involvement of DA in various target regions of VTA neurons during fear conditioning where and how perturbations of DA signaling upon LHb inactivation modulates fear learning remains to be explored.

Besides DA, another key implication of the LHb during conditioning could be to contribute to the proper modulation of the hypothalamic-pituitary-adrenal axis response. Kaouane et al. 2012 have shown that acute restraint stress

and postconditioning intrahippocampal, or systemic, corticosterone (CORT) injections, induce memory impairments reminiscent with those observed in the current study in hM4–CNO rats. Indeed, animals conditioned with an explicitly CS–US unpaired training procedure disregarded the context as the correct predictor of a footshock and showed fear of the unpredictable cue. We have previously shown that the blood CORT response to a stressful experience was higher in rats with inactivated LHb (Mathis et al. 2018); one can, therefore, hypothesize that a too large CORT release during conditioning has contributed to the memory impairments observed in hM4–CNO rats. Such a CORT-mediated effect would be congruent with the general role of the LHb in the modulation of fear learning.

In summary, we have shown that LHb inactivation during the conditioning phase of a trace fear conditioning paradigm led to contextual memory deficits along with an enhanced response to a discrete cue. This study improves our understanding of the neuroanatomical bases of fear memory by showing that the LHb is crucially involved in the selection of the more relevant cue predicting a danger.

References

- Agetsuma M, Aizawa H, Aoki T et al (2010) The habenula is crucial for experience-dependent modification of fear responses in zebrafish. *Nat Neurosci* 13:1354–1356
- Aizawa H, Kobayashi M, Tanaka S et al (2012) Molecular characterization of the subnuclei in rat habenula. *J Comp Neurol* 520:4051–4066
- Aizawa H, Yanagihara S, Kobayashi M et al (2013) The synchronous activity of lateral habenular neurons is essential for regulating hippocampal theta oscillation. *J Neurosci* 33:8909–8921
- Albrechet-Souza L, Carvalho MC, Brandão ML (2013) D(1)-like receptors in the nucleus accumbens shell regulate the expression of contextual fear conditioning and activity of the anterior cingulate cortex in rats. *Int J Neuropsychopharmacol* 16(5):1045–1057
- Ali M, Cholvin T, Muller MA et al (2017) Environmental enrichment enhances systems-level consolidation of a spatial memory after lesions of the ventral midline thalamus. *Neurobiol Learn Mem* 141:108–123
- Amo R, Fredes F, Kinoshita M et al (2014) The habenulo-raphé serotonergic circuit encodes an aversive expectation value essential for adaptive active avoidance of danger. *Neuron* 84:1034–1048
- Andres KH, von Düring M, Veh RW (1999) Subnuclear organization of the rat habenular complexes. *J Comp Neurol* 407(1):130–150
- Baker PM, Mizumori SJY (2017) Control of behavioral flexibility by the lateral habenula. *Pharmacol Biochem Behav* 162:62–68
- Barrett DW, Gonzalez-Lima F (2018) Prefrontal-limbic functional connectivity during acquisition and extinction of conditioned fear. *Neuroscience* 376:162–171
- Brown PL, Palacorolla H, Brady D, Riegger K, Elmer GI, Shepard PD (2017) Habenula-induced inhibition of midbrain dopamine neurons is diminished by lesions of the rostromedial tegmental nucleus. *J Neurosci* 37(1):217–225
- Calandrea L, Desmedt A, Decorte L, Jaffard R (2005) A different recruitment of the lateral and basolateral amygdala promotes contextual or elemental conditioned association in Pavlovian fear conditioning. *Learn Mem Cold Spring Harb N* 12:383–388
- Campbell EJ, Marchant NJ (2018) The use of chemogenetics in behavioural neuroscience: receptor variants, targeting approaches and caveats. *Br J Pharmacol* 175:994–1003
- Chan J, Guan X, Ni Y, Luo L, Yang L, Zhang P, Zhang J, Chen Y (2017) Dopamine D1-like receptor in lateral habenula nucleus affects contextual fear memory and long-term potentiation in hippocampal CA1 in rats. *Behav Brain Res* 321:61–68
- Chastrette N, Pfaff DW, Gibbs RB (1991) Effects of daytime and nighttime stress on Fos-like immunoreactivity in the paraventricular nucleus of the hypothalamus, the habenula, and the posterior paraventricular nucleus of the thalamus. *Brain Res* 563:339–344
- Cho J-H, Rendall SD, Gray JM (2017) Brain-wide maps of Fos expression during fear learning and recall. *Learn Mem* 24:169–181
- Chou M-Y, Amo R, Kinoshita M et al (2016) Social conflict resolution regulated by two dorsal habenular subregions in zebrafish. *Science* 352:87–90
- Chowdhury N, Quinn JJ, Fanselow MS (2005) Dorsal hippocampus involvement in trace fear conditioning with long, but not short, trace intervals in mice. *Behav Neurosci* 119:1396–1402
- Congiu M, Trusel M, Pistis M, Mameli M, Lecca S (2019) Opposite responses to aversive stimuli in lateral habenula neurons. *Eur J Neurosci* 50(6):2921–2930
- Connor DA, Gould TJ (2016) The role of working memory and declarative memory in trace conditioning. *Neurobiol Learn Mem* 134:193–209
- Cullinan WE, Herman JP, Battaglia DF et al (1995) Pattern and time course of immediate early gene expression in rat brain following acute stress. *Neuroscience* 64:477–505
- Detert JA, Kampa ND, Moyer JR (2008) Differential effects of training intertrial interval on acquisition of trace and long-delay fear conditioning in rats. *Behav Neurosci* 122:1318–1327
- Duvarci S, Pare D (2014) Amygdala microcircuits controlling learned fear. *Neuron* 82:966–980
- Esclassan F, Coutureau E, Scala GD, Marchand AR (2009) Differential contribution of dorsal and ventral hippocampus to trace and delay fear conditioning. *Hippocampus* 19:33–44
- Fanselow MS, Dong H-W (2010) Are the dorsal and ventral hippocampus functionally distinct structures? *Neuron* 65:7–19
- Geng F, Liu J-Y, Chen X-W et al (2019) ErbB4 receptors in the medial habenula regulate contextual fear memory. *Pharmacology* 103:68–75
- Gilmartin MR, Helmstetter FJ (2010) Trace and contextual fear conditioning require neural activity and NMDA receptor-dependent transmission in the medial prefrontal cortex. *Learn Mem* 17:289–296
- Gilmartin MR, Miyawaki H, Helmstetter FJ, Diba K (2013) Prefrontal activity links nonoverlapping events in memory. *J Neurosci* 33:10910–10914
- González-Pardo H, Conejo NM, Lana G, Arias JL (2012) Different brain networks underlying the acquisition and expression of contextual fear conditioning: a metabolic mapping study. *Neuroscience* 202:234–242
- Goutagny R, Loureiro M, Jackson J et al (2013) Interactions between the lateral habenula and the hippocampus: implication for spatial memory processes. *Neuropsychopharmacology* 38:2418–2426
- Guimaraes M, Gregório A, Cruz A et al (2011) Time Determines the neural circuit underlying associative fear learning. *Front Behav Neurosci* 5:89
- Heath FC, Jurkus R, Bast T, Pezze MA, Lee JL, Voigt JP, Stevenson CW (2015) Dopamine D1-like receptor signalling in the hippocampus and amygdala modulates the acquisition of contextual fear conditioning. *Psychopharmacology* 232(14):2619–2629
- Heldt SA, Ressler KJ (2006) Lesions of the habenula produce stress- and dopamine-dependent alterations in prepulse inhibition and locomotion. *Brain Res* 1073–1074:229–239

- Hennigan K, D'Ardenne K, McClure SM (2015) Distinct midbrain and habenula pathways are involved in processing aversive events in humans. *J Neurosci* 35:198–208.
- Hsu Y-WA, Morton G, Guy EG, et al (2016) Dorsal Medial Habenula Regulation of mood-related behaviors and primary reinforcement by tachykinin-expressing habenula neurons. *eNeuro* 3(3)
- Ilg A-K, Enkel T, Bartsch D, Böhner F (2018) Behavioral effects of acute systemic low-dose clozapine in wild-type rats: implications for the use of DREADDs in behavioral neuroscience. *Front Behav Neurosci* 12:173
- Jacobs NS, Cushman JD, Fanselow MS (2010) The accurate measurement of fear memory in pavlovian conditioning: resolving the baseline issue. *J Neurosci Methods* 190:235–239
- Kaouane N, Porte Y, Vallée M et al (2012) Glucocorticoids can induce PTSD-like memory impairments in mice. *Science* 335:1510–1513
- Kim T-K, Han P-L (2016) Functional connectivity of basolateral amygdala neurons carrying orexin receptors and melanin-concentrating hormone receptors in regulating sociability and mood-related behaviors. *Exp Neurobiol* 25:307–317
- Kim U, Lee T (2012) Topography of descending projections from anterior insular and medial prefrontal regions to the lateral habenula of the epithalamus in the rat. *Eur J Neurosci* 35:1253–1269
- Lammel S, Lim BK, Ran C et al (2012) Input-specific control of reward and aversion in the ventral tegmental area. *Nature* 491:212–217
- Lecca S, Meye FJ, Trusel M, et al (2017) Aversive stimuli drive hypothalamus-to-habenula excitation to promote escape behavior. *eLife* 6:e30697
- Lecourtier L, DeFrancesco A, Moghaddam B (2008) Differential tonic influence of lateral habenula on prefrontal cortex and nucleus accumbens dopamine release. *Eur J Neurosci* 27(7):1755–1762
- Li H, Pullmann D, Cho JY, Eid M, Zhou TC (2019) Generality and opponency of rostromedial tegmental (RMTg) roles in valence processing. *Elife* 8. pii: e41542
- Li H, Pullmann D, Zhou TC (2019) Valence-encoding in the lateral habenula arises from the entopeduncular region. *Elife* 8. pii: e41223
- Manvich DF, Webster KA, Foster SL, et al (2018) The DREADD agonist clozapine N-oxide (CNO) is reverse-metabolized to clozapine and produces clozapine-like interoceptive stimulus effects in rats and mice. *Sci Rep* 8:3840.z
- Marchand AR, Luck D, DiScala G (2003) Evaluation of an improved automated analysis of freezing behaviour in rats and its use in trace fear conditioning. *J Neurosci Methods* 126:145–153
- Maren S, Phan KL, Liberzon I (2013) The contextual brain: implications for fear conditioning, extinction and psychopathology. *Nat Rev Neurosci* 14:417–428
- Marr D (1971) Simple memory: a theory for archicortex. *Philos Trans R Soc Lond B Biol Sci* 262:23–81
- Mathis V, Barbelivien A, Majchrzak M, et al (2016) The lateral habenula as a relay of cortical information to process working memory. *Cereb Cortex* 1–11
- Mathis V, Cosquer B, Avallone M et al (2015) Excitatory transmission to the lateral habenula is critical for encoding and retrieval of spatial memory. *Neuropsychopharmacology* 40:2843–2851
- Mathis V, Cosquer B, Barbelivien A et al (2018) The lateral habenula interacts with the hypothalamo-pituitary adrenal axis response upon stressful cognitive demand in rats. *Behav Brain Res* 341:63–70
- Matsumoto M, Hikosaka O (2009) Representation of negative motivational value in the primate lateral habenula. *Nat Neurosci* 12:77–84
- Metzger M, Souza R, Lima LB, Bueno D, Gonçalves L, Sego C, Donato J Jr, Shammah-Lagnado SJ (2019) Habenular connections with the dopaminergic and serotonergic system and their role in stress-related psychiatric disorders. *Eur J Neurosci*. <https://doi.org/10.1111/ejn.14647>
- Milanovic S, Radulovic J, Laban O et al (1998) Production of the Fos protein after contextual fear conditioning of C57BL/6N mice. *Brain Res* 784:37–47
- Misane I, Tovov P, Meyer M et al (2005) Time-dependent involvement of the dorsal hippocampus in trace fear conditioning in mice. *Hippocampus* 15:418–426
- Padilla-Coreano N, Do-Monte FH, Quirk GJ (2012) A time-dependent role of midline thalamic nuclei in the retrieval of fear memory. *Neuropharmacology* 62:457–463
- Paxinos G, Watson C (2007) The rat brain in stereotaxic coordinates, 6th edn. Elsevier, Academic Press, Amsterdam
- Penzo MA, Robert V, Tucciarone J et al (2015) The paraventricular thalamus controls a central amygdala fear circuit. *Nature* 519:455–459
- Petzel A, Bernard R, Poller WC, Veh RW (2017) Anterior and posterior parts of the rat ventral tegmental area and the rostromedial tegmental nucleus receive topographically distinct afferents from the lateral habenular complex. *J Comp Neurol* 525(10):2310–2327
- Piedra J, Ontiveros M, Miravet S et al (2015) Development of a rapid, robust, and universal picogreen-based method to titer adeno-associated vectors. *Hum Gene Ther Methods* 26:35–42
- Radulovic J, Kammermeier J, Spiess J (1998) Relationship between Fos production and classical fear conditioning: effects of novelty, latent inhibition, and unconditioned stimulus preexposure. *J Neurosci* 18:7452–7461
- Rescorla RA (1968) Probability of shock in the presence and absence of CS in fear conditioning. *J Comp Physiol Psychol* 66:1–5
- Rescorla RA, Wagner AR (1972) A theory of Pavlovian conditioning: Variations in the effectiveness of reinforcement and nonreinforcement. *Class Cond II Curr Res Theory* 64–99
- Root DH, Mejias-Aponte CA, Qi J, Morales M (2014) Role of glutamatergic projections from ventral tegmental area to lateral habenula in aversive conditioning. *J Neurosci* 34:13906–13910
- Rudy JW, Barrientos RM, O'Reilly RC (2002) Hippocampal formation supports conditioning to memory of a context. *Behav Neurosci* 116:530–538
- Runyan JD, Dash PK (2004) Intra-medial prefrontal administration of SCH-23390 attenuates ERK phosphorylation and long-term memory for trace fear conditioning in rats. *Neurobiol Learn Mem* 82(2):65–70
- Sánchez-Catalán MJ, Faivre F, Yalcin I, Muller MA, Massotte D, Majchrzak M, Barrot M (2017) Response of the tail of the ventral tegmental area to aversive stimuli. *Neuropsychopharmacology* 42(3):638–648
- Song M, Jo YS, Lee Y-K, Choi J-S (2017) Lesions of the lateral habenula facilitate active avoidance learning and threat extinction. *Behav Brain Res* 318:12–17
- Stamatakis AM, Stuber GD (2012) Activation of lateral habenula inputs to the ventral midbrain promotes behavioral avoidance. *Nat Neurosci* 15:1105–1107
- Stopper CM, Floresco SB (2014) What's better for me? Fundamental role for lateral habenula in promoting subjective decision biases. *Nat Neurosci* 17:33–35
- Stubbendorff C, Hale E, Cassaday HJ, Bast T, Stevenson CW (2019) Dopamine D1-like receptors in the dorsomedial prefrontal cortex regulate contextual fear conditioning. *Psychopharmacology* 236(6):1771–1782
- Trusel M, Nuno-Perez A, Lecca S, Harada H, Lalive AL, Congiu M, Takemoto K, Takahashi T, Ferraguti F, Mameli M (2019) Punishment-predictive cues guide avoidance through potentiation of hypothalamus-to-habenula synapses. *Neuron* 102(1):120–127
- Veening JG, Böcker KBE, Verdouw PM et al (2009) Activation of the septohippocampal system differentiates anxiety from fear in startle paradigms. *Neuroscience* 163:1046–1060
- Wang D, Li Y, Feng Q, et al (2017) Learning shapes the aversion and reward responses of lateral habenula neurons. *eLife* 6:e23045

- Wang Z, Wang L, Yamamoto R et al (2013) Role of the lateral habenula in shaping context-dependent locomotor activity during cognitive tasks. *NeuroReport* 24:276–280
- Wirtshafter D, Asin KE, Pitzer MR (1994) Dopamine agonists and stress produce different patterns of Fos-like immunoreactivity in the lateral habenula. *Brain Res* 633:21–26
- Yamaguchi T, Danjo T, Pastan I et al (2013) Distinct roles of segregated transmission of the septo-habenular pathway in anxiety and fear. *Neuron* 78:537–544
- Zahn DS, Root DH (2017) Review of the cytology and connections of the lateral habenula, an avatar of adaptive behaving. *Pharmacol Biochem Behav* 162:3–21
- Zhang J, Tan L, Ren Y et al (2016) Presynaptic excitation via GABAB receptors in habenula cholinergic neurons regulates fear memory expression. *Cell* 166:716–728
- Zhou W, Jin Y, Meng Q et al (2019) A neural circuit for comorbid depressive symptoms in chronic pain. *Nat Neurosci* 22:1649–1658

Publisher's Note Springer Nature remains neutral with regard to jurisdictional claims in published maps and institutional affiliations.

Supplementary Information

Involvement of the lateral habenula in fear memory

Laura Durieux^{1,2}, Victor Mathis^{1,2,3}, Karine Herbeaux^{1,2}, Marc–Antoine Muller^{1,2}, Alexandra Barbelivien^{1,2}, Chantal Mathis^{1,2}, Rémy Schlichter⁴, Sylvain Hugel⁴, Monique Majchrzak^{1,2}, Lucas Lecourtier^{1,2}

¹Laboratoire de Neurosciences Cognitives et Adaptatives, Université de Strasbourg, Strasbourg, France.

²LNCA, UMR 7364, Centre National de la Recherche Scientifique, Strasbourg, France.

³Present address: Department of Neuroscience, Icahn School of Medicine at Mount Sinai, New York 10029–6574, USA.

⁴Institut des Neurosciences Cellulaires et Intégratives (INCI), UPR–3212, CNRS, 5 Rue Blaise Pascal, 67000 Strasbourg, France.

Supplementary information include:

Methodological details and illustration of the delineation of the regions of interest in which c-Fos+ cells were counted (**pages 3–9**).

A detailed description of the method used to perform the counting of c-Fos+ cells using ImageJ macros (**pages 10–12**).

The comparisons of the values of c-Fos+ cells in both hemispheres for each region (**page 13**), followed by the pooling of both values (**page 14**).

Statistical analyses of behavioural performances of the two Veh-treated control groups (Sham-Veh and hM4-Veh) before their gathering in a single control group (**page 15**).

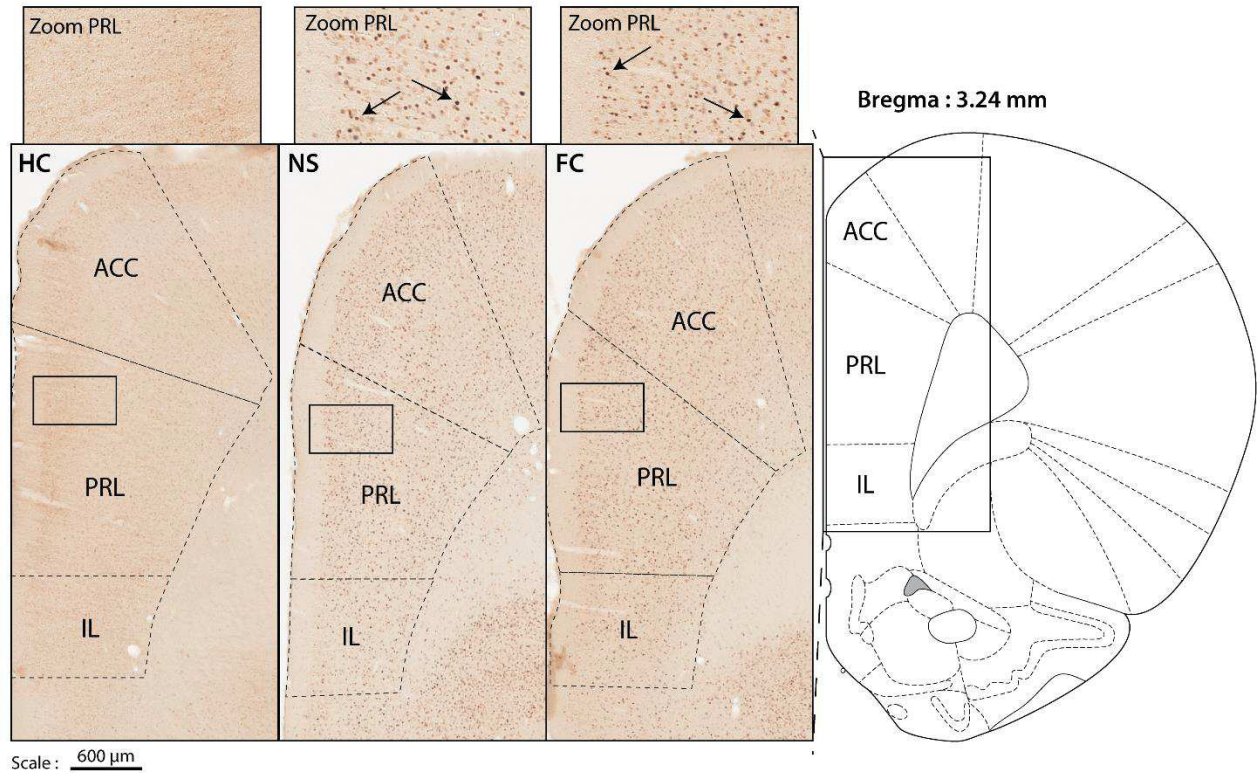
Quantification of c-Fos+ cells

Scanning of brain sections

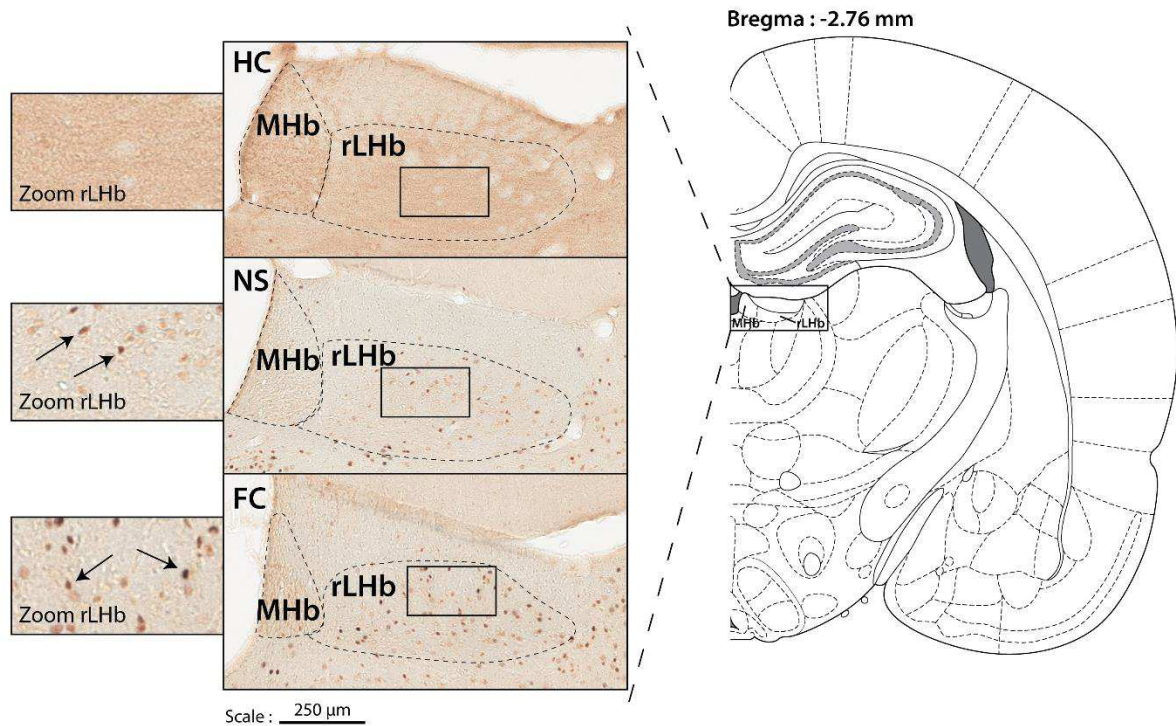
Sections (3–6 slices per region) were scanned using a NanoZoomer S60 (Hamamatsu) with an image processing software (NDP.scan, Hamamatsu), with a x 20 magnification. Images were saved in NDPI format.

Delineation of the regions of interest

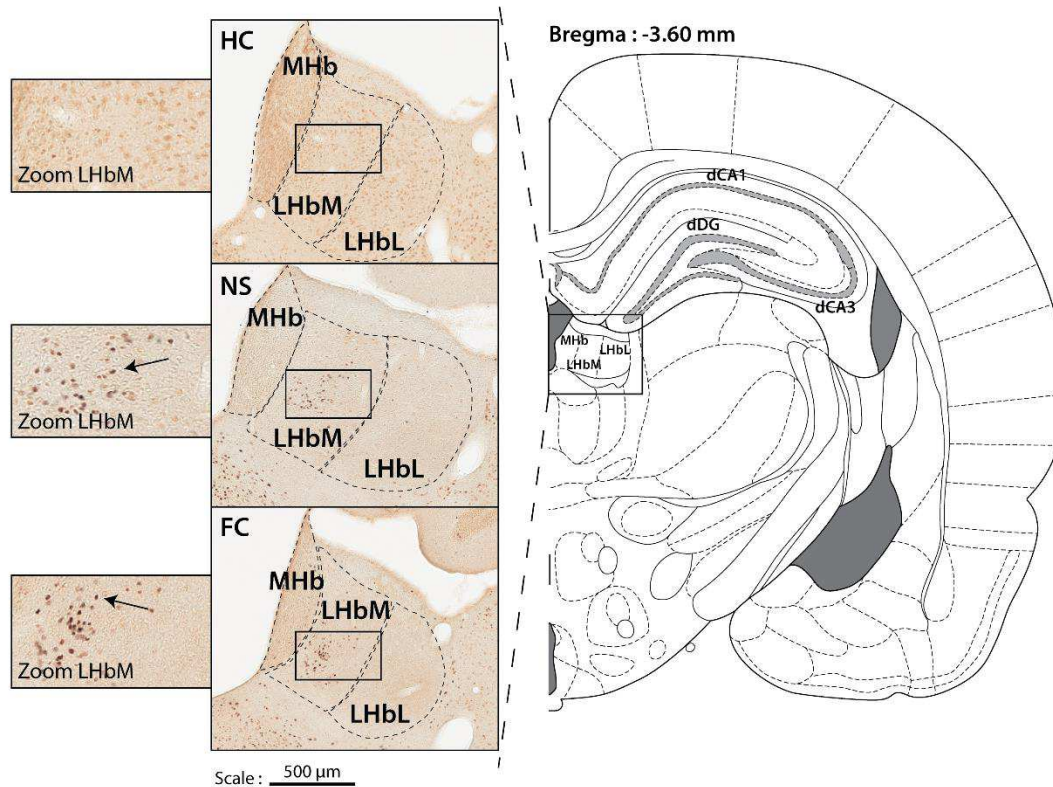
A ImageJ (Free license, Wayne Rasband, Research Services Branch, NIH, Bethesda, Maryland, USA) macro transformed the RGB images in 8-bit grey scale images. The different structures of interest were first manually outlined on each slice (see examples of outlining for each structure on **Supplementary Fig. 1–6**). Quantification was performed in each section (3 to 6 per subregion) at the following coordinates (in mm from Bregma): **medial prefrontal cortex** [mPFC, including a prelimbic (PRL), an infralimbic (IL), and an anterior cingulate (ACC) region]: between + 4.20 and + 2.52; **amygdala** [including a central (CeA), a lateral (LA) and a basal (BL) region]: between – 2.04 and – 3.84; **rostral part of the lateral habenula** (rLHb): between – 2.28 and – 2.92; **medial habenula** (MHb): between – 2.28 and – 4.40; **lateral habenula** [LHb, including a lateral (LHbL), and a medial (LHbM) subdivision]: between – 3.00 and – 4.36; **rostral part of the hippocampus** [including the dorsal hippocampus region (dHPC) composed of ammonic field regions 1 (drCA1) and 3 (drCA3), and dentate gyrus (drDG)]: between – 2.28 and – 4.56; **caudal part of the hippocampus** [including the *caudal part of the dHPC*, composed of ammonic field regions 1 (dcCA1) and 3 (dcCA3), and dentate gyrus (drDG)], and the *ventral part of the HPC* (vHPC), composed of ammonic field regions 1 (vCA1) and 3 (vCA3), and dentate gyrus (vDG): between – 4.68 and – 6.24). According to the dHPC, we pooled countings from the drHPC and dcHPC (mean of the two values) for each of the three subregions (CA1, CA3, DG; **Supplementary Fig. 5–6**).



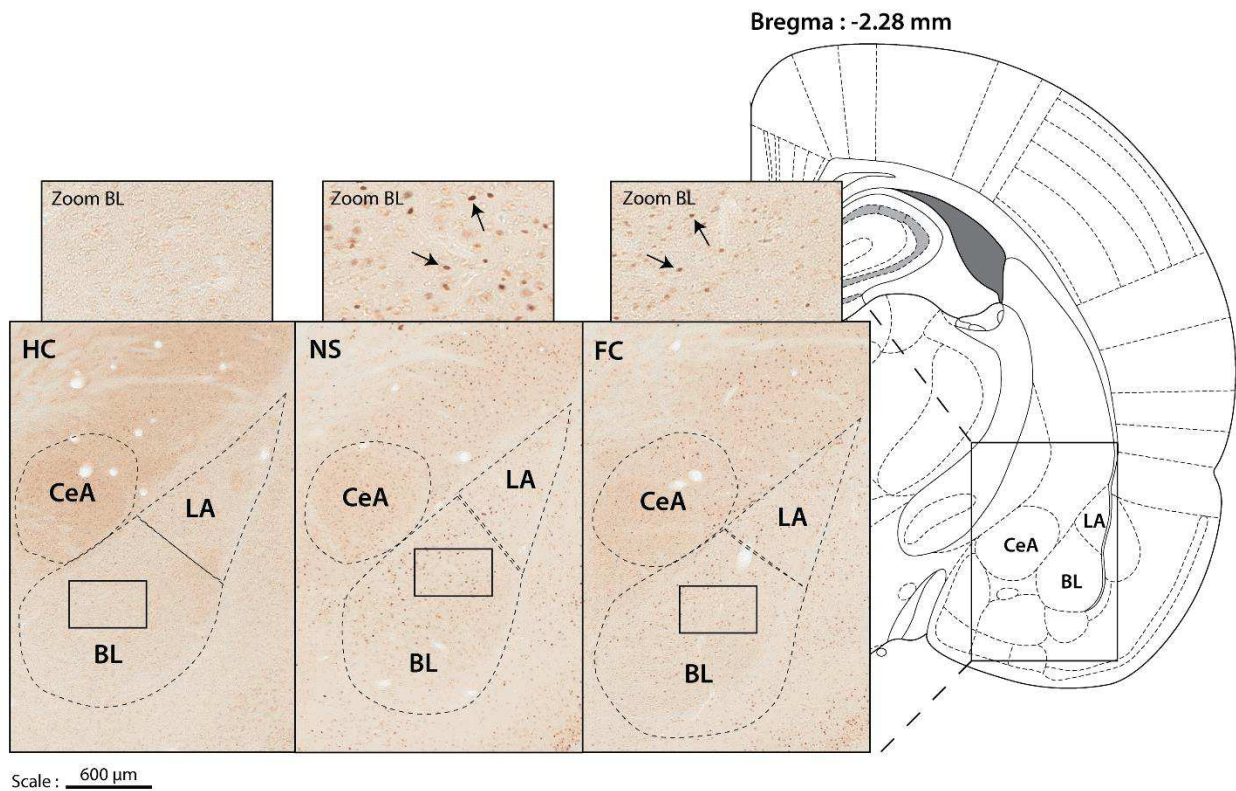
Supplementary Fig. 1. Delineation (dashed lines on the microphotographs on the left) of medial prefrontal cortical subregions, including the anterior cingulate (ACC), prelimbic (PRL), and infralimbic (IL) subregions. Examples of c-Fos expression within the PRL region (zoom) in a Home Cage (HC, left) or in a No-Shock (NS, middle) or in a Fear Conditioning (FC, right) rat. Black arrows point to examples of neurons included in the counting.



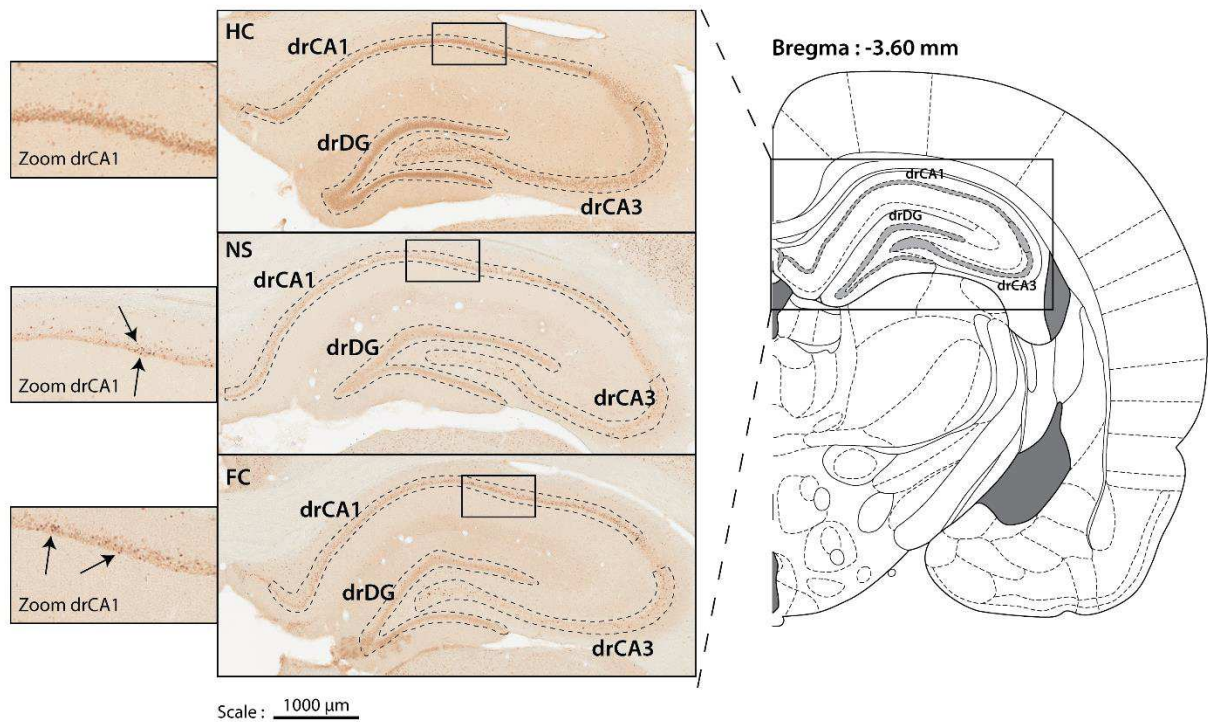
Supplementary Fig. 2. Delineation (dashed lines on the microphotographs in the middle) of habenular regions in its most anterior part, when there is no delimitation of a medial and lateral subdivision of the LHb, with examples of c-Fos expression (zoom) within the rLHb in a Home Cage (HC, left) or in a No-Shock (NS, middle) or in a Fear Conditioning (FC, right) rat. Abbreviations: rLHb, rostral part of the LHb; MHb, medial habenula.



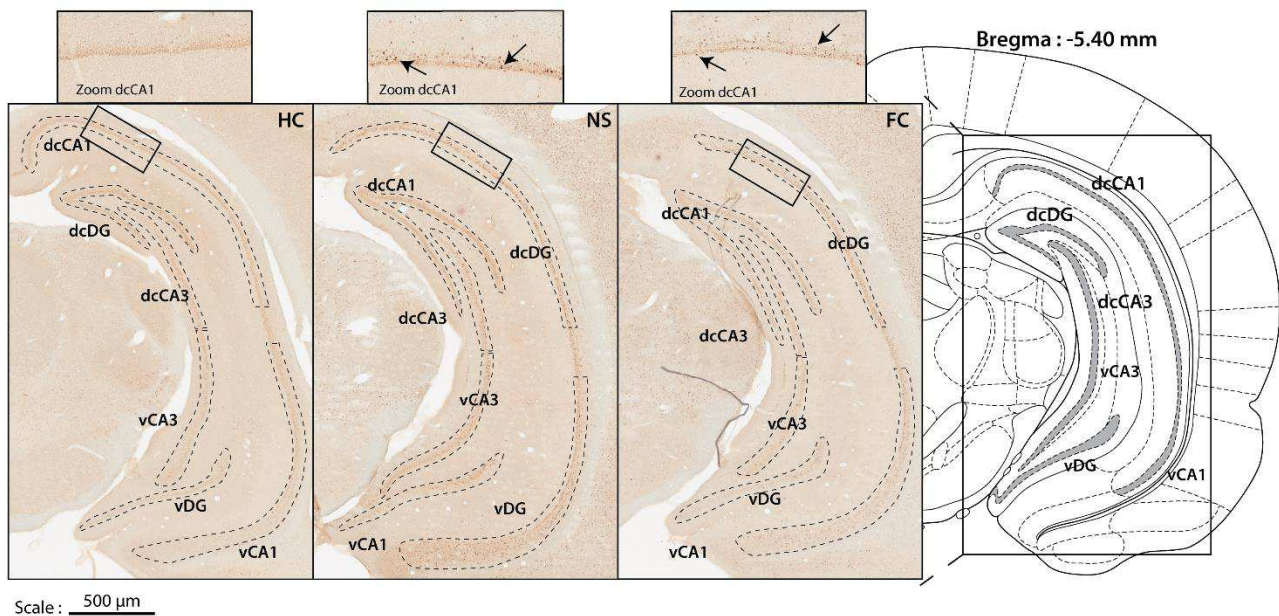
Supplementary Fig. 3. Delineation (dashed lines on the microphotographs in the middle) of habenular regions in its posterior part, when there is a delimitation between a medial LHbM) and a lateral (LHbL) subdivision of the LHb, with examples of c-Fos expression (zoom) within the LHbM in a Home Cage (HC, left) or in a No-Shock (NS, middle) or in a Fear Conditioning (FC, right) rat. Abbreviations: MHb, medial habenula.



Supplementary Fig. 4. Delineation (dashed lines on the microphotographs on the left) of amygdalar subregions, including the central (CeA), lateral (LA), and basal (BL) nuclei, with examples of *c-Fos* expression (zoom) within the BL nucleus in a Home Cage (HC, left) or in a No-Shock (NS, middle) or in a Fear Conditioning (FC, right) rat. Black arrows point to examples of neurons included in the counting.



Supplementary Fig.5. Delineation (dashed lines on the microphotographs in the middle) of hippocampal subregions in its most rostral part, so-called dorsal hippocampus, including CA1, CA3, and DG subregions, with examples of c-Fos expression (zoom) within the CA1 subregion in a Home Cage (HC, left) or in a No-Shock (NS, middle) or in a Fear Conditioning (FC, right) rat. Black arrows point to examples of neurons included in the counting. **Abbreviations:** drCA1, rostral part of dorsal CA1; drCA3, rostral part of dorsal CA3; drDG, rostral part of dorsal DG.



Supplementary Fig. 6. Delineation (dashed lines on the microphotographs on the left) of hippocampal subregions in its caudal part, when there is a dorsal hippocampal region still present, along with the ventral hippocampal region (vHPC), including CA1 [dorso-caudal (dcCA1, and ventral (vCA1)], CA3 [dorso-caudal (dcCA3, and ventral (vCA3)], and DG [dorsal region in the caudal part (dcDG), and ventral (vDG)] subregions, with examples of c-Fos expression (zoom) in dCA1 in a Home Cage (HC, left) or in a No-Shock (NS, middle) or in a Fear Conditioning (FC, right) rat. Black arrows point to examples of neurons included in the counting.

Quantification of c-Fos density

Counting of c-Fos+ cells was performed in each delineated region using ImageJ with homemade scripts. A median blur with a radius of 2 μm was applied in order to perform noise reduction in the active image by replacing each pixel with the median of the neighboring pixel values; this led to the removal of small artefacts while sparing nuclei. Then, the FindMaxima() function was applied. It is an algorithm which determines the local maxima in the image. It is based on the parameter called "Noise Tolerance" (calibrated unit) which allows to set a threshold at the maximum value minus the noise tolerance (set according to the calculations detailed below). The continuous area around the maximum found is then analyzed and this process is repeated each time the algorithm finds a local maximum.

As the counting macro was homemade, we first verified that it was providing accurate results. To this matter, we compared the results it gave with those acquired manually in one of the structures of interest, the medial part of the lateral habenula. We tested 6 numbers from 50 to 100 (step of 10) of the noise tolerance parameter of the FindMaxima() function and selected the more appropriate value based on the equation of the correlation.

$$Y = (a * X) + b \text{ (A1)},$$

where Y is the value given by automated counting, X is the value given by manual counting, a is the slope of the best fitting line, and b is the intersection with the Y axis. Based on this linear equation, we can find the more accurate parameter (noise tolerance) of the FindMaxima() function. For that, we need to have $Y = X$, representing the ideal case where the manual and the automated methods provide the same number of counted objects.

If $a = 1$ and $b = 0$, then:

$$Y = (1 \times X) + 0 \text{ (A2)},$$

$$\text{so } Y = X \text{ (A3)}.$$

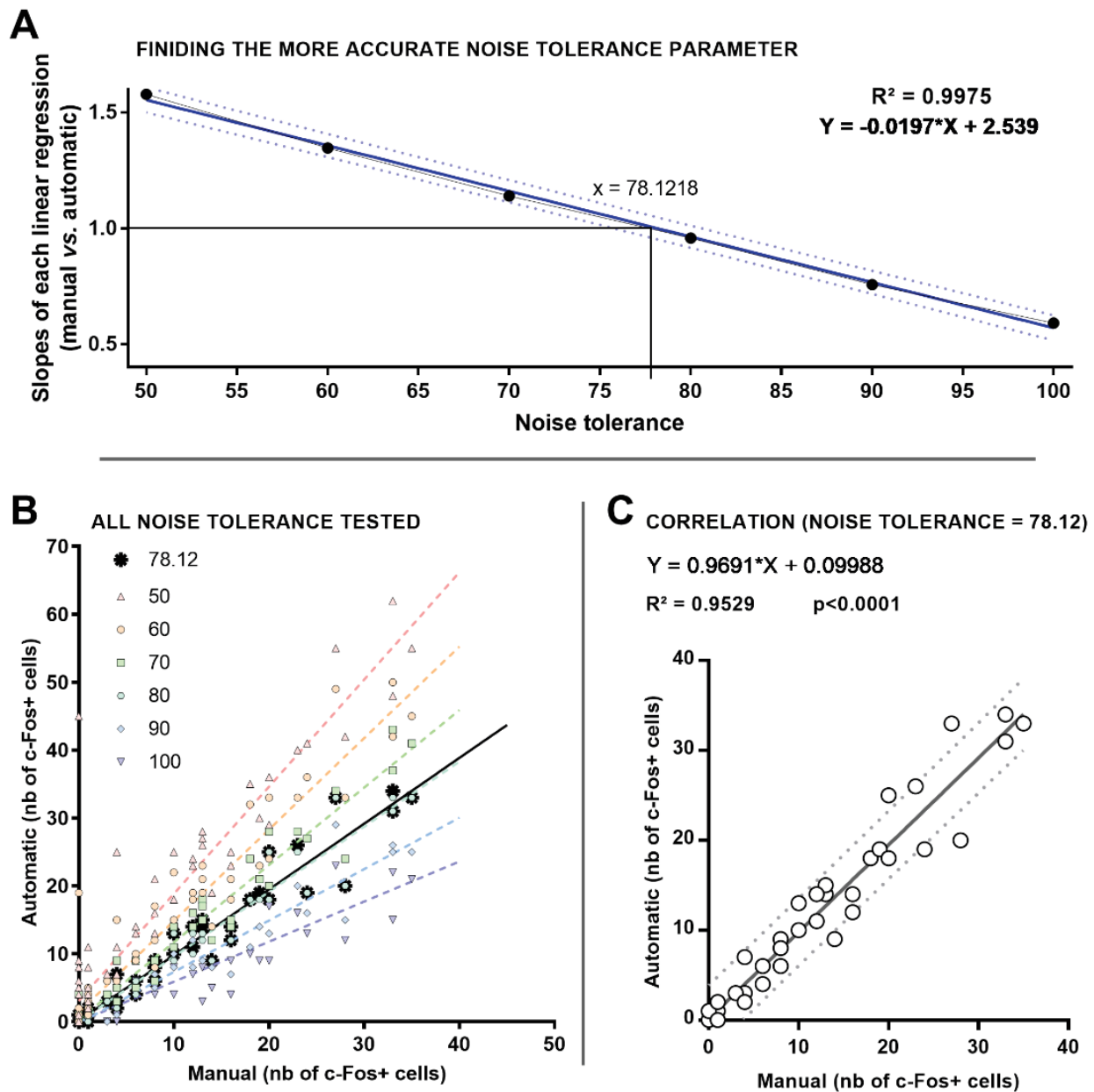
The closest parameter found was 78.12 (**Supplementary Fig. 7**), displaying a linear equation of:

$$Y = (0.9691 * X) + 0.09988 \text{ (A4)}$$

The correlation found with this noise tolerance parameter was very high ($R^2 = 0.95$; $p < 0.0001$), allowing to conclude positively on the accuracy and reliability of the automated counting method.

The macro displays all the results (such as area, mean, minimum, maximum grey value, and number of c-Fos+ neurons). To obtain densities, values in pixels were transformed in mm². Finally, for each region, values of both hemispheres were pooled (**Supplementary Table 1**) after it was verified they did not differ statistically (**Supplementary Fig. 8**).

Image J parameter (noise tolerance) for FindMaxima() function

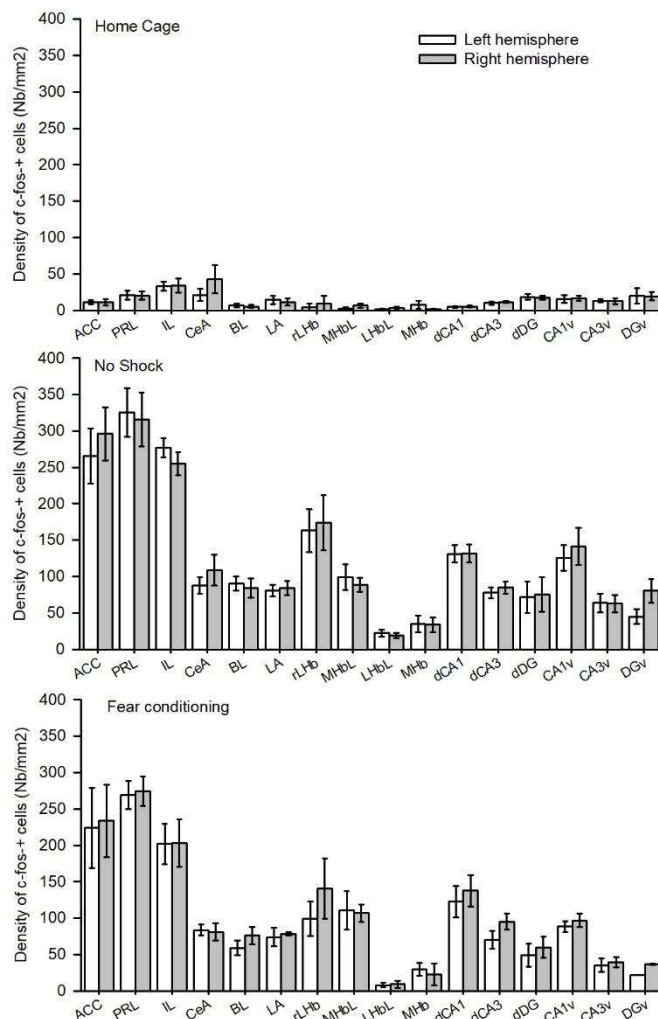


Supplementary Fig. 7. Assessment of the accuracy of automated as opposed to manual counting methods. **(A)** Plot showing the correlation between each slope (from linear regression of manual vs automated counting) and the noise tolerance parameter on the FindMaxima() function in ImageJ. We tested for 50, 60, 70, 80, 90 and 100, and then took the slope (“a”) number from the equation ($Y = a * X + b$) of the best line fitting our data set. The data show an affine function allowing us to calculate the best parameter (noise tolerance) for the automated counting. Consequently, the most efficient score for noise tolerance (with $Y = 1$) equals 78.12. **(B)** Linear regression between automated counting with different parameters set and manual counting; one can see that the more representative parameter for manual counting seems to be at 78.12 in comparison with the other values. **(C)** Plot representing the linear correlation of manual vs automated counting; “a” is close to 1, demonstrating the similarity between manual and automated counting methods. Indeed, there is a very high correlation between manual and automatic counting ($R^2 = 0.95$; $p < 0.0001$).

Results

Comparison of the density of c-Fos+ cells between both hemispheres

For each structure, using paired t-tests, we first verified that values of c-Fos+ cells densities from both hemispheres did not vary statistically. Therefore, for all the structures final values were calculated as mean of both hemispheres' values (see **Supplementary Table 1**).



Supplementary Fig. 8. In none of the behavioural condition did the densities of c-Fos+ cells vary between the two hemispheres. *Abbreviations:* ACC, anterior cingulate cortex; BL, basal nucleus of the amygdala; CeA, central nucleus of the amygdala; d/vCA1, ammonic field 1 of the dorsal/ventral hippocampus; d/vCA3, ammonic field 3 of the dorsal/ventral hippocampus; dcDG, dorsal dentate gyrus in the caudal part of the HPC; drDG, dorsal dentate gyrus in the rostral part of the HPC; IL, infralimbic cortex; LA, lateral nucleus of the amygdala; LHb, lateral habenula; LHbL, lateral part of the lateral habenula; LHbM, medial part of the lateral habenula; PRL, prelimbic cortex; rLHb, rostral part of the LHb; vDG, ventral dentate gyrus.

Following the analyses presented in **Supplementary Fig. 8**, values of both hemispheres were pooled. Results are presented in **Supplementary Table 1** below.

		Home Cage		No Shock		Fear Conditioning	
		Density (nb/mm ²)		Density (nb/mm ²)		Density (nb/mm ²)	
		Mean	SEM	Mean	SEM	Mean	SEM
medial Prefrontal cortex	ACC	9.62	2.98	281.93	31.23	228.74	52.19
	PRL	17.55	5.76	311.09	26.18	256.36	29.10
	IL	28.98	7.55	262.83	15.26	202.56	29.77
Amygdala	CeA	27.07	3.70	93.91	8.35	68.06	9.59
	BL	7.95	2.47	90.38	9.73	68.79	4.89
	LA	16.11	4.46	81.32	7.58	81.11	5.19
Habenula	rLHb	6.24	2.62	143.35	18.04	128.93	20.82
	LHbM	6.74	2.00	87.90	13.02	107.92	15.72
	LHbL	1.82	0.48	21.17	3.51	8.09	1.73
	MHb	4.94	1.35	36.52	8.45	21.81	5.96
dorsal Hippocampus	dCA1	4.56	0.46	130.53	14.36	113.53	14.68
	dCA3	10.08	0.87	84.63	7.37	73.41	8.50
	dDG	18.60	3.12	65.87	7.37	18.60	3.12
ventral Hippocampus	vCA1	16.50	3.87	121.62	12.52	99.92	6.02
	vCA3	11.95	2.40	52.20	6.58	33.57	3.70
	vDG	17.95	5.83	55.78	8.47	32.31	4.30

Supplementary Table 1. Values represent the mean (\pm SEM) density of c-Fos+ cells for each region. *Abbreviations:* ACC, anterior cingulate cortex; BL, basal nucleus of the amygdala; CeA, central nucleus of the amygdala; d/vCA1, ammonic field 1 of the dorsal/ventral hippocampus; d/vCA3, ammonic field 3 of the dorsal/ventral hippocampus; dcDG, dorsal dentate gyrus in the caudal part of the HPC; drDG, dorsal dentate gyrus in the rostral part of the HPC; IL, infralimbic cortex; LA, lateral nucleus of the amygdala; LHb, lateral habenula; LHbL, lateral part of the lateral habenula; LHbM, medial part of the lateral habenula; PRL, prelimbic cortex; rLHb, rostral part of the LHb; vDG, ventral dentate gyrus.

Comparative analyses of performances of Sham–Veh and hM4–Veh rats, by means of t–tests, in order to gather them into a single Ctl–Veh group

Elevated plus maze

Total number of visits in the 4 arms: $t_{10} = -1.00, p > 0.3$.

Number of visits in open arms (% of total arm entries): $t_{10} = -0.37, p > 0.7$.

Time in open arms (% of total time in all arms): $t_{10} = -0.38, p > 0.7$.

Fear conditioning

Conditioning

Baseline: $t_{10} = 1.09, p > 0.2$.

Post–US: $t_{10} = 0.03, p > 0.9$.

Context test

$t_{10} = 1.15, p > 0.2$.

New context exposure

$t_{10} = 1.80, p > 0.1$.

CS test

Baseline: $t_{10} = 2.18, p > 0.05$

CS presentation: $t_{10} = -0.32, p > 0.7$

Locomotor activity

Baseline (total): $t_{10} = -0.60, p > 0.5$.

Post–injection (total): $t_{10} = 0.97, p > 0.3$.

In consequence, for each test Sham–Veh and hM4–Veh rats have been pooled in a single Ctl–Veh group for all analyses.

RESULTS - STUDY 2: Functional brain-wide network mapping during acute stress exposure in rats. Impact of DREADD-induced lateral habenula inactivation, with a note on CNO

II. STUDY 2: Functional brain-wide network mapping during acute stress exposure in rats. Impact of DREADD-induced lateral habenula inactivation, with a note on CNO

Functional brain-wide network mapping during acute stress exposure in rats: Interaction between the lateral habenula and cortical, amygdalar, hypothalamic and monoaminergic regions

Running title: Lateral habenula and stress network

Authors

Laura Durieux^{1*}, Karine Herbeaux¹, Christopher Borcuk¹, Cécile Hildenbrand¹, Virginie Andry^{2,3}, Yannick Goumon^{2,3}, Alexandra Barbelivien¹, Chantal Mathis¹, Demian Bataglia^{1,4,5}, Monique Majchrzak^{1*#}, Lucas Lecourtier^{1*#}

Affiliations

¹Université de Strasbourg, CNRS, Laboratoire de Neurosciences Cognitives et Adaptatives (LNCA), UMR 7364, F-67000 Strasbourg, France.

²CNRS UPR3212, Institut des Neurosciences Cellulaires et Intégratives, Centre National de la Recherche Scientifique, University of Strasbourg, Strasbourg, France.

³Mass Spectrometry Facilities of the CNRS UPR3212, Institut des Neurosciences Cellulaires et Intégratives, Centre National de la Recherche Scientifique, Strasbourg, France.

⁴University of Strasbourg Institute for Advanced Studies (USIAS), F-67000 Strasbourg, France.

⁵Université d'Aix-Marseille, Inserm, Institut de Neurosciences des Systèmes (INS) UMR-S 1106, F-1213005 Marseille, France.

*Corresponding authors: #Equal contribution

ACKNOWLEDGEMENTS

The authors wish to thank Dr. Michel Barrot for the gift of CNO and Elouan Cosquer for its helps and expertise with Python language.

Functional brain-wide network mapping during acute stress exposure in rats: Interaction between the lateral habenula and cortical, amygdalar, hypothalamic and monoaminergic regions

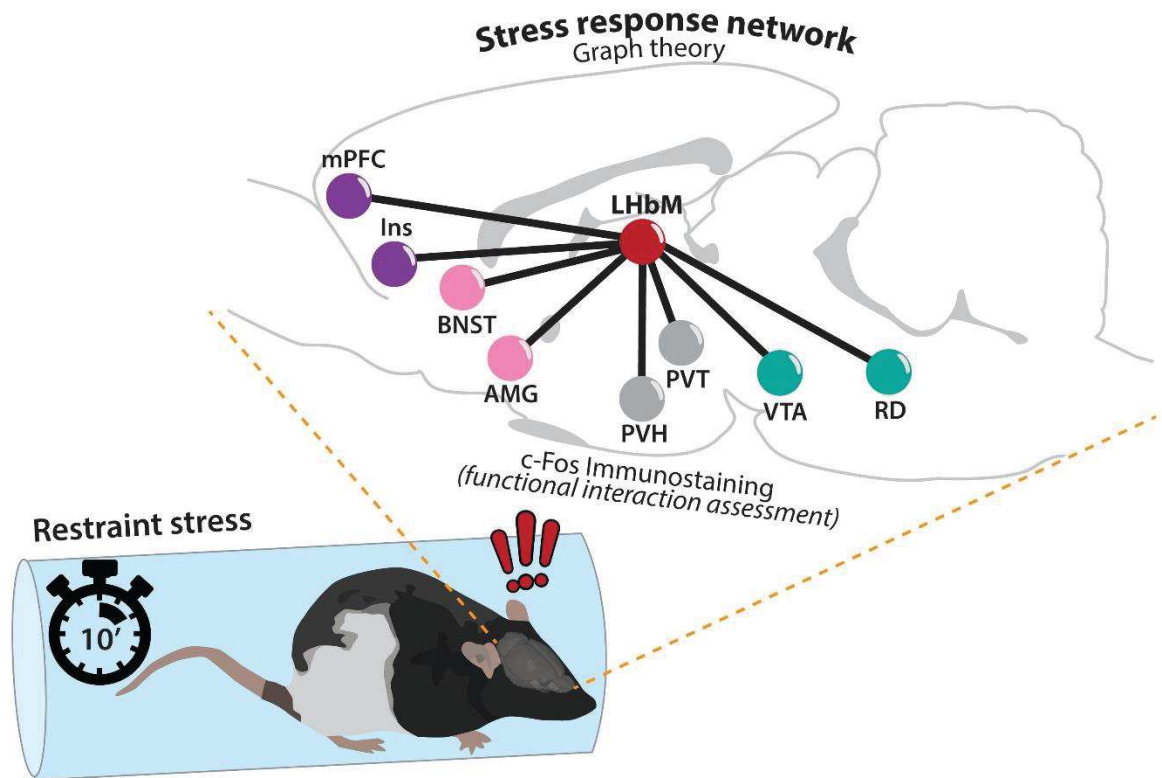
Abstract

Upon stress exposure a broad network of structures comes into play in order to provide adequate responses and restore homeostasis. It has been known for decades that the main structures engaged during the stress response are the medial prefrontal cortex, the amygdala, the hippocampus, the monoaminergic systems (noradrenaline, dopamine, serotonin), and the periaqueductal gray. The lateral habenula (LHb) is an epithalamic structure directly connected to prefrontal cortical areas and to the amygdala, whereas it functionally interacts with the hippocampus. Also, it is a main modulator of monoaminergic systems. The LHb is activated upon exposure to basically all types of stressors, suggesting it is also involved in the stress response. However, it remains unknown if and how the LHb functionally interacts with the broad stress response network. In the current study we performed in rats a restraint stress procedure followed by immunohistochemical staining of the c-Fos protein throughout the brain. Using functional correlational analyses based on Graph Theory, we show here that the LHb is engaged during stress exposure in close interaction with important structures such as the medial prefrontal cortex, the insular cortex, the extended amygdala, the paraventricular hypothalamic nucleus, and the raphe nucleus. In addition, we performed DREADD-induced LHb inactivation during the same restraint paradigm in order to explore its consequences on the stress response network. This last experiment gave contrasting results as the DREADD ligand alone, clozapine-N-oxide, was able to modify the network.

KEYWORDS

lateral habenula, stress response, DREADD, functional connectivity, graph theory

GRAPHICAL ABSTRACT



In this study, using immunohistochemical staining of the immediate early gene c-fos and graph theory-based functional correlational analyses, we aimed at unravelling the possible engagement of the LHb within the stress response network during acute stress exposure (10-min restraint) in rats. We found that the medial part of the LHb (LHbM) was preferentially engaged and that this engagement was correlated with this of structures such as the medial prefrontal cortex (mPFC), the insular cortex (Ins), hypothalamic (PVH) and thalamic (PVT) paraventricular nuclei, the extended amygdala, comprising the Bed nucleus of the stria terminalis (BNST) and the entire amygdala (AMY), as well as midbrain monoaminergic structures, i.e. the dopaminergic ventral tegmental area (VTA) and the serotonergic dorsal raphe nucleus (RD). This suggests upon stressful situations the LHbM serves as a relay of cortical, thalamic, hypothalamic and temporal information, further transmitted to the monoaminergic systems to engage coping strategies.

List of Abbreviations

AAV8: Adeno-Associated Virus serotype 8	mBNST: Bed Nucleus of the <i>Stria Terminalis</i> (medial part)
ACC: Anterior Cingulate Cortex	MCC: Mid Cingulate Cortex
ACN: acetonitrile	MD: Medio-Dorsal nucleus of the thalamus
AMG: Amygdala	MHb: Medial Habenula
BA: Basal nucleus of the Amygdala	MM: Mammillary nucleus of hypothalamus
BLA: Basal Lateral nucleus of the Amygdala	MO: Medial Orbitofrontal cortex
BNST: Bed Nucleus of the <i>Stria Terminalis</i>	mPFC: medial prefrontal cortex
CamKII: CA ²⁺ /Calmodulin-dependent protein Kinase II	MR: Raphe Median
CeA: Central nucleus of the Amygdala	MS: Medial Septum
Cl: Claustrum	MSpect: Mass Spectrometer
cNAc: core of the Nucleus Accumbens	PAG: Periaqueductal Gray
CNO: Clozapine-N-Oxide	PBS: Phosphate Buffered Saline
CORT: Corticosterone	PFC: Prefrontal Cortex
dCA1: dorsal <i>Cornus Ammonis</i> 1	PRh: Perirhinal cortex
dCA2: dorsal <i>Cornus Ammonis</i> 2	PRL: Prelimbic cortex
dCA3: dorsal <i>Cornus Ammonis</i> 3	PVH: Paraventricular nucleus of the Hypothalamus
dDG: dorsal Dentate Gyrus	PVT: Paraventricular nucleus of the Thalamus
dIS: dorso-lateral Striatum	Re: Reuniens nucleus
dmS: dorso-median Striatum	RS: Retrosplenial Cortex
DMSO: Dimethyl sulfoxide	sNAc: shell of the Nucleus Accumbens
DR: Raphe Dorsal	SNc: <i>Substantia Nigra pars compacta</i>
DREADD: Designer Receptor Exclusively Activated by Designer Drugs	SNr: <i>Substantia Nigra pars reticula</i>
Ect: Ectorhinal cortex	SRM: Selected Reaction Monitoring
Ent: Entorhinal cortex	SuMM: Supramammillary nucleus of the hypothalamus
hM4(Gi): modified human Muscarinic 4 (coupled with inhibitory G protein)	TS: Triangular Septal nucleus
HPA: hypothalamus-pituitary-adrenal	tVTA: tail of the Ventral Tegmental Area
HPC: Hippocampus	vCA1: ventral <i>Cornus Ammonis</i> 1
HPLC: High performance liquid chromatography	vCA2: ventral <i>Cornus Ammonis</i> 2
IL: Infralimbic cortex	vCA3: ventral <i>Cornus Ammonis</i> 3
Ins_C: Caudal part of the Insular cortex	vDG: ventral Dentate Gyrus
Ins_R: Rostral part of the Insular cortex	vis: ventro-lateral Striatum
LA: Lateral nucleus of the Amygdala	vmS: ventro-median Striatum
IBNST: Bed Nucleus of the <i>Stria Terminalis</i> (lateral part)	VO: Ventral Orbitofrontal cortex
LC: Locus Coeruleus	VP: Ventral Pallidum
LDT: Latero-dorsal Tegmental nucleus	VTA: Ventral Tegmental Area
LH: Lateral Hypothalamus	
LHb: Lateral Habenula	
LHbL: Lateral part of the Lateral Habenula	
LHbM: Medial part of the Lateral Habenula	
LO: Lateral Orbitofrontal cortex	
LS: Lateral Septum	

INTRODUCTION

Adaptive response to stress exposure requires the coordinated activity of an extended brain network involved in cognitive, emotional, and motor processes (Joëls and Baram, 2009; Godoy et al., 2018). A large part of the studies addressing stress-induced changes in such functional network did so in the context of chronic stress, in order to better understand pathological conditions (e.g. Henckens et al., 2015; Magalhães et al., 2018). In humans, acute stressors engage key regions such as the insula (Ins), amygdala (AMG), anterior cingulate cortex (ACC), ventral striatum, prefrontal cortex (PFC), hippocampus (HPC), bed nucleus of the stria terminalis (BNST), thalamus, and the paraventricular nucleus of the hypothalamus (PVH) (Herman et al., 2003; Sousa, 2016). These structures – or their homologous - have also been shown to subservise physiological and behavioral responses to stress exposure in rodents (Herman et al., 2003; McEwen et al., 2015; Godoy et al., 2018).

In recent years, the lateral habenula (LHb), an epithalamic structure integrating forebrain information and modulating the activity of the main monoaminergic pathways, emerged as a prominent region for the control of the stress response (Hikosaka, 2010; Hu et al., 2020). The LHb is strongly activated by acute exposure to various stressors ranging from mild ones, like exposure to a novel environment (Wirtshafter et al., 1994; Durieux et al., 2020), to more severe such as electrical foot-shock, immobilization, tail pinch, and predator exposure (Chastrette et al., 1991; Wirtshafter et al., 1994; González-Pardo et al., 2012; Brown and Shepard, 2013; Dolzani et al., 2016; Zhang et al., 2016; Lecca et al., 2017; Barrett and Gonzalez-Lima, 2018; Durieux et al., 2020). Interestingly, in rodents the LHb directly or indirectly interacts with the above-cited key regions of the stress response. Regions which send direct projections onto the LHb comprise the entire PFC (Kim and Lee, 2012), and the extended amygdala, including the BNST (Dong and Swanson, 2004, 2006), and the basolateral (Kim and Han, 2016) and central (Zhou et al., 2019) amygdalar nuclei. The LHb and HPC, although they do not share direct connections, likely communicate and functionally interact (Aizawa et al., 2013; Goutagny et al., 2013; Baker et al., 2019). The LHb has been shown to modulate the hypothalamus-pituitary-adrenal (HPA) axis (one of the primary effectors of the stress response; Selye, 1950; de Kloet et al., 1998), and therefore most likely the activity of the PVH (Murphy et al., 1996; Jacinto et al., 2016; Mathis et al., 2018). In addition, the LHb, as shown in rodents, cats and monkeys, can modulate the main neurotransmitter systems involved in the stress response, *i.e.*, dopamine (Christoph et al., 1986; Ji and Shepard, 2007; Lecourtier et al., 2008), noradrenaline (Kalen, 1989a; Cenci et al., 1992), and serotonin (Reisine et al., 1982; Kalen et al., 1989b). The link with the serotonergic system is of particular interest as inhibition of the LHb-dorsal raphe nucleus pathway in rats reduces passive stress response (Coffey et al., 2020). The LHb also interacts with other regions to process emotional responses. For example, in mice inhibition of the lateral hypothalamus-LHb pathway alters escape behavior upon unpredictable exposure to foot-shocks (Lecca et al., 2017), and stimulation of the pathway connecting the entopeduncular nucleus to the LHb (Shabel et al., 2012), the LHb to the ventral tegmental area (Lammel et al., 2012), and

the LHb to the rostromedial tegmental nucleus (Stamatakis and Stuber, 2012), induces aversive responses. Finally, probably through an indirect activation of rostral medullary raphe neurons, the LHb has been involved in rats in the control of stress-induced hyperthermia, a component of the physiological stress response (Ootsuka et al., 2017).

To date no study has been devoted to unravelling if and how the LHb is part of the broad network involved in the stress response. In the current study we used acute exposure to restraint stress as a behavioural paradigm and specifically aimed to describe: 1) the network activated by restraint and the position of the LHb within this network, and 2) the consequences of DREADD-induced LHb inactivation on the connectivity of the network. To this aim we quantified the level of expression of the c-Fos protein in a large number of brain regions, including the key structures involved in the acute stress response. The immediate-early gene c-Fos appeared relevant to explore as it is the best characterized and most widely used tool for functional anatomical mapping in rodents, given its rapid activation by various stimuli (Kovács, 1998; Hudson, 2018). The quantification of the density of c-Fos positive (c-Fos+) cells throughout the brain, and the exploration of between-structure correlations can reveal functional interactions between structures belonging to a given network, as several studies previously agreed (e.g., in fear memory; Wheeler et al., 2013; Vetere et al., 2017). This level of analysis can be achieved applying a Graph theory approach. Graph theory is a mathematical field allowing to analyze complex networks (Bullmore and Sporns, 2009). The main principle of this approach is to consider the structures as nodes of a given network, nodes that are connected through edges (the functional variable, in our study, c-Fos+ cells density correlations). Then, different parameters of the network can be revealed, such as the principal hubs of the network, through strength analysis, or the presence of sub-networks, which could be engaged in different aspects of the ongoing process, through the extraction of modules/communities (see Bullmore and Sporns 2009 for examples). Finally, in animals exposed to restraint, we assessed the level of plasmatic corticosterone, before and following restraint, in order to control for the effectiveness of such procedure and to further investigate if the LHb modulates the HPA axis upon stress exposure.

MATERIALS & METHODS

Animals

This experiment, authorized by the French authorities (APAFIS#7114), was carried out with 44 five months old male Long–Evans rats (Janvier Labs, France) issued from a previous study (Durieux et al., 2020). They were housed in pairs on a 12 h light/dark cycle (lights on at 7:00 A.M.) with *ad libitum* access to food and water. Rats were singly housed five days before the start of the experiment and, the last three days, were familiarized to the holding procedure later used to collect blood samples. The experiment took place between 9:00 and 12:00 PM. A schematic representation of the experimental procedure is provided in **FIGURE 1**.

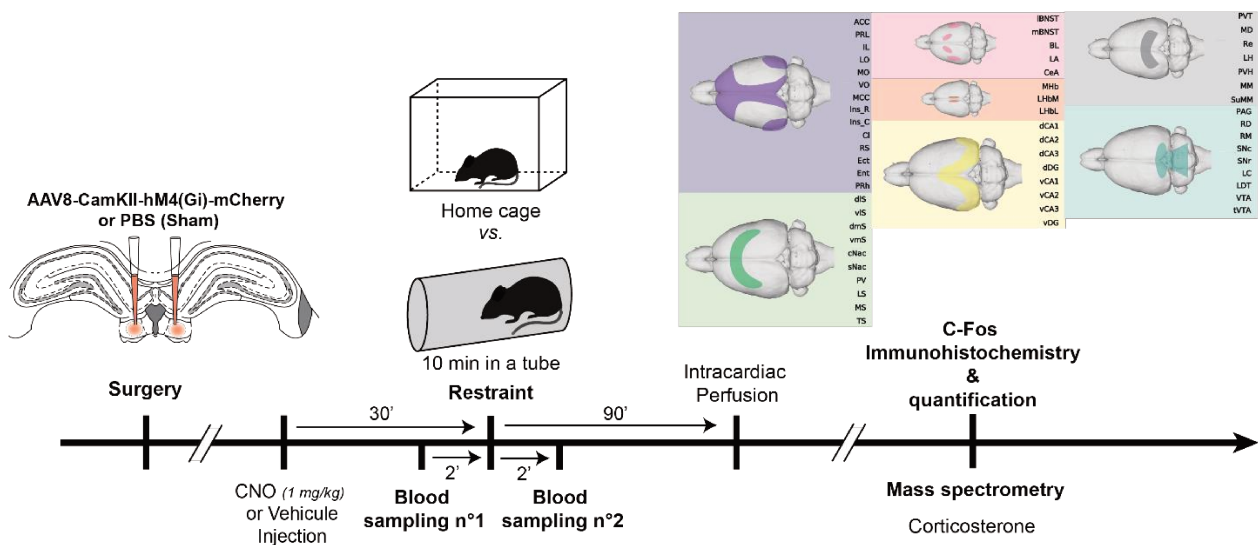


FIGURE 1 Timeline of the experiment. The protocol comprised the following steps: 7 to 9 weeks after surgery, animals were exposed to the restraint protocol (animals kept 10 min in a tube) or kept in their home cage. The injection of CNO (1 mg/kg) or vehicle was performed 30 min before. In restrained animals, blood samples were collected once 2 min before and once 2 min after restraint. Eighty min following restraint, animals were deeply anesthetized, intracardiac perfusion was performed and brains were removed. Blood samples were run through a mass spectrometer to assess corticosterone levels. Brains were cut, and immunolabeling of the c-Fos protein was performed on 40 μ m-thick floating sections. The density of c-Fos+ cells was calculated in each region of interest.

Surgery

Surgery was conducted 7-9 weeks before the experiment as described in detail in Durieux et al. (2020). Shortly, under isoflurane anesthesia [4% for induction; 1.5 % throughout surgery] and painkiller supply (meloxicam, 1 mg/kg, *s.c.*), rats were bilaterally microinjected with either the viral vector (AAV8–CamKII–hM4(Gi)–mCherry ; Viral Production Unit, Universitat Autònoma de Barcelona ; hM4 group, n=22), or phosphate–buffered saline (Sham group, n=22) at the two following coordinates and volumes : 1) anteroposterior (AP) = – 3.3 mm from Bregma, mediolateral (ML) = \pm 0.7 mm from the midline of the sagittal sinus, dorsoventral (DV) = – 4.5 mm from dura (0.2 μ L); 2) AP = – 3.5 mm from Bregma, ML = \pm 0.7 mm from the midline of the sagittal sinus, DV = – 4.4 mm from dura (0.15 μ L).

Drug treatments

CNO (1 mg/kg; dissolved in 0.9% NaCl–0.5% DMSO) or vehicle (Veh, 0.9% NaCl–0.5% DMSO) were administered intraperitoneally. Sixteen hM4 animals and sixteen sham animals were administered CNO (hM4–CNO and Ctl–CNO group, respectively). Six rats of each surgery condition were administered vehicle (Ctl-Veh group). Thirty minutes after drug injection, half of the animals of each group were exposed to blood sampling and restraint [restraint stress (RS) groups], the other animals remaining undisturbed in their home cage [Home cage (HC) group].

Restraint

Rats were gently placed in an opaque grey PVC tube (length, 80 cm; diameter, 13.5 cm) including ventilation holes at each end. They remained in it for a duration of 10 min.

Plasmatic CORT concentration assessment

Blood sampling

Blood sampling was performed in RS groups 2 min before (pre-restraint) and 2 min after (post-restraint) the restraint procedure. Rats were put on a table with their head positioned in a folded towel, and gently held in place. The caudal vein was lightly incised with a razor blade and blood, approximately 250 µl each time, was collected through a heparinized capillary tube (Microvette CB 300) while gently stroking the tail from the base to the tip. The pre-restraint incision was performed about 3 cm from the tip of the tail, and the post-restraint one was performed 2 cm higher. As soon as blood was collected, the tubes were placed in ice (4°C) before being centrifuged (3000 rpm at 4°C during 4 min) to collect approximately 150 µl of plasma, which was then stored at -80°C until analysis was performed.

CORT preparation

For each sample, 50 µl of plasma were added to 10 µl of D4-CORT (50 pmole/10 µl, Sigma-Aldrich, St. Quentin Fallavie, France) in 99.1% H₂O / 0.1 % formic acid (v/v). Then, proteins were precipitated by adding 1 ml of acetonitrile (ACN 100 %). Two successive centrifugations were performed at 20,000 g (4°C, 20 min) and, the resulting supernatant was recovered and dried under vacuum (SpeedVac, Thermo Fisher). Samples were re-suspended in 30 µl of 20 % ACN / 0.1 % of formic acid, followed by a last centrifugation (20,000 g, 10 min). Supernatants were recovered and kept at -80°C until LC-MS/MS analysis.

Liquid Chromatography Tandem-mass Spectrometry (LC-MS/MS)

Analyses were performed with a Dionex Ultimate 3000 HPLC system (Thermo Electron, Villebon-sur-Yvette, France) coupled with a triple quadrupole Endura mass spectrometer (Thermo Electron). Samples were loaded onto a ZORBAX SB-C18 column (150 x 1 mm, 3.5 µm, flow of 90 µl/min; Agilent, Les Ulis, France) heated at 40°C. LC and MS conditions used are detailed in **Table S1-2**. Qualification and quantification were performed using the multiple reaction monitoring mode (MRM) according to the isotopic dilution method (Ho et al., 1990). Identifications of the compounds were based on precursor ions, selective fragment ions and retention times obtained for the heavy

counterpart (*i.e.*, IS). Selection of the monitored transitions and optimisation of collision energy and RF Lens parameters were determined automatically (**Table S2**). Xcalibur v4.0 software was used to control the system (Thermo Electron).

Brain tissue preparation and section processing

Eighty minutes after the end of the restraint stress procedure, rats were deeply anesthetized with a pentobarbital overdose (120 mg/kg, *i.p.*). Following intracardiac perfusion of phosphate-buffered saline (PBS, 0.1M) and then 4% paraformaldehyde (PFA)-PBS solution (pH 7.4; 4°C), brains were removed, post-fixed in 4 % PFA-PBS (4°C, 2 h), transferred into a 0.1 M PBS–20 % sucrose solution (4°C, 48 h) and subsequently frozen (isopentane, - 40°C, 1 min). Serial 40 µm-thick free-floating sections were cut – 1 every 120 µm – in the coronal plane at – 20°C and stored in a cryoprotectant solution at – 20°C. In animals injected with the DREADD viral solution, within the block containing the LHb, one every three sections was directly collected on gelatin-coated slides in order to assess the extent of mCherry expression.

Immunohistochemistry

The immunohistochemistry protocol used was performed such as during our previous study (see Durieux et al., 2020 for details). In summary, c-Fos proteins were bound by primary anti-Fos rabbit polyclonal antibody (1:750, polyclonal rabbit antibodies; SYSY; ref: 226 003, Synaptic System). The secondary antibody was a biotinylated goat anti-rabbit antibody (1:500, Biotin-SP-conjugated affiniPure Goat anti-rabbit IgG, ref: BA1000, Vector). Staining was performed with the avidin–biotin peroxidase method (Vectastain ABC kit, PK 6100; Vector Laboratories, Burlingame, CA, USA). Sections were subsequently dehydrated by incrementally concentrated alcohol baths (70%, 90%, 95%, 100%, 100%), covered with Clearify (Americain MasterTech Scientific) and fixed on microscopic slides with Diamount (Diapath S.P.A).

Quantification

Quantification of c-Fos positive (c-Fos+) cells was performed in 56 structures (see Supporting information: **Table S3**; **Figure S1-2**) using a semi-automated method with ImageJ (Free License, Wayne Rasband, Research Services Branch, National Institute of Mental Health, Bethesda, Maryland, USA; **Figure S3**) such as described in Durieux et al. (2020). We took from 3 to 20 sections per structure depending on their rostro-caudal extent. Both hemispheres were pooled. Results were expressed as mean number of c-Fos+ cells by mm² (for more details see Supplementary information).

Statistical analyses

Between-group (Ctl-Veh, Ctl-CNO, and hM4-CNO in the restraint condition) comparison of plasmatic corticosterone (CORT) levels was performed using a two-way ANOVA with Time (pre- vs post-restraint) as the repeated measure. For each brain region, c-Fos raw data (c-Fos+ cells densities) were analyzed with ANOVAs with Group (Ctl-Veh, Ctl-CNO, hM4-CNO) and Condition (HC and RS)

as between-subject factors. Post hoc Newman-Keuls multiple range test was used when appropriate. In all analyses significance was set for $p < 0.05$.

Functional connectivity analysis

We used this analysis method to model the functional network during stress response. For this purpose, only c-Fos data of the RS groups were further analyzed using network modeling (Ctl-Veh-RS, $n=6$; Ctl-CNO-RS, $n=7$; hM4-CNO-RS, $n=7$). They were processed using Python (version 3.7.5, PyCharm edition community – free; <https://www.jetbrains.com/fr-fr/pycharm/>) with helps from several toolbox. For general coding, we used pandas (manipulating data as DataFrame and XLSX/CSV export/import; <https://pandas.pydata.org/>), numpy (managing matrix; <https://numpy.org/>), Scipy (for general statistic purposes; <https://www.scipy.org/>). The others Python toolbox used during the analysis for precise goal are cited when necessary. Correlations were calculated using Korr (<https://pypi.org/project/korr/>) according to the Pearson method. The correlation matrix was plot using matplotlib (<https://matplotlib.org/>) and seaborn (<https://seaborn.pydata.org/>). The 3D Rats brains representations used have been created from The Scalable Brain Atlas (Bakker et al., 2015).

The network modeling was processed using NetworkX toolbox (<https://networkx.org/>). The graphs were undirected and unsigned (absolute correlations were used as weights). All analyses were done on full weighted networks. Graph theoretical metrics, *i.e.*, the strength of each node in the network, the modularity (based on Louvain algorithm module/community detection, see below), the average clustering coefficient, and the average of edge weights, were computed using NetworkX. We used classical bootstrap analysis to estimate the variance of the population in groups or in random model. The random model was computed by shuffling the row and the column of the correlation matrix keeping the main diagonal intact (so that each structure remains the same in the random model). Between-group comparisons were done using the permutation test. The permutation test is a statistical test under the null hypothesis based on the calculation of the shuffling of the two compared groups (creating the null hypothesis) and comparing the given distribution of the p value to the p value of both original groups. Only data showing a significance difference ($p < 0.05$) in both tests (bootstrap and permutation) were estimate significantly different.

The allegiance matrices were computed using the Louvain method which allows to unfold communities in large networks (Python package <https://pypi.org/project/python-louvain/> called by NetworkX). The modules (or communities) were calculated for each bootstrap, modulating the resolution of Louvain algorithm from 0.88 to 1 over 10 repetitions, so that the number of communities varied from 2 to 5 depending on the group considered (see Supporting information **Figure S4**). The allegiance represents the probability that two structures are in the same community across bootstrap iterations over all possible pair of structures. The allegiance matrix also displays modules, allowing us to extract the communities on this matrix and study which structures may be activated in a functionally coordinated manner. This calculation can highlight high synchronicity and high functional connectivity between structures of the same community. Once the allegiance matrix calculated, the

allegiance communities were extracted using the Louvain algorithm (resolution of 1). The allegiance communities of the Ctl-Veh-RS group was extracted and the “within-module strength Z-score” evaluated (see Supporting information **Figure S4**).

Between-group comparisons were based on the communities extracted from the Ctl-Veh-RS group. The average strength of the structures of each community was calculated for each group and compared (Ctl-Veh-RS vs Ctl-CNO-RS, Ctl-Veh-RS vs hM4-CNO-RS and Ctl-CNO-RS vs hM4-CNO-RS) using the non-parametric test, Wilcoxon-Mann-Whitney. The differences were considered significant for $p < 0.05$. On the same principle, we also tested the possible differences between the Ctl-CNO and the hM4-CNO communities based on Ctl-CNO communities. For each group we assessed the distribution of the structures of interest in the different communities, using the so-called confusion matrices, based on the principle that communities do not have a hierarchical level, so that one may wonder which community of a given group best represents the community of another group. We calculated the Jaccard index gauging the similarity and the diversity of a sample set.

RESULTS

Histology

The rats used in this study are those used in our previous study (Durieux et al., 2020). Groups were composed as follows: Ctl-Veh-HC, n = 6; Ctl-Veh-RS, n = 6; Ctl-CNO-HC, n = 8; Ctl-CNO-RS, n = 7; hM4-CNO-HC, n = 4; hM4-CNO-RS, n = 7. The extent of the expression of mCherry in hM4-CNO animals is represented in Supporting Information **Figure S5**).

Blood CORT release

The two-way ANOVA indicated no significant effect of Group ($F_{2,17} = 0.13$; $p > 0.8$), a significant effect of Time ($F_{1,17} = 235.76$; $p < 0.0001$), and no interaction between the two factors ($F_{2,17} = 0.21$; $p > 0.8$) (**Figure 2**). This indicates that whereas the restraint procedure was indeed stressful, leading to a marked increase of CORT release, Lhb inactivation had no impact on such response, although a ceiling effect remains a possibility.

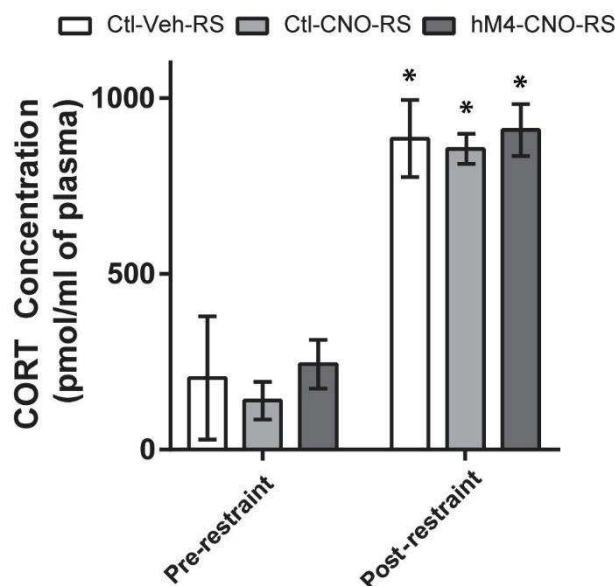


FIGURE 2 Effect of restraint and Lhb inactivation on CORT plasmatic concentration. Mean CORT plasmatic concentration (\pm S.E.M) before (left) and after (right) restraint in Ctl-Veh-RS (white bars), Ctl-CNO-RS (light grey bars) and hM4-CNO-RS (dark grey bars) groups. Statistics: * $p < 0.05$ vs. pre-restraint in the same group.

C-fos+ cell densities

C-Fos expression was high in almost all structures in restraint groups but also in the HC hM4-CNO group (**Figure 3A**; see also Supporting Information **Table S4** for the raw data and **Table S5** for statistics).

The restraint-induced increase in c-Fos expression was evidenced by significant Condition effect in almost all structures at the exception of the dIS, vIS, dCA2, MD, MM, SNc, SNr, and LDT; in the latter, a significant Group effect due to higher c-Fos+ cells density in the hM4-CNO group than in

both control groups was observed in the dlS, vlS, MD, and MM, and a significant interaction without main effects of each factor due to a higher c-Fos+ cells density in the hM4-CNO-RS group than in the Ctl-CNO group of the same condition ($p < 0.05$) in dCA2). In regions showing activation upon restraint, the analyses showed a significant Group effect - also due to higher c-Fos+ cells density in hM4-CNO group compared to the two control groups which did not differ- in the PRL, LO, VO, MCC, Ins_R, Ins_C, Cl, RS, vmS, PV, LS, TS, BA, CeA, dCA3, PVT, Re, and tVTA; in the LH the ANOVA also indicated a significant interaction due to higher c-Fos expression in hM4-CNO-HC group as compared to both HC control groups ($p < 0.001$ for each comparison). The lack of difference between the Ctl-Veh and Ctl-CNO groups indicates that the effects observed in the hM4-CNO group are specific to the action of CNO on hM4(Gi) receptors. However, in the LS, the Group effect was also due to lower c-Fos+ cells density in Ctl-CNO and, in the RD, it was only due to lower c-Fos+ cells density in Ctl-CNO group than the others, suggesting that CNO was not devoid of effects in our conditions albeit in only a few regions. In both subdivisions of the LHb (**Figure 3B-C**), the ANOVA indicated significant effects of Condition and Group and a significant interaction between both factors. In both control groups, restraint induced c-Fos expression only in the LHbM. However, in the hM4-CNO group, restraint induced a significant increase in c-Fos expression not only in the LHbM ($p < 0.001$) but also in the LHbL ($p < 0.001$). Moreover, in the HC condition, c-Fos expression was higher in the LHbM of the hM4-CNO group compared to control groups ($p < 0.05$ for each comparison). If these results confirm that stress induces c-Fos expression predominantly in the medial subdivision of the LHb, they show something that to our knowledge has never been reported in studies including DREADD-induced LHb inactivation, that is an increase of c-Fos+ cell density within a DREADDED LHb upon CNO administration. We have no clear explanation for that. A plausible hypothesis is the possibility that LHb inactivation induced downstream effects; one of them, probably for feedback control purposes for example, could have been to increase the activatory drive onto the LHb in order to compensate for the marked decrease of its activity. Given the results presented in Supporting Information **Table S5** one can postulate that this excitatory drive arises in the Ins-R. We have shown in our previous study (Durieux et al., 2020) that the vector we used indeed produced a marked lowering of LHb activity, validating the DREADD-induced inactivation strategy; therefore we propose that whereas LHb cells received “compensatory” excitatory inputs, inducing an increase of intracellular calcium concentration and therefore the expression of c-Fos, the presence of hM4-Gi receptor in these LHb cells nonetheless prevented the downstream propagation of the incoming signals.

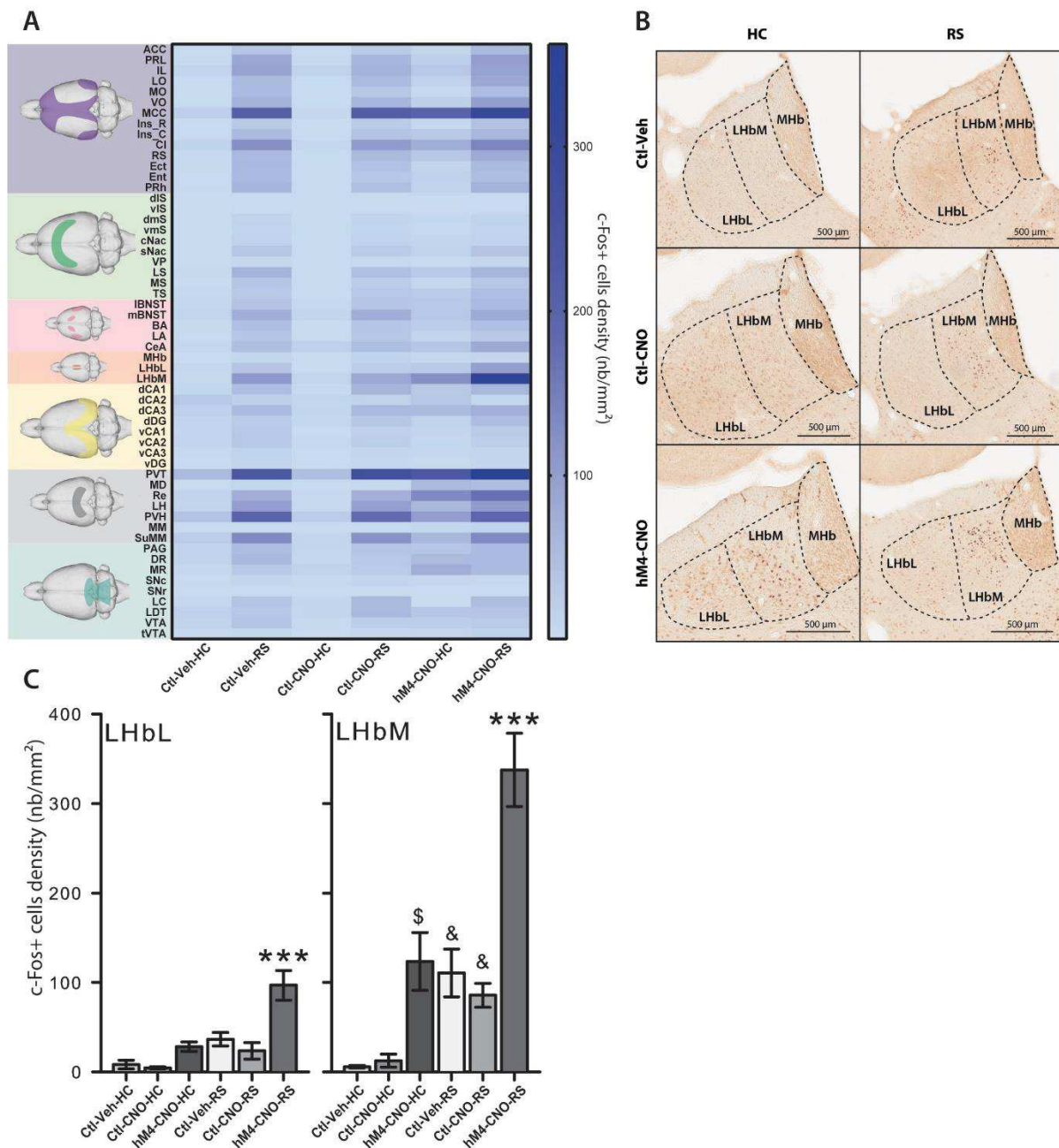


FIGURE 3 Effects of restraint and Lhb inactivation on c-Fos expression. **(A)** Heatmap of mean c-Fos+ density per structures for all groups. **(B)** Photography of c-Fos labeling in the entire habenula in Ctl-Veh (top), Ctl-CNO (middle), and hM4-CNO (bottom) groups in the HC (left) and RS (right) conditions. **(C)** Bar plot of c-Fos+ density (mean \pm S.E.M) in the LHbL and LHbM. Statistics: *** $p < 0.001$ vs. all other groups; & $p < 0.05$ vs. the corresponding HC group; \$ $p < 0.05$ vs. the other HC groups.

Functional Network activated by Restraint in Ctl-Veh-RS animals

We first investigated if the Lhb had a significant position within the stress response control network coming out of the analysis in animals not exposed to CNO, i.e., in Ctl-Veh-RS rats. To this purpose, we first calculated the correlation matrix including correlations between all structures, as an estimation of functional connectivity (**Figure 4A**). This highlighted several interesting correlations. For example, we found high connectivity within local networks, such as the mPFC, the AMG and the

midbrain monoaminergic regions. This makes perfect sense because those structures are largely described to be crucial in the stress response. We also found high positive correlations between structures of those different networks, suggesting that the stress response is mediated by covariation of cortical, amygdalar and monoaminergic structures. In other important point looking at the correlation matrix, is that it presents these pools of structures jointly varying called modules. These modules represent complex and robust networks. To test the randomness of these modules, we compared using classical bootstrap (resampled with replacement – 500 repetitions) the Ctl-Veh-RS matrix with random matrices created from the bootstrapped Ctl-Veh-RS matrices. The comparison of the modularity of both matrices shows a significantly lower modularity coefficient in the random matrix than in the initial data (bootstrap, $p < 0.05$; **Figure 4B**), suggesting that the modularity observed is not random; this allows us to investigate the composition of the different modules and the inter-structural interactions (see later).

Significant correlation (Pearson; $p < 0.05$) are represented on a graph theory network (**Figure 4C**). In this network, showing the functional connectivity shared by the structures investigated, we can again notice a large network which is mainly supported by cortical areas (at the exception of the orbitofrontal cortex), the extended amygdala and some thalamic and hypothalamic regions, such as the periventricular nuclei. Furthermore, we identified hubs of connectivity in this network following calculation of the strength of each structure (**Figure 4D**); those key structures strength include: the Ins_C, the BLA, the PRh, the PVH, the LH, the mBNST, the VTA, the vIS, and the PVT. The analysis indicates that these structures are those including the highest density of shared connections within the network, suggesting that a large part of the flow of information that passes within the network during stress exposure transits through those structures. If we go further in the analysis, the 10 next structures which show a smaller – but still significant – amount of connections, include structures known for their implication in the stress response, such as the anterior and mid cingulate cortices, the dorsal hippocampus (dCA1 and dDG), and monoaminergic regions, *i.e.*, the dopaminergic SNc and noradrenergic LC. According to our main structure of interested, the LHb, whereas its medial subdivision (LHbM) is situated in the medial portion of the graph, making it a hub of medium importance, the LHbL is the last structure that comes out, suggesting it is a very weak actor in the stress response.

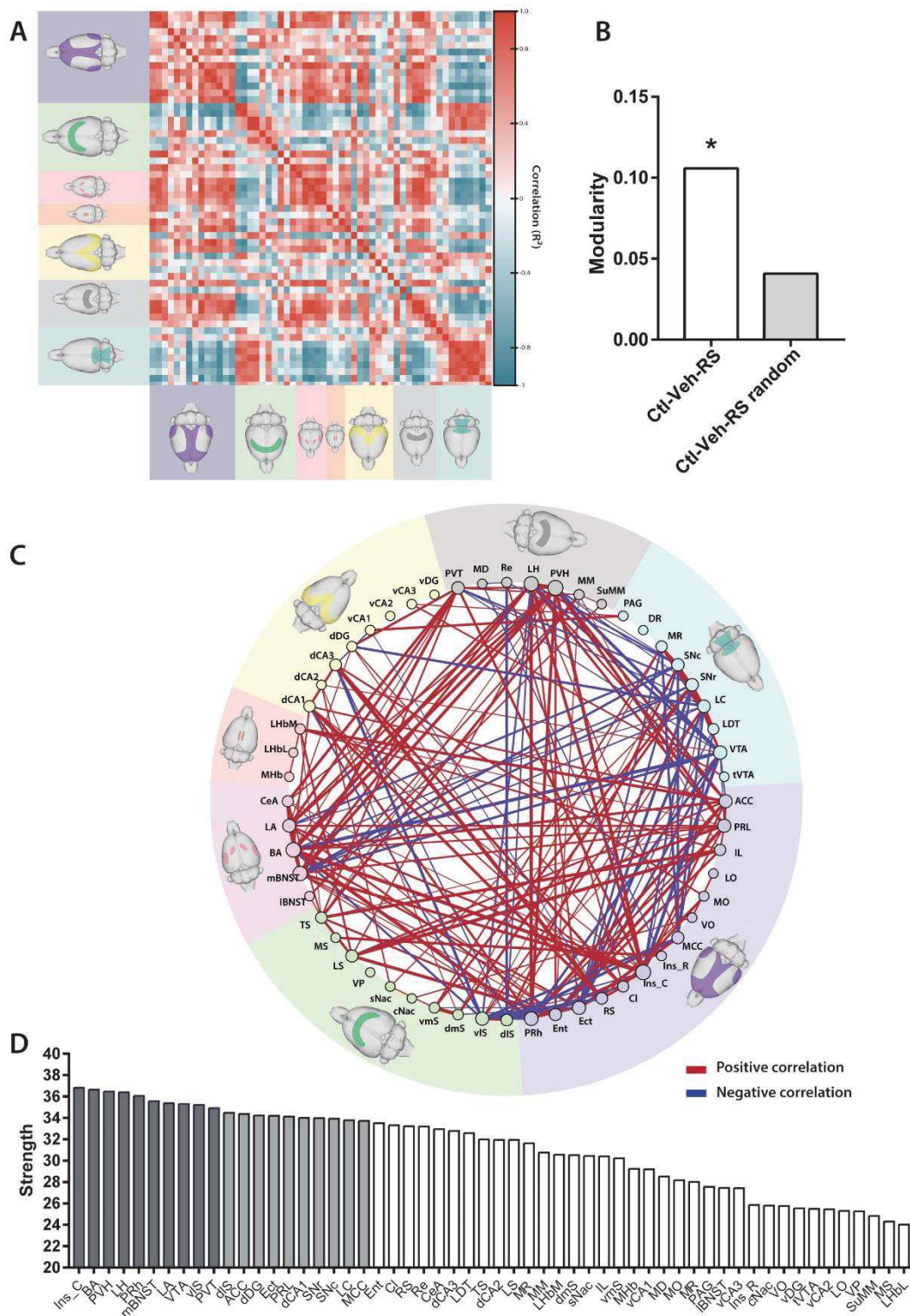


FIGURE 4 Evaluation of the network engaged by restraint. **(A)** Heatmap representing the cross-correlations (color scale, Pearson correlation R^2 ; red represent positive, and blue negative, correlations) between all investigated structures represented with a color code according to main brain regions (cortical regions, purple; basal ganglia and septum, green; extended amygdala, pink; habenula, red; hippocampus, yellow; thalamus and hypothalamus, grey; brainstem, blue). **(B)** Modularity based on Louvain algorithm, in the Ctl-Veh-RS group and its associated random network. Statistics: bootstrap, $*p < 0.05$. **(C)** Graphical representation of the network with nodes (structures) and edges (connecting lines representing significant correlations; Pearson $p < 0.05$). Positive correlations are represented in red and negative ones in blue. **(D)** Strength of each structure in decreasing order. The ten structures (Ins_C to PVT) displaying the highest strength are represented in dark grey and the tens following in light grey.

To better understand the place of the LHb within the network, we focused our analysis on its correlations with the rest of the network (**Figure 5A**). We found several significant correlations ($p < 0.05$ for each association, $R^2 > 0.81$) with the entire mPFC (ACC; PRL; IL), the LS, and the MHb. As those regions directly project onto the LHb, these results suggest that during stress exposure the LHb process selective information directly coming from those areas. Knowing that the network is composed of non-random modules, we calculated the probability of two structures to be in the same modules across bootstrap repetitions (500 iterations), considering each possible pair of structures (allegiance); further, we focused on the composition of the module that includes the LHbM, as well as the position of this structures within the module.

The allegiance heatmap displayed three modules, also called “communities” (**Figure 5B**). The community including the LHbM also contained the whole mPFC (ACC, PRL, IL), the Ins_C, the Ent, the PRh, the LS, the TS, both lateral and medial subdivisions of the BNST, the whole AMG, the PVT, the LH, the PVH, the MM, the RD, and the VTA. The community within-module strength Z-score, provides the strength of the connections that a given structure shares with structures of the same community or with structures of other communities (i.e., strong positive scores represent high interaction with structures of the same community, and strong negative scores represent high interaction with structures of other communities, whereas scores around 0 indicate potential bi-directional interactions, intra- and extra-community) (**Figure 5C**). Community n°1, which includes the LHbM, presents an unbalanced pattern of intra/extra community interactions; indeed, only two structures, the IBNST and the RD, seem to connect with structures of different communities, whereas the other structures seem to either show a preference for internal communication or do not show any preference. Communities n°2 and n°3 display a more balanced pattern; around half of the structures promote intra-community interactions, the other half promoting extra-community interactions. Interestingly, the structures present in the same community than the LHbM are crucial for the stress response, i.e., the PVH, the PRL, the mBNST, the ACC, and the LA; moreover, they seem to preferentially display intra-community interaction, suggesting they promote a loop for information processing inside their own community. On the other hand, the IBNST and the RD could be seen as input and/or output structures, as they interact with other communities although we cannot know the directionality of these interactions, whether they receive information from other communities to transmit them to their own, or whether they transmit information from their own community to others. According to the LHbM, its within module strength z-scores – near 0 – suggests it could have a role covering this of the other structures of the community, participating to intra-community interactions and/or to communication with other communities either as an input or an output structure.

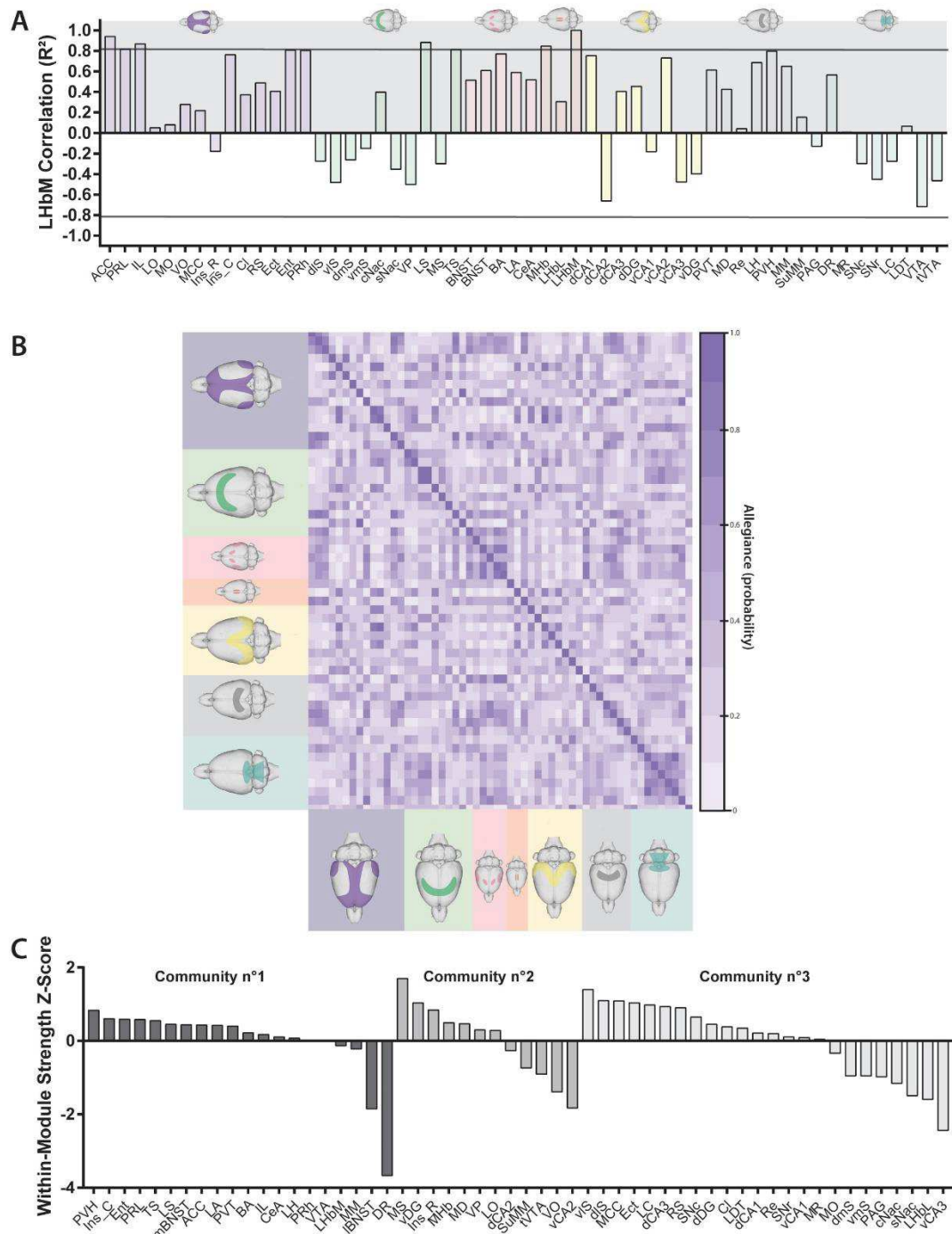


FIGURE 5 LHbM implication in the stress response may be supported by its functional connections. **(A)** Pearson correlation (R^2) between the LHbM and structures of the network. Horizontal black lines represent the threshold of significant correlations ($p < 0.05$). The structures are ordered by areas (cortical areas, purple; basal ganglia and septum, green; extended amygdala, pink; habenula, red; hippocampus, yellow; thalamus and hypothalamus, grey; brainstem, blue). Note that the correlation of the LHbM with itself equals 1. **(B)** Heatmap of allegiance of the Ctl-Veh-RS group, representing the probability for two given structures to belong to the same community across the bootstrap iterations (the darker, the higher probability). **(C)** Within-modules strength z-score organized by structures according to the community they belong to. The communities have been detected on the allegiance matrix of the Ctl-Veh-RS with Louvain algorithm.

Effects of CNO on functional connectivity

The observation of the correlation matrices of the Ctl-Veh-RS and the Ctl-CNO-RS groups (**Figure 6A-B**) suggested a decreased functional connectivity in the Ctl-CNO-RS group (**Figure 6B**: colors are globally lighter), although cortical areas (**Figure 6B** top left purple color) display a higher intra-correlation state, suggesting a hypersynchrony of those cortical networks. We then evaluated the strength difference between both Ctl-Veh-RS and Ctl-CNO-RS networks (**Figure 6C**) and found that some structures showed a significantly higher strength within the Ctl-Veh-RS group (classical bootstrap $p < 0.05$ and permutation test $p < 0.05$; ACC, dIS, TS, PVT, LH, PVH, VTA), than within the Ctl-CNO-RS group. These results suggest CNO might have on its own altered the brain's functional network so that it might be difficult to evaluate the net effect of the DREADD-induced LHb inactivation. We also investigated the potential effect of CNO based on the stress response control network (represented by the network of the Ctl-Veh-RS group), meaning on the strength of the initial communities (communities extracted from the Ctl-Veh-RS group). Accordingly, the correlation matrix of the Ctl-CNO-RS group has been sorted according to the structural configuration of the communities of the Ctl-Veh-RS group.

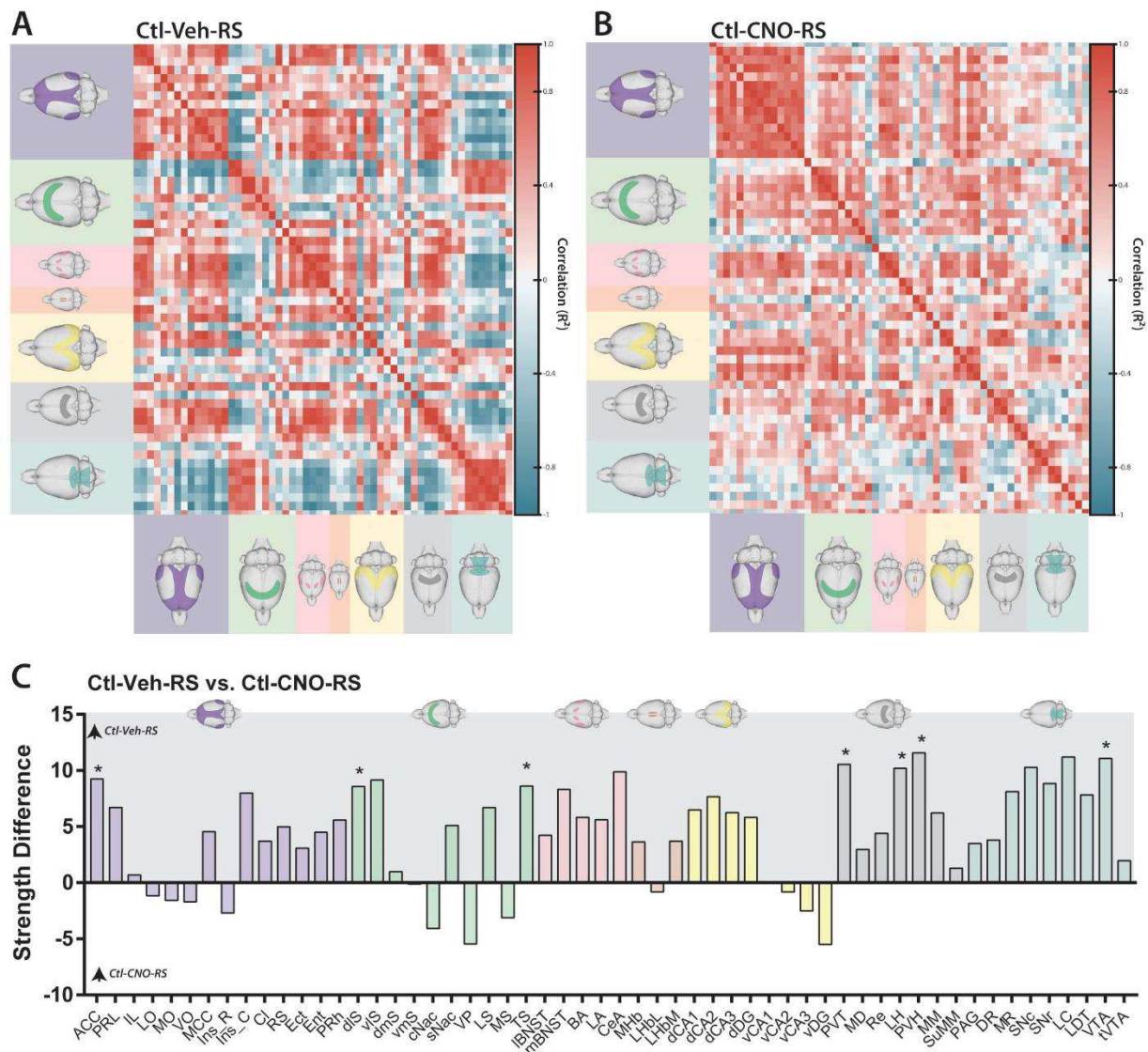


FIGURE 6 Effects of CNO injection on brain functional network. Heatmap representing the cross-correlations (color scale, Pearson correlation R^2 ; red represent positive, and blue negative, correlations) between all structures organized by main regions (cortical regions, purple; basal ganglia and septum, green; extended amygdala, pink; habenula, red; hippocampus, yellow; thalamus and hypothalamus, grey; brainstem, blue) for Ctl-Veh-RS (**A**) and Ctl-CNO-RS (**B**). (**C**) Strength difference for each structure between the Ctl-Veh-RS group and the Ctl-CNO-RS group organized by main areas (positive scores indicate a higher strength in the Ctl-Veh-RS group compared to Ctl-CNO-RS group; negative scores indicate a higher strength in the Ctl-CNO-RS than in Ctl-Veh-RS group). Statistics: bootstrap $*p < 0.05$ between groups.

We were able to visually notice the disruption of Ctl-Veh-RS communities in the Ctl-CNO-RS group (**Figure 7A** right). In addition, the evaluation of the community strength across both networks (Ctl-Veh-RS and Ctl-CNO-RS) showed that community n°1 and community n°3 were affected by CNO; indeed, the presence of CNO induced a decrease of the strength of both communities in comparison with the Ctl-Veh group (Mann-Whitney non-parametric test; Ctl-Veh-RS vs. Ctl-CNO-RS for each community; $p < 0.05$; **Figure 7B**). The fact that community n°1, which contains some of the main

structures implicated in the stress responses, has a lower strength in the Ctl-CNO-RS network, further strengthens the view that this response may have been altered by the presence of CNO.

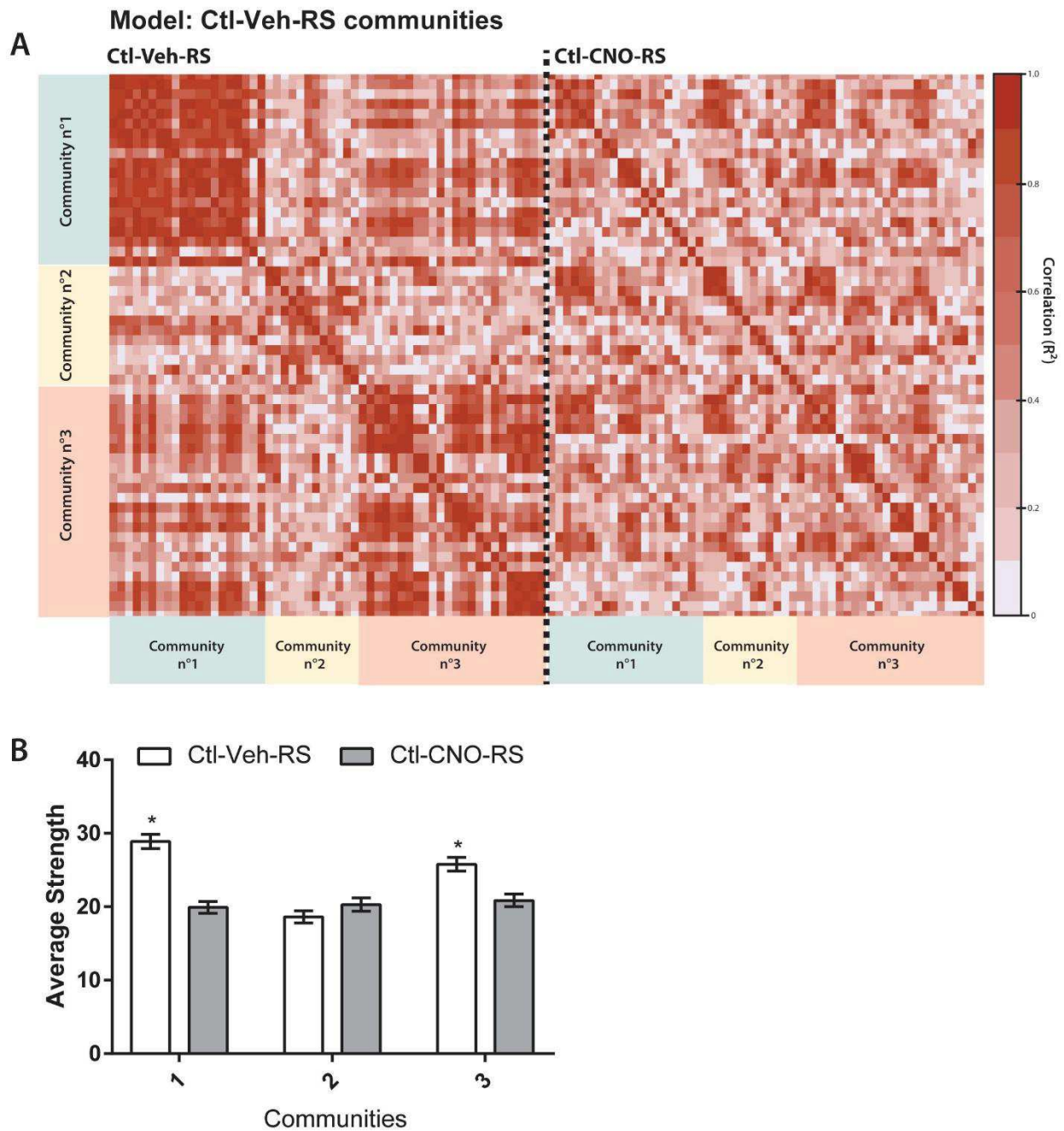


FIGURE 7 Effects of CNO injection network communities upon restraint. **(A)** Heatmaps representing the cross-correlations (color scale, Pearson correlation R^2 ; the darker, the stronger) between all structures organized according to Ctl-Veh-RS communities (communities have been detected using the allegiance of the Ctl-Veh-RS group) for both groups (Ctl-Veh-RS and Ctl-CNO-RS). **(B)** Average strength of the communities in Ctl-Veh-RS and Ctl-CNO-RS group. Statistics: Mann-Whitney non-parametric test; * $p < 0.05$ vs. Ctl-CNO for the same community.

Effects of LHb inactivation on functional connectivity

The observation of the correlation matrices of the Ctl-CNO-RS and hM4-CNO-RS groups suggests that the heatmaps of both groups are not identical but very similar (**Figure 8A**). We found several significant differences regarding the strength of the structures between the Ctl-Veh-RS and Ctl-CNO-RS and hM4-CNO-RS, but no difference between the Ctl-CNO-RS and the hM4-CNO-RS groups (see Supporting Information **Table S6**), suggesting that the strengths within the network may mainly be the consequence of CNO itself, masking the effects of LHb inactivation. The hM4-CNO-RS group had a quite similar community correlation heatmap than the Ctl-CNO group when arranged according to Ctl-CNO-RS communities (**Figure 8B**). The allegiance analysis detected three communities in the Ctl-CNO-RS group (see Supporting Information, Composition of the communities for each group). The calculation of the average strength of the communities revealed that the strength of community n°1 and n°2 was significantly higher in hM4-CNO-RS group than in Ctl-CNO-RS ($p < 0.05$; **Figure 8C**), supporting the idea of an increased community synchrony in animals with LHb inactivation.

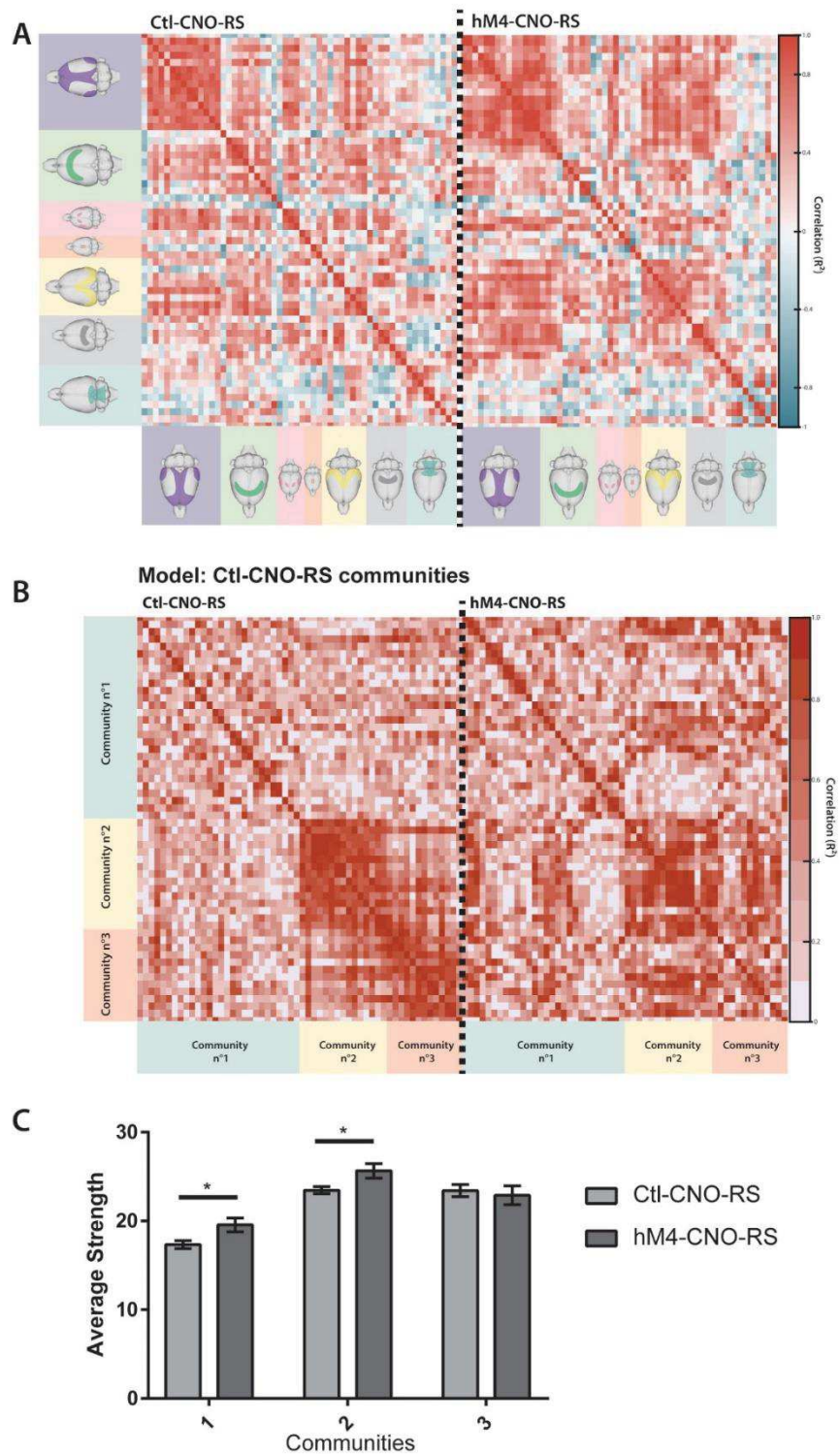


FIGURE 8 Lhb Inactivation and CNO injection alone present some similarities. **(A)** Heatmap representing the cross-correlations (color scale, Pearson correlation R^2 ; red represent positive, and blue negative, correlations) between all structures sorted by main regions (cortical areas, purple; basal ganglia and septum areas, green; extended amygdala, pink; habenula, red; hippocampus field, yellow; thalamus and hypothalamus area, grey; brainstem area, blue) for Ctl-CNO-RS and hM4-CNO-RS. **(B)** Heatmaps of the correlations (R^2 ; the darker the stronger correlation) in Ctl-CNO-RS and hM4-CNO-RS groups organized according to Ctl-CNO-RS communities (communities extracted on the allegiance matrix of the Ctl-CNO-RS group). **(C)** Average strength of the communities in Ctl-CNO-RS and hM4-CNO-RS group. Statistics: Mann-Whitney non-parametric test; * $p < 0.05$ indicated between-group difference for the same community.

In addition, we have extracted the composition of the communities of each group (see supplemental information: Compositions of the communities for each group) in order to compare them (after we have checked their “non-randomness” and calculated their allegiance matrices; see Supporting Information **Figure S6-8**). We have calculated the Jaccard coefficient for every possible pair of communities (Ctl-Veh-RS vs Ctl-CNO-RS, **Figure 9A**; Ctl-CNO-RS vs hM4-CNO-RS, **Figure 9B**). The composition of the communities of the Ctl-Veh-RS group does not show much difference with this of the Ctl-CNO group. For example, communities n°1 and n°3 of the Ctl-Veh-RS group are best represented by community n°1 of the Ctl-CNO-RS group network (31.4 % and 31.6 % respectively). This suggests that communities n°1 and 3 of the Ctl-Veh-RS group have been shuffled in the Ctl-CNO-RS group, leading to a reorganization of the balance between the initial communities (i.e. the communities of the Ctl-Veh-RS group, based on the original assumption that CNO should not have had any effect and that communities of the Ctl-CNO group should have been the same than those of the Ctl-Veh-RS group) under the influence of CNO. Also, there are more correspondences when comparing communities of the Ctl-CNO-RS and hM4-CNO-RS groups. For example, community n°1 of the Ctl-CNO-RS group is highly represented in community n°2 of the hM4-CNO-RS group (47.1 %), suggesting that a large part of the consequences of Lhb inactivation on the functional network engaged in the stress response might be due to CNO itself. These results can be used as another indication of the non-negligible consequences of CNO administration.

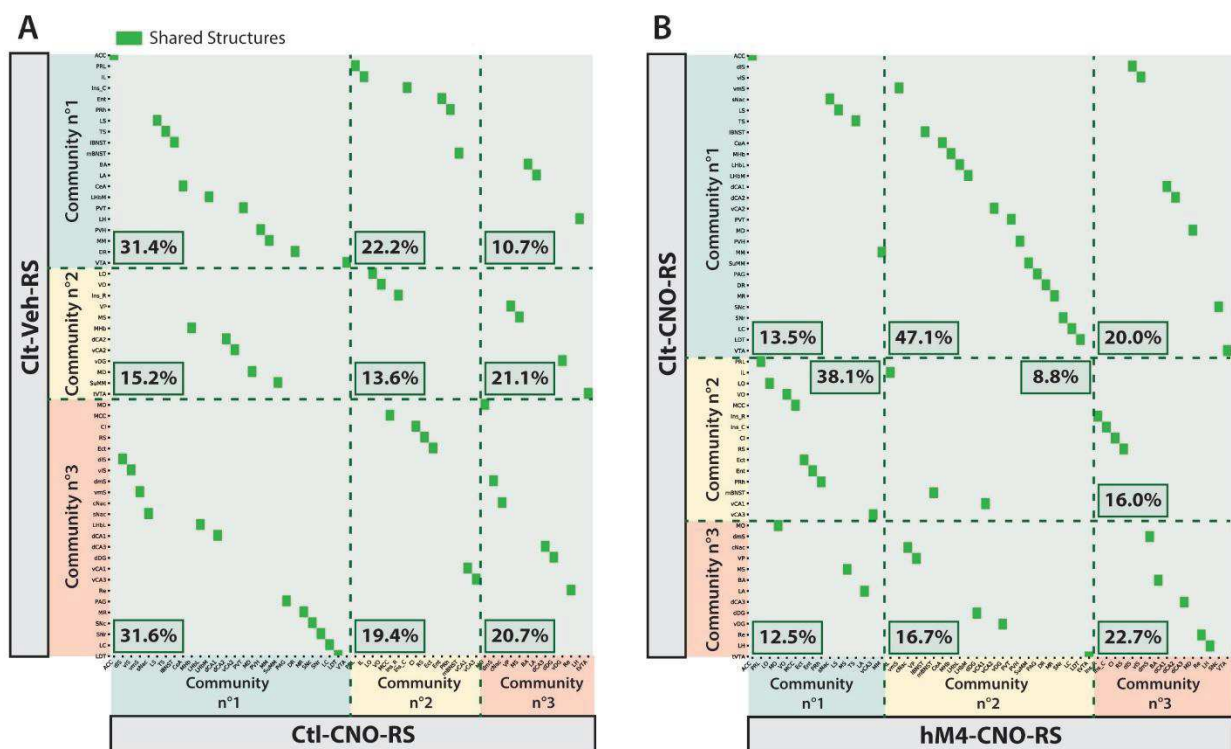


FIGURE 9 Representation of the structures shared between communities of the different groups. Shared structures (green squares) between Ctl-Veh-RS communities and Ctl-CNO-RS communities (**A**) and between Ctl-CNO-RS communities and hM4-CNO-RS communities (**B**). Jaccard index in percentage is displayed for each comparison, representing the percentage of corresponding between the two communities indicated (rows and columns).

DISCUSSION

Restraint has extensively been used in the literature as a model of acute stress (Paré and Glavin, 1986). The increased plasmatic CORT concentration observed in all groups seems to validate, if needed, this stressful procedure, as it stimulates the HPA axis. The lack of impact of LHb inactivation on CORT release appears consistent with those already found in our laboratory, showing that LHb inactivation only seems to affect CORT release when there is a cognitive task to perform (Mathis et al., 2018).

Following restraint, we found a generalized marked increase in the density of c-Fos+ cells, indicating the engagement of many different brain structures in the stress response, as expected (Herman et al., 2003; Sousa, 2016). The functional network that seems to support this response possesses a significant modularity (communities of structures which vary together). This modular architecture is a characteristic of small world networks (i.e., a high number of short connections between structures and a high level of local clustering between structures). This type of network is known to be very robust to structural alterations (if one of the nodes is deleted, the information that originally should have passed through this node is eventually rerouted to finally reach its destination without increasing too much the distance it travelled; Sporns et al. 2004; Bassett and Bullmore 2006; Stam and Reijneveld 2007; Reijneveld et al. 2007). Small world architectures are known to be robust networks, promoting rapid information transfer and network synchronization, and providing efficient balance between global integration and local processing (Sporns, 2013). Accordingly, the network engaged upon restraint may be very plastic and robust permitting a very integrated balance of local and global processing leading to highly efficient information transfer at low energy cost.

We found the principal hubs of the stress response network to be the Ins_C, the BA and the PVH, which are main components of the stress response network. The Ins is associated with the modulation of the autonomic response, including somatosensory, nociceptive and visceral processing (Kimura et al., 2010; Menon and Uddin, 2010; Rogers-Carter et al., 2018; Aguilar-Rivera et al., 2020; Ming et al., 2020); in addition, the more caudal part of the Ins (Ins_C), which is the one coming out in our analysis, is involved in respiratory and cardiovascular controls (Bagaev and Aleksandrov, 2006). The engagement of the Ins_C makes perfect sense as the autonomic response facing stress is crucial to allow efficient coping (Selye, 1950; de Kloet et al., 1998). The PVH and the BA are also key structures of the stress response (Prewitt and Herman, 1998; Roozendaal et al., 2009; Sousa, 2016). As said above, the PVH is the entry point of the HPA axis which triggers the physiological response to a stressor through the stimulation of CORT release (Herman et al., 2003; Ulrich-Lai and Herman, 2009). The BLA is essential for processing stressors (Janak and Tye, 2015); it is activated by the anticipation of a stressor (Cullinan et al., 1995) and involved in the consolidation of aversive memories (Roozendaal et al., 2009). Other key structures of the stress response were present in the twenty first hubs that came out from the analysis, including the mBNST, the LA, the

mPFC (ACC, PRL), the HPC (dDG, dCA1), and the dopaminergic (SNc and VTA) and noradrenergic (LC) systems (Herman et al., 2003; Sousa, 2016; Godoy et al., 2018).

With regard to the structure of interest of the current study, the LHb, our results first confirmed that its medial part (LHbM) is preferentially activated by stress (Chastrette et al., 1991; Wirtshafter et al., 1994; Brown and Shepard, 2013; Durieux et al., 2020). The LHbM has long been referred to as the “limbic” subdivision of the LHb, as it is directly connected with the mPFC, but also with the hypothalamus and the monoamine systems (Metzger et al., 2021). It therefore makes perfect sense that in the subsequent community analyses of the Ctl-Veh-RS group we found strong correlation between the LHbM and the mPFC (ACC, PRL and IL), which all belong to the same community. In addition, we found the LHbM to be significantly correlated to the LS and the MHb. The proximity with the LS is not surprising as identical correlation has been demonstrated using PET + 18-FDG in rats exposed to inescapable foot-shocks (Mirrione et al., 2014). The link with the MHb is more surprising but very interesting. Surprising because the current view is generally that the LHb and the MHb are distinct in terms of anatomical connections and functions; first of all, although the two habenular subregions are indeed very distinct in terms of input and output connections, Kim and Chang (2005) have described a small subset of MHb neurons making en passant synapses on dendrites of LHb neurons before exiting the MHb by the fasciculus retroflexus, suggesting that both regions can share information; these information can indeed be related to the stress response as molecular mechanisms within the MHb have recently been involved in despair-like behavior in mice (Yoo et al., 2021) whereas c-Fos expression was found to be increased in the MHb in rats susceptible to chronic mild stress (Febbraro et al., 2017). These different results imply that both the LHb and MHb could conjointly participate to stress-related responses, such as suggested by our own findings.

Community analyses revealed that, in addition to the mPFC, the LHbM shared strong functional connections with the PVH, the Ins_C, the extended amygdala (BA, LA, CeA, BNST), and the dopamine (VTA) and serotonin (RD) systems. These results support the view that the LHb receives and integrates information from several macrosystems (Geisler and Trimble, 2008), including cortical and amygdalar, related to several aspects of the stress response, and that it could represent a relay of those information towards the monoaminergic centers (VTA and RD), which are engaged in the control of the activity of cortical and subcortical structures to favor coping.

An important result of our study that should be highlighted for future studies is the unexpected effect of CNO on the stress network. Behavioral effects of CNO have generally been observed following administration of doses of CNO higher than the one we used (Manvich et al., 2018), while the vast majority of the studies did not report any adverse behavioral consequences following CNO administration (e.g., Aponte et al., 2011; Ferguson et al., 2013; Augur et al., 2016; Han et al., 2017; Durieux et al., 2020). Our analyses demonstrate an undeniable effect of CNO as correlation matrices of Ctl-Veh-RS and Ctl-CNO-RS groups hardly differ. Because in our protocol CNO was injected 30 min before restraint, this can suggest the integrity of the stress response network “to be engaged”

during restraint had been compromised in rats of the group including LHb inactivation. These effects are probably related to the metabolism of CNO into clozapine (Gomez et al., 2017; Manvich et al., 2018), a psychoactive compound which can influence many neurotransmitter systems through its action on dopamine (D1 and D4), serotonin (including 5HT1A and 5HT2A), noradrenaline (alpha 1 and 2), histamine (H1), and muscarinic (M1, M3 and M4) receptors (Aringhieri et al., 2018). Importantly, in HC condition, CNO did not induce c-Fos expression in all the brain areas known to be activated by clozapine like the mPFC and the NAc (see *e.g.*, Robertson and Fibiger, 1992); this suggests that although CNO was converted into clozapine, its level was probably too low to induce a generalized effect. However, even if CNO altered the level of c-Fos expression in only a few regions, network analyses indicated a lower strength of many structures following its administration, including the ACC, the PVH, and the VTA. We can therefore hypothesize that the detrimental effects of CNO on the organization of the network came from the perturbation of the modulatory function of the HPA axis and of the dopamine system, two very important modulators of the physiological stress response. Interestingly, in rats, at the same concentration we used (1 mg/kg), CNO reduced the acoustic startle reflex (MacLaren et al., 2016) and induced interoceptive effects that partially substitute to that of a low dose of clozapine (Manvich et al., 2018), suggesting it can affect components of the stress response. In trying to differentiate between the effects of CNO itself and the consequences of LHb inactivation, we could only observe that even if some communities were showing some differences between both conditions, the interactions within the communities of the two groups remained quite similar, suggesting the effect of LHb inactivation had been partly masked by the effects of CNO.

CONCLUSIONS

We have seen that the LHb, and more specifically its medial subdivision, the LHbM, was engaged, during acute stress exposure, among a broad network of key regions of the stress response. Given its anatomical position, the role of the LHbM could be to integrate multiple stress-related information stemming in cortical, thalamic and hypothalamic regions to further communicate it downstream to monoaminergic systems in order to probably initiate coping strategies. Indeed, as shown by others, the LHb – or its equivalent in zebrafishes – is engaged in behavioral adaptation under stressful situations (Ootsuka and Mohammed, 2015; Berger et al., 2018; Andalman et al., 2019; Coffey et al., 2020). Better understanding the engagement of the LHb when individuals are exposed to stressful situation appears like a relevant question as alteration of LHb function or morphology has been evidenced in stress-related psychiatric pathologies such as depression (Browne et al., 2018; Gold and Kadriu, 2019; Hu et al., 2020) and schizophrenia (Sandyk, 1992; Shepard et al., 2006; Zhang et al., 2017; but see Schafer et al., 2018).

CONFLICT OF INTEREST

The authors declare no conflict of interest.

ETHICAL STATEMENT

The authors declare that animals were handled in accordance with ethical requirements enacted by the French authorities and the Strasbourg university who approved the present project (APAFIS #7114).

AUTHOR CONTRIBUTIONS

LL and MM designed the study. LD, LL, MM performed the experiments and analysed the data. AB helped with the restraint procedure. KH, CB, CH helped with the c-fos counting. DB helped with graph theory analyses. VA and YG performed the LC-MS/MS measurements. LL, MM, LD wrote the manuscript.

DATA AVAILABILITY STATEMENT

Data supporting the findings of this study are available upon reasonable request from the corresponding authors.

SUPPORTING INFORMATION

Additional supporting information may be found online in the Supporting Information section at the end of this article.

Supporting information

Materials and Methods

MSPECT-HPLC

We summarize the elution gradient used in the HPLC for CORT assessment (**Table S1**) and the parameters used in the mass spectrometer to ionize, select, fragment and identify CORT and its deuterated derivative (**Table S2**).

Table S1: Elution gradient for corticosterone assessment through HPLC column.

Retention (min)	Debit (ml/min)	%phase mobile B
0	0,150	0
1	0,150	0
3	0,150	25
10	0,150	30
12	0,150	98
14	0,150	98
15	0,150	0
19	0,150	0

Table S2: Mass spectrometer ionization, selection, fragmentation, and identification parameters.

Compound	Polarity	Precursor (m/z)	Product (m/z)	Collision Energy (V)	RF Lens (V)
Corticosterone	positive	347.11	293.472	17.03	227.49
			311.294	15.91	
			329.169	14.95	
D4-corticosterone	positive	351.179	297.103	17.68	223.55
			315.183	16.88	
			333.24	15.56	

Quantification of c-Fos+ cells density

Outlining of the targeted areas

We evaluated c-Fos+ cells density across 56 brain structures along the anteroposterior axis of the brain (see coordinates in **Table S3**) and according to the boundaries drawn in the Paxinos and Watson stereotaxic atlas (Paxinos et Watson, 2007), such as shown in **Figure S1** and **Figure S2**.

Table S3: Anteroposterior coordinates of the structures investigated

	<i>Structures</i>	<i>Start (mm from bregma)</i>	<i>End (mm from bregma)</i>
	ACC	4.20	2.52
	PRL	4.68	2.52
	IL	4.20	2.52
	LO	4.68	3.00
	MO	4.68	4.20
	VO	4.68	3.00
	MCC	2.28	-1.56
	Ins_R	4.20	-0.36
	Ins_C	-0.36	-2.92
	Cl	4.20	-1.08
RS	-1.72	-6.60	
Ect	-3.00	-6.60	
Ent	-3.12	-6.60	
PRh	-3.00	-6.60	
dIS	2.04	0.00	
vIS	2.04	0.00	
dmS	2.04	0.00	
vmS	2.04	0.00	
cNac	2.04	0.48	
sNac	2.04	0.48	
VP	2.76	-0.72	
LS	2.28	-0.60	
MS	1.56	0.00	
TS	-0.24	-1.08	
IBNST	0.36	-0.72	
mBNST	0.72	-1.08	
BA	-1.56	-3.36	
LA	-1.56	-3.36	
CeA	-1.56	-3.12	
MHb	-2.04	-4.36	
LHbL	-2.92	-4.36	
LHbM	-2.92	-4.36	
dCA1	-2.28	-6.24	
dCA2	-2.28	-6.24	
dCA3	-2.28	-6.24	
dDG	-2.28	-6.24	
vCA1	-4.68	-6.24	
vCA2	-4.68	-6.24	
vCA3	-4.68	-6.24	
vDG	-4.68	-6.24	
PVT	-1.20	-3.72	
MD	-1.80	-3.72	
Re	-1.20	-3.96	
LH	-1.56	-4.56	
PVH	-1.56	-3.36	
MM	-4.20	-5.28	
SuMM	-4.20	-4.80	
PAG	-4.56	-8.52	
DR	-6.84	-9.36	
MR	-7.08	-8.76	
SNc	-4.92	-6.48	
SNr	-4.56	-6.72	
LC	-9.48	-10.08	
LDT	-8.16	-9.36	
VTA	-4.68	-6.48	
tVTA	-6.12	-6.96	

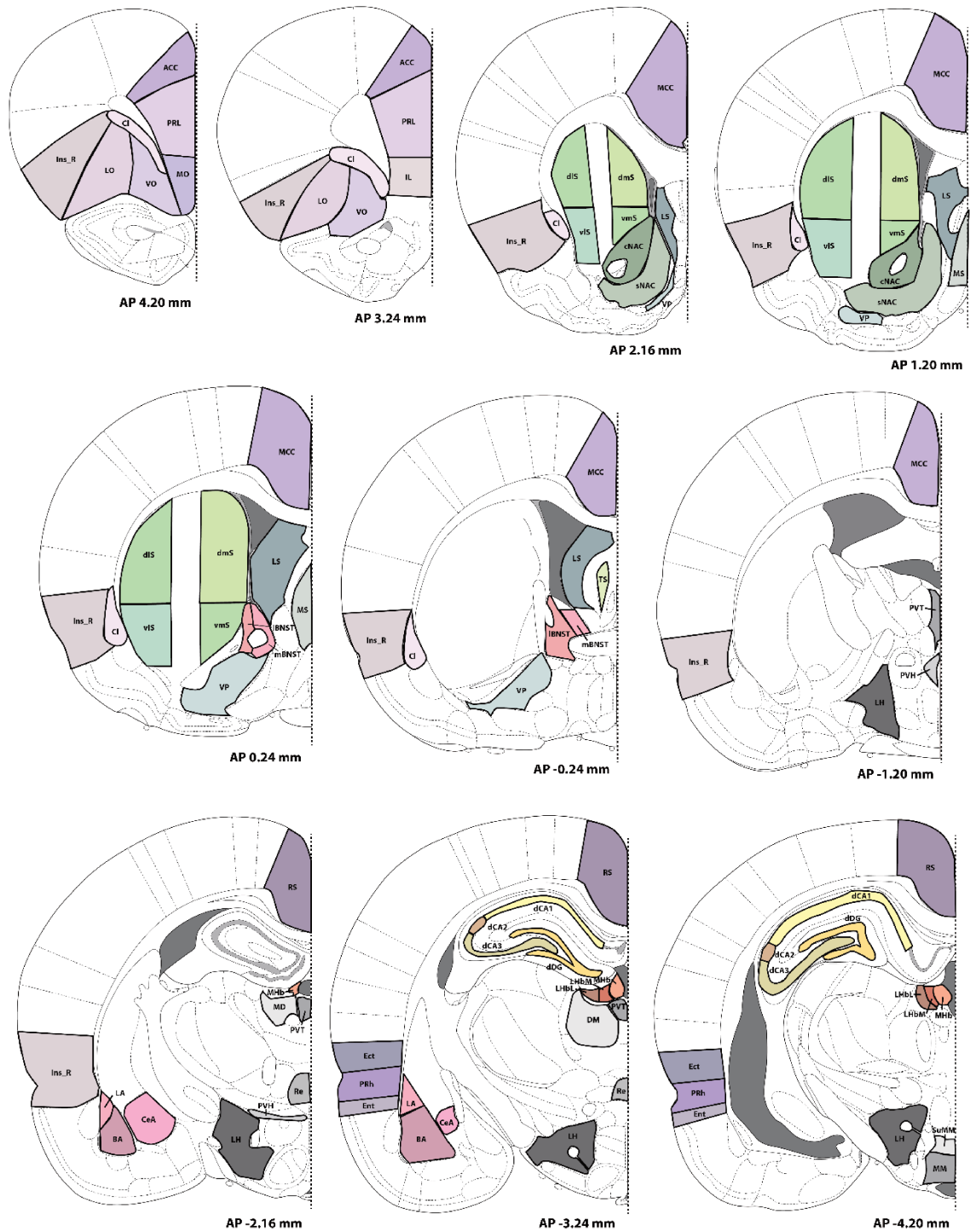


Figure S1: Boundaries of the structures for the evaluation of c-Fos+ cells densities (part 1)
Adapted from Paxinos and Watson atlas (Paxinos et Watson, 2007).

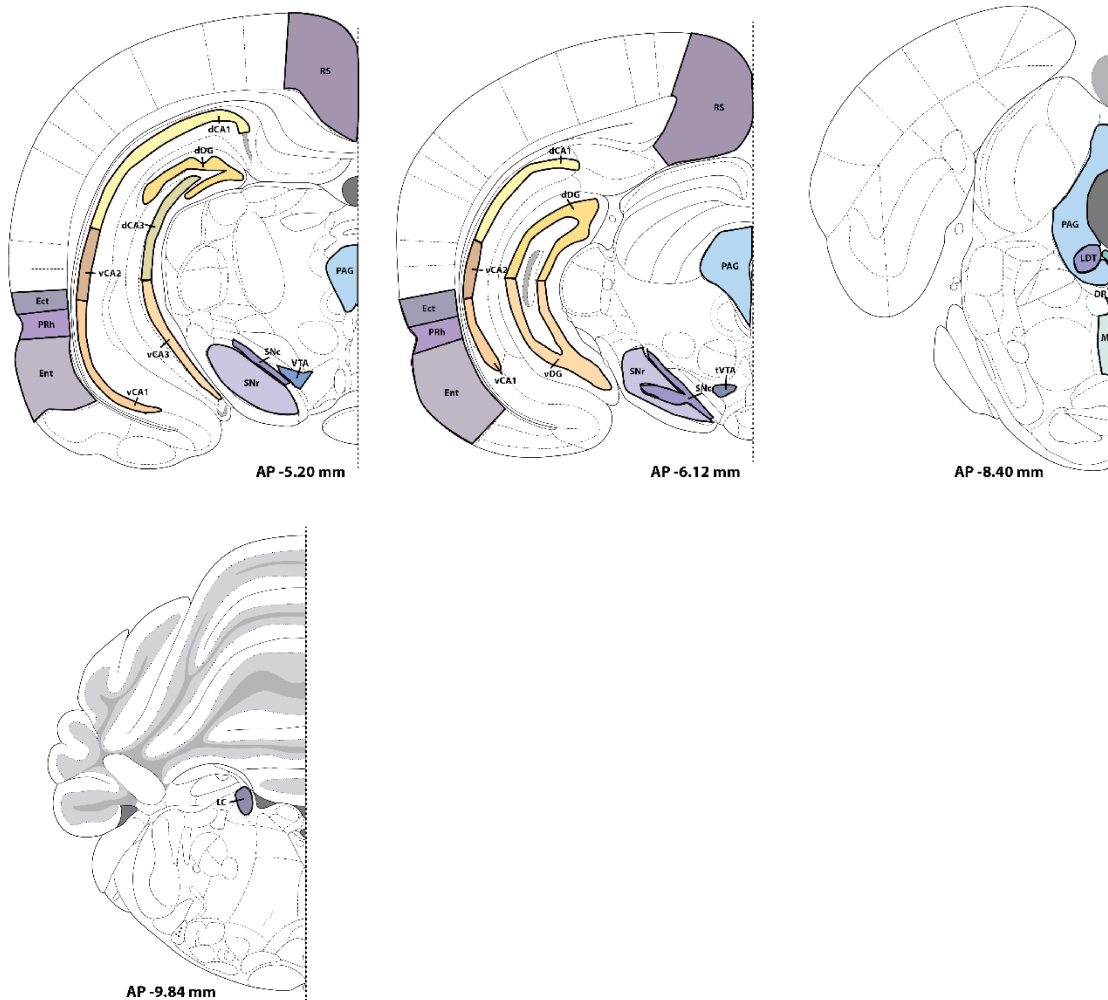


Figure S2: Boundaries of the structures for the evaluation of c-Fos+ cells densities (part 2). Adapted from Paxinos and Watson atlas (Paxinos et Watson, 2007).

Semi-automated c-Fos+ cells quantification method

Quantification was performed using ImageJ (Free license, Wayne Rasband, Research Services Branch, NIH, Bethesda, Maryland, USA) with homemade scripts, such as described in Durieux et al., 2020. However, we still verified the accuracy of the semi-automated counting method by comparing it to manual counting, choosing the LHb (**Figure S3**). We found almost identical results with both methods with a correlation $R^2 = 0.98$ (Pearson) and a slope = $(1.009 \times X) \pm 0.0101$ (where slope is $Y = (a * X) + b$ [where Y is the value given by automated counting, X is the value given by manual counting, a is the slope of the best fitting line, and b is the intersection with the Y axis]). A parameter a near 1 suggests that n cells counted semi-automatically will be equal to n counted manually; a parameter b near 0 means that 0 detected cells in the manual counting gives 0 detected cells with the semi-automated method.

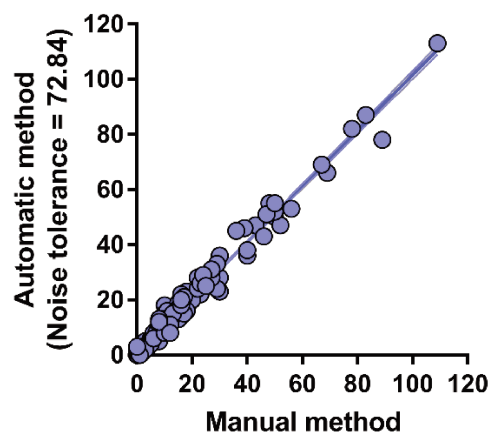


Figure S3: Assessment of the accuracy of the semi-automated counting method in comparison with the manual counting method. Plot representing the linear correlation of manual vs semi-automated counting; “a” is close to 1, demonstrating the similarity between manual and semi-automated counting, with a very high correlation between both methods ($R^2 = 0.98$; $p < 0.0001$), with the noise tolerance parameter of the FindMaxima() function of ImageJ set to 72.84.

Allegiance analysis

Resolution of Louvain algorithm

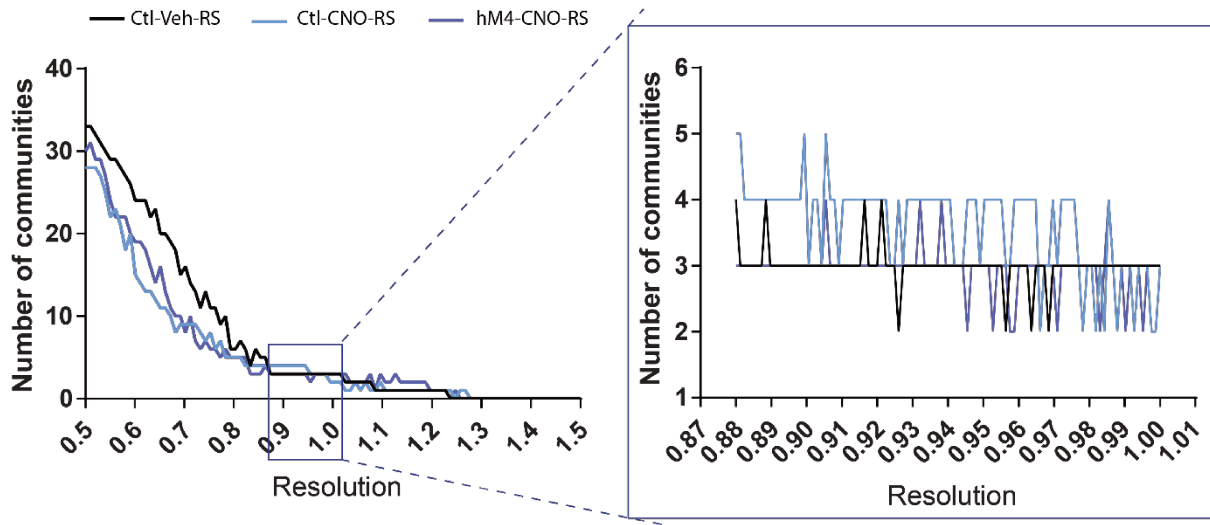


Figure S4: Plots of the number of communities by the Louvain resolution. The graphic on the left displays the number of communities extracted in function of the resolution of the Louvain algorithm. We decided to variate the resolution of Louvain Algorithm, staying around the number of communities obtain when the resolution equal 1 (greedier parameter), leading to a variation of the number of communities between 2 and 5. So, we select the interval for the resolution from 0.88 to 1 (as displayed on the right plot). The variation of the number of communities through the resolution interval are displayed by group and over 100 repetitions.

Within-module strength z-score calculation

To calculating the strength of the interaction between structures of the same community and between structures of different communities, we evaluated the within-module strength z-score using the following equation:

$$WM_{z-score} = \frac{Strength_{within} - Strength_{tot}}{std(Strength_{tot})}$$

where $WM_{z-score}$ is the within-module strength z-score for one structure in its own community, $Strength_{within}$ is the strength (sum of edge weights connecting to the targeted node) considering only the edges connecting with the node (structures) included in the same community than the node targeted, $Strength_{tot}$ is the total strength of the network, and the $std(x)$ is the standard deviation of x .

Results

Histology

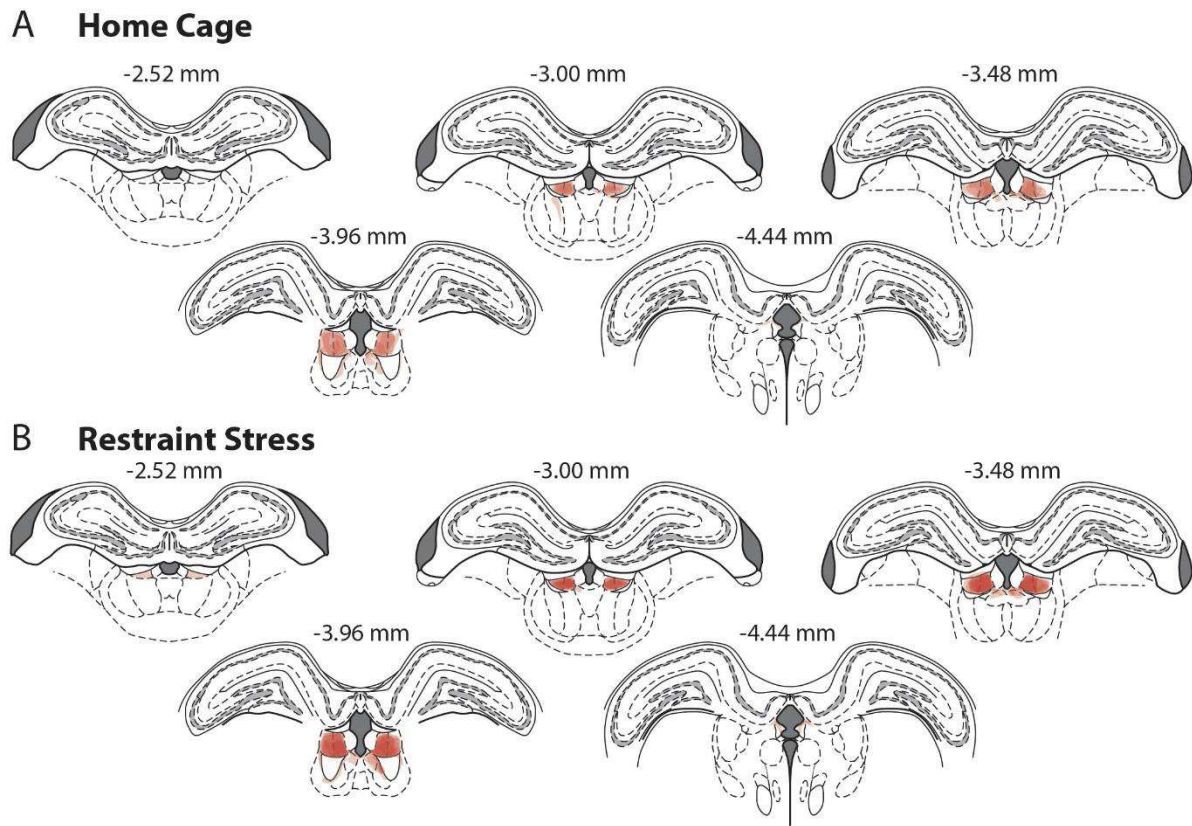


Figure S5: Schematic representation of the presence of hM4(Gi) receptors in the animals kept following histological verification. For each rat, on each slide used, the area including the expression of the hM4(Gi) receptors was delineated using a pale red color (opacity 20%). Then, for each stereotaxic coordinate [numbers above the slides correspond to AP coordinates from Bregma (mm) (Paxinos and Watson, 2007)], the slides of all the animals were piled, creating a color scale from pale red to dark red. Therefore, the darker is the area, the greater is the number of animals presenting an expression of the hM4(Gi) receptors within this area. One can see that hM4(Gi) receptors were expressed within the LHB in its entire rostrocaudal extent. The extent of mCherry expression is represented for Home cage rats (**A**; n = 4) and rats subjected to restraint stress (**B**; n = 7).

C-Fos + cells density raw data and statistics

Table S4: Raw c-Fos+ cells density represented by the mean (\pm SEM) for each region.

	Home Cage						Restraint Stress					
	Ctl-Veh		Ctl-CNO		hM4-CNO		Ctl-Veh		Ctl-CNO		hM4-CNO	
	Mean	SEM	Mean	SEM	Mean	SEM	Mean	SEM	Mean	SEM	Mean	SEM
ACC	0.721	0.215	1.092	0.266	10.895	4.130	37.704	8.332	27.677	3.381	53.414	14.489
PRL	4.909	1.009	4.309	0.567	23.120	6.088	85.988	11.702	61.113	6.440	97.203	17.734
IL	13.323	2.804	15.317	3.265	34.509	9.930	92.791	10.439	67.882	6.346	93.195	14.321
LO	1.280	0.275	1.220	0.268	17.253	6.337	53.287	10.291	52.767	12.463	86.572	12.218
MO	2.694	1.339	1.088	0.418	7.046	0.949	52.228	11.051	33.449	4.628	48.298	9.671
VO	1.649	0.657	1.557	0.623	19.598	8.262	68.375	11.903	63.157	13.148	98.303	14.192
MCC	21.753	11.620	7.153	1.842	202.504	9.954	214.155	47.953	219.380	19.598	302.079	60.292
Ins_R	1.599	0.580	1.374	0.267	8.509	3.962	28.724	2.473	25.595	4.027	41.423	3.840
Ins_C	3.860	1.492	2.048	0.474	30.214	14.465	54.409	13.275	40.551	5.877	60.889	11.558
CI	16.560	3.763	7.371	1.918	74.348	26.511	125.236	28.053	102.424	13.261	135.979	14.122
RS	4.345	1.687	2.492	0.600	33.303	7.722	57.801	12.095	56.221	5.425	79.778	17.365
Ect	4.525	0.938	3.031	0.543	13.075	3.462	59.610	6.501	43.687	6.286	54.799	12.532
Ent	4.140	1.168	3.040	0.630	18.761	4.022	52.791	7.045	34.366	5.455	47.175	9.751
PRh	4.256	0.731	1.914	0.289	15.420	4.056	64.873	7.885	47.579	5.515	68.570	16.136
dIS	0.786	0.257	0.618	0.050	2.794	1.289	1.039	0.173	1.132	0.155	3.542	1.094
vIS	0.540	0.133	0.809	0.240	2.174	0.741	0.661	0.141	0.692	0.203	4.056	0.812
dmS	1.617	0.471	2.238	0.562	8.224	1.222	15.559	3.533	14.059	1.922	15.943	2.208
vmS	1.498	0.543	1.309	0.411	6.329	1.136	12.834	2.960	10.019	1.843	13.450	1.230
cNac	2.889	0.888	2.209	0.541	11.387	3.230	18.264	2.085	16.322	2.882	17.172	2.061
sNac	3.065	0.769	3.724	0.769	16.255	2.694	36.828	6.436	27.652	6.506	38.231	6.772
VP	0.735	0.257	0.820	0.172	4.470	0.806	7.242	2.186	5.996	0.625	8.955	1.453
LS	5.294	1.656	3.639	0.809	28.208	7.579	67.091	10.040	45.916	4.769	62.896	8.023
MS	2.371	0.780	2.469	0.601	8.091	1.071	37.899	6.623	23.527	3.478	35.374	6.399
TS	6.830	3.382	3.725	1.204	27.402	11.218	28.972	10.272	33.926	5.024	46.838	5.558
IBNST	8.461	2.705	6.704	1.924	32.901	5.350	39.662	6.431	37.345	4.404	51.495	9.610
mBNST	11.754	2.506	8.746	2.285	33.118	4.396	73.715	10.892	74.231	11.924	81.224	6.711
BA	5.094	1.934	2.701	0.491	25.625	8.139	44.653	8.312	37.192	5.348	45.794	7.543
LA	4.272	0.954	3.278	0.562	12.311	6.145	37.839	5.710	36.060	4.238	29.892	3.907
CeA	7.236	2.527	18.539	4.198	36.367	7.198	45.515	10.174	45.929	3.530	83.367	20.339
MHb	1.649	0.714	2.461	0.859	7.559	1.986	10.042	2.902	15.223	4.029	8.832	2.362
LHbL	7.126	4.916	3.202	1.312	28.144	5.336	36.670	7.581	23.499	9.080	96.880	16.507
LHbM	5.771	1.272	12.621	6.989	123.519	32.485	110.652	26.764	85.647	13.443	337.576	40.965
dCA1	8.213	2.894	5.050	1.004	32.924	4.137	46.543	13.538	64.920	11.123	59.659	12.860
dCA2	31.886	11.165	9.676	3.545	37.394	10.068	20.370	7.460	18.386	4.007	9.591	3.036
dCA3	19.467	6.865	11.830	2.529	54.663	14.803	52.982	8.202	57.807	8.135	71.694	10.754
dDG	12.399	4.181	7.978	2.078	17.048	5.345	26.870	5.155	35.962	6.915	48.545	13.084
vCA1	10.078	5.444	3.423	1.023	10.944	5.513	33.651	4.641	18.746	4.350	25.917	6.289
vCA2	13.167	7.693	6.871	2.124	7.822	1.536	31.464	5.859	22.900	6.848	21.833	3.464
vCA3	6.590	4.001	2.788	0.947	7.236	1.921	16.642	4.575	9.298	1.981	9.326	2.169
vDG	2.030	0.306	2.231	0.793	3.902	2.149	11.289	3.502	7.816	2.108	9.097	2.151
PVT	56.328	24.931	46.498	10.383	236.460	20.366	240.248	42.837	266.718	28.247	362.334	51.632
MD	0.828	0.357	1.323	0.448	53.558	26.284	10.049	1.587	5.810	1.463	47.354	20.746
Re	13.697	9.106	5.959	1.382	132.411	27.645	72.389	18.300	70.241	12.864	170.591	36.268
LH	10.867	2.713	6.559	0.947	57.317	18.163	97.442	11.193	96.276	6.781	101.064	10.834
PVH	42.686	20.326	24.312	5.963	99.025	23.669	196.286	41.287	178.912	24.710	191.432	23.541
MM	0.981	0.468	2.971	1.376	8.425	4.656	2.632	0.660	3.799	1.031	13.639	5.733
SuMM	24.141	12.938	10.956	4.282	59.548	23.217	134.138	26.551	120.753	26.555	132.483	14.089
PAG	17.023	5.953	10.609	2.976	37.055	21.584	47.888	7.051	39.294	6.844	53.248	10.458
DR	17.802	6.646	7.881	2.490	53.718	32.327	59.531	13.790	31.439	6.434	53.098	13.835
MR	7.434	2.479	15.588	10.296	75.959	33.404	32.828	9.472	25.990	5.805	54.033	12.522
SNC	5.214	1.940	4.864	1.299	7.757	5.110	11.472	2.875	12.433	4.377	5.912	1.540
SNr	1.213	0.227	2.693	0.819	3.278	1.585	3.917	1.149	3.621	0.971	2.714	0.495
LC	7.483	4.553	9.736	2.642	3.294	2.329	41.242	3.741	56.439	10.187	49.093	15.143
LDT	19.470	9.423	8.766	3.598	37.490	29.355	33.553	15.022	57.374	16.710	36.697	12.307
VTA	14.246	6.944	4.966	1.444	21.639	11.855	40.869	11.361	22.166	4.333	27.152	3.519
tVTA	5.632	1.531	2.852	0.644	11.004	2.274	7.944	1.270	9.421	2.067	15.528	3.760

Table S5: c-Fos+ cells density statistics according to Condition (home cage vs restraint), Group (Ctl-Veh vs Ctl-CNO vs hM4-CNO) and Condition x Group interaction. * $p < 0.05$; ** $p < 0.01$; *** $p < 0.001$; **** $p < 0.0001$; ***** $p < 0.00001$; ns, no significant effect. According to the structures showing significant interactions, the relevant between-group statistics are given in the article.

	Condition		Group					Interaction	
	F value	p	F value	p	Ctl-Veh vs hM4-CNO	Ctl-CNO vs hM4-CNO	Ctl-Veh vs Ctl-CNO	F value	p
ACC	31.261	*****	2.702	ns				0.574	ns
PRL	73.977	*****	3.75	*	*	**	ns	0.865	ns
IL	75.107	*****	3.12	ns				1.3	ns
LO	58.453	*****	4.414	*	***	**	ns	0.554	ns
MO	56.99	*****	1.765	ns				0.921	ns
VO	66.259	*****	3.701	*	**	**	ns	0.345	ns
MCC	33.648	*****	9.124	**	***	***	ns	1.352	ns
Ins_R	135.506	*****	8.254	**	***	***	ns	1.092	ns
Ins_C	30.892	*****	3.848	*	*	**	ns	0.603	ns
CI	46.8	*****	5.104	*	*	**	ns	1.053	ns
RS	39.772	*****	4.333	*	**	**	ns	0.078	ns
Ect	62.651	*****	1.377	ns				0.658	ns
Ent	54.113	*****	3.114	ns				0.213	ns
PRh	57.232	*****	2.088	ns				0.417	ns
dIS	2.309	ns	19.147	**	***	**	ns	0.073	ns
vIS	2.837	ns	17.367	*****	***	***	ns	2.663	ns
dmS	46.473	*****	2.154	ns				1.123	ns
vmS	47.234	*****	3.45	*	*	**	ns	0.811	ns
cNac	48.672	*****	3.041	ns				2.889	ns
sNac	40.182	*****	2.548	ns				0.739	ns
PV	32.379	*****	4.357	*	**	**	ns	0.368	ns
LS	82.743	*****	5.735	**	*	***	*	2.4	ns
MS	62.965	*****	2.522	ns				1.55	ns
TS	22.24	*****	5.559	**	**	**	ns	0.435	ns
IBNST	31.063	*****	6.61	**	**	***	ns	0.667	ns
mBNST	81.755	*****	2.243	ns				0.635	ns
BA	43.401	*****	3.697	*	*	**	ns	1.337	ns
LA	78.97	*****	0.098	ns				2.494	ns
CeA	17.92	***	4.902	*	**	**	ns	0.42	ns
MHb	12.724	**	0.795	ns				2.514	ns
LHbL	25.437	****	14.102	****				3.39	*
LHbM	43.003	*****	32.414	*****				4.369	*
dCA1	27.678	*****	1.745	ns				1.582	ns
dCA2	3.594	ns	2.09	ns				3.961	*
dCA3	21.336	****	6.483	**	**	**	ns	1.447	ns
dDG	15.854	***	1.551	ns				0.679	ns
vCA1	21.16	****	2.975	ns				0.518	ns
vCA2	13.527	***	1.298	ns				0.073	ns
vCA3	7.155	*	2.117	ns				0.893	ns
vDG	15.347	***	0.416	ns				0.57	ns
PVT	39.285	*****	11.053	***	***	***	ns	0.939	ns
MD	0.0068	ns	9.459	***	***	***	ns	0.204	ns
Re	9.951	**	17.431	*****	***	***	ns	0.206	ns
LH	104.963	*****	5.667	**				3.971	*
PVH	42.638	*****	1.52	ns				0.93	ns
MM	1.051		4.698	*	**	**	ns	0.273	ns
SuMM	38.516	*****	1.232	ns				0.563	ns
PAG	12.148	**	2.604	ns				0.36	ns
RD	4.533	*	3.839	*	ns	ns	*	1.332	ns
RM	0.205	ns	7.752	**	**	**	ns	1.686	ns
SNc	2.762	ns	0.204	ns				1.404	ns
SNr	1.909	ns	0.242	ns				1.499	ns
LC	33.136	*****	0.592	ns				0.333	ns
LDT	3.196	ns	0.266	ns				1.708	ns
VTA	9.294	**	2.768	ns				1.164	ns
tVTA	5.919	*	5.703	**	**	**	ns	0.494	ns

Comparison of the structure strength in all the group

Using the classical bootstrap and the permutation test, we evaluated the significant differences between the three groups (Ctl-Veh, Ctl-CNO and hM4-CNO) exposed to restraint (**Table S6**). No difference was observed between the Ctl-CNO and the hM4-CNO group, suggesting that the effects observed on the functional network in hM4-CNO group may come from CNO effects more than, directly, the inactivation of LHb.

Table S6: Significant between-groups strength differences. Represents the three possible comparisons between the groups (columns) for each structure (rows). The cells indicated in red represents when both statistical tests (classical bootstrap and permutation test) were displaying a significant difference ($p < 0.05$), in green (per) when a significant difference only occurred after the permutation test ($p < 0.05$), and in yellow (bs) when a significant difference only occurred after the bootstrap test ($p < 0.05$). Note that only significant interactions detected by both tests have been considered in this study.

	Ctl-Veh-RS vs. Ctl-CNO-RS	Ctl-Veh-RS vs. hM4-CNO-RS	Ctl-CNO-RS vs. hM4-CNO-RS
ACC	p<0.05	ns	ns
PRL	ns	ns	ns
IL	ns	ns	ns
LO	ns	ns	ns
MO	ns	ns	ns
VO	ns	ns	ns
MCC	ns	ns	ns
Ins_R	ns	ns	ns
Ins_C	ns	p<0.05	ns
CI	ns	ns	ns
RS	ns	ns	ns
Ect	ns	ns	ns
Ent	ns	ns	ns
PRh	ns	ns	ns
dIS	p<0.05	ns	ns
vIS	per	ns	ns
dmS	ns	ns	ns
vmS	ns	ns	ns
cNac	ns	ns	ns
sNac	ns	ns	ns
VP	ns	ns	ns
LS	bs	ns	ns
MS	ns	ns	ns
TS	p<0.05	bs	ns
IBNST	ns	ns	ns
mBNST	bs	p<0.05	ns
BA	ns	ns	ns
LA	ns	ns	ns
CeA	bs	p<0.05	ns
MHb	ns	ns	ns
LHbL	ns	ns	ns
LHbM	ns	p<0.05	ns
dCA1	bs	ns	ns
dCA2	bs	ns	ns
dCA3	ns	ns	ns
dDG	ns	ns	ns
vCA1	ns	ns	ns
vCA2	ns	ns	ns
vCA3	ns	ns	ns
vDG	ns	ns	ns
PVT	p<0.05	ns	ns
MD	ns	ns	ns
Re	ns	ns	ns
LH	p<0.05	ns	ns
PVH	p<0.05	bs	ns
MM	ns	ns	ns
SuMM	ns	ns	ns
PAG	ns	ns	ns
DR	ns	ns	ns
MR	bs	ns	ns
SNc	ns	p<0.05	ns
SNr	bs	p<0.05	ns
LC	per	per	ns
LDT	bs	p<0.05	ns
VTA	p<0.05	bs	ns
tVTA	ns	ns	ns

Example of random network based on the initial data

The random networks have been created by shuffling the columns and the rows of the correlation of the initial matrices (see **Figure S6** for an example).

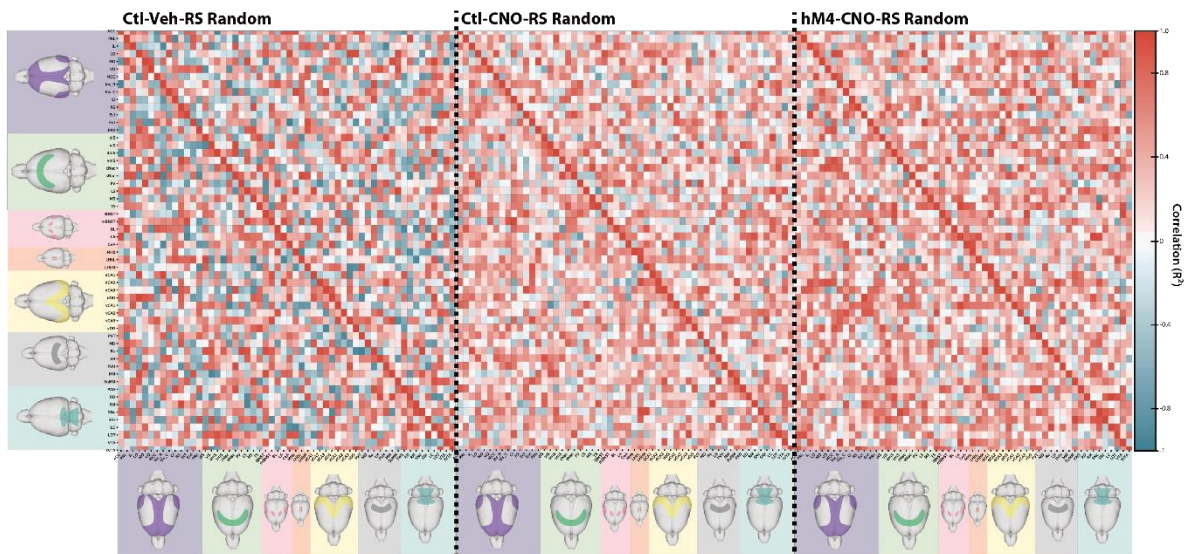


Figure S6: Example of a random network by group. Note that 500 random networks have been created for each group to estimate the distribution of the null hypothesis (H0).

Global measurement of the network

We observed that the random networks created for each group presented, as planned, the same average clustering and the same average weight (**Figure SA-B**). In addition, they all presented a lower modularity (classic bootstrap $p < 0.05$; **Figure S-C**), suggesting that the networks associated to all groups presented a non-random modularity. This result allowed us to evaluate the allegiance, making the modules accurate and meaningful.

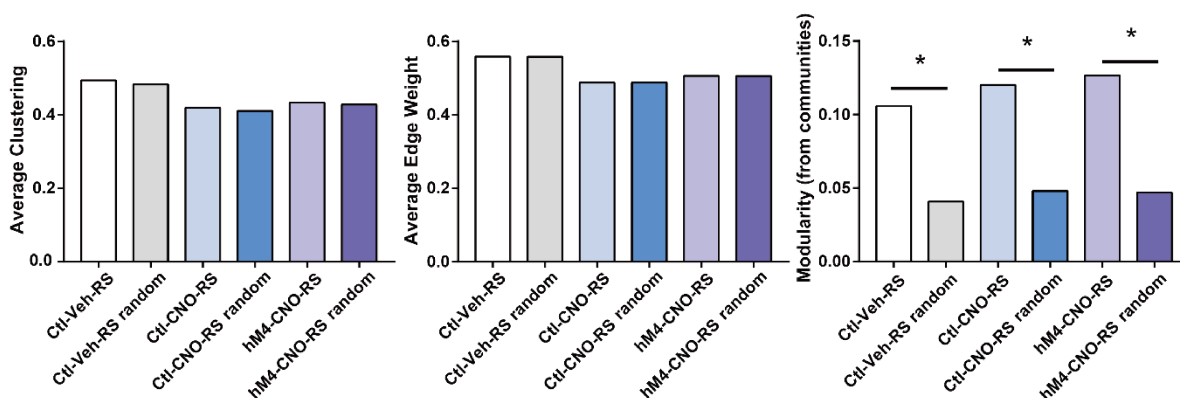


Figure S7: Global evaluation for random networks associated with the initial groups. Average clustering (**A**), Average edge weight (**B**) and modularity (**C**) of each group (Ctl-Veh-RS, Ctl-CNO-RS, hM4-CNO-RS) exposed to restraint and their associated random networks. Statistics: * $p < 0.05$.

Allegiance analysis on all the groups

We evaluated the allegiance matrices for each group exposed to restraint (**Figure S**) which served as a base to compare the composition (last main analysis) of their respective communities.

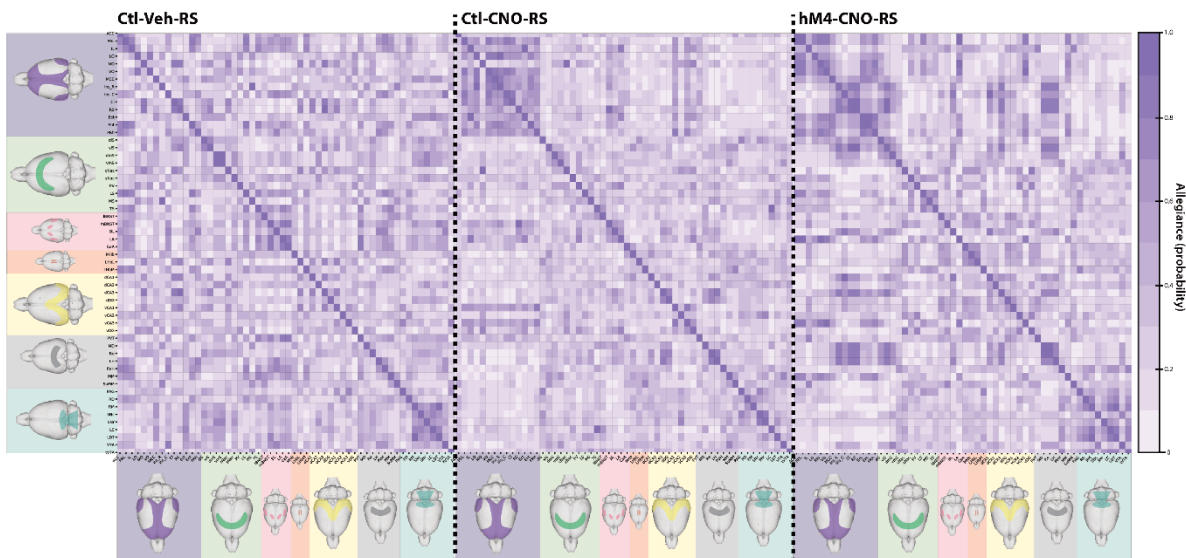


Figure S8: Allegiance heatmap for the three groups. Heatmap of allegiance of the Ctl-Veh-RS, the Ctl-CNO-RS and the hM4-CNO-RS groups, representing the probability for two given structures to belong to the same community across the bootstrap iterations (the darker, the higher probability).

Compositions of the communities for each group

Ctl-Veh-RS group:

Community °1: ACC, PRL, IL, Ins_C, Ent, PRh, LS, TS, IBNST, mBNST, BA, LA, CeA, LHbM, PVT, LH, PVH, MM, DR, VTA.

Community n°2: LO, VO, Ins_R, VP, MS, MHb, dCA2, vCA2, vDG, MD, SuMM, tVTA.

Community n°3: MO, MCC, Cl, RS, Ect, dIS, vIS, dmS, vmS, cNac, sNac, LHbL, dCA1, dCA3, dDG, vCA1, vCA3, Re, PAG, MR, SNc, SNr, LC, LDT.

Ctl-CNO-RS group:

Community °1: ACC, dIS, vIS, vmS, sNac, LS, TS, IBNST, CeA, MHb, LHbL, LHbM, dCA1, dCA2, vCA2, PVT, MD, PVH, MM, SuMM, PAG, DR, MR, SNc, SNr, LC, LDT, VTA.

Community n°2: PRL, IL, LO, VO, MCC, Ins_R, Ins_C, Cl, RS, Ect, Ent, PRh, mBNST, vCA1, vCA3.

Community n°3: MO, dmS, cNac, VP, MS, BA, LA, dCA3, dDG, vDG, Re, LH, tVTA.

hM4-CNO-RS group:

Community °1: ACC, PRL, LO, MO, VO, MCC, Ect, Ent, PRh, sNac, LS, MS, TS, LA, vCA3, MM.

Community n°2: = IL, vmS, cNac, VP, IBNST, mBNST, CeA, MHb, LHbL, LHbM, dDG, vCA1, vCA2, vDG, PVT, PVH, SuMM, PAG, DR, MR, SNr, LC, LDT, tVTA.

Community n°3: Ins_R, Ins_C, Cl, RS, dIS, vIS, dmS, BA, dCA1, dCA2, dCA3, MD, Re, LH, SNc, VTA.

III. STUDY 3: Changes in Lateral Habenula Oscillatory Activity Upon Repeated Stress Exposure

Changes in lateral habenula oscillatory activity upon repeated stress exposure

Authors

Laura Durieux^{1,2}, Karine Herbeaux^{1,2}, Chantal Mathis^{1,2}, Monique Majchrzak^{1,2}, Nelson Totah³, Lucas Lecourtier^{1,2}

Affiliations

¹Laboratoire de Neurosciences Cognitives et Adaptatives, Université de Strasbourg, Strasbourg, France.

²LNCA, UMR–7364, Centre National de la Recherche Scientifique, Strasbourg, France.

³HiLIFE, Helsinki Institute of LifeScience and School of Pharmacy, University of Helsinki, Helsinki, Finland.

Keywords

Local Field Potential; Immobilization; Clustering; Sleep; Lateral habenula.

Introduction

Responding adequately to a threatening environment is essential for survival. This ability is supported by a wide brain network in which forebrain limbic structures such as the amygdala (AMG), the medial prefrontal cortex (mPFC) and the hippocampus (HPC) are involved in multiple ways, from threat assessment to the modulation of behavioral and physiological responses (**Ulrich-Lai and Herman 2009; Godoy et al. 2018**).

For example, these three structures have differential implication in the stress response, as described by **Godoy et al. (2018)**. For example, within the mPFC, whereas the prelimbic cortex (PRL) is considered an inhibitor of the hypothalamic–pituitary–adrenal (HPA) axis with anxiolytic effects, the infralimbic cortex is a stimulator of the HPA axis with anxiogenic effects (**Diorio et al. 1993; Sullivan and Gratton 1999, 2002; Figueiredo et al. 2003**). The HPC can provide a negative feedback to the HPA axis to limit the potential deleterious consequences of prolonged corticosterone (CORT) release (**Sapolsky et al. 1986; Herman et al. 1995**). The AMG is implicated in the memorization of aversive events by triggering associations between the threat and relevant cues, and in the genesis of behavioral responses facing threat, in direct relation with the periaqueductal gray (PAG; **Cullinan et al. 1995; LeDoux, 2000**). The HPC has also a prominent role in fear responses and fear memory by triggering association between the threat and the context in which it was encountered (**Fanselow 2000; Maren et al. 2013**).

In our previous investigation (**study 2**), we highlighted the functional network engaged in response to a mild acute 10 min-long restraint (10 min). Not only we have found that mPFC region (anterior cingulate cortex [ACC], PRL, infralimbic cortex [IL]) were strongly connected, but we also found that the lateral habenula (LHb), which is in general activated by all kinds of stressors (**Benabid and Jeaugey 1989; Chastrette et al. 1991; Wirtshafter et al. 1994; Duncan et al. 1996; Brown and Shepard 2013**), displayed high connectivity with these structures, suggesting that they belong to a network exchanging information relevant to the ongoing situation and likely supporting coping with this aversive experience. These interactions have anatomical substrates, at least for the whole mPFC and the basolateral amygdala (BLA), which project to the LHb (**Kim and Lee 2012; Kim and Han 2016**). There is no anatomical connection between the LHb and the HPC; however, two studies evidenced synchronized oscillatory activities between these two regions, at the theta frequency, including during rapid-eye movement (REM) sleep (**Goutagny et al. 2013; Aizawa et al. 2013**), suggesting they exchange information. Finally, if no data have yet been provided about a functional relationship between the AMG and the LHb, the latter seems to receive information from the PRL during a working memory task (**Mathis et al. 2016**) whereas strong theta coherence between the LHb and HPC has been correlated with efficient contextual memory in an object-based task (**Goutagny et al. 2013**).

In view of those different studies, it appeared interesting to explore how the LHb interact with the mPFC, HPC, and BLA during a stressful challenge (immobilization), in order to potentially

demonstrate, as many have suggested (e.g., **Geisler and Trimble 2008; Hikosaka 2010**), that the LHb is involved in the processing of many information regarding the environment and its potential dangerous aspect in order to participate in the elaboration of relevant behavioral responses. Therefore, we performed recordings of local field potential (LFP) signals within the PRL, ACC, dorsal HPC (dHPC), BLA, and LHb, during a paradigm comprising two consecutive 10 min long immobilization sessions separated by three hours. In addition, we quantified several behaviors during and following the immobilizations to obtain behavioral of the stress response. Moreover, we looked at inter-individual differences in the expression of those behaviors in order to eventually detect signs of coping. The repetition of the immobilization procedure was also envisaged to potentially detect, electrophysiologically, brain activities related to learning processes, especially during the sleep episodes that followed each immobilization. Finally, this protocol was also chosen according to (**Jackson and Moghaddam 2004**) who demonstrated a particular dynamic of dopamine (DA) release from the first to the second immobilization, *i.e.*, a significant increased release during the first and none during the second; this appeared particularly interesting considering the engagement of prefrontal cortex (PFC) DA in the stress response, and the fact that the LHb not only is engaged in the stress response but also in the control of DA transmission. In addition, we took a particular attention to sleep-wake stages, especially during the post-immobilization periods. Indeed, the LHb has been linked with sleep, as mentioned earlier (theta coherence between the LHb and HPC during REM sleep), and also as shown by **Valjakka et al. (1998)** who found in rats a reduction of the time spent in REM sleep following lesion of the *fasciculus retroflexus*, the fiber bundle carrying LHb outputs. The investigation of sleep patterns appeared also particularly relevant in light with a vast literature in rodents showing the significant impact of stress on sleep-wake behavior (**Pawlyk et al. 2008**). For example, **Tang et al. (2005)** have found in rats an increased time spent in wakefulness and a decreased time spent in REM sleep and slow-wave sleep (SWS) following exposure to several stressors (*i.e.*, cage change and open field exposure). In humans, sleep disturbances following stress has especially been heavily documented in the scope of post-traumatic stress disorders (**Maher et al. 2006**). We found the investigation of sleep-wake pattern interesting for two reasons: first, as said above, it is known that stress has a strong impact on subsequent sleep, so that it appears interesting to investigate whether, during the period following the second stress exposure, sleep episodes show differences from those following the first stress session, likely linked to coping mechanisms; the second reason is that during sleep occur very important physiological processes, in the HPC and between the HPC and the mPFC, at the origin of the memorization of past experiences (**Tang and Jadhav 2018; Rothschild 2019; Skelin et al. 2019; Laventure and Benchenane 2020**); therefore, the present study also aimed at exploring the communication between the LHb and the structures such as the mPFC and the HPC, during episodes of sleep following both stress sessions, in order to potentially detect interactions which could potentially be linked to memory processes.

Materials and Methods

Animals

This study has been authorized by the French authorities (APAFIS#11554). We used 20 male Long-Evans rats (250–350 g; Janvier Labs, France). After arrival in the laboratory, they were housed in pairs in transparent Makrolon cages (40 x 23 x 18 cm), and then housed individually after surgery. Cages were stored in rooms with controlled ventilation, temperature ($22 \pm 1^\circ\text{C}$) and humidity ($35 \pm 5\%$) under cycled light (12 h)/dark (12 h) exposure. They had *ad libitum* access to food and water. Thirteen rats were used in the principal experiment (LHb connectivity) and six rats were used in the secondary experiment (current source density [CSD] analysis). A schematic representation of the experimental procedure is given in **Figure 1**.

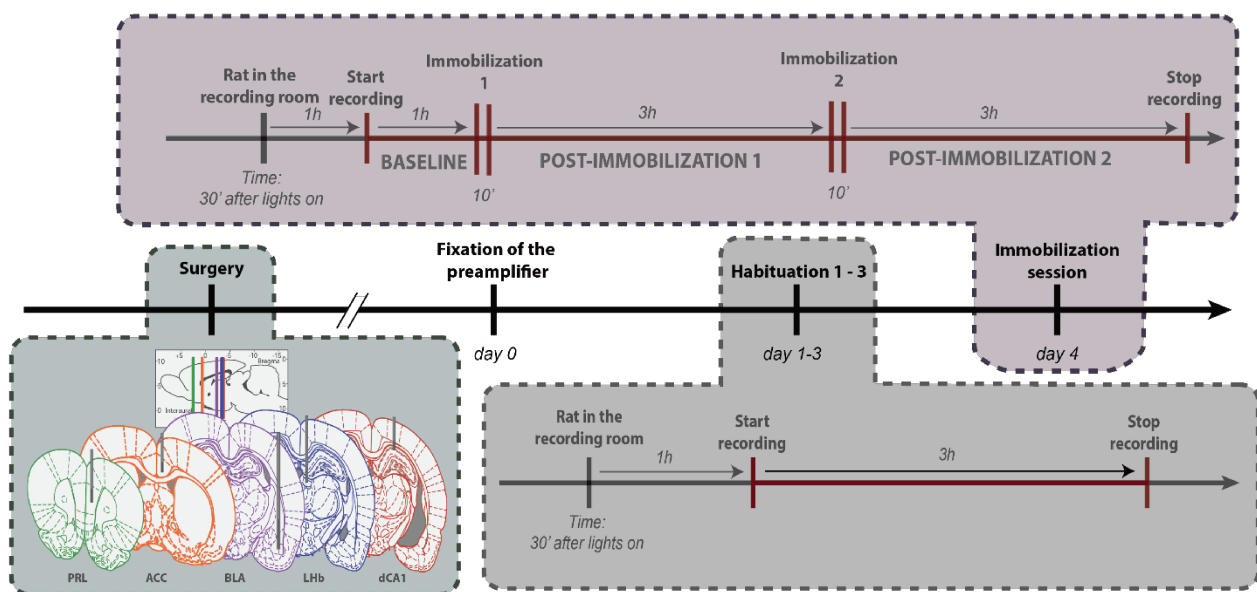


Figure 1: Summary of the timeline of the electrophysiology recording experiment.

Ten days after surgery, the preamplifier was plugged to the EIB-16 and fixed on the rat's head-cap. The following 3 days, rats were brought to the recording room 30 min after the beginning of the light period. One hour after, rats were plugged to the electrophysiology system and recordings were started, each time for 3 hours. On the fourth day, rats were brought to the room 1 h before the beginning of the recording. Following 1 hour of recording (baseline), the first 10-min immobilization was performed, followed by 3 hours of recordings (= post-immobilization 1). Then the second 10-min immobilization was performed, again followed by 3 hours of recording (post-immobilization 2).

Surgery

Rats were operated under isoflurane anesthesia [4% for induction in an induction box (3 min), 1.5 % throughout surgery] delivered in O_2 . and received a painkiller (meloxicam, 1 mg/kg, *s.c.*). Rats were placed in the stereotaxic frame, after their head was shaved. Lidocaine (0.02 mg in 0.1 ml, *s.c.*) was injected at the incision location. Home-made electrodes, composed by three coated tungsten wires (A-M Systems, bare: 50,8 μm , coated: 101,6 μm) twisted together with the tip cut either to form a flat edge (main experiment) or a beveled edge (secondary experiment, needed to investigate the effects of volume conduction, using the "CSD" calculation), were implanted in the right hemisphere in in the

following structures: ACC, PRL, BLA, LHb and dCA1 (main experiment); : dCA1, and LHb (secondary experiment; see coordinates in **Table 1**). Before being descended, the tip of each electrode was briefly dipped into a Dil solution, in order to mark the position of the electrodes for further histological verifications. The reference electrode was positioned on the Dura in the most anterior part of the exposed skull, whereas the ground electrode was positioned within the skull with no contact with the dura, in the most posterior part of the exposed skull. Once all electrodes were in place, they were all glued together and to the skull surface using a thin layer of Superbond glue (C&B[®]). Then the apical tip of each wire was uncoated using the welding device and welded to its respective channel within an EIB-16. Finally, the wires and the EIB-16 were covered with dental cement. Rats were then placed under a warming lamp until they fully awakened. They were left undisturbed for 7 to 10 days (except post-surgery checking) to favor a good recovery from the surgical procedure.

Table 1: Stereotaxic coordinates of the electrode implantations

Structures	Anteroposterior axis (mm from the bregma)	Mediolateral axis (mm for the middle of the superior sagittal sinus)	Dorsoventral axis (mm from the dura)
ACC	+ 0.5	0.7	- 2
PRL	+ 2.6	0.7	- 3
BLA	- 2.5	4.9	- 6.5
LHb	- 3.5	0.8	- 4.2
dCA1	- 3.8	2.7	- 2.1

Electrophysiology recording

Devices

Recordings were performed using an Alpha Omega system (Alpha Omega GmbH, Ubstadt-Weihe, Germany) with a preamplifier (16 channels, amplification by a factor 10; AD instruments, UK) connected to the EIB, while the behavior of the rats was constantly recorded with a webcam placed above the cage and connected to a different computer than the electrophysiology recording system. Video recording was made with OBS Studio (Open Broadcaster Software 25.0.1, free and open source: <https://obsproject.com/fr>). The electrophysiology recorded signal was amplified by a factor 200 in total and was filtered (hardware minimum) from 0.5Hz to 8kHz. The signal was digitalized at a sampling rate of 1375 Hz. Electrode impedance was checked before the start of each recording session; we obtained impedances from ~50kΩ to ~200kΩ at 1kHz.

Recordings

During each recording session rats were placed in their respective recording cage (the same each time), within the Faraday cage, for 1 h before being connected to the system. During the recording sessions they had only access to water, to avoid frequent contamination of the signals with chewing. Signals were checked on a given day and then the preamplifier was secured to the EIB and head cap so that it stayed in place and did not move during the entire experiment. During the 3 days following the secured plugging of the preamplifier, baseline recordings were performed for 3 h per day from 09:00 am to 12:00 am. These 3 sessions were designed to allow habituation to the recording situation. In order to potentially evidence activity changes due to the habituation, we focused the analysis on the habituation 1 (HAB1) and habituation 3 (HAB3) across the study. Then, the following day, the actual immobilization experiment was performed. After the rats were brought to the recording room, they were placed into their cage and left undisturbed for one hour. Then, they were plugged, and the recording was started. After 1 h, considered as pre-immobilization baseline, the first immobilization stress was performed; for this, the rat was immobilized against one of the corners of the cage, its head and body being held by an experimenter for 10 min. Then, rats were left undisturbed for 3 h, considered as post-immobilization 1 (PS1) period, after which the second 10-min immobilization was performed; then rats were left undisturbed for an extra 3 h, considered as post-immobilization 2 (PS2) period, before the recordings (electrophysiological and video) were stopped. During the different sessions considered for subsequent analyses (HAB3, PS1 and PS2), several behaviors were scored (i.e., stereotyped behaviors amongst those frequently analyzed in studies investigating the stress response; **MacLennan and Maier, 1983**) using AION software: *locomotion* (when rats just move in the cage; according to this specific behavior, when rats reach an end of the cage, this is scored as a *cage crossing*); *rearing* (when rats stand on their back paws while sniffing up); *sniffing down* (when rats repeatedly sniff the bedding); *digging* (when rats use their forepaws and nose to dig the bedding and push it to the side); *turning* (when rats, while standing on their four paws, abruptly make a half-turn); *wet-dog shake* (when rats, either on their four paws or on their back paws, shake their upper body for a very brief period). In addition, during both immobilization sessions we scored the time rats spent “struggling”, meaning the time spent moving their body upward or backward (rats were immobilized against one of the corners of the cage) pushing on their paws to escape the situation.

Histology analysis

Brain tissue preparation and section processing

After the last recording, rats were deeply anesthetized with pentobarbital overdose (120 mg/kg, *i.p.*). Following intracardiac perfusion of phosphate-buffered saline (PBS, 0.1M) and then 4% paraformaldehyde (PFA)-PBS solution (pH 7.4; 4°C), brains were removed, post-fixed in 4 % PFA-PBS (4 °C, 48 h), transferred into a 0.1 M PBS–20 % sucrose solution (4° C, 48 h) and subsequently frozen (isopentane, -40°C, 1 min). Serial 40 µm-thick free-floating sections were cut in the coronal plane at – 20 °C and collected then stored in cryoprotectant at – 20°C.

Location of Electrodes implantation

The visualization of the placement of Dil was performed using a fluorescence microscope (Apotome.2, Zeiss®) *via* a camera (Orca Flash 4.0 LT, Hamamatsu) linked to a computer equipped with a picture acquisition and processing software (ZEN 2 Black, Zeiss®). As several brain slices were positioned on a given slide, it took several pictures to cover the entire surface of a slide at the given magnification used (x 2.5; all pictures of a slide were acquired with the same zoom parameter), so that they were subsequently assembled to reconstruct the whole slide in 2D using the same software (ZEN 2 Black). Images were subsequently superimposed to the images taken in the Paxinos and Watson atlas (**Paxinos et Watson, 2007**) in order to determine with precision the location of the tip of electrodes. Only the animal with a correct placement were kept for the analysis (see results).

Videos tracking analysis

Videos were formatted, using Format Factory software (Freeware, Free Time), in MP4 (MPEG-4 Part 14) which allows a wider compatibility software than the initial format and decreases the size of the files.

From the recorded videos, in order to automatically track the animals' position during the different sessions of our protocol, we used a Deep Learning algorithm called DeepLabCut (DLC) developed by the Mathis group (**Mathis et al. 2018; Nath et al. 2019**). This approach allowed us to extract the movement of the animals, which was essential to determine, in combination with the electrophysiological data, the different sleep/wake stages. The training of DLC was performed using 11 videos with 100 images uniformly extracted. For the creation of the training set, we used the pretrained network ResNet152 from ImageNet (<http://www.image-net.org/index> & <https://www.kaggle.com/pytorch/resnet152>). We used *imgaug* (Copyright © 2018 Alexander Jung; <https://github.com/aleju/imgaug-doc>) as image augmenter (recommended by DLC). We filtered the data using the median filter proposed by DLC to remove the outliers. From the video tracking results of DLC, we extracted if the animal moved or not, helping to the assessment of sleep-wake stages.

LFP analysis

Preprocessing

The analyses of LFP signals were done with MATLAB (MathWorks®, Natick, Massachusetts, United States, R2020b, 9.9.0.1467703). Signals were filtered (MATLAB function `filtfilt()`; zero phase digital filtering; high pass: 0.5 & low pass: 500) and down-sampled (by 5, transforming the sample rate from 1375 Hz to 275 Hz). For each recorded structure, we calculate the signal based on a local reference (difference between two channels recorded in the same structures).

To investigate the 'amount' of LHb signal contaminated by volume-conducted signal coming from the dHPC, in a second experiment, we performed a CSD calculation with the signals of the three

LHb electrodes (limiting the portion of the signal which is volume-conducted from a distant source; **Nicholson and Freeman, 1975**) as follows:

$$CSD = - \left(\frac{LFP_{ch3} - 2LFP_{ch2} + LFP_{ch1}}{spacing^2 \times cond} \right)$$

where *CSD* is the current source density in Ampere, *LFP* is the LFP signal recorded in Volt, from the shortest electrodes (ch1), the medium-size electrode (ch2) and the longest electrode (ch3), *spacing* is the distance between electrodes in Meters, and *cond* is the conductivity of the extracellular medium (0.3 S.m⁻¹).

We compared the signal resulting from the CSD calculation with the raw signal and the signal resulting from the local reference calculation.

Sleep-wake stages assessment

We evaluated the power using the Chronux toolbox with the following parameters: sliding window (5-s windows moving across 0.3 s), tapers ($k = 9$; $nw = (k+1)/2$; $[nw \ k]$), frequency band analyzed (0.5 Hz and 100 Hz). Sleep-wake stages were assessed based on the power in dCA1 and PRL power, the theta/delta ratio in dCA1, the delta/gamma ratio in PRL, and the determination of the presence or absence of movement provided by DLC. For the calculation of the ratios, we considered the following band width: delta: 1 Hz to 3 Hz; theta: 5 Hz to 12 HZ; gamma: 30 Hz to 100 Hz. We then considered four different stages: **active wake (AW)**, **calm (quiet) wake (CW)**, **slow wave sleep (SWS)**, and **rapid eye movement sleep (REM sleep)**. AW, as well as REM sleep, were characterized by a high theta power in the dHPC and a high gamma power in the PRL. The presence (AW) or absence (REM sleep) of movements of the animals further separated both stages. SWS was characterized by cortical delta (slow) waves of high power. Were defined as CW all other portions of the signal not corresponding to the above-mentioned characteristics. We partitioned the signal so that we could store the different stages separately and saved the results. From the hypnogram (*i.e.*, the description of the succession of the sleep-wake stages across time) we evaluated, for each recording session, the latency to reach the first episode of each stage, the number and duration of episodes of the different stages, as well as the cumulative duration of each stage. In addition, we removed artefacts from the signal by deleting the time points where the amplitude of the signal was superior to six time the standard deviation of the total signal. In each step of the analysis, a visual checking has been done to make sure that the integrity of the signal was conserved.

Clustering of the animals according to the behavioral and electrophysiology data following PS1

Due to a certain inter-individual variability in the response to the immobilizations, we decided to try to cluster the animals. They were therefore separated according to the difference between the first hours after the first immobilization and the 1-h baseline, on following selected variables: the duration of the first AW episode, the time spent rearing, and the time spent in locomotion. To evaluate the

main variance of these variables, we performed a PCA (principal component analysis) using Statistica© (Statsoft, Tulsa, USA). Then the factor representing the main variance was selected to represent the “responsiveness” of the animal to the immobilization. We further clustered the animals using k-mean algorithm (Matlab function) based on the individual values of the principal component (PC) of the PCA. This provided 3 clusters: one including animals considered as showing a high level of activity following immobilization (*high responders*), one including animals considered as showing a low level of activity following immobilization (*low responders*), and one including animals that we considered had a peculiar “opposite” response to what was expected, as they were more active during baseline than following immobilization (*opposite responders*). We decided to pool the “opposite responders” and the “low responders” within a single “low responders” group.

Global forebrain dynamic classification

According to **Gervasoni et al. (2004)**, rat sleep-wake stages can be predicted by the global forebrain dynamic (e.g., LFP signals in the HPC and the PFC). We repeated their analyses to verify if we could find the same classification with our own data. The signals recorded in dCA1 and PRL were first processed using a fast Fourier transform (FFT; chronux toolbox) then two frequency band ratios were calculated for each structure, i.e. ratio 1: (1-20Hz)/(1-55.0 Hz), and ratio 2; (1-4.5Hz)/(1-9Hz). Then a PCA was applied separately on ratio 1 and ratio 2. The PC of both ratios was plotted as: x axis, first PC ratio 2; y axis, first PC ratio 1.

Power and coherence evaluation

Following the global analysis of sleep-wake stages, we studied the power of each oscillation considered (the square of the amplitude) according to the different stages (AW, CW, SWS, REM) during each session of the protocol by periods of one hour. We used MATLAB Complex Morlet wavelet definition: $cmor(Fb)-Fc$ where Fb is the bandwidth parameter and Fc is the wavelet center frequency (cmor2-0.7958).

To use the wavelet transform, we defined a frequency scale (i.e., 277 frequencies from 1 to the Nyquist frequency rate $[275 \text{ Hz}]/2 = 137.5 \text{ Hz}$). From the wavelet transform we obtained the amplitude (by extend the power = amplitude²) and the phase of the oscillation. The power was transformed from arbitrary unit (a.u.) in decibel (dB) using the following equation:

$$Power_{dB} = 10 \times \log_{10} (Power_{a.u.})$$

where the *Power* is a vector containing the power values by frequencies.

After evaluating the spectrogram obtained (i.e., the frequency bands which are actually present within the recorded signal), we considered three specific bands: delta (1 Hz to 3 Hz), theta (5 Hz to 9 Hz), and gamma (45 Hz to 65 Hz). These bands were defined based on the bands present – or mostly present - in the spectrogram depending on the structure and the sleep-wake stage considered (e.g., no theta band was observed in dCA1 during SWS). For the results by band of interest, we

normalized the power of a given session by the Baseline session (e.g., PS1[AW] – BL[AW] by structures and by rats) in order to reduce inter-individual variations.

Coherence analyses between all recorded structures (PRL, ACC, dorsal *cornu Ammonis* 1 of the HPC [dCA1], BLA, LHb) therefore led to ten possible comparisons. Coherence was evaluated using the Chronux toolbox, considering all frequency bands from 1 Hz to 80 Hz. We evaluated the mean of the coherence in these frequency bands for each pair of structures (if the coherence was present in the coherogram). We used the same tapers ($k = 9$; $nw = (k+1)/2$; [nw k]) than for the FFT analysis with Chronux.

Statistics

We compared the time spent struggling during the two immobilization sessions, as well as the presence of the different behaviors cited above during the first hour following both immobilization sessions, using t-tests Statistica® (Statsoft, Tulsa, USA). Electrophysiology data were analyzed using 2-ways ANOVAs with repeated measures followed, when required, by Newman-Keuls post-hoc multiple comparisons test. The threshold for rejecting the null hypothesis was 0.05 throughout. Due to technical limitations, some LFP signals was not computable / analyzable depending on the structures, the rats and the sessions. Consequently, the number of animals (n) took for each analysis is indicated on the concerned results.

Results

Note: except for the histology, the following results are considered preliminary because the LFP signal analyses are still ongoing. For example, post-immobilization analyses were performed over the entire period (3 hours) whereas a finer analysis, taking into account several distinct periods following stress (right after vs several hours after) would certainly provide different results and conclusions. Therefore, the analyses and statistics, as well as the discussion, reported hereafter remain temporary. In addition, we took the liberty to indicate and discuss tendencies in these analyses. A tendency was considered when $0.05 < p < 0.25$ accounting for a potential fake positive of 25% (i.e., estimating that we have 25% chance to be wrong and that the tendency is not actually relevant.

Verification of electrodes localization and of the electrophysiological signals

Before performing signal analyses, the placement of the different electrodes was verified thanks to the presence of Dil (**Figure 2**).

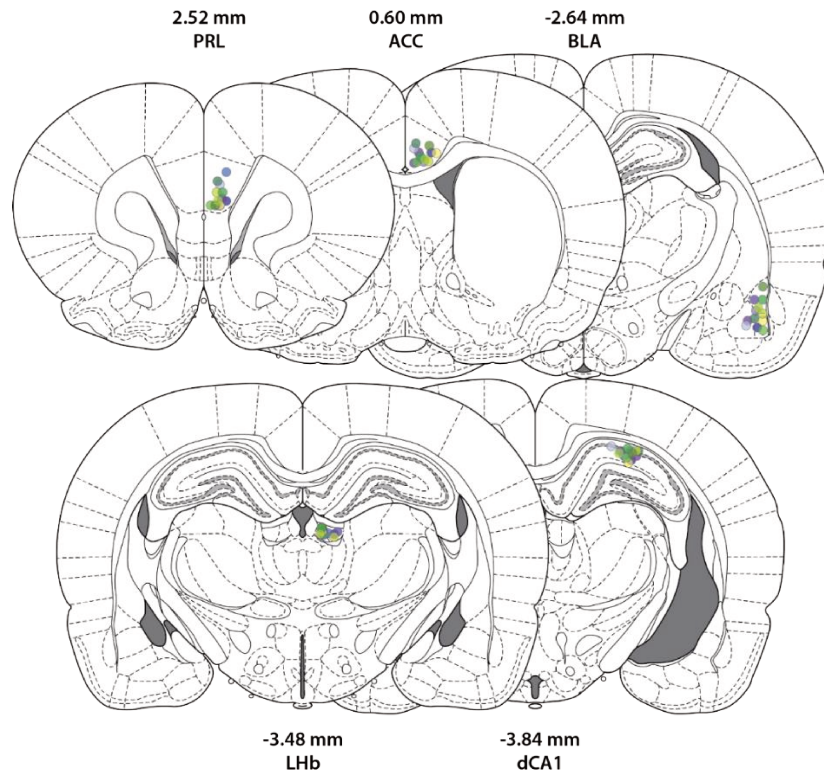


Figure 2: Verification of the placement of the electrodes

Schematic representation of the placement of the different electrodes within the PRL, ACC, BLA, LHb and dCA1 respectively (each color represent a given rat). Adapted from Paxinos and Watson atlas (Paxinos et Watson, 2007).

In **Figure 3** is represented an example of raw signals recorded in each structure during an AW episode in one rat.

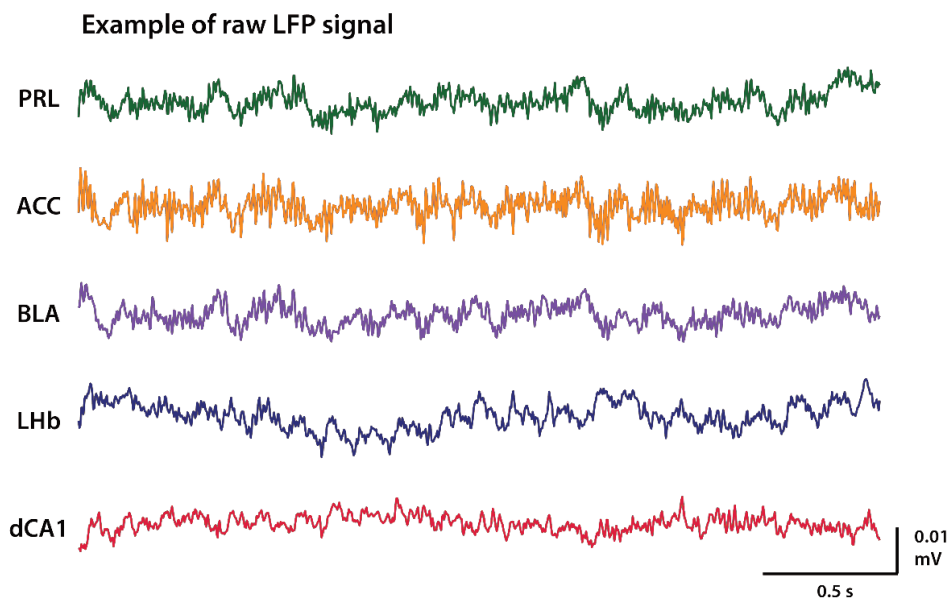


Figure 3: Example of LFP signals recorded in each structure.

Example of LFP recordings (5 sec) during an AW episode during habituation in one rat. The five structures are represented in a color code as follows: PRL (green), ACC (orange), BLA (purple), LHb (blue), dCA1 (red).

Diversity of the behavioral responses and stages dynamics facing repeated stress exposure.

During the 10 min of immobilization, animals displayed significantly less struggling time in the second exposition than the first exposition ($t_{24}=4.33$, $p<0.0001$; **Figure 4A**). In addition, animals presented a decrease of the time spent doing, or of the number of, several behaviors from the first to the second post-immobilization periods (the first hour following immobilization); those include: the number of cage crossing ($t_{24}=2.44$, $p<0.05$; **Figure 4B**), total locomotor activity duration ($t_{24}=3.69$, $p<0.01$; **Figure 4C**), total rearing duration ($t_{24}=2.69$, $p<0.05$; **Figure 4D**), total digging duration ($t_{24}=3.23$, $p<0.01$; **Figure 4E**), total sniffing down duration ($t_{24}=3.58$, $p<0.01$; **Figure 4F**), number of wet-dog shake ($t_{24}=2.58$, $p<0.05$; **Figure 4G**) and the number of turn around ($t_{24}=2.45$, $p<0.05$; **Figure 4H**). These results indicate that animals struggled less during, and were less active following, the second immobilization. However, one could notice the variability of the inter-individual behavioral responses.

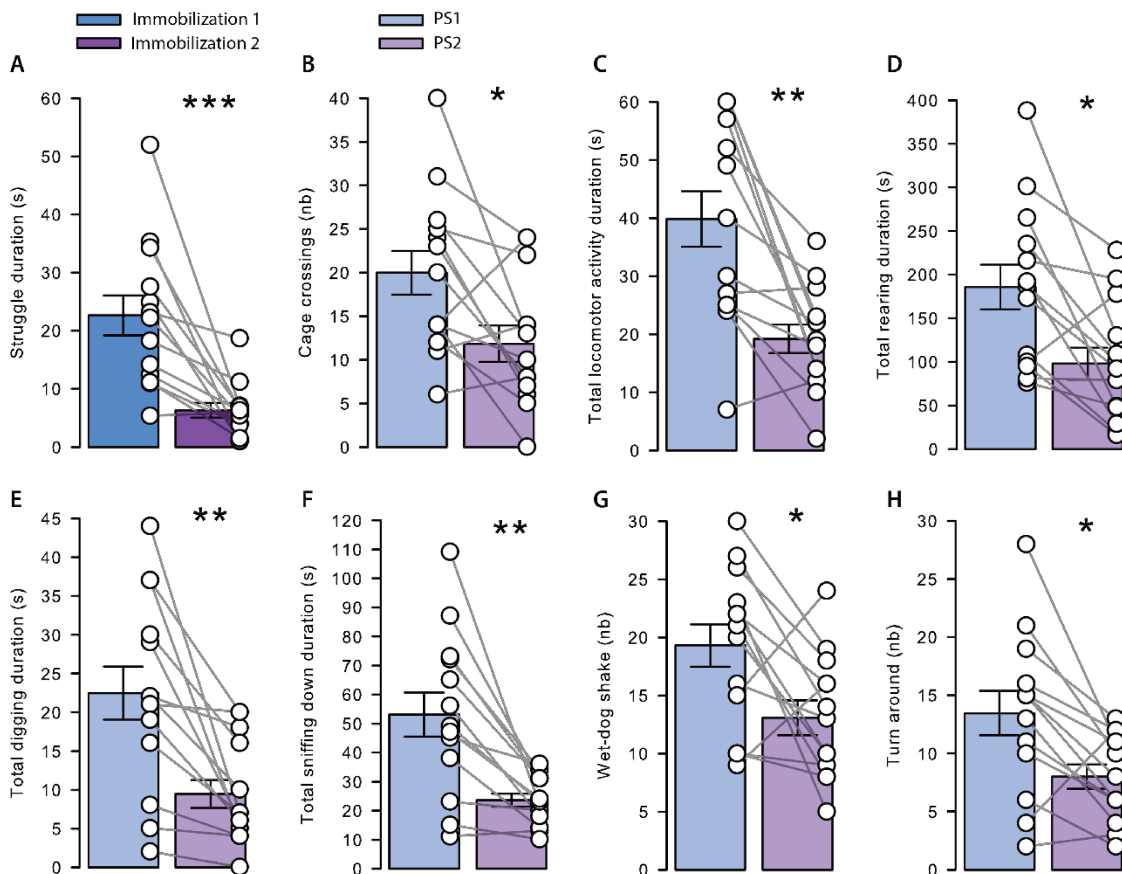


Figure 4: The behavioral response that accompany the second immobilization is of lower magnitude.

(A) Struggle duration in seconds displayed by rats during both immobilization sessions. Number of cage crossings (B), total time spent doing locomotion (in seconds) (C), total time spent rearing (in seconds) (D), total time spent digging (in seconds) (E), total time spent sniffing down (in seconds) (F), number of wet-dog shakes (G), and number of turn-arounds (H), during the first hour following each immobilization session (PS1 and PS2). All behavioral measures significantly decrease from PS1 to PS2. Statistics: * $p<0.05$, ** $p<0.01$, *** $p<0.001$ vs immobilization 1 (A) or PS1 (B-H). $n=13$.

The sleep-wake stages were determined based on four stages: AW, CW, SWS and REM sleep, as described in the Materials and Methods.

To verify the manual coding of the sleep-wake stages assessment (**Figure 5A**), we studied the stages dynamic such as described in **Gervasoni et al. (2004)**; our goal was to check if we could find a similar distribution of the first PC ratios in the PRL and the HPC. We obtained roughly similar stages dynamics distribution, supporting the accuracy of our manual coding method (**Figure 5B-C**). However, this is a preliminary result, as the analysis was performed on only one rat.

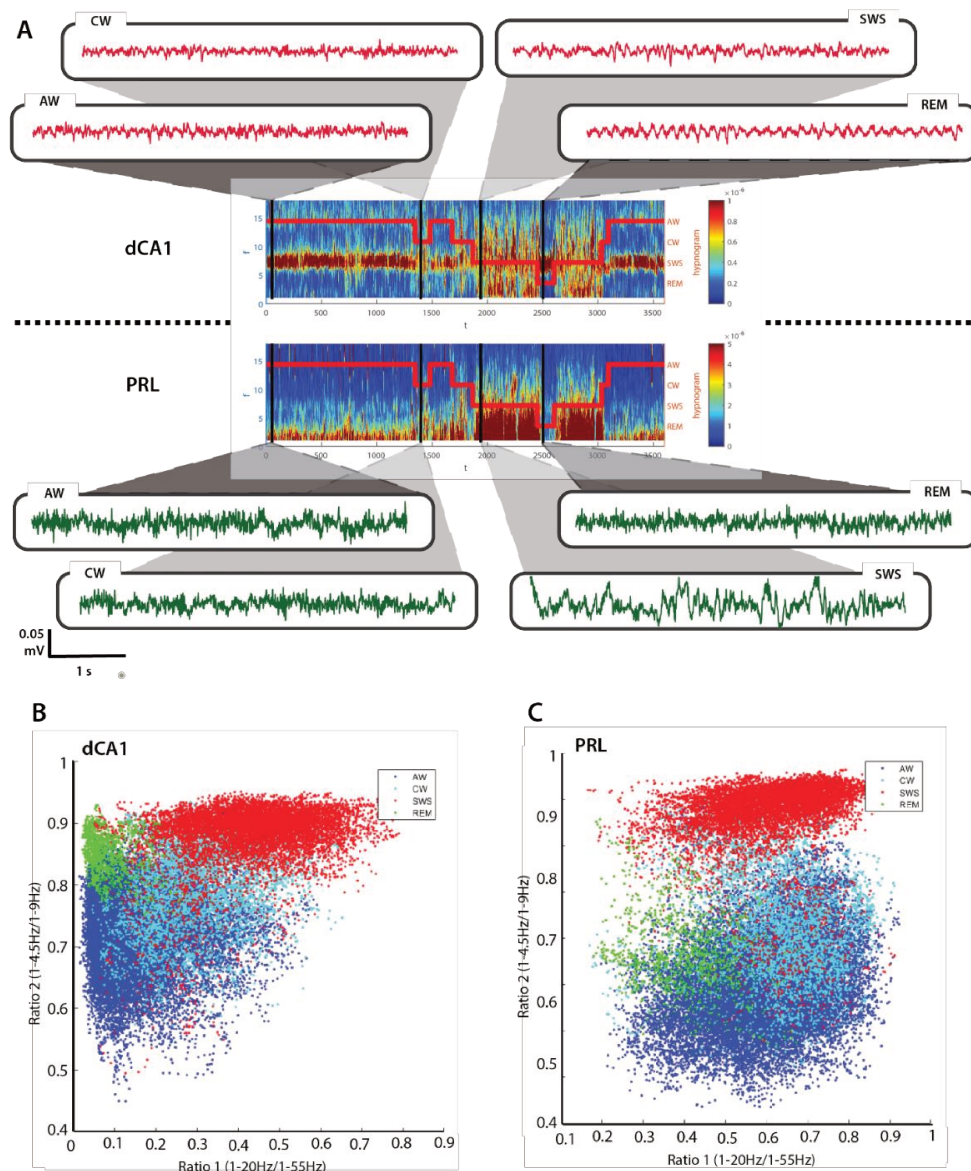


Figure 5: Sleep-wake stages assessment.

(**A**) Spectrograms (frequency x time x power) of dCA1 (top) and PRL (bottom) with a zoom on the LFP signal for each stage (5 seconds are represented). AW, as well as REM sleep, are characterized by a high theta power in dCA1 and a high gamma power in PRL. The presence (AW) or absence (REM sleep) of movements of the animals further separated both stages. SWS is characterized by high amplitude of cortical delta (slow) waves. (**B-C**) Plots representing the ratios (ratio 1, [1-20Hz]/[1-55.0 Hz] and ratio 2, [1-4.5Hz]/[1-9Hz]) extracted from the PCA of LFP recordings in dCA1 (**B**) and PRL (**C**). According to Gervasoni et al. (2004), rat sleep-wake stages can be predicted by these two ratios; this further supports the accuracy of our manual coding of sleep-wake stages across our recordings.

From hypnograms (**Figure 6A** for an example), the latency of the first entry in the different stages, the number of episode occurrences, and the cumulative duration of each stages were evaluated (**Figure 6B-D**). For the latency, the 2-way ANOVA with repeated measures indicated an effect of Stage ($F(3, 44) = 70.75$; $p < 0.0001$) and of Session ($F(3, 132) = 10.74$; $p < 0.0001$), as well as a significant interaction between them ($F(9, 132) = 2.753$; $p = 0.0056$). Newman-Keuls test revealed a significant decrease of the latency to enter in SWS in PS2 compared to HAB1 ($p < 0.05$; **Figure 6B**). In addition, the latency to enter REM sleep was lower in PS2 than all the other sessions ($p < 0.05$; **Figure 6 B**). In summary, only the second immobilization seemed to affect the latency to reach the SWS and REM sleep stages.

According to the number of occurrences of each stage (**Figure 6 C**), the 2-way ANOVA with repeated measures showed significant effects of Stage ($F(3, 44) = 51.71$; $p < 0.0001$), Session ($F(3, 132) = 3.649$; $p = 0.014$), and interaction ($F(9, 132) = 4.164$; $p < 0.0001$). Newman-Keuls test highlighted a significant increase in the number of SWS and REM sleep episodes in PS2 as compared to each of the other sessions ($p < 0.05$ for each comparison).

According to the cumulative duration of each stage (across each 3 hours of recordings; **Figure 6 D**), the 2-way ANOVA indicated a significant effect of Stage ($F(3, 44) = 116.2$; $p < 0.0001$), no effect of Session but a significant Stage x Session interaction ($F(9, 132) = 7.88$; $p < 0.0001$). Newman-Keuls test showed a lower time spend in AW in PS1 in comparison to HAB1 ($p < 0.05$) and a lower time spent in AW in PS2 in comparison with the other sessions. The time spent in SWS was significantly increased in PS2 in comparison with HAB1 and HAB3 ($p < 0.05$). Post-hoc test highlighted a longer time spent in REM sleep during the PS2 session in comparison with all the other sessions. Therefore, first immobilization seems to lead to a decrease of the time spent in AW in comparison with HAB1; in addition, we observed a decrease of the time spend in AW and an increase of the time spent in SWS and REM sleep following the second immobilization.

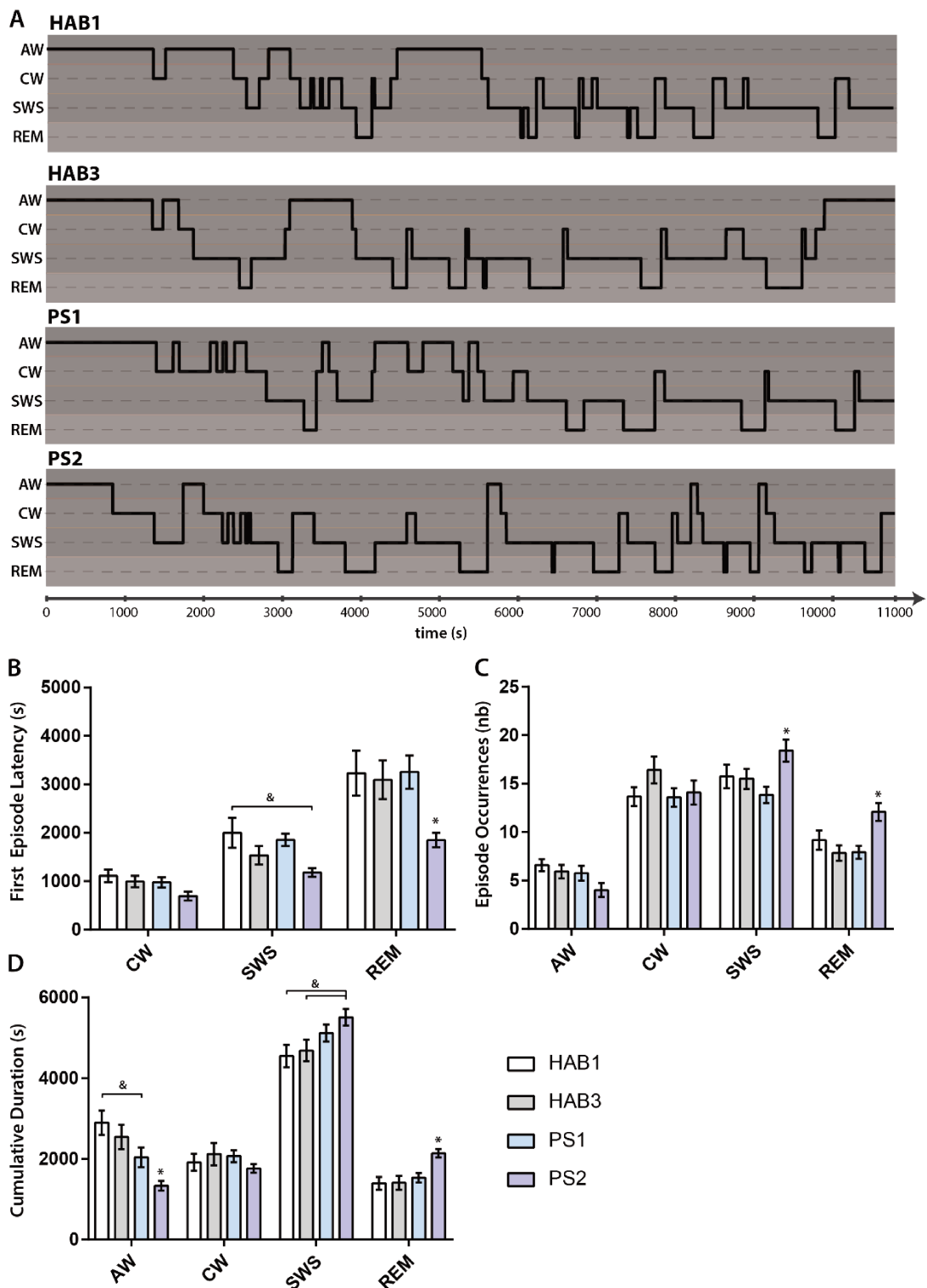


Figure 6: Effects of the repetition of immobilization on the dynamics of the sleep-wake stages.

(A) Example of a rat's hypnogram across the three hours of recordings for each session (HAB1, HAB3, PS1 and PS2). (B-D) Bar plots of the characteristics of the sleep-wake stages across all sessions (HAB 1, HAB3, S1 and PS2). (B) Latency in second to reach the indicated stage (note: AW is not represented because each session starting as soon as the rat was connected, rats were automatically doing AW, making the latency equal to 0). (C) Number of episodes (occurrences) spent in each stage. (D) Cumulative duration of each stage across the three hours of recording. Data are represented as mean \pm SEM. Stats: &p<0.05 vs the specific session (linked with the horizontal black line), *p<0.05 vs. each of the other sessions, for the same stage. n=11.

In summary, we observed a decrease of the time spent in AW following PS2 compared to PS1 suggesting a modulation of the response across the repetition of the stress exposure. However, there is no difference between the first immobilization and the habituation sessions, except for a shorted time spent in AW.

Given the inter-individual variability in animal behavior during post-immobilization periods, we used a PCA and clustered the animals according to the difference in their response between the first immobilization and the previous 1-hour baseline. The data used for this were: the duration of the first episode of AW, the time spent rearing, and the total number of cage crossing. The first component (PC1) of the PCA accounted for 88.5 % (eigenvalue = 2.65), the second for 10.6% (eigenvalue = 0.31), and the last one for 0.8 % (eigenvalue = 0.02) of the total variance (see supplemental information, **Figure S1**). The three variables used were negatively correlated with the principal component of the PCA: R^2 of the correlation between PC1 and duration of the first episode of AW = -0.88; the time spent in rearing position = -0.98; the total number of crossing cages = -0.95; see supplemental information (**Figure S1**), suggesting that high PC1 values represent low responsiveness of the animal, whereas low PC1 values represent high responsiveness. The k-means algorithm on PC1 revealed 3 clusters (**Figure 7**). We grouped the animals of 2 of these clusters to finally constitute 2 categories, *i.e.*, rats displaying intense stress-related behavior and rats displaying no obvious behavioral response. The high responders represented the animals with low PC1 score (low because of the negative correlation between the PC1 and the variable) and the low responders included animals with a high or near zero score in PC1.

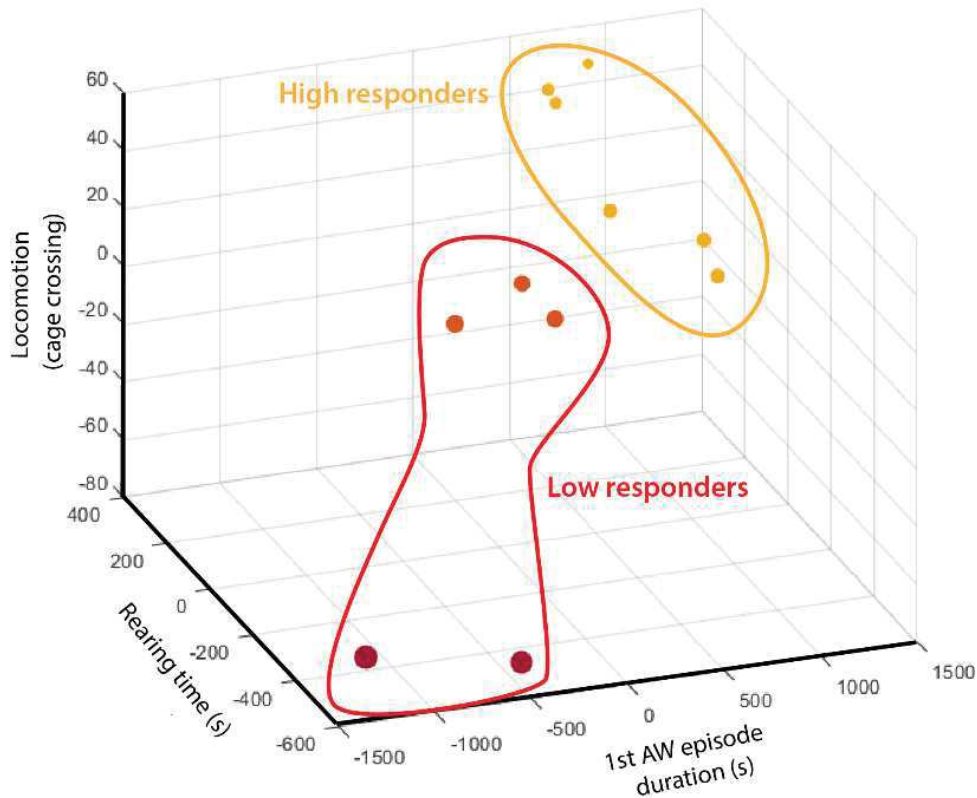


Figure 7: Clustering based on behavioral responses following exposure to the first immobilization.

K mean algorithm clustered animals based on PC1 extract from three variables: the number of cage crossings, the total time spent rearing and the duration of the first AW episode following the first immobilization, normalized by the same variables scored during baseline (the hour preceding the immobilization). It unraveled three clusters (marked by the different color dots) that we grouped (depending on their PC1 score) as “high responders” (animal displaying high reactivity after the immobilization) and “low responders” (not displaying any change in behavior, or even being less active after the immobilization that during baseline). n=11.

Theta synchronization of LHb neuronal assemblies in AW is differentially affected depending on the responsiveness to the immobilization.

In the LHb, a theta rhythm (6-9Hz) was very apparent across the signal (**Figure 7A**), such as further revealed by the spectrogram, showing a pic of the oscillation power in the theta frequency band across all session (**Figure 7B**). We did preliminary statistics on theta power across sessions and groups but, as the power displayed in this analysis is the average power of AW over the 3 hours of recording, potential effects could be drowned out. The 2-way ANOVA with repeated measures indicated a significant effect of Session ($F(2, 14) = 4.211$; $p = 0.037$), and a tendency for a significant effect of Group ($F(1, 7) = 2.364$; $p=0.168$), but no significant interaction of the two factors ($F(2, 14) = 1.426$; $p=0.273$). Post hoc test revealed a decreased theta power from HAB3 to PS2 ($p<0.05$) only in the low responders (**Figure 7C**). This preliminary result suggests a disrupted synchronization of the LHb cells assemblies only in animals not affected by stress.

The results in dCA1 seem to diverge from those obtained in the LHb. We observed a strong theta band in dCA1 across all sessions (HAB3, PS1 and 2) (**Figure 7D-E**). The 2-way ANOVA indicated

no effect of Session ($F(2, 18) = 0.3054$; $p = 0.740$), a tendency towards an effect of Group ($F(1, 9) = 2.79$; $p=0.129$), and no interaction between the two factors ($F(2, 18) = 0.395$; $p=0.679$), (**Figure 7F**). The tendency of theta power to be lower in high responders suggests that theta synchronization might be disrupted in the animal affected by stress exposure. In addition, the theta oscillation observed in the dCA1 does not seem to be correlated with movement (see supplemental information; **Figure S1**), suggesting that the theta observed in AW in our conditions could be more linked to cognitive rather than motor processes. Noteworthy, the fact that disruption of theta synchronization found in low responders is observed in the LHb but not in dCA1 could support the idea that the theta observed in the LHb may not be, at least totally, volume conducted from dHPC.

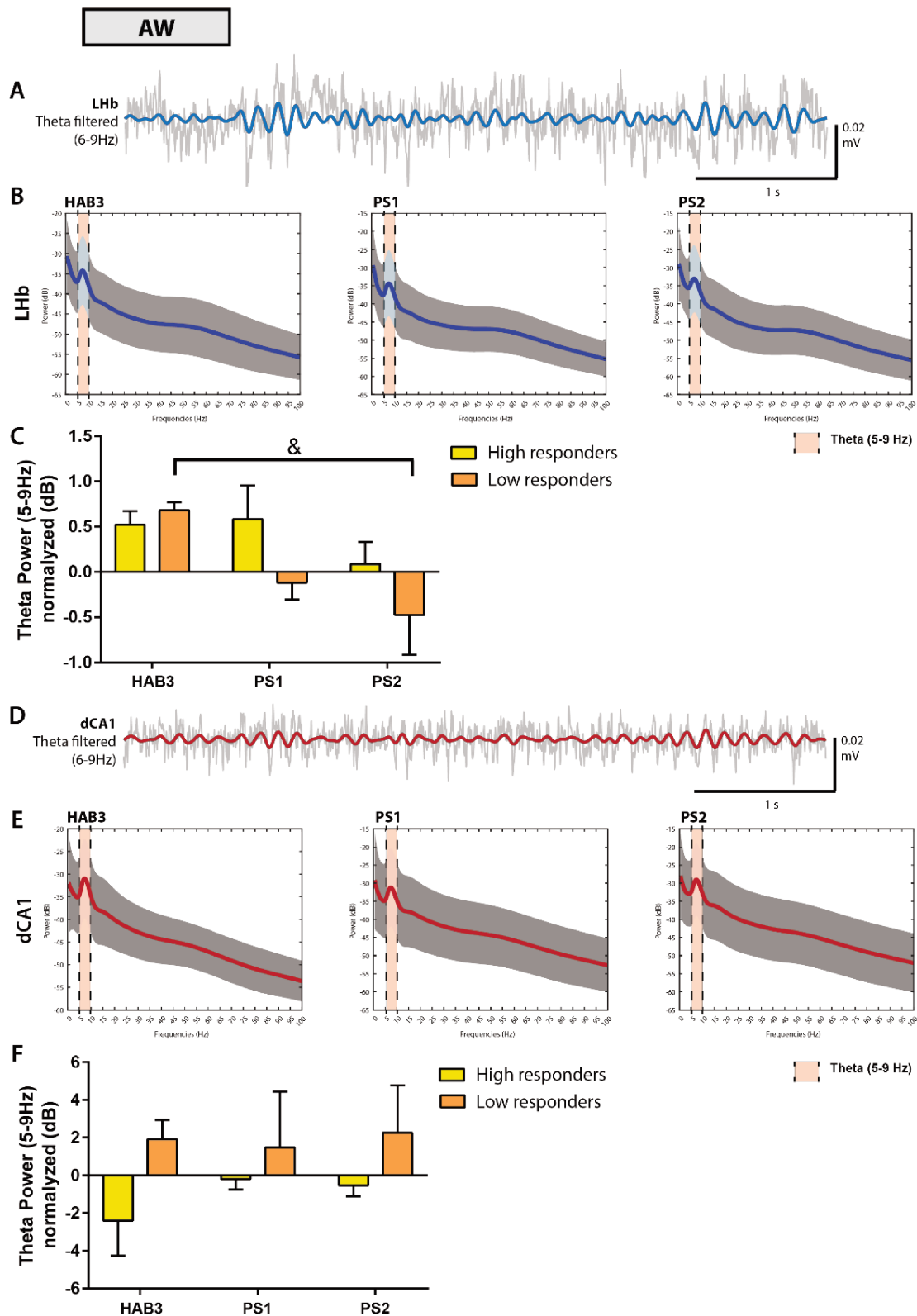


Figure 8: Theta oscillations in Lhb and dCA1 during AW across sessions.

Example of LFP signal in Lhb (A) and dCA1 (D) superimposed with their respective theta oscillation filtered track. Spectrogram (power in dB x frequency in Hz) in the Lhb (B) and dCA1 (E) across the different sessions (HAB3, PS1, PS2) for all rats (average \pm 95% confidence interval). The frequency of the theta pic is highlighted in orange. Evolution of the power of the theta band in the Lhb across the sessions in high (n=4) and low responders (n=5) (C) and dCA1 across the sessions in high (n=5) and low responders (n=4) (F) bars represented the mean \pm SEM. Stats: $\&p < 0.05$.

Disruption of SWS synchronization in LHb following immobilization

Considering the implication of LHb in sleep and memory, we decided to look at the LFP activity of the LHb in SWS across sessions. We found that during SWS, the LHb displayed a slow wave activity from 1Hz to 3 Hz (delta; **Figure 9A-B**). The 2-way ANOVA indicated a significant effect of Session ($F(2, 14) = 7.591$; $p = 0.005$), a tendency for a significant effect of Group ($F(1, 7) = 1.974$; $p = 0.208$), and a near-significant interaction of both factors ($F(2, 14) = 3.605$; $p = 0.0546$). This near-significance of the interaction prompted us to perform post hoc analyses; Newman-Keuls test revealed a decreased delta power during PS2 as compared to HAB3 ($p < 0.01$) and PS1 ($p < 0.05$) only in high responders (**Figure 9C**). This result may suggest a decreased delta synchronization of LHb cell assemblies upon the repetition of stress exposure in animals displaying stronger behavioral responses.

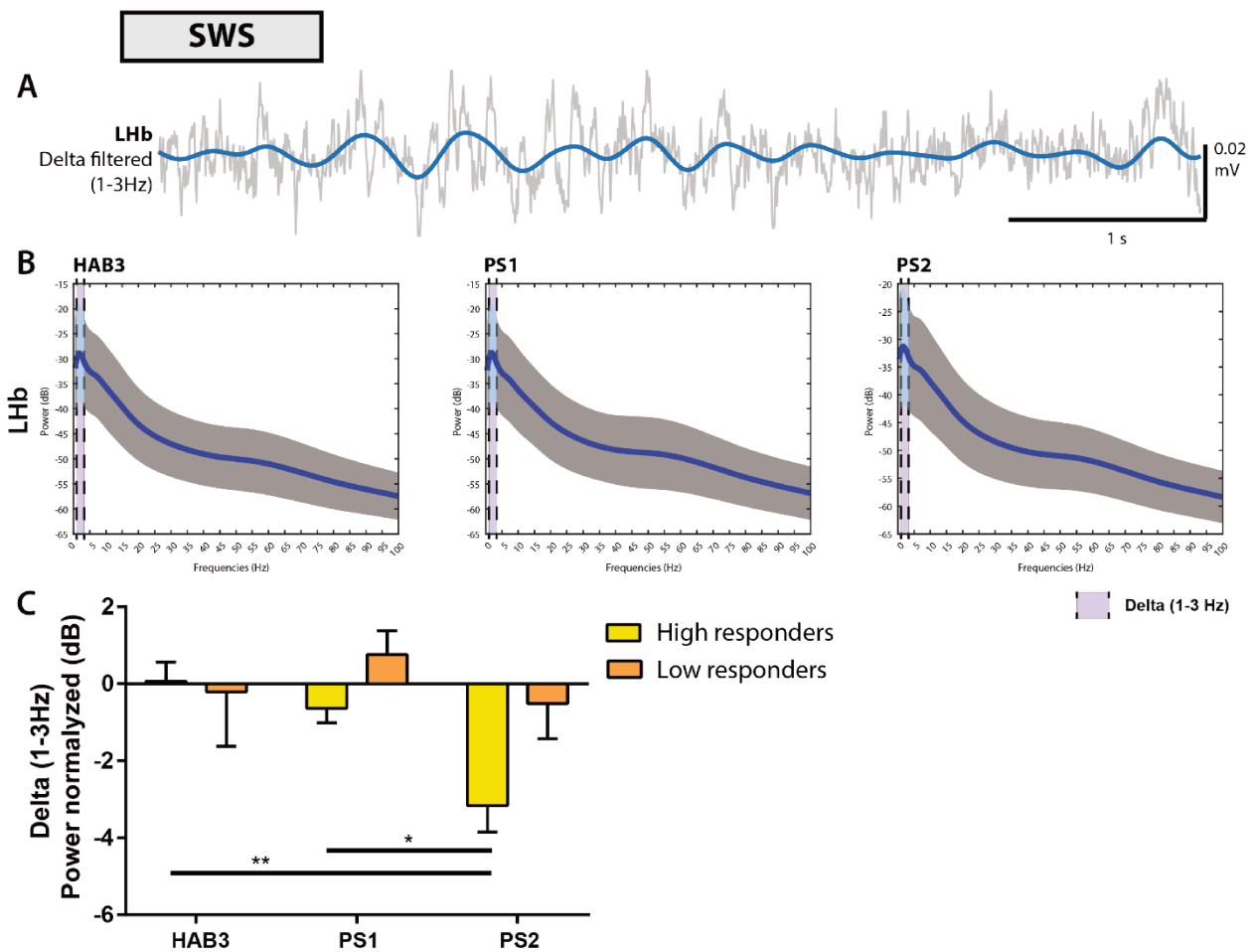


Figure 9: Delta oscillations in LHb during SWS across sessions.

(A) Example of LFP signal in LHb superposed with its delta oscillation filtered track. (B) Spectrogram (power in dB x frequency in Hz) in the LHb across the different session (HAB3, PS1, PS2) for all rats (average \pm 95% confidence interval). The frequency of the delta pic is highlighted in purple. (C) Evolution of the power of the delta band in the LHb across the session in high (n=5) and low responders (n=4); mean + SEM. Stats: * $p < 0.05$, ** $p < 0.01$.

A stable Lhb-dCA1 slow oscillation coherence across all conditions

According to the interaction between Lhb and dCA1 in the theta band already demonstrated during REM-sleep and during a contextual memory task (Goutagny et al., 2013), and given their implication in the stress response, we tested Lhb-dCA1 theta coherence in AW, REM sleep, and Lhb-dCA1 delta coherence in SWS. Regardless of the session, Lhb and dCA1 presented equivalent coherence in the theta band in AW and REM sleep, and equivalent coherence in the delta band in SWS (Figure 10A-F). These preliminary results only account as an example supporting a further discussion. Nevertheless, we considered (for now) 0.6 coherence as a threshold to support a potential coherence between two structures. Further analyses will be required to confirm this Lhb-dCA1 coherence in the theta delta bands.

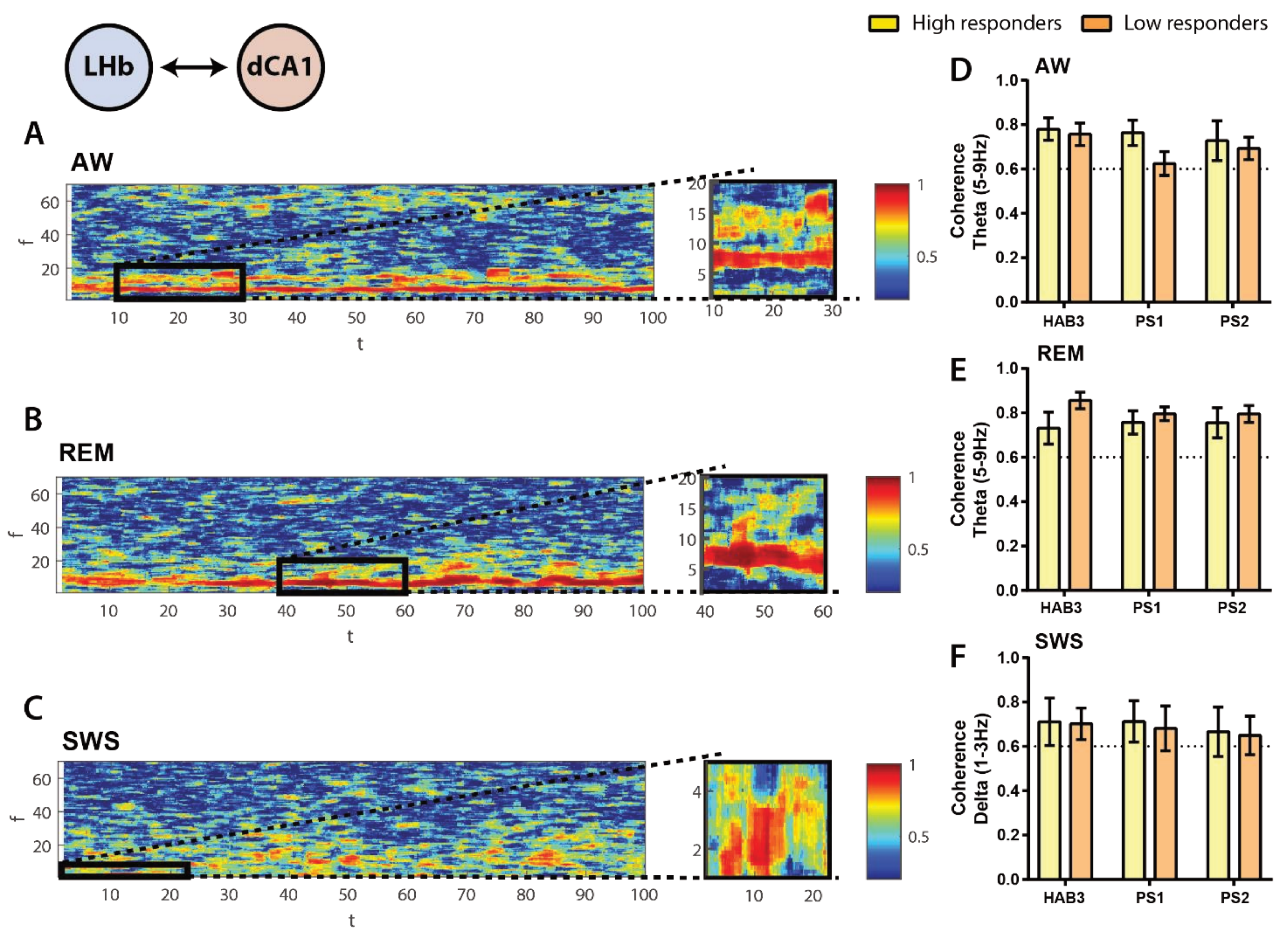


Figure 10: Coherence of slow oscillations between Lhb and dCA1 across sessions and stages.

(A-C) Example of Lhb-dCA1 coherograms across time (frequency in Hz x time in s x coherence) during 100s in AW (A), during REM sleep (B), and during SWS (C). The black rectangle represents the zoomed area (20 seconds) positioned on the right). (D-F) Bar plots representing the average (\pm SEM) of the coherence in the theta band across the three hours of the sessions (HAB3, PS1, PS2) in both groups in AW stage (D; high responders, n=4; low responders, n=5) and REM sleep stage (E; high responders, n=5; low responders, n=5), and in the delta band across SWS stage (F; high responders, n=5; low responders, n=5).

We also witnessed a high theta coherence between the LHb and the dCA1 during the two 10 min periods of immobilization, without clear difference between both (**Figure 11A-B**). In addition, no power difference was observed in high responders between immobilization 1 and 2 in each structure (**Figure 11C**).

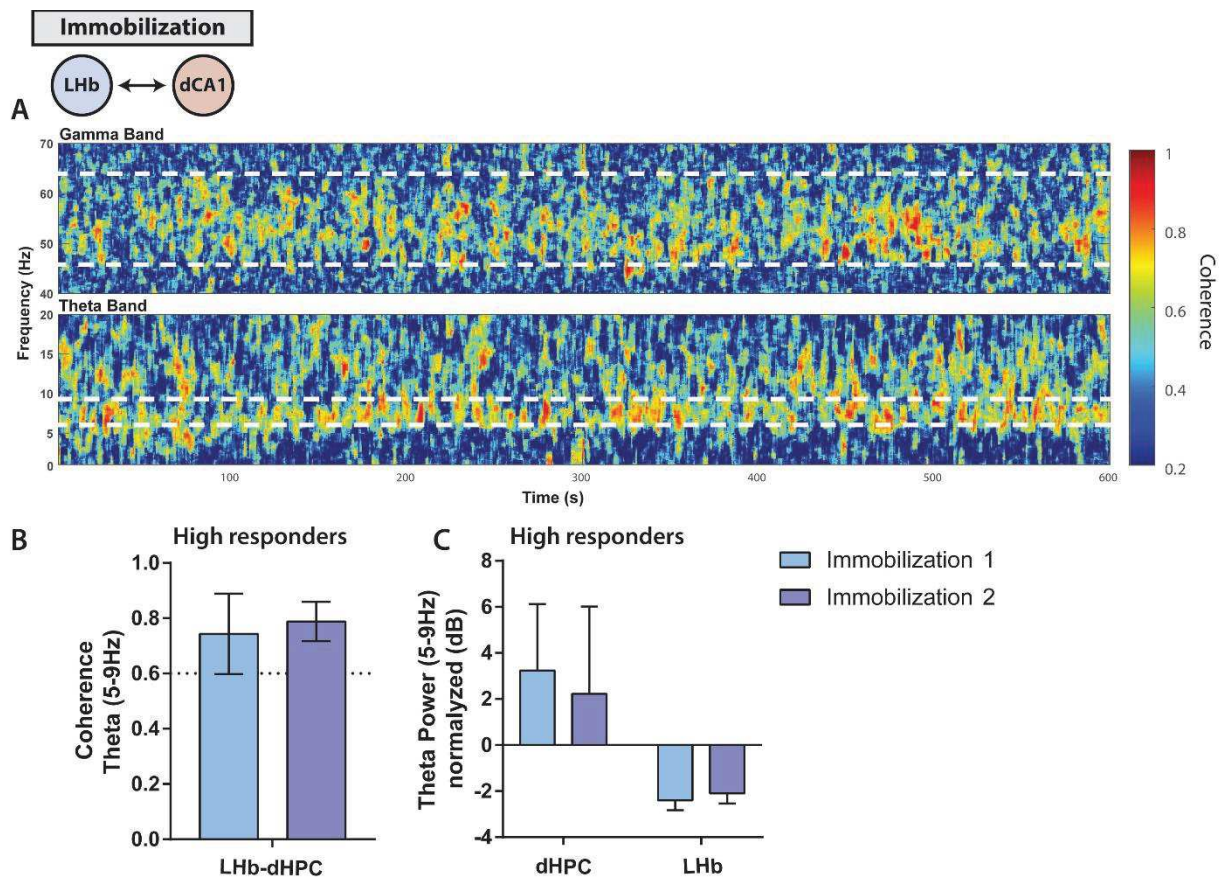


Figure 11: Coherence and theta power in the LHb during the two exposures to immobilization.

(A) Example of LHb-dCA1 coherograms across time (frequency in Hz x time in s x coherence) during the first immobilization. Upper panel shown the coherence across the 40-70 Hz frequencies (white tick lines frame the limits of the delta band considered in the analyses). Lower panel focus on the coherence across the slow frequencies (1-20Hz; the white ticked line frames the limits of the theta band considered in the analyses). (B) Bar plot representing the average (\pm SEM) theta coherence during both immobilization sessions, only in high responders (n=4). (C) Bar plot representing the theta power (average \pm SEM) in the LHb during both immobilization sessions, only in high responders (n=4).

The presence of high LHb-dCA1 coherence across all the sessions and according to all oscillations considered (theta and delta), raises the following issue, given the anatomical proximity between the LHb and dHPC: is the slow oscillatory activity observed in the LHb entirely volume-conducted from the HPC?

To investigate this issue, we did a second experiment (called “CSD experiment”), where the shape of the electrodes placed in the dHPC and in the LHb (*i.e.*, beveled shape) allowed to calculate the CSD. After we checked the location of the implantation of the electrodes (supplementary information; **Figure S2**), we generated the spectrogram for the slow frequency band (1-30Hz) and compared the raw LFP signal, CSD and local reference signal spectrograms in both structures with the theta peak

of the dHPC as the reference. The proportion of the LHb theta peak compared to the dHPC theta peak is smaller in each condition (CSD and local reference; **Figure 12A-B**). We can see that the theta peak in the CSD condition is much smaller than in the local reference condition, compared to the raw LFP condition. Since the CSD is supposed to represent the analysis leading to a signal comprising the least amount of contamination from volume-conducted signal, these spectrograms suggest that the local reference do not limit enough the volume conduction as well as we thought. However, the coherence between both structures seems maintained even with the CSD application. This result may suggest that even without (or few) volume-conducted signal, the theta coherence between the LHb and the dHPC persists (**Figure 12C**). As this kind of analysis was only done with one rat, and only across the first 10 minutes of the third habituation (HAB3), we need to perform a finer analysis and maybe perform complementary experiment (like recording single extracellular units in the LHb which would be phase-locked to LHb oscillatory activity) to conclude with certainty whether or not the slow oscillatory activity observed in the LHb are volume-conducted from the HPC.

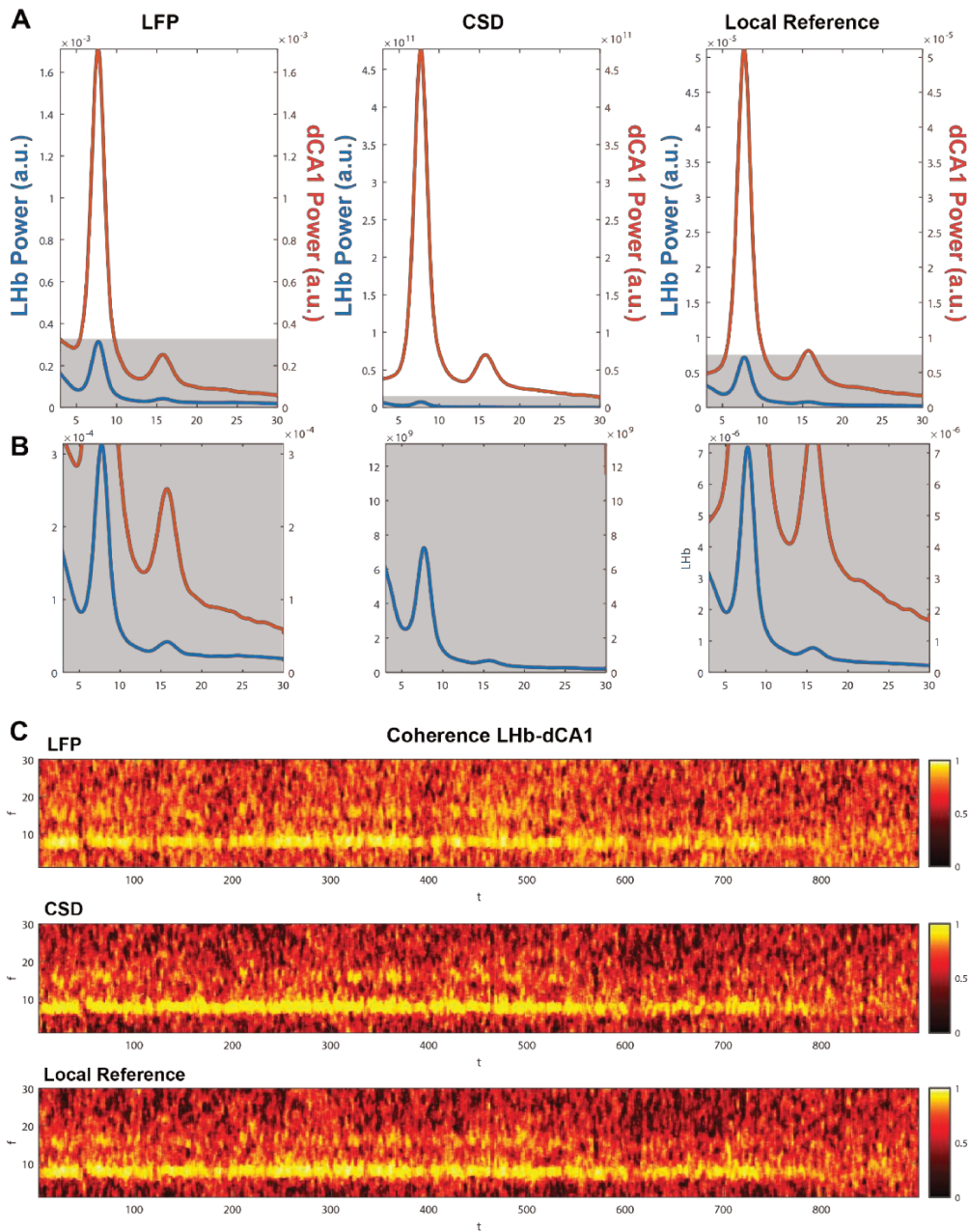


Figure 12: Comparison of the raw LFP signals, to signals obtained following the CSD and local reference calculations in Lhb and dCA1.

(A) Lhb (left axis, blue) and dHPC (right axis, red) power (a.u.) scaled in the theta pic of the dHPC in three conditions: raw LFP signal (left), signal following CSD (middle) and signal following local reference (right). (B) Zoomed areas of the grey rectangle on the spectrogram in (A) with magnification of the power scale, in order to focus on the Lhb theta pic across the three conditions. (C) Lhb-dHPC coherogram in the three conditions [raw LFP (top), CSD (middle), and local reference (bottom) signals].

Discussion

This experiment was designed to explore the stress coping network through the analysis of electrophysiological activity in key structures belonging to the stress response system. We wanted to investigate the behavioral response to repeated stressful exposures, as well as potential inter-individual differences. We also wanted to study potential communication, so that the electrophysiological substrates of a possible stress coping network could be explored.

Behaviorally we investigated behaviors, including stereotypies, which in rodents are typical of defense responses to a stressor (**MacLennan and Maier 1983; Blanchard et al. 1989; Moser 1989; Adamec and Shallow 1993**). We first focused our analyses on the first stress exposure, in order to have a closer look at the way rats coped with this new situation and potentially reveal different behavioral responses, or rather different intensities in the response. It is interesting to point to the diversity of responses to stressful experiences, as each individual, whether they are humans or animals, can show different ways to cope with stress. This type of variability, as well as the dynamic of sleep-wake stages related to stressful experiences have already been discussed in the human and rodent literature (**Jakovcevski et al. 2008; Wellman et al. 2016; Kalmbach et al. 2018; Kazavchinsky et al. 2019; Kalinichenko et al. 2019**); most studies concluded that this diversity of response accounted for a diversity in the vulnerability to stressors (**Wellman et al. 2016**). What was interesting is that we were able to differentiate two main populations on the basis of the time spent doing locomotion, the time spent rearing, and the duration of the first AW episode following the first immobilization (of course in the future we will try to refine this analysis by exploring other behavioral and/or electrophysiological parameters): one composed of “high responders” and one composed of “low responders”. For the moment we do not know what those results mean. At first one could argue that low responders are rats showing resistance to stress exposure, so which can be designated as less vulnerable, whereas high responders could represent rats more vulnerable to stress exposure. Or else, one could consider that both populations are equally resistant, or vulnerable, to stress, and present different types of coping behavior.

Aside these differences of reaction following the first immobilization, we were able to observe a decrease in the intensity of the response following the second immobilization, which was accompanied by an increase of the time spent sleeping. Although this might be due to natural increase of sleep time linked to the nycthemeral cycle, this could also indicate that the second stress exposure was perceived differently by the animals as they did not respond in the same way; the rats would have learned that the immobilization has no dangerous consequences and anticipated that the second immobilization would soon end.

In fact, as a response to the new and stressful experience of immobilization, we expected to observe an intense reaction to the first immobilization (*i.e.*, a decrease of the time spent sleeping as well as an increase of the time spent in AW, such as observed in case of intense stress exposure; *e.g.*, **Philbert et al. 2011**); in addition, we expected to see a less pronounced activity to the second

immobilization, as an indication that animals have gained a certain knowledge following the first immobilization. Electrophysiological measures did not provide the expected results. First of all, rats did not display a significant increase of time spent in AW as well as a significant decrease of the time spent sleeping following the first immobilization, in comparison with habituation sessions. One first explanation resides in the intensity of the stressor; indeed, the predictability, controllability and intensity of a stressor are parameters which play an important role on the potential behavioral consequences of stress exposure, especially concerning sleep homeostasis and sleep-wake stages regulation (**Sanford et al. 2010; Yang et al. 2011; Wellman et al. 2016**). Therefore, it can be argued that the stressor was not strong enough to induce a marked reaction or to prevent fast recovery. Second of all, rats displayed a greater number of episodes of, and a longer time spent in, SWS and REM sleep after the second immobilization, in comparison with habituation sessions and with the first immobilization. These results can be interpreted in two ways: either they mean that rats have somehow learnt from the first experience, so that this second stress exposure did not affect at all their behavior and they fast went back to sleep by lack of behavioral excitation; or it mean, after all, a higher sleep pressure as a consequence of the repetitive stress exposures, so that the organism needs to initiate defense mechanisms, including a sleep rebound. Such a sleep rebound is often reached after several exposure to immobilization/restraint stress (**Paré and Glavin 1986; Koehl et al. 2002**).

The next step was to investigate LHb electrophysiological data to start to try to understand its role in the stress response. In doing so we separated rats according to their level of responsivity to the first stress exposure, as described above. Indeed, it was important to us to be able to refine our electrophysiology analyses and partition our animal population into relevant categories, because the processes we are eventually studying (coping facing stress, learning from an experience), not only are not processed the same way by the different structures we investigated, but as said earlier rats can cope differently with stress exposure. We have seen in the introduction that the stress response involves a certain diversity of processes, ranging from purely “emotional”, which involves defense mechanisms including the HPA axis, to more “cognitive”; the later can occur upon the occurrence of the stressor, in order to try to figure out if it is potentially dangerous, or once the stressor has been dealt with, during processes helping the individual learning from that specific experience in order not only to properly recover from it – and eventually put in place resilience mechanisms when the stress is too intense or chronic in order to counteract the potential rise of stress-related disorders – but also to be better prepared in case such a stressor is encountered again. Those mechanisms generally take place offline during sleep episodes consecutive to the lived experience, and include, as demonstrated for spatial memory, a specific pattern of cellular excitation (replay) in structures that processed this specific experience (e.g., HPC, mPFC; **Klinzing et al. 2019; Findlay et al. 2020; Liu and Watson 2020**).

We first explored AW parameters because the time spent in AW, which is a stage of awareness and attention, can give an idea of the cognitive responsiveness of the animals in such a situation. We

observed a decreased theta power in the LHb through the different stress exposures, reflecting a decrease of the synchronization within LHb neuronal assemblies, but only in “low responders”. This may suggest that in low responders, which are postulated to be resistant to stress, the LHb needs to be disengaged – as the power of a given structure represents the level of synchronization not only of cells of this structure, but also with other brain structures – from a network processing the stress response; by extension, in high responders, maybe more sensitive to stress, the LHb needs to maintain its engagement in the network in order to overcome stress.

Noteworthy, no difference of AW theta power was found in dCA1 across the different sessions; instead, there was a tendency to display a decreased theta power in high responders. Here again results are rather counterintuitive; we would have expected higher theta power in animals presenting a strong behavioral response following immobilization because dHPC theta oscillation in freely moving animal is often associated with voluntary movement (**Vanderwolf, 1969; Buzsáki, 2002**). Nevertheless, we could not see, in our preliminary results, that theta oscillation during AW was linked to motor processes (see supplementary figure 1). If these preliminary results are confirmed, one can suggest that a lower theta synchrony in the dHPC may be a hallmark of the vulnerability of the animals to stressor exposure.

Then we started exploring delta activity in the LHb in order to try to see if post-stress SWS sleep would be altered, as, potentially, a hallmark of ongoing memory processes. Of course, we made such assumption in the hypothesis, not proven yet at this stage of our investigations, that the decreased behavioral response between the first and second exposure is a consequence of memory processes leading to habituation and therefore to a better management of the second stressful experience. We could see, in high responders, a progressive decrease of LHb delta power in SWS through the repetition of the stress exposure. First of all, this result could support the hypothesis of Zang and collaborators (2016) that the LHb is engaged in the modulation of sleep homeostasis in rats (**Zhang et al., 2016**). Second, it could suggest that in animals that seem more vulnerable to stress exposure (high responders), the LHb needs to be disengaged during sleep, maybe to favor sleep processes useful for a consolidation of the memory trace of this particular experience, in order to prepare better coping in the case rats face this situation again.

Slow (theta and delta) oscillatory activity has been hypothesized to support long range coherence of activity, and therefore communication, between distant brain structures (**von Stein and Sarnthein 2000**). We have seen that, in the LHb, the repetition of stress exposure induced a decrease of theta synchrony in AW in low responders, and a decrease of delta synchrony in SWS in high responders. Of course, at this stage of our analyses, we have no clear idea of what that precisely means. One can just assume that repeated stress exposure decreases long range communication between the LHb and distant structures involved in the stress response. Those, of course can include the HPC, the mPFC, the basal ganglia (BG), or monoaminergic midbrain structures such as the dopaminergic ventral tegmental area and the serotonergic raphe. For example, it is known that the LHb exerts an inhibitory control over midbrain dopaminergic and serotonergic structures; a disengagement of the

LHb with these structures could allow the activation of both systems, this being a physiological mechanism subserving the stress response (**Puglisi-Allegra and Andolina 2015; Belujon and Grace 2015; Holly and Miczek 2016**). The different functions this could regard, according to AW theta oscillation, could also include the processing of contextual information (in relation with the dHPC), vigilance (in relation with the mPFC), or the production of a behavioral coping response (basal ganglia); according to SWS delta oscillation, they could regard consolidation processes related to the recent experience (with the HPC and mPFC), again in the hypothesis that the behavioral response observed following the second immobilization reflects habituation consecutively to memory processes.

Finally, as previously shown (**Goutagny et al. 2013; Aizawa et al. 2013**), we observed a high coherence between the LHb and dCA1 in the theta frequency band during AW, during and after immobilization, and during REM sleep. We also observed delta coherence in SWS between these two structures have never been shown before but could make sense in regard to their common implication, for example, in memory processes (**Buzsáki 2002; Goutagny et al. 2013; Mathis et al. 2015; Mathis and Lecourtier 2017**). However, an important issue is that we failed to find differences across sessions, both structures being always highly coherent at theta. This supports the assumption that theta oscillation recorded in LHb are totally, or partly, volume-conducted from the dHPC lying just dorsally. This is a recurrent point of discussion in the literature (**Goutagny et al. 2013; Aizawa et al. 2013; Bertone-Cueto et al. 2020**). **Bertone-Cueto et al. (2020)** have argued that the signal recorded in the LHb is totally volume-conducted from the dHPC; however, in their study they did not try to limit the volume conduction by applying CSD or local referencing calculations. Other studies support the fact that the recorded signal in the LHb is not entirely volume-conducted from the dHPC. For example, Goutagny et al. (2013) have shown that theta activity could still be recorded in the LHb in rats with complete ibotenate-induced dHPC lesion. These authors, as well as others (Aizawa et al., 2013) postulate that theta oscillations exist in the LHb such as it exists in the dHPC and that both structures might have a common pacemaker, the best candidate being the medial septal area, which also projects onto the LHb (**Do et al. 2016**). In trying to have a better idea of the amount of the volume-conducted signal in the LHb, we compared LHb raw LFP spectrogram with these obtained following CSD and local referencing calculations; we found that CSD markedly reduced but did not eliminate theta power in the LHb, suggesting CSD provides a LHb signal devoid of dHPC contamination (indeed, CSD is said to a more reliable estimate of oscillatory activity than raw LFP itself; **Lindén et al., 2010; Kajikawa and Schroeder, 2011, 2015**). On the other hand, such a dramatic decrease could not be observed following local referencing, suggesting this calculation spares a majority of the volume-conducted signal. Therefore, we can assume that, using the CSD, if the high theta correlation persists, it means that both structures are indeed synchronized during these particular periods (AW, REM-sleep), so that we can postulate they participate to the same functions, for example to the processing of contextual information in AW.

In conclusion, we want to stress again that those results are preliminary, as the analyses will be refined, through the selection of more precise time windows following stress exposure, comparing data from moment immediately following stress exposure with moments far from it (for the moment we analyzed and averaged the whole three hours). Also, we want to say again that the few results obtained have been discuss in light of hypotheses which can be discussed (for example that high responders are more sensitive to stress whereas low responders are less). In addition, we plan to focus our analysis on the potential dynamic of coherence changes across the sessions (in response to repeated immobilizations) within the entire network of recorded structures (*i.e.*, ACC, PRL, BLA, dCA1 and LHb). Depending on what will be discovered, we also plan to study the directionality of the different routes of communication [*i.e.*, which structures leads which other one(s)] using the Granger causality. Finally, we would like to support more efficiently the idea that not all theta power observed in the LHb is volume-conducted from the dHPC. To support this hypothesis, we need to record extracellular activity in the LHb and show that LHb cells firing is synchronized with LHb theta oscillation.

Acknowledgments

The authors thank Elouan Cosquer for its helps and expertise with Python language and videos processing technics.

Supplementary information

Animal clustering using PCA and k-means algorithm.

The following tables group the results obtained from the PCA done on the behaviors post-immobilization. As one can see the PC1 represents the main part of the variances of all the variables taken in the analysis (*i.e.*, AW first episode duration, rearing time and spontaneous locomotion; **Table S1**). PC1 explains 88.5% of the total variance which is a very high score. Accordingly, these results support the idea that PC1 represents the responsiveness of the animals to the first immobilization. The score of PC1 for each animal is represented in **Table S2** as well as the results of the k-means cluster algorithm (1-3 represent the number of the cluster containing the animal considered) and the respective group of each animal.

Table S1: Representation of the variable by the different components.

Variable	Component 1	Component 2	Component 3
<i>AW 1st episode duration</i>	-0.884053	-0.466755	0.024282
<i>Rearing</i>	-0.982248	0.144432	-0.119702
<i>Locomotion</i>	-0.953521	0.283967	0.100796
<i>Eigenvalue</i>	2.655564	0.319358	0.025078
<i>Explained variance</i>	88.51880	10.64526	0.83593

Table S2: Individual values representing PC1 and their clustering by k-means.

<i>Rat</i>	<i>PC1 values</i>	<i>Index k means</i>	<i>Group</i>
1	-0.83856	1	High responders
2	-1.86337	1	High responders
3	3.14434	2	Low responders
4	-0.63114	1	High responders
5	0.02257	3	Low responders
6	0.29391	3	Low responders
7	-1.38856	1	High responders
8	-1.38856	1	High responders
9	2.73489	2	Low responders
10	0.58264	3	Low responders
11	-1.29852	1	High responders

Correlation between voluntary movement and theta power in dCA1.

We saw that AW dCA1 theta power displayed a tendency to be lower in high responders than in low responders in every session, whereas we were expecting to find the opposite results (i.e., higher theta power in high responders which are the more active) because theta power is linked to voluntary movements. Accordingly, we calculated the Pearson correlation between the theta power and PC1 scores (low PC1 scores represents a high activity and high PC1 scores represent a low activity in the PS1 session) across all three sessions. We found that dCA1 theta power is not correlated to PC1 values (**Figure S1**), and by extension does not seem to be correlated with voluntary movement, suggesting that the theta observed in AW in our condition could preferentially be linked to cognitive processes than voluntary movements.

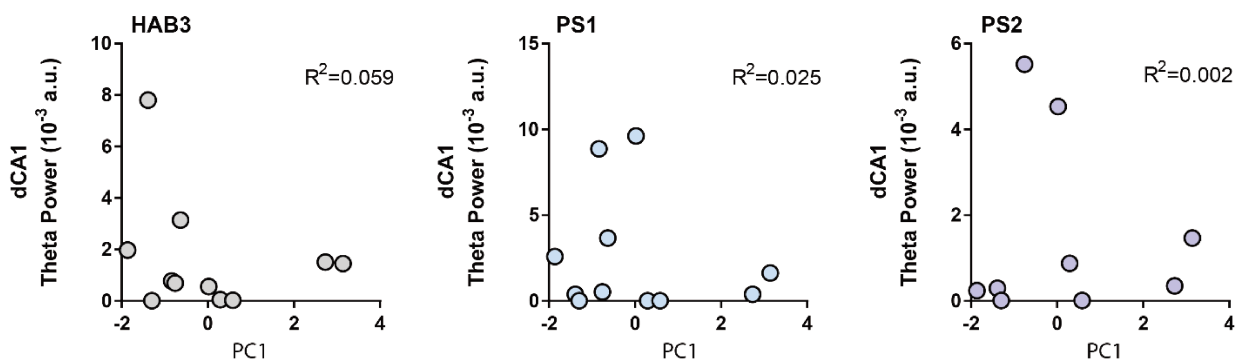


Figure S1: Correlation of PC1 with the theta power recorded in dCA1 across sessions.

Individual PC1 value (x axis) plot against the individual values of dCA1 theta power during AW (y axis) of the HAB3 (left), PS1 (middle) and PS2 (right) sessions. No correlations have been found (Pearson's correlation).

Localization of the electrodes in the experiment including CSD calculation.

Only 3 rats out of 6 presented correct positions in both structures (**Figure S2**) and were kept for the analyses.

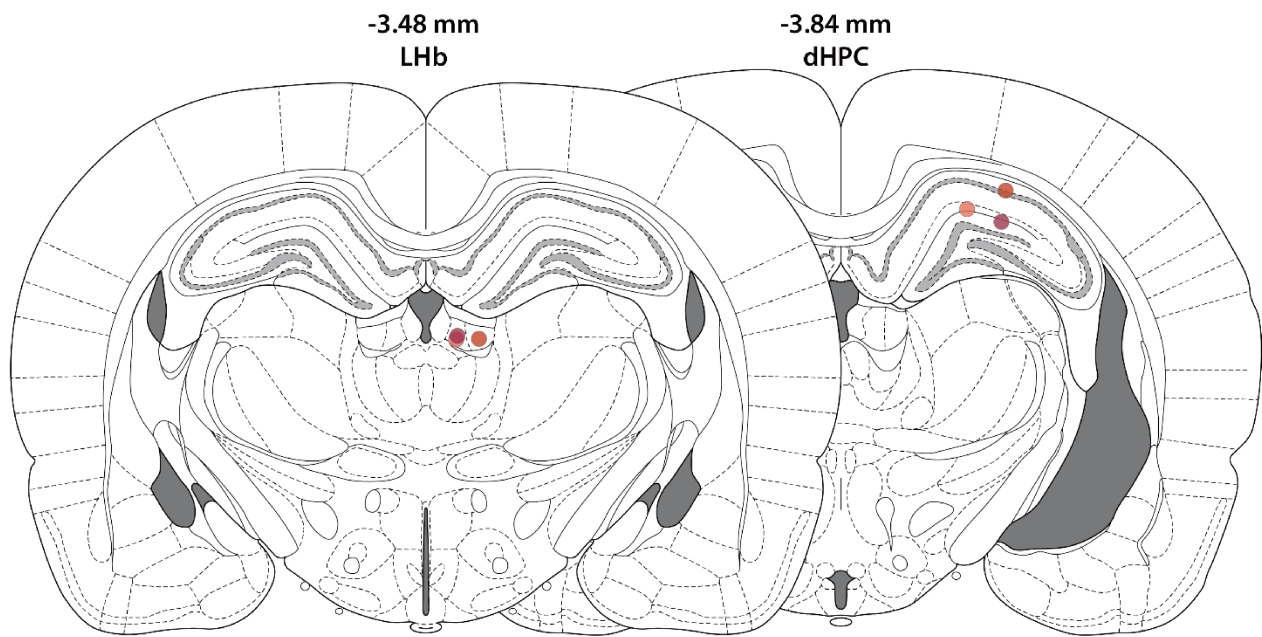


Figure S2: Localization of electrodes.

Schematic representation of the placement of the different electrodes within the Lhb and dHPC (each color represents a given rat). Adapted from Paxinos and Watson atlas (Paxinos et Watson, 2007).

DISCUSSION

DISCUSSION

DISCUSSION - Technical considerations

This part will first address technical issue encountered during my work, then will summarize the main findings and conclusions of the three studies described in the document. Then, these results will be confronted to the current knowledge about the LHb and the stress response to try to provide a unified view concerning the role of the LHb in the behavioral adaptation to stress. At the end, I will go through some perspectives resulting from these findings.

I. Technical considerations

Throughout this work there has been some technical issues which may have masked and prevented important findings. Those include the use of CNO as a ligand for the hM4 receptor when we inactivated the LHb. If we could not see any behavioral effect in *Study 1* during our trace fear conditioning paradigm, we could see the consequences of CNO administration during *study 2* following the network analyses on c-Fos data. New ligands are now available, including deschloroclozapine (Nagai et al., 2020), which will be used in case we want to use the DREADD technic again. Another possible issue in our experiment may have been the use of c-Fos as immediate early gene to provide insights on brain activation. It is a fact that c-Fos expression in resting animals is very low so that, unlike other markers such as zif268, it is not possible to detect a decreased activation when comparing several groups. Also, the graph theory approach is not that common in c-Fos-based studies, as it is used mostly on fMRI and EEG data. It could especially be a concern when used on c-Fos data, which in fact give a snapshot of a given situation, and not at all the dynamic of a system, such as given by fMRI or EEG data. Therefore, we lack a little bit of distance to really appreciate the outcome and possibilities of such analysis. Finally, in study 3 the main technical issue was the volume conduction. Indeed, the use of the kind of electrodes we have used does not allow easily to get rid of volume-conducted oscillations when recording in a sub-cortical non organized structure such as the LHb, especially when a powerful emitter of oscillations such as theta, *i.e.*, the HPC, is situated nearby. Not only we will have to refine our analyses, using CSD, but we will have also in the future to perform an experiment using a custom-made multi-unit probe (such as those from Neuronexus used by the Buzsáki's laboratory); those probes can include a lot of electrodes – with known spacing between them – in the same axis so that we will be able to have electrodes along the whole dorso-ventral axis of the dHPC, including the DG, and also the LHb. We will then be able to perform the CSD and also, more importantly, to record cells in both the LHb and dHPC and prove that the firing pattern of LHb cells is locked to the LHb oscillation.

II. Principal findings of the three studies

In *study 1* we found using the trace fear conditioning paradigm that LHb inactivation induced contextual memory deficits, and also biased the rat's response toward the less predictive cue. This prompted us to conclude that the LHb not only was involved in the processing of contextual information (such as already found in our laboratory: [Goutagny et al., 2013](#); [Mathis et al., 2015, 2018c](#)) but was also involved in the attribution of saliency to cues associated to an aversive event. In addition, following conditioning we performed c-Fos immunostaining in a group of rats and processed a FA on the data, taking into account the entire Hb, the mPFC (ACC, PRL, IL), the dHPC (CA1-3 and DG), and the AMG (BL, LA, CeA). We found the LHb to be included in several factors, one alongside the dHPC, which we linked to contextual information processing, and one alongside the LA and the CeA, which we linked to the associations between the US and its predictors and to the onset of fear response. In *study 2*, to explore in a finer manner the potential place of the LHb in the stress response network, we again performed c-Fos immunostaining, this time following a 10-min long restraint (*vs.* home cage controls), which was followed by a functional network analysis based on the graph theory. We found the LHb to have a high functional connectivity with the main hubs of the stress response, *i.e.*, the mPFC, the PVH, the HPC, the extended AMG, and also the Ins, the VTA, and the RD. Interestingly, the analyses also positioned the LHb at the interface between several communities of structures, making it an important relay for the transfer of information, likely towards the midbrain monoaminergic centers, in order to modulate homeostasis and favor stress coping. In *study 3*, we wanted to explore communication dynamics between the LHb and some of the important hubs to which it had been functionally connected in the previous study, *i.e.*, PRL, ACC, dCA1, and BLA using LFPs recordings in freely-moving animals. We did so throughout a protocol including two 10-min long immobilizations, separated by three hours, in order to gain insight into possible habituation processes following the first immobilization. First, we found rats to display a less intense behavioral response following the second immobilization, suggesting that habituation processes had been triggered. In addition, we could cluster our animals into low and high responders, for us mirroring higher and lower resistance to stress exposure respectively. Our preliminary LFPs analyses showed that whereas in low responders LHb theta power in active waking dropped progressively following the repeated stress exposure, in high responders LHb delta power during SWS also progressively decreased following repeated stress exposure. These results may suggest that, depending on the susceptibility of an individual to a stressor, in order to cope with stress and show adaptation, the LHb needs to disengage itself from the networks subserving specific processes, either during

DISCUSSION - Hypotheses linking the LHb and the stress response

awake periods, to maybe promote vigilance towards the situation, or during sleep to promote consolidation of past experiences.

III. Hypotheses linking the LHb and the stress response

We have seen in the introduction of this thesis manuscript that the LHb is engaged in numerous functions such as error prediction, cognitive flexibility, the processing of contextual cues and their inclusion into long-term memory traces, or the short-term maintenance of information. We have also seen that the LHb is considered a circadian oscillator, so that it is suggested to be engaged in physiological processes likely serving the brain and body homeostasis. The anatomical position of the LHb and its connections make it a route of information transfer between the main brain systems engaged in cognitive, reward, and emotional processes, whether it is the basal ganglia or the limbic system. The LHb is a main modulator of all monoaminergic pathways, as well as of the activity of the HPA axis. It is considered the result of the brain's evolution so that it participates in monkeys and humans to higher cognitive abilities but nonetheless, as a residue of ancient history, is still engaged in survival functions, such as the Hb probably is in every vertebrate species, including emotional and behavioral responses when facing stressful or threatening situations.

The present project has focuses on determining what could be the place of the LHb at the network level in situations of stress, whether they are intense, such as facing inescapable footshocks during a fear conditioning paradigm, or facing restraint or immobilization, which can be considered stressors of lower intensities because not directly harmful. We wanted, using immediate early genes and electrophysiology, to understand the relationship the LHb could have with the emotional brain. We could indeed see that the LHb is functionally connected with the main brain structures engaged in emotional processing. The key, given the results of our laboratory and the literature, seems to be “how is the LHb going to help properly reacting to a sudden change in the environment”. Its engagement can take place on several occasions along the different steps leading *in fine* to a behavioral response. The first step can be the evaluation of the status of the current situation: “is it potentially dangerous or is it safe?” The second can be the *alarm reaction* that prepares the body physiologically, once a situation has been evaluated as potentially dangerous, engaging the SAM and HPA axes. The third can be the selection and production of the behavioral output which ultimately will allow the individual to cope best with the situation. And finally, it could also participate to the continuous updating of the behavioral response: “is the

DISCUSSION - Hypotheses linking the LHb and the stress response

current behavior helping? And if not, which other one could help facing the threat?" Please refers to [Figure 63](#).

One can see the LHb at the crossroad of these processes and at the crossroad of these systems. When facing a threat, it can promote vigilance in the early moments by its action on noradrenalin towards the mPFC. It can be engaged in the early process of contextual information, in collaboration with the HPC in order to decide which are the ones the individual should be careful about; to that particular matter this information will be compared to what is already stored in memory so that the LHb would interact with the AMG and mPFC. If contextual information is perceived as predictive, both the HPC and mPFC would collaborate with the AMG so that the CeA can send downstream information to the PAG in order to prepare the behavioral response. In parallel, one can imagine that the LHb receives information from the basal ganglia about the predictability of environmental, and/or other cues, to bring another level of information to the DA system in the preparation of the behavioral response. One of the likely outputs of the LHb once this information has been processed is the 5-HT system. This system is important as facing a threat increases the activity of the RD and 5-HT release throughout the brain (mPFC, HPC, AMG; [Mahar et al., 2014](#)) to participate to the engagement of stress coping strategies ([Puglisi-Allegra and Andolina, 2015](#)).

The LHb is also well positioned to process internal information. The treatment of interoceptive information is essential for survival, for being able to fight or escape a threat. Painful stimuli have extensively been shown to induce a strong response in the LHb (e.g., [Lehner et al., 2004](#)); the LHb is viewed as a relay between the NAc and the PAG in order to deal with pain. One can therefore postulate that such pain processing is also an essential role of the LHb when fighting an opponent, in order to further decide on the strategy to adopt, keep on fighting or escaping. Another possibility is that the LHb participates to the triggering of the stress-associated analgesia in order to be able to better fight or fly. This could occur in different ways. Either by an action on the DA system, as [Gao et al., \(1990\)](#) have demonstrated in rats that the dopaminergic signal from the SNc that participates to the induction of analgesia upon stress was modulated by the LHb; or through an action on the PAG, as [Yu and Han \(1990\)](#) have demonstrated in rabbits that the LHb was a relay of NAc information to the PAG to counteract nociception.

Finally, we have seen in *study 3* that the LHb likely disengage (from a network that we need to investigate) in order to maybe trigger habituation processes and promote the memorization of the situation the individual just experienced, including the cues that were, or not, associated to it and more or less predictive of the threat. This could be the final engagement of the LHb in the overall

DISCUSSION - Perspectives

processes which helps an individual deal with a particular threat. One could conclude that an important aspect of the engagement of the LHb in the response to a threat is its participation to this “cognitive loop” linking both ends of a stressful situation: at the beginning it helps determining if the situation has already been experienced before, by comparing what is stored in memory to the ongoing situation, and at the end it will help memorizing the details linked to a particular situation, in order to later favor efficient coping. And so on.

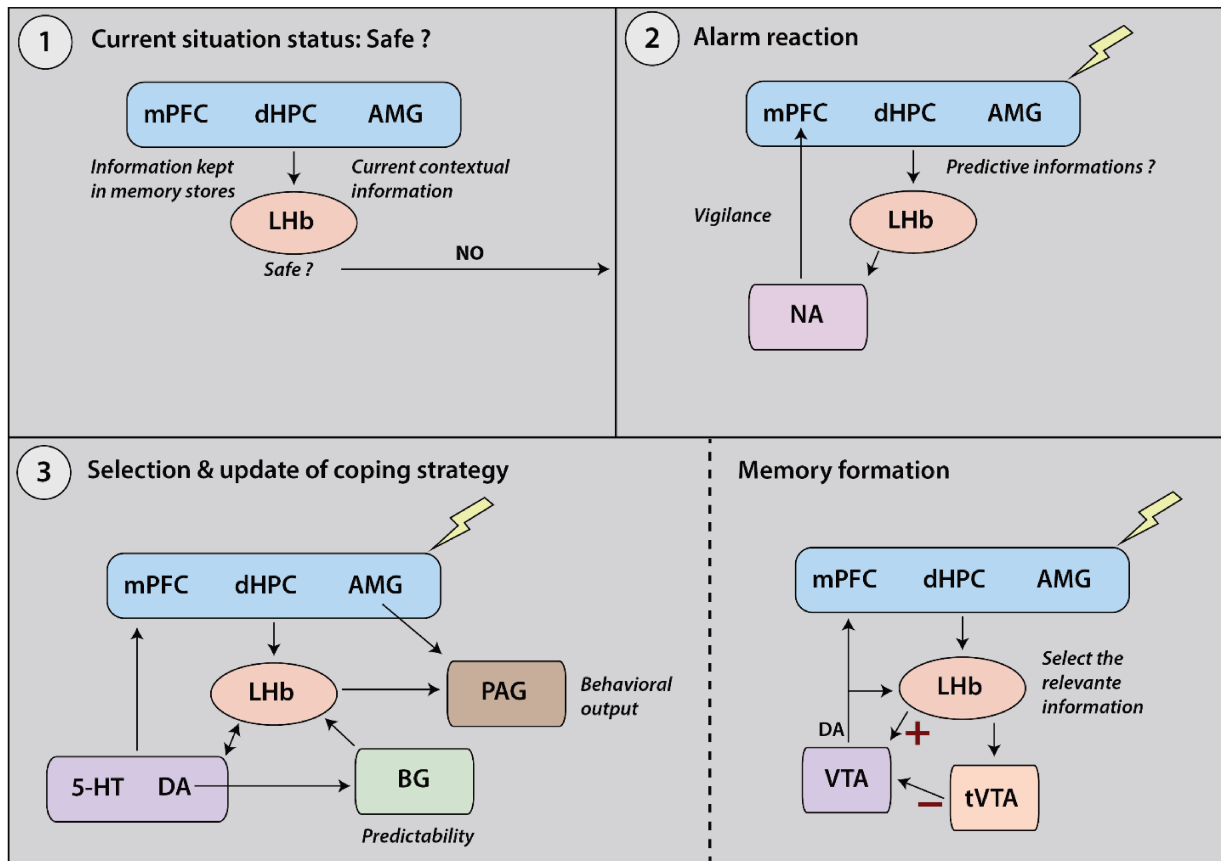


Figure 63: Schematization of the hypothesis concerning LHb implication in various aspects of the stress response.

IV. Perspectives

The first perspective is to finish the analyses of *study 3*. In addition to what has been described earlier in the technical consideration (the need to resolve the volume conduction issue by performing proper experiment and analyses), I will focus on refining the analyses. Indeed, as said when I described the LFP study, the analyses of baseline and post-immobilization periods were made taking into account three hours of recordings. Especially concerning the post-immobilization

DISCUSSION - Perspectives

periods, this is not satisfactory as different interesting processes can occur shortly after the immobilization vs. three hours later. Therefore, we will consider smaller episodes to address the evolution of the signals across the three hours. The same goal will be achieved during both immobilization sessions; for the moment we took the entire 10 minutes, but there also could be different dynamics at the beginning and at the end of these sessions which need to be discovered. This will require to work on the analysis scripts. Then, we will explore the dynamics throughout the whole network by including in the analyses all the structures (ACC, PRL, BLA, dCA1, LHb). Depending on what will be discovered, we also plan to study the directionality of the communication routes (*i.e.*, which structures leads the others) using the Granger causality. Following these analyses, which we hope will bring interesting insights into the dynamics of information transfer during stress exposure, we will explore the role of the LHb in those dynamics by performing its inactivation, using the DREADD but without CNO, in order to see if not only those dynamics are disturbed, but also with the behavioral response of the animals will be altered; will they still show habituation or not will be a main question. We want to guess they will not.

Following study 2, we wondered what would have been the consequences of LHb inactivation on the functional network supporting stress response if there had not been the issue of the CNO. Accordingly, we would like to conduct the same study but this time with another ligand, as discuss before. We will therefore compare the effects of LHb inactivation to an *in silico* model allowing to simulate the silencing of a structure in the functional network (see [Annexes part In silico silencing of the LHb in the restraint stress functional network page 149](#)). This approach will confirm the accuracy of the *in silico* models and will furnish a discussion around the place of LHb in the stability of the restraint network.

In *study 1 and study 2* we have seen that the LHb is particularly connected with the mPFC. Although the mPFC projects onto the LHb, the functional implications of this connection has rarely been addressed except considering short-term memory such as performed in our laboratory ([Mathis et al., 2016](#)). This pathway seems key also in the stress response and trace fear conditioning such as seen in our experiments (*study 1 and study 2*). It would then be interesting to better understand the role of this pathway across the various tasks we performed. To that purpose, one of the perspectives would be to either perform specific permanent lesions (using a Cre-dependent caspase approach), or specific inactivation of this pathway, using Cre-dependent expression of DREADD receptors; we would perform trace fear conditioning, and elevated plus maze as a start. The exact same approach will be applied to the pathway supposedly connecting the BLA and the LHb (that will first need to be confirmed anatomically, which we will do using

DISCUSSION - Perspectives

tracing approaches such as anterograde and retrograde tracers, or Cre vectors, including a fluorescent marker, which can be very selective of the neuronal population and have retrograde tracing properties).

ANNEXES

I. Graph Theory analysis - Random Network Modeling

We tried several possibilities to model random network. Theoretically, the rows represent the inputs whereas the columns represent the outputs of the structures. With that in mind, we compared the three possibilities: i) shuffling only the rows (inputs), ii) shuffling only the columns (outputs), iii) shuffling both rows and columns (input/outputs). Noteworthy, where the matrix was symmetrical before the shuffling, the later made it non-symmetrical, therefore giving two possible versions of the same random network on the same map. Trying to recover the shape of the initial matrix, we attempted to make the matrix symmetrical again using the following equation.

$$SMatrix_{rand} = Matrix_{rand} + Matrix_{corr}^T$$

where $SMatrix_{rand}$ is the random matrix made symmetrical again, $Matrix_{rand}$ is the random matrix, and the $Matrix_{corr}^T$ is the transposition (flipping the matrix over its diagonal, leading to the switch of the row and the column indices) of the original correlation matrix.

The symmetrization creates a loss in the weights and an increase of the modularity in comparison with the model before symmetrization. Having no differences between the inputs, outputs or inputs/outputs matrix, we decided to keep it the closest (i.e., inputs/outputs matrix), theoretically, to the initial matrix. Therefore, we kept the random model representing the non-symmetrical matrix with inputs/outputs (see [Figure 64](#)).

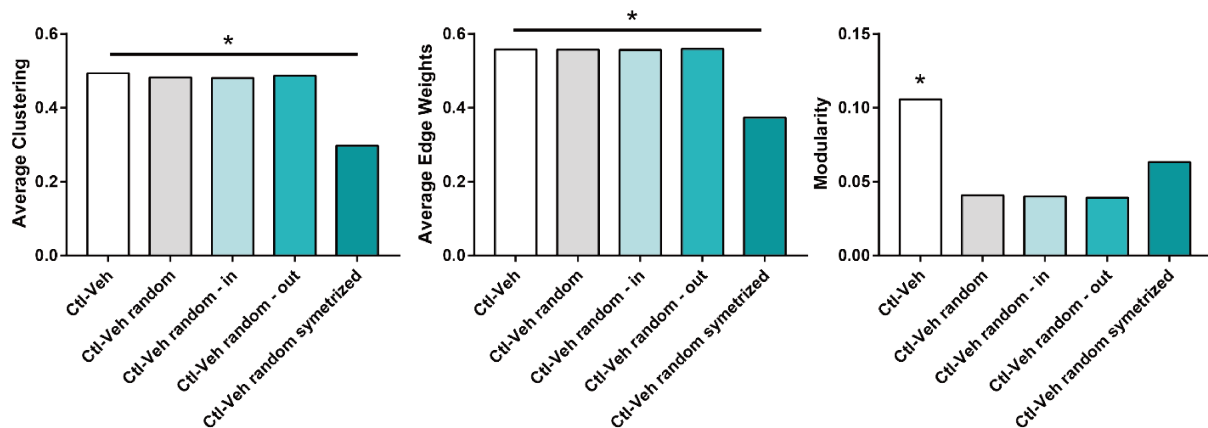


Figure 64: Global assessment of the random networks

The following parameters, Average clustering (**Left**), Average edge weight (**Middle**) and modularity (**Right**) of each possible random network based on the Ctl-Veh group exposed to restraint stress, have been tested in the different conditions: random (in which the inputs and outputs are shuffled), random-in (in which only the inputs are shuffled), random-out (in which only the outputs are shuffled), random-symmetrized (in which both the inputs and outputs are shuffled and in which the symmetrization has been performed). Bootstrap, Stats: *p<0.05.

II. Setting DeepLabCut and checking results

To create our DLC model we tested several possibilities, such as pretrained network and data augmentation (*i.e.*, image augmenter), filters. The DLC model proved to be accurate to detect the presence or the absence of movements, so that we could analyze the sleep-wake stages based on it, with a checking of the EMG signal when it was possible.

f. Pretrained networks and data augmenter evaluation

To obtain the best accuracy possible, we tested two pretrained networks: ResNet50 (<https://www.kaggle.com/keras/resnet50>) and ResNet152 (see [page 119](#)). We tried three image augmenters: default (standard DLC data augmentation; see [Nath et al. 2019](#)), imaug, and deterministic. We run the training with each pretrained networks and each data augmenter. We obtained a smaller error between the manual labels and the labels predicted by DLC with the parameters used for the experiment (*i.e.*, ResNet152 & imaug; see [Table 7](#)). The performance of the different networks was measured by computing the mean average Euclidean error (proportional to the average root mean squared error). The errors were taken into account only for body parts where the likelihood was superior to the p-cutoff (0.6). The model based on the ResNet152 with imaug as data augmenter was the model displaying less pixels (px) errors. Acknowledging that, we used this model to extract the x and y position of the rats' body parts.

Table 7: Summary of the errors from the different pretrained network coupled to a data augmenter.

PRETRAINED NETWORK	DATA AUGMENTER	P-CUTOFF USED	TRAIN ERROR (PX - P-CUTOFF)	TEST ERROR (PX - P-CUTOFF)
RESNET50	default	0.6	2.29	8.57
RESNET50	imaug	0.6	2.14	7.44
RESNET50	deterministic	0.6	2.32	7.56
RESNET152	default	0.6	1.65	7.42
RESNET152	imaug	0.6	1.03	7.22
RESNET152	deterministic	0.6	1.86	7.38

g. Filtering method assessment

DLC offers two types of filters: median filter and ARIMA filter (see <https://www.statsmodels.org/dev/generated/statsmodels.tsa.statespace.sarimax.SARIMAX.html> for more information on the mathematical algorithm). The filters are designed to extract the outliers from the results (*i.e.*, excessive coordinates differences between successive images). We compared the results without filter to this with median filter and this with ARIMA filter (see **Figure 65**). We computed the distribution of the difference of x and y coordinates between successive images (DeltaX and DeltaY). Theoretically, the values of DeltaX and DeltaY should be close to 0 (no excessive coordinates differences of body parts between successive images). We selected the filter giving the larger number of values close to 0 (*i.e.*, median filter); it indeed led to the removal of most of the noise.

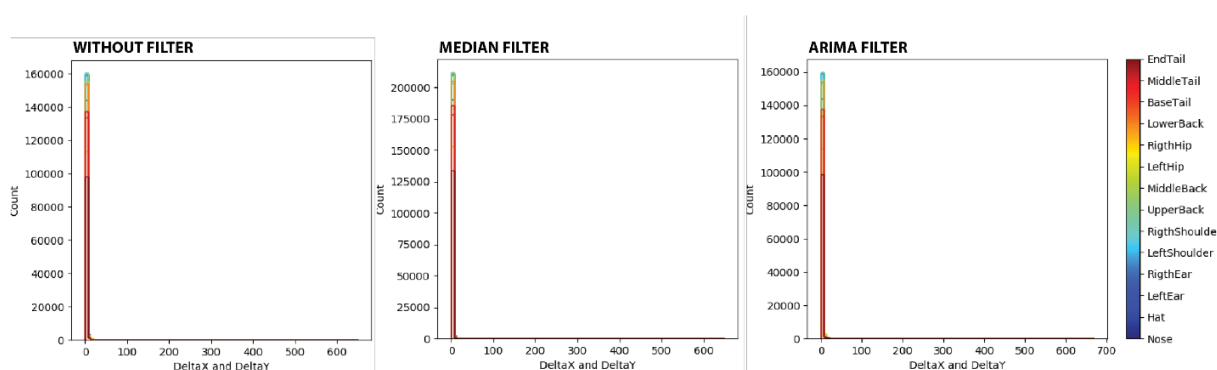


Figure 65: Histogram of the accuracy of different filters: MEDIAN and ARIMA

Example (one rat and one session) of a distribution of DeltaX and DeltaY across all successive images of a given video using different filters (MEDIAN and ARIMA). DeltaX and DeltaY are the differences of the x and y coordinates, respectively, between two successive images. Ideally, both Deltas should tend to 0 (no excessive difference of coordinates in the rat's body parts). The MEDIAN filter seems to be the most accurate filter when applied to our data set because it has more than 200 000 DeltaX and DeltaY near 0. We found a better accuracy with the median filter through different sessions and rats.

Verification of DLC results after the motionness assessment

The verification of the accuracy of the results is issued from the processing with DLC and the movement extraction script. Then, we compared what we obtained with the EMG recording on several rats. We also did a comparison with manual coding (on Aion software), where we showed similar accuracy (see **Figure 66**). The results exported from DLC were judged accurate for the motionness assessment.

ANNEXES - In silico silencing of the LHb in the restraint stress functional network

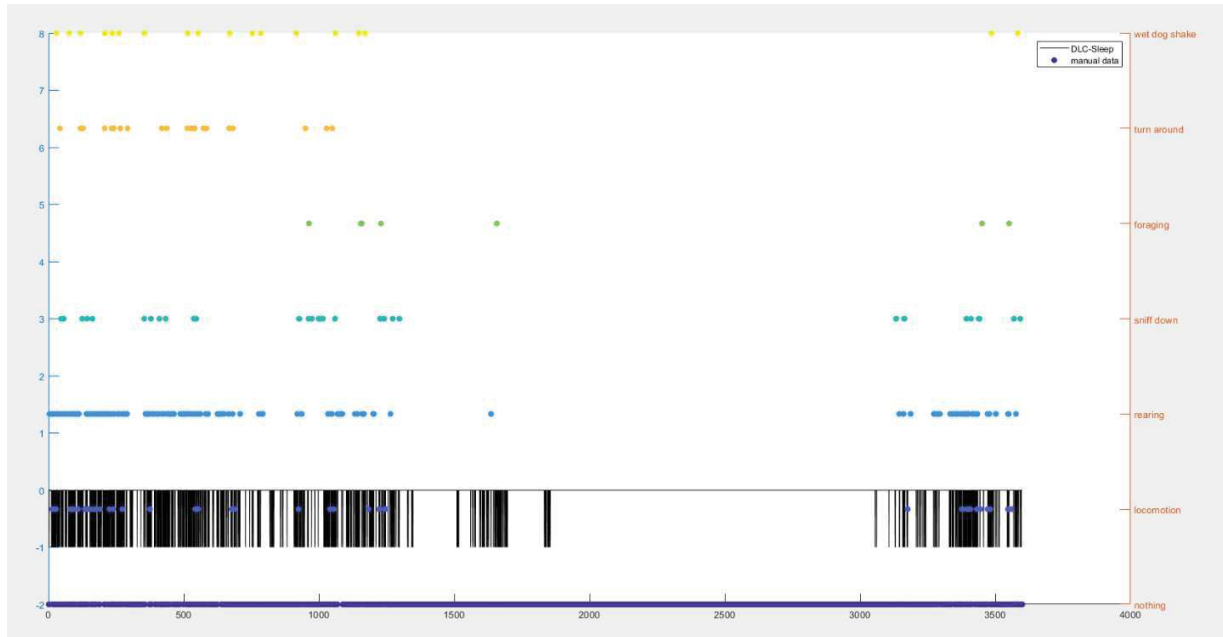


Figure 66: Comparison of DLC detection motionness and manual behavioral coding made with Aion. The left y axis represents the coding from DLC; 0 is when the rat is not moving and 1 is when the rat is detected as moving. The right y axis indicates the manually coded behavior [*i.e.*, wet dog shake (yellow), turn around (orange), foraging (light green), sniff down (green), rearing (light blue), locomotion (blue); each occurrence is represented by a dot]. All data are indicated across time in second.

III. *In silico* silencing of the LHb in the restraint stress functional network

We wanted to address the consequences of LHb inactivation using a computational surrogate model, in order to see if such “*in silico*” model, based on the removal of a specific node (in our case the LHb) from the Ctl-Veh group could predict the data obtained in the hM4-CNO group. For this *in silico* modeling we used the Disruption Propagation Model (DPM) developed by the group of Paul W. Frankland (Vetere et al., 2017). The DPM model works as follows: first, all edges associated to the deleted node are set at zero; then, edge weights and node strengths of all the other structures are updated iteratively until convergence is reached. The strength of each node at the iteration time t is defined as:

$$n_i(t) = \sum_j e_{ij}(t)$$

where e_{ij} is the edge weight between the node i and the node j .

ANNEXES - In silico silencing of the LHB in the restraint stress functional network

Then, the node strengths and edge weights are updated as follows:

$$\Delta n_i(t) = n_i(t - 1) - n_i(t)$$

$$e_{ij}(t + 1) = e_{ij}(t) \times \left(1 - \frac{\Delta n_i(t) + \Delta n_j(t)}{n_i(t) + n_j(t) - 2e_{ij}(t)} \right)$$

The modification of edge weights is only allowed one time and the network updates until there are no longer change of edge weights possible. The model was implemented in python. We ran the DPM two times in order to subsequently delete the LhbM and the LhbL.

We obtained the surrogate correlation matrix estimate from the DPM (DPM *in silico*; see [Figure 67](#)). A quick visual evaluation between the matrix from Ctl-Veh group and the DPM clearly gives the impression that the correlations values did not change much. Indeed, the difference of R² values between both was around 0.1 in all the correlation values across the matrix. This result suggests that the DPM does not work in our model, which is certainly due to the fact that we used all the correlations to model the network and did not select only the significant correlations as [Vetere et al. in 2017](#) have done). Therefore, it will be useful in the future to do this analysis again, this time with a thresholded network, in order to give us information concerning the effect of Lhb silencing on the homeostasis of the restraint stress network.

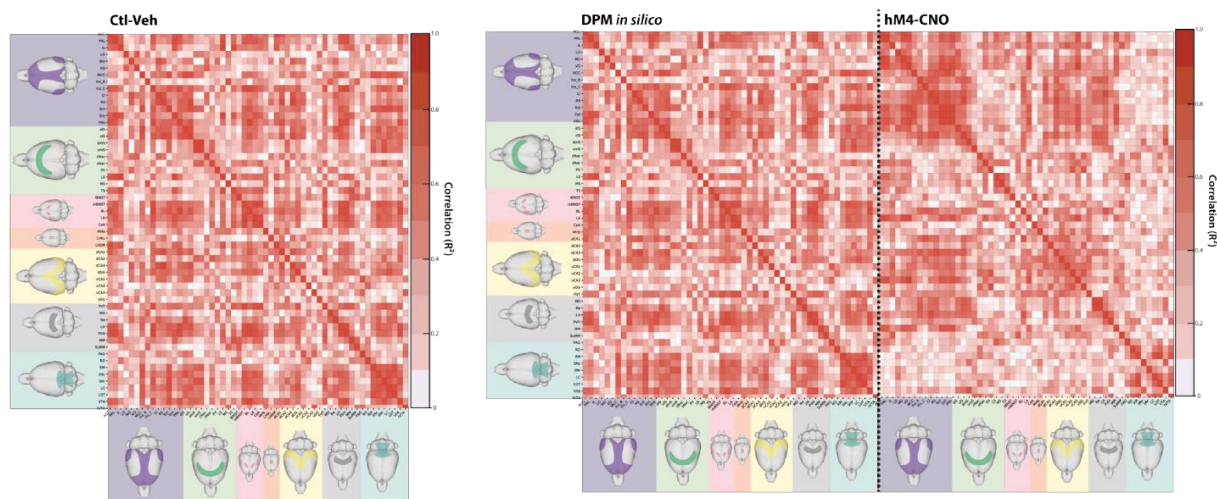


Figure 67: Correlation heatmaps of the Ctl-Veh, the DPM and the hM4-CNO.

Heatmap of each three conditions (Ctl-Veh, DPM, hM4-CNO) representing the cross-correlations (color scale, absolute value of Pearson correlation R²; red represent positive, and white null, correlations) between all investigated structures represented with a color code according to main brain regions (cortical regions, purple; basal ganglia and septum, green; extended amygdala, pink; habenula, red; hippocampus, yellow; thalamus and hypothalamus, grey; brainstem, blue).

REFERENCES

REFERENCES

- Abercrombie ED, Keefe KA, DiFrischia DS, Zigmond MJ (1989) Differential effect of stress on in vivo dopamine release in striatum, nucleus accumbens, and medial frontal cortex. *J Neurochem* 52:1655–1658.
- Adamec RE, Shallow T (1993) Lasting effects on rodent anxiety of a single exposure to a cat. *Physiology & Behavior* 54:101–109.
- Adhikari A, Topiwala MA, Gordon JA (2010) Synchronized Activity between the Ventral Hippocampus and the Medial Prefrontal Cortex during Anxiety. *Neuron* 65:257–269.
- Aghajanian GK, Wang RY (1977) Habenular and other midbrain raphe afferents demonstrated by a modified retrograde tracing technique. *Brain Research* 122:229–242.
- Aguilar-Rivera M, Kim S, Coleman TP, Maldonado PE, Torrealba F (2020) Interoceptive insular cortex participates in sensory processing of gastrointestinal malaise and associated behaviors. *Sci Rep* 10:21642.
- Aizawa H, Cui W, Tanaka K, Okamoto H (2013a) Hyperactivation of the habenula as a link between depression and sleep disturbance. *Frontiers in Human Neuroscience* 7 Available at: <http://journal.frontiersin.org/article/10.3389/fnhum.2013.00826/abstract> [Accessed April 16, 2018].
- Aizawa H, Kobayashi M, Tanaka S, Fukai T, Okamoto H (2012) Molecular characterization of the subnuclei in rat habenula. *The Journal of Comparative Neurology* 520:4051–4066.
- Aizawa H, Yanagihara S, Kobayashi M, Niisato K, Takekawa T, Harukuni R, McHugh TJ, Fukai T, Isomura Y, Okamoto H (2013b) The Synchronous Activity of Lateral Habenular Neurons Is Essential for Regulating Hippocampal Theta Oscillation. *J Neurosci* 33:8909–8921.
- Aizawa H, Zhu M (2019) Toward an understanding of the habenula's various roles in human depression. *Psychiatry and Clinical Neurosciences* 73:607–612.
- Ali M, Cholvin T, Muller MA, Cosquer B, Kelche C, Cassel J-C, Pereira de Vasconcelos A (2017) Environmental enrichment enhances systems-level consolidation of a spatial memory after lesions of the ventral midline thalamus. *Neurobiology of Learning and Memory* 141:108–123.
- Allen HN, Bobnar HJ, Kolber BJ (2021) Left and right hemispheric lateralization of the amygdala in pain. *Prog Neurobiol* 196:101891.
- Amaral DG, Witter MP (1989) The three-dimensional organization of the hippocampal formation: A review of anatomical data. *Neuroscience* 31:571–591.
- Amaral LA, Scala A, Barthelemy M, Stanley HE (2000) Classes of small-world networks. *Proc Natl Acad Sci U S A* 97:11149–11152.
- Amat J, Sparks PD, Matus-Amat P, Griggs J, Watkins LR, Maier SF (2001) The role of the habenular complex in the elevation of dorsal raphe nucleus serotonin and the changes in the behavioral responses produced by uncontrollable stress. *Brain Res* 917:118–126.
- Amo R et al. (2014) The habenulo-raphe serotonergic circuit encodes an aversive expectation value essential for adaptive active avoidance of danger. *Neuron* 84:1034–1048.
- Amo R, Aizawa H, Takahoko M, Kobayashi M, Takahashi R, Aoki T, Okamoto H (2010) Identification of the Zebrafish Ventral Habenula As a Homolog of the Mammalian Lateral Habenula. *Journal of Neuroscience* 30:1566–1574.
- Anastassiou CA, Montgomery SM, Barahona M, Buzsáki G, Koch C (2010) The effect of spatially inhomogeneous extracellular electric fields on neurons. *J Neurosci* 30:1925–1936.
- Andalman AS, Burns VM, Lovett-Barron M, Broxton M, Poole B, Yang SJ, Grosenick L, Lerner TN, Chen R, Benster T, Mourrain P, Levoy M, Rajan K, Deisseroth K (2019a) Neuronal Dynamics Regulating Brain and Behavioral State Transitions. *Cell* 177:970-985.e20.
- Andalman AS, Burns VM, Lovett-Barron M, Broxton M, Poole B, Yang SJ, Grosenick L, Lerner TN, Chen R, Benster T, Mourrain P, Levoy M, Rajan K, Deisseroth K (2019b) Neuronal Dynamics Regulating Brain and Behavioral State Transitions. *Cell* 177:970-985.e20.
- Andersen P, Soleng AF, Raastad M (2000) The hippocampal lamella hypothesis revisited11Published on the World Wide Web on 12 October 2000. *Brain Research* 886:165–171.
- Aponte Y, Atasoy D, Sternson SM (2011) AGRP neurons are sufficient to orchestrate feeding behavior rapidly and without training. *Nature Neuroscience* 14:351–355.
- Araki M, McGeer PL, Kimura H (1988) The efferent projections of the rat lateral habenular nucleus revealed by the PHA-L anterograde tracing method. *Brain Res* 441:319–330.
- Araki M, McGeer PL, McGeer EG (1984) Retrograde HRP tracing combined with a pharmacohistochemical method for GABA transaminase for the identification of presumptive GABAergic projections to the habenula. *Brain Research* 304:271–277.

REFERENCES

- Aringhieri S, Carli M, Kolachalam S, Verdesca V, Cini E, Rossi M, McCormick PJ, Corsini GU, Maggio R, Scarselli M (2018) Molecular targets of atypical antipsychotics: From mechanism of action to clinical differences. *Pharmacology & Therapeutics* 192:20–41.
- Armario A, Daviu N, Muñoz-Abellán C, Rabasa C, Fuentes S, Belda X, Gagliano H, Nadal R (2012) What can we know from pituitary-adrenal hormones about the nature and consequences of exposure to emotional stressors? *Cell Mol Neurobiol* 32:749–758.
- Armbruster BN, Li X, Pausch MH, Herlitze S, Roth BL (2007) Evolving the lock to fit the key to create a family of G protein-coupled receptors potently activated by an inert ligand. *Proceedings of the National Academy of Sciences of the United States of America* 104:5163–5168.
- Arnsten AF (2000) Through the looking glass: differential noradrenergic modulation of prefrontal cortical function. *Neural Plast* 7:133–146.
- Arnsten AFT (2015) Stress weakens prefrontal networks: molecular insults to higher cognition. *Nat Neurosci* 18:1376–1385.
- Aschauer DF, Kreuz S, Rumpel S (2013) Analysis of Transduction Efficiency, Tropism and Axonal Transport of AAV Serotypes 1, 2, 5, 6, 8 and 9 in the Mouse Brain. *PLoS ONE* 8:1–16.
- Ashby CR, Wang RY (1996) Pharmacological actions of the atypical antipsychotic drug clozapine: a review. *Synapse* 24:349–394.
- Aston-Jones G, Ennis M, Pieribone VA, Nickell WT, Shipley MT (1986) The brain nucleus locus coeruleus: restricted afferent control of a broad efferent network. *Science* 234:734–737.
- Atkinson HC, Waddell BJ (1997) Circadian variation in basal plasma corticosterone and adrenocorticotropin in the rat: sexual dimorphism and changes across the estrous cycle. *Endocrinology* 138:3842–3848.
- Augur IF, Wyckoff AR, Aston-Jones G, Kalivas PW, Peters J (2016) Chemogenetic Activation of an Extinction Neural Circuit Reduces Cue-Induced Reinstatement of Cocaine Seeking. *J Neurosci* 36:10174–10180.
- Austenfeld JL, Stanton AL (2004) Coping through emotional approach: a new look at emotion, coping, and health-related outcomes. *J Pers* 72:1335–1363.
- Authement ME, Langlois LD, Shepard RD, Browne CA, Lucki I, Kassis H, Nugent FS (2018a) A role for corticotropin-releasing factor signaling in the lateral habenula and its modulation by early-life stress. *Sci Signal* 11.
- Authement ME, Langlois LD, Shepard RD, Browne CA, Lucki I, Kassis H, Nugent FS (2018b) A role for corticotropin-releasing factor signaling in the lateral habenula and its modulation by early-life stress. *Sci Signal* 11:eaan6480.
- Baas D, Aleman A, Kahn RS (2004) Lateralization of amygdala activation: a systematic review of functional neuroimaging studies. *Brain Research Reviews* 45:96–103.
- Babu M et al. (2012) Interaction landscape of membrane-protein complexes in *Saccharomyces cerevisiae*. *Nature* 489:585–589.
- Babu M et al. (2014) Quantitative genome-wide genetic interaction screens reveal global epistatic relationships of protein complexes in *Escherichia coli*. *PLoS Genet* 10:e1004120.
- Baeg EH, Kim YB, Jang J, Kim HT, Mook-Jung I, Jung MW (2001) Fast Spiking and Regular Spiking Neural Correlates of Fear Conditioning in the Medial Prefrontal Cortex of the Rat. *Cerebral Cortex* 11:441–451.
- Bagaev V, Aleksandrov V (2006) Visceral-related area in the rat insular cortex. *Auton Neurosci* 125:16–21.
- Baker PM, Oh SE, Kidder KS, Mizumori SJY (2015) Ongoing behavioral state information signaled in the lateral habenula guides choice flexibility in freely moving rats. *Front Behav Neurosci* 9 Available at: <https://www.ncbi.nlm.nih.gov/pmc/articles/PMC4631824/> [Accessed May 5, 2021].
- Baker PM, Rao Y, Rivera ZMG, Garcia EM, Mizumori SJY (2019) Selective Functional Interaction Between the Lateral Habenula and Hippocampus During Different Tests of Response Flexibility. *Front Mol Neurosci* 12:245.
- Baker PM, Raynor SA, Francis NT, Mizumori SJY (2017) Lateral habenula integration of proactive and retroactive information mediates behavioral flexibility. *Neuroscience* 345:89–98.
- Balcita-Pedicino JJ, Omelchenko N, Bell R, Sesack SR (2011) The inhibitory influence of the lateral habenula on midbrain dopamine cells: ultrastructural evidence for indirect mediation via the rostromedial mesopontine tegmental nucleus. *J Comp Neurol* 519:1143–1164.
- Balleine BW, Killcross S (2006) Parallel incentive processing: an integrated view of amygdala function. *Trends in Neurosciences* 29:272–279.

REFERENCES

- Barbas H, Blatt GJ (1995) Topographically specific hippocampal projections target functionally distinct prefrontal areas in the rhesus monkey. *Hippocampus* 5:511–533.
- Barrett DW, Gonzalez-Lima F (2018) Prefrontal-limbic Functional Connectivity during Acquisition and Extinction of Conditioned Fear. *Neuroscience* 376:162–171.
- Barth DS (2003) Submillisecond synchronization of fast electrical oscillations in neocortex. *J Neurosci* 23:2502–2510.
- Bartos M, Vida I, Jonas P (2007) Synaptic mechanisms of synchronized gamma oscillations in inhibitory interneuron networks. *Nature Reviews Neuroscience* 8:45–56.
- Bassett DS, Bullmore E (2006) Small-world brain networks. *Neuroscientist* 12:512–523.
- Beaulieu S, Di Paolo T, Barden N (1986) Control of ACTH secretion by the central nucleus of the amygdala: implication of the serotonergic system and its relevance to the glucocorticoid delayed negative feedback mechanism. *Neuroendocrinology* 44:247–254.
- Belujon P, Grace AA (2015a) Regulation of dopamine system responsivity and its adaptive and pathological response to stress. *Proceedings of the Royal Society B: Biological Sciences* 282:20142516–20142516.
- Belujon P, Grace AA (2015b) Regulation of dopamine system responsivity and its adaptive and pathological response to stress. *Proc Biol Sci* 282 Available at: <https://www.ncbi.nlm.nih.gov/pmc/articles/PMC4389605/> [Accessed April 26, 2021].
- Benabid AL, Jeaugey L (1989a) Cells of the rat lateral habenula respond to high-threshold somatosensory inputs. *Neurosci Lett* 96:289–294.
- Benabid AL, Jeaugey L (1989b) Cells of the rat lateral habenula respond to high-threshold somatosensory inputs. *Neuroscience Letters* 96:289–294.
- Berger AL, Henricks AM, Lugo JM, Wright HR, Warrick CR, Sticht MA, Morena M, Bonilla I, Laredo SA, Craft RM, Parsons LH, Grandes PR, Hillard CJ, Hill MN, McLaughlin RJ (2018) The Lateral Habenula Directs Coping Styles Under Conditions of Stress Via Recruitment of the Endocannabinoid System. *Biological Psychiatry* 0 Available at: [https://www.biologicalpsychiatryjournal.com/article/S0006-3223\(18\)31473-2/fulltext](https://www.biologicalpsychiatryjournal.com/article/S0006-3223(18)31473-2/fulltext) [Accessed June 29, 2018].
- Bergstrom HC (2016) The neurocircuitry of remote cued fear memory. *Neuroscience & Biobehavioral Reviews* 71:409–417.
- Bernard R, Veh RW (2012) Individual neurons in the rat lateral habenular complex project mostly to the dopaminergic ventral tegmental area or to the serotonergic raphe nuclei. *J Comp Neurol* 520:2545–2558.
- Bertone-Cueto NI, Makarova J, Mosqueira A, García-Violini D, Sánchez-Peña R, Herreras O, Belluscio M, Piriz J (2020) Volume-Conducted Origin of the Field Potential at the Lateral Habenula. *Front Syst Neurosci* 13 Available at: <https://www.ncbi.nlm.nih.gov/pmc/articles/PMC6961596/> [Accessed May 5, 2021].
- Bhatnagar S, Dallman M (1998) Neuroanatomical basis for facilitation of hypothalamic-pituitary-adrenal responses to a novel stressor after chronic stress. *Neuroscience* 84:1025–1039.
- Bianco IH, Wilson SW (2009) The habenular nuclei: a conserved asymmetric relay station in the vertebrate brain. *Philosophical Transactions of the Royal Society B: Biological Sciences* 364:1005–1020.
- Blanchard RJ, Blanchard DC (1969) Crouching as an index of fear. *J Comp Physiol Psychol* 67:370–375.
- Blanchard RJ, Blanchard DC (1989) Antipredator defensive behaviors in a visible burrow system. *J Comp Psychol* 103:70–82.
- Blanchard RJ, Brain P, Blanchard DC, Parmigiani S eds. (1989) *Ethoexperimental Approaches to the Study of Behavior*. Springer Netherlands. Available at: <https://www.springer.com/gp/book/9780792302964> [Accessed May 23, 2021].
- Bland BH, Trepel C, Oddie SD, Kirk IJ (1996) Intraseptal microinfusion of muscimol: effects on hippocampal formation theta field activity and phasic theta-ON cell discharges. *Exp Neurol* 138:286–297.
- Blondel VD, Guillaume J-L, Lambiotte R, Lefebvre E (2008) Fast unfolding of communities in large networks. *J Stat Mech* 2008:P10008.
- Bocchetta M, Gordon E, Marshall CR, Slattery CF, Cardoso MJ, Cash DM, Espak M, Modat M, Ourselin S, Frisoni GB, Schott JM, Warren JD, Rohrer JD (2015) The habenula: an under-recognised area of importance in frontotemporal dementia? *J Neurol Neurosurg Psychiatry* Month 87:13–16.
- Bocchio M, McHugh SB, Bannerman DM, Sharp T, Capogna M (2016) Serotonin, Amygdala and Fear: Assembling the Puzzle. *Front Neural Circuits* 10:24.

REFERENCES

- Bouthenet M-L, Souil E, Martres M-P, Sokoloff P, Giros B, Schwartz J-C (1991) Localization of dopamine D3 receptor mRNA in the rat brain using in situ hybridization histochemistry: comparison with dopamine D2 receptor mRNA. *Brain Research* 564:203–219.
- Bouton ME, Bolles RC (1979) Role of conditioned contextual stimuli in reinstatement of extinguished fear. *J Exp Psychol Anim Behav Process* 5:368–378.
- Bowen MT, Kevin RC, May M, Staples LG, Hunt GE, McGregor IS (2013) Defensive Aggregation (Huddling) in Rattus Norvegicus toward Predator Odor: Individual Differences, Social Buffering Effects and Neural Correlates. *PLOS ONE* 8:e68483.
- Bracha DHS (2004) Freeze, Flight, Fight, Fright, Faint: Adaptationist Perspectives on the Acute Stress Response Spectrum. *CNS Spectr* 9:679–685.
- Bradbury MJ, Strack AM, Dallman MF (1993) Lesions of the hippocampal efferent pathway (fimbria-fornix) do not alter sensitivity of adrenocorticotropin to feedback inhibition by corticosterone in rats. *Neuroendocrinology* 58:396–407.
- Bragin A, Engel J, Wilson CL, Fried I, Buzsáki G (1999) High-frequency oscillations in human brain. *Hippocampus* 9:137–142.
- Bragin A, Jando G, Nadasdy Z, Hetke J, Wise K, Buzsaki G (1995) Gamma (40–100 Hz) oscillation in the hippocampus of the behaving rat. *J Neurosci* 15:47–60.
- Bressler SL (1995) Large-scale cortical networks and cognition. *Brain Research Reviews* 20:288–304.
- Brinshawitz K, Dittgen A, Madai VI, Lommel R, Geisler S, Veh RW (2010) Glutamatergic axons from the lateral habenula mainly terminate on GABAergic neurons of the ventral midbrain. *Neuroscience* 168:463–476.
- Brioni JD, Nagahara AH, McGaugh JL (1989) Involvement of the amygdala GABAergic system in the modulation of memory storage. *Brain Res* 487:105–112.
- Brischoux F, Chakraborty S, Brierley DI, Ungless MA (2009) Phasic excitation of dopamine neurons in ventral VTA by noxious stimuli. *Proc Natl Acad Sci U S A* 106:4894–4899.
- Brodman K (1909) Vergleichende Lokalisationslehre der Grosshirnrinde in ihren Prinzipien dargestellt auf Grund des Zellenbaues. Leipzig: Barth. Available at: <http://archive.org/details/b28062449> [Accessed April 20, 2021].
- Bromberg-Martin ES, Hikosaka O (2011) Lateral habenula neurons signal errors in the prediction of reward information. *Nature Neuroscience* 14:1209–1216.
- Brown PL, Shepard PD (2013a) Lesions of the Fasciculus Retroflexus Alter Footshock-Induced cFos Expression in the Mesopontine Rostromedial Tegmental Area of Rats Tanimoto H, ed. *PLoS ONE* 8:e60678.
- Brown PL, Shepard PD (2013b) Lesions of the fasciculus retroflexus alter footshock-induced cFos expression in the mesopontine rostromedial tegmental area of rats. *PLoS One* 8:e60678.
- Browne CA, Hammack R, Lucki I (2018) Dysregulation of the Lateral Habenula in Major Depressive Disorder. *Front Synaptic Neurosci* 10:46.
- Brynildsen JK, Mace KD, Cornblath EJ, Weidler C, Pasqualetti F, Bassett DS, Blendy JA (2020) Gene coexpression patterns predict opiate-induced brain-state transitions. *Proc Natl Acad Sci U S A* 117:19556–19565.
- Buijs RM (1978) Intra- and extrahypothalamic vasopressin and oxytocin pathways in the rat. Pathways to the limbic system, medulla oblongata and spinal cord. *Cell Tissue Res* 192:423–435.
- Bullmore E, Sporns O (2009) Complex brain networks: graph theoretical analysis of structural and functional systems. *Nature Reviews Neuroscience* 10:186–198.
- Burgos-Robles A, Kimchi EY, Izadmehr EM, Porzenheim MJ, Ramos-Guasp WA, Nieh EH, Felix-Ortiz AC, Namburi P, Leppla CA, Presbrey KN, Anandalingam KK, Pagan-Rivera PA, Anahtar M, Beyeler A, Tye KM (2017) Amygdala inputs to prefrontal cortex guide behavior amid conflicting cues of reward and punishment. *Nature Neuroscience* 20:824–835.
- Buschman TJ, Miller EK (2007) Top-Down Versus Bottom-Up Control of Attention in the Prefrontal and Posterior Parietal Cortices. *Science* 315:1860–1862.
- Butler MW, Lutz TJ, Fokidis HB, Stahlschmidt ZR (2016) Eating increases oxidative damage in a reptile. *Journal of Experimental Biology* 219:1969–1973.
- Buzsáki G (2002) Theta Oscillations in the Hippocampus. *Neuron* 33:325–340.
- Buzsáki G (2010) Neural Syntax: Cell Assemblies, Synapsembles, and Readers. *Neuron* 68:362–385.
- Buzsáki G, Anastassiou CA, Koch C (2012) The origin of extracellular fields and currents — EEG, ECoG, LFP and spikes. *Nature Reviews Neuroscience* 13:407–420.

REFERENCES

- Buzsáki G, Bickford RG, Ponomareff G, Thal LJ, Mandel R, Gage FH (1988) Nucleus basalis and thalamic control of neocortical activity in the freely moving rat. *J Neurosci* 8:4007–4026.
- Buzsáki G, Draguhn A (2004) Neuronal Oscillations in Cortical Networks. *Science* 304:1926–1929.
- Buzsáki G, Watson BO (2012) Brain rhythms and neural syntax: implications for efficient coding of cognitive content and neuropsychiatric disease. *Dialogues Clin Neurosci* 14:345–367.
- Calandreau L, Desmedt A, Decorte L, Jaffard R (2005) A different recruitment of the lateral and basolateral amygdala promotes contextual or elemental conditioned association in Pavlovian fear conditioning. *Learn Mem* 12:383–388.
- Campbell EJ, Marchant NJ (2018) The use of chemogenetics in behavioural neuroscience: receptor variants, targeting approaches and caveats. *Br J Pharmacol* 175:994–1003.
- Campeau S, Davis M (1995) Involvement of the central nucleus and basolateral complex of the amygdala in fear conditioning measured with fear-potentiated startle in rats trained concurrently with auditory and visual conditioned stimuli. *J Neurosci* 15:2301–2311.
- Cannon WB (Walter B (1915) Bodily changes in pain, hunger, fear and rage, an account of recent researches into the function of emotional excitement. New York and London, D. Appleton and Co. Available at: <http://archive.org/details/cu31924022542470> [Accessed April 13, 2021].
- Canolty RT, Edwards E, Dalal SS, Soltani M, Nagarajan SS, Kirsch HE, Berger MS, Barbaro NM, Knight RT (2006) High gamma power is phase-locked to theta oscillations in human neocortex. *Science* 313:1626–1628.
- Caputo A, Ghiringhelli L, Dieci M, Giobbio GM, Tenconi F, Ferrari L, Gimosti E, Prato K, Vita A (1998) Epithalamus calcifications in schizophrenia. *Eur Arch Psychiatry Clin Neurosci* 248:272–276.
- Carlén M (2017) What constitutes the prefrontal cortex? *Science* 358:478–482.
- Carlson JN, Fitzgerald LW, Jr RWK, Glick SD (1993) Lateralized changes in prefrontal cortical dopamine activity induced by controllable and uncontrollable stress in the rat. :10.
- Casady RL, Taylor AN (1976) Effect of Electrical Stimulation of the Hippocampus Upon Corticosteroid Levels in the Freely-Behaving, Non-Stressed Rat. *NEN* 20:68–78.
- Casarrubea M, Davies C, Faulisi F, Pierucci M, Colangeli R, Partridge L, Chambers S, Cassar D, Valentino M, Muscat R, Benigno A, Crescimanno G, Di Giovanni G (2015) Acute nicotine induces anxiety and disrupts temporal pattern organization of rat exploratory behavior in hole-board: a potential role for the lateral habenula. *Front Cell Neurosci* 9 Available at: <https://www.ncbi.nlm.nih.gov/pmc/articles/PMC4450172/> [Accessed August 7, 2018].
- Cassens G, Kuruc A, Roffman M, Orsulak PJ, Schildkraut JJ (1981) Alterations in brain norepinephrine metabolism and behavior induced by environmental stimuli previously paired with inescapable shock. *Behav Brain Res* 2:387–407.
- Cedarbaum JM, Aghajanian GK (1978) Activation of locus coeruleus neurons by peripheral stimuli: modulation by a collateral inhibitory mechanism. *Life Sci* 23:1383–1392.
- Cenci MA, Kalén P, Mandel RJ, Björklund A (1992a) Regional differences in the regulation of dopamine and noradrenaline release in medial frontal cortex, nucleus accumbens and caudate-putamen: a microdialysis study in the rat. *Brain Res* 581:217–228.
- Cenci MA, Kalén P, Mandel RJ, Björklund A (1992b) Regional differences in the regulation of dopamine and noradrenaline release in medial frontal cortex, nucleus accumbens and caudate-putamen: a microdialysis study in the rat. *Brain Res* 581:217–228.
- Cerpa J-C, Marchand AR, Coutureau E (2019) Distinct regional patterns in noradrenergic innervation of the rat prefrontal cortex. *Journal of Chemical Neuroanatomy* 96:102–109.
- Chan CY, Nicholson C (1986) Modulation by applied electric fields of Purkinje and stellate cell activity in the isolated turtle cerebellum. *J Physiol* 371:89–114.
- Chan J, Guan X, Ni Y, Luo L, Yang L, Zhang P, Zhang J, Chen Y (2017) Dopamine D1-like receptor in lateral habenula nucleus affects contextual fear memory and long-term potentiation in hippocampal CA1 in rats. *Behavioural Brain Research* 321:61–68.
- Chastrette N, Pfaff DW, Gibbs RB (1991a) Effects of daytime and nighttime stress on Fos-like immunoreactivity in the paraventricular nucleus of the hypothalamus, the habenula, and the posterior paraventricular nucleus of the thalamus. *Brain Res* 563:339–344.
- Chastrette N, Pfaff DW, Gibbs RB (1991b) Effects of daytime and nighttime stress on Fos-like immunoreactivity in the paraventricular nucleus of the hypothalamus, the habenula, and the posterior paraventricular nucleus of the thalamus. *Brain Research* 563:339–344.

REFERENCES

- Chau LS, Prakapenka A, Fleming SA, Davis AS, Galvez R (2013) Elevated Arc/Arg 3.1 protein expression in the basolateral amygdala following auditory trace-cued fear conditioning. *Neurobiology of Learning and Memory* 106:127–133.
- Chaudhury D et al. (2013) Rapid regulation of depression-related behaviours by control of midbrain dopamine neurons. *Nature* 493:532–536.
- Choi DC, Furay AR, Evanson NK, Ostrander MM, Ulrich-Lai YM, Herman JP (2007) Bed nucleus of the stria terminalis subregions differentially regulate hypothalamic-pituitary-adrenal axis activity: implications for the integration of limbic inputs. *J Neurosci* 27:2025–2034.
- Choudhury SR, Hudry E, Maguire CA, Sena-Esteves M, Breakefield XO, Grandi P (2016) Viral vectors for therapy of neurologic diseases. *Neuropharmacology*.
- Christoph G, Leonzio R, Wilcox K (1986a) Stimulation of the lateral habenula inhibits dopamine-containing neurons in the substantia nigra and ventral tegmental area of the rat. *J Neurosci* 6:613–619.
- Christoph G, Leonzio R, Wilcox K (1986b) Stimulation of the lateral habenula inhibits dopamine-containing neurons in the substantia nigra and ventral tegmental area of the rat. *J Neurosci* 6:613–619.
- Ciani E, Severi S, Bartesaghi R, Contestabile A (2005) Neurochemical correlates of nicotine neurotoxicity on rat habenulo-interpeduncular cholinergic neurons. *Neurotoxicology* 26:467–474.
- Clavier RM (1979) Afferent projections to the self-stimulation regions of the dorsal pons, including the locus coeruleus, in the rat as demonstrated by the horseradish peroxidase technique. *Brain Res Bull* 4:497–504.
- Cleare AJ (2004) The HPA axis and the genesis of chronic fatigue syndrome. *Trends in Endocrinology & Metabolism* 15:55–59.
- Clemens Z, Mölle M, Eross L, Jakus R, Rásonyi G, Halász P, Born J (2011) Fine-tuned coupling between human parahippocampal ripples and sleep spindles. *Eur J Neurosci* 33:511–520.
- Coffey KR, Marx RG, Vo EK, Nair SG, Neumaier JF (2020) Chemogenetic inhibition of lateral habenula projections to the dorsal raphe nucleus reduces passive coping and perseverative reward seeking in rats. *Neuropsychopharmacology* 45:1115–1124.
- Cohen MX (2014) *Analyzing neural time series data: theory and practice*. Cambridge, Massachusetts: The MIT Press.
- Colgin LL, Moser EI (2010) Gamma oscillations in the hippocampus. *Physiology (Bethesda)* 25:319–329.
- Concha ML, Wilson SW (2001) Asymmetry in the epithalamus of vertebrates. *Journal of Anatomy* 199:63–84.
- Connor DA, Gould TJ (2016) The role of working memory and declarative memory in trace conditioning. *Neurobiology of Learning and Memory* 134:193–209.
- Copeland BJ, Neff NH, Hadjiconstantinou M (2005) Enhanced dopamine uptake in the striatum following repeated restraint stress. *Synapse* 57:167–174.
- Corcoran KA, Quirk GJ (2007) Activity in Prelimbic Cortex Is Necessary for the Expression of Learned, But Not Innate, Fears. *J Neurosci* 27:840–844.
- Corodimas KP, Rosenblatt JS, Canfield ME, Morrell JI (1993) Neurons in the lateral subdivision of the habenular complex mediate the hormonal onset of maternal behavior in rats. *Behav Neurosci* 107:827–843.
- Cox R, Hofman WF, Talamini LM (2012) Involvement of spindles in memory consolidation is slow wave sleep-specific. *Learn Mem* 19:264–267.
- Crestani CC, Alves FH, Gomes FV, Resstel LB, Correa FM, Herman JP (2013) Mechanisms in the Bed Nucleus of the Stria Terminalis Involved in Control of Autonomic and Neuroendocrine Functions: A Review. *Curr Neuropharmacol* 11:141–159.
- Crossley NA, Mechelli A, Scott J, Carletti F, Fox PT, McGuire P, Bullmore ET (2014) The hubs of the human connectome are generally implicated in the anatomy of brain disorders. *Brain* 137:2382–2395.
- Cullinan WE, Herman JP, Battaglia DF, Akil H, Watson SJ (1995) Pattern and time course of immediate early gene expression in rat brain following acute stress. *Neuroscience* 64:477–505.
- Cullinan WE, Herman JP, Watson SJ (1993) Ventral subicular interaction with the hypothalamic paraventricular nucleus: evidence for a relay in the bed nucleus of the stria terminalis. *J Comp Neurol* 332:1–20.
- Cunningham ET, Sawchenko PE (1988) Anatomical specificity of noradrenergic inputs to the paraventricular and supraoptic nuclei of the rat hypothalamus. *J Comp Neurol* 274:60–76.

REFERENCES

- Czéh B, Müller-Keuker JIH, Rygula R, Abumaria N, Hiemke C, Domenici E, Fuchs E (2007) Chronic social stress inhibits cell proliferation in the adult medial prefrontal cortex: hemispheric asymmetry and reversal by fluoxetine treatment. *Neuropsychopharmacology* 32:1490–1503.
- Czéh B, Perez-Cruz C, Fuchs E, Flügge G (2008) Chronic stress-induced cellular changes in the medial prefrontal cortex and their potential clinical implications: Does hemisphere location matter? *Behavioural Brain Research* 190:1–13.
- Czerniawski J, Ree F, Chia C, Otto T (2012) Dorsal versus ventral hippocampal contributions to trace and contextual conditioning: differential effects of regionally selective NMDA receptor antagonism on acquisition and expression. *Hippocampus* 22:1528–1539.
- Dalal SS, Hamamé CM, Eichenlaub J-B, Jerbi K (2010) Intrinsic coupling between gamma oscillations, neuronal discharges, and slow cortical oscillations during human slow-wave sleep. *J Neurosci* 30:14285–14287.
- Daniel SE, Rainnie DG (2016) Stress Modulation of Opposing Circuits in the Bed Nucleus of the Stria Terminalis. *Neuropsychopharmacology* 41:103–125.
- Dayas CV, Buller KM, Crane JW, Xu Y, Day TA (2001) Stressor categorization: acute physical and psychological stressors elicit distinctive recruitment patterns in the amygdala and in medullary noradrenergic cell groups. *Eur J Neurosci* 14:1143–1152.
- Dayas CV, Buller KM, Day TA (1999) Neuroendocrine responses to an emotional stressor: evidence for involvement of the medial but not the central amygdala. *Eur J Neurosci* 11:2312–2322.
- de Jong TR, Measor KR, Chauke M, Harris BN, Saltzman W (2010) Brief pup exposure induces Fos expression in the lateral habenula and serotonergic caudal dorsal raphe nucleus of paternally experienced male California mice (*Peromyscus californicus*). *Neuroscience* 169:1094–1104.
- de Kloet ER (1992) Corticosteroids, stress, and aging. *Ann N Y Acad Sci* 663:357–371.
- de Kloet ER (2013) Functional profile of the binary brain corticosteroid receptor system: Mediating, multitasking, coordinating, integrating. *European Journal of Pharmacology* 719:53–62.
- de Kloet ER, Joëls M, Holsboer F (2005) Stress and the brain: from adaptation to disease. *Nature Reviews Neuroscience* 6:463–475.
- de Kloet ER, Oitzl MS, Joëls M (1999) Stress and cognition: are corticosteroids good or bad guys? *Trends in Neurosciences* 22:422–426.
- de Kloet ER, Vreugdenhil E, Oitzl MS, Joëls M (1998) Brain Corticosteroid Receptor Balance in Health and Disease*. *Endocrine Reviews* 19:269–301.
- De Oca BM, DeCola JP, Maren S, Fanselow MS (1998) Distinct regions of the periaqueductal gray are involved in the acquisition and expression of defensive responses. *J Neurosci* 18:3426–3432.
- de Quervain DJ-F, Roozendaal B, McGaugh JL (1998) Stress and glucocorticoids impair retrieval of long-term spatial memory. *Nature* 394:787–790.
- De Vries GJ, Buds RM, Swaab DF (1981) Ontogeny of the vasopressinergic neurons of the suprachiasmatic nucleus and their extrahypothalamic projections in the rat brain—presence of a sex difference in the lateral septum. *Brain Research* 218:67–78.
- Dedovic K, Duchesne A, Andrews J, Engert V, Pruessner JC (2009) The brain and the stress axis: the neural correlates of cortisol regulation in response to stress. *Neuroimage* 47:864–871.
- Del Giudice M, Ellis BJ, Shirtcliff EA (2011) The Adaptive Calibration Model of stress responsivity. *Neuroscience & Biobehavioral Reviews* 35:1562–1592.
- Dennis EL, Thompson PM (2014) Functional Brain Connectivity using fMRI in Aging and Alzheimer's Disease. *Neuropsychol Rev* 24:49–62.
- Derman RC, Bass CE, Ferrario CR (2020) Effects of hM4Di activation in CamKII basolateral amygdala neurons and CNO treatment on sensory-specific vs. general PIT: refining PIT circuits and considerations for using CNO. *Psychopharmacology* 237:1249–1266.
- Diamantopoulou A, Raftogianni A, Stamatakis A, Alikaridis F, Oitzl MS, Stylianopoulou F (2012) Denial of reward in the neonate shapes sociability and serotonergic activity in the adult rat. *PLoS One* 7:e33793.
- Diamond DM, Bennett MC, Fleshner M, Rose GM (1992) Inverted-U relationship between the level of peripheral corticosterone and the magnitude of hippocampal primed burst potentiation. *Hippocampus* 2:421–430.
- Diamond DM, Campbell AM, Park CR, Halonen J, Zoladz PR (2007) The temporal dynamics model of emotional memory processing: a synthesis on the neurobiological basis of stress-induced amnesia, flashbulb and traumatic memories, and the Yerkes-Dodson law. *Neural Plast* 2007:60803.

REFERENCES

- Diamond DM, Park CR, Heman KL, Rose GM (1999) Exposing rats to a predator impairs spatial working memory in the radial arm water maze. *Hippocampus* 9:542–552.
- Díaz E, Bravo D, Rojas X, Concha ML (2011) Morphologic and immunohistochemical organization of the human habenular complex. *The Journal of Comparative Neurology* 519:3727–3747.
- Diorio D, Viau V, Meaney M (1993) The role of the medial prefrontal cortex (cingulate gyrus) in the regulation of hypothalamic-pituitary-adrenal responses to stress. *J Neurosci* 13:3839–3847.
- Do JP, Xu M, Lee S-H, Chang W-C, Zhang S, Chung S, Yung TJ, Fan JL, Miyamichi K, Luo L, Dan Y (2016) Cell type-specific long-range connections of basal forebrain circuit. *Elife* 5.
- Dolzani SD, Baratta MV, Amat J, Agster KL, Saddoris MP, Watkins LR, Maier SF (2016a) Activation of a Habenulo-Raphe Circuit Is Critical for the Behavioral and Neurochemical Consequences of Uncontrollable Stress in the Male Rat. *eNeuro* 3.
- Dolzani SD, Baratta MV, Amat J, Agster KL, Saddoris MP, Watkins LR, Maier SF (2016b) Activation of a Habenulo-Raphe Circuit Is Critical for the Behavioral and Neurochemical Consequences of Uncontrollable Stress in the Male Rat. *eNeuro* 3.
- Do-Monte FH, Quiñones-Laracuenta K, Quirk GJ (2015) A temporal shift in the circuits mediating retrieval of fear memory. *Nature* 519:460–463.
- Dong H-W, Petrovich GD, Swanson LW (2001) Topography of projections from amygdala to bed nuclei of the stria terminalis. *Brain Research Reviews* 38:192–246.
- Dong H-W, Swanson LW (2004) Organization of axonal projections from the anterolateral area of the bed nuclei of the stria terminalis. *J Comp Neurol* 468:277–298.
- Dong H-W, Swanson LW (2006) Projections from bed nuclei of the stria terminalis, dorsomedial nucleus: Implications for cerebral hemisphere integration of neuroendocrine, autonomic, and drinking responses. *The Journal of Comparative Neurology* 494:75–107.
- Dotson VM, Szymkowicz SM, Kirton JW, McLaren ME, Green ML, Rohani JY (2014) Unique and interactive effect of anxiety and depressive symptoms on cognitive and brain function in young and older adults. *J Depress Anxiety Suppl* 1.
- Duncan GE, Knapp DJ, Breese GR (1996a) Neuroanatomical characterization of Fos induction in rat behavioral models of anxiety. *Brain Research* 713:79–91.
- Duncan GE, Knapp DJ, Johnson KB, Breese GR (1996b) Functional classification of antidepressants based on antagonism of swim stress-induced fos-like immunoreactivity. *J Pharmacol Exp Ther* 277:1076–1089.
- Durieux L, Mathis V, Herbeaux K, Muller M-A, Barbelivien A, Mathis C, Schlichter R, Hugel S, Majchrzak M, Lecourtier L (2020) Involvement of the lateral habenula in fear memory. *Brain Struct Funct*.
- Duvarci S, Pare D (2014) Amygdala Microcircuits Controlling Learned Fear. *Neuron* 82:966–980.
- Ellison G (2002) Neural degeneration following chronic stimulant abuse reveals a weak link in brain, fasciculus retroflexus, implying the loss of forebrain control circuitry. *Eur Neuropsychopharmacol* 12:287–297.
- Elul R (1971) The genesis of the EEG. *Int Rev Neurobiol* 15:227–272.
- Ely BA, Stern ER, Kim J, Gabbay V, Xu J (2019) Detailed mapping of human habenula resting-state functional connectivity. *NeuroImage* 200:621–634.
- Emmert MH, Herman JP (1999) Differential forebrain c-fos mRNA induction by ether inhalation and novelty: evidence for distinctive stress pathways. *Brain Res* 845:60–67.
- Faber DS, Korn H (1989) Electrical field effects: their relevance in central neural networks. *Physiol Rev* 69:821–863.
- Fanselow EE, Sameshima K, Baccala LA, Nicoletis MA (2001) Thalamic bursting in rats during different awake behavioral states. *Proc Natl Acad Sci U S A* 98:15330–15335.
- Fanselow MS (2000) Contextual fear, gestalt memories, and the hippocampus. *Behavioural Brain Research* 110:73–81.
- Fanselow MS (2010) From contextual fear to a dynamic view of memory systems. *Trends in Cognitive Sciences* 14:7–15.
- Fanselow MS, Dong H-W (2010) Are the dorsal and ventral hippocampus functionally distinct structures? *Neuron* 65:7–19.
- Febbraro F, Svenningsen K, Tran TP, Wiborg O (2017) Neuronal substrates underlying stress resilience and susceptibility in rats. *PLoS One* 12:e0179434.
- Feldman S, Conforti N, Itzik A, Weidenfeld J (1994) Differential effect of amygdaloid lesions on CRF-41, ACTH and corticosterone responses following neural stimuli. *Brain Res* 658:21–26.

REFERENCES

- Felix-Ortiz AC, Burgos-Robles A, Bhagat ND, Leppla CA, Tye KM (2016) Bidirectional modulation of anxiety-related and social behaviors by amygdala projections to the medial prefrontal cortex. *Neuroscience* 321:197–209.
- Fell J, Axmacher N (2011) The role of phase synchronization in memory processes. *Nature Reviews Neuroscience* 12:105–118.
- Fendt M, Fanselow MS (1999) The neuroanatomical and neurochemical basis of conditioned fear. *Neuroscience & Biobehavioral Reviews* 23:743–760.
- Ferguson SM, Phillips PEM, Roth BL, Wess J, Neumaier JF (2013) Direct-Pathway Striatal Neurons Regulate the Retention of Decision-Making Strategies. *J Neurosci* 33:11668–11676.
- Ferraro G, Montalbano ME, Sardo P, La Grutta V (1997) Lateral habenula and hippocampus: A complex interaction raphe cells-mediated. *J Neural Transmission* 104:615–631.
- Ferraro L, Tanganelli S, O'Connor WT, Antonelli T, Rambert F, Fuxe K (1996) The vigilance promoting drug modafinil decreases GABA release in the medial preoptic area and in the posterior hypothalamus of the awake rat: possible involvement of the serotonergic 5-HT₃ receptor. *Neuroscience Letters* 220:5–8.
- Figueiredo HF, Bruestle A, Bodie B, Dolgas CM, Herman JP (2003) The medial prefrontal cortex differentially regulates stress-induced c-fos expression in the forebrain depending on type of stressor. *Eur J Neurosci* 18:2357–2364.
- Fillinger C, Yalcin I, Barrot M, Veinante P (2017a) Afferents to anterior cingulate areas 24a and 24b and midcingulate areas 24a' and 24b' in the mouse. *Brain Struct Funct* 222:1509–1532.
- Fillinger C, Yalcin I, Barrot M, Veinante P (2017b) Efferents of anterior cingulate areas 24a and 24b and midcingulate areas 24a' and 24b' in the mouse. *Brain Struct Funct* Available at: <http://link.springer.com/10.1007/s00429-017-1585-x> [Accessed April 20, 2021].
- Findlay G, Tononi G, Cirelli C (2020) The evolving view of replay and its functions in wake and sleep. *Sleep Adv* 1:zpab002.
- Finsterwald C, Alberini CM (2014) Stress and glucocorticoid receptor-dependent mechanisms in long-term memory: From adaptive responses to psychopathologies. *Neurobiology of Learning and Memory* 112:17–29.
- Flügge G, Van Kampen M, Mijster MJ (2004) Perturbations in brain monoamine systems during stress. *Cell Tissue Res* 315:1–14.
- Fluttert M, Dalm S, Oitzl MS (2000) A refined method for sequential blood sampling by tail incision in rats. *Lab Anim* 34:372–378.
- Forster GL, Pringle RB, Mouw NJ, Vuong SM, Watt MJ, Burke AR, Lowry CA, Summers CH, Renner KJ (2008) Corticotropin-releasing factor in the dorsal raphe nucleus increases medial prefrontal cortical serotonin via type 2 receptors and median raphe nucleus activity. *Eur J Neurosci* 28:299–310.
- Fowler CD, Lu Q, Johnson PM, Marks MJ, Kenny PJ (2011) Habenular $\alpha 5$ nicotinic receptor subunit signalling controls nicotine intake. *Nature* 471:597–601.
- Frahm S, Antolin-Fontes B, Görlich A, Zander J-F, Ahnert-Hilger G, Ibañez-Tallon I (2015) An essential role of acetylcholine-glutamate synergy at habenular synapses in nicotine dependence. *Elife* 4:e11396.
- Francisco Gonzalez-Lima HS (1986) Classical Conditioning of tone-signaled bradycardia modifies 2-Desoxyglucose uptake patterns in cortex, thalamus, habenula, caudate-putamen and hippocampal formation.
- Franklin TB, Saab BJ, Mansuy IM (2012) Neural Mechanisms of Stress Resilience and Vulnerability. *Neuron* 75:747–761.
- Freund TF, Buzsáki G (1996) Interneurons of the hippocampus. *Hippocampus* 6:347–470.
- Fries P (2005a) A mechanism for cognitive dynamics: neuronal communication through neuronal coherence. *Trends in Cognitive Sciences* 9:474–480.
- Fries P (2005b) A mechanism for cognitive dynamics: neuronal communication through neuronal coherence. *Trends in Cognitive Sciences* 9:474–480.
- Friess E, Wiedemann K, Steiger A, Holsboer F (1995) The hypothalamic-pituitary-adrenocortical system and sleep in man. *Adv Neuroimmunol* 5:111–125.
- Friston K (2002) Beyond phrenology: what can neuroimaging tell us about distributed circuitry? *Annu Rev Neurosci* 25:221–250.
- Gabbott PLA, Warner TA, Jays PRL, Salway P, Busby SJ (2005) Prefrontal cortex in the rat: Projections to subcortical autonomic, motor, and limbic centers. *J Comp Neurol* 492:145–177.

REFERENCES

- Gamble KL, Berry R, Frank SJ, Young ME (2014) Circadian clock control of endocrine factors. *Nature Reviews Endocrinology* 10:466–475.
- Gao DM, Jeaugey L, Pollak P, Benabid AL (1990) Intensity-dependent nociceptive responses from presumed dopaminergic neurons of the substantia nigra, pars compacta in the rat and their modification by lateral habenula inputs. *Brain Res* 529:315–319.
- Garcia A, Steiner B, Kronenberg G, Bick-Sander A, Kempermann G (2004) Age-dependent expression of glucocorticoid- and mineralocorticoid receptors on neural precursor cell populations in the adult murine hippocampus. *Aging Cell* 3:363–371.
- Geddes LA, Roeder R (2003) Criteria for the selection of materials for implanted electrodes. *Ann Biomed Eng* 31:879–890.
- Geisler S, Andres KH, Veh RW (2003) Morphologic and cytochemical criteria for the identification and delineation of individual subnuclei within the lateral habenular complex of the rat. *J Comp Neurol* 458:78–97.
- Geisler S, Trimble M (2008a) The Lateral Habenula: No Longer Neglected. *CNS spectr* 13:484–489.
- Geisler S, Trimble M (2008b) The lateral habenula: no longer neglected. *CNS Spectr* 13:484–489.
- Gentile CG, Jarrell TW, Teich A, McCabe PM, Schneiderman N (1986) The role of amygdaloid central nucleus in the retention of differential pavlovian conditioning of bradycardia in rabbits. *Behav Brain Res* 20:263–273.
- Gervasoni D, Lin S-C, Ribeiro S, Soares ES, Pantoja J, Nicolelis MAL (2004) Global Forebrain Dynamics Predict Rat Behavioral States and Their Transitions. *J Neurosci* 24:11137–11147.
- Gilmartin MR, Balderston NL, Helmstetter FJ (2014) Prefrontal cortical regulation of fear learning. *Trends in Neurosciences* 37:455–464.
- Gilmartin MR, Helmstetter FJ (2010) Trace and contextual fear conditioning require neural activity and NMDA receptor-dependent transmission in the medial prefrontal cortex. *Learn Mem* 17:289–296.
- Gilmartin MR, Kwapis JL, Helmstetter FJ (2012) Trace and contextual fear conditioning are impaired following unilateral microinjection of muscimol in the ventral hippocampus or amygdala, but not the medial prefrontal cortex. *Neurobiology of Learning and Memory* 97:452–464.
- Gilmartin MR, McEchron MD (2005) Single Neurons in the Medial Prefrontal Cortex of the Rat Exhibit Tonic and Phasic Coding During Trace Fear Conditioning. *Behavioral Neuroscience* 119:1496–1510.
- Gilmartin MR, Miyawaki H, Helmstetter FJ, Diba K (2013) Prefrontal Activity Links Nonoverlapping Events in Memory. *J Neurosci* 33:10910–10914.
- Girardeau G, Zugaro M (2011) Hippocampal ripples and memory consolidation. *Current Opinion in Neurobiology* 21:452–459.
- Godoy LD, Rossignoli MT, Delfino-Pereira P, Garcia-Cairasco N, de Lima Umeoka EH (2018a) A Comprehensive Overview on Stress Neurobiology: Basic Concepts and Clinical Implications. *Front Behav Neurosci* 12 Available at: <https://www.ncbi.nlm.nih.gov/pmc/articles/PMC6043787/> [Accessed April 12, 2021].
- Godoy LD, Rossignoli MT, Delfino-Pereira P, Garcia-Cairasco N, de Lima Umeoka EH (2018b) A Comprehensive Overview on Stress Neurobiology: Basic Concepts and Clinical Implications. *Front Behav Neurosci* 12 Available at: <https://www.ncbi.nlm.nih.gov/pmc/articles/PMC6043787/> [Accessed January 21, 2021].
- Godsil BP, Kiss JP, Spedding M, Jay TM (2013) The hippocampal–prefrontal pathway: The weak link in psychiatric disorders? *European Neuropsychopharmacology* 23:1165–1181.
- Gold PW, Kadriu B (2019) A Major Role for the Lateral Habenula in Depressive Illness: Physiologic and Molecular Mechanisms. *Front Psychiatry* 10:320.
- Golden SA et al. (2016a) Basal forebrain projections to the lateral habenula modulate aggression reward. *Nature* 534:688–692.
- Golden SA et al. (2016b) Basal forebrain projections to the lateral habenula modulate aggression reward. *Nature* 534:688–692.
- Gomez JL, Bonaventura J, Lesniak W, Mathews WB, Sysa-Shah P, Rodriguez LA, Ellis RJ, Richie CT, Harvey BK, Dannals RF, Pomper MG, Bonci A, Michaelides M (2017) Chemogenetics revealed: DREADD occupancy and activation via converted clozapine. *Science* 357:503–507.
- Gonçalves L, Seigo C, Metzger M (2012) Differential projections from the lateral habenula to the rostromedial tegmental nucleus and ventral tegmental area in the rat. *The Journal of Comparative Neurology* 520:1278–1300.

REFERENCES

- Goni J, van den Heuvel MP, Avena-Koenigsberger A, Velez de Mendizabal N, Betzel RF, Griffa A, Hagmann P, Corominas-Murtra B, Thiran J-P, Sporns O (2014) Resting-brain functional connectivity predicted by analytic measures of network communication. *Proceedings of the National Academy of Sciences* 111:833–838.
- González-Pardo H, Conejo NM, Lana G, Arias JL (2012a) Different brain networks underlying the acquisition and expression of contextual fear conditioning: a metabolic mapping study. *Neuroscience* 202:234–242.
- González-Pardo H, Conejo NM, Lana G, Arias JL (2012b) Different brain networks underlying the acquisition and expression of contextual fear conditioning: a metabolic mapping study. *Neuroscience* 202:234–242.
- Goode TD, Acca GM, Maren S (2020) Threat imminence dictates the role of the bed nucleus of the stria terminalis in contextual fear. *Neurobiol Learn Mem* 167:107116.
- Görlich A, Antolin-Fontes B, Ables JL, Frahm S, Slimak MA, Dougherty JD, Ibañez-Tallon I (2013a) Reexposure to nicotine during withdrawal increases the pacemaking activity of cholinergic habenular neurons. *Proc Natl Acad Sci U S A* 110:17077–17082.
- Görlich A, Antolin-Fontes B, Ables JL, Frahm S, Slimak MA, Dougherty JD, Ibañez-Tallon I (2013b) Reexposure to nicotine during withdrawal increases the pacemaking activity of cholinergic habenular neurons. *Proc Natl Acad Sci U S A* 110:17077–17082.
- Goutagny R, Loureiro M, Jackson J, Chaumont J, Williams S, Isope P, Kelche C, Cassel J-C, Lecourtier L (2013a) Interactions between the Lateral Habenula and the Hippocampus: Implication for Spatial Memory Processes. *Neuropsychopharmacology* 38:2418–2426.
- Goutagny R, Loureiro M, Jackson J, Chaumont J, Williams S, Isope P, Kelche C, Cassel J-C, Lecourtier L (2013b) Interactions between the Lateral Habenula and the Hippocampus: Implication for Spatial Memory Processes. *Neuropsychopharmacology: official publication of the American College of Neuropsychopharmacology* 38:2418–2426.
- Grandjean J, Corcoba A, Kahn MC, Upton AL, Deneris ES, Seifritz E, Helmchen F, Mansuy IM, Mann EO, Rudin M, Saab BJ (2019) A brain-wide functional map of the serotonergic responses to acute stress and fluoxetine. *Nature Communications* 10:350.
- Grandjean J, Zerbi V, Balsters JH, Wenderoth N, Rudin M (2017) Structural Basis of Large-Scale Functional Connectivity in the Mouse. *J Neurosci* 37:8092–8101.
- Graybeal C, Kiselycznyk C, Holmes A (2012) Stress-induced impairments in prefrontal-mediated behaviors and the role of the N-methyl-D-aspartate receptor. *Neuroscience* 211:28–38.
- Graybiel AM (2008) Habits, rituals, and the evaluative brain. *Annu Rev Neurosci* 31:359–387.
- Greatrex RM, Phillipson OT (1982) Demonstration of synaptic input from prefrontal cortex to the habenula in the rat. *Brain Res* 238:192–197.
- Gregoriou GG, Gotts SJ, Zhou H, Desimone R (2009) Long-range neural coupling through synchronization with attention. In: *Progress in Brain Research* (Srinivasan N, ed), pp 35–45 Attention. Elsevier. Available at: <https://www.sciencedirect.com/science/article/pii/S0079612309176033> [Accessed May 15, 2021].
- Grillner S, von Twickel A, Robertson B (2018) The blueprint of the vertebrate forebrain - With special reference to the habenulae. *Semin Cell Dev Biol* 78:103–106.
- Grothe I, Neitzel SD, Mandon S, Kreiter AK (2012) Switching neuronal inputs by differential modulations of gamma-band phase-coherence. *J Neurosci* 32:16172–16180.
- Guilding C, Hughes ATL, Piggins HD (2010) Circadian oscillators in the epithalamus. *Neuroscience* 169:1630–1639.
- Guimarais M, Gregório A, Cruz A, Guyon N, Moita MM (2011) Time Determines the Neural Circuit Underlying Associative Fear Learning. *Front Behav Neurosci* 5 Available at: <https://www.frontiersin.org/articles/10.3389/fnbeh.2011.00089/full> [Accessed November 5, 2019].
- Hämäläinen M, Hari R, Ilmoniemi RJ, Knuutila J, Lounasmaa OV (1993) Magnetoencephalography---theory, instrumentation, and applications to noninvasive studies of the working human brain. *Rev Mod Phys* 65:413–497.
- Han F, Ding J, Shi Y (2014) Expression of amygdala mineralocorticoid receptor and glucocorticoid receptor in the single-prolonged stress rats. *BMC Neurosci* 15:77.
- Han F, Ozawa H, Matsuda K, Nishi M, Kawata M (2005) Colocalization of mineralocorticoid receptor and glucocorticoid receptor in the hippocampus and hypothalamus. *Neurosci Res* 51:371–381.

REFERENCES

- Han S, Yang SH, Kim JY, Mo S, Yang E, Song KM, Ham B-J, Mechawar N, Turecki G, Lee HW, Kim H (2017) Down-regulation of cholinergic signaling in the habenula induces anhedonia-like behavior. *Sci Rep* 7:900.
- Hartley T, Lever C, Burgess N, O'Keefe J (2014) Space in the brain: how the hippocampal formation supports spatial cognition. *Philos Trans R Soc Lond B Biol Sci* 369 Available at: <https://www.ncbi.nlm.nih.gov/pmc/articles/PMC3866435/> [Accessed April 24, 2021].
- Hashimoto S, Inoue T, Koyama T (1999) Effects of conditioned fear stress on serotonin neurotransmission and freezing behavior in rats. *Eur J Pharmacol* 378:23–30.
- Hattar S, Kumar M, Park A, Tong P, Tung J, Yau K-W, Berson DM (2006) Central projections of melanopsin-expressing retinal ganglion cells in the mouse. *J Comp Neurol* 497:326–349.
- Heidbreder CA, Groenewegen HJ (2003) The medial prefrontal cortex in the rat: evidence for a dorso-ventral distinction based upon functional and anatomical characteristics. *Neuroscience & Biobehavioral Reviews* 27:555–579.
- Heim C, Newport DJ, Mletzko T, Miller AH, Nemeroff CB (2008) The link between childhood trauma and depression: Insights from HPA axis studies in humans. *Psychoneuroendocrinology* 33:693–710.
- Helmstetter FJ, Parsons RG, Gafford GM (2008) Macromolecular synthesis, distributed synaptic plasticity, and fear conditioning. *Neurobiology of Learning and Memory* 89:324–337.
- Henckens MJAG, van der Marel K, van der Toorn A, Pillai AG, Fernández G, Dijkhuizen RM, Joëls M (2015) Stress-induced alterations in large-scale functional networks of the rodent brain. *NeuroImage* 105:312–322.
- Henke PG (1983) Unit-activity in the central amygdalar nucleus of rats in response to immobilization—stress. *Brain Research Bulletin* 10:833–837.
- Hennigan K, D'Ardenne K, McClure SM (2015) Distinct Midbrain and Habenula Pathways Are Involved in Processing Aversive Events in Humans. *Journal of Neuroscience* 35:198–208.
- Herkenham M, Nauta WJ (1979a) Efferent connections of the habenular nuclei in the rat. *J Comp Neurol* 187:19–47.
- Herkenham M, Nauta WJH (1977) Afferent connections of the habenular nuclei in the rat. A horseradish peroxidase study, with a note on the fiber-of-passage problem. *J Comp Neurol* 173:123–145.
- Herkenham M, Nauta WJH (1979b) Efferent connections of the habenular nuclei in the rat. *J Comp Neurol* 187:19–47.
- Herman JP, Cullinan WE, Morano MI, Akil H, Watson SJ (1995) Contribution of the ventral subiculum to inhibitory regulation of the hypothalamo-pituitary-adrenocortical axis. *J Neuroendocrinol* 7:475–482.
- Herman JP, Dolgas CM, Carlson SL (1998) Ventral subiculum regulates hypothalamo-pituitary-adrenocortical and behavioural responses to cognitive stressors. *Neuroscience* 86:449–459.
- Herman JP, Figueiredo H, Mueller NK, Ulrich-Lai Y, Ostrander MM, Choi DC, Cullinan WE (2003) Central mechanisms of stress integration: hierarchical circuitry controlling hypothalamo–pituitary–adrenocortical responsiveness. *Frontiers in Neuroendocrinology* 24:151–180.
- Herman JP, Guillonneau D, Dantzer R, Scatton B, Semerdjian-Rouquier L, Le Moal M (1982) Differential effects of inescapable footshocks and of stimuli previously paired with inescapable footshocks on dopamine turnover in cortical and limbic areas of the rat. *Life Sci* 30:2207–2214.
- Herman JP, Mueller NK (2006) Role of the ventral subiculum in stress integration. *Behavioural Brain Research* 174:215–224.
- Herman JP, Patel PD, Akil H, Watson SJ (1989) Localization and Regulation of Glucocorticoid and Mineralocorticoid Receptor Messenger RNAs in the Hippocampal Formation of the Rat. *Molecular Endocrinology* 3:1886–1894.
- Herman JP, Prewitt CM, Cullinan WE (1996) Neuronal circuit regulation of the hypothalamo-pituitary-adrenocortical stress axis. *Crit Rev Neurobiol* 10:371–394.
- Herry C, Ferraguti F, Singewald N, Letzkus JJ, Ehrlich I, Lüthi A (2010) Neuronal circuits of fear extinction. *European Journal of Neuroscience* 31:599–612.
- Herry C, Johansen JP (2014) Encoding of fear learning and memory in distributed neuronal circuits. *Nature Neuroscience* 17:1644–1654.
- Héту S, Luo Y, Saez I, D'Ardenne K, Lohrenz T, Montague PR (2016) Asymmetry in functional connectivity of the human habenula revealed by high-resolution cardiac-gated resting state imaging. *Hum Brain Mapp* 37:2602–2615.
- Hikosaka O (2010a) The habenula: from stress evasion to value-based decision-making. *Nature Reviews Neuroscience* 11:503–513.

REFERENCES

- Hikosaka O (2010b) The habenula: from stress evasion to value-based decision-making. *Nature reviews Neuroscience* 11:503–513.
- Hikosaka O, Sesack SR, Lecourtier L, Shepard PD (2008) Habenula: Crossroad between the Basal Ganglia and the Limbic System. *J Neurosci* 28:11825–11829.
- Hitchcock J, Davis M (1986) Lesions of the amygdala, but not of the cerebellum or red nucleus, block conditioned fear as measured with the potentiated startle paradigm. *Behav Neurosci* 100:11–22.
- Holly EN, Miczek KA (2016) Ventral tegmental area dopamine revisited: effects of acute and repeated stress. *Psychopharmacology (Berl)* 233:163–186.
- Holmes A, Wellman CL (2009) Stress-induced prefrontal reorganization and executive dysfunction in rodents. *Neurosci Biobehav Rev* 33:773–783.
- Hong S, Zhou TC, Smith M, Saleem KS, Hikosaka O (2011) Negative reward signals from the lateral habenula to dopamine neurons are mediated by rostromedial tegmental nucleus in primates. *J Neurosci* 31:11457–11471.
- Hoover WB, Vertes RP (2007) Anatomical analysis of afferent projections to the medial prefrontal cortex in the rat. *Brain Struct Funct*:31.
- Horger BA, Roth RH (1996) The role of mesoprefrontal dopamine neurons in stress. *Crit Rev Neurobiol* 10:395–418.
- Hörtnagl H, Tasan RO, Wieselthaler A, Kirchmair E, Sieghart W, Sperk G (2013) Patterns of mRNA and protein expression for 12 GABAA receptor subunits in the mouse brain. *Neuroscience* 236:345–372.
- Hu H (2019) Advances in Molecular and Circuitry Mechanisms of Depressive Disorder-A Focus on Lateral Habenula. *Adv Exp Med Biol* 1180:135–146.
- Hu H, Cui Y, Yang Y (2020a) Circuits and functions of the lateral habenula in health and in disease. *Nat Rev Neurosci* 21:277–295.
- Hu H, Cui Y, Yang Y (2020b) Circuits and functions of the lateral habenula in health and in disease. *Nature Reviews Neuroscience* 21:277–295.
- Hubel DH (1957) Tungsten Microelectrode for Recording from Single Units. *Science* 125:549–550.
- Hudson AE (2018) Genetic Reporters of Neuronal Activity: c-Fos and G-CaMP6. *Methods Enzymol* 603:197–220.
- Hurley KM, Herbert H, Moga MM, Saper CB (1991) Efferent projections of the infralimbic cortex of the rat. *J Neurosci* 11:28.
- Hutcheon B, Yarom Y (2000) Resonance, oscillation and the intrinsic frequency preferences of neurons. *Trends in Neurosciences* 23:216–222.
- Ikemoto S (2007) Dopamine reward circuitry: Two projection systems from the ventral midbrain to the nucleus accumbens–olfactory tubercle complex. *Brain Research Reviews* 56:27–78.
- Jacinto LR, Cerqueira JJ, Sousa N (2016) Patterns of Theta Activity in Limbic Anxiety Circuit Preceding Exploratory Behavior in Approach-Avoidance Conflict. *Front Behav Neurosci* 10 Available at: <https://www.ncbi.nlm.nih.gov/pmc/articles/PMC5031779/> [Accessed January 28, 2019].
- Jacinto LR, Mata R, Novais A, Marques F, Sousa N (2017a) The habenula as a critical node in chronic stress-related anxiety. *Experimental Neurology* 289:46–54.
- Jacinto LR, Mata R, Novais A, Marques F, Sousa N (2017b) The habenula as a critical node in chronic stress-related anxiety. *Experimental Neurology* 289:46–54.
- Jackson ME, Moghaddam B (2004) Stimulus-specific plasticity of prefrontal cortex dopamine neurotransmission. *J Neurochem* 88:1327–1334.
- Jacobs BL, Azmitia EC (1992) Structure and function of the brain serotonin system. *Physiological Reviews* 72:165–229.
- Jacobson L, Sapolsky R (1991) The role of the hippocampus in feedback regulation of the hypothalamic-pituitary-adrenocortical axis. *Endocr Rev* 12:118–134.
- Jakovcevski M, Schachner M, Morellini F (2008) Individual variability in the stress response of C57BL/6J male mice correlates with trait anxiety. *Genes Brain Behav* 7:235–243.
- Janak PH, Tye KM (2015) From circuits to behaviour in the amygdala. *Nature* 517:284–292.
- Jennings JH, Sparta DR, Stamatakis AM, Ung RL, Pleil KE, Kash TL, Stuber GD (2013) Distinct extended amygdala circuits for divergent motivational states. *Nature* 496:224–228.
- Jensen O, Lisman JE (2005) Hippocampal sequence-encoding driven by a cortical multi-item working memory buffer. *Trends in Neurosciences* 28:67–72.

REFERENCES

- Jeong H, Mason SP, Barabási A-L, Oltvai ZN (2001) Lethality and centrality in protein networks. *Nature* 411:41–42.
- Jhou TC, Fields HL, Baxter MG, Saper CB, Holland PC (2009) The rostromedial tegmental nucleus (RMTg), a major GABAergic afferent to midbrain dopamine neurons, selectively encodes aversive stimuli and promotes behavioral inhibition. *Neuron* 61:786–800.
- Ji H, Shepard PD (2007a) Lateral Habenula Stimulation Inhibits Rat Midbrain Dopamine Neurons through a GABAA Receptor-Mediated Mechanism. *J Neurosci* 27:6923–6930.
- Ji H, Shepard PD (2007b) Lateral Habenula Stimulation Inhibits Rat Midbrain Dopamine Neurons through a GABAA Receptor-Mediated Mechanism. *J Neurosci* 27:6923–6930.
- Joëls M (2018a) Corticosteroids and the brain. *Journal of Endocrinology* 238:R121–R130.
- Joëls M (2018b) Corticosteroids and the brain. *J Endocrinol* 238:R121–R130.
- Joëls M, Baram TZ (2009) The neuro-symphony of stress. *Nat Rev Neurosci* 10:459–466.
- Joels M, Kloet E de (1989) Effects of glucocorticoids and norepinephrine on the excitability in the hippocampus. *Science* 245:1502–1505.
- Joëls M, Pu Z, Wiegert O, Oitzl MS, Krugers HJ (2006) Learning under stress: how does it work? *Trends in Cognitive Sciences* 10:152–158.
- Johnson EO, Kamilaris TC, Chrousos GP, Gold PW (1992) Mechanisms of stress: a dynamic overview of hormonal and behavioral homeostasis. *Neurosci Biobehav Rev* 16:115–130.
- Jones KR, Myers B, Herman JP (2011) Stimulation of the Prelimbic Cortex Differentially Modulates Neuroendocrine Responses to Psychogenic and Systemic Stressors. *Physiol Behav* 104:266–271.
- Kajikawa Y, Schroeder CE (2011) How Local Is the Local Field Potential? *Neuron* 72:847–858.
- Kajikawa Y, Schroeder CE (2015) Generation of field potentials and modulation of their dynamics through volume integration of cortical activity. *J Neurophysiol* 113:339–351.
- Kalén P, Lindvall O, Björklund A (1989a) Electrical stimulation of the lateral habenula increases hippocampal noradrenaline release as monitored by in vivo microdialysis. *Exp Brain Res* 76:239–245.
- Kalén P, Lindvall O, Björklund A (1989b) Electrical stimulation of the lateral habenula increases hippocampal noradrenaline release as monitored by in vivo microdialysis. *Exp Brain Res* 76:239–245.
- Kalinichenko LS, Kornhuber J, Müller CP (2019) Individual differences in inflammatory and oxidative mechanisms of stress-related mood disorders. *Frontiers in Neuroendocrinology* 55:100783.
- Kalmbach DA, Anderson JR, Drake CL (2018) The impact of stress on sleep: Pathogenic sleep reactivity as a vulnerability to insomnia and circadian disorders. *J Sleep Res* 27:e12710.
- Kandel ER, Pittenger C (1999) The past, the future and the biology of memory storage. *Philos Trans R Soc Lond B Biol Sci* 354:2027–2052.
- Kant GJ, Meyerhoff JL, Jarrard LE (1984) Biochemical indices of reactivity and habituation in rats with hippocampal lesions. *Pharmacol Biochem Behav* 20:793–797.
- Kaouane N, Porte Y, Vallée M, Brayda-Bruno L, Mons N, Calandreau L, Marighetto A, Piazza PV, Desmedt A (2012) Glucocorticoids Can Induce PTSD-Like Memory Impairments in Mice. *Science* 335:1510–1513.
- Karalis N, Dejean C, Chaudun F, Khoder S, Rozeske RR, Wurtz H, Bagur S, Benchenane K, Sirota A, Courtin J, Herry C (2016) 4-Hz oscillations synchronize prefrontal–amygdala circuits during fear behavior. *Nature Neuroscience* 19:605–612.
- Kaufling J, Veinante P, Pawlowski SA, Freund-Mercier M-J, Barrot M (2009) Afferents to the GABAergic tail of the ventral tegmental area in the rat. *J Comp Neurol* 513:597–621.
- Kawakami M, Seto K, Terasawa E, Yoshida K, Miyamoto T, Sekiguchi M, Hattori Y (1968) Influence of electrical stimulation and lesion in limbic structure upon biosynthesis of adrenocorticoid in the rabbit. *Neuroendocrinology* 3:337–348.
- Kazavchinsky L, Dafna A, Einat H (2019) Individual variability in female and male mice in a test-retest protocol of the forced swim test. *Journal of Pharmacological and Toxicological Methods* 95:12–15.
- Kerr KM, Agster KL, Furtak SC, Burwell RD (2007) Functional neuroanatomy of the parahippocampal region: the lateral and medial entorhinal areas. *Hippocampus* 17:697–708.
- Kim JJ, Diamond DM (2002) The stressed hippocampus, synaptic plasticity and lost memories. *Nature Reviews Neuroscience* 3:453–462.
- Kim JJ, Fanselow MS (1992) Modality-specific retrograde amnesia of fear. *Science* 256:675–677.
- Kim JJ, Lee HJ, Welday AC, Song E, Cho J, Sharp PE, Jung MW, Blair HT (2007) Stress-induced alterations in hippocampal plasticity, place cells, and spatial memory. *Proc Natl Acad Sci U S A* 104:18297–18302.

REFERENCES

- Kim T-K, Han P-L (2016) Functional Connectivity of Basolateral Amygdala Neurons Carrying Orexin Receptors and Melanin-concentrating Hormone Receptors in Regulating Sociability and Mood-related Behaviors. *Experimental Neurobiology* 25:307.
- Kim U, Chang S-Y (2005) Dendritic morphology, local circuitry, and intrinsic electrophysiology of neurons in the rat medial and lateral habenular nuclei of the epithalamus. *J Comp Neurol* 483:236–250.
- Kim U, Lee T (2012a) Topography of descending projections from anterior insular and medial prefrontal regions to the lateral habenula of the epithalamus in the rat. *European Journal of Neuroscience* 35:1253–1269.
- Kim U, Lee T (2012b) Topography of descending projections from anterior insular and medial prefrontal regions to the lateral habenula of the epithalamus in the rat. *European Journal of Neuroscience* 35:1253–1269.
- Kimura A, Imbe H, Donishi T (2010) Efferent connections of an auditory area in the caudal insular cortex of the rat: anatomical nodes for cortical streams of auditory processing and cross-modal sensory interactions. *Neuroscience* 166:1140–1157.
- Kiss J, Csáki Á, Bokor H, Kocsis K, Kocsis B (2002) Possible glutamatergic/aspartatergic projections to the supramammillary nucleus and their origins in the rat studied by selective [3H]D-aspartate labelling and immunocytochemistry. *Neuroscience* 111:671–691.
- Klinzing JG, Niethard N, Born J (2019) Mechanisms of systems memory consolidation during sleep. *Nat Neurosci* 22:1598–1610.
- Knight DC, Cheng DT, Smith CN, Stein EA, Helmstetter FJ (2004) Neural substrates mediating human delay and trace fear conditioning. *J Neurosci* 24:218–228.
- Kobayashi Y, Sano Y, Vannoni E, Goto H, Suzuki H, Oba A, Kawasaki H, Kanba S, Lipp H-P, Murphy NP, Wolfer DP, Itohara S (2013) Genetic dissection of medial habenula-interpeduncular nucleus pathway function in mice. *Frontiers in behavioral neuroscience* 7:17.
- Koehl M, Bouyer JJ, Darnaudéry M, Le Moal M, Mayo W (2002) The effect of restraint stress on paradoxical sleep is influenced by the circadian cycle. *Brain Research* 937:45–50.
- Kohara K, Pignatelli M, Rivest AJ, Jung H-Y, Kitamura T, Suh J, Frank D, Kajikawa K, Mise N, Obata Y, Wickersham IR, Tonegawa S (2014) Cell type-specific genetic and optogenetic tools reveal hippocampal CA2 circuits. *Nature Neuroscience* 17:269–279.
- Kole MHP, Costoli T, Koolhaas JM, Fuchs E (2004) Bidirectional shift in the cornu ammonis 3 pyramidal dendritic organization following brief stress. *Neuroscience* 125:337–347.
- Kopin IJ, Eisenhofer G, Goldstein D (1988) Sympathoadrenal Medullary System and Stress. In: *Mechanisms of Physical and Emotional Stress* (Chrousos GP, Loriaux DL, Gold PW, eds), pp 11–23 *Advances in Experimental Medicine and Biology*. Boston, MA: Springer US. Available at: http://link.springer.com/10.1007/978-1-4899-2064-5_2 [Accessed April 17, 2021].
- Kotterman MA, Schaffer DV (2014) Engineering adeno-associated viruses for clinical gene therapy. *Nat Rev Genet* 15:445–451.
- Kovács KJ (1998) Invited review c-Fos as a transcription factor: a stressful (re)view from a functional map. *Neurochemistry International* 33:287–297.
- Kramis R, Vanderwolf CH, Bland BH (1975) Two types of hippocampal rhythmical slow activity in both the rabbit and the rat: Relations to behavior and effects of atropine, diethyl ether, urethane, and pentobarbital. *Experimental Neurology* 49:58–85.
- Kvetnansky R, Sabban EL, Palkovits M (2009) Catecholaminergic systems in stress: structural and molecular genetic approaches. *Physiol Rev* 89:535–606.
- Lammel S, Hetzel A, Häckel O, Jones I, Liss B, Roeper J (2008) Unique Properties of Mesoprefrontal Neurons within a Dual Mesocorticolimbic Dopamine System. *Neuron* 57:760–773.
- Lammel S, Ion DI, Roeper J, Malenka RC (2011) Projection-specific modulation of dopamine neuron synapses by aversive and rewarding stimuli. *Neuron* 70:855–862.
- Lammel S, Lim BK, Malenka RC (2014) Reward and aversion in a heterogeneous midbrain dopamine system. *Neuropharmacology* 76 Pt B:351–359.
- Lammel S, Lim BK, Ran C, Huang KW, Betley MJ, Tye KM, Deisseroth K, Malenka RC (2012a) Input-specific control of reward and aversion in the ventral tegmental area. *Nature* 491:212–217.
- Lammel S, Lim BK, Ran C, Huang KW, Betley MJ, Tye KM, Deisseroth K, Malenka RC (2012b) Input-specific control of reward and aversion in the ventral tegmental area. *Nature* 491:212–217.
- Langer N, Pedroni A, Jäncke L (2013) The problem of thresholding in small-world network analysis. *PLoS One* 8:e53199.

REFERENCES

- Laubach M, Amarante LM, Swanson K, White SR (2018) What, If Anything, Is Rodent Prefrontal Cortex? *eNeuro* 5 Available at: <https://www.eneuro.org/content/5/5/ENEURO.0315-18.2018> [Accessed April 20, 2021].
- Laventure S, Benchenane K (2020) Validating the theoretical bases of sleep reactivation during sharp-wave ripples and their association with emotional valence. *Hippocampus* 30:19–27.
- Lecca S, Namboodiri VMK, Restivo L, Gervasi N, Pillolla G, Stuber GD, Mameli M (2020) Heterogeneous Habenular Neuronal Ensembles during Selection of Defensive Behaviors. *Cell Rep* 31:107752.
- Lecca S, Trusel M, Mameli M (2017) Footshock-induced plasticity of GABAB signalling in the lateral habenula requires dopamine and glucocorticoid receptors. *Synapse* 71.
- Lecourtier L, Alicia D, Moghaddam B (2008) Differential tonic influence of lateral habenula on prefrontal cortex and nucleus accumbens dopamine release. *European Journal of Neuroscience* 27:1755–1762.
- Lecourtier L, Kelly PH (2007a) A conductor hidden in the orchestra? Role of the habenular complex in monoamine transmission and cognition. *Neuroscience & Biobehavioral Reviews* 31:658–672.
- Lecourtier L, Kelly PH (2007b) A conductor hidden in the orchestra? Role of the habenular complex in monoamine transmission and cognition. *Neuroscience and Biobehavioral Reviews* 31:658–672.
- LeDoux J (2003) The emotional brain, fear, and the amygdala. *Cell Mol Neurobiol* 23:727–738.
- LeDoux J (2012) Rethinking the Emotional Brain. *Neuron* 73:653–676.
- LeDoux JE (2000) Emotion circuits in the brain. *Annu Rev Neurosci* 23:155–184.
- Lee E-H, Han P-L (2019) Reciprocal interactions across and within multiple levels of monoamine and cortico-limbic systems in stress-induced depression: A systematic review. *Neuroscience & Biobehavioral Reviews* 101:13–31.
- Lehner M, Taracha E, Skórzewska A, Wisłowska A, Zienowicz M, Maciejak P, Szyndler J, Bidziński A, Płażnik A (2004) Sensitivity to pain and c-Fos expression in brain structures in rats. *Neuroscience Letters* 370:74–79.
- Li B, Piriz J, Mirrione M, Chung C, Proulx CD, Schulz D, Henn F, Malinow R (2011) Synaptic potentiation onto habenula neurons in learned helplessness model of depression. *Nature* 470:535–539.
- Li J, Yang S, Liu X, Han Y, Li Y, Feng J, Zhao H (2019) Hypoactivity of the lateral habenula contributes to negative symptoms and cognitive dysfunction of schizophrenia in rats. *Exp Neurol* 318:165–173.
- Li Y-Q, Takada M, Mizuno N (1993a) Demonstration of habenular neurons which receive afferent fibers from the nucleus accumbens and send their axons to the midbrain periaqueductal gray. *Neuroscience Letters* 158:55–58.
- Li Y-Q, Takada M, Shinonaga Y, Mizuno N (1993b) The sites of origin of dopaminergic afferent fibers to the lateral habenular nucleus in the rat. *J Comp Neurol* 333:118–133.
- Liang F, Hatanaka Y, Saito H, Yamamori T, Hashikawa T (2000) Differential expression of gamma-aminobutyric acid type B receptor-1a and -1b mRNA variants in GABA and non-GABAergic neurons of the rat brain. *J Comp Neurol* 416:475–495.
- Likhtik E, Johansen JP (2019) Neuromodulation in circuits of aversive emotional learning. *Nat Neurosci* 22:1586–1597.
- Likhtik E, Stujenske JM, Topiwala MA, Harris AZ, Gordon JA (2014) Prefrontal entrainment of amygdala activity signals safety in learned fear and innate anxiety. *Nature Neuroscience* 17:106–113.
- Lindén H, Pettersen KH, Einevoll GT (2010) Intrinsic dendritic filtering gives low-pass power spectra of local field potentials. *J Comput Neurosci* 29:423–444.
- Ling TJ, Forster GL, Watt MJ, Korzan WJ, Renner KJ, Summers CH (2009) Social status differentiates rapid neuroendocrine responses to restraint stress. *Physiology & Behavior* 96:218–232.
- Linke R, Braune G, Schwegler H (2000) Differential projection of the posterior paralaminar thalamic nuclei to the amygdaloid complex in the rat. *Exp Brain Res* 134:520–532.
- Lisoprawski A, Herve D, Blanc G, Glowinski J, Tassin JP (1980) Selective activation of the mesocortico-frontal dopaminergic neurons induced by lesion of the habenula in the rat. *Brain Res* 183:229–234.
- Liu T-Y, Watson BO (2020) Patterned activation of action potential patterns during offline states in the neocortex: replay and non-replay. *Philos Trans R Soc Lond B Biol Sci* 375:20190233.
- Liu X, Betzenhauser MJ, Reiken S, Meli AC, Xie W, Chen B-X, Arancio O, Marks AR (2012) Role of Leaky Neuronal Ryanodine Receptors in Stress- Induced Cognitive Dysfunction. *Cell* 150:1055–1067.
- Llinas RR (1988) The intrinsic electrophysiological properties of mammalian neurons: insights into central nervous system function. *Science* 242:1654–1664.

REFERENCES

- Llorens-Martín M, Blazquez-Llorca L, Benavides-Piccione R, Rabano A, Hernandez F, Avila J, DeFelipe J (2014) Selective alterations of neurons and circuits related to early memory loss in Alzheimer's disease. *Front Neuroanat* 8 Available at: <https://www.ncbi.nlm.nih.gov/pmc/articles/PMC4034155/> [Accessed April 24, 2021].
- Logothetis NK, Wandell BA (2004) Interpreting the BOLD signal. *Annu Rev Physiol* 66:735–769.
- Loonen AJM, Ivanova SA (2016) Circuits Regulating Pleasure and Happiness: The Evolution of the Amygdalar-Hippocampal-Habenular Connectivity in Vertebrates. *Frontiers in Neuroscience* 10 Available at: <https://www.ncbi.nlm.nih.gov/scd-rproxy.u-strasbg.fr/pmc/articles/PMC5118621/> [Accessed February 6, 2017].
- Lovick TA (1993) The periaqueductal gray-rostral medulla connection in the defence reaction: efferent pathways and descending control mechanisms. *Behav Brain Res* 58:19–25.
- Luine V, Villegas M, Martinez C, McEwen BS (1994) Repeated stress causes reversible impairments of spatial memory performance. *Brain Research* 639:167–170.
- Luine VN (1994) Steroid hormone influences on spatial memory. *Ann N Y Acad Sci* 743:201–211.
- Lupien SJ, Lepage M (2001) Stress, memory, and the hippocampus: can't live with it, can't live without it. *Behavioural Brain Research* 127:137–158.
- Lupien SJ, Maheu F, Tu M, Fiocco A, Schramek TE (2007) The effects of stress and stress hormones on human cognition: Implications for the field of brain and cognition. *Brain and Cognition* 65:209–237.
- Luque-García A, Teruel-Martí V, Martínez-Bellver S, Adell A, Cervera-Ferri A, Martínez-Ricós J (2018) Neural oscillations in the infralimbic cortex after electrical stimulation of the amygdala. Relevance to acute stress processing. *J Comp Neurol* 526:1403–1416.
- MacLaren DAA, Browne RW, Shaw JK, Krishnan Radhakrishnan S, Khare P, España RA, Clark SD (2016) Clozapine N-Oxide Administration Produces Behavioral Effects in Long-Evans Rats: Implications for Designing DREADD Experiments. *eNeuro* 3 Available at: <https://www.ncbi.nlm.nih.gov/pmc/articles/PMC5089539/> [Accessed April 7, 2018].
- MacLennan AJ, Maier SF (1983) Coping and the stress-induced potentiation of stimulant stereotypy in the rat. *Science* 219:1091–1093.
- Magalhães R, Barrière DA, Novais A, Marques F, Marques P, Cerqueira J, Sousa JC, Cachia A, Boumezbeur F, Bottlaender M, Jay TM, Mériaux S, Sousa N (2018a) The dynamics of stress: a longitudinal MRI study of rat brain structure and connectome. *Mol Psychiatry* 23:1998–2006.
- Magalhães R, Barrière DA, Novais A, Marques F, Marques P, Cerqueira J, Sousa JC, Cachia A, Boumezbeur F, Bottlaender M, Jay TM, Mériaux S, Sousa N (2018b) The dynamics of stress: a longitudinal MRI study of rat brain structure and connectome. *Molecular Psychiatry* 23:1998–2006.
- Mahar I, Bambico FR, Mechawar N, Nobrega JN (2014) Stress, serotonin, and hippocampal neurogenesis in relation to depression and antidepressant effects. *Neurosci Biobehav Rev* 38:173–192.
- Maher M, Rego S, Asnis G (2006) Sleep disturbances in patients with post-traumatic stress disorder: epidemiology, impact and approaches to management. *CNS drugs* 20 Available at: <https://pubmed.ncbi.nlm.nih.gov/16800716/> [Accessed June 3, 2021].
- Manvich DF, Webster KA, Foster SL, Farrell MS, Ritchie JC, Porter JH, Weinschenker D (2018) The DREADD agonist clozapine N-oxide (CNO) is reverse-metabolized to clozapine and produces clozapine-like interoceptive stimulus effects in rats and mice. *Sci Rep* 8 Available at: <https://www.ncbi.nlm.nih.gov/pmc/articles/PMC5832819/> [Accessed April 9, 2018].
- Marchand AR, Luck D, DiScala G (2003) Evaluation of an improved automated analysis of freezing behaviour in rats and its use in trace fear conditioning. *Journal of Neuroscience Methods* 126:145–153.
- Maren S, Fanselow MS (1996) The Amygdala and Fear Conditioning: Has the Nut Been Cracked? *Neuron* 16:237–240.
- Maren S, Phan KL, Liberzon I (2013) The contextual brain: implications for fear conditioning, extinction and psychopathology. *Nature Reviews Neuroscience* 14:417–428.
- Margolis EB, Lock H, Hjelmstad GO, Fields HL (2006) The ventral tegmental area revisited: is there an electrophysiological marker for dopaminergic neurons? *J Physiol* 577:907–924.
- Margolis EB, Mitchell JM, Ishikawa J, Hjelmstad GO, Fields HL (2008) Midbrain Dopamine Neurons: Projection Target Determines Action Potential Duration and Dopamine D2 Receptor Inhibition. *J Neurosci* 28:8908–8913.
- Maroteaux M, Mamelì M (2012) Cocaine Evokes Projection-Specific Synaptic Plasticity of Lateral Habenula Neurons. *J Neurosci* 32:12641–12646.

REFERENCES

- Martin EI, Ressler KJ, Binder E, Nemeroff CB (2009) The neurobiology of anxiety disorders: brain imaging, genetics, and psychoneuroendocrinology. *Psychiatr Clin North Am* 32:549–575.
- Martin SJ, Grimwood PD, Morris RG (2000) Synaptic plasticity and memory: an evaluation of the hypothesis. *Annu Rev Neurosci* 23:649–711.
- Mathis A, Mamidanna P, Abe T, Cury KM, Murthy VN, Mathis MW, Bethge M (2018a) Markerless tracking of user-defined features with deep learning. arXiv:1804.03142 [cs, q-bio, stat] Available at: <http://arxiv.org/abs/1804.03142> [Accessed August 24, 2020].
- Mathis A, Mamidanna P, Cury KM, Abe T, Murthy VN, Mathis MW, Bethge M (2018b) DeepLabCut: markerless pose estimation of user-defined body parts with deep learning. *Nature Neuroscience* 21:1281–1289.
- Mathis V, Barbelivien A, Majchrzak M, Mathis C, Cassel J-C, Lecourtier L (2016) The Lateral Habenula as a Relay of Cortical Information to Process Working Memory. *Cerebral Cortex*:1–11.
- Mathis V, Cosquer B, Avallone M, Cassel J-C, Lecourtier L (2015) Excitatory Transmission to the Lateral Habenula Is Critical for Encoding and Retrieval of Spatial Memory. *Neuropsychopharmacology* : official publication of the American College of Neuropsychopharmacology 40:2843–2851.
- Mathis V, Cosquer B, Barbelivien A, Herbeaux K, Bothorel B, Sage-Ciocca D, Poirel V-J, Mathis C, Lecourtier L (2018c) The lateral habenula interacts with the hypothalamo-pituitary adrenal axis response upon stressful cognitive demand in rats. *Behavioural Brain Research* 341:63–70.
- Mathis V, Cosquer B, Barbelivien A, Herbeaux K, Bothorel B, Sage-Ciocca D, Poirel V-J, Mathis C, Lecourtier L (2018d) The lateral habenula interacts with the hypothalamo-pituitary adrenal axis response upon stressful cognitive demand in rats. *Behavioural Brain Research* 341:63–70.
- Mathis V, Lecourtier L (2017) Role of the lateral habenula in memory through online processing of information. *Pharmacology Biochemistry and Behavior* 162:69–78.
- Matsumoto M, Hikosaka O (2007) Lateral habenula as a source of negative reward signals in dopamine neurons. *Nature* 447:1111–1115.
- Matsumoto M, Hikosaka O (2009a) Two types of dopamine neuron distinctly convey positive and negative motivational signals. *Nature* 459:837–841.
- Matsumoto M, Hikosaka O (2009b) Representation of negative motivational value in the primate lateral habenula. *Nature Neuroscience* 12:77–84.
- Matthews-Felton T, Corodimas KP, Rosenblatt JS, Morrell JI (1995) Lateral habenula neurons are necessary for the hormonal onset of maternal behavior and for the display of postpartum estrus in naturally parturient female rats. *Behav Neurosci* 109:1172–1188.
- Matthews-Felton T, Linton L, Rosenblatt JS, Morrell JI (1998) Intact neurons of the lateral habenular nucleus are necessary for the nonhormonal, pup-mediated display of maternal behavior in sensitized virgin female rats. *Behav Neurosci* 112:1458–1465.
- McCall JG, Al-Hasani R, Siuda ER, Hong DY, Norris AJ, Ford CP, Bruchas MR (2015) CRH Engagement of the Locus Coeruleus Noradrenergic System Mediates Stress-Induced Anxiety. *Neuron* 87:605–620.
- McDonald AJ, Shammah-Lagnado SJ, Shi C, Davis M (1999) Cortical afferents to the extended amygdala. *Ann N Y Acad Sci* 877:309–338.
- McEwen BS (2007) Physiology and Neurobiology of Stress and Adaptation: Central Role of the Brain. *Physiological Reviews* 87:873–904.
- McEwen BS, Bowles NP, Gray JD, Hill MN, Hunter RG, Karatsoreos IN, Nasca C (2015) Mechanisms of stress in the brain. *Nature Neuroscience* 18:1353–1363.
- McEwen BS, Weiss JM, Schwartz LS (1968) Selective Retention of Corticosterone by Limbic Structures in Rat Brain. *Nature* 220:911–912.
- McEwen C (1968) Early synovectomy in the treatment of rheumatoid arthritis. *N Engl J Med* 279:420–422.
- McGarry LM, Carter AG (2016) Inhibitory Gating of Basolateral Amygdala Inputs to the Prefrontal Cortex. *J Neurosci* 36:9391–9406.
- McGaugh JL, Roozendaal B (2002) Role of adrenal stress hormones in forming lasting memories in the brain. *Current Opinion in Neurobiology* 12:205–210.
- McGregor A, Herbert J (1992) Differential effects of excitotoxic basolateral and corticomедial lesions of the amygdala on the behavioural and endocrine responses to either sexual or aggression-promoting stimuli in the male rat. *Brain Res* 574:9–20.
- McIntosh AR (1999) Mapping cognition to the brain through neural interactions. *Memory* 7:523–548.

REFERENCES

- McLean S, Skirboll LR, Perti CB (1983) Opiatergic projection from the bed nucleus to the habenula: demonstration by a novel radioimmunohistochemical method. *Brain Research* 278:255–257.
- Mendoza J (2017) Circadian neurons in the lateral habenula: Clocking motivated behaviors. *Pharmacol Biochem Behav* 162:55–61.
- Mendoza J, Vanotti G (2019) Circadian neurogenetics of mood disorders. *Cell Tissue Res* 377:81–94.
- Menon V, Uddin LQ (2010) Saliency, switching, attention and control: a network model of insula function. *Brain Struct Funct* 214:655–667.
- Mesulam MM (1998) From sensation to cognition. *Brain* 121 (Pt 6):1013–1052.
- Metzger M, Bueno D, Lima LB (2017) The lateral habenula and the serotonergic system. *Pharmacology Biochemistry and Behavior* 162:22–28.
- Metzger M, Souza R, Lima LB, Bueno D, Gonçalves L, Segó C, Donato J, Shammah-Lagnado SJ (2019) Habenular connections with the dopaminergic and serotonergic system and their role in stress-related psychiatric disorders. *Eur J Neurosci*.
- Metzger M, Souza R, Lima LB, Bueno D, Gonçalves L, Segó C, Donato J, Shammah-Lagnado SJ (2021) Habenular connections with the dopaminergic and serotonergic system and their role in stress-related psychiatric disorders. *Eur J Neurosci* 53:65–88.
- Meye FJ, Lecca S, Valentinova K, Mameli M (2013) Synaptic and cellular profile of neurons in the lateral habenula. *Front Hum Neurosci* 7:860.
- Miklós IH, Kovács KJ (2002) GABAergic innervation of corticotropin-releasing hormone (CRH)-secreting parvocellular neurons and its plasticity as demonstrated by quantitative immunoelectron microscopy. *Neuroscience* 113:581–592.
- Ming Q, Ma H, Li J, Yang F, Li J, Liang J, Li D, Lin W (2020) Changes in autonomic nervous function and influencing factors in a rat insular cortex electrical kindling model. *Neurosci Lett* 721:134782.
- Mirrione MM, Schulz D, Lapidus KAB, Zhang S, Goodman W, Henn FA (2014) Increased metabolic activity in the septum and habenula during stress is linked to subsequent expression of learned helplessness behavior. *Frontiers in Human Neuroscience* 8 Available at: <http://journal.frontiersin.org/article/10.3389/fnhum.2014.00029/abstract> [Accessed April 16, 2018].
- Mitchell SJ, Rawlins JN, Steward O, Olton DS (1982) Medial septal area lesions disrupt theta rhythm and cholinergic staining in medial entorhinal cortex and produce impaired radial arm maze behavior in rats. *J Neurosci* 2:292–302.
- Mitra R, Jadhav S, McEwen BS, Vyas A, Chattarji S (2005) Stress duration modulates the spatiotemporal patterns of spine formation in the basolateral amygdala. *Proc Natl Acad Sci U S A* 102:9371–9376.
- Moberly AH, Schreck M, Bhattarai JP, Zweifel LS, Luo W, Ma M (2018) Olfactory inputs modulate respiration-related rhythmic activity in the prefrontal cortex and freezing behavior. *Nature Communications* 9:1528.
- Modianos DT, Hitt JC, Flexman J (1974) Habenular lesions produce decrements in feminine, but not masculine, sexual behavior in rats. *Behav Biol* 10:75–87.
- Moghaddam B (2002) Stress activation of glutamate neurotransmission in the prefrontal cortex: implications for dopamine-associated psychiatric disorders. *Biol Psychiatry* 51:775–787.
- Morgan MA, LeDoux JE (1995) Differential contribution of dorsal and ventral medial prefrontal cortex to the acquisition and extinction of conditioned fear in rats. *Behav Neurosci* 109:681–688.
- Morgan MA, Romanski LM, LeDoux JE (1993) Extinction of emotional learning: Contribution of medial prefrontal cortex. *Neuroscience Letters* 163:109–113.
- Morrow BA, Elsworth JD, Lee EJ, Roth RH (2000) Divergent effects of putative anxiolytics on stress-induced fos expression in the mesoprefrontal system of the rat. *Synapse* 36:143–154.
- Moser PC (1989) An evaluation of the elevated plus-maze test using the novel anxiolytic buspirone. *Psychopharmacology (Berl)* 99:48–53.
- Murlidharan G, Samulski RJ, Asokan A (2014) Biology of adeno-associated viral vectors in the central nervous system. *Front Mol Neurosci* 7:76.
- Murphy CA, DiCamillo AM, Haun F, Murray M (1996a) Lesion of the habenular efferent pathway produces anxiety and locomotor hyperactivity in rats: a comparison of the effects of neonatal and adult lesions. *Behavioural Brain Research* 81:43–52.
- Murphy CA, DiCamillo AM, Haun F, Murray M (1996b) Lesion of the habenular efferent pathway produces anxiety and locomotor hyperactivity in rats: a comparison of the effects of neonatal and adult lesions. *Behavioural Brain Research* 81:43–52.

REFERENCES

- Musselman DL, Anderson G, Porter M, Nemeroff CB (1997) The hypothalamic-pituitary-adrenocortical system. In: *Women's Health*, 1st ed. (Casper RC, ed), pp 109–121. Cambridge University Press. Available at: https://www.cambridge.org/core/product/identifier/CBO9780511570087A011/type/book_part [Accessed April 17, 2021].
- Myers B (2017) Corticolimbic regulation of cardiovascular responses to stress. *Physiology & Behavior* 172:49–59.
- Nagai Y et al. (2020) Deschloroclozapine, a potent and selective chemogenetic actuator enables rapid neuronal and behavioral modulations in mice and monkeys. *Nat Neurosci* 23:1157–1167.
- Nakane H, Shimizu N, Hori T (1994) Stress-induced norepinephrine release in the rat prefrontal cortex measured by microdialysis. *Am J Physiol* 267:R1559–1566.
- Namboodiri VMK, Rodriguez-Romaguera J, Stuber GD (2016) The habenula. *Current Biology* 26:R873–R877.
- Nath T, Mathis A, Chen AC, Patel A, Bethge M, Mathis MW (2019) Using DeepLabCut for 3D markerless pose estimation across species and behaviors. *Nat Protoc* 14:2152–2176.
- Nemeroff CB (2016) *Paradise Lost: The Neurobiological and Clinical Consequences of Child Abuse and Neglect*. *Neuron* 89:892–909.
- Neske GT (2015) The Slow Oscillation in Cortical and Thalamic Networks: Mechanisms and Functions. *Front Neural Circuits* 9:88.
- Neugebauer NM, Einstein EB, Lopez MB, McClure-Begley TD, Mineur YS, Picciotto MR (2013) Morphine dependence and withdrawal induced changes in cholinergic signaling. *Pharmacol Biochem Behav* 109:77–83.
- Nicholson C, Freeman JA (1975) Theory of current source-density analysis and determination of conductivity tensor for anuran cerebellum. *J Neurophysiol* 38:356–368.
- Niedermeyer E, Lopes da Silva FH (2005) *Electroencephalography: basic principles, clinical applications, and related fields*. Philadelphia: Lippincott Williams & Wilkins.
- Nilsson OG, Kalén P, Rosengren E, Björklund A (1990) Acetylcholine release in the rat hippocampus as studied by microdialysis is dependent on axonal impulse flow and increases during behavioural activation. *Neuroscience* 36:325–338.
- Noh SJ, Kang D-W, Yoo SB, Lee JY, Kim JY, Kim B-T, Lee J-H, Jahng JW (2012) Stress-responsive hypothalamic-nucleus accumbens regulation may vary depending on stressors. *Indian J Exp Biol* 50:447–454.
- Nuno-Perez A, Tchenio A, Mameli M, Lecca S (2018) Lateral Habenula Gone Awry in Depression: Bridging Cellular Adaptations With Therapeutics. *Front Neurosci* 12:485.
- Nuno-Perez A, Trusel M, Lalive AL, Congiu M, Gastaldo D, Tchenio A, Lecca S, Soiza-Reilly M, Bagni C, Mameli M (2021) Stress undermines reward-guided cognitive performance through synaptic depression in the lateral habenula. *Neuron* 109:947–956.e5.
- Oitzl MS, de Kloet ER (1992) Selective corticosteroid antagonists modulate specific aspects of spatial orientation learning. *Behav Neurosci* 106:62–71.
- O'Keefe J, Dostrovsky J (1971) The hippocampus as a spatial map. Preliminary evidence from unit activity in the freely-moving rat. *Brain Res* 34:171–175.
- O'Mahony CM, Sweeney FF, Daly E, Dinan TG, Cryan JF (2010) Restraint stress-induced brain activation patterns in two strains of mice differing in their anxiety behaviour. *Behav Brain Res* 213:148–154.
- Omelchenko N, Bell R, Sesack SR (2009) Lateral habenula projections to dopamine and GABA neurons in the rat ventral tegmental area: Habenula input to VTA cell populations. *European Journal of Neuroscience* 30:1239–1250.
- Ootsuka Y, Mohammed M (2015) Activation of the habenula complex evokes autonomic physiological responses similar to those associated with emotional stress. *Physiological Reports* 3:e12297.
- Ootsuka Y, Mohammed M, Blessing WW (2017) Lateral habenula regulation of emotional hyperthermia: mediation via the medullary raphe. *Sci Rep* 7:4102.
- Orsini CA, Kim JH, Knapska E, Maren S (2011) Hippocampal and Prefrontal Projections to the Basal Amygdala Mediate Contextual Regulation of Fear after Extinction. *J Neurosci* 31:17269–17277.
- Otsu Y, Lecca S, Pietrajtis K, Rousseau CV, Marcaggi P, Dugué GP, Mailhes-Hamon C, Mameli M, Diana MA (2018) Functional Principles of Posterior Septal Inputs to the Medial Habenula. *Cell Rep* 22:693–705.

REFERENCES

- Padilla-Coreano N, Do-Monte FH, Quirk GJ (2012) A time-dependent role of midline thalamic nuclei in the retrieval of fear memory. *Neuropharmacology* 62:457–463.
- Paré D, Quirk GJ, Ledoux JE (2004) New vistas on amygdala networks in conditioned fear. *J Neurophysiol* 92:1–9.
- Paré WP, Glavin GB (1986) Restraint stress in biomedical research: a review. *Neurosci Biobehav Rev* 10:339–370.
- Parent A, Gravel S, Boucher R (1981) The origin of forebrain afferents to the habenula in rat, cat and monkey. *Brain Res Bull* 6:23–38.
- Park H, Rhee J, Park K, Han J-S, Malinow R, Chung C (2017) Exposure to Stressors Facilitates Long-Term Synaptic Potentiation in the Lateral Habenula. *The Journal of Neuroscience* 37:6021–6030.
- Park H-J, Friston K (2013) Structural and Functional Brain Networks: From Connections to Cognition. *Science* 342 Available at: <https://science.sciencemag.org/content/342/6158/1238411> [Accessed May 13, 2021].
- Pasquier DA, Kemper TL, Forbes WB, Morgane PJ (1977) Dorsal raphe, substantia nigra and locus coeruleus: interconnections with each other and the neostriatum. *Brain Res Bull* 2:323–339.
- Pavlidis C, Ogawa S, Kimura A, McEwen BS (1996) Role of adrenal steroid mineralocorticoid and glucocorticoid receptors in long-term potentiation in the CA1 field of hippocampal slices. *Brain Res* 738:229–235.
- Pavlov IP (1927) Conditioned reflexes: An investigation of the physiological activity of the cerebral cortex. Available at: <http://www.annualofneurosciences.org/journal/index.php/annual/article/view/246>.
- Pawlyk AC, Morrison AR, Ross RJ, Brennan FX (2008) Stress-induced changes in sleep in rodents: Models and mechanisms. *Neuroscience & Biobehavioral Reviews* 32:99–117.
- Paxinos G, Watson C (2007) *The rat brain in stereotaxic coordinates*, 6. ed. Amsterdam: Elsevier, Academic Press.
- Penzo MA, Robert V, Tucciarone J, De Bundel D, Wang M, Van Aelst L, Darvas M, Parada LF, Palmiter RD, He M, Huang ZJ, Li B (2015) The paraventricular thalamus controls a central amygdala fear circuit. *Nature* 519:455–459.
- Petsche H, Stumpf C (1962) The origin of theta-rhythm in the rabbit hippocampus. *Wien Klin Wochenschr* 74:696–700.
- Pfaus JG, Kleopoulos SP, Mobbs CV, Gibbs RB, Pfaff DW (1993) Sexual stimulation activates c-fos within estrogen-concentrating regions of the female rat forebrain. *Brain Res* 624:253–267.
- Pfurtscheller G, Aranibar A (1977) Event-related cortical desynchronization detected by power measurements of scalp EEG. *Electroencephalogr Clin Neurophysiol* 42:817–826.
- Phelps EA, O'Connor KJ, Gatenby JC, Gore JC, Grillon C, Davis M (2001) Activation of the left amygdala to a cognitive representation of fear. *Nature Neuroscience* 4:437–441.
- Philbert J, Pichat P, Beeské S, Decobert M, Belzung C, Griebel G (2011) Acute inescapable stress exposure induces long-term sleep disturbances and avoidance behavior: a mouse model of post-traumatic stress disorder (PTSD). *Behav Brain Res* 221:149–154.
- Phillips RG, LeDoux JE (1992) Differential contribution of amygdala and hippocampus to cued and contextual fear conditioning. *Behav Neurosci* 106:274–285.
- Piedra J, Ontiveros M, Miravet S, Penalva C, Monfar M, Chillón M (2015) Development of a Rapid, Robust, and Universal PicoGreen-Based Method to Titer Adeno-Associated Vectors. *Human Gene Therapy Methods* 26:35–42.
- Pirker S, Schwarzer C, Wieselthaler A, Sieghart W, Sperk G (2000) GABA_A receptors: immunocytochemical distribution of 13 subunits in the adult rat brain. *Neuroscience* 101:815–850.
- Pobbe RLH, Zangrossi H (2010) The lateral habenula regulates defensive behaviors through changes in 5-HT-mediated neurotransmission in the dorsal periaqueductal gray matter. *Neuroscience Letters* 479:87–91.
- Popa D, Duvarci S, Popescu AT, Léna C, Paré D (2010) Coherent amygdalocortical theta promotes fear memory consolidation during paradoxical sleep. *Proc Natl Acad Sci U S A* 107:6516–6519.
- Prewitt CMF, Herman JP (1998) Anatomical interactions between the central amygdaloid nucleus and the hypothalamic paraventricular nucleus of the rat: a dual tract-tracing analysis. *Journal of Chemical Neuroanatomy* 15:173–186.
- Proulx CD, Hikosaka O, Malinow R (2014a) Reward processing by the lateral habenula in normal and depressive behaviors. *Nature Neuroscience* 17:1146–1152.

REFERENCES

- Proulx CD, Hikosaka O, Malinow R (2014b) Reward processing by the lateral habenula in normal and depressive behaviors. *Nat Neurosci* 17:1146–1152.
- Puglisi-Allegra S, Andolina D (2015) Serotonin and stress coping. *Behavioural Brain Research* 277:58–67.
- Purvis EM, Klein AK, Ettenberg A (2018) Lateral habenular norepinephrine contributes to states of arousal and anxiety in male rats. *Behavioural Brain Research* 347:108–115.
- Qu T, Dong K, Sugioka K, Yamadori T (1996) Demonstration of direct input from the retina to the lateral habenular nucleus in the albino rat. *Brain Res* 709:251–258.
- Quaedflieg CWEM, Schneider TR, Daume J, Engel AK, Schwabe L (2020) Stress Impairs Intentional Memory Control through Altered Theta Oscillations in Lateral Parietal Cortex. *J Neurosci* 40:7739–7748.
- Quinn JJ, Wied HM, Ma QD, Tinsley MR, Fanselow MS (2008) Dorsal hippocampus involvement in delay fear conditioning depends upon the strength of the tone-footshock association. *Hippocampus* 18:640–654.
- Quirarte GL, Roozendaal B, McGaugh JL (1997) Glucocorticoid enhancement of memory storage involves noradrenergic activation in the basolateral amygdala. *Proc Natl Acad Sci U S A* 94:14048–14053.
- Quirk GJ, Garcia R, González-Lima F (2006) Prefrontal Mechanisms in Extinction of Conditioned Fear. *Biological Psychiatry* 60:337–343.
- Radley J, Morilak D, Viau V, Campeau S (2015) Chronic stress and brain plasticity: Mechanisms underlying adaptive and maladaptive changes and implications for stress-related CNS disorders. *Neurosci Biobehav Rev* 58:79–91.
- Radley JJ, Arias CM, Sawchenko PE (2006) Regional Differentiation of the Medial Prefrontal Cortex in Regulating Adaptive Responses to Acute Emotional Stress. *J Neurosci* 26:12967–12976.
- Rajakumar N, Elisevich K, Flumerfelt BA (1993) Compartmental origin of the striato-entopeduncular projection in the rat. *J Comp Neurol* 331:286–296.
- Ranft K, Dobrowolny H, Krell D, Bielau H, Bogerts B, Bernstein H-G (2010) Evidence for structural abnormalities of the human habenular complex in affective disorders but not in schizophrenia. *Psychol Med* 40:557–567.
- Raper J, Morrison RD, Daniels JS, Howell L, Bachevalier J, Wichmann T, Galvan A (2017) Metabolism and Distribution of Clozapine-N-oxide: Implications for Nonhuman Primate Chemogenetics. *ACS Chem Neurosci* 8:1570–1576.
- Reijneveld JC, Ponten SC, Berendse HW, Stam CJ (2007) The application of graph theoretical analysis to complex networks in the brain. *Clinical Neurophysiology* 118:2317–2331.
- Reimsnider S, Manfredsson FP, Muzyczka N, Mandel RJ (2007) Time Course of Transgene Expression After Intrastratial Pseudotyped rAAV2/1, rAAV2/2, rAAV2/5, and rAAV2/8 Transduction in the Rat. *Molecular Therapy* 15:1504–1511.
- Reisine TD, Soubrié P, Artaud F, Glowinski J (1982) Involvement of lateral habenula-dorsal raphe neurons in the differential regulation of striatal and nigral serotonergic transmission cats. *J Neurosci* 2:1062–1071.
- Reul JM, de Kloet ER (1985) Two receptor systems for corticosterone in rat brain: microdistribution and differential occupation. *Endocrinology* 117:2505–2511.
- Robertson GS, Fibiger HC (1992) Neuroleptics increase C-FOS expression in the forebrain: Contrasting effects of haloperidol and clozapine. *Neuroscience* 46:315–328.
- Rodriguez P, Levy WB (2001) A model of hippocampal activity in trace conditioning: where's the trace? *Behav Neurosci* 115:1224–1238.
- Roelfsema PR, Engel AK, König P, Singer W (1996) The role of neuronal synchronization in response selection: a biologically plausible theory of structured representations in the visual cortex. *J Cogn Neurosci* 8:603–625.
- Roelfsema PR, Engel AK, König P, Singer W (1997) Visuomotor integration is associated with zero time-lag synchronization among cortical areas. *Nature* 385:157–161.
- Rogers-Carter MM, Varela JA, Gibbons KB, Pierce AF, McGoey MT, Ritchey M, Christianson JP (2018) Insular cortex mediates approach and avoidance responses to social affective stimuli. *Nat Neurosci* 21:404–414.
- Roman E, Weininger J, Lim B, Roman M, Barry D, Tierney P, O'Hanlon E, Levins K, O'Keane V, Roddy D (2020) Untangling the dorsal diencephalic conduction system: a review of structure and function of the stria medullaris, habenula and fasciculus retroflexus. *Brain Struct Funct* 225:1437–1458.

REFERENCES

- Romanski LM, Clugnet MC, Bordi F, LeDoux JE (1993) Somatosensory and auditory convergence in the lateral nucleus of the amygdala. *Behav Neurosci* 107:444–450.
- Root DH, Hoffman AF, Good CH, Zhang S, Gigante E, Lupica CR, Morales M (2015) Norepinephrine Activates Dopamine D4 Receptors in the Rat Lateral Habenula. *J Neurosci* 35:3460–3469.
- Root DH, Mejias-Aponte CA, Qi J, Morales M (2014) Role of Glutamatergic Projections from Ventral Tegmental Area to Lateral Habenula in Aversive Conditioning. *Journal of Neuroscience* 34:13906–13910.
- Roosendaal B, McEwen BS, Chattarji S (2009) Stress, memory and the amygdala. *Nature Reviews Neuroscience* 10:423–433.
- Rosen JB, Fanselow MS, Young SL, Sitcoske M, Maren S (1998) Immediate-early gene expression in the amygdala following footshock stress and contextual fear conditioning. *Brain Res* 796:132–142.
- Roth BL (2016) DREADDs for Neuroscientists. *Neuron* 89:683–694.
- Rothschild G (2019) The transformation of multi-sensory experiences into memories during sleep. *Neurobiology of Learning and Memory* 160:58–66.
- Roux L, Buzsáki G (2015) Tasks for inhibitory interneurons in intact brain circuits. *Neuropharmacology* 88:10–23.
- Rudy JW, Barrientos RM, O'Reilly RC (2002) Hippocampal formation supports conditioning to memory of a context. *Behavioral Neuroscience* 116:530–538.
- Sá JPM de (2007) *Applied statistics: using SPSS, Statistica, MATLAB, and R*, 2nd ed. Berlin ; New York: Springer.
- Sah P, Faber ESL, Lopez De Armentia M, Power J (2003) The Amygdaloid Complex: Anatomy and Physiology. *Physiological Reviews* 83:803–834.
- Saito H, Kaba H, Sato T, Honmura A, Kawakami T, Seto K, Yamamoto H, Kawakami M (1989) Influence of electrical stimulation of the limbic structure on adrenocortical steroidogenesis in hypophysectomized rats. *Exp Clin Endocrinol* 94:387–390.
- Salazar RF, Dotson NM, Bressler SL, Gray CM (2012) Content-Specific Fronto-Parietal Synchronization During Visual Working Memory. *Science* 338:1097–1100.
- Sandi C, Loscertales M, Guaza C (1997) Experience-dependent facilitating effect of corticosterone on spatial memory formation in the water maze. *Eur J Neurosci* 9:637–642.
- Sandyk R (1992) Pineal and habenula calcification in schizophrenia. *Int J Neurosci* 67:19–30.
- Sanford LD, Yang L, Wellman LL, Liu X, Tang X (2010) Differential effects of controllable and uncontrollable footshock stress on sleep in mice. *Sleep* 33:621–630.
- Sankar V, Patrick E, Dieme R, Sanchez JC, Prasad A, Nishida T (2014) Electrode impedance analysis of chronic tungsten microwire neural implants: understanding abiotic vs. biotic contributions. *Front Neuroeng* 7 Available at: <https://www.ncbi.nlm.nih.gov/pmc/articles/PMC4021112/> [Accessed March 18, 2020].
- Sapolsky RM, Krey LC, McEwen BS (1986) The neuroendocrinology of stress and aging: the glucocorticoid cascade hypothesis. *Endocr Rev* 7:284–301.
- Sarabdjitsingh RA, Jezequel J, Pasricha N, Mikasova L, Kerkhofs A, Karst H, Groc L, Joëls M (2014) Ultradian corticosterone pulses balance glutamatergic transmission and synaptic plasticity. *Proc Natl Acad Sci U S A* 111:14265–14270.
- Sarkar S, Légrádi G, Lechan RM (2002) Intracerebroventricular administration of alpha-melanocyte stimulating hormone increases phosphorylation of CREB in TRH- and CRH-producing neurons of the hypothalamic paraventricular nucleus. *Brain Res* 945:50–59.
- Saveanu RV, Nemeroff CB (2012) Etiology of depression: genetic and environmental factors. *Psychiatr Clin North Am* 35:51–71.
- Sawchenko PE, Brown ER, Chan RK, Ericsson A, Li HY, Roland BL, Kovács KJ (1996) The paraventricular nucleus of the hypothalamus and the functional neuroanatomy of visceromotor responses to stress. *Prog Brain Res* 107:201–222.
- Schafer M, Kim J-W, Joseph J, Xu J, Frangou S, Doucet GE (2018) Imaging Habenula Volume in Schizophrenia and Bipolar Disorder. *Front Psychiatry* 9:456.
- Schotte A, Janssen PF, Megens AA, Leysen JE (1993) Occupancy of central neurotransmitter receptors by risperidone, clozapine and haloperidol, measured ex vivo by quantitative autoradiography. *Brain Res* 631:191–202.
- Schwabe L (2016) Memory under stress: from single systems to network changes. *European Journal of Neuroscience*:12.

REFERENCES

- Seggie J (1987) Differential responsivity of corticosterone and prolactin to stress following lesions of the septum or amygdala: implications for psychoneuroendocrinology. *Prog Neuropsychopharmacol Biol Psychiatry* 11:315–324.
- Sehlmeyer C, Schöning S, Zwieterlood P, Pfeleiderer B, Kircher T, Arolt V, Konrad C (2009) Human Fear Conditioning and Extinction in Neuroimaging: A Systematic Review. *PLoS One* 4 Available at: <https://www.ncbi.nlm.nih.gov/pmc/articles/PMC2692002/> [Accessed August 9, 2018].
- Selye H (1946) The general adaptation syndrome and the diseases of adaptation. *J Clin Endocrinol Metab* 6:117–230.
- Selye H (1950) Stress and the General Adaptation Syndrome. *Br Med J* 1:1383–1392.
- Selye H (1976) Stress without Distress. In: *Psychopathology of Human Adaptation* (Serban G, ed), pp 137–146. Boston, MA: Springer US. Available at: https://doi.org/10.1007/978-1-4684-2238-2_9 [Accessed June 6, 2021].
- Semba K, Fibiger HC (1992) Afferent connections of the laterodorsal and the pedunculo-pontine tegmental nuclei in the rat: A retro- and antero-grade transport and immunohistochemical study. *J Comp Neurol* 323:387–410.
- Shabel SJ, Proulx CD, Trias A, Murphy RT, Malinow R (2012a) Input to the Lateral Habenula from the Basal Ganglia Is Excitatory, Aversive, and Suppressed by Serotonin. *Neuron* 74:475–481.
- Shabel SJ, Proulx CD, Trias A, Murphy RT, Malinow R (2012b) Input to the Lateral Habenula from the Basal Ganglia Is Excitatory, Aversive, and Suppressed by Serotonin. *Neuron* 74:475–481.
- Sharvit A, Segal M, Kehat O, Stork O, Richter-Levin G (2015) Differential modulation of synaptic plasticity and local circuit activity in the dentate gyrus and CA1 regions of the rat hippocampus by corticosterone. *Stress* 18:319–327.
- Shelton L, Becerra L, Borsook D (2012) Unmasking the mysteries of the habenula in pain and analgesia. *Prog Neurobiol* 96:208–219.
- Shepard PD, Holcomb HH, Gold JM (2006) Schizophrenia in translation: the presence of absence: habenular regulation of dopamine neurons and the encoding of negative outcomes. *Schizophr Bull* 32:417–421.
- Shiba Y, Santangelo AM, Roberts AC (2016) Beyond the Medial Regions of Prefrontal Cortex in the Regulation of Fear and Anxiety. *Front Syst Neurosci* 10 Available at: <https://www.ncbi.nlm.nih.gov/pmc/articles/PMC4761915/> [Accessed April 21, 2021].
- Shumake J, Ilango A, Scheich H, Wetzel W, Ohl FW (2010) Differential Neuromodulation of Acquisition and Retrieval of Avoidance Learning by the Lateral Habenula and Ventral Tegmental Area. *J Neurosci* 30:5876–5883.
- Sierra-Mercado D, Corcoran KA, Lebrón-Milad K, Quirk GJ (2006) Inactivation of the ventromedial prefrontal cortex reduces expression of conditioned fear and impairs subsequent recall of extinction. *Eur J Neurosci* 24:1751–1758.
- Sierra-Mercado D, Padilla-Coreano N, Quirk GJ (2011) Dissociable Roles of Prelimbic and Infralimbic Cortices, Ventral Hippocampus, and Basolateral Amygdala in the Expression and Extinction of Conditioned Fear. *Neuropsychopharmacology* 36:529–538.
- Silva LR, Amitai Y, Connors BW (1991) Intrinsic oscillations of neocortex generated by layer 5 pyramidal neurons. *Science* 251:432–435.
- Singer W (1999) Neuronal Synchrony: A Versatile Code for the Definition of Relations? *Neuron* 24:49–65.
- Sirota A, Buzsáki G (2005) Interaction between neocortical and hippocampal networks via slow oscillations. *Thalamus Relat Syst* 3:245–259.
- Skaggs WE, McNaughton BL, Permenter M, Archibeque M, Vogt J, Amaral DG, Barnes CA (2007) EEG sharp waves and sparse ensemble unit activity in the macaque hippocampus. *J Neurophysiol* 98:898–910.
- Skelin I, Kilianski S, McNaughton BL (2019) Hippocampal coupling with cortical and subcortical structures in the context of memory consolidation. *Neurobiology of Learning and Memory* 160:21–31.
- Slusher MA (1966) Effects of cortisol implants in the brainstem and ventral hippocampus on diurnal corticosteroid levels. *Exp Brain Res* 1:184–194.
- Smotherman WP, Kolp LA, Coyle S, Levine S (1981) Hippocampal lesion effects on conditioned taste aversion and pituitary-adrenal activity in rats. *Behavioural Brain Research* 2:33–48.
- Song M, Jo YS, Lee Y-K, Choi J-S (2017) Lesions of the lateral habenula facilitate active avoidance learning and threat extinction. *Behavioural Brain Research* 318:12–17.

REFERENCES

- Soria-Gómez E, Busquets-Garcia A, Hu F, Mehidi A, Cannich A, Roux L, Louit I, Alonso L, Wiesner T, Georges F, Verrier D, Vincent P, Ferreira G, Luo M, Marsicano G (2015) Habenular CB1 Receptors Control the Expression of Aversive Memories. *Neuron* 88:306–313.
- Soubrié P, Reisine T, Artaud F, Glowinski J (1981) Role of the lateral habenula in modulating nigral and striatal in vivo [3H]serotonin release in the cat. *Brain Res* 222:192–197.
- Sousa N (2016) The dynamics of the stress neuromatrix. *Molecular Psychiatry* 21:302–312.
- Sporns O (2012) From simple graphs to the connectome: Networks in neuroimaging. *NeuroImage* 62:881–886.
- Sporns O (2013) Network attributes for segregation and integration in the human brain. *Current Opinion in Neurobiology* 23:162–171.
- Sporns O, Chialvo DR, Kaiser M, Hilgetag CC (2004) Organization, development and function of complex brain networks. *Trends in Cognitive Sciences* 8:418–425.
- Stam CJ, Reijneveld JC (2007) Graph theoretical analysis of complex networks in the brain. *Nonlinear Biomed Phys* 1:3.
- Stamatakis AM, Stuber GD (2012a) Activation of lateral habenula inputs to the ventral midbrain promotes behavioral avoidance. *Nature Neuroscience* 15:1105–1107.
- Stamatakis AM, Stuber GD (2012b) Activation of lateral habenula inputs to the ventral midbrain promotes behavioral avoidance. *Nature Neuroscience* 15:1105–1107.
- Sterling P, Eyer J (1988) Allostasis: A new paradigm to explain arousal pathology. In: *Handbook of life stress, cognition and health*, pp 629–649. Oxford, England: John Wiley & Sons.
- Stern WC, Johnson A, Bronzino JD, Morgane PJ (1979) Effects of electrical stimulation of the lateral habenula on single-unit activity of raphe neurons. *Experimental Neurology* 65:326–342.
- Stopper CM, Floresco SB (2014) What's better for me? Fundamental role for lateral habenula in promoting subjective decision biases. *Nat Neurosci* 17:33–35.
- Storm JF (1988) Temporal integration by a slowly inactivating K⁺ current in hippocampal neurons. *Nature* 336:379–381.
- Sullivan RM, Gratton A (1999) Lateralized Effects of Medial Prefrontal Cortex Lesions on Neuroendocrine and Autonomic Stress Responses in Rats. *J Neurosci* 19:2834–2840.
- Sullivan RM, Gratton A (2002) Prefrontal cortical regulation of hypothalamic–pituitary–adrenal function in the rat and implications for psychopathology: side matters. *Psychoneuroendocrinology* 27:99–114.
- Sullivan RM, Szechtman H (1994) Left/right nigrostriatal asymmetry in susceptibility to neurotoxic dopamine depletion with 6-hydroxydopamine in rats. *Neurosci Lett* 170:83–86.
- Sutherland RJ (1982) The dorsal diencephalic conduction system: A review of the anatomy and functions of the habenular complex. *Neuroscience & Biobehavioral Reviews* 6:1–13.
- Takehara-Nishiuchi K, McNaughton BL (2008) Spontaneous Changes of Neocortical Code for Associative Memory During Consolidation. *Science* 322:960–963.
- Takillah S, Naudé J, Didienne S, Sebban C, Decros B, Schenker E, Spedding M, Mourot A, Mariani J, Faure P (2017) Acute Stress Affects the Expression of Hippocampal Mu Oscillations in an Age-Dependent Manner. *Front Aging Neurosci* 9 Available at: <https://www.ncbi.nlm.nih.gov/pmc/articles/PMC5627040/> [Accessed May 14, 2021].
- Tanaka M, Kohno Y, Nakagawa R, Ida Y, Takeda S, Nagasaki N, Noda Y (1983) Regional characteristics of stress-induced increases in brain noradrenaline release in rats. *Pharmacol Biochem Behav* 19:543–547.
- Tang W, Jadhav SP (2018) Conducting the Neural Symphony of Memory Replay. *Neuron* 100:1016–1019.
- Tang X, Liu X, Yang L, Sanford LD (2005) Rat strain differences in sleep after acute mild stressors and short-term sleep loss. *Behavioural Brain Research* 160:60–71.
- Tanimizu T, Kenney JW, Okano E, Kadoma K, Frankland PW, Kida S (2017) Functional Connectivity of Multiple Brain Regions Required for the Consolidation of Social Recognition Memory. *The Journal of Neuroscience* 37:4103–4116.
- Tank AW, Lee Wong D (2015) Peripheral and central effects of circulating catecholamines. *Compr Physiol* 5:1–15.
- Taylor SE, Klein LC, Lewis BP, Gruenewald TL, Gurung RA, Updegraff JA (2000) Biobehavioral responses to stress in females: tend-and-befriend, not fight-or-flight. *Psychol Rev* 107:411–429.
- Tempesta D, Socci V, De Gennaro L, Ferrara M (2018) Sleep and emotional processing. *Sleep Medicine Reviews* 40:183–195.

REFERENCES

- Tenenbaum L, Chtarto A, Lehtonen E, Velu T, Brotchi J, Levivier M (2004) Recombinant AAV-mediated gene delivery to the central nervous system. *J Gene Med* 6 Suppl 1:S212-222.
- Tennent BJ, Smith ER, Davidson JM (1982) Effects of progesterone implants in the habenula and midbrain on proceptive and receptive behavior in the female rat. *Horm Behav* 16:352–363.
- Terreberry RR, Neafsey EJ (1987) The rat medial frontal cortex projects directly to autonomic regions of the brainstem. *Brain Research Bulletin* 19:639–649.
- Thierry AM, Tassin JP, Blanc G, Glowinski J (1976) Selective activation of mesocortical DA system by stress. *Nature* 263:242–244.
- Thorndike EL (1911) Animal Intelligence. *Psych Revmonog* 8:207–208.
- Thrivikraman null, Su null, Plotsky null (1997) Patterns of Fos-Immunoreactivity in the CNS Induced by Repeated Hemorrhage in Conscious Rats: Correlations with Pituitary-Adrenal Axis Activity. *Stress* 2:145–158.
- Thrivikraman KV, Nemeroff CB, Plotsky PM (2000) Sensitivity to glucocorticoid-mediated fast-feedback regulation of the hypothalamic-pituitary-adrenal axis is dependent upon stressor specific neurocircuitry. *Brain Res* 870:87–101.
- Tomaiuolo M, Gonzalez C, Medina JH, Piriz J (2014) Lateral Habenula determines long-term storage of aversive memories. *Front Behav Neurosci* 8 Available at: <https://www.ncbi.nlm.nih.gov/pmc/articles/PMC4026688/> [Accessed April 16, 2018].
- Tonhajzerova I, Mestanik M (2017) New Perspectives in the Model of Stress Response. 66:13.
- Tort ABL, Komorowski R, Eichenbaum H, Kopell N (2010) Measuring phase-amplitude coupling between neuronal oscillations of different frequencies. *J Neurophysiol* 104:1195–1210.
- Tort ABL, Komorowski RW, Manns JR, Kopell NJ, Eichenbaum H (2009) Theta–gamma coupling increases during the learning of item–context associations. *Proc Natl Acad Sci U S A* 106:20942–20947.
- Tort ABL, Kramer MA, Thorn C, Gibson DJ, Kubota Y, Graybiel AM, Kopell NJ (2008) Dynamic cross-frequency couplings of local field potential oscillations in rat striatum and hippocampus during performance of a T-maze task. *Proc Natl Acad Sci U S A* 105:20517–20522.
- Totty MS, Chesney LA, Geist PA, Datta S (2017) Sleep-Dependent Oscillatory Synchronization: A Role in Fear Memory Consolidation. *Front Neural Circuits* 11 Available at: <https://www.ncbi.nlm.nih.gov/pmc/articles/PMC5498516/> [Accessed April 27, 2021].
- Trainor BC (2011) Stress responses and the mesolimbic dopamine system: Social contexts and sex differences. *Hormones and Behavior* 60:457–469.
- Traub RD, Bibbig A, LeBeau FEN, Buhl EH, Whittington MA (2004) Cellular mechanisms of neuronal population oscillations in the hippocampus in vitro. *Annu Rev Neurosci* 27:247–278.
- Tronel S, Sara SJ (2002) Mapping of olfactory memory circuits: region-specific c-fos activation after odor-reward associative learning or after its retrieval. *Learn Mem* 9:105–111.
- Turner BH, Herkenham M (1991) Thalamoamygdaloid projections in the rat: a test of the amygdala's role in sensory processing. *J Comp Neurol* 313:295–325.
- Uliana DL, Gomes FV, Grace AA (2021) Stress impacts corticoamygdalar connectivity in an age-dependent manner. *Neuropsychopharmacology* 46:731–740.
- Ullsperger M, von Cramon DY (2003a) Error monitoring using external feedback: specific roles of the habenular complex, the reward system, and the cingulate motor area revealed by functional magnetic resonance imaging. *J Neurosci* 23:4308–4314.
- Ullsperger M, von Cramon Y (2003b) Error Monitoring Using External Feedback: Specific Roles of the Habenular Complex, the Reward System, and the Cingulate Motor Area Revealed by Functional Magnetic Resonance Imaging. *The Journal of Neuroscience* 23:4308–4314.
- Ulrich-Lai YM, Herman JP (2009) Neural regulation of endocrine and autonomic stress responses. *Nature Reviews Neuroscience* 10:397–409.
- Urban DJ, Roth BL (2015) DREADDs (Designer Receptors Exclusively Activated by Designer Drugs): Chemogenetic Tools with Therapeutic Utility. *Annual Review of Pharmacology and Toxicology* 55:399–417.
- Vale-Martínez A, Martí-Nicolovius M, Guillazo-Blanch G, Coll-Andreu M, Morgado-Bernal I (1997) Effects of habenular lesions upon two-way active avoidance conditioning in rats. *Neurobiol Learn Mem* 68:68–74.
- Valentino RJ, Van Bockstaele E (2008) Convergent regulation of locus coeruleus activity as an adaptive response to stress. *Eur J Pharmacol* 583:194–203.

REFERENCES

- Valentinova K, Mameli M (2016) mGluR-LTD at Excitatory and Inhibitory Synapses in the Lateral Habenula Tunes Neuronal Output. *Cell Reports* 16:2298–2307.
- Valjakka A, Vartiainen J, Tuomisto L, Tuomisto JT, Olkkonen H, Airaksinen MM (1998a) The fasciculus retroflexus controls the integrity of REM sleep by supporting the generation of hippocampal theta rhythm and rapid eye movements in rats. *Brain research bulletin* 47:171–184.
- Valjakka A, Vartiainen J, Tuomisto L, Tuomisto JT, Olkkonen H, Airaksinen MM (1998b) The fasciculus retroflexus controls the integrity of REM sleep by supporting the generation of hippocampal theta rhythm and rapid eye movements in rats. *Brain Res Bull* 47:171–184.
- Van de Kar LD, Piechowski RA, Rittenhouse PA, Gray TS (1991) Amygdaloid lesions: differential effect on conditioned stress and immobilization-induced increases in corticosterone and renin secretion. *Neuroendocrinology* 54:89–95.
- Van De Werd HJMM, Uylings HBM (2014) Comparison of (stereotactic) parcellations in mouse prefrontal cortex. *Brain Struct Funct* 219:433–459.
- van den Heuvel MP, Hulshoff Pol HE (2010) Exploring the brain network: A review on resting-state fMRI functional connectivity. *European Neuropsychopharmacology* 20:519–534.
- Van Someren EJW, Van Der Werf YD, Roelfsema PR, Mansvelder HD, da Silva FHL (2011) Slow brain oscillations of sleep, resting state, and vigilance. *Prog Brain Res* 193:3–15.
- van Strien NM, Cappaert NLM, Witter MP (2009) The anatomy of memory: an interactive overview of the parahippocampal–hippocampal network. *Nature Reviews Neuroscience* 10:272–282.
- Vanderwolf CH (1969) Hippocampal electrical activity and voluntary movement in the rat. *Electroencephalogr Clin Neurophysiol* 26:407–418.
- Veenema AH, Koolhaas JM, de Kloet ER (2004) Basal and stress-induced differences in HPA axis, 5-HT responsiveness, and hippocampal cell proliferation in two mouse lines. *Ann N Y Acad Sci* 1018:255–265.
- Veening JG, Böcker KBE, Verdouw PM, Olivier B, De Jongh R, Groenink L (2009) Activation of the septohippocampal system differentiates anxiety from fear in startle paradigms. *Neuroscience* 163:1046–1060.
- Velasquez KM, Molfese DL, Salas R (2014) The role of the habenula in drug addiction. *Frontiers in human neuroscience* 8:174.
- Velazquez-Hernandez G, Sotres-Bayon F (2021) Lateral Habenula Mediates Defensive Responses Only When Threat and Safety Memories Are in Conflict. *eNeuro* 8.
- Vertes RP, Kocsis B (1997) Brainstem-diencephalo-septohippocampal systems controlling the theta rhythm of the hippocampus. *Neuroscience* 81:893–926.
- Vetere G, Kenney JW, Tran LM, Xia F, Steadman PE, Parkinson J, Josselyn SA, Frankland PW (2017) Chemogenetic Interrogation of a Brain-wide Fear Memory Network in Mice. *Neuron* 94:363-374.e4.
- Vidal-Gonzalez I, Vidal-Gonzalez B, Rauch SL, Quirk GJ (2006) Microstimulation reveals opposing influences of prelimbic and infralimbic cortex on the expression of conditioned fear. *Learn Mem* 13:728–733.
- Vitaliano PP, DeWolfe DJ, Maiuro RD, Russo J, Katon W (1990) Appraised changeability of a stressor as a modifier of the relationship between coping and depression: a test of the hypothesis of fit. *J Pers Soc Psychol* 59:582–592.
- Vitkauskas M, Mathuru AS (2020) Total Recall: Lateral Habenula and Psychedelics in the Study of Depression and Comorbid Brain Disorders. *Int J Mol Sci* 21.
- Vogt BA, Paxinos G (2014) Cytoarchitecture of mouse and rat cingulate cortex with human homologies. *Brain Struct Funct* 219:185–192.
- von Stein A, Sarnthein J (2000) Different frequencies for different scales of cortical integration: from local gamma to long range alpha/theta synchronization. *International Journal of Psychophysiology* 38:301–313.
- Vouimba R-M, Yaniv D, Diamond D, Richter-Levin G (2004) Effects of inescapable stress on LTP in the amygdala versus the dentate gyrus of freely behaving rats. *Eur J Neurosci* 19:1887–1894.
- Wagner F, French L, Veh RW (2016) Transcriptomic-anatomic analysis of the mouse habenula uncovers a high molecular heterogeneity among neurons in the lateral complex, while gene expression in the medial complex largely obeys subnuclear boundaries. *Brain Struct Funct* 221:39–58.
- Wagner F, Stroh T, Veh RW (2014) Correlating habenular subnuclei in rat and mouse by using topographic, morphological, and cytochemical criteria: Subnuclear organization of the mouse habenula. *J Comp Neurol* 522:2650–2662.

REFERENCES

- Wallenstein GV, Eichenbaum H, Hasselmo ME (1998) The hippocampus as an associator of discontinuous events. *Trends Neurosci* 21:317–323.
- Walsh R (2011) Lifestyle and mental health. *Am Psychol* 66:579–592.
- Wang D, Li Y, Feng Q, Guo Q, Zhou J, Luo M (2017) Learning shapes the aversion and reward responses of lateral habenula neurons. *eLife* 6 Available at: <https://www.ncbi.nlm.nih.gov/pmc/articles/PMC5469615/> [Accessed April 16, 2018].
- Wang J-H, Cui S (2018) Associative memory cells and their working principle in the brain. *F1000Res* 7 Available at: <https://www.ncbi.nlm.nih.gov/pmc/articles/PMC5806053/> [Accessed April 14, 2021].
- Wang RY, Aghajanian GK (1977a) Physiological Evidence for Habenula as Major Link Between Forebrain and Midbrain Raphe. *Science, New Series* 197:89–91.
- Wang RY, Aghajanian GK (1977b) Inhibition of neurons in the amygdala by dorsal raphe stimulation: Mediation through a direct serotonergic pathway. *Brain Research* 120:85–102.
- Wang Z, Wang L, Yamamoto R, Sugai T, Kato N (2013) Role of the lateral habenula in shaping context-dependent locomotor activity during cognitive tasks. *Neuroreport* 24:276–280.
- Wasserman EA, Miller RR (1997) What's elementary about associative learning? *Annu Rev Psychol* 48:573–607.
- Weele CMV, Siciliano CA, Tye KM (2019) Dopamine tunes prefrontal outputs to orchestrate aversive processing. *Brain Research* 1713:16–31.
- Weiss T, Veh RW (2011) Morphological and electrophysiological characteristics of neurons within identified subnuclei of the lateral habenula in rat brain slices. *Neuroscience* 172:74–93.
- Wellman LL, Fitzpatrick ME, Hallum OY, Sutton AM, Williams BL, Sanford LD (2016) Individual Differences in Animal Stress Models: Considering Resilience, Vulnerability, and the Amygdala in Mediating the Effects of Stress and Conditioned Fear on Sleep. *Sleep* 39:1293–1303.
- Wheeler AL, Teixeira CM, Wang AH, Xiong X, Kovacevic N, Lerch JP, McIntosh AR, Parkinson J, Frankland PW (2013a) Identification of a Functional Connectome for Long-Term Fear Memory in Mice Sporns O, ed. *PLoS Comput Biol* 9:e1002853.
- Wheeler AL, Teixeira CM, Wang AH, Xiong X, Kovacevic N, Lerch JP, McIntosh AR, Parkinson J, Frankland PW (2013b) Identification of a functional connectome for long-term fear memory in mice. *PLoS Comput Biol* 9:e1002853.
- Whissell PD, Tohyama S, Martin LJ (2016) The Use of DREADDs to Deconstruct Behavior. *Front Genet* 7 Available at: <https://www.ncbi.nlm.nih.gov/pmc/articles/PMC4868840/> [Accessed April 7, 2018].
- Wilcox KS, Christoph GR, Double BA, Leonzio RJ (1986) Kainate and electrolytic lesions of the lateral habenula: effect on avoidance responses. *Physiol Behav* 36:413–417.
- Wilensky AE, Schafe GE, Kristensen MP, LeDoux JE (2006) Rethinking the fear circuit: the central nucleus of the amygdala is required for the acquisition, consolidation, and expression of Pavlovian fear conditioning. *J Neurosci* 26:12387–12396.
- Wills KE, Gosnell SN, Curtis KN, Velasquez K, Fowler JC, Salas R (2020) Altered habenula to locus coeruleus functional connectivity in past anorexia nervosa suggests correlation with suicidality: a pilot study. *Eat Weight Disord* 25:1475–1480.
- Wilson MA, Grillo CA, Fadel JR, Reagan LP (2015) Stress as a one-armed bandit: Differential effects of stress paradigms on the morphology, neurochemistry and behavior in the rodent amygdala. *Neurobiology of Stress* 1:195–208.
- Wiltgen BJ, Sanders MJ, Anagnostaras SG, Sage JR, Fanselow MS (2006) Context fear learning in the absence of the hippocampus. *J Neurosci* 26:5484–5491.
- Wirtshafter D, Asin KE, Pitzer MR (1994a) Dopamine agonists and stress produce different patterns of Fos-like immunoreactivity in the lateral habenula. *Brain Research* 633:21–26.
- Wirtshafter D, Asin KE, Pitzer MR (1994b) Dopamine agonists and stress produce different patterns of Fos-like immunoreactivity in the lateral habenula. *Brain Research* 633:21–26.
- Witter MP (2007) The perforant path: projections from the entorhinal cortex to the dentate gyrus. In: *Progress in Brain Research* (Scharfman HE, ed), pp 43–61 *The Dentate Gyrus: A Comprehensive Guide to Structure, Function, and Clinical Implications*. Elsevier. Available at: <https://www.sciencedirect.com/science/article/pii/S0079612307630039> [Accessed April 24, 2021].
- Womelsdorf T, Fries P (2007) The role of neuronal synchronization in selective attention. *Current Opinion in Neurobiology* 17:154–160.
- Wong RK, Prince DA, Basbaum AI (1979) Intradendritic recordings from hippocampal neurons. *Proc Natl Acad Sci U S A* 76:986–990.

REFERENCES

- Wood SK, Valentino RJ (2017) The brain norepinephrine system, stress and cardiovascular vulnerability. *Neuroscience & Biobehavioral Reviews* 74:393–400.
- Xu C, Sun Y, Cai X, You T, Zhao H, Li Y, Zhao H (2018) Medial Habenula-Interpeduncular Nucleus Circuit Contributes to Anhedonia-Like Behavior in a Rat Model of Depression. *Front Behav Neurosci* 12 Available at: <https://www.ncbi.nlm.nih.gov/pmc/articles/PMC6189744/> [Accessed April 30, 2021].
- Xu L, Anwyl R, Rowan MJ (1998) Spatial exploration induces a persistent reversal of long-term potentiation in rat hippocampus. *Nature* 394:891–894.
- Yamaguchi T, Danjo T, Pastan I, Hikida T, Nakanishi S (2013) Distinct roles of segregated transmission of the septo-habenular pathway in anxiety and fear. *Neuron* 78:537–544.
- Yañez J, Anadon R (1994) Afferent and efferent connections of the habenula in the larval sea lamprey (*Petromyzon marinus* L.): an experimental study. *J Comp Neurol* 345:148–160.
- Yang H, Jong JW de, Tak Y, Peck J, Bateup HS, Lammel S (2018) Nucleus Accumbens Subnuclei Regulate Motivated Behavior via Direct Inhibition and Disinhibition of VTA Dopamine Subpopulations. *Neuron* 97:434–449.e4.
- Yang L, Wellman LL, Ambrozewicz MA, Sanford LD (2011) Effects of Stressor Predictability and Controllability on Sleep, Temperature, and Fear Behavior in Mice. *Sleep* 34:759–771.
- Yetnikoff L, Cheng AY, Lavezzi HN, Parsley KP, Zahm DS (2015) Sources of input to the rostromedial tegmental nucleus, ventral tegmental area and lateral habenula compared: a study in rat. *The Journal of comparative neurology* 523:2426.
- Ylinen A, Bragin A, Nádasdy Z, Jandó G, Szabó I, Sik A, Buzsáki G (1995) Sharp wave-associated high-frequency oscillation (200 Hz) in the intact hippocampus: network and intracellular mechanisms. *J Neurosci* 15:30–46.
- Yokoyama M, Suzuki E, Sato T, Maruta S, Watanabe S, Miyaoka H (2005) Amygdalic levels of dopamine and serotonin rise upon exposure to conditioned fear stress without elevation of glutamate. *Neurosci Lett* 379:37–41.
- Yoo H, Yang SH, Kim JY, Yang E, Park HS, Lee SJ, Rhyu IJ, Turecki G, Lee HW, Kim H (2021) Down-regulation of habenular calcium-dependent secretion activator 2 induces despair-like behavior. *Sci Rep* 11:3700.
- Yu LC, Han JS (1990) Habenula as a relay in the descending pathway from nucleus accumbens to periaqueductal grey subserving antinociception. *Int J Neurosci* 54:245–251.
- Yuen EY, Wei J, Liu W, Zhong P, Li X, Yan Z (2012) Repeated Stress Causes Cognitive Impairment by Suppressing Glutamate Receptor Expression and Function in Prefrontal Cortex. *Neuron* 73:962–977.
- Zagami MT, Montalbano ME, Ferraro G, Sardo P, Caravaglios G, La Grutta V (1995) Electrophysiological and iontophoretic aspects of the habenular influence on hippocampal neurones. *Arch Physiol Biochem* 103:59–63.
- Zahm DS (2006) The evolving theory of basal forebrain functional—anatomical ‘macrosystems.’ *Neuroscience & Biobehavioral Reviews* 30:148–172.
- Zahm DS, Root DH (2017) Review of the cytology and connections of the lateral habenula, an avatar of adaptive behaving. *Pharmacology Biochemistry and Behavior* 162:3–21.
- Zerbi V, Floriou-Servou A, Markicevic M, Vermeiren Y, Sturman O, Privitera M, von Ziegler L, Ferrari KD, Weber B, De Deyn PP, Wenderoth N, Bohacek J (2019) Rapid Reconfiguration of the Functional Connectome after Chemogenetic Locus Coeruleus Activation. *Neuron* 103:702–718.e5.
- Zhang B, Gao Y, Li Y, Yang J, Zhao H (2016a) Sleep Deprivation Influences Circadian Gene Expression in the Lateral Habenula. *Behav Neurol* 2016 Available at: <https://www.ncbi.nlm.nih.gov/pmc/articles/PMC4930817/>.
- Zhang J, Tan L, Ren Y, Liang J, Lin R, Feng Q, Zhou J, Hu F, Ren J, Wei C, Yu T, Zhuang Y, Bettler B, Wang F, Luo M (2016b) Presynaptic Excitation via GABAB Receptors in Habenula Cholinergic Neurons Regulates Fear Memory Expression. *Cell* 166:716–728.
- Zhang L, Wang H, Luan S, Yang S, Wang Z, Wang J, Zhao H (2017) Altered Volume and Functional Connectivity of the Habenula in Schizophrenia. *Front Hum Neurosci* 11:636.
- Zhao H, Rusak B (2005) Circadian firing-rate rhythms and light responses of rat habenular nucleus neurons in vivo and in vitro. *Neuroscience* 132:519–528.
- Zhao H, Zhang BL, Yang SJ, Rusak B (2015) The role of lateral habenula-dorsal raphe nucleus circuits in higher brain functions and psychiatric illness. *Behavioural Brain Research* 277:89–98.

REFERENCES

- Zhao M-G, Toyoda H, Lee Y-S, Wu L-J, Ko SW, Zhang X-H, Jia Y, Shum F, Xu H, Li B-M, Kaang B-K, Zhuo M (2005) Roles of NMDA NR2B Subtype Receptor in Prefrontal Long-Term Potentiation and Contextual Fear Memory. *Neuron* 47:859–872.
- Zhao-Shea R, Liu L, Pang X, Gardner PD, Tapper AR (2013) Activation of GABAergic neurons in the interpeduncular nucleus triggers physical nicotine withdrawal symptoms. *Curr Biol* 23:2327–2335.
- Zheng C, Zhang T (2015) Synaptic plasticity-related neural oscillations on hippocampus-prefrontal cortex pathway in depression. *Neuroscience* 292:170–180.
- Zhou W et al. (2019a) A neural circuit for comorbid depressive symptoms in chronic pain. *Nature Neuroscience* 22:1649–1658.
- Zhou W et al. (2019b) A neural circuit for comorbid depressive symptoms in chronic pain. *Nature Neuroscience* 22:1649–1658.
- Zhu W, Umegaki H, Suzuki Y, Miura H, Iguchi A (2001) Involvement of the bed nucleus of the stria terminalis in hippocampal cholinergic system-mediated activation of the hypothalamo–pituitary–adrenocortical axis in rats. *Brain Research* 916:101–106.

RESUME FRANÇAIS

Résumé Français

Les mécanismes physiologiques qui sous-tendent l'adaptation comportementale face à une situation stressante sont étudiés depuis longtemps, depuis les travaux de Cannon, au début du siècle dernier. Il a ainsi été établi que cette adaptation dépend notamment de l'effet modulateur des glucocorticoïdes et de l'adrénaline sur l'activité cérébrale. Différents comportements ont été décrits en situation de stress et un réseau cérébral complexe leur a été associé. Cependant, plus de 100 ans plus tard, les processus qui sous-tendent la sélection de comportements adaptés face à une situation de stress ne sont toujours pas entièrement compris.

L'habénula latérale (HbL) est une sous-division de l'habénula, une structure cérébrale épithalamique que l'on dit « conservée » au cours de l'évolution, car on la retrouve chez toutes les espèces de vertébrés et notamment les poissons « préhistoriques » tels que le coelacanthé. Elle a été le mieux étudiée chez le rongeur, notamment le Rat et la Souris. Chez ces espèces, des études anatomiques ont révélé que l'HbL tient une place stratégique entre le système limbique et les ganglions de la base d'un côté, et les grands systèmes monoaminergiques mésencéphaliques de l'autre. En effet, elle reçoit des afférences depuis le cortex préfrontal médian, et l'hypothalamus, ainsi que depuis le pallidum, notamment le pallidum ventral et le noyau entopédonculaire (qui est l'équivalent de la portion interne du globus pallidus chez les mammifères, une voie de sortie des ganglions de la base). En aval, elle projette sur les noyaux dopaminergiques et sérotoninergiques. Cette connectivité unique fait de l'HbL un intégrateur d'informations télencéphaliques, informations qui ont trait aux processus cognitifs, émotionnels, ou liés à la récompense ; une fois ces informations traitées, l'HbL les transmet aux régions monoaminergiques afin que ces dernières modulent en retour le fonctionnement des structures gérant ces grands processus. L'HbL est considérée comme une structure pivot permettant d'adapter les réponses comportementales de l'individu en fonction des changements internes (physiologiques, psychologiques) et externes (informations contextuelles), notamment dans des situations d'urgence, générant un stress non négligeable, comme lors de la rencontre avec un prédateur. Cependant, la façon dont l'HbL s'intègre dans le vaste réseau qui soutient la réponse au stress n'est pas encore totalement comprise.

L'objectif principal de mon doctorat était d'étudier, chez le Rat, l'implication de l'HbL dans l'adaptation comportementale face à une situation stressante, ou potentiellement dangereuse, en essayant de la situer à l'intérieur du réseau de la réponse au stress. Dans ce cadre, nous voulions non seulement étudier les réponses comportementales au stress, mais également les mécanismes cognitifs qui sous-tendent ces réponses.

Résumé Français

Notre première étude avait pour but d'explorer le rôle de l'HbL lors d'un conditionnement de peur, un paradigme souvent utilisé pour étudier les processus de mémoire émotionnelle. Parce que l'HbL est directement connectée avec le cortex préfrontal médian, une connexion impliquée dans le maintien temporaire d'informations, et indirectement connectée avec l'hippocampe, une interaction très probablement impliquée dans le traitement d'informations contextuelles, nous avons utilisé un type de conditionnement engageant ces deux structures, c'est-à-dire un conditionnement de type « trace » ; dans ce test, un délai de 30 seconde est inséré entre la fin de la présentation du stimulus conditionnel (SC ; le son) et la survenue du stimulus inconditionnel (SI ; le choc électrique léger aux pattes). Dans cette configuration, le contexte devient l'élément prédictif le plus prégnant du stimulus aversif, le CS étant le moins prégnant. Nous avons fait cette étude dans le but d'explorer les possibles interactions fonctionnelles, pendant ce conditionnement, entre l'HbL et l'hippocampe et le cortex préfrontal médian, mais également l'amygdale. Lors d'une première expérience, grâce à la technique d'immunohistochimie, nous avons révélé l'expression de la protéine c-Fos (marqueur d'activité cellulaire) dans les régions précitées. Nous avons dans un premier temps constaté que c'est la partie médiane de l'HbL qui présentait une importante activation cellulaire, confirmant d'autres données de la littérature liant cette partie de l'HbL et la réponse au stress. Ensuite, sur les données de toutes les structures explorées, nous avons pratiqué une analyse factorielle, afin de mettre en évidence leurs interactions fonctionnelles. Nous avons ainsi pu mettre en évidence un premier niveau d'interaction entre la partie la plus rostrale de l'HbL et le cortex préfrontal médian, l'hippocampe dorsal et l'amygdale basolatérale, et un deuxième niveau d'interaction entre la partie plus postérieure de l'HbL et le reste de l'amygdale ; ces données suggèrent que l'HbL est impliquée dans plusieurs processus lors du conditionnement de trace, dans la gestion des informations contextuelles, avec l'hippocampe et le cortex préfrontal, et dans l'association entre les stimuli ainsi que l'élaboration de la réponse comportementale, avec l'amygdale. Lors d'une deuxième expérience, nous avons répété ce conditionnement, cette fois en inactivant l'HbL à l'aide d'une approche pharmacogénétique (DREADD). Ensuite, afin d'évaluer la mémoire des différentes associations, nous avons évalué la réaction de peur des animaux lors de leur réintroduction dans le contexte de conditionnement (test au contexte), et lors de leur réexposition au stimulus conditionnel, dans un environnement différent (test au son). Nous avons constaté que les animaux dont l'HbL avait été inactivée lors du conditionnement présentaient une moindre réaction de peur par rapport aux groupes témoins, signe d'un déficit d'association avec le contexte, et présentaient, lors de la réexposition au son, une réaction de peur plus importante que les animaux témoins, ce qui peut être considéré comme une réaction inadaptée, le son n'étant pas l'élément le plus

Résumé Français

prédictif du stimulus aversif. Nous avons pu conclure que non seulement l'HbL était impliquée, comme montré précédemment, dans le traitement des informations contextuelles, mais qu'elle était également impliquée dans l'attribution de la valence prédictive des différents indices associés, de près ou de loin, à un événement stressant.

Notre deuxième étude avait pour but d'explorer de manière plus détaillée le réseau fonctionnel engagé, et la place particulière que pourrait y tenir l'HbL, lors d'une exposition à une autre situation stressante aiguë, une contention (placement dans un tube étroit) d'une durée de 10 minutes. A nouveau, suite à cette contention, nous avons révélé l'expression de la protéine c-Fos, cette fois-ci dans 56 régions cérébrales. La corrélation entre les densités en cellules exprimant la protéine c-Fos de ces structures nous a permis de modéliser un réseau fonctionnel en utilisant un domaine mathématique appelé « Graph Theory ». Les interactions fonctionnelles à travers le réseau ont révélé plusieurs modules (communautés), suggérant que l'architecture de ce réseau permettait un traitement complexe des informations. De plus, nous avons constaté que l'activation de l'HbL était hautement corrélée avec celle des principales structures impliquées dans la réponse au stress, c'est-à-dire les structures précitées ainsi que les régions monoaminergiques, confirmant sa position de pivot entre ces différents systèmes. Afin de démontrer la nécessité de la présence de l'HbL pour maintenir l'intégrité de ce réseau fonctionnel, nous l'avons inactivé à nouveau en utilisant la technique DREADD. Malheureusement, nous avons pu constater que les animaux témoins ayant reçu uniquement le ligand "spécifique" du récepteur DREADD, la clozapine-N-oxycide (CNO), présentaient un réseau fonctionnel complètement remodelé lors de la contention, occultant l'effet potentiel de l'inactivation de l'HbL. Ces derniers résultats nous ont donc fourni des indications importantes sur les limitations de l'utilisation de la CNO.

Notre troisième et dernière étude a été élaborée sur la base des résultats obtenues lors des deux précédentes. En effet, l'interaction entre l'HbL et les principales structures limbiques de la réponse au stress (cortex préfrontal médian, hippocampe et amygdale) a suggéré qu'elle avait un rôle important dans l'intégration et le transfert d'informations provenant de ces structures en situation de stress. Cependant, avec le marqueur d'activité c-Fos, qui ne donne qu'une indication à un instant précis, nous ne pouvions pas étudier la dynamique temporelle de ces interactions. Par conséquent, dans cette dernière expérience, nous avons décidé d'explorer la communication entre ces structures (HbL, les régions cingulaire et prélimbique du cortex préfrontal médian, la région CA1 de l'hippocampe et l'amygdale basolatérale) lors de toutes les étapes d'un protocole d'immobilisation en utilisant l'enregistrement de leur activité électrophysiologique locale. La particularité de cette étude, par rapport à la précédente, est que nous avons procédé non pas à

Résumé Français

une mais à deux immobilisations de 10 minutes séparées par un délai de trois heures ; nous avons fait cela afin d'évaluer l'adaptation du réseau lors de la réexposition à cette situation stressante, et potentiellement aborder les mécanismes cognitifs d'habituation. Dans un premier temps, nous avons évalué l'apparition de comportements spontanés tels que les stéréotypies, qui apparaissent généralement chez les rongeurs en réponse à un stress. Dans un second temps, nous avons analysé la dynamique des différents stades de veille/sommeil afin d'étudier plusieurs mécanismes liés à la réponse au stress, qu'il s'agisse de la modulation du niveau de vigilance ou des processus de consolidation d'épisodes de vie survenant pendant le sommeil. Sur le plan comportemental, nous avons observé lors de la deuxième immobilisation une réponse moins soutenue que lors de la première, ainsi que, suite aux analyses de la dynamique des états de veille/sommeil, une diminution du temps passé en veille active et une augmentation du temps passé en sommeil à onde lente et en sommeil paradoxal ; ces données suggèrent la mise en place de phénomènes de plasticité issus de la mise en mémoire de l'expérience vécue lors de la première immobilisation. Suite à ces analyses, ayant observé une certaine variabilité inter-individuelle dans la réponse à la première immobilisation, nous avons procédé à la séparation de nos animaux en fonction de l'intensité de cette réponse ; cela a donné deux groupes, l'un composé des animaux ayant faiblement réagi et l'autre composé des animaux ayant fortement réagi. Nous avons constaté que ces groupes présentaient une synchronisation thêta différentielle de l'HbL pendant les périodes de veille active et de sommeil lent après la deuxième immobilisation, suggérant que l'HbL participait, durant ces différentes périodes, à différents processus impliqués dans la gestion du stress. De plus, nous avons observé une forte cohérence entre les oscillations thêta de l'hippocampe dorsale et de l'HbL pendant les épisodes de veille active et de sommeil paradoxal, suggérant que ces deux structures collaborent étroitement, probablement dans le but de gérer les informations contextuelles liées à l'expérience vécue.

THE END

"No great mind has ever existed
without a touch of madness."

- Aristotle -



QUAND LA FOLIE N'EST PAS TRES LOIN ...

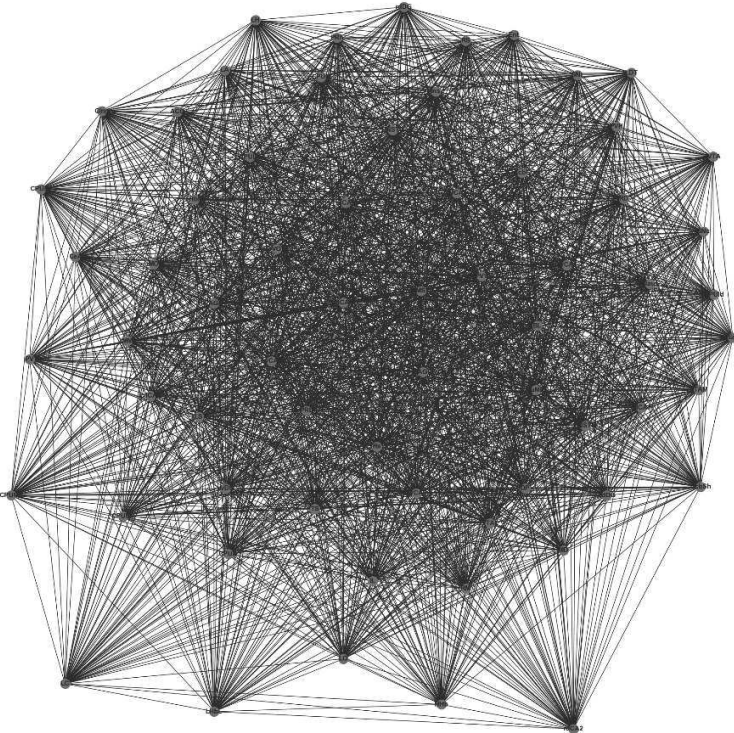
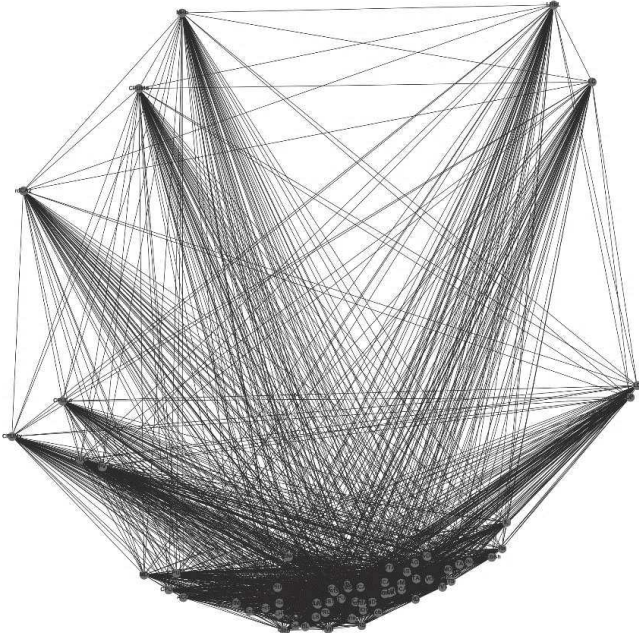


« Maitresse habénula, sur le thalamus perché,
Gérait la mémoire et l'anxiété,
Maitre hippocampe, de par son avidité,
Lui tint à peu près ce couplet
Hey bonjour, madame habénula
Que vous êtes centrale, que vous êtes extra
Sans mentir, si votre personnalité
Se rapporte à vos multiples fonctionnalités
Vous êtes le préfrontale de ces structures sous corticales
A ces mots, l'habénula ne se sent pas de joie
Et pour montrer qu'elle est une structure de choix
Emet un large signal et laisse s'échapper son thêta,
L'hippocampe s'en saisit et dit : Ma bonne madame
Apprenez que tout flatteur
Vit aux dépens de celui qui l'écoute.
Cette leçon vaut bien la mémoire, sans doute.
Le complexe habénulaire honteux et confus
Jura, mais un peu tard, qu'on ne l'y prendrait plus. »

Inspiré de Jean de La Fontaine, Les fables de La Fontaine



QUAND LES ERREURS DONNENT DE L'ART ...



Laura DURIEUX

Étude du rôle de l'habénula latérale dans la peur conditionnée et la réponse au stress chez le Rat

Résumé

L'adaptation de notre réponse comportementale face à un environnement menaçant est essentielle à la survie des individus. Cette capacité est soutenue par un vaste réseau cérébral. L'habénula latérale (HbL) semble être une structure importante dans la réponse au stress. Si l'HbL semble avoir sa place dans le réseau de structures impliquées dans la réponse au stress, à ce jour peu d'études ont été engagées afin de découvrir comment elle interagit avec ce réseau. Le but de mon projet de doctorat a été d'étudier le rôle de l'HbL dans la réponse à différentes situations stressantes, en focalisant nos investigations sur ces interactions fonctionnelles avec le réseau engagé dans la réponse au stress. Dans une première étude, nous avons démontré l'implication de l'HbL dans le conditionnement de peur ; de plus, nous avons montré que l'HbL interagissait avec les principales structures impliquées dans le conditionnement de peur, c'est-à-dire le cortex préfrontal médian, l'hippocampe et l'amygdale. Lors de notre deuxième étude, nous avons exploré plus profondément les réseaux cérébraux de la réponse au stress, ce qui nous a permis de mettre en évidence la position clé de l'HbL entre le système limbique et les centres monoaminergiques. La dernière étude que nous avons réalisée, en utilisant des enregistrements électrophysiologiques sur animaux vigiles, suggère une implication de l'HbL dans plusieurs processus, online et offline, impliqués dans la gestion d'événements stressant et potentiellement dans leur mise en mémoire. Dans l'ensemble, ces études permettent de mieux comprendre le rôle de l'HbL dans la réponse comportementale face à un environnement menaçant et supporte l'idée que qu'elle est un centre crucial d'intégration et de traitement des informations clés qui lui sont associées, afin d'adapter au mieux cette réponse.

Mots clés : habénula latérale ; conditionnement de peur ; réponse au stress ; réseaux fonctionnels

Résumé en anglais

Adapting our behavioral response when facing a threatening environment is essential to survival. This ability is supported by a wide brain network. The lateral habenula (LHb) seems to be an important structure of the stress response as it shows important activation in the presence of various stressors; it is postulated to interact with limbic structures such as the medial prefrontal cortex, the extended amygdala, and the hippocampus in order to participate to stress coping. However, these interactions remain poorly explored. The goal of my PhD project was to study in rats the role of the LHb in the stress response and how it is integrated into the wide network supporting such response, at the emotional, cognitive, and behavioral levels. In a first study, we demonstrated the implication of the LHb in fear memory, as well as its interaction with the key limbic structures engaged in this process. In our second study, we explored the functional network engaged during restraint stress and found the close interaction between the LHb and the whole stress response network, also including monoaminergic systems, suggesting the LHb contributes to the balance of the monoaminergic control over key limbic structures involved in the stress response. In our last study, using local field potential recordings, we discovered that the LHb was differentially engaged during the different steps of the response to immobilization stress, whether they take place during periods of active waking, or during sleep. Altogether, these results increase our knowledge of the engagement of the LHb in stress coping, in coordination with the key limbic regions involved in emotional processes; they further support the idea that this structure is a crucial hub of information integration, updating the network supporting the stress response.

Keywords: lateral habenula; fear conditioning; stress response; functional network